



Durham E-Theses

The pyretic sulphide deposits of the lahanos mine area, eastern black sea region, Turkey

Tugal, H. Tarik

How to cite:

Tugal, H. Tarik (1969) *The pyretic sulphide deposits of the lahanos mine area, eastern black sea region, Turkey*, Durham theses, Durham University. Available at Durham E-Theses Online:
<http://etheses.dur.ac.uk/9628/>

Use policy

The full-text may be used and/or reproduced, and given to third parties in any format or medium, without prior permission or charge, for personal research or study, educational, or not-for-profit purposes provided that:

- a full bibliographic reference is made to the original source
- a [link](#) is made to the metadata record in Durham E-Theses
- the full-text is not changed in any way

The full-text must not be sold in any format or medium without the formal permission of the copyright holders.

Please consult the [full Durham E-Theses policy](#) for further details.

Academic Support Office, Durham University, University Office, Old Elvet, Durham DH1 3HP
e-mail: e-theses.admin@dur.ac.uk Tel: +44 0191 334 6107
<http://etheses.dur.ac.uk>

THE PYRITIC SULPHIDE DEPOSITS OF THE
LAHANOS MINE AREA, EASTERN BLACK SEA
REGION, TURKEY.

A THESIS SUBMITTED FOR THE DEGREE OF DOCTOR OF
PHILOSOPHY IN THE UNIVERSITY OF DURHAM

by

H. TARIK TUĞAL (Dip. Geol. Istanbul; D.I.C. and M.Sc. London)

GRADUATE SOCIETY

AUGUST, 1969



ABSTRACT

The Lahanos pyritic sulphide deposit is one of the important copper deposits occurring within the submarine volcanic environment of the Eastern Pontus Ore province. It is situated 10 miles to the south of Espiye, Giresun Vilayeti. Petrographic study of the Lahanos rocks, despite their heavy alteration, shows that they belong mainly to the calc alkaline and tholeiitic basalt suites, and in addition, there are some high-alumina basalts. The intense igneous activity took place during the Mesozoic and the early and middle Tertiary periods. This phase of igneous activity culminated in the intrusion of syntectonic granites, tonolites and adamellites, and was followed by aplitic and hydrothermal phases, in the Pontid Geosyncline. The ore mineralisation, associated with dacites, is characterised by large quantities of pyrite associated with other base metal sulphides such as chalcopyrite, sphalerite, galena and other sulphides and sulphosalts. Field, underground and borehole evidence shows that the Lahanos ore body displays a zonal arrangement, which is similar to the well documented "Kuroko" type ore deposits in Japan. The results of detailed chemical and mineralogical study of the ore and country rock are given and the temperature of formation is estimated. Comparative details are given for the Murgul and Karadere deposits. The evidence supports an epigenetic hydrothermal origin for this "strata bound" deposit, but the volcanicity alone is inadequate to explain the source of the base metals, which are probably derived from the granites. The role of pyroclastic horizons of restricted permeability as a control of precipitation is discussed.

ACKNOWLEDGEMENTS

The author wishes to thank Professor G.M. Brown, the head of Department for making available the apparatus and technical assistance necessary for this study, and to Professor K.C. Dunham for suggesting the area of study.

I would like to express my sincere gratitude to Mr. R. Phillips who supervised the research. He is also to be thanked for his encouragement, criticism and advice throughout the course of this study.

The help of Dr. C.H. Emeleus and Dr. D.M. Hirst is gratefully acknowledged, for reading the sections on the petrology and rock chemistry respectively.

Dr. J.G. Holland kindly made available his computer programme for the reduction of the X-ray fluorescence data and thanks are due to Dr. G. Larwood for identification of the fossils.

Grateful thanks are due to Mr. G. Wilson and the technical staff of the department, especially Mr. G. Dresser who took great care with the photography.

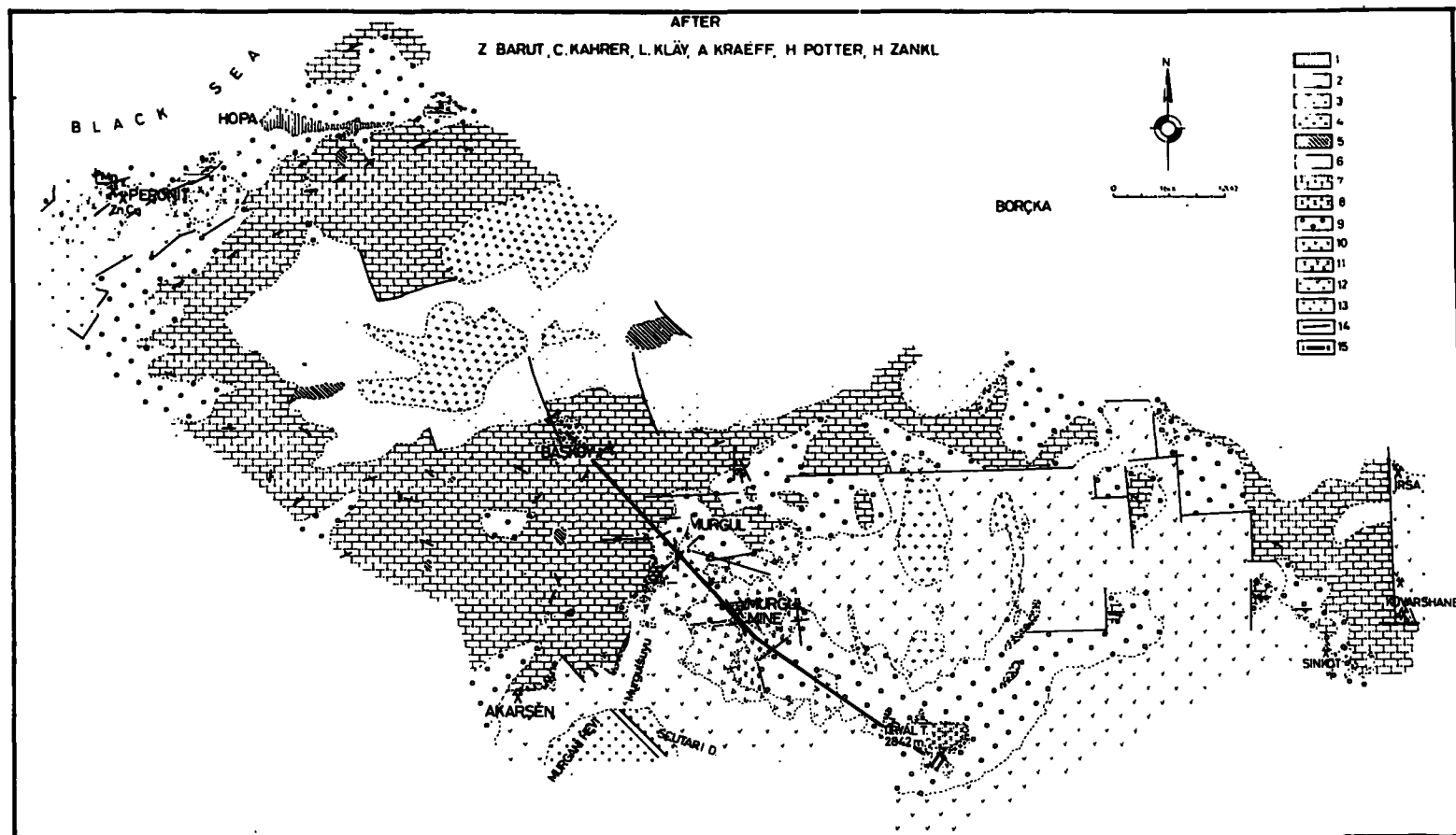
Acknowledgment is also made to those many people who gave advice and help during the preparation of this thesis.

MAP_3

GEOLOGICAL MAP OF THE HOPA-MURGUL REGION

AFTER

Z BARUT, C. KAHRER, L. KLÄY, A. KRAEFF, H. POTTER, H. ZANKL



1..Alluvial Pleistocene deposits, 2..Debris & landslide masses, 3..Late Tertiary basalts, andesites, 4..Tertiary tonalites, albite granodiorite, 5..Albite dacite III, 6..Tuff series (Upper Campanian-Eocene?), 7..Limestone-marl series (Upper Campanian-Eocene?), 8..Hippuritic limestone series (Turonian-Lower Campanian), 9..Spilite series II, 10..Albite dacite II, 11..Dacitic tuff, 12..Albite dacite I, 13..Spilite series I, 14..Fault line, 15..Section line

the River Halys and Batum. Its length is about 300 miles from east to west, and its average width is about 30 miles from north to south (See Map 1).

The Lahanos pyritic sulphide deposit occurs to the west of the middle of the Eastern Pontus Ore Province, and is located between Giresun Province (Giresun Vilayeti) and Trabzon province (Trabzon Vilayeti), about 10 miles inland from Espiye on the Black Sea Coast (See Map 2). The area studied in detail covers 27 square miles around the Lahanos copper mine. Within the detailed study area, there are eight pyritic sulphide deposits which have been worked possibly since medieval times.

The pyritic base metal sulphide deposits occurring throughout the Pontus Ore Province are of small size but very widespread. At present only two are working - one of them, in the Eastern Pontus Ore Province, is the Murgul Copper Mine, and the other is Kure["] Copper Mine in the Western Pontus Ore Province. In the near future the Lahanos Copper Mine will join them as a third Copper-Zinc producing mine.

Climate:

Because of northwesterly winds, the eastern Black sea area is always humid and rainy. The rainfall reaches a maximum of about one hundred inches a year, particularly in the Rizé region, whereas the southern slopes of the Pontic Mountains get less rain, and further south, towards the semi arid continental climate of

the Anatolian Plateau, annual rainfall gets smaller and smaller. The distribution of vegetation very closely follows these sudden climatic changes. Most of the pyritic base metal sulphide deposits occur within the high rainfall area, on the northern slopes of the Pontic Mountains covered by thick forest, dense bushes and thick soil. Because of its young and abrupt morphology the area shows a very young drainage pattern and most of the rivers and streams follow the main tectonic lines.

Because of these factors, the population is concentrated in the narrow coastal strip. The main agricultural products are hazelnuts, maize, tobacco and beans. Coastwise navigation is well developed in this area, and there is an important fishing industry.

CHAPTER B -- PREVIOUS WORK

B. PREVIOUS WORK

B.I Stratigraphy

Stratigraphic studies of the Eastern Pontids by different geologists show similar results. From north to south progressively older rocks occur and at the southern edge the base of the Pontid volcanic series is unconformable on Palaeozoic metamorphic rocks. The volcanic series of the Pontids starts with Liassic formations of transgressive conglomerate and concretionary limestone as a sedimentary facies and a spilitic agglomeratic series, (Schultze - Westrum, 1961). Volcanic activity continued throughout the Mesozoic and Tertiary into the Quaternary. The following stratigraphic column generalises the stratigraphic units over the whole Eastern Pontid area (this stratigraphic column has been based on the following author's ideas : Geoffroy (1960), Gettinger (1961), Kraeff (1963 a & b), Pollak (1961), Schultze-Westrum (1961)).

11. Sea and river Terraces,
10. Glacial Moraine,
9. The Young Basic Series,
8. The Tertiary Granitic intrusions,
7. Quartz-Biotite-Feldspar porphyry (=Hypabyssal dacite),
6. The Upper Basic Series,
5. The Upper Dacitic Series,
4. The Lower Dacitic Series,
3. The Lower Basic Series,
2. Granitic and Granodioritic Intrusions of the Palaeozoic,
1. Crystalline Basement.

1. The basement is believed to be of Palaeozoic or Precambrian? age, because of its grade of metamorphism compared to the

unmetamorphosed or slightly metamorphosed Mesozoic formations and its lack of fossils. Palaeozoic formations with a certain degree of metamorphism occur in various parts of the Pontids. The upper part of the crystalline basement also includes fossiliferous formations of the Permo-Carboniferous; therefore the Crystalline basement is sub divided into

a - The metamorphic series, represented by sericitic schists, biotite-schists, gneiss, augite-gneiss and quartzites at the Sirya and Ardanuç areas in the valleys of the River Çoruh and Imerhevi, Artvin (Kraeff, 1963a). Similar conditions apply in the " " Gumuşhane area where strongly folded formations have a general NE-SW strike with an average dip of 30° - 40° to the SE or NW (Gettinger, 1961). The average thickness is about 700 to 800 meters.

b - The Permo-Carboniferous rocks, mainly characterised by arkose, sandy schists and quartzites in the lower horizons whilst near the top there are quartzitic rocks interstratified with acidic lavas, tuffs and limestones. These fossiliferous Permo-Carboniferous formations contain Schwagerinae, Spirifer and Corals, west of Bayburt, " " Gumuşhane (Ketin, 1951). Their average thickness is about 2000 meters.

Petrographic similarity of these two units a & b suggests that they might have been deposited during the same period. Wherever they are exposed, they always overly the much older, possibly Pfc-Cambrian massif?, whose age has not been confirmed yet.

2. Granitic and granodioritic intrusions of the Palaeozoic are exposed in the River Çoruh and Imerhevi valleys (See Map 3.) These granodioritic intrusions cut through the crystalline basement metamorphic series and the Permo-Carboniferous series. The same intrusions are also well exposed in the Karamustafa Valley, Southwest of ^{" "}Gumüşhane where the granite is in contact with blocks of the Upper Carboniferous quartzites. The overlying Liassic conglomerates show pebbles of granite and granodiorite. Thus granodioritic intrusion took place between Permian and Jurassic and therefore represents the period of Hercynian granitic intrusion. Late granodioritic hypabyssal intrusion took place at the beginning of the Alpine orogenesis.

3. Various names have been proposed by other authors for the Lower Basic Series but this name seems to be the most appropriate description of the general nature of the beds. The Lower Basic Series ranges in age from the Lower Lias to the Upper Cretaceous, a thick sequence of volcanics being interstratified with fossiliferous limestone, marl and sandstone. The units forming the Lower Basic Series in the middle Pontids according to Schultze-Westrum, 1961 are shown in Tab. 1.

In the eastern parts of the Eastern Pontids, the Lower Basic Series consists of sodium rich keratophyre spilite with tuffs and agglomerates (^{" "}Kraeff 1963) with a thickness of about 500 meters in the Sirya-Ardanuç region and Murgul area (see Map 3).

TABLE 1

Stratigraphic column (after

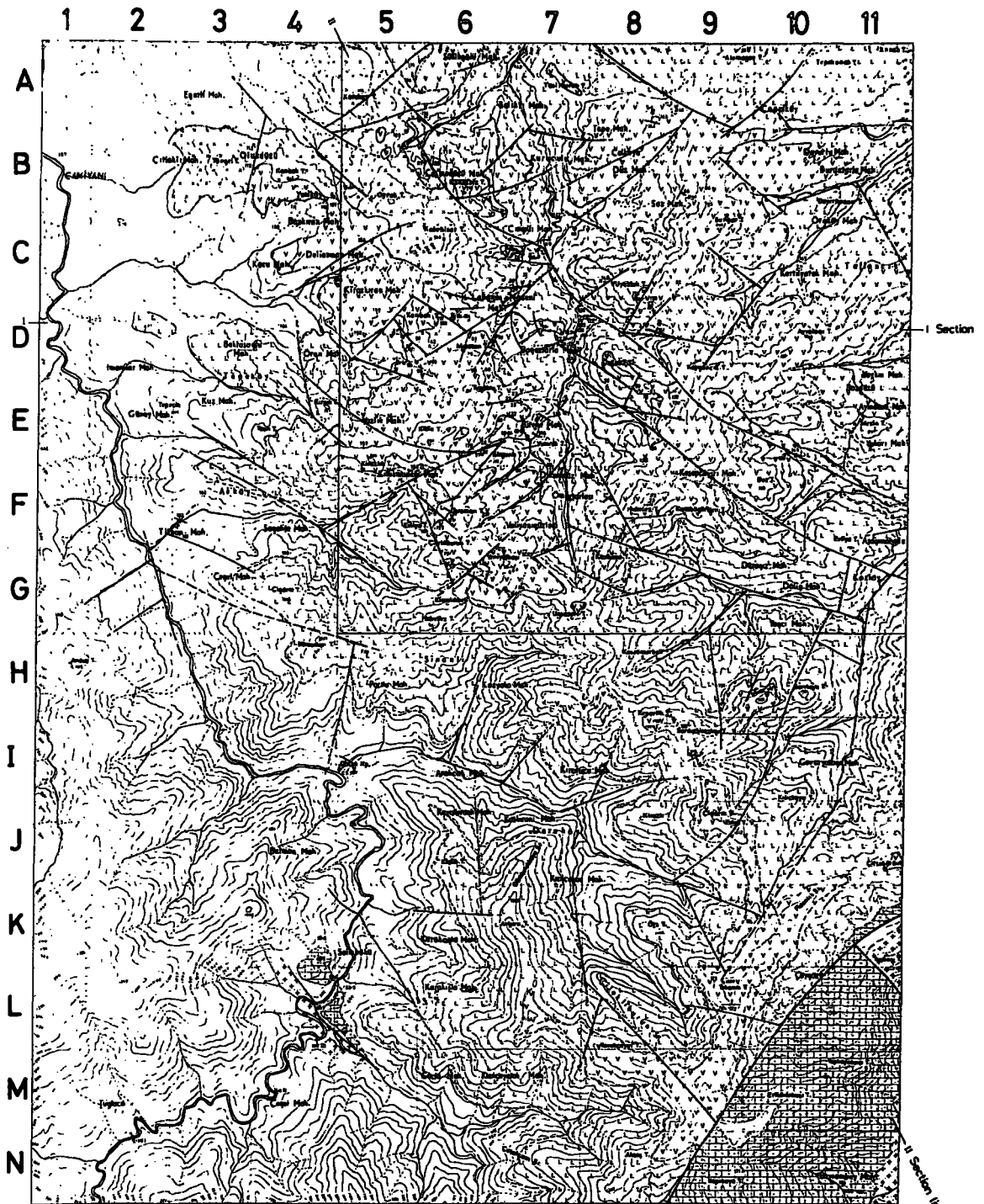
Name of the Series Quaternary formations	Sedimentary rock Sea & River Terra
Young volcanics and its sedimentary equivalents	Marly limestone of Oligocene and Myoc
	Andesitic tuffs
Upper Basic Series and its sedimentary equivalents.	Nummulitic limestone (Eocene) Tuffaceous marl-li series (Senonian)
Dacitic Series	Red Tuffaceous Inc limestone Red inoceramus lin
Lower Basic Series and its sedimentary members	Tuffaceous marl-li series and Hippuri limestone (Upper C Massive limestone: Cretaceous-Malm)
Bottom volcanics and its sedimentary equivalents	Concretionary lime and Transgressive Liassic Conglomer
Crystalline basement	Quartzitic conglom Para-rocks: Seric -Schists. Sericite Quartzit

In the Rize Çayeli region, this series mainly consists of basalts, andesites and volcanic agglomerate (Geoffroy, 1960).

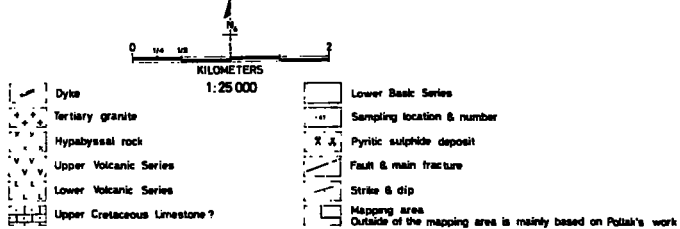
In the Lahanos area, this series is the oldest stratigraphic unit, exposed in river valleys and deep stream bottoms and forming the basement of the thick volcanic series. It is characterised by thick, predominantly green black spilite, basalts, agglomerates and interbedded Hippuritic limestone and marble or the massive limestone of the Lower Cretaceous or Malm at Mount Kapıkaya, in Bayrambey area (See Map 4, N9 and Geo. Sec. 1).

4. The Lower Dacitic Series is one of the most important Series within the Eastern Pontus Ore Province, from the point of view of the occurrences of pyritic sulphide deposits. The present concept concerning the occurrence of these sulphide deposits is that they are located either in the Lower Dacitic Series or at the contact with the Upper Dacitic Series. The Lower Dacitic Series is characterised by porphyritic dacitic lavas which exhibit rounded quartz phenocrysts and idiomorphic feldspar phenocrysts (albite) in a felsitic groundmass. Within the Lower Dacitic Series, due to hydrothermal alteration and mineralisation, the porphyritic dacites can be divided into three sub divisions e.g. in the Murgul Copper mine area Kraeff (1963 b) recognised the following types of dacite according to their field occurrence : (i) Fresh Dacite, (ii) Partly silicified dacite, (iii) Totally silicified dacite.

MAP_4



GEOLOGICAL MAP OF THE VICINITY OF LAHANOS COPPER MINE
EASTERN BLACK SEA NE TURKEY



The sedimentary equivalents of the Lower Dacitic Series have been described by Schultze-Westrum (1961) from the Giresun region, where they are mainly red Inoceramus Limestones interbedded with the dacitic series.

The upper Dacitic Series is also important in relation to the occurrence of pyritic sulphide deposits in the Eastern Pontus Ore Province. This series can be sub divided into:

b - Dacite II

a - Dacitic tuffs (including interbedded limestone and marl beds).

a - Dacitic tuffs immediately overlie the Lower Dacitic Series.

The pyritic sulphide deposits tend to occur at or near to the contact of the porphyritic dacite with tuffs. Limestone-marl intercalations within the Upper Dacitic Series are well developed in the Lahanos copper mine, particularly in boreholes above rich sulphide mineralisation.

b = Dacite II is well developed and described in the Murgul copper mine area where Dacite II partly overlies porphyritic dacite of the Lower Dacitic Series and the dacitic tuffs (Kraeff, 1963b) (see Map 3). Between porphyritic dacite and dacite II an unconformity has been described by Kraeff (1963b). Dacite II usually shows a greenish colour, but around the sulphide mineralisation, it tends to show red-violet colours. There is no mineralisation at the contact of porphyritic dacite and dacite II in the Murgul area.

6. The Upper Basic Series. It is possible to see this formation throughout the Eastern Pontids. In the Murgul region the series is represented by spilite, soda-keratophyre spilite with pillow-lava structure, spilitic agglomerate and spilitic tuff. They may contain xenoliths of reddish dacite II and reddish limestones.

In the Çayeli, Rize region this series consists of basalts and basaltic volcanic rocks, together with a few tuff intercalations (Geoffroy, 1960). The age is possibly Lower Eocene.

The Upper Basic Series consists of agglomerates, tuffs, spilites and basalts, keratophyre and andesite at Aksu Stream in Giresun region (Schultze-Westrum, 1961). The corresponding sediments are the tuffaceous limestone-marl series (Senonian in age) and Nummulitic limestones (Eocene in age).

7. Quartz-Biotite-Feldspar porphyry (=Hypabyssal dacite) has an intrusive character as well as extrusive. The equivalent of this porphyry is called "Dacite III" in the Murgul area by Kraeff (1963b) and the "Lahanos Tepe Dasiti" or "Intrusive Dacite" in the Lahanos area by Pollak (1961).

8. Tertiary Granitic intrusions occupy roughly the middle of the broken anticlinal axis of the Pontids and they are possibly syn-orogenic intrusions containing xenoliths of volcanics and other rocks.

In the Eastern part of the Eastern Pontids, the Tertiary granitic intrusions consist of different intrusions of tonalite,

granodiorite and granite. A tonalite is intruded into the Upper Basic Series and partly into Limestone-marl series rocks of Upper Cretaceous - Eocene age at Kise and Başköy village Murgul area (See Map 3). In Kokolet Su Stream, Murgul, another tonalitic, granodioritic intrusion is intruded into the Lower Dacitic Series. At their contact some unimportant pyrite impregnations are developed (Kraeff, 1963b).

In the western part of the Eastern Pontids syn-orogenic granitic intrusions consisting of augite-monzonite, hornblende-augite diorite, granodiorite, quartz diorite, hypabyssal granodiorite, granodioritic porphyry, quartz albitite, aplite and lamprophyre dykes have been described by Schultze-Westrum (1961).

9. The Young Basic Series (Young Basic volcanics and their intrusive series) in some parts of the Eastern Pontids, are well developed. In the Eastern part of the Eastern Pontids the series mainly consists of a series of andesites and a series of basalts, particularly in the Murgul-Çoruh area (See Map 3). Similarly andesite and basalts are also well developed in the Tirebolu region, near Israil Copper mine (See Map 2.)

In the western part of the Eastern Pontids the Young Basic Series consists of basaltic agglomerates, tuffs, quartz trachyte, trachyandesite, leucitite, tephrite, olivine leucitite, olivine basalt and sediments of marly limestone of Oligocene-Miocene age. Again basic dykes and volcanics of similar age are well described by

Geoffroy (1960) in the Rize region.

Partly albitized andesites, basalts and spilite with andesitic porphyries, porphyrite and diabases are described by Kraeff (1963a) in the Sirya-Ardanuç area.

10. Glacial moraines are found on the highest ridges of the Pontic Mountains. During the Pleistocene the formation of glacial valleys, terraces, moraine and boulder clay took place. Relicts of glaciers are still present today in the highest crests of the Eastern Pontic Mountains.

11. Sea and river terraces were also formed during the Pleistocene and their relicts are exposed along the narrow coastal plain of the Black Sea and big river channels.

B.II TECTONIC AND OROGENIC ACTIVITIES

Before discussing the tectonic features of the Pontic Mountains it will be useful to give a summary of the main tectonic units of Turkey. So far Turkey has been divided into many different units by previous workers e.g. Arni (1939), Blumental (1946), Egeran (1947), Ketin (1961 & 1965) (See Summary Tab. 2), but these involve no major change in the original divisions proposed by P. Arni (1939), of which the geographic distribution can be easily seen on Map 1.

(i) The Pontids are tectonically equivalent to the Pontic Mountains, which occupy the northern coast of Anatolia (Asia Minor) along the Black sea coast from Batum in the East to the Bulgarian border in the West, inside Turkish territory (See Map 1).

(ii) The Anatolids mainly occupy the highland of Anatolia (See Map 1).

(iii) The Taurids mainly occupy the Tauros Mountains along the Mediterranean Sea in the South (See Map 1).

(iv) The Iranids mainly occupy the southeastern Turkish mountains towards Persia (see Map 1). Taurids and Iranids can be tectonically combined together.

(v) Border folds occupy an area between Anatolia and the Arabian Massif (See Map 1).

The tectonic divisions of Arni (1939) and Egeran (1947) are based on the stratigraphy and magmatic activity in Turkey; whereas Ketin (1959), in his division, considered orogenic movements. In various parts of Turkey, different phases of different orogenic

TABLE 2

Tectonic Division of Turkey (after Ketin, 1966)

P. Arni 1939	M. Blumental 1946	N. Egeran 1947	I. Ketin 1961-1965
Pontids } North Pontids } South Pontids	Pontids Anatolids	{ Pontids { Anatolids { Intermediate Zone	Pontids
Anatolids	Intermediary massif of Central Anatolia	{ Ortaailides { Massif Intermediate { Içilides	Anatolids
Taurids Iranids	Taurids Iranids	Taurids Egean Iranids Onilides	Taurids
Border Folds (Anatolian-Iranian)	Irakids Syrian-Arabian Block	Border Folds (Anatolian-Iranian)	Border Folds

movements are present, but for the purposes of the present study, it will be sufficient to describe only those tectonic events affecting the Pontids, and in particular the Eastern Pontids.

The Pontids extend from the Lower Balkan foredeep in the West, to the Lower Caucasian foredeep in the East, (See Map 1). They are mainly composed of a series of faulted blocks yielding horst and graben structures which have been pointed out by many previous workers e.g. Zankl (1961) in the Harşit Valley, Schultze-Westrum (1961) in the Giresun area, and Kraëff (1963b) in the Sirya-Ardanuç area etc. The Pontids are tectonically divided into two groups by Schultze-Westrum (1961): Western and Eastern Pontids.

The Western Pontids are separated from the Anatolids by a tectonic line which has been described as "Paphlogonya Tectonic line" (Nowak, 1935), which extends from the estuary of the River Sangoria (Sakarya) along Bolu-Eskipazar-Devres Çay towards Samsun, where the tectonic line rejoins the Black Sea (See Map 1). The northern limit of the Western Pontids is thought to be beneath the Black Sea, except in the hinterland of the Ereğli-Zonguldak coal field, where the northern limit comes onto the shore.

The Eastern Pontids are separated from the Anatolids by another tectonic line, which is described as "Kelkit-Çoruh tectonic line" by Oswald (1912), and extends from the East of Samsun along the Kelkit and Çoruh valleys towards Batum area, where it turns southwards and follows the southern limit of the Lower Caucasian foredeep to the south, and forms the southern limit of the "Pambar

"-Gokça Zon" (See Map 1). The northern limit of the Eastern Pontids is beneath the Black Sea, except further east in "Meskische Horst" where the northern limit comes on the land and is exposed between the Meskische Horst and the Lower Caucasian foredeep (Schultze-Westrum, 1961) (See Map 1). The possible connection of the broken-block horst structure of the Eastern Pontids and a zone of broken-block horst structure of the Southern Crimea, so far has not been fully explained; similarly the possible extension of the Western Pontids into the Vardar Zone again has not been clearly proved.

The Eastern Pontids, due to faulting, tend to show a fault and fracture pattern lying in N-S, NW-SE, E-W, and NE-SW directions. In the Murgul and Çoruh area the predominant fracture and fault pattern shows a direction of N-S and E-W; whereas in Hopa and the Central area fracture and fault patterns run in the direction of NW-SE and SW-NE. These fractures and faults exert an important control on the intrusion of younger intrusives and ascendent hydrothermal solutions which formed economic Cu-Pb-Zn Sulphide deposits throughout the Eastern Pontids.

To the SW of Trabzon, the seaward sloping of the Pontids in some places is caused by a step faulting. The general direction of step faulting runs on a line more or less parallel to the present Coast line, i.e. to the general direction of the strike of the Pontic Mountains. There are also other fault sets, which run transverse to those step faults. In general both the transverse:

and longitudinal fault systems facilitated the ascent of the intrusive masses; and due to intrusive plutonic masses conditions were rendered quite favourable by a system of apical faults (Gattinger et al, 1962).

During the Quaternary due to epeirogenic movements along the Black Sea Coast terraces were formed. Today these terraces are about 200 meters above the present level of the Black Sea. Due to uplifting of the Pontids' batholith, regional tilting, with a dip of 25-30 degrees northwards, and gravity faulting with a dip of up to 70 degrees, occurred.

B.III MAGMATIC ACTIVITY

Magmatic activity in Turkey and its neighbour countries (i.e. Syria in SE, Greece in W) has been extensively studied by Dubertret (1953), Brunn (1952) and Borchert (1958). They give a broad outline of magmatic activity in this part of the world and they tend to relate ultrabasic and acidic magmatic activity by invoking differentiation and fractionation of the initial magma which was basaltic in composition, Borchert (1958).

The Pontids have more volcanic activity in their geological history than other tectonic units of Turkey. The volcanic rocks roughly cover 60% (compared to sedimentary rocks 15%, and intrusive rocks 25%) of the Eastern Pontids and their magmatic history can be divided into four main cycles:

- IV. The fourth magmatic cycle (mainly basic)
- III. The third magmatic cycle is a repetition of the second cycle i.e. (b) Acidic differentiation of the initial magma of the third cycle, (a) Basic differentiation.
- II. The second magmatic cycle is composed of (b) Acidic differentiation of the initial magma of the second cycle, (a) Basic differentiation.
- I. The first Post-Palaeozoic magmatic cycle (Hercynian grano-diorites).

I. The first magmatic cycle occurred in the Hercynian belt of the Pontids particularly in the area of Sirya-Ardanuç and yielded grano-dioritic intrusions, Kraeff(1963a).

II. The second magmatic cycle is due to differentiation and fractionation of the initial basaltic magma that produced the Lower Basic Series (See BI & field geology). Further differentiation

and fractionation yielded rocks of acidic composition i.e. the Dacitic Series. The furthestmost fractionation of acidic magma caused the silicification of the last products of the acidic fractionation. This alteration would be accepted as a late hydrothermal phase of the Second magmatic cycle. The second magmatic activity took place during the Lias and Senonian.

III. The third magmatic cycle is also composed of a basic fractionation and secondly an acidic fractionation. The first basic differentiation and fractionation of the initial magma produced the Upper Basic Series. The further differentiation and fractionation of the basic magma yielded an acidic magma which produced a series of intrusive rocks i.e. quartz-biotite-feldspar porphyry in the Lahanos area, granites, granodiorites and tonolites over the whole Pontids. Finally the third magmatic cycle ends up with a late hydrothermal phase. The third magmatic cycle can be placed between the Senonian and Post Eocene. The Upper Cretaceous and Eocene sediments were formed during the gap between basic and acidic differentiation and fractionation of the initial magma.

IV. The fourth magmatic cycle is basic in character and lasted between Eocene-Pleistocene. It produced mainly the Young basic intrusives and extrusives e.g. Andesitic and basaltic rocks in the East of the Eastern Pontids (Kraeff 1963).

Borchert's (1958) conclusions on the origin of the mineralisation

and magmatic activity were as follows: (i) a continuous crystallisation and differentiation of initial basaltic magma giving continuous fractionation products from ultr^abasic to rhyolite; (ii) later, an intermediate magma forming intrusive bodies, subvolcanoes and volcanics in the geosynclinals e.g. in the case of the Pontids eugeosynclinal where one could see pillow-lavas, melaphyre, spilites, keratophyres, andesites and finally dacite forming submarine lava flows; (iii) thirdly the upward movements of more acidic components gave the gaseous phase which caused auto-hydration (violent propylitisation) in the Pontids; (iv) fourthly, a final gaseous phase which formed different exhalative mineral deposits.

B.IV MINERALISATION

According to the special edition on copper mineralisation of M.T.A. (1966) the occurrences of copper mineralisation in Turkey can be broadly classified as follows:-

Ia. Copper mineralisation in crystalline schists e.g. in marbles, slates etc., mainly composed of chalcopyrite, bornite, covellite and hematite as primary minerals and cuprite, auzurite, malachite, native copper as secondary copper minerals.

Ib. Copper mineralisation near intrusive bodies of mainly Palaeozoic age, as pyrometasomatic deposits in limestones, with pyrite, sphalerite, argentiferous galena, chalcopyrite and sometimes hematite.

II. Copper mineralisation chiefly associated with or occurring in volcanic rocks of various ages, that may be also divided into three distinct groups: -

IIa. Copper deposits that are mainly associated with pillow-lavas, spilites and diabases e.g. Kure and Ergani Copper mines (See Map 1). These deposits are often found in the Mesozoic volcanics.

IIb. Copper deposits that mainly occur in more acidic volcanic rocks, mainly andesite, dacite and rhyolites.

IIc. Copper mineralisation genetically associated with the late Tertiary granitic intrusions in the volcanic environment.

In this thesis only groups IIb and II c will be dealt with

and subdivided and studied in a larger sense. The ages of the host rocks of these groups vary from Mesozoic to Lower Tertiary.

The Eastern Pontid area has so far been visited by many German geologists, and most of them favour accepting a sub-volcanic exhalative origin (According to the Schneiderhöhn's classification) e.g. Kieft (1956), Schultze-Westrum (1961) and Maucher (1960) etc. Some of them however suggested a hydrothermal origin e.g. Wijkerslooth (1946), Pollak (1961) and Geoffroy (1960), who describes two main phases of metalogenic history:

(i) Towards the end of emplacement of the dacitic lava flows i.e. a sub-volcanic episode which produced autoalteration products such as silicification, propylitisation, kaolinisation, pyritisation and calcification.

(ii) Due to emplacement of the Pontid's batholith

a - Contact metasomatic mineralisation

b - Hydrothermal mineralisation

Borchert (1958) thought that differentiation and fractionation of the initial basaltic magma finally yielded a gaseous phase giving different exhalative mineral deposits according to its different composition, and made the following suggestions:-

1. Supposing the later gaseous phases are rich in Fe Cl_2 , they form hematite deposits if they find a chemically suitable host rock, if not they produce reddish sediments (Flysche) in geosynclinals.

2. If the emanations are rich in H_2S then they form exhalative sulphide deposits (mainly copper deposits). Ergani and Kure can be regarded as typical of this group. They are always associated with pillow-lavas, spilite and diabase porphyries.

3. Apo-magmatic formations of radiolarite and manganese deposition occur when the source of emanations is deep seated.

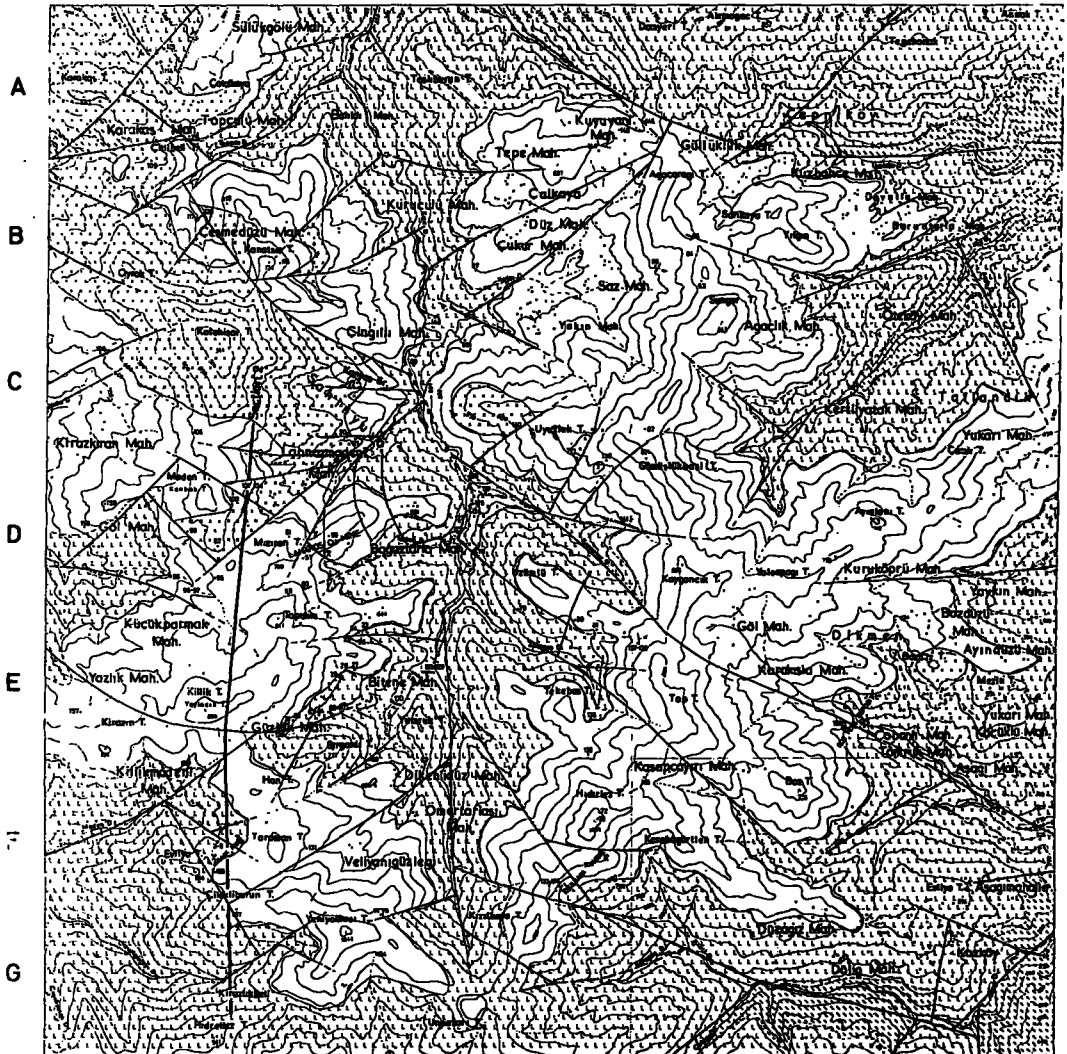
CHAPTER C - FIELD WORK

C. FIELD WORKINTRODUCTION

For the purpose of studying the genesis of the pyritic sulphide deposit of the Lahanos Cu-mine, a good deal of geological mapping and geochemical sampling was undertaken at surface, underground and from boreholes. During the field work a part of the 1/25,000 scale Geological map, a 1/10,000 scale geological, 1/5,000 detail geological map of the Lahanos copper mine site and finally 1/500 scale underground mapping were completed. (See maps, 4,5, 6 and 7). The area studied in detail covers 70 square kilometers (27 square miles) around the Lahanos copper mine. In addition to the Lahanos pyritic sulphide deposit, there are eight more minor mineralised localities, within the area studied in detail, which lie in a narrow belt, with an average width of three miles perpendicular to the Black Sea Coast.

A systematic grid sampling programme, in order to show primary distribution of major and minor elements at surface above the ore body, and another systematic sampling of boreholes in order to show the primary distribution of major and minor elements at depth towards the ore body, were collected (about 167 samples). Underground samples were collected to show the distribution of major and minor elements within the ore horizon, together with ore samples, from boreholes to show the vertical distribution (about 77 samples).

For comparison with the Lahanos mineralisation the following thirteen different mineral deposits have also been visited, starting

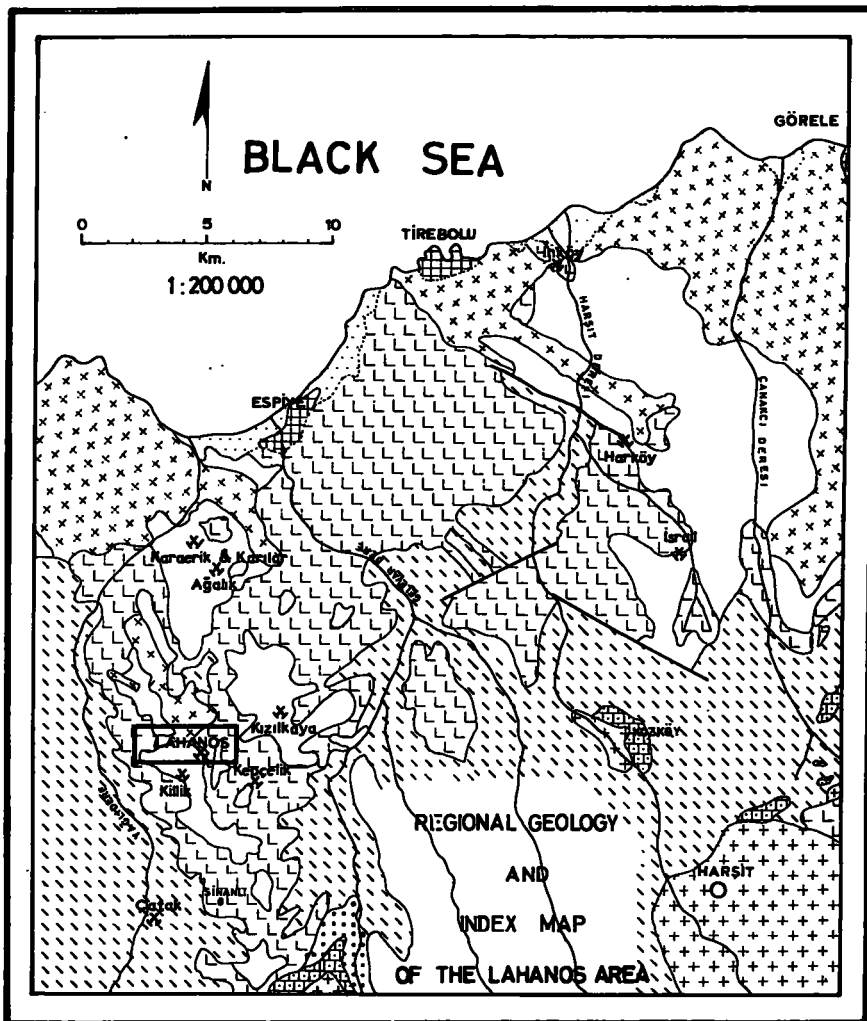


MAP.5_GEOLOGICAL MAP OF THE VICINITY OF LAHANOS COPPER MINE
EASTERN BLACK SEA NE TURKEY

1:10000



MAP_2



- | | | | |
|--|---|--|----------------|
| | Coastal plain and sea terrace | | Upper volcanic |
| | Tertiary granite | | Lower volcanic |
| | Skarn mineralisation | | Lower basic |
| | Upper Cretaceous limestone | | Fault |
| | Hypabyssal quartz-biotite-feldspar porphyry | | Mine site |
- (Compiled from M.T.A. records)

TABLE OF CONTENTS

	Page
ABSTRACT	i
ACKNOWLEDGEMENT	ii
TABLE OF CONTENTS	iii
LIST OF FIGURES	viii
LIST OF MAPS AND GEOLOGICAL SECTIONS	xiv
LIST OF TABLES	xv
LIST OF PLATES	xix
CHAPTER A - INTRODUCTION	1
Climate	2
CHAPTER B - PREVIOUS WORK	4
B. I - STRATIGRAPHY	4
B. II - TECTONIC AND OROGENIC ACTIVITIES	12
B. III - MAGMATIC ACTIVITY	16
B. IV - MINERALISATION	19
CHAPTER C - FIELD WORK	22
INTRODUCTION	22
C. I - COMMENTS ON MAPS	22
a - GEOLOGICAL SUCCESSION	24
The Lower Basic Series	24
Massive Limestone	25
The Lower Volcanics	26
The Upper Volcanics	27
Hypabyssal Rock	30
Tertiary Granitic Intrusions	30
Late Dykes	31
b - SOME STRUCTURAL COMMENTS	31
c - CONCLUSIONS	32
CHAPTER D - PETROGRAPHY OF THE LAHANOS AREA	35
Latite-Basalts	35
Alkali-Basalts	37
Tholeiitic Basalt-Andesites	38
Quartz-Andesites	39
Dacitic lava and Pyroclastics	40

CHAPTER D (Contd.)

Rocks of rhyodacitic composition	42
Rhyolitic pyroclastics and lavas	43
Quartz-andesitic rocks	44
Pyroxene basalt andesite	46
Hypabyssal dacites	47
Granitic intrusions	48
D. II - ROCK CHEMISTRY	52
a - Field and Petrographic Evidence of Alteration in the Lahanos Volcanic Rocks	53
Mineralogical alteration of basaltic rocks	54
Mineralogical alteration of andesitic rocks	55
Mineralogical alteration of acidic rocks	55
b - The effects of Alteration in the Chemistry of the Lahanos Volcanic Rocks	55
b1 - Common Alteration Products of the Lahanos Volcanic Rocks	56
General alteration trend of the Latite-basalts	56
General alteration trend of the Alkali-basalts	56
General alteration trend of the Tholeiitic basalt andesite	57
General alteration trend of the quartz-andesite	57
General alteration trend of the dacite	57
General alteration trend of the rhyodacite	58
General alteration trend of the Rhyo- lite	58
b2 - Effects of Alteration on the Variation of Major Oxides	59
Variation of Oxides with SiO ₂	59
Variation in Al ₂ O ₃	61
Variation in Iron Oxides	61
Variation in CaO	61
Variation in MgO	62
Variation in Na ₂ O	62
Variation in K ₂ O	62
Fe:Mg:(Na+K) ratios	63
K:Na:Ca ratios	64
Al:Ca:Na ratios	64
Total Iron Oxide - Magnesia ratio and Iron Enrichment - Total Mafic Ratios	65

CHAPTER D (Contd.)

D. III - VARIATION IN MINOR ELEMENTS	67
Variation in Barium	67
Variation in Strontium	68
Variation in Rubidium	69
Variation in Zirconium	70
Variation in Copper	71
Variation in Zinc	71
Variation in Sulphur	72
a - Summary of the Petrochemistry of the Volcanic Rocks of the Lahanos area	73
b - The Possible Origin of Basalts of the Lahanos area	74
c - The Possible Origin of the Andesite- Dacite-Rhyodacite of the Lahanos area	75
d - Stratigraphy - Modification of Field Observation following laboratory work	78
CHAPTER E - MINERALISATION OF THE LAHANOS AREA	
E. I - LAHANOS	80
a - MODE OF OCCURRENCE OF THE ORE	82
b - METHOD OF STUDY	84
c - ORE MICROSCOPY	84
Marginal Stockwork and Dissaminated Mineralisation	85
Ore Zone III	86
Ore Zone II	89
Ore Zone I	95
d - QUANTITATIVE PHYSICAL MEASUREMENTS ON THE LAHANOS ORES	97
X-ray Diffraction	97
Electron Microprobe Analysis	97
Enargite	99
Tetrahedrite-Tennantite	99
Bismuth-Tellurium-Sulphur Minerals	101
Reflectivity	104
Enargite	106
Bornite	106
Tetrahedrite-tennantite	107
Pyrite	107
Marcasite	109
Sphalerite	109
Galena	109
e - Wall-rock Petrography	110
Borehole A	110
Borehole B	113
" e - Mineralogy of Alteration Halo	116

	Page
CHAPTER E (Contd.)	
E. II - CHEMISTRY	119
A - Trace Elements in Sulphides	119
Ai - TRACE ELEMENT DISTRIBUTION IN PURIFIED INDIVIDUAL SULPHIDE MINERALS	120
pyrite	120
Chalcopyrite	123
Sphalerite	124
Bornite	126
Aii - MAJOR AND TRACE ELEMENT DISTRIBUTION IN LAHANOS NEW GALLERY 2	126
Bi - VERTICAL DISTRIBUTION OF MAJOR AND TRACE ELEMENTS	128
Lithophile major elements	128
Lithophile trace elements	129
Chalcopyrite major and trace elements	129
Siderophile major and trace elements	129
Bii - SURFACE GEOLOGY	129
CHAPTER F	
F. I - MURGUL	131
The geology and general setting of the area	133
The Lower Basic Series	133
The Lower Dacitic Series	134
The Upper Dacitic Series	134
The Upper Basic Series	135
The post-Cretaceous dacite III	135
Tertiary granitic intrusions	136
The Young Basic Series	136
Alluvial-Pleistocene deposits	136
Ia - MINERALISATION	136
Mode of Occurrences of Ore	136
Methods of Study	137
Ore Microscopy	137
Pyrite	137
Sphalerite	137
Chalcopyrite	138
Galena	138A
The Tennantite-tetrahedrite	138A
Neodigenite	138A
Covellite	139
X-ray Diffraction	139
Galena	140
Chalcopyrite	140
Reflectivity	140
Wall-rock Alteration	141
CHEMISTRY	141

CHAPTER F (Contd.)

F. II - KARADERE AND INKÖY (BLACK VEIN TYPE DEPOSITS)	143
FIIa - KARADERE (Pb-Zn-Cu) MINE	143
Minerology of ore	144
Ore microscopy	144
Pyrrhotite	144
Marcasite	145
Pyrite	145
Sphalerite	145
Enargite	145
Tennantite	145
Chalcopyrite	146
Galena	146
Covellite and Neodigenite	147
X-ray Diffraction	147
Sphalerite	147
Galena	148
Chalcopyrite	148
Reflectivity Measurements on Karadere Sulphides	149
Chemistry	149
FIIb - INKÖY (Pb-Zn-Cu) MINE	150
F. III - OTHER DEPOSITS OF THE EASTERN PONTUS ORE PROVINCE	150
Syngenetic or Syn-sedimentary submarine Exhalative Ore deposits	151
The pyrite deposits	151
The manganese deposits	151
Contact Metasomatic or Contact Pneumatolithic Deposits	152
CHAPTER G - CONCLUSION AND DISCUSSION ON ORIGIN OF THE LAHANOS PYRITIC SULPHIDE DEPOSIT	154
Field Observation	154
Ore microscopy	155
Chemistry of Ore	156
REFERENCES	167
APPENDIX	A-1

FIGURES

1. Stratigraphic column from Lahanos, Murgul and Latum mines.
- 2A General attitude of faults and main fractures in the vicinity of Lahanos Cu-mine Espiye, Eastern Black Sea, NE Turkey.
- 2B Structural diagram of the underground workings at the Lahanos Cu-mine, and possible main stress directions.
3. Distribution of volcanic rocks from the Lahanos area Espiye, Eastern Black Sea, Turkey.
4. Model classification of silicic volcanic rocks from the Lahanos area Espiye, Eastern Black Sea, Turkey.
5. The Al_2O_3 - total alkali - SiO_2 relation of three basalt types from the Lahanos area Espiye, Eastern Black Sea, NE Turkey.
6. The CaO value plotted against the corresponding alkali-lime index (proposed by Kuno, 1959) for Lahanos volcanic rocks.
7. Total alkali - SiO_2 relation in the alkali and tholeiite series of the Lahanos area Espiye, Eastern Black Sea, Turkey.
- 8A ACF diagram showing the relationship of latite and latite-basalts from the Lahanos area to the compositional fields of average basalt-andesite and common alteration products.
- 8B ACF diagram showing the relationship of alkali basalts from the Lahanos area to the compositional fields of average basalt-andesite and common alteration products.
- 8C ACF diagram showing the relationship of tholeiite basalt-andesites from the Lahanos area to the compositional fields of average basalt-andesite and common alteration products.
- 8D ACF diagram showing the relationship of quartz-andesites from the Lahanos area to the compositional fields of average basalt-andesite, acidic rock and common alteration products.
- 8E ACF diagram showing the relationship of dacites from the Lahanos area to the compositional fields of average acidic rock and common alteration products.
- 8F ACF diagram showing the relationship of rhyodacites from the Lahanos area to the compositional fields of average acidic rock and common alteration products.

- 8G ACF diagram showing the relationship of rhyolites from the Lahanos area to the compositional fields of average acidic rock and common alteration products.
9. Variation diagram for basalt-andesite-dacite-rhyolite, around Espiye in the Black Sea region, NE Turkey.
10. Variation in oxides with the Larsen's function in the Lahanos volcanic rocks.
11. Variation of $Fe:Mg:(Na + K)$ in rocks of the Lahanos area Espiye, Eastern Black Sea, Turkey. Skaergaard Trend, Crater Lake, Lassen Peak, Hakone Hypersthenic and Pigeonitic Series for comparison.
12. Variation of $K:Na:Ca$ ratios in rocks of the Lahanos area Espiye, Eastern Black Sea, Turkey. Lassen Peak, Crater Lake, Hakone Hypersthenic Series and St. Kitts for comparison.
13. Variation of $Al:Ca:Na$ ratios in rocks of the Lahanos area Espiye, Eastern Black Sea, Turkey. Japanese pigeonitic, Hypersthenic and Alkali series for comparison.
14. Variation in $MgO-(FeO + Fe_2O_3)$ ratios for volcanic rocks of the Lahanos area and their comparison to other volcanic areas.
15. Plot of iron enrichment $(FeO + Fe_2O_3) / (MgO + FeO + Fe_2O_3)$ against total mafics $(MgO + FeO + Fe_2O_3)$ for the rocks of the Lahanos area. Japanese Pigeonitic Series, Skaergaard Trend, Hawaiian Tholeiite and Alkali Series for comparison.
16. Variation in S, Sr, Rb, Zr, Ba, Cu, Ni and Zn contents of the Lahanos volcanic area Espiye, Eastern Black Sea, Turkey.
17. K/Rb ratio in volcanic rocks around Espiye, NE Turkey.
18. Distribution of S, Zn, Cu in the Lahanos pyritic sulphide deposit.
19. Distribution of Cu and Zn % in the Lahanos orebody.
20. Dispersion curves of chalcopyrite from the Karadere, Lahanos and Murgul mines.
- 20A The spectral reflectivity of chalcopyrites from the Lahanos mine.
- 20B The spectral reflectivity of chalcopyrites from the Murgul mine.
21. The spectral reflectivity of enargite from the Lahanos mine (A)
22. The spectral reflectivity of bornite from the Lahanos mine.

23. The spectral reflectivity of tetrahedrites-tennantites from the Lahanos mine.
24. Dispersion curves of anisotropic pyrite with a cell size of $a_0 = 5.4174 \text{ \AA}$ from the Lahanos mine.
- 24 A and B The spectral reflectivity of pyrites from the Lahanos mine (A).
25. The spectral reflectivity of marcasites from the Lahanos mine.
- 25A Dispersion curves of marcasite from the Karadere and Lahanos mines. (Solid lines for maximum reflection and dashed lines for minimum reflection).
26. The spectral reflectivity of sphalerites from the Lahanos mine.
- 26 A and B The spectral reflectivity of sphalerites from the Murgul (A) and Karadere (B) mines.
- 26C Dispersion curves of sphalerite from the Karadere, Lahanos and Murgul mines.
27. The spectral reflectivity of galenas from the Lahanos mine.
- 27A The spectral reflectivity of galenas from the Murgul mine.
- 27B The spectral reflectivity of galenas from the Karadere mine.
- 27C Dispersion curves of galena from the Karadere, Lahanos and Murgul mines.
28. Calibration graphs for XRF spectrography.
29. Lahanos NG2 - Distribution of the major ore elements S, Cu, Zn, Pb in NG2.
- 30A Lahanos Borehole A - Distribution of the lithophile elements SiO_2 , Al_2O_3 , total iron as Fe_2O_3 with depth
- 30B Lahanos borehole B - Distribution of the lithophile elements SiO_2 , Al_2O_3 , total iron as Fe_2O_3 with depth.
- 31A Lahanos borehole A - Distribution of the lithophile elements MgO , CaO , K_2O , Na_2O , MnO , TiO_2 with depth.
- 31B Lahanos Borehole B - Distribution of the lithophile elements MgO , CaO , K_2O , Na_2O , MnO , TiO_2 with depth.

- 32A. Lahanos borehole A - Distribution of the trace lithophile elements Ba, Sr, Cr, Zr, Ga, Rb with depth.
- 32B Lahanos borehole B - Distribution of the trace lithophile elements Ba, Sr, Cr, Zr, Ga, Rb with depth.
- 33A Lahanos borehole A - Distribution of the major elements S, Pb, Zn, Ba, Cu with depth in the ore horizon.
- 33B Lahanos borehole B - Distribution of the major elements S, Pb, Zn, Ba, Cu with depth in the ore horizon.
- 34A Lahanos borehole A - Distribution of the siderophile elements total iron as Fe_2O_3 , Mo, Ni with depth.
- 34B Lahanos borehole B - Distribution of the siderophile elements total iron as Fe_2O_3 , Mo, Ni with depth.
- 35A Lahanos borehole A - Distribution of the trace chalcophile elements As, Sb, Bi, Cd, Te, Ag with depth in the ore horizon.
- 35B Lahanos borehole B - Distribution of the trace chalcophile elements As, Sb, Bi, Cd, Te, Ag with depth in the ore horizon.
- 36A Lahanos borehole A - Distribution of the trace chalcophile elements S, Zn, Cu, Pb, Bi, As, Cd, Te with depth.
- 36B Lahanos borehole B - Distribution of the trace chalcophile elements S, Zn, Cu, Pb, Bi, As, Cd, Te with depth.
37. Surface distribution of various elements on the sampling grid.
- 37A Distribution of SiO_2 in surface value above the mineralisation at Lahanos Espiye.
- 37B Distribution of Al_2O_3 in surface values above the mineralisation at Lahanos Espiye.
- 37C Distribution of MgO in surface values above the mineralisation at Lahanos, Espiye.
- 37D Distribution of CaO in surface values above the mineralisation at Lahanos, Espiye.
- 37E Distribution of Na_2O in surface values above the mineralisation at Lahanos, Espiye.
- 37F Distribution of K_2O in surface values above the mineralisation at Lahanos, Espiye.

- 37G Distribution of TiO_2 in surface values above the mineralisation at Lahanos, Espiye.
- 37H Distribution of MnO in surface values above the mineralisation at Lahanos, Espiye.
- 37I Distribution of Ba in surface values above the mineralisation at Lahanos, Espiye.
- 37J Distribution of Sr in surface values above the mineralisation at Lahanos, Espiye.
- 37K Distribution of Zr in surface values above the mineralisation at Lahanos, Espiye.
- 37L Distribution of Ga in surface values above the mineralisation at Lahanos, Espiye.
- 37M Distribution of Cr in surface values above the mineralisation at Lahanos, Espiye.
- 38A Distribution of $FeO + Fe_2O_3$ in surface values above the mineralisation at Lahanos, Espiye.
- 38B Distribution of Mo in surface values above the mineralisation at Lahanos, Espiye.
- 38C Distribution of Ni in surface values above the mineralisation at Lahanos, Espiye.
- 39A Distribution of S in surface values above the mineralisation at Lahanos, Espiye.
- 39B Distribution of Cu in surface values above the mineralisation at Lahanos, Espiye.
- 39C Distribution of Zn in surface values above the mineralisation at Lahanos, Espiye.
- 39D Distribution of Pb in surface values above the mineralisation at Lahanos, Espiye.
- 39E Distribution of Bi in surface values above the mineralisation at Lahanos, Espiye.
- 39F Distribution of As in surface values above the mineralisation at Lahanos, Espiye.

- 39G Distribution of Sb in surface values above the mineralisation at Lahanos, Espiye.
- 39H Distribution of Cd in surface values above the mineralisation at Lahanos, Espiye.
- 39I Distribution of Te in surface values above the mineralisation at Lahanos, Espiye.
40. Map of Hokkaido and northern Honshu, showing location of old massifs (shaded), volcanic zones, principal calderas, and selected black ore mines.
41. Calculated "A" isosolubility curves for galena in NaCl-HCl-H₂O solutions at fixed $m_{\text{NaCl}}(t) = 3.0$ with superimposed phase relations in the system K₂O-Al₂O₃-SiO₂-H₂O at 15,000 psi after Hemley.

MAPS

1. Geographic position of the Pontids in Eastern Europe and Anatolia.
2. 1:200000 scale geological map of the Lhanos mine area.
3. Geological map of the Hopa-Murgul region.
4. Geological map of the vicinity of Lahanos copper mine, Eastern Black Sea, NE Turkey (1:25000). (In pocket).
5. Geological map of the vicinity of Lahanos copper mine, Eastern Black Sea, NE Turkey (1:10000). (In pocket).
6. Geological map of the Lahanos Cu-mine, Eastern Black Sea, NE Turkey. (1:5000). (In pocket).
7. Underground workings at Lahanos copper mine (1:500). (In pocket).
8. Key map for old boreholes and geochemical study locations at Lahanos.

GEOLOGICAL SECTIONS

1. Geological sections (from 1:25000 map). (In pocket).
2. Geological section (from 1:10000map).
3. Geological sections (from 1:5000 key map).
4. Geological section (through the Lahanos boreholes A and B).
5. Geological section of the Murgul area.

TABLES

1. Stratigraphic column (after Schultze-Westrum, 1961). p.6
2. Tectonic division of Turkey (after Ketin, 1966). p.12
3. Sequence of igneous activity and related volcanic rocks with corresponding sediments in the Lahanos region. p. 35
4. Chemical analyses of rocks from the Lahanos area. p.52
5. Trace element analyses of rocks from the Lahanos area. p.59
6. Chemical composition of various basalts in the Lahanos area, Espiye, Eastern Black Sea, NE Turkey. p. 61
- 7.1 Sphalerite - NG39 light coloured sphalerite, Lahanos mine, ore Zone II, New Gallery. p.97
- 7.2 Sphalerite - NG39 dark coloured sphalerite, Lahanos mine, ore Zone II, New Gallery. p.97
- 7.3 Galena - NGD16 associated with sphalerite, Lahanos mine, ore Zone II, New Gallery. p.97
- 7.4 Galena - NGD17 associated with sphalerite and chalcopryrite, Lahanos mine, ore Zone II, New Gallery. p.97
- 7.5 Chalcopryrite - NGD8 associated with bornite, Lahanos mine, ore Zone I, New Gallery. p.97
- 7.6 Chalcopryrite - NG36 associated with bornite, Lahanos mine, ore Zone I, New Gallery. p.97
- 7.7 Chalcopryrite - NG39 associated with sphalerite and pyrite, Lahanos mine, ore Zone II, New Gallery. p.97
- 7.8 Bornite - NGD8 associated with chalcopryrite, Lahanos mine, ore Zone I, New Gallery. p.97
- 7.9 Bornite - NG36 associated with chalcopryrite, Lahanos mine, ore Zone I, New Gallery. p.97
- 7.10 Pyrite - NGD17 associated with sphalerite, chalcopryrite and galena, Lahanos mine, ore Zone II, New Gallery. p.97

- 7.11 Pyrite - NG18 anisotropic pyrite, Lahanos mine, ore Zone III, New Gallery. p.97
- 7.12 Pyrite - 94 massive pyrite, Lahanos mine, Ore Zone III, surface sample. p.97
- 7.13 Sphalerite - M2 honey coloured sphalerite, Murgul mine. p.97
- 7.14 Sphalerite - M2 dark coloured sphalerite, Murgul mine. p.97
- 7.15 Galena - M2 associated with sphalerite and little chalcopyrite, Murgul mine. p.97
- 7.16 Chalcopyrite - M12 associated with sphalerite, Murgul mine. p.97
- 7.17 Chalcopyrite - M15 associated with sphalerite and pyrite, Murgul mine. p.97
- 7.18 Sphalerite - Kd. brownish sphalerite, Karadere mine, "Unye. p.97
- 7.19 Sphalerite - Kd. honey coloured sphalerite, Karadere mine, "Unye. p.97
- 7.20 Sphalerite - Kd. greenish translucent sphalerite, Karadere mine, "Unye, p.97
- 7.21 Sphalerite - Kd. dark coloured sphalerite, Karadere mine, "Unye. p.97
- 7.22 Galena - Kd. galena from mixed ore, Karadere mine, "Unye. p.97
- 7.23 Galena - Kd. galena rich ore, Karadere mine, "Unye. p.97
- 7.24 Chalcopyrite - Kd. in mixed ore, Karadere mine, "Unye. p.97
8. Comparative cell size determination of various sulphide minerals from the Eastern Pontus Ore Province p.97
9. Operating conditions for the electron probe analyser. p.98
- 10.1 Enargite No. 49 II, Lahanos, Ore Zone II. p.99
- 10.2 Enargite No. 48 I, Lahanos, Ore Zone II. p.99
- 10.3 Enargite No. 48 II, Lahanos, Ore Zone II. p.99
- 10.4 Enargite No. 48 IIIA, Lahanos, Ore Zone II. p.99
- 10.5 Enargite No. 48 IIIB, Lahanos, ore Zone II. p.99
- 10.6 Enargite No. 43 I, Lahanos, Ore Zone II. p.99
- 11.1 Zincian tetrahedrite No. 49 III, Lahanos, Ore Zone II. p.100

- 11.2 Zincian tennantite-tetrahedrite ('Zanbergerite') No. 48 IV, Lahanos, Ore Zone II. p.100
- 11.3 Ferroan tennantite No. 43 III, Lahanos, Ore Zone II. p.100
- 11.4 Zincian tetrahedrite H.A.1A, Inkoy. p.100
- 11.5 Zincian tetrahedrite H.A.1B, Inkoy. p.100
- 12.1 Tetradymite No. Ed, Lahanos. p.102
- 12.2 Tetrahymite No. Ee, Lahanos. p.102
- 12.3 Tetradymite No. Ef, Lahanos. p.102
- 12.4 Tetradymite No. Eg, Lahanos. p.102
- 12.5 Tetradymite No. Ei, Lahanos. p.102
- 12.6 Average of Ed, Ee, Ef, Eg and Ei. p.102
- 12.7 Tetradymite No. Ej, Lahanos. p.102
- 12.8 Tetradymite No. Eh, Lahanos. p.102
- 12.9 Tetradymite No. Ek, Lahanos. p.102
- 12.10 Tellurium-sulphur mineral OG37, Lahanos. p.102
13. Linearity of response of the photomultiplier. p.104
14. N.P.L. Reflectivity values for standards. p.115
15. Reflectivity measurements of chalcopyrite. p.115
16. Reflectivity measurements of enargite. p.106
17. Reflectivity measurements of bornite. p.106
18. Reflectivity measurements of tennantite-tetrahedrite. p.107
19. Reflectivity measurements of pyrite. p.107
20. Reflectivity measurements of marcasite. p.109
21. Reflectivity measurements of sphalerite. p.109
22. Reflectivity measurements of galena. p.109
23. Trace element distribution of pyrite, chalcopyrite, sphalerite, and galena in the Lahanos, Murgul and Karadere mines. p.120

24. Co and Ni analysis of concentrated sulphides from the Lahanos, Murgul and Karadere mines. p.120
25. Major and trace elements analyses of the NG2 and OG2 ore samples including other deposits. p.127
26. Major and trace element analyses of the boreholes A & B ore samples. p.128
- 27A. Major and trace element analyses of the borehole A rock samples. p.128
- 27B. Major and trace element analyses of the borehole B rock samples. p.128
28. Analyses of gases from Kalavea. p.159
29. Analyses of gases from Showa-Shinzon. p.159

NB

Tables follow the given page number

PLATES

1. General field appearance of the Lower Basic Series at Camiyani Yağlıdere, (showing upstream dip).
2. Pillow-lava structure of the Lower Basic Series in the river Yağlı, north of Camiyani.
3. General appearance of the agglomerate, in the river Yağlı, just south of Camiyani.
4. Hypabyssal dacite intrusion into the Lower Volcanic Series, at Boğaztarla (Map 4, D7).
5. Hypabyssal dacite intrusion into the Lower Volcanic Series, at Boğaztarla location (Map 4, D7).
6. Columnar Jointing, Upper Volcanic Series, Lahanos mine.
7. Acidic (rhyolitic) coarse fragment volcanic breccias at Sulukgözü, Mahallesi (Map 4, A6) in the Lahanos mine - Eskiye road.
8. Acidic (rhyolitic) coarse fragment volcanic breccias, cut by hypabyssal dacite, Sulukgözü Mahallesi (Map 4, A6) Lahanos mine - Eskiye road
9. Columnar jointing, hypabyssal dacite, Olukdüzü (Map 4, B3).
10. Granite cut by the Lake dyke (dark in colour) at Tuğlacık, River Yağlı (Map 4, N2).
11. Glass shards from the Upper Volcanic Series, at Çukur Mahalle (Map 4, B7). 350 x.
12. The southern outcrop of the pyritic sulphide ore at Lahanos copper-mine.
13. General view looking from NE of the Lahanos copper mine, Hydrothermally altered Lower Volcanic Series in the stream valley.
14. Zoning in ore Zone IV pyrite. 350 x
15. Colloidal and granular pyrite relationships, ore Zone III. 160 x
- 16A. Botryoidal texture in colloidal pyrite, ore Zone III. 875 x.
- 16B. Colloform banding in colloidal pyrite, ore Zone III. 73 x
17. Shattered pyrite replaced by gangue and chalcopyrite (Cataclastic or mottled texture in pyrite, ore zone III). 350 x
18. Atoll texture in pyrite due to replacing gangue mineral, ore Zone III. 160 x

19. Tennantite replaces and infills the interstices of granular pyrite, ore Zone III. 350 x.
- 20A. Sphalerite, gangue, barite relationships, ore Zone II. 160 x
- 20B. Sphalerite, gangue, barite relationships, ore Zone II. 160 x
- 20C. Sphalerite, gangue, barite relationships, ore Zone II. 160 x
- 21A. Sphalerite chalcopyrite relationship, ore Zone II. 160 x
- 21B. Sphalerite chalcopyrite relationship, ore Zone II. 160 x
- 21C. Sphalerite chalcopyrite relationship, ore Zone II. 160 x
22. Guided replacement of sphalerite by chalcopyrite (whitish gray) and tennantite (gray), ore Zone II. 160 x
- 23A. Emulsion type ex-solution blebs of chalcopyrite in sphalerite from the Kepçelik mine, Lahanos area. 875 x.
- 23B. Ex-solution lamellae of chalcopyrite in sphalerite from the Kepçelik mine, Lahanos area. 2200 x
24. Colloidal pyrite-pyrite and sphalerite relationships, ore Zone II. 73 x
25. Shelly colloform texture in pyrite, ore Zone II. 160 x
26. Colloidal pyrite-sphalerite-galena-tennantite-barite relationships, ore Zone II. 350 x
- 27A. Age relationships between colloidal pyrite and galena, gangue and tennantite, ore Zone II. 350 x.
- 27B. Age relationships between colloidal pyrite and galena, gangue, ore Zone II. 350 x
28. Framboidal pyrite-sphalerite relationships, ore Zone II. 875 x
29. Contorted banded texture in colloidal pyrite, ore Zone II. 160 x
30. Colloform banding of chalcopyrite, sphalerite, associated tennantite and gangue, ore Zone II. 350 x
- 31A. Shattered pyrite replaced by tennantite, ore Zone II closer to the ore Zone III. 600 x
- 31B. Tennantite-galena-bornite-gangue age relationship, ore zone II closer to the ore Zone I. 875 x
32. Enargite phenocryst, ore Zone II. 875 x

33. Enargite replaces interstices of pyrite, ore Zone II. 350 x
- 34A. Covellite-bornite-pyrite relation, ore Zone II, closer to the ore Zone I. 875 x.
- 34B. Covellite-bornite-pyrite relation, under cross nichols, ore Zone II, closer to the ore Zone I. 875 x
- 35A. Galena-bornite relation, ore Zone II closer to the ore Zone I. 875 x
- 35B. Galena-bornite relation, ore Zone II closer to the ore Zone I. 2200 x
36. Colloform banding of covellite and pyrite, ore Zone II. 875 x
- 37A. Colloidal pyrite-marcasite relationship. 375 x
- 37B. Colloidal pyrite-marcasite relationship, under cross nichols. 375 x
38. Matching wall texture in between pyrite and bornite, ore Zone I. 375 x
39. Chalcopyrite-bornite relation, ore Zone I. 875 x
40. Advance replacement of colloidal pyrite by bornite associated with chalcopyrite, ore Zone I. 875 x.
41. Bornite and colloidal pyrite relationship, ore Zone I. 375 x
42. Tennantite-chalcopyrite-bornite relationship, ore Zone I. 375 x
43. Occurrence of native gold in bornite, ore Zone I. 2200 x
44. Matching wall texture between pyrite and chalcopyrite, ore Zone I. 375 x
45. Spherulitic texture of colloidal pyrite, ore Zone I. 375 x
- 46A. Framboidal pyrite sphere, ore Zone I. 2200 x
- 46B . Framboidal pyrite sphere, ore Zone I. 600 x
- 47A. Colloidal pyrite-bornite-chalcopyrite relationship, ore Zone I. 875 x
- 47B. Colloidal pyrite-bornite relationship, ore Zone I. 600 x
- 48A Zoned-crystalline texture in pyrite associated with bornite, Ore Zone I. 875 x
- 48B. Zoned-crystalline texture in pyrite associated with bornite, ore Zone I. 2200 x
49. The electron image of Plate 32, ore Zone II.

- 49A. The X-ray image of Cu in Plate 32, ore Zone II.
- 49B. The X-ray image of As in Plate 32, ore Zone II.
- 49C. The X-ray image of Sb in Plate 32, ore Zone II.
- 50A. General view of tetradymite (Bi-Te-S) mineral in association with pyrite, chalcopyrite and tennantite. 375 x
- 50B. Right hand corner of Plate 50 at higher magnification. 875 x
- 50C. The second group of (Bi-Te-S) mineral association with pyrite and chalcopyrite. 50 x
- 51. The backscattered electron image of Plate 50A, Lahanos mine.
- 51A. The backscattered electron image of the grain IIe.
- 51B. The X-ray image of Bi in the sample IIe.
- 51C. The X-ray image of Te in the sample IIe.
- 51D. The X-ray image of ~~As~~ in the sample IIe.
- 51E. The X-ray image of Au in the sample IIe.
- 52. Occurrences of Te-S-(Bi) mineral in ore Zone III pyrite, Lahanos. 875 x
- 53. Ore-hanging-wall relationship in borehole A.
- 54. The general view of the alteration above the Lahanos mine.
- 55. The second generation sphalerite (dark gray) and chalcopyrite relationship, Murgul mine. 160 x
- 56. Chalcopyrite lamellae in sphalerite, Murgul mine. 2700 x.
- 57. Icosahedron pyrite crystal from Murgul mine.
- 58. The general field occurrence of the Black vein type mineralisation at Inkoy, Tirebolu.

CHAPTER A - INTRODUCTION

A. INTRODUCTION

This particular research is based on a study of the mode of occurrence and the genesis of pyritic base metal sulphide deposits within the submarine volcanic environment at the Lahanos copper mine and a comparison with other pyritic base metal sulphide deposits occurring in the Eastern Black Sea area. Maps, 1, 2 & 3 show the areas of interest, all located in the Eastern Pontic mountains (Doğu Karadeniz Dağları)* of N.E. Turkey.

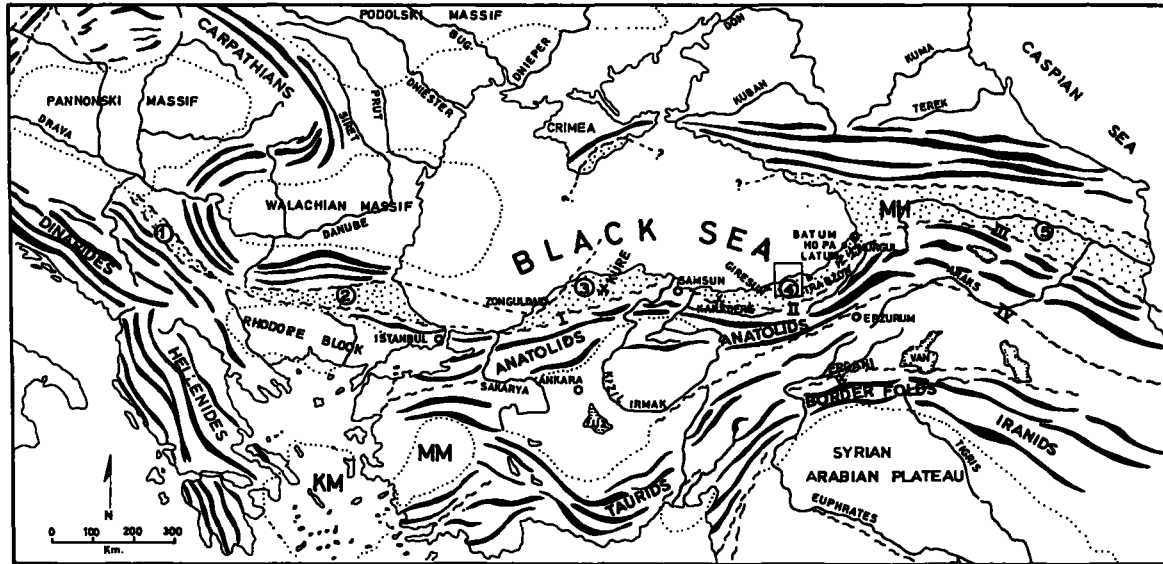
The Pontic mountains start from the estuary of the River Sangarius (Sakarya Nehri) and extend eastward along the Black Sea Coast to Batum (Russia). They are divided into western and eastern major units by the River Halys (Kizil Irmak) (See Map 1). In the south they rest on the Anatolian Plateau and, in the north, they form the abrupt coastal mountains of the Black Sea. The relief of the mountain chain increases eastwards and near the Russian border it reaches almost its maximum. The highest point is Mount Kaçkar (Kaçkar Tepeleri), 12917 feet (3,937 m) above sea level. The Pontic Mountain chain is geologically known as the "Pontids".




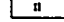
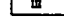
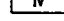
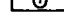
This thesis will deal only with pyritic base metal sulphide deposits in the region known as the "Eastern Pontus Ore Province" (Doğu Karadeniz Cevher Bölgesi) which includes the area between







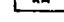
*Names in brackets following place names are Turkish names.

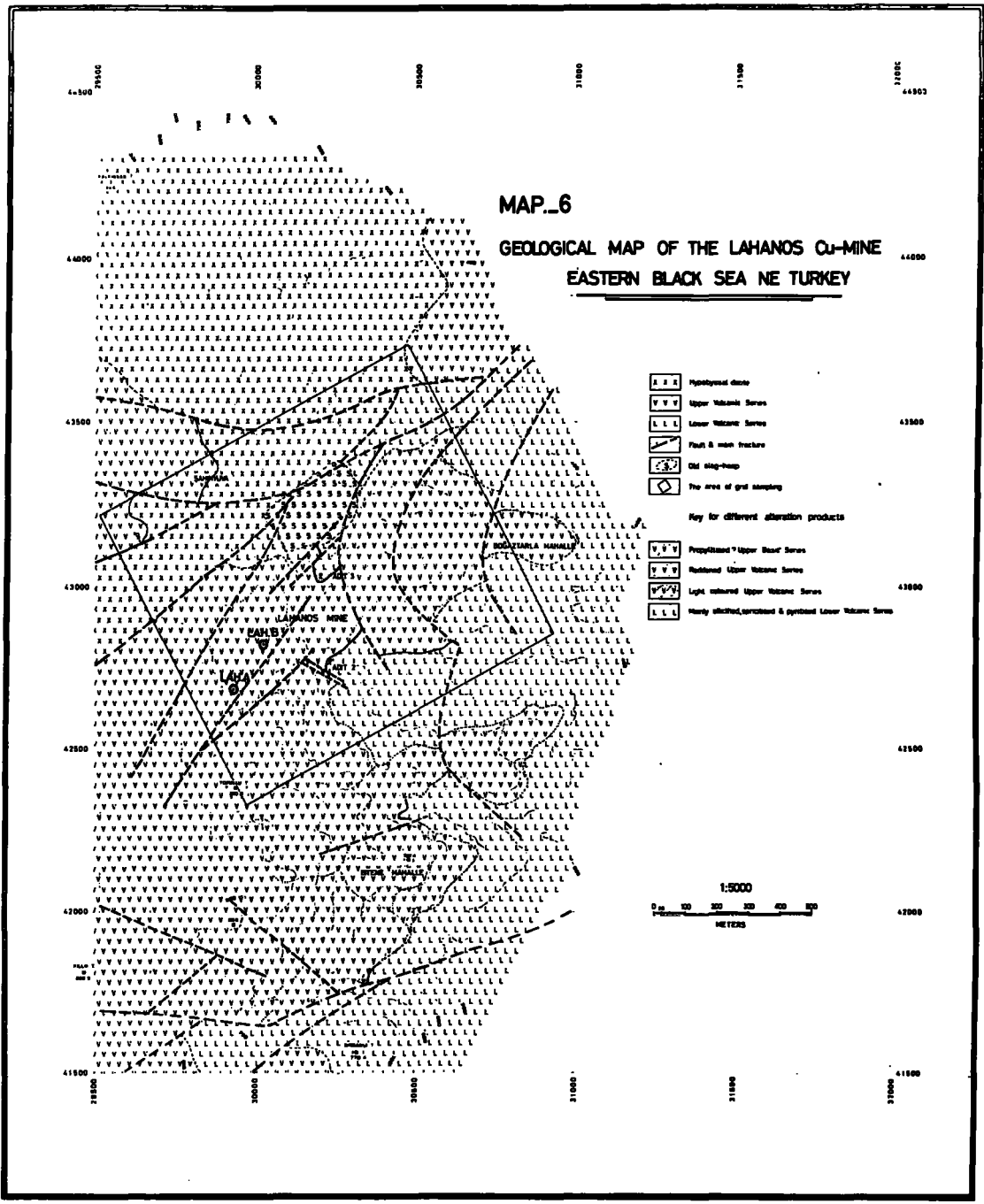
MAP_1

GEOGRAPHIC POSITION OF THE PONTIDS IN EASTERN EUROPE AND ANATOLIA
(After Schultze-Westrum)



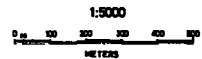
-  Young folding system
-  Major fault & tectonic line
-  "Paphlagonya izi"
-  "Kelkit-Çoruh zonu"
-  Pambar-Gökçe zone
-  Erzurum-Ararat-Araks zone
-  Vardar zone

-  Lower Balkan foredeep
-  Western Pontids
-  Eastern Pontids
-  Lower Caucasian foredeep
-  Meski horst
-  Menderes Massif
-  Kiklâdhes Massif



MAP_6
GEOLOGICAL MAP OF THE LAHANOS Cu-MINE
EASTERN BLACK SEA NE TURKEY

- Hypothetical dike
 - Upper Volcanic Series
 - Lower Volcanic Series
 - Fault & main fracture
 - Old slag-heap
 - The area of grid sampling
- Key for different alteration products**
- Propylitic Upper Volcanic Series
 - Reddish Upper Volcanic Series
 - Light colored Upper Volcanic Series
 - Heavy silicified, carbonated & pyritic Lower Volcanic Series



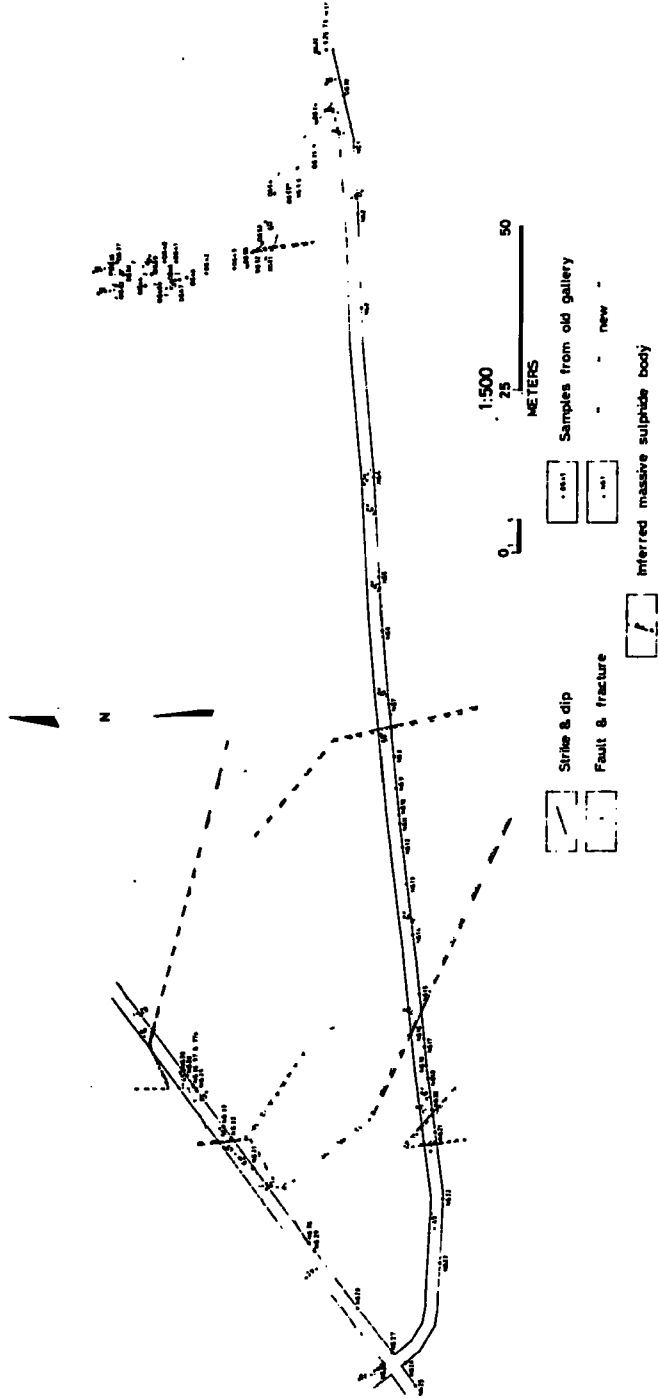
9900

9850

9800

9750

MAP. 7. UNDERGROUND WORKINGS AT LAHANOS COPPER MINE



from the East near the Russian border (Maps, 1, 2, 3, 4 and 5).

Murgul Copper Mine, Borçka, Artvin, is the biggest and only

working mine among these deposits (Maps 1 and 3);

Pilarcivat Cu-Pb-Zn-Fe-(Mn) deposit, Ardeşen, Rize (Map 1);

Latum Cu-Zn-Pb, (an old mine) Çayeli, Rize (Map 1);

Israil (Kovanpinari) Copper Mine (an old mine), Trabolu,

Giresun (Map 2);

Kaflar & Karaerik Cu-Zn-Pb deposits (old mines), Espiye,

Giresun (Map 2);

Killik Copper Mine (an old mine), Espiye, Giresun

(Map 4);

Kizil Kaya Copper Mine (an old mine), Espiye, Giresun (Map 4);

Boztepe massive pyrite deposit, Tomruk Mahallesi, Espiye,

Giresun (Map 4);

Kepçelik Pb-Zn-Cu deposit, Yağci Mahallesi, Espiye, Giresun

(Map 4);

Kapi Kaya Fe-Skarn mineralisation, Bayrambey, Espiye, Giresun,

(Map 4);

Çatak Fe-skarn mineralisation, Sinanlı, Camiyani, Giresun,

(Map 4);

Karadere Cu-Pb-Zn Mine, Kumarli, Ünye, Ordu, (Map 1).

C.I COMMENTS ON MAPS

The area shows a very young drainage system, dendritic at the middle of the mapping area i.e. around the Lahanos Copper Mine, and

subdendritic towards the East and West edges of the field area, i.e. towards the river Yağlıdere and Gelavera. These young drainage patterns follow the main structural lines i.e. faults and fracture zones. The whole area without any exception is covered by heavy forest, bushes and dense fern. Because of its abrupt morphology and heavy rainfall there is not much soil on the slopes, and due to the hot climate there has been a lot of surface weathering.

CIa GEOLOGICAL SUCCESSION

Within the mapping area the rocks are mainly volcanics. The following mappable units were recognised:-

7. Late dykes (mainly basic and intermediate)
6. Tertiary granitic intrusion
5. Hypabyssal rocks
4. Upper Volcanics (including the Upper Basic Series)
3. Lower Volcanics
2. Massive Limestones
1. Lower Basic Series

1. The Lower Basic Series that are the oldest rock unit are exposed mainly in the deeply eroded river valleys in the mapping area and form the basement of the thick volcanic series. Various names have been proposed by other authors for the Lower Basic Series, but this name seems to be the most appropriate description of the general nature of these beds, whose age ranges from the Lower Jurassic (?Lias) to the Upper Cretaceous (Schultze-Westrum,

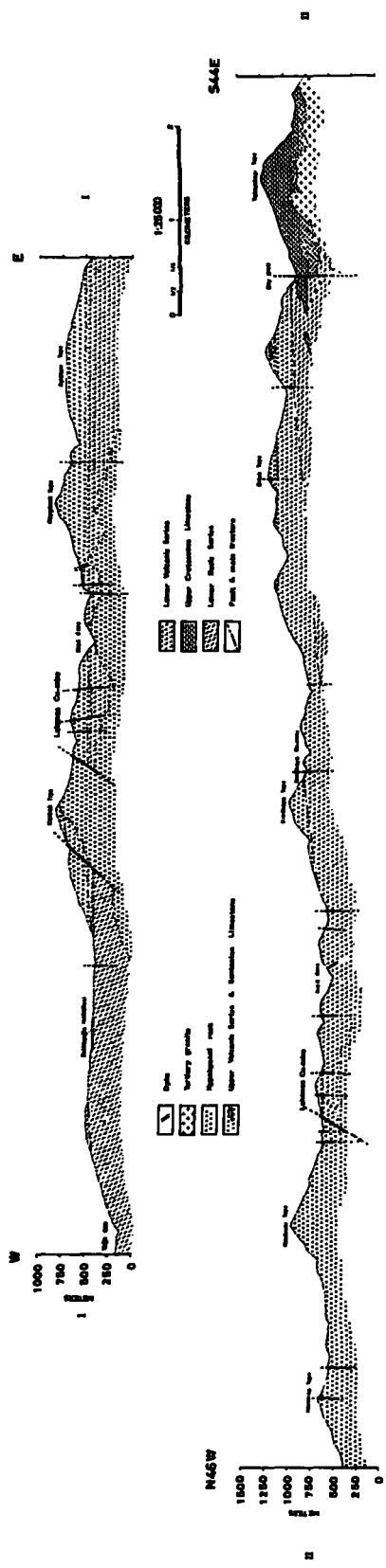
1961), a thick sequence of volcanics being interstratified with limestones. This characterised by thick predominantly green-black spilites, pillow lavas, alkali basalts, agglomerates (Plates 1, 2 and 3) and interbedded Hippurites-bearing thermally metamorphosed limestone at Kapikaya (N9) in the Bayrambey area and marble at Saimbuku in Yağlıdere (L4 in Map 4 and geological sections).

In the valley of the Yağlıdere e.g. at Değirmendere by the foot bridge (F3), the Lower Basic Series consists of various flows of latite and alkali basalts interbedded with thick green bedded agglomerate (basic in character) (Plate 3) and spilites. The visible thickness of this series up to the Lower Volcanic Series is over 150 meters, although the base is not seen (Plate 1). Both here and further north, it is difficult to see any Upper Cretaceous limestone interbedded with the volcanics, but upstream towards Saimbuku (Map 4), there are some isolated recrystallised limestone lenses in which no fossils have been found. Recrystallisation and formation of skarn mineralisation in these small lenses of limestone is due to emplacement of a Tertiary granitic (tonalite) intrusion. These unfossiliferous massive limestone lenses in the Lower Basic Series might represent the Malm or Lower Cretaceous Limestone (See Tab. 1). The general appearance of the Lower Basic Series can be seen in Plate 1 from Yağlıdere at Camiyani (Map 4 B1).

2. Massive Limestone as a mappable unit consists of mainly whitish, bluish, gray limestone at the southeast corner of Map 4 in the Kapikaya, Topkayabaşı (M11) and Bayrambey areas, here again,

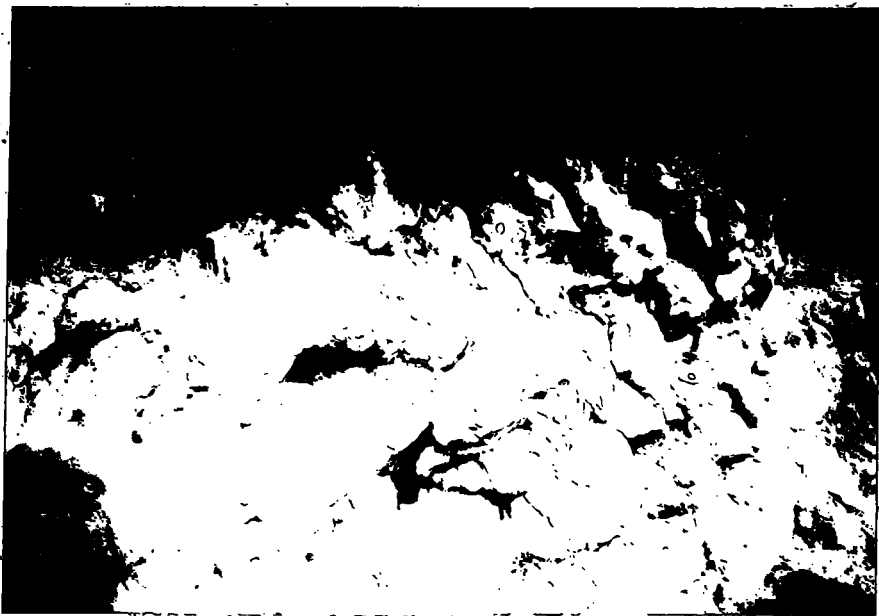
Geo. Sec.-1

GEOLOGICAL SECTIONS (From 1:25,000 map)

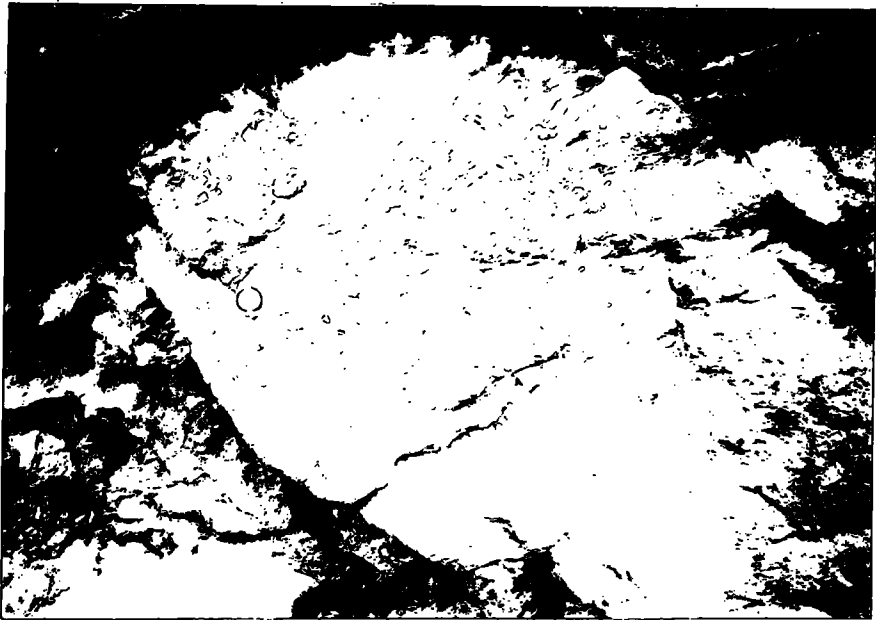




Pl. 1. General field appearance of the Lower Basic Series at Camiyani Yaglidere, (showing upstream dip)



Pl. 2. Pillow-lava structure of the Lower Basic Series in the River Yagli, north of Camiyani



Pl. 3. General appearance of the agglomerate, in the river Yağlı, just south of Camiyani.



Pl. 4. Hypabyssal dacite intrusion into the Lower Volcanic Series at Boğagtarla (Map 4, D7).

due to the Tertiary granitic intrusion a skarn mineralisation of mainly specularite, magnetite, garnets and calc-silicates has been developed. Although no determinable fossils have been found in this limestone, the presence of some organic calcite remains (bivalves) suggests that this mappable unit is at least Cretaceous or possibly Lower Upper Cretaceous in age, having lateral and vertical facies changes into the Lower Basic Series.

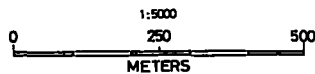
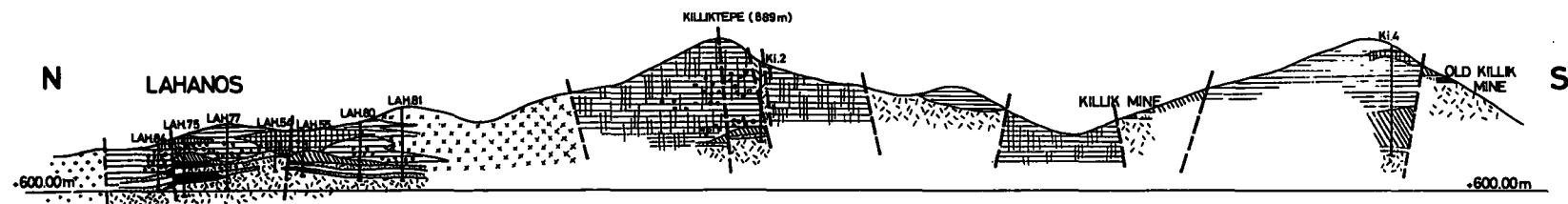
Another limestone interbedded with the Lower Basic Series is found at Saimbuku " " (Map 4, L4) in the upper course of the Yağlıdere where lenses of limestones are completely interbedded within the Lower Basic Series. Due to the granitic intrusion these limestones are thermally metamorphosed to marble and they contain some skarn and metasomatic iron ore mineralisation.

3. The Lower Volcanics are the second oldest volcanic rock series in the mapping area and overlie the dark green agglomerate, and brown or dark green spilite of the Lower Basic series at the northern bank of the Dēgirmendere, in the Tilhan Mahallesi (Map 4, F3) where an almost complete stratigraphic section can be seen towards the Killik Madeni (Section 2). At the same location it is also possible to see the overlying Upper Volcanic Series. Here the Lower Volcanic Series is possibly represented either by a single composite lava flow containing three different flow units or by three different lava flows (owing to weathering and hydrothermal alteration, the exact relationship is difficult to establish).

Geo. Sec._2

GEOLOGICAL SECTION

(AFTER A.POLLAK & A.GÜMÜŞ, from 1:10 000 map)



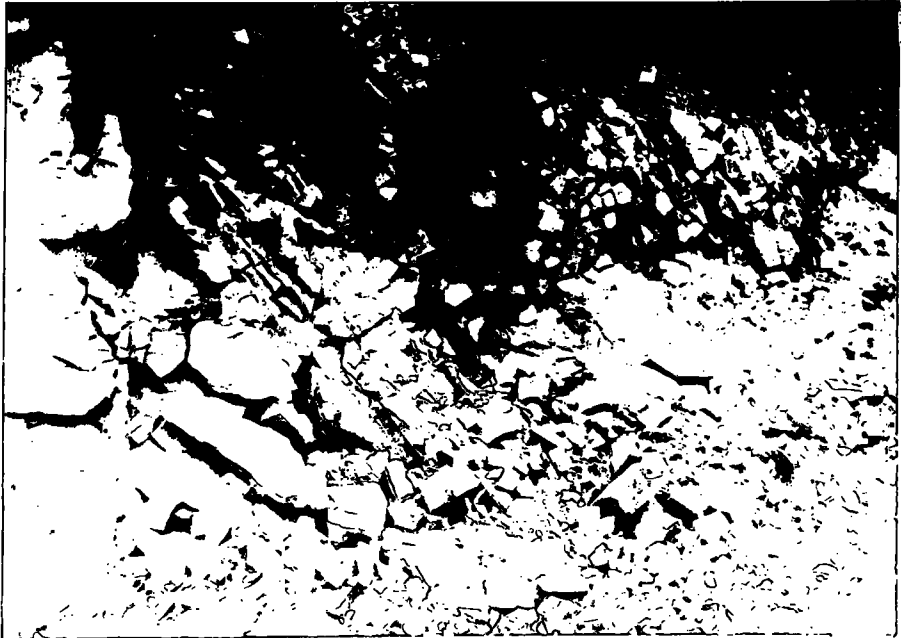
The Lower Volcanic Series around the Lahanos copper mine area (especially in the area of Map 5) without any exception, due to mineralisation, have suffered intense hydrothermal alteration and later heavy weathering, so that one cannot see any fresh rock. As a result of hydrothermal alteration it is possible to see hydrothermal brecciation particularly in the vicinity of the pyritic sulphide deposit e.g. north of the Lahanos Copper mine, between "Guzlek Mahalle (Map 4, E6) and Bitene Mahalle (Map 4, E7). The common alteration processes are silicification, sericitisation and less commonly, chloritisation. During the field mapping their distinct alteration products, distinct colours, petrological and morphological characters could be used for mapping purposes in spite of their heavy alteration, thick vegetation and soil cover.

In the east of Bitene Mahalle a series of quartz-andesite dykes cut through the Lower Volcanics. Plates 4 and 5 show an intrusive hypabyssal dacite intruded into the Lower Volcanics with a chilled margin against them.

4. The Upper Volcanics (including the Upper Basic Series) have been used as a single mappable unit in order to facilitate mapping. As far as mineralisation is concerned the Lower Volcanics and Upper Volcanics are vitally important and pyritic sulphide mineralisation almost always takes place near the contact of these two units, or more often within the Upper Volcanic Series, but close to the Lower Volcanic contact. The average thickness of the Upper Volcanic Series



Pl. 5. Hypabyssal dacite intrusion into the Lower Volcanic Series at Bogaztarla location (Map 4, D7)



Pl. 6. Columnar jointing, Upper Volcanic Series, Lahanos mine.

changes from 25 to 250 meters (Fig. 1). This series because of its younger age occupies the highest ridges and hills.

The Upper Volcanics are mainly composed of alternations of lava flows, pyroclastics and marine sediments. The composition of the volcanics gradually changes from bottom to top i.e. dacitic to rhyolitic, which might indicate that a continuous differentiation and crystallisation of the initial Magma took place during the Santonian, because in the three different levels of the Upper Volcanics and the Upper Basics fossils were found for the first time in this particular region.

However these fossiliferous and layered limestone levels give some idea of the general structure, which mainly consists of a series of faulted (broken) gentle anticlines and synclines. Figures 2A & B show the general direction of faults, fractures and joints occurring in the field and their possible maximum stress directions.

Although some of the rhyolitic and dacitic fine grained volcanics show beautiful columnar jointing, sometimes, especially in the field, it is difficult to make a distinction between fine grained pyroclastics and lava flows without any columnar jointing. Plate 6 shows quite well developed columnar jointing in the rhyodacitic lavas above the adit 2 at the Lahanos mine. However, there is a vertical transition series from dacitic to rhyolitic lavas in to pyroclastic rocks mainly tuff and coarse fragmented volcanic breccia of rhyolitic composition (Plates 6 and 7) and

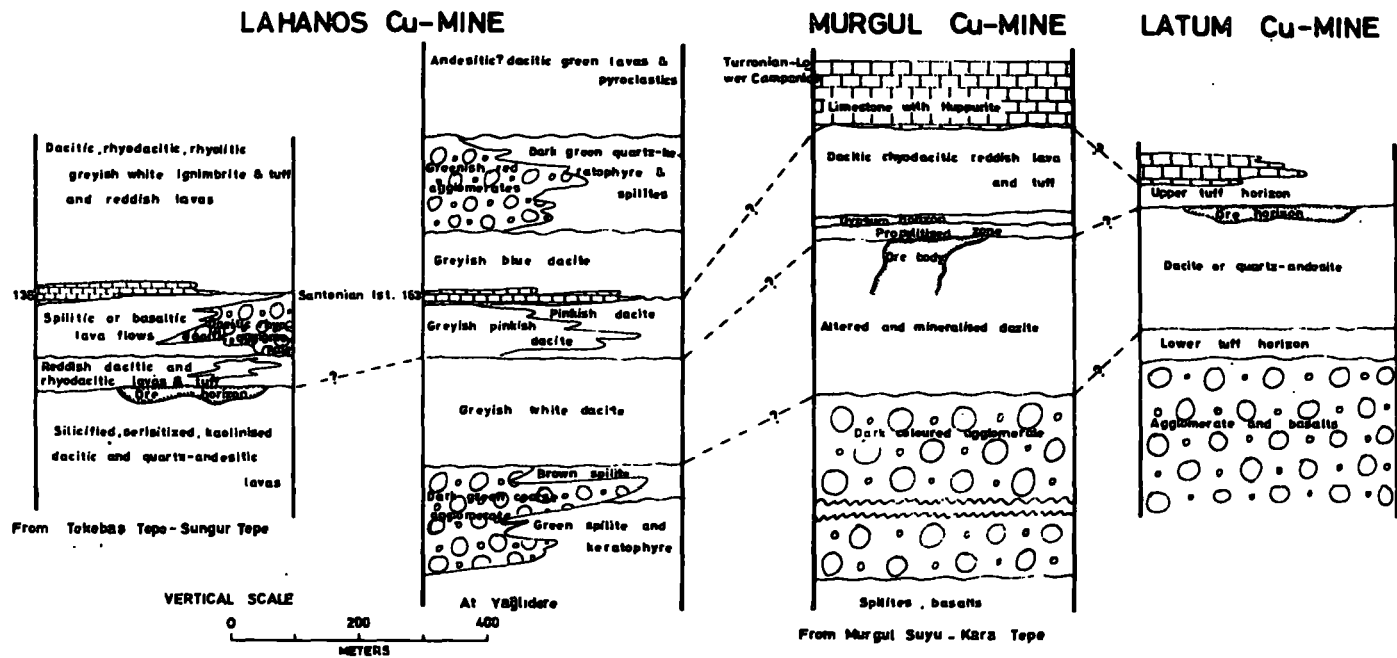


FIG.1.—Stratigraphic columns from various parts of the Eastern Black Sea region, NE Turkey.

Vertical scale applies only for Lahanos sections. Actual thicknesses at Murgul and Latum unknown—sections given are approximations based on various sources of information.

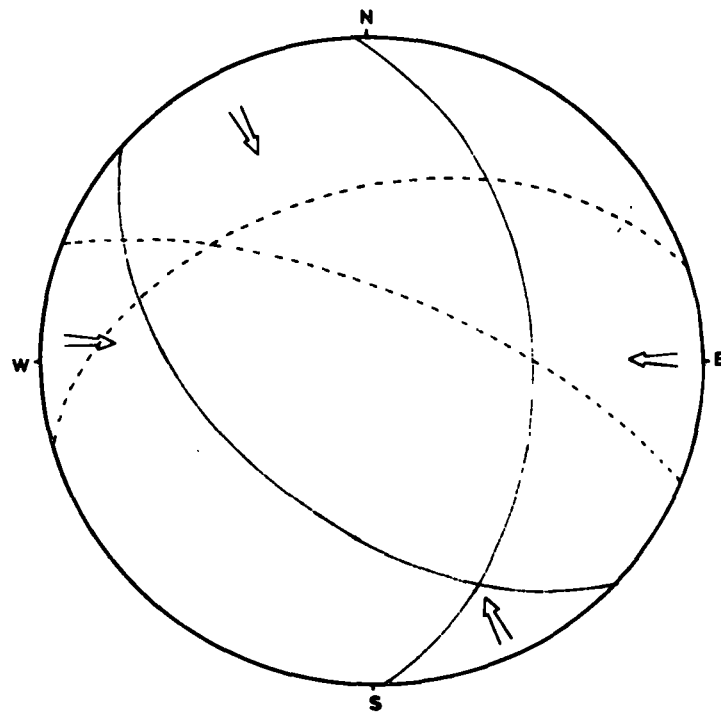
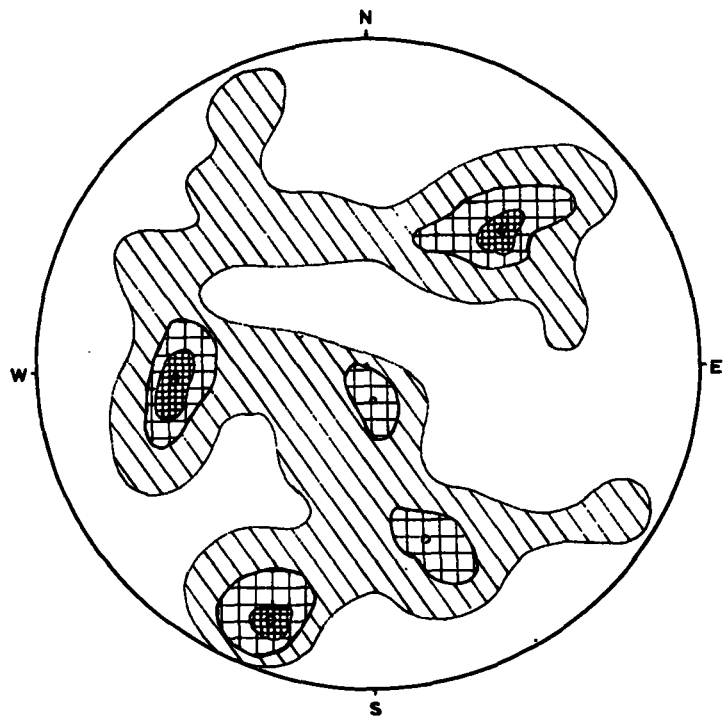


FIG. 2A.—Structural diagram of the underground workings at the Lahanos Cu-mine, and possible main stress directions:

— { $088^{\circ} 50^{\circ}$ - - - { $022^{\circ} 72^{\circ}$
 { $222^{\circ} 50^{\circ}$ - - - { $344^{\circ} 46^{\circ}$



11 %



7 %



3 %

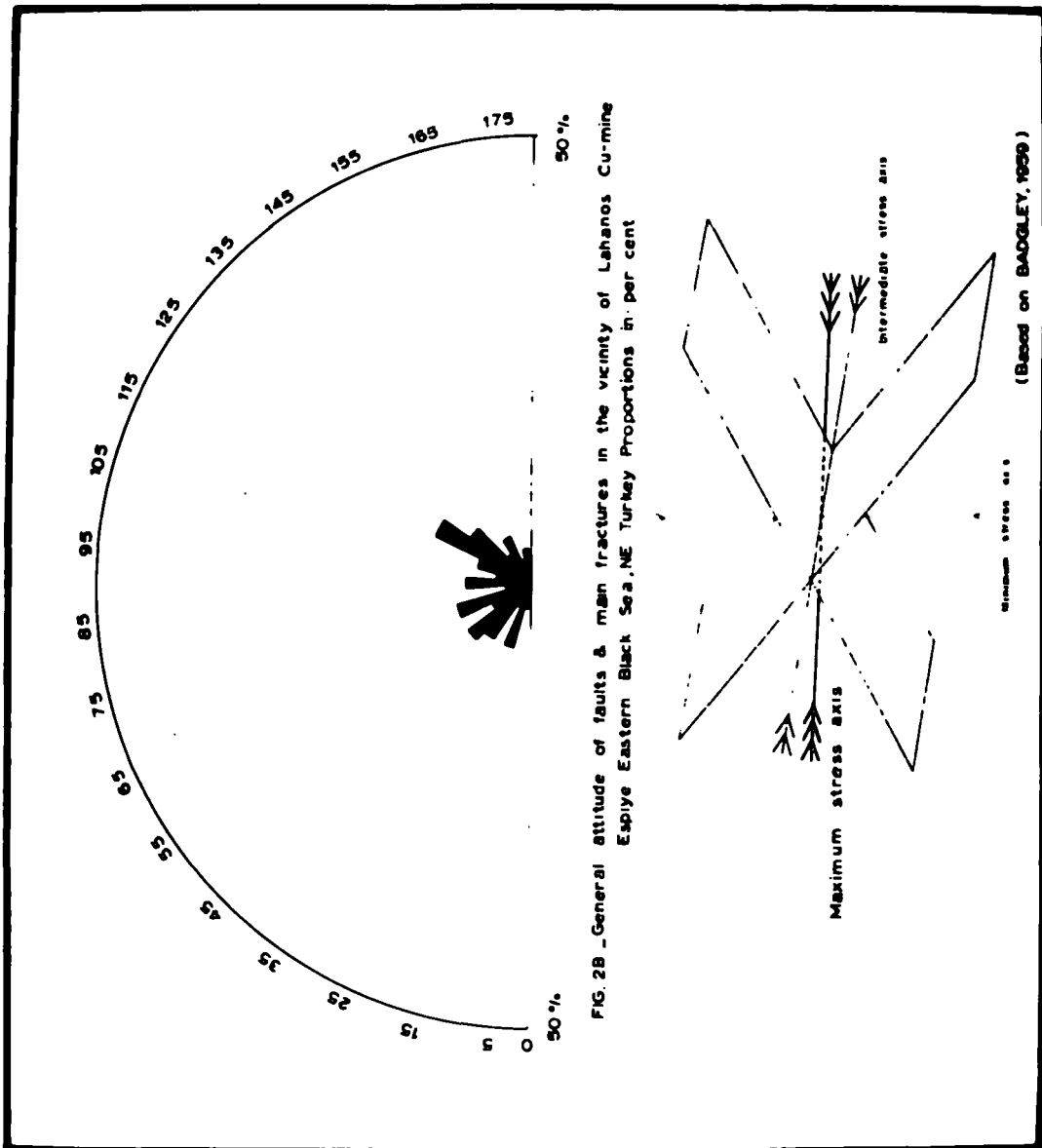
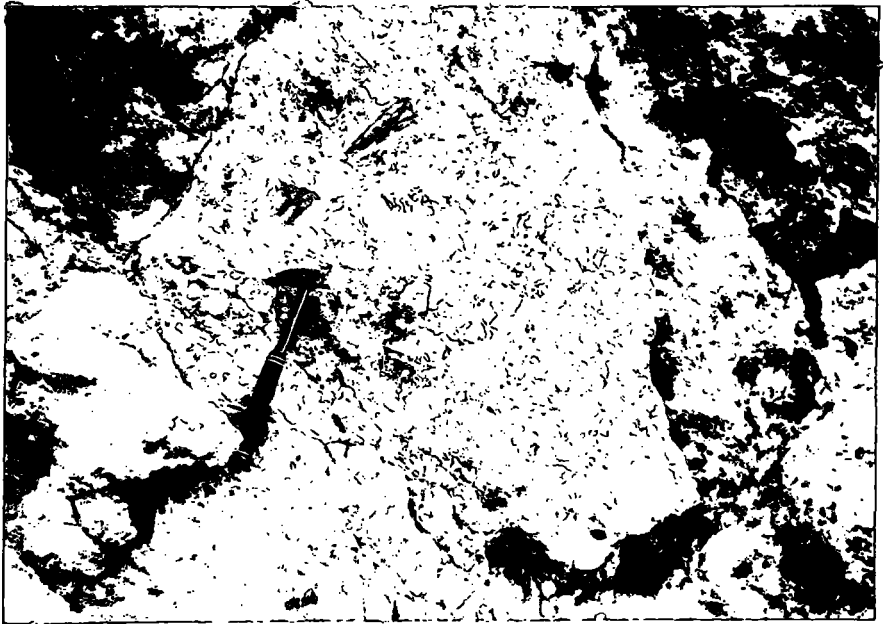
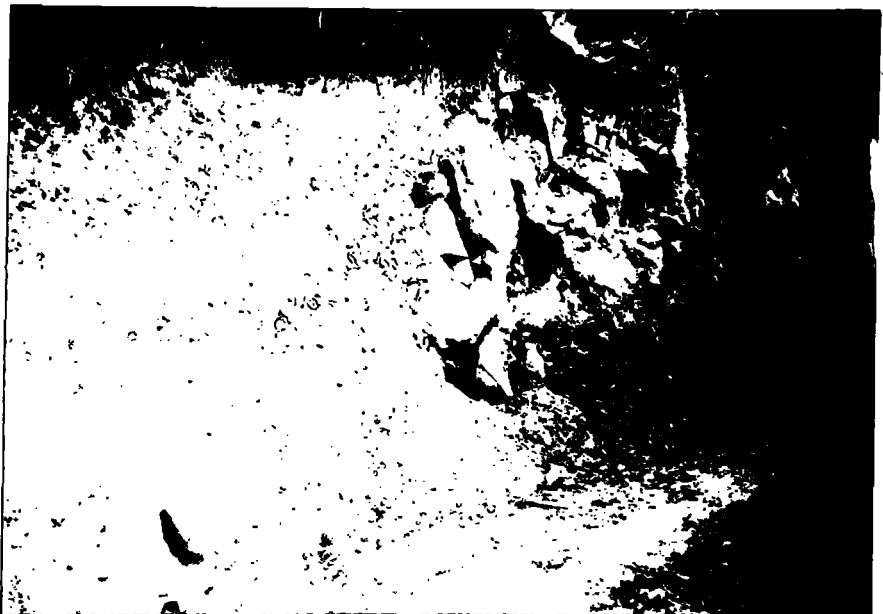


FIG. 2B - General attitude of faults & main fractures in the vicinity of Lahanos Cu-mine
Espiye Eastern Black Sea, NE Turkey Proportions in per cent

(Based on BAGGLEY, 1959)



pl. 7. Acidic (rhyolitic) coarse fragment volcanic breccias at Sülüközü Mahallesi (Map 4, A6) in the Lahanos mine - Espiye road.



Pl. 8. Acidic (rhyolitic) coarse fragment volcanic breccias, cut by hypabyssal dacite, Sülüközü Mahallesi (Map 4, A6), Lahanos mine - Espiye road.

finally into dacitic-rhyolitic green pyroclastics and ignimbrites. For mapping purposes in order to distinguish the Upper Volcanics from the Lower Volcanics the following characters of the Upper Volcanics were used: columnar jointing; their distinct alteration products i.e. mainly kaolinisation, carbonatisation just above the mineralisation, their distinct red colours due to weathering, their stratigraphic position and distinct morphological features.

In places it is possible to see clear age relations between hypabyssal dacite and the Upper Volcanic rocks (Plate 7). One of the best places to see this, is a road cutting of the Lahanos Mine - Espiye road south east of the Maden Tepe (Kanbak Tepe, Map 4, D6). At this point intrusive hypabyssal dacite shows a chilled margin against the Upper Volcanics. This phenomenon can be followed along the eastern slope of the Maden Tepe. The same age relationship can be seen between coarse fragmental rhyolitic volcanic breccia and hypabyssal dacite in the " " " " Sulukgözü Mahallesi (Map 4 and 5, A6) (Plates 7 and 8).

Rocks of the Upper Basic Series around the Lahanos mine are characterised by dark green andesitic or basaltic agglomerate and spilites and they were named the "Green Spilitic Series" by Pollak (1961). The Upper Basic Series with a common trend of NE-SW overlies the Upper Volcanic series, and towards the Killik mine (Map 4, E6) increases in thickness. Another well developed area of the Upper Basic Series is west of Kasap Çayiri Mahalle (Map 4, F8) where one

gets the impression that these basic rocks laterally and vertically pass into the Upper Volcanic Series. A fossiliferous horizon (i.e. Sample 138) from these basic rocks gave a Santonian age, similar to samples 163 and 172.

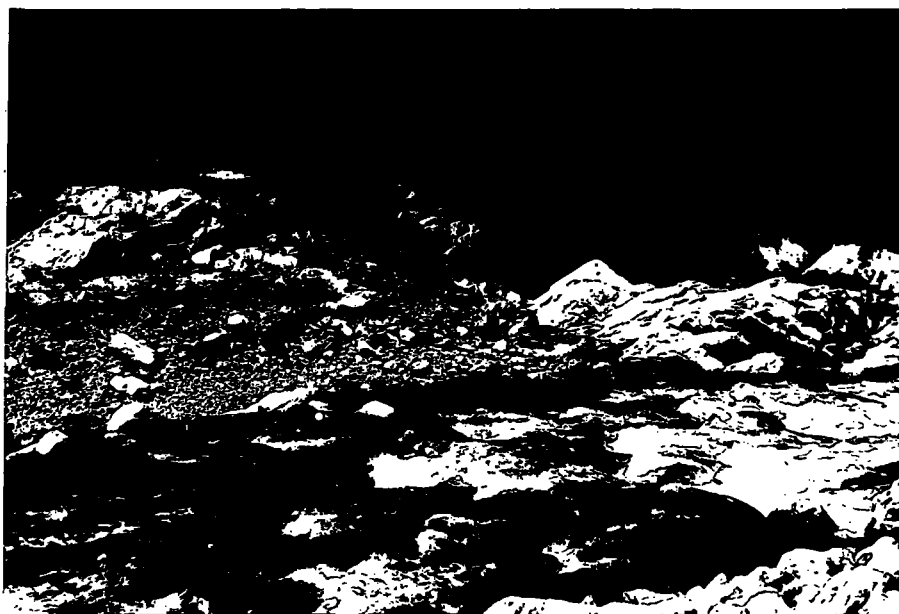
5. Hypabyssal rock as a mappable unit is called "Intrusive Lahanos Tepe Dasiti" by Pollak (1961). It is a biotite-quartz-feldspar porphyry of dacitic composition and covers large areas northwest of the Lahanos copper mine. It shows a SE-NW trend on the ridges of the Kalehisar Tepe (Map 4, C6) - Oyrak Tepe (Map 4, B5) towards the Karakaş Tepe (Map 4, A5) and forms a huge dome shaped intrusive body. It is possible to see dykes of the Lahanos Tepe Dacite cutting through the whole volcanic series including the Upper Volcanic Series (Plate 8), particularly north of the Karaağaç dere (Map 5, D8) therefore the age of the Hypabyssal rocks is clearly later than the Upper Volcanic Series i.e. Later than the Santonian, possibly late Upper Cretaceous or Early Tertiary.

In the field it is easy to recognise and it sometimes shows columnar jointing (Plate 9) north of the Oluk Düzü area (Map 4, B 3 and 4). It shows deep weathering, onion structure and forms arenaceous alteration products particularly at Oyrak Tepe (Map 4, B5).

6. Tertiary Granitic Intrusions can be seen only at the SE and SW corner of the Map 4 and the South of Map 2. At the SE corner of Map 4, a granitic intrusion occurs in the Lower Basic rocks and



Pl. 9. Columnar jointing, hypabyssal dacite, Olukdūzu (Map 4, B3)



Pl. 10. Granite cut by the late dyke (dark in colour) at Tuḡlacik, river Yaḡli (Map 4, N2)

limestones in the east of the Bayrambey Mahalle (Map 4, K11 and N11). At the SW corner of Map 4 in the Saimbuku (Map 4, L4) another small quartz-dioritic intrusion is found in the Lower Basic Series. Both of these intrusions produce a thermal metasomatism halo around them and many small iron ore bodies and skarn mineralisation were formed. The age of these granitic intrusions is believed to be Tertiary or late Tertiary (Oligocene) during the Alpine orogeny.

7. Late dykes are generally basic in character i.e. tholeiitic basalt and andesite. In the Tuğlacik area in the Yağlıdere (Map 4, N2 and Plate 10) a quartz-dioritic intrusion is cut by a late (doleritic) basic dyke. In other parts of the field area, particularly in the Bitene Mahalle (Map 5, E7), quartz-andesitic dykes cut through the volcanic rocks. These late dykes represent the youngest igneous activity in the Lahanos area.

C.1b SOME STRUCTURAL COMMENTS

The Lahanos area appears to have suffered little or no tectonic deformation on folding, but was mainly affected by block faulting (Kraus, 1958; Gattinger et al., 1961) to give a series of horsts and grabens trending along the Eastern Black Sea Coast. The presence of pyroclastic horizons and normal sea sediments in the Lower and Upper Volcanic Series gives some idea of the general structure of the Lahanos area. The structural study of Maps 4 and 5 indicated a broken anticline with a general trend of SW-NE.

In order to find out the main possible structural trend in the

Lahanos area Fig 2A was constructed by using the surface trend of faults and fractures and then plotting on to a rose diagram, giving an E-W possible maximum stress direction. On the other hand Fig 2B was produced from underground data giving two dominant directions: major faults and main fractures displaying again the E-W direction; but minor faults, fractures and joints gave distinct direction of NNW-SSE.

C.1c CONCLUSIONS

In different parts of the field area, different stratigraphic columns and sections showed that rocks from the Lower Volcanic Series through the Upper Volcanic Series up to the top of the Upper Basic Series were possibly formed during the Upper Cretaceous or more precisely in the Santonian to Campanian (Fig. 1). The presence of Santonian-Campanian fossils throughout the Lower Volcanics and the Upper Basics indicates that these series might have been formed during the Santonian-Campanian, Upper Cretaceous. The following paleontological evidence is the first to be described from the Lahanos area. Sample 163, gray limestone, representing the bottom of the Upper Volcanics at Değirmendere (Map 4, F3) contains

Globo-truncana Linneiana (d'Orbigny) group,
Heterohelix Sp., and
Rotaliform bentic species

giving a possible *Santonian age.

*Fossils are determined in the British Museum (Natural History) by Dr. D.D. Bayliss.

Sample 138 brown reddish limestone representing the middle of the Volcanic series in the southeast of "Üzümlü Tepe" (Map 4, 5, E9) contains

Globotruncana Linneiana (d'Orbigny),
 Globotruncana Linneiana Tricarinata (Querreau),
 Globotruncana Linneiana Coronata Bolli,
 Globotruncana Cf. renzi Gandolfi,
 Globotruncana Spp. indet,
 Globigerinelloides Sp.,
 Hetero helix Sp.,
 Hedbergella Spp., and
 ?Marsonella Sp.

This fauna suggested a probably Santonian age. And finally Sample 172, gray limestone, representing the top of the Upper Volcanics south of the Tekçam Tepe, contains (Map 4, L9)

Globotruncana Linneiana (d'Orbigny) group,
 Hedbergella Sp.

giving a possible Santonian age.

On the other hand Schultze-Westrum (1961) suggested that the Lower Basic Series has an age range from Liassic up to the Upper Cretaceous (no certain stage has been given). The presence of limestone lenses within the Lower Basic Series particularly at Kapıkaya, in the Bayrambey Mahalle (Map 4, N9) has been suggested as indicating an Upper Cretaceous age by Schultze-Westrum. During the field study samples containing some fossil remains which look like Hippurites remnants were collected at Kapıkaya. Therefore one could assume that there was a little time gap between the Lower Basic Series and the overlying Lower and Upper Volcanic Series, or even one might think that the whole series were deposited contempor

-aneously in the same eugeosyncline, but they might represent different facies?

Similar rock units and stratigraphical columns are also found in different parts of the Eastern Pontids. e.g. in the Murgul and Latum areas (Fig. 1) with very little different stratigraphical columns are quite similar to the Lahanos stratigraphical column, but with the exception that the Hippuritic limestone series comes on top of the Upper Volcanic Dacite and rhyodacite and the Upper Basic Series as well (Kleay, 1962) in Murgul area.

CHAPTER D - PETROGRAPHY OF THE LAHANOS AREA

D.I PETROGRAPHY OF THE LAHANOS AREA

As mentioned in Section C, severe and heavy alteration made it difficult to obtain fresh rocks, furthermore the fine-grained character of these rocks also made identification difficult; therefore most of the nomenclature is based on chemical analysis rather than microscopic studies. For the purpose of chemical nomenclature Streckeisen's classification (1967) is employed (Fig 3,4) and for the purpose of microscopic studies Williams et al, (1954), Moorhouse (1959) and Kerr (1959) were mainly used. During the petrographical studies over 200 thin sections were examined. Determination of feldspars, particularly plagioclase, are mainly based on twinning axis measurements as described by Slemmon's (1962) and an x-ray diffractometer method. The rocks of the whole volcanic series have suffered autoalteration, hydrothermal alteration and weathering; therefore finding representative fresh rocks was difficult particularly in the mineralised area. Most of the fresher rocks were collected away from areas of hydrothermal alteration. Analysis of the field evidence on the volcanic rocks suggested the following sequence of igneous activity for the Lahanos area (See Tab. 3)

1. Latite-basalts form the bottom of the Lower Volcanic rocks outcropping in the Lahanos area. The major minerals are basic plagioclase, olivine and pyroxene. Some of these basalts show conspicuous plagioclase pheno crystals and lath shaped plagioclase in

TABLE 3

Sequence of igneous activity and related volcanic rocks
with corresponding sediments in the Lahanos region

<u>IGNEOUS ROCK SERIES</u>	<u>CORRESPONDING SEDIMENTARY ROCKS</u>
11. Granitic intrusions	
10. Hypabyssal dacite	
9. Pyroxene basalt-andesite) Gray limestones
8. Quartz-andesite (mainly dyke)) Red Limestones
7. Rhyolitic lavas and pyroclastics	
6. Rhyodacitic lavas and pyroclastics	} Gray Limestone
5. Dacitic lavas and pyroclastics	
4. Quartz andesite	
3. Tholeiitic basalt and andesite	} Bluish grey Limestone
2. Alkali basalt and spilite	
1. Latite-basalt	

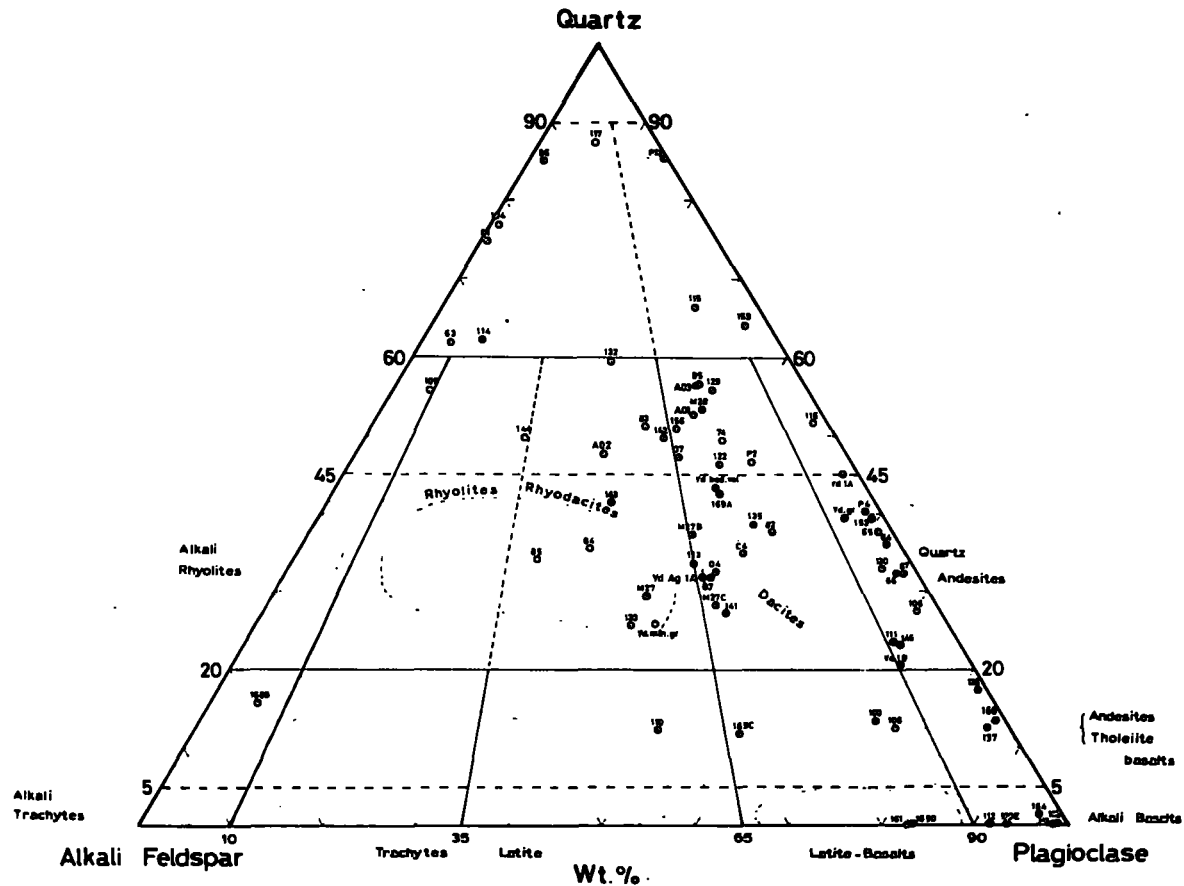


FIG.3...Distribution of volcanic rocks from the Lahanos area Espiye, Eastern Black Sea, Turkey.
 Analyses of Lahanos volcanic rocks shown on a diagram of the type used by Streckeisen, 1957.

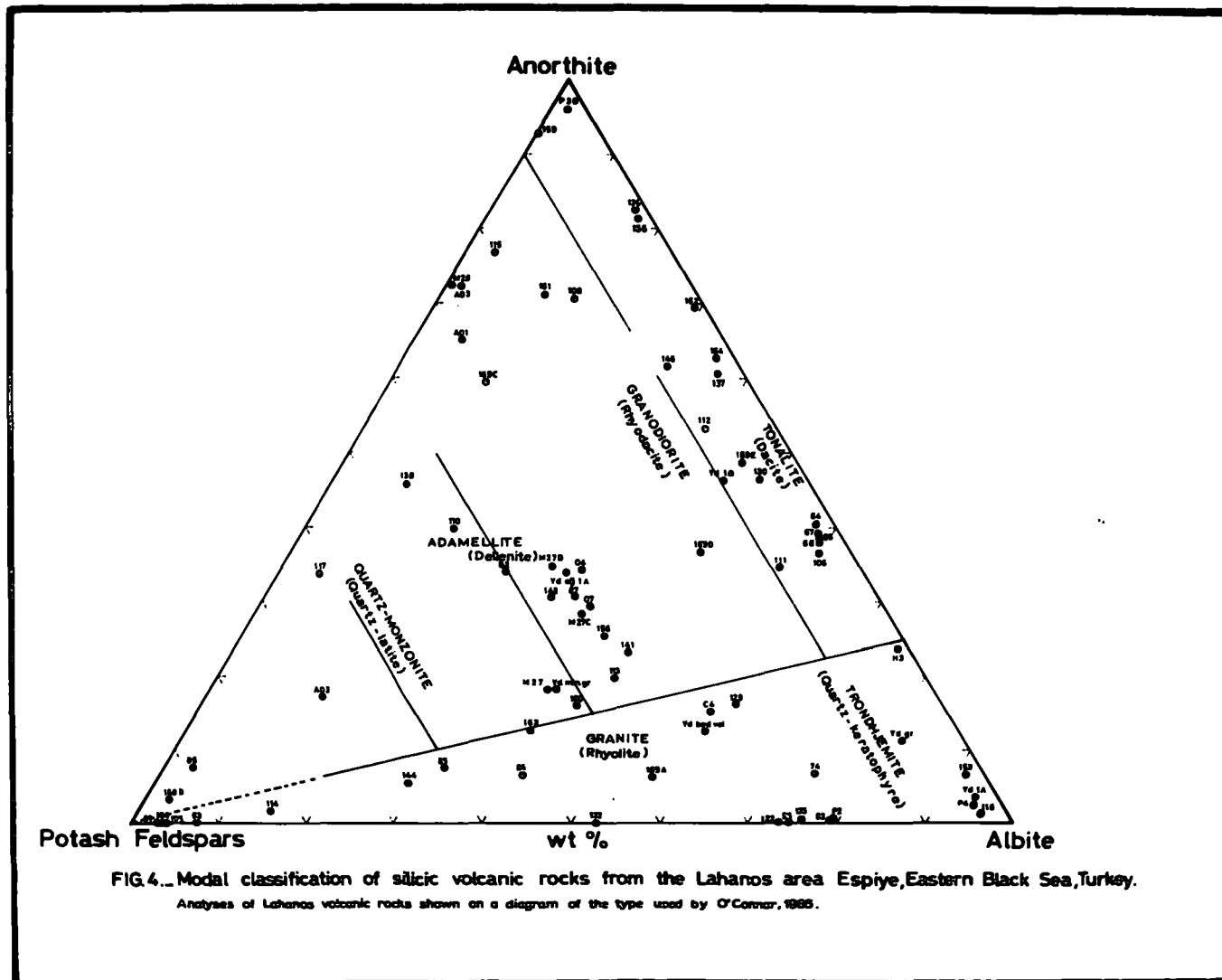


FIG.4... Modal classification of silicic volcanic rocks from the Lahanos area Espiye, Eastern Black Sea, Turkey.

Analyses of Lahanos volcanic rocks shown on a diagram of the type used by O'Connor, 1965.

the groundmass. The chemical analysis gave a latite-basalt (according to Strekeisen's classification, 1967) whilst microscopic properties showed that this was an olivine-basalt (unsaturated basalt) with very porphyritic, intergranular texture in which it is possible to see interstitial texture of coarse grained groundmass. Sometime a glomeroporphyritic texture can be observed.

Plagioclases form large pheno-crysts with an average composition of bytownite-labradorite (using optical and X-ray methods). The composition of the lath shaped plagioclase in the groundmass is less basic, possibly labradorite or andesine in composition. The size of the large pheno-crysts changes from sample to sample; the larger plagioclase crystals are about a few centimeters by a few millimeters. They are twinned according to either the carlsbad or albite twinning laws, and chiefly altered to calcite, but sometimes to kaolinite, when hardly any fresh plagioclase remains.

The pyroxenes are usually augite but they suffered severe alteration and sometimes are represented only by their alteration products e.g. chlorite, iron ores and calcite.

Olivines are similarly only represented by their alteration product, idding site; no fresh olivine was found.

Calcite, sericite and kaolinite after feldspar; chlorite and opaque minerals after pyroxene, and iddingsite after olivine are the common secondary minerals of the latite-basalts. The presence

of aragonite, opal, chalcedony and zeolites might be due to late stage hydrothermal activity (Williams et al., 1954).

2. Alkali-basalts and spilites in association can be seen in many parts of the area. The major minerals of spilite are: sodic plagioclase, mainly albite and oligoclase, deuteritic chlorite, after ferro-magnesian minerals, with calcite, chalcedony in filling amygdales and vesicles and brown glass (possibly palagonite). The common texture of these rocks is intergranular, variolitic texture is also developed with abundant vesicles and amygdales.

Plagioclases are altered to kaolinite and calcite, but most of them show the optical properties of oligoclase and albite. Some of the calcic plagioclase (e.g. specimen 112) is altered to analcime which was determined by using the universal stage and verified by X-ray diffractometer analysis. A similar kind of alteration was pointed out by Johannsen (1937, Vol. III, pp 254).

Dark coloured glass-like material forms either the entire groundmass with numerous vesicles and amygdales which are infilled by zeolites, calcite, chlorite, chalcedony and opal, or patches of glass within the granular groundmass. However, there are two distinct colours of volcanic glasses present in these spilites i.e. greenish and reddish greenish brown coloured. The latter one is probably palagonite.

As a general character of the Lower Basic Series, due to alteration products of iron-manganese chlorite and iron oxide, a

a reddish and greenish appearance is very common. Owing to weathering, onion structures are well developed, thus some spilitic rocks may have a sort of ball or egg-like structure which is not true pillow-lava structure but due to spheroidal alteration. The general texture of the spilites is sometimes very fine grained, generally porphyritic and very frequently vesicular. The ground-mass contains acidic plagioclases, altered to calcite and chlorite. The phenocrysts of oligoclase-andesine are very much carbonated, and ferro-magnesian minerals are chiefly altered to chlorite.

The microscopic characteristics of the alkali-basalts are somewhat different from the spilite. They are fine grained dark coloured basalts (mainly associated with or usually overlying the latite-basalts) and commonly show intersertal or less frequently porphyritic texture. The interstices between the Plagioclase-laths (mainly labradorite) are occupied by pyroxene (augite). The principal constituents are calcic plagioclase, mainly labradorite, and pyroxene (augite) with subordinate amounts of opaque minerals and deuteritic chlorite, calcite and other alteration products.

3. Tholeiitic basalt-andesites overlying the latite and alkali-basalts show somewhat darker grayish black colours and finer grain size with some amygdales and vesicles. Calcic plagioclase with pyroxene, (occasionally pigeonite optical determinations, form the major minerals, while chlorite, calcite, ore grains and tridymite with short prismatic grains, form the subsidiary minerals. The common textures are hyalophitic and intergranular. Thin plagioclase laths, in the

groundmass, sometimes have a suggestion of flow structure. In the groundmass there are many vesicles and amygdales infilled by calcite and chlorite. Some of these vesicles show quite distinct 'tridymite' lining similar to segregated vesicles as described by Smith (1967). Due to alteration, calcification of plagioclase, and chloritisation of pyroxene are very abundant.

4. Quartz-andesites form the top of the Lower Basic Series and are mainly fine grained with bluish gray colours, containing tiny green speckles. Feldspars form the principal mineral while quartz, altered pyroxenes, opaque grains, chlorite, calcite and kaolinite form the subordinate and deuteric minerals. The common texture is porphyritic in which the phenocrysts are mainly feldspars. The groundmass is composed of tiny needle-like plagioclases and anhedral quartz. Sometimes glomeroporphyritic texture is also pronounced.

The plagioclases are mainly andesine-oligoclase. Zoning is also present and the compositional changes of the zoned plagioclase are clearly displayed by the different degree of alteration, and as well as their alteration products. Albite, carlsbad and combined twins are fairly abundant. However, the presence of fresher albite and oligoclase indicates an albitisation which might be due to a hydrothermal stage alteration (i.e. soda metasomatism). Most of the oligoclase - andesine at the centre of zoned plagioclase is replaced by chlorite while some oligoclase-andesine phenocrysts are replaced along cleavages and around the edges by chlorite.

Less common alteration products of plagioclase are calcite and kaolinite.

The groundmass is mainly made of short small plagioclase laths, devitrified glass and xenomorphic quartz. Alteration of the groundmass produces devitrification of glass, kaolinisation of feldspar, chloritisation and calcification.

5. Dacitic lavas and pyroclastics include the Lower, and part of the Upper Volcanic lava flows and pyroclastics, thus dacitic rocks will be subdivided into

- c - dacitic pyroclastic rocks,
- b - dacitic Upper Volcanic lavas,
- a - dacitic Lower Volcanic lavas.

a - Dacitic Lower Volcanic series are represented by porphyritic dacite which is fine to medium grained, containing phenocrysts of rounded and sometimes corroded quartz, and feldspars which are lying in a quartz-rich groundmass containing albite and alteration products of chlorite, sericite and ore grains, mainly pyrite. The common plagioclase compositions are oligoclase-andesine or albite-oligoclase. Dacites of this subgroup are distinguished from the dacite of the Upper Volcanic Series by means of their more abundant and distinct alteration products involving intense silicification and sericitisation. Depending on the degree of alteration, the dacitic lower Volcanics can be grouped as follows:

(i) Partly silicified dacite is characterised by idiomorphic quartz phenocrysts and silicified and sericitised plagioclase crystals

in a completely silicified groundmass associated with a small amount of sericitisation.

(ii) Totally silicified dacite is represented by a mozaic of xenomorphic quartz crystals which are always bordered by small flakes of sericite.

b - Dacitic Upper Volcanic lavas are somewhat fresher and finer grained than the dacitic Lower Volcanic lavas and have a pronounced flow structure. Feldspars and quartz form the major minerals of this group of lavas. The groundmass shows good trachytic texture in a fluidal groundmass of sub-parallel acidic plagioclase laths with intergranular glass. The alteration products are also somewhat different from the Lower Dacitic Series and particularly closer to ore bodies chloritisation, kaolinisation and calcification are ubiquitous and very striking in the field.

Plagioclase phenocrysts are mainly albite and oligoclase in composition with albite and carlsbad twinning. Zoning of plagioclase is very rare. The commonest alteration products of plagioclase are kaolinisation and very little silicification. Silicified plagioclase phenocrysts have a salt and pepper appearance. Near the ore bodies replacement of plagioclase by carbonate minerals, pyrite and occasionally chlorite is quite common.

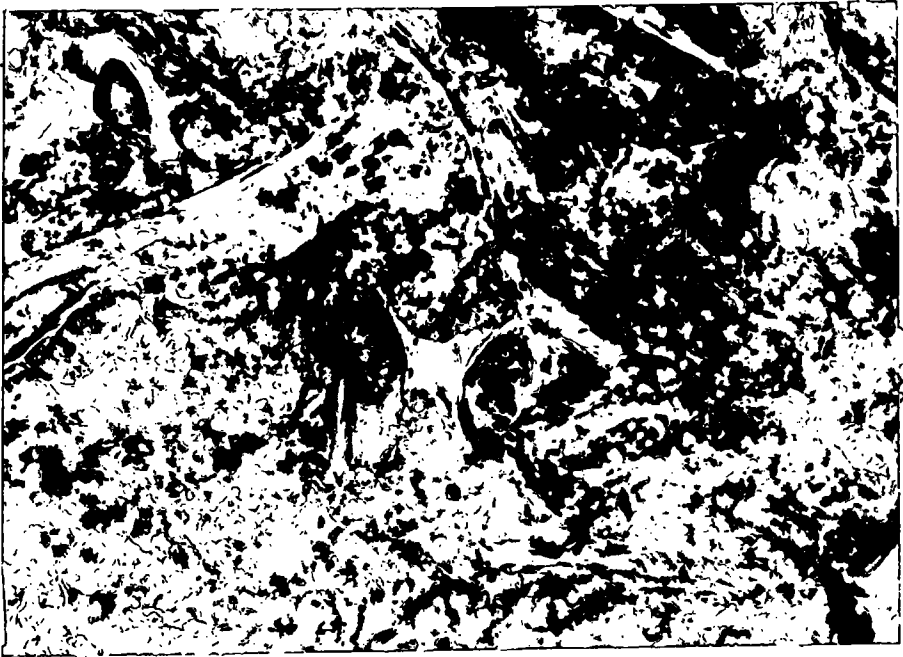
Quartz is usually the main constituent of the groundmass with albite and oligoclase-laths. Deuteric quartz shows xenomorphic mozaic texture when it replaces the groundmass and dacitic glass, but when it replaces feldspar phenocrysts, it forms very fine grained

anhedral aggregates whose appearance is like salt and pepper.

c - Dacitic pyroclastic rocks with few exceptions are green or whitish, grayish green in colour with fine to medium fragments 0.045 to 0.067mm up to 1.200 to 1.700mm in size. They contain different kinds of fragments of glass and crystals. The presence of glass shards, (Plate 11), suggests that these may be dacitic ignimbrites, since they show flow texture and very few occasional elongated glass shards described as typical of such rocks by various authors (e.g. Adamian 1966, Cook 1966, Maleyev 1966, Petrov 1966, Shirinian 1966 and Vlodayetz 1966 from Armenia, and Schmincke 1967 from South Central Washington).

6. Rocks of rhyodacitic composition: According to their mode of occurrence these can be subdivided into two main groups.

(i) Rhyodacitic pyroclastic rocks are very similar in appearance to the dacitic pyroclastics i.e. mainly green or sometimes brownish to reddish in colour. Two leading types of pyroclastics can be distinctly described, namely lithic and crystal tuffs and ignimbrites (these terms are used in the sense proposed by Williams et al., 1954). The principal fragments in the crystal tuffs are feldspar and quartz and in addition there are lithic tuffs with vesicular fragments of rhyodacite or dacite derived from fluidal lava flows. These are cemented by a fine-grained felsophyric groundmass containing abundant sanidine (with very small 2V) in which zoning is not uncommon. Some of these pyroclastics contain fragments of andesine, but the common plagioclases are oligoclase and albite with carlsbad and albite twinning.



Pl. 11. Glass shards from the Upper Volcanic Series, at Çukur Mahalle (Map 4, B7) 350 x



Pl. 12. The southern outcrop of the pyritic sulphide ore at Lahanos copper-mine.

The presence of pyroclastic and flow characters might suggest a welded tuff, but the absence of elongated glass shards would seem to make it difficult to accept the term welded tuff in this case.

The principal alteration products of these rocks are chlorite, kaolinite, deuteric quartz, sericite and pyrite. Because of these alteration products the predominant colour of the rocks varies from green to red in the field.

(ii) Rhyodacitic lavas also appear with a dominant red or reddish colour in the field. They have a distinct porphyritic texture with a fine grained felsitic groundmass in which corroded and rounded quartz and sanidine and orthoclase with carlsbad twinning form the phenocrysts. Alteration of potash feldspars is mainly to kaolinite. Owing to silicification, development of xenomorphic deuteric quartz in the groundmass can be present. Oxidation of ore grains produces a predominant red staining to the lavas.

7. Rhyolitic pyroclastics and lavas form the top of the acidic volcanics. Because of their severe alteration, microscopic studies of the rhyolitic pyroclastics were limited. They show bleached white and gray colours in the field. Some of these pyroclastics are fine grained tuffs showing bedding.

The microscopic studies of pyroclastics showed that these are mainly very fine grained volcanic ashes, thus they can be classified as "vitric ash" or "tuffs". (Williams et al., 1954).

The lavas of this group show a good porphyritic texture and their groundmass exhibits very fine grained felsitic texture enclosing

corroded phenocrysts of quartz and altered potash_feldspars.

8. Quartz-andesitic rocks forming lava flows, sills and dykes occur in the field. These almost invariably have a green or greenish colour which might be due to propylitisation of these rocks. Quartz-andesitic rocks will be dealt with under three separate subdivisions as follows

- (i) Sills and small intrusive bodies;
- (ii) Dykes;
- (iii) Lavas.

(i) Sills and small intrusive bodies are fine to almost medium grain with a predominant green colour. Plagioclase, quartz biotite and amphibole form the major constituent minerals, whilst chlorite, kaolinite and pyrite form subsidiary secondary minerals. The textures of these quartz-andesitic sills and minor intrusive bodies is rather striking; as a whole, it can be called a porphyritic texture, but the appearance of the groundmass and its interlocking xenomorphic granular texture with euhedral and subhedral crystals of the principal minerals suggests a microgranitic texture, in which interlocking xenomorphic quartz crystals enclose tiny oligoclase-albite laths. It is sometimes possible to recognise xenoliths of the Lower Basic Series which are more easily recognised than the xenoliths of the acidic volcanics.

Determination of the plagioclases of these rocks was done by using a universal stage method as described by Slemmons (1962) and gave an average of 50-61% anorthite corresponding to a range from

andesine to labradorite. Some of the calcic plagioclase and amphiboles give an appearance of cumulophyric texture. Zoning and twinning of plagioclase are very common. The centres of zoned plagioclase are very often altered to kaolinite, chlorite, sericite.

Amphiboles (usually heavily altered to chlorite) occur as euhedral and subhedral grains and sometimes aggregates of hornblende. It is possible to see some relicts of biotite completely altered to chlorite. This mineralogical assemblage corresponds to hornblende-biotite andesite.

(ii) Quartz-andesitic dykes show light to dark green colours and most of them suffered dense alteration in the field. Intergranular sub-ophitic and hyaloophitic textures are well developed. The interstices of plagioclase-laths are infilled with altered pyroxene and amphibole, devitrified glass and sometimes with xenomorphic quartz. In the groundmass there are some vesicles that are mainly infilled with flaky chlorite and some xenomorphic quartz, and rarely phenocrysts of calcic plagioclase (possibly labradorite). Abundant spinel group opaque grains are present. Main alteration products of these rocks are chlorite, deuteric quartz and kaolinite.

(iii) The lavas of this group are fine-grained vesicular rocks with glomeroporphyritic textures. The groundmass consists of interlocking xenomorphic quartz. Amygdales and vesicles are infilled with calcite, chlorite and chalcedony. Devitrification of andesitic glass is very abundant. The intense chloritisation of amphiboles, and

complete calcification and kaolinisation of feldspars are very common. These lavas are similar to the dykes in that they contain plenty of opaque ore grains.

9. Pyroxene basalt andesites occur as less altered lavas of the Upper Basic Series showing beautiful onion structure in the field. Under the microscope a well developed sub-ophitic texture of plagioclase laths (labradorite) and clinopyroxene (augite) can be seen. Although chemical analysis of these lavas gave a tholeiitic basalt-andesite composition, the plotting of these into Kuno's diagram in Fig. 5 showed that they are mainly tholeiitic and high alumina basalt in composition and are termed pyroxene basaltic-andesites.

Lath shaped plagioclase crystals form almost the entire rock with their interstices infilled by pyroxene. Larger zoned plagioclase phenocrysts are less abundant. The overall composition of the plagioclase is labradorite and bytownite. Zoned plagioclases show high $2V$ with negative optic sign at the centre whereas outer rims also show high $2V$ with positive optic sign; thus the composition of zoned plagioclases changes from calcic cores to more sodic margins. Plagioclases show very little alteration, mainly sericitisation.

Pyroxenes are almost colourless or pale greenish, very weak or non pleochroic with high relief compared to plagioclase. The maximum extinction angle of longitudinal sections varies from 40 to 45 degrees, and twinning with (100) as the twin-plane is fairly common. These optical properties indicate diopsidic-augite and pigeonite (with a small $2V$).

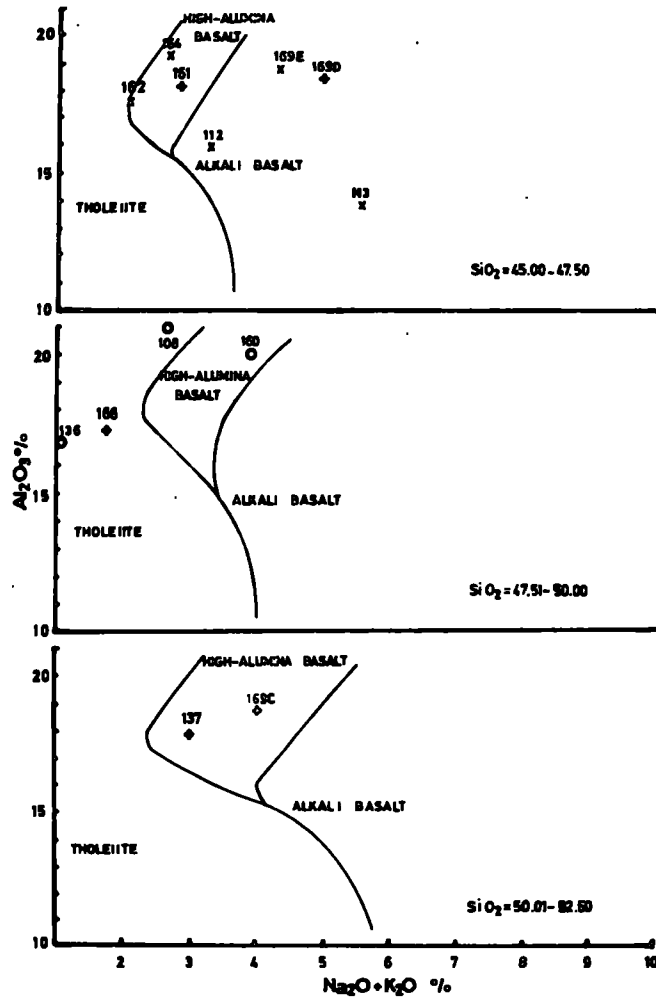


FIG. B.- Al_2O_3 -Total alkali- SiO_2 relation of three basalt types from the Lahanos area Espiye, Eastern Black Sea, relative to boundaries proposed by Kuno (1960).

Accessory minerals of amphibole (hornblende), biotite and ore grains can be seen with a common alteration to chlorite.

10. Hypabyssal dacites form fairly large intrusive bodies, but rarely show columnar jointing. In places extensive weathering produces large onion structures up to about 60cm. by 75cm. in the field. The other abundant weathering product due to complete disintegration of the groundmass is arenaceous sand and kaolinisation of feldspar and very little weathering of biotite. Unaltered hypabyssal dacites are very hard. The rock can be called biotite-quartz-feldspar porphyry owing to the ubiquitous presence of these minerals in it.

The main constituents of these dacitic rocks are feldspar (mainly as andesine and orthoclase) and quartz forming leucocrate minerals, while biotite and hornblende form the mafic minerals. Subsidiary amounts of alteration products of the principal minerals and accessory amounts of zircon and apatite from the rest. There is a well developed porphyritic texture and the groundmass exhibits a fine grained felsitic texture.

Biotite forms idiomorphic euhedral crystals and sometimes shows corroded edges against the felsitic groundmass. It shows strong pleochroism in yellow, yellowish brown to brown colours. Biotite crystals show a platy habit and some apatite inclusions and are often replaced by feldspar, quartz, calcite and chlorite along the cleavages. It is also possible to see bent crystals of biotite.

Hornblende shows quite distinct pleochroism. Sometimes it is possible to see crystal outlines of pyroxene now completely pseudomorphed by hornblende and some opaque. Even hornblendes are later

altered to a chloritic rim and fine-grained dusty opaques and calcite.

Quartz forms large rounded and corroded crystals and it is always present in the fine-grained felsophyric groundmass. Corroded and embayed quartz phenocrysts are often occupied by the groundmass. On the other hand replacement of biotite along the cleavages by quartz is quite common.

Feldspars are represented by potash feldspars and plagioclase. The potash feldspars are orthoclase together with a very little sanidine with carlsbad twinning. Plagioclases are one of the three main phenocrysts of the hypabyssal dacite. Zoning of plagioclase is not exceptional and each zone distinctly shows different optical properties. Among the plagioclases albite and pericline twinning are well developed. Determination of plagioclase composition was done by X-ray diffractometer and optical methods which gave average values of 24-33% anorthite that is they are of oligoclase-andesine composition. Replacement of plagioclase in the centre of zoned crystals by sericite, kaolinite, calcite and sometimes by chlorite are very abundant.

The groundmass always shows a felsitic texture and is mainly composed of quartz and feldspar. It infills cavities and embays the phenocrysts of biotite, hornblende, feldspar, quartz, and contains some zircon and apatite; but the groundmass is replaced by opaques, chlorite, kaolinite and sometimes by calcite.

11. Granitic intrusions: although away from the detailed map area (See Map 2 and 4) one cannot leave without mentioning the granites. The granitic intrusions in many parts of the Eastern Pontids are

surrounded by a zone of hornfels with a width of about 200 to 1500 meters, the hornfels are dark fine-grained rocks, mainly feldspathised and pyritised. The marginal facies of the granitic batholith varies from tonalite to hornblende-granodiorite in many parts of the Eastern Pontids. Near the volcanics the granitic intrusions assimilated volcanic rocks, and it is possible to see granitic appophyses in volcanics, however more often it is possible to see xenoliths of volcanic rocks near the margins of the granitic intrusion.

Some of the tonalitic intrusions show a myrmekitic intergrowth of albite and small quartz crystals. Samples from Yağlıdere (see Map 4, L3), showed two main types of granitic rocks:- (i) Tonalite (quartz-diorite) and (ii) Granite.

(i) Tonalites are presumably formed by the assimilation of the Lower Basic Series in a granitic magma. They always form the margin of larger granitic intrusions in the field. Sometimes it is possible to see small isolated intrusive bodies of tonalite. Tonalites mainly consist of amphibole, plagioclase with subordinate amounts of biotite and quartz. Accessory apatite and ore grains are present. The texture of the tonalite is often hypidiomorphic granular or sometimes porphyritic intergranular.

Amphiboles are mainly hornblende showing green or brownish colours with distinct pleochroism often altered to chlorite. Hornblendes occur as hypidiomorphic grains filling the interstices of large plagioclase laths.

Plagioclase forms allotriomorphic grains mainly of oligoclase-andesine and albite in composition (confirmed by XRD) with carlsbad and albite twinings.

Quartz also occurs in these rocks in subordinate amounts and infills the interstices of large feldspar grains.

Chloritisation of amphiboles and biotites, albitisation, carbonitisation, sericitisation and kaolinisation of plagioclases and orthoclase are well represented in tonalites.

(ii) Granites are found in the centre of the large acid intrusions. The rocks are quite coarse grained, with hypidiomorphic granular texture. Large reddish pinkish orthoclase phenocrysts give an impression of porphyritic texture in which mafic minerals and plagioclase tend to be in euhedral form, while most of the orthoclase is subhedral and quartz occupies the irregular inter-spaces of amphiboles and feldspars. Orthoclase, albite, oligoclase and quartz are among the principal minerals while biotite, amphibole and a little pyroxene (titano augite) are the subordinate minerals, and apatite forms the accessory minerals. Due to late hydrothermal activities, joints and fractures of granite are infilled with mainly pyrite containing chalcopyrite and neodigenite etc.

The compositions of plagioclases are albite and oligoclase. Orthoclase encloses plagioclase and contains some inclusions of plagioclase. Albite, carlsbad and pericline twinning can be widely seen among the feldspars of which common alterations are sericite and kaolinite.

Quartz infills the empty spaces and intergranular spaces of feldspars and shows xenomorphic granular texture.

Biotite is strongly pleochroic with dark brown colour and usually alters to chlorite and some opaques. There are some amphiboles present beside biotite, greenish in colour and showing the optical properties of hornblende.

D.II ROCK CHEMISTRY

As mentioned in the descriptive petrography, because of the fine granularity of the volcanics and their heavy alteration closer to the pyritic sulphide deposits, further definition of rock types has had to be based on chemical analysis. During the laboratory work, rock samples from the Lahanos area were analysed by XRF methods. Sample and standard preparation techniques were carried out as described by Ineson, 1967. See appendix for operating conditions and also calibration graphs Fig. 28 A-D. Mass absorption corrections and recomputing to 100% were done by the Holland and Brindle (1966) Computer programme. In all, 231 rock samples representing surface, underground, boreholes and geochemical grid were analysed for SiO_2 , Al_2O_3 , MgO , Fe_2O_3 (total iron), CaO , Na_2O , K_2O , TiO_2 , MnO and S. The FeO analyses were done by wetchemical methods. 65 rock samples of various volcanic rocks from the surface were analysed for Ba, Sr, Rb, Zr, Cu and Zn, while 166 rock samples representing the geochemical grid and boreholes were analysed for Ba, Sr, Rb, Zr, Ga, Cr, Mo, Ni, Pb, Zn, Cu, Te, As, Bi, Cd and Ag. Results are given in Tables 4, 5, 6 and 27 (a and b). In most cases attempts have been made to recalculate the proximate mineralogical composition as "norms". C.I.P.W. norms were calculated from the chemical analysis of various volcanic rocks previously described petrographically (see Tab. 4). In order to name these rocks, analysis of the Lahanos volcanic rocks have been shown on diagram of the type used by Strekeisen, (1967,

TABLE 4

Chemical analyses of rocks from the Lahanos area

	Latite-basalt			Latite	Alkali basalt					Andesite-Tholeiite basalt						Ya.1B	
	161	169C	169D	110	112	162	164	169E	H3	108	111	136	137	146	160		166
SiO ₂	43.24	51.21	46.24	47.10	44.56	44.72	47.41	47.34	44.68	49.24	57.47	48.18	53.00	55.11	49.02	49.75	57.02
Al ₂ O ₃	18.09	18.65	18.40	19.89	15.86	17.78	19.24	18.68	13.91	20.98	16.96	16.87	18.00	16.76	19.97	17.45	16.19
FeO	4.20	2.83	2.61	1.32	3.93	6.30	2.27	4.68	6.66	1.73	2.98	3.71	3.95	1.51	4.07	3.32	4.15
Fe ₂ O ₃	8.40	6.67	11.06	11.80	10.24	8.11	9.20	6.81	15.77	9.27	6.16	10.30	3.30	8.79	8.97	5.93	5.57
MgO	8.49	6.06	9.70	7.80	12.72	11.35	10.14	10.00	4.00	3.16	6.14	6.91	3.15	4.85	8.28	5.84	3.12
CaO	13.25	8.66	4.39	4.01	7.44	7.93	7.58	7.07	6.34	10.92	3.74	11.60	13.95	8.48	4.16	14.02	8.13
Na ₂ O	1.27	0.81	3.27	0.99	2.53	1.94	2.45	3.56	5.42	1.18	3.56	0.94	2.63	1.97	2.54	1.57	3.07
K ₂ O	1.58	3.21	1.72	3.66	0.76	0.11	0.24	0.73	0.12	1.61	0.82	0.10	0.31	0.79	1.38	0.11	1.00
TiO ₂	0.71	1.55	2.13	0.95	1.14	0.95	1.11	0.66	2.79	1.20	1.09	1.10	1.41	1.08	1.09	0.87	0.70
MnO	0.29	0.07	0.10	0.11	0.29	0.29	0.15	0.18	0.15	0.12	0.25	0.14	0.38	0.19	0.17	0.12	0.27
S	0.47	0.27	0.36	2.37	0.50	0.49	0.18	0.27	0.13	0.60	0.84	0.15	0.65	0.45	0.32	0.13	0.77
Quartz	0	7.76	0	7.12	0	0	0.88	0	0	9.62	16.51	10.68	8.58	16.88	7.74	7.86	15.44
Orthoclase	9.38	19.03	10.19	21.66	4.51	0.65	1.42	4.33	0.71	9.53	4.86	0.59	1.67	4.67	8.19	0.55	5.93
Albite	6.35	6.87	27.75	8.38	21.50	16.54	20.79	30.29	42.03	10.00	30.22	7.98	22.00	16.70	21.60	8.60	26.10
Anorthite	39.18	37.90	21.84	19.92	29.89	39.64	37.71	33.02	13.38	47.28	18.61	41.69	36.42	34.62	20.74	40.58	27.57
Nepheline	2.40	0	0	0	0	0	0	0	2.27	0	0	0	0	0	0	0	0
Corundum	0	0	3.18	7.01	0	0.05	1.17	0	0	0	3.42	0	0	0	6.76	0	0
Diopside	20.91	4.05	0	0	5.59	0	0	1.76	14.27	5.44	0	12.53	19.79	5.85	0	16.26	10.26
Hypersthene	0	13.26	13.40	19.45	7.66	23.37	25.32	3.37	0	5.36	15.34	11.47	0	9.38	20.72	0	4.43
Olivine	8.09	0	7.58	0	15.10	6.15	0	16.26	2.40	0	0	0	0	0	0	0	0
Magnetite	11.09	4.08	1.53	0	8.88	10.82	4.07	9.17	13.43	0.79	4.88	8.78	4.87	1.08	9.59	7.65	7.44
Hematite	0.32	3.56	9.74	14.99	3.71	0	6.16	0	5.88	8.54	2.47	3.86	0	7.89	1.94	0.64	0
Ilmenite	1.35	2.95	4.05	1.80	2.17	1.81	2.11	1.26	5.34	2.28	2.07	2.09	3.36	2.05	2.03	1.67	1.33
Titanite	0	0	0	0	0	0	0	0	0	0	0	0	0	0	0	0	0
Rutile	0	0	0	0	0	0	0	0	0	0	0	0	0	0	0	0	0
Pyrite	0.88	0.50	0.67	4.44	0.94	0.92	0.33	0.50	0.24	1.12	1.57	0.28	2.40	0.84	0.60	0.48	1.44

TABLE 4 (Contd.)

Chemical analyses of rocks from the Lahanos area

	Q u a r t z - A n d e s i t e										
	64	65	66	67	106	130	153	159	Yd.1.A	P.4	P.3b
SiO ₂	60.81	57.60	60.45	52.88	59.90	55.70	61.00	72.22	73.25	71.80	67.92
Al ₂ O ₃	16.16	18.04	17.82	15.09	18.52	17.15	17.72	16.94	14.50	15.45	7.43
FeO	2.34	2.00	3.05	4.07	2.42	4.42	2.37	0.20	0.81	3.17	5.71
Fe ₂ O ₃	6.68	6.93	5.54	9.33	4.47	7.09	7.89	2.87	3.25	2.28	12.12
MgO	0.37	4.38	3.67	4.78	4.41	6.75	4.33	0.66	1.85	0.50	3.79
CaO	4.30	3.34	3.95	3.38	4.07	4.07	0.56	6.10	0.35	0.27	1.93
Na ₂ O	3.56	2.95	3.58	2.98	3.89	2.44	4.44	0	5.20	5.72	0.02
K ₂ O	0.19	0.20	0.26	0.16	0.37	0.39	0.15	0.38	0.23	0.28	0.04
TiO ₂	0.80	0.74	0.62	0.68	0.99	1.36	1.07	0.46	0.11	0.26	0.25
MnO	0.23	0.18	0.19	0.16	0.13	0.18	0.23	0.07	0.08	0.05	0.22
S	4.56	3.63	0.87	6.49	0.77	0.45	0.23	0.14	0.39	0.22	0.56
Quartz	29.68	26.04	24.78	20.66	20.63	21.34	27.02	56.81	38.64	33.16	58.25
Orthoclase	1.12	1.18	1.54	0.95	2.19	2.31	0.88	2.24	1.36	1.59	0.23
Albite	30.20	25.02	30.39	25.33	33.02	20.75	37.67	0.00	44.03	46.64	0.17
Anorthite	21.38	16.60	19.66	16.84	20.25	20.29	2.78	29.70	1.73	1.29	9.64
Nepheline	0	0	0	0	0	0	0	0	0	0	0
Corundum	2.28	6.91	4.48	3.88	4.33	5.34	9.26	5.63	5.06	8.91	3.87
Diopside	0	0	0	0	0	0	0	0	0	0	0
Hypersthene	0.92	10.93	9.17	11.95	11.01	16.89	10.81	1.64	4.61	4.82	9.52
Olivine	0	0	0	0	0	0	0	0	0	0	0
Magnetite	0	0	6.19	0	3.17	9.60	4.63	0	1.45	2.69	16.76
Hematite	11.18	10.40	0.94	13.51	2.02	0	4.45	3.11	2.15	0	0
Ilmenite	1.52	1.40	1.18	1.29	1.88	2.59	2.03	0.57	0.20	0.47	0.47
Titanite	0	0	0	0	0	0	0	0.38	0	0	0
Rutile	0	0	0	0	0	0	0	0	0	0	0
Pyrite	8.56	6.81	1.63	12.21	1.44	0.84	0.43	0.26	0.73	0.39	1.05

TABLE 4 (Contd.)

Chemical analyses of rocks from the Lahanos area

	D a c i t e																				
	74	82	87	95	113	122	129	135	141	156	169A	Yd. la	Ag. Vol.	Yd. Bed	C4	04	07	A01	A03	M.27B	M.27C
SiO ₂	69.59	75.09	75.77	75.68	63.66	57.49	65.85	76.51	62.80	76.23	75.58	67.16	71.80	69.99	65.39	66.05	59.44	64.97	65.34	65.03	69.28
Al ₂ O ₃	16.43	14.56	12.70	16.13	18.33	21.41	19.55	14.18	15.34	13.50	14.57	15.50	14.96	16.93	15.50	15.79	19.25	16.21	17.01	17.23	15.87
FeO	1.37	0.51	0.45	0.44	2.51	2.95	3.03	0.34	2.78	0.39	0.54	0.83	1.20	1.43	3.90	4.22	1.54	1.34	1.59	0.51	0.73
Fe ₂ O ₃	1.92	1.68	1.62	2.16	3.02	3.67	2.62	0.33	4.16	1.21	1.23	4.08	2.45	0.35	2.07	1.32	7.86	7.23	3.13	4.86	2.12
MgO	3.95	0.18	0.62	0.07	3.87	9.87	3.61	0.51	4.95	1.10	0.54	1.37	1.52	0.89	2.82	2.49	4.45	2.51	3.39	1.40	2.98
CaO	0.59	0	3.10	0	2.03	0	1.01	0.09	2.60	2.32	0.67	4.41	1.27	1.77	4.08	3.42	4.22	4.86	3.58	3.64	5.77
Na ₂ O	3.92	5.47	2.07	3.35	2.68	2.39	2.23	5.17	2.97	2.18	4.15	2.36	3.40	3.98	2.26	2.61	0.22	0.06	1.85	2.78	0.03
K ₂ O	1.46	2.06	2.91	1.64	3.03	1.24	1.22	2.34	3.04	2.60	2.52	3.57	2.41	2.64	3.08	3.26	1.63	1.54	3.02	3.72	1.82
TiO ₂	0.42	0.35	0.37	0.50	0.62	0.68	0.64	0.35	0.84	0.35	0.14	0.49	0.48	0.53	0.70	0.60	1.07	0.77	0.47	0.43	0.30
MnO	0.12	0.09	0.05	0.02	0.07	0.12	0.09	0.01	0.18	0.03	0.04	0.05	0.10	0.05	0.11	0.08	0.06	0.04	0.18	0.06	0.53
S	0.22	0.05	0.34	0.08	0.17	0.24	0.14	0.16	0.39	0.07	0.01	0.19	0.40	1.40	0.06	0.10	0.24	0.45	0.41	0.32	0.45
Quartz	33.99	35.12	45.04	49.80	25.90	23.57	39.64	36.54	20.87	47.01	39.58	28.45	37.86	31.14	27.59	27.32	36.18	44.22	30.35	24.75	45.38
Orthoclase	8.64	12.17	17.20	9.68	17.95	7.34	7.23	13.83	18.02	15.37	14.90	2.11	14.26	15.63	18.20	19.35	9.45	8.90	17.88	22.00	10.76
Albite	33.22	46.29	17.52	28.34	22.74	20.28	18.93	43.76	25.21	18.45	35.14	19.98	28.81	33.75	19.21	22.11	2.01	0.52	15.68	23.54	0.25
Anorthite	2.93	0	15.38	0	10.10	0	5.02	0.44	12.94	11.51	3.32	21.17	6.30	8.80	19.59	17.04	20.85	24.18	17.79	18.07	28.65
Nepheline	0	0	0	0	0	0	0	0	0	0	0	0	0	0	0	0	0	0	0	0	0
Corundum	7.34	3.33	0.50	8.48	6.97	16.18	12.77	2.98	2.44	2.88	3.79	0	4.45	4.31	1.26	1.73	9.38	5.50	4.19	2.01	3.36
Diopside	0	0	0	0	0	0	0	0	0	0	0	0.56	0	0	0	0	0	0	0	0	0
Hypersthene	10.08	0.44	1.54	0.17	10.83	26.00	11.57	1.27	12.64	2.74	1.34	3.15	3.79	3.40	7.04	6.23	11.10	6.30	8.45	3.48	7.42
Olivine	0	0	0	0	0	0	0	0	0	0	0	0	0	0	0	0	0	0	0	0	0
Magnetite	2.56	0.78	0	0	3.98	4.85	3.32	0	5.51	0.14	1.43	0.88	1.67	0	0	2.49	0.92	0.70	3.19	0	1.68
Hematite	0	1.08	1.85	2.24	0	0	0	0.52	0	1.06	0.17	3.38	1.16	0	5.69	2.35	7.20	6.72	0.75	5.01	0.87
Ilmenite	0.79	0.66	0.70	0.94	1.18	1.29	1.21	0.6	1.60	0.66	0.26	0.93	0.91	1.02	0.97	1.14	1.98	1.37	0.89	0.81	0.74
Titanite	0	0	0	0	0	0	0	0	0	0	0	0	0	0	0.45	0	0	0	0	0	0
Rutile	0	0	0	0	0	0	0	0	0	0	0	0	0	0	0	0	0	0	0	0	0
Pyrite	0.41	0.09	0.63	0.14	0.31	0.45	0.26	0.29	0.73	0.13	0.01	0.35	0.75	2.64	0.11	0.20	0.96	1.68	0.76	0.59	0.84

TABLE 4 (Contd.)

Chemical analyses of rocks from the Lahanos area

	R h y o d a c i t e										R h y o l i t e s					
	83	84	85	117	132	138	142	143	A02	M27	81	86	104	105	114	144
SiO ₂	74.85	73.13	71.58	91.34	73.91	57.40	69.07	66.67	57.54	66.26	79.63	85.50	64.22	78.29	64.72	74.87
Al ₂ O ₃	14.12	14.49	15.64	4.78	15.89	13.39	17.24	18.09	20.48	16.12	14.55	6.77	18.60	14.09	20.72	14.48
FeO	0.43	0.54	0.39	0.73	0.68	0.29	0.85	0.81	1.50	0.46	0.68	0.32	0.34	0.29	1.32	0.44
Fe ₂ O ₃	1.71	1.97	2.28	0.18	0.94	6.23	1.48	2.76	8.19	4.64	0.41	3.14	11.80	0.09	5.32	2.29
MgO	0.60	0.27	0.05	0.43	3.35	2.65	3.12	3.17	4.99	2.50	0.64	1.38	0.27	0.29	2.02	0.42
CaO	3.10	0.78	0.94	0.82	0	12.68	2.67	1.19	2.85	2.20	0	0.24	0	0	0.10	0.51
Na ₂ O	1.38	2.95	2.31	0.06	1.99	0.50	1.46	2.12	0.39	2.72	0.08	0.05	0.06	0.18	0.47	1.55
K ₂ O	3.09	5.32	6.31	1.26	2.57	3.87	2.55	3.76	2.79	4.42	3.60	1.99	2.63	6.63	3.79	5.06
TiO ₂	0.39	0.43	0.30	0.08	0.43	0.57	0.34	0.62	1.07	0.14	0.46	0.43	0.73	0.13	0.92	0.25
MnO	0.05	0.06	0.06	0.01	0.03	0.45	0.10	0.08	0.03	0.06	0.01	0.02	0.03	0	0.08	0.03
S	0.24	0.05	0.09	0.31	0.17	1.95	1.11	0.68	0.16	0.17	0.03	0.17	1.40	0.06	0.54	0.09
Quartz	47.41	35.55	31.89	83.54	47.46	17.21	40.48	32.68	30.96	25.08	64.33	75.07	53.37	51.24	44.32	44.79
Orthoclase	18.32	31.46	37.30	7.45	15.19	22.88	15.08	22.24	16.68	26.14	21.27	11.76	15.53	39.21	22.43	29.92
Albite	11.68	24.98	19.55	0.50	16.93	4.23	12.36	17.95	3.14	23.03	0.67	0.42	0.50	1.60	3.98	13.12
Anorthite	15.43	3.87	4.71	4.07	0	22.87	13.25	5.95	14.18	10.92	0	1.01	0	0	0.49	2.53
Nepheline	0	0	0	0	0	0	0	0	0	0	0	0	0	0	0	0
Corundum	2.84	2.46	3.29	1.82	9.82	0	7.23	8.36	11.52	2.86	10.52	4.16	15.64	6.58	15.68	5.52
Diopside	0	0	0	0	0	14.24	0	0	0	0	0	0	0	0	0	0
Hypersthene	1.51	0.67	0.14	1.72	8.37	Wollas-	7.77	7.90	12.50	6.25	1.77	3.43	0.67	0.87	5.03	1.04
						tonite										
						9.08										
Olivine	0	0	0	0	0	0	0	0	0	0	0	0	0	0	0	0
Magnetite	0	0.54	0.36	0.14	0.56	0	0	0	1.39	0.01	0.48	0	0	0.08	0.32	0.53
Hematite	1.77	1.53	1.98	0	0.48	9.46	2.10	3.25	7.20	4.58	0	3.43	14.47	0	4.95	1.87
Ilmenite	0.74	0.81	0.57	0.15	0.83	1.08	0.64	1.19	1.98	0.77	0.87	0.71	0.78	0.26	1.74	0.47
Titanite	0	0	0	0	0	0	0	0	0	0	0	0.12	0	0	0	0
Rutile	0	0	0	0	0	0	0	0	0	0	0	0	0.31	0	0	0
Pyrite	0.44	0.09	0.16	0.58	0.31	3.65	2.08	1.27	0.60	0.31	0.05	0.31	2.62	0.11	1.01	0.16

in Fig. 3) and by O'Connor, (1965, in Fig. 4). In this thesis Strekeisen's final chemical classification and estimated distribution of volcanic rocks in the orogenic belts has been used rather than O'Connor's classification.

Plotting of the normative composition of the volcanic rocks from the Lahanos area on a Quartz-Alkali feldspar-Plagioclase triangular diagram showed a sequence of volcanic rocks ranging in composition from alkali basalt to rhyodacite and rhyolite. Comparison of this trend with Zavaritskii's classification of volcanic rocks (Gorshkov, 1967) suggests a similar trend to the Calc-alkali lavas of the Island arcs and to the orogenic belt volcanism described by Williams et al. (1954), and Turner and Verhoogen (1960), and their close association with spilite and quartz-keratophyre. Examination of Figs. 3 to 7 suggested that the volcanic rocks of the Lahanos area embrace the Calc-alkaline and tholeiitic series.

D.IIa Field and Petrographic Evidence of Alteration in the Lahanos

Volcanic Rocks

Field occurrences of the Lahanos volcanic rocks have dominantly shown severe alteration and as a result of alteration (i) a bleaching in colour i.e. mainly silicification, kaolinisation, sericitisation; (ii) green descolouration i.e. mainly chloritisation, propylitisation, and rarely epidotisation and actinolitisation in particularly hydro-thermally active areas and closer to the late granitic intrusive. The latter produced actinolite, tremolite, green garnet and skarn minerals particularly in adjacent limestone and volcanic rocks e.g.

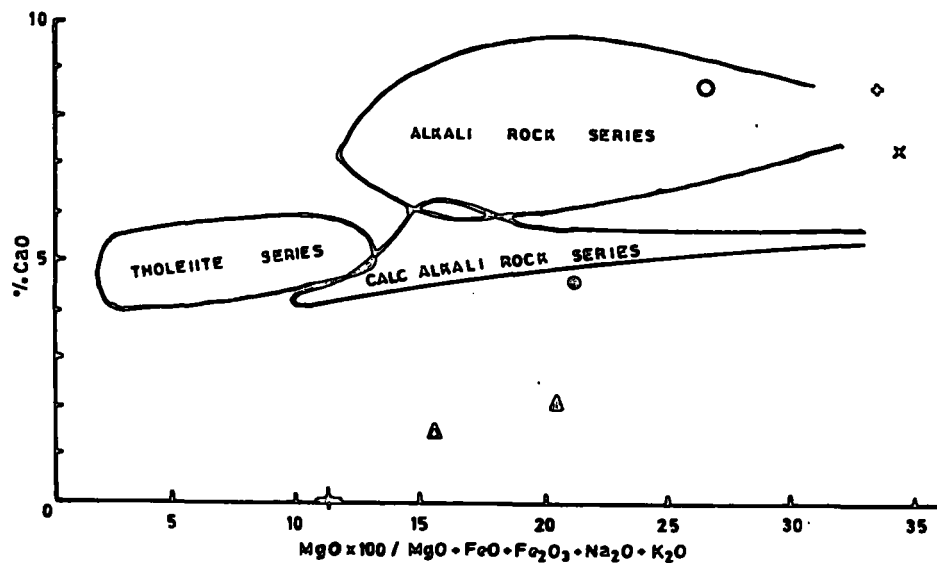


FIG. 6._ The CaO value plotted against the corresponding alkali-lime index (proposed by Kuno 1959) for Lahaos volcanic rocks.

- | | | | |
|---|------------------------------------|---|-------------------|
| • | Mean of 3 latite- (divine-) basalt | Δ | Mean of 21 dacite |
| x | 5 alkali basalt | Δ | 10 rhyodacite |
| o | 4 andesite tholeiite basalt | ◇ | 3 rhyelite |
| o | 15 quartz andesite | | |

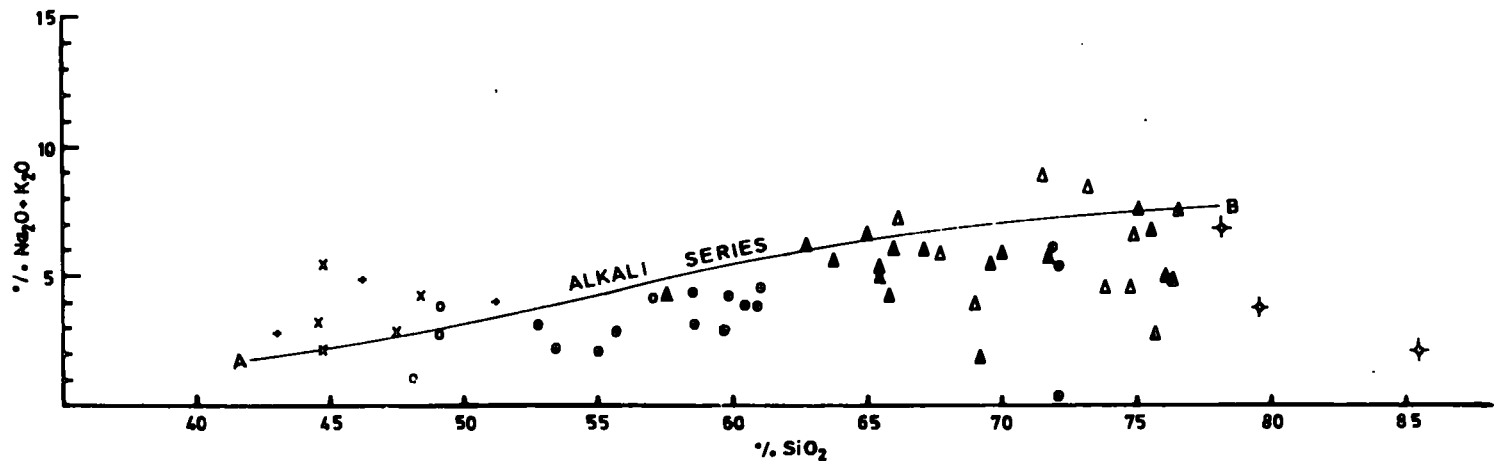


FIG.7._ Total alkali-SiO₂ relation in the alkali and tholeiite series of the Lahanos area Espiye, Eastern Black Sea, Turkey. AB-Alkali / Tholeiite boundary according to Kuno 1959.

- | | | | |
|---|---------------------------|---|------------|
| ◆ | Latite-(olivine-) basalt | △ | Dacite |
| x | Alkali basalt | △ | Rhyodacite |
| ○ | Andesite tholeiite basalt | ⊕ | Rhyolite |
| ○ | Quartz andesite | | |

in the Kapıkaya-Bayrambey area (Map 4,) where well developed skarn minerals in limestone are present. In the Çatak and the River Yağlı and Harşit valleys (Map 2), epidotisation and actinolitisation of volcanic rocks are well represented adjacent to the granitic intrusives; (iii) due to weathering, oxidation of ore grains and other iron rich minerals gave a red staining to some of the Lahanos volcanic rocks. The chemical data for the Lahanos volcanic rocks are plotted in terms of $Al_2O_3 - (Na_2O + K_2O)$; CaO; FeO; FeO (Total iron) + MgO + MnO on Fig. 8 (A to G). On Fig. 8A the average alkali, calc-alkaline, tholeiitic basalt and andesite field and average dacite, dellenite, rhyodacite, alkali and calc-alkali rhyolite field have been marked according to Nockold's (1954) and Manson and Poldervaart's (1964) average chemical composition of basalts, andesites, dacites, rhyodacites and rhyolites, in addition to the unaltered average igneous rock fields. The positions of the common alteration products are shown, that is secondary epidote clinozoisite, pumpellyite, prehnite, piemontite, actinolite, chlorite, kaolinite, montmorillonite and illite (Composition based on Deer, Howie and Zussman, 1962, Vol. 1, 2 and 3).

Mineralogical alteration of basaltic rocks:

During the petrographic studies, examination of the alkali and latite-basalts showed dominant chloritisation, carbonatisation and formation of opaque grains in the pyroxene; carbonatisation, sericitisation, chloritisation in feldspars, while olivine is converted into iddingsite or chlorite. Spilitisation (in the sense of Cann's

and Vine's (1966) definition), formation of analcime and particularly palagonite indicates aqueous conditions. In the field alteration products of the Lower Basic Series Fe-Mn chlorite and iron oxide give a brownish-reddish appearance and onion structure is seen due to spheroidal weathering.

Mineralogical alteration of andesitic rocks:

Andesites are somewhat similar to basaltic rocks in giving more or less similar alteration products - in addition to chloritisation, sericitisation, kaolinisation, pyritisation, there is also albitisation of the groundmass and calcic plagioclase, due to soda metasomatism.

Mineralogical alteration of the acidic rocks (i.e. dacite, rhyodacite and rhyolite):

The common alteration products observed in the field and thin section study are silicification, pyritisation, sericitisation, carbonatisation albitisation and a little chloritisation of the groundmass and of the phenocrysts of feldspars, amphiboles and biotite.

D.IIb The Effects of Alterations in the Chemistry of the

Lahanos Volcanic Rocks

In order to work out and explain the effects of alteration in the chemistry of the Lahanos volcanic rocks, a composite triangular ACF diagram as mentioned above (Fig.8 (A - G) and other variation diagrams will be discussed in the following section; D.IIb is subdivided into D.IIb1 - common alteration products of the Lahanos

volcanic rocks, and D.IIb2 - the effects of alteration on the variation of major oxides.

D.IIb1 - Common Alteration Products of the Lahanos Volcanic Rocks

The chemical analyses of average normal basalts, andesites, dacite, dellenites, latite, rhyodacite, rhyolite are given together with the analyses of the Lahanos volcanic rocks in Table 4. In order to determine the probable effects of alteration in the Lahanos volcanic rocks Fig. 8 (A - G) has been constructed using Nockold's and Manson and Poldervaart's average igneous rock composition, together with the probable fields of secondary minerals.

General alteration trend of the Latite-Basalts: As seen in Fig. 8A, the average normal basalt and andesitic area, together with the Lahanos rocks were plotted. Samples 161 and 169C are in the average normal basalt field and representing more or less altered latite-basalts while sample 169D left the average normal basalt field and moved towards the chlorite side i.e. the sample 169D has mainly suffered from chloritisation rather than other alteration. Microscopic study of it predominantly showed severe chloritisation of the pyroxene and to a less extent plagioclase.

General Alteration Trend of the Alkali-Basalts: Plotting of the alkali basalts in Fig. 8B showed that none of the alkali-basalts has fallen into the average normal basalt field of Manson and Poldervaart and Nockold, the analyses indicate an approach towards the chlorite field of the ACF diagram i.e. chloritisation of the alkali-basalts is predominant which is similar to the latite-basalts of the Lahanos area.

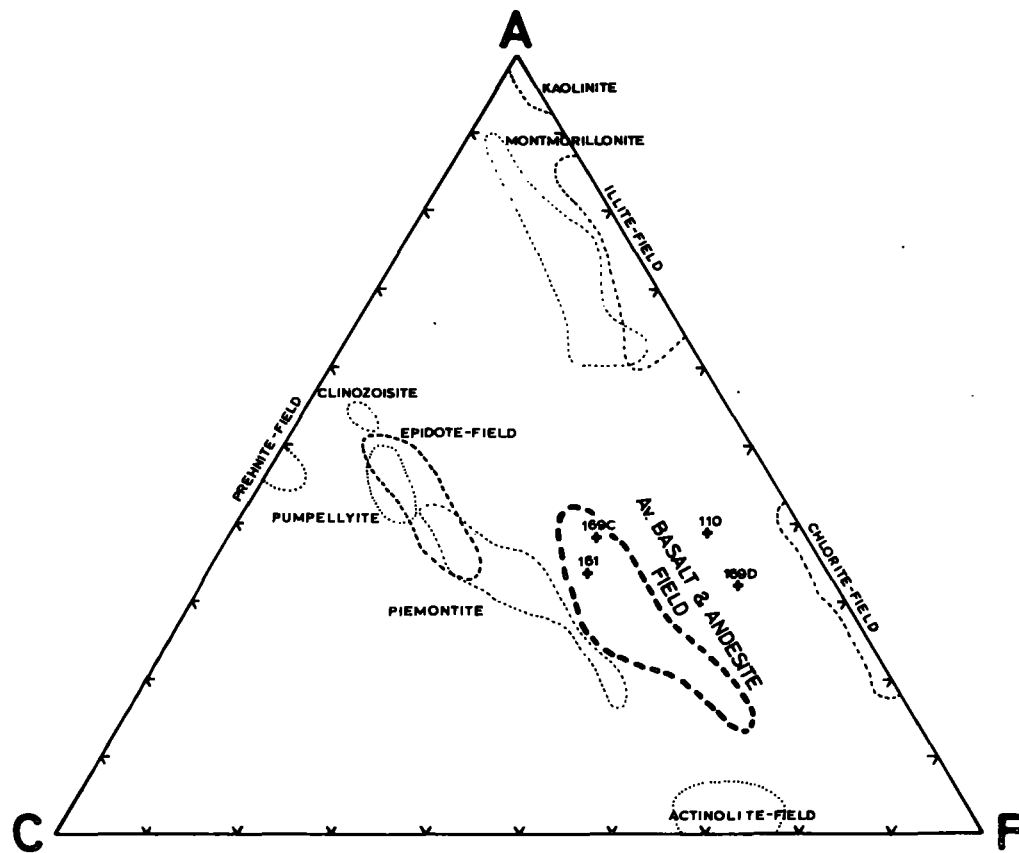


FIG.8A.- ACF diagram showing the relationship of latite & latite-basalts from the Lahanos area to the compositional fields of average basalt-andesite and common alteration products

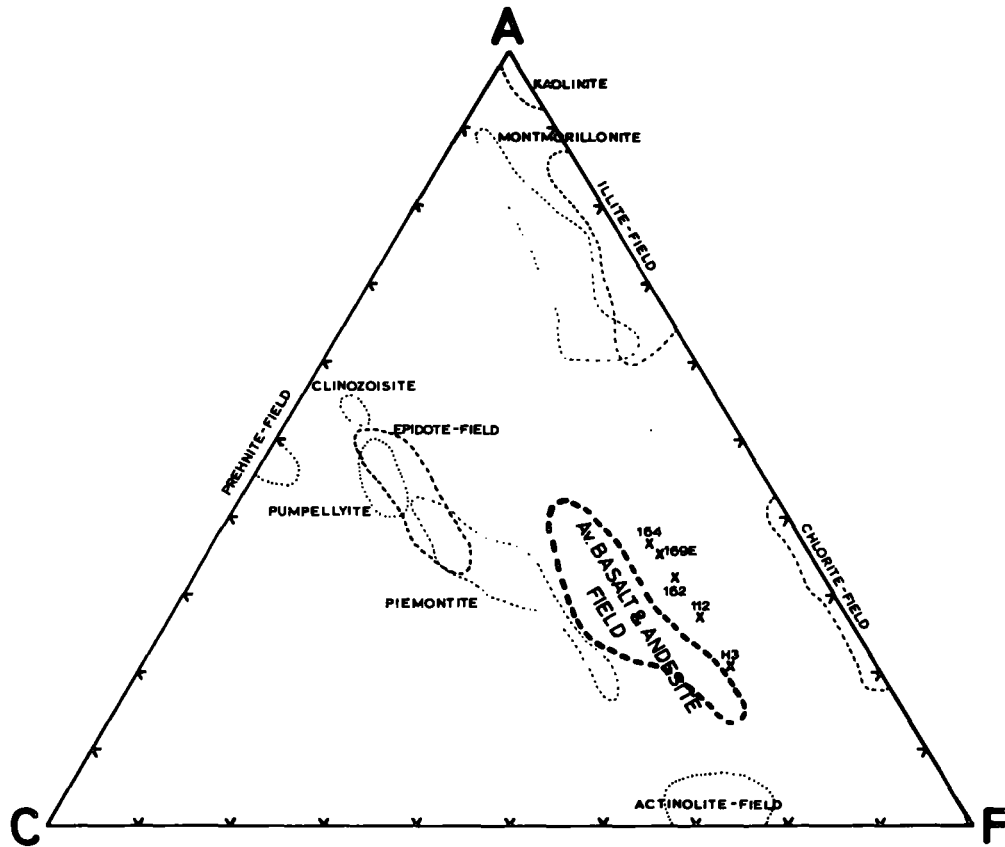


FIG.8B... ACF diagram showing the relationship of alkali basalts from the Lahanos area to the compositional fields of average basalt-andesite and common alteration products

General alteration trend of the Tholeiitic Basalt and Andesite:

Plotting of the tholeiitic andesite and basalt in the ACF diagram (Fig. 8C) showed that samples 136, 146 and Yd. 1.B have fallen into the average normal basalt and andesite field of Manson and Poldervaart and Nockold; while samples 137 and 166 fell towards the epidote and Mn-rich piemontite field and samples 111 and 160 showed an alteration trend towards the chlorite field. In addition to these two different alterations, however, there is also slight alumina enrichment due to leaching out of soluble elements and concentration of alumina as kaolinite e.g. Sample 108. Thus, the alteration products of the tholeiitic andesite and basalt vary considerably, epidotisation, chloritisation and kaolinisation are all found.

General alteration trend of the Quartz - Andesite: (8D) Plotting of these rocks showed that none of the quartz-andesitic rocks fell into the average normal basalt-andesite field nor into the dacite-rhyodacite-rhyolite field. However, as far as alteration processes are concerned the quartz-andesitic rocks yielded three main alteration products whose presence was also confirmed by the thin section study i.e. chloritisation, kaolinisation and illitic alteration e.g. sample Yd. 1.A and P4.

General alteration trend of the Dacite: Plotting of the Lahanos and Murgul dacites gave examples (i.e. Samples Yd. Bed. Vol. 1, A03, Yd. Ag. 1A, M27B and M27C) which fall into the average normal dacite-rhyodacite-rhyolite field and about seven close to the field. The

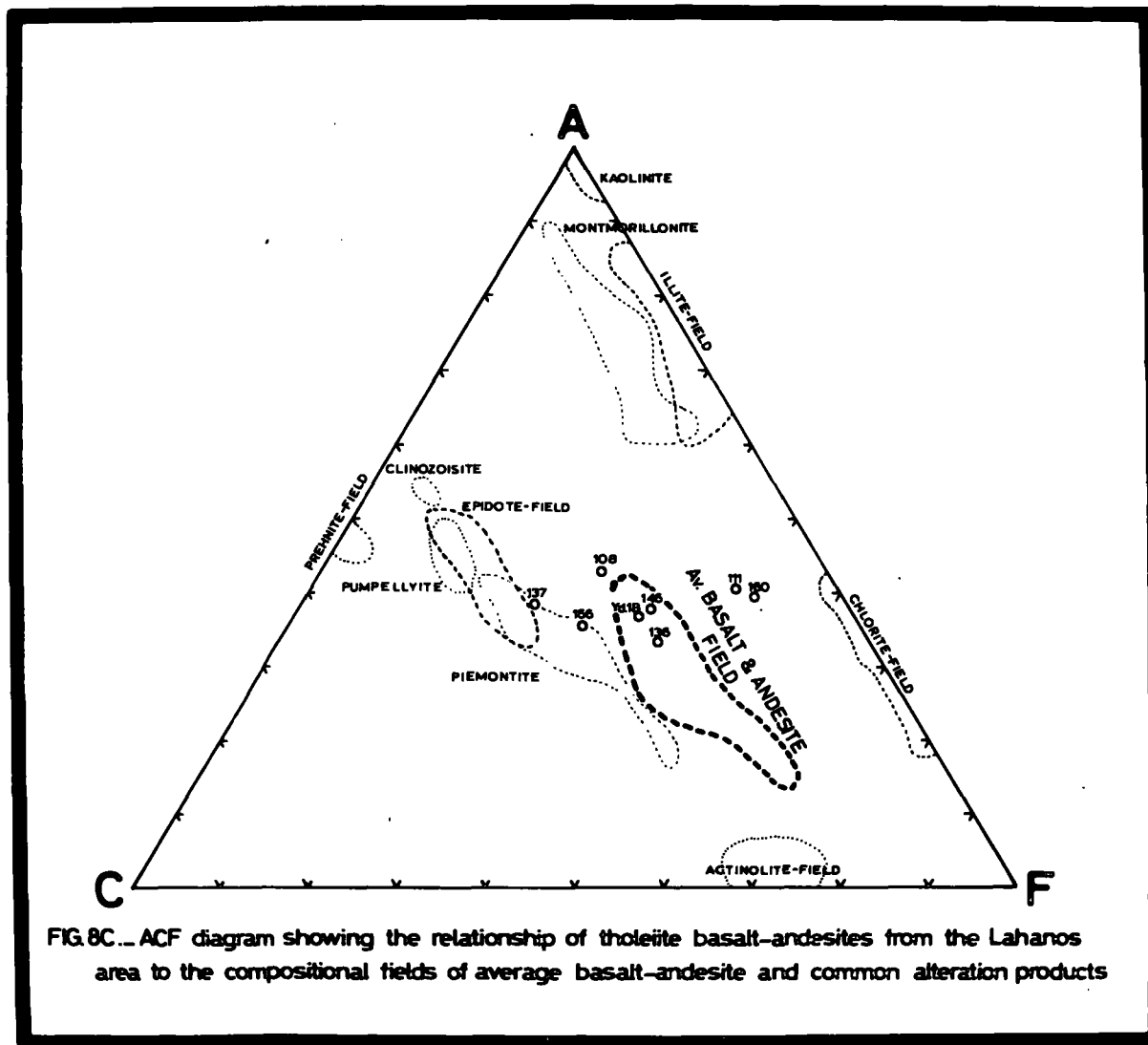


FIG. 8C... ACF diagram showing the relationship of tholeiite basalt-andesites from the Lahanos area to the compositional fields of average basalt-andesite and common alteration products

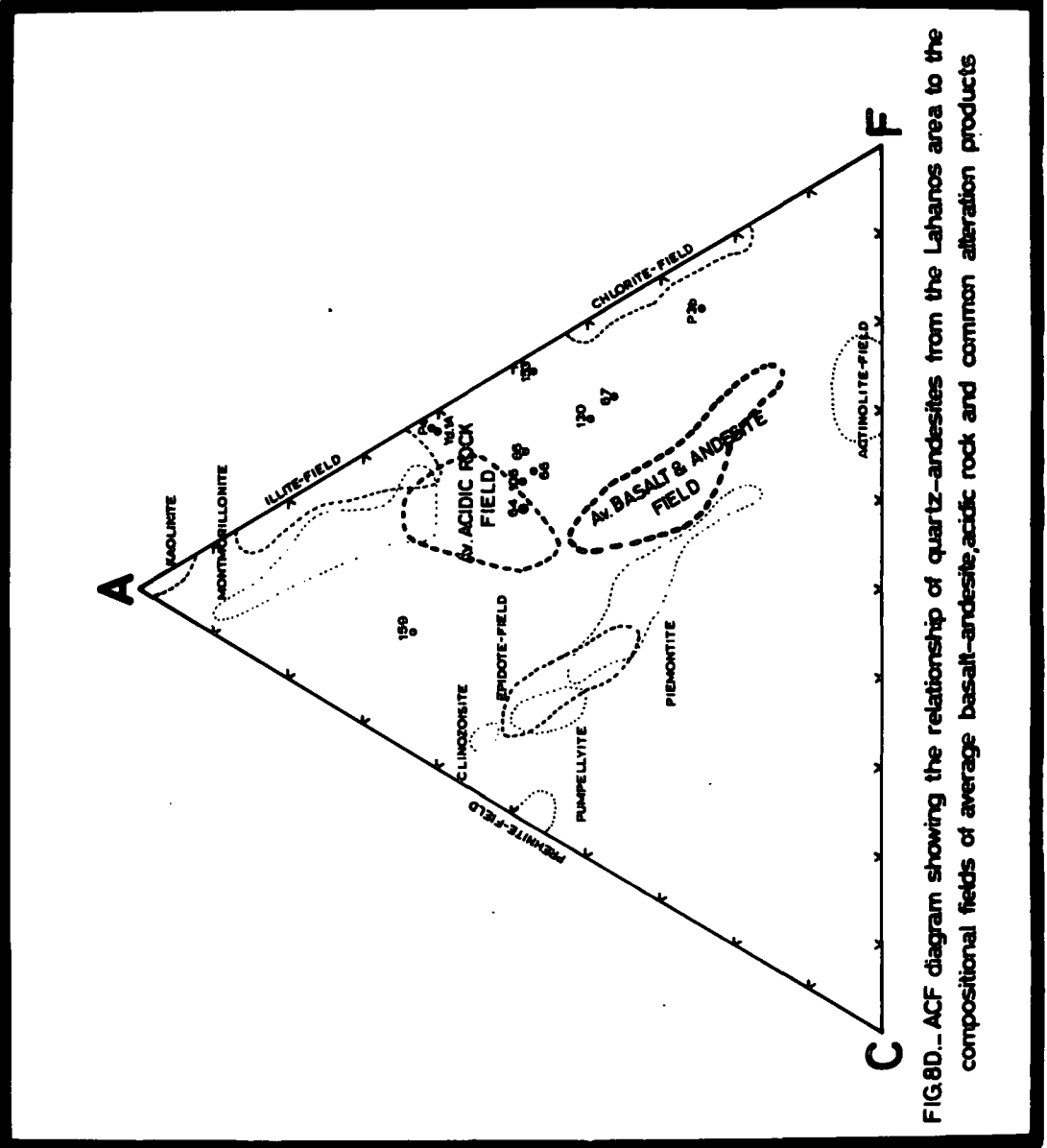


FIG.8D.- ACF diagram showing the relationship of quartz-andesites from the Lahanos area to the compositional fields of average basalt-andesite, acidic rock and common alteration products

Alteration trend of the dacite is towards the chlorite, montmorillonite and illite field (Fig. 8E).

General Alteration trend of the Rhyodacite: Only three of the rhyodacites (i.e. Samples 84, 117 and 142) have fallen into the average normal dacite-rhyodacite-rhyolite field. Rhyodacites are similar to those of the dacite showed three main alteration trends i.e. their alteration trend extends towards montmorillonite-, illite-, and chlorite- field. Sample 138, because of heavy carbonatisation, showed an approach towards the C corner of the ACF diagram (Fig. 8F); from microscopic study it may be confirmed that the sample suffered dense carbonatisation.

General alteration trend of the Rhyolite: None of the rhyolite plots in the average acidic rock field; thus, the rhyolites have suffered a great amount of alteration. Fig. 8G indicates alteration trends towards the chlorite-field, the illite-field and the kaolinite-field.

The study of the ACF diagram suggests that the volcanic rocks of the Lahanos area have commonly suffered intense chloritisation, kaolinisation (including other clay minerals i.e. montmorillonite and illite) and very little epidotisation. Chloritic alterations are more common in the basic rocks because of abundant ferro-magnesian minerals, but little or no kaolinisation. The alteration trends of the acidic rocks showed little chloritic alteration, but very common kaolinitic, montmorillonitic and illitic alterations.

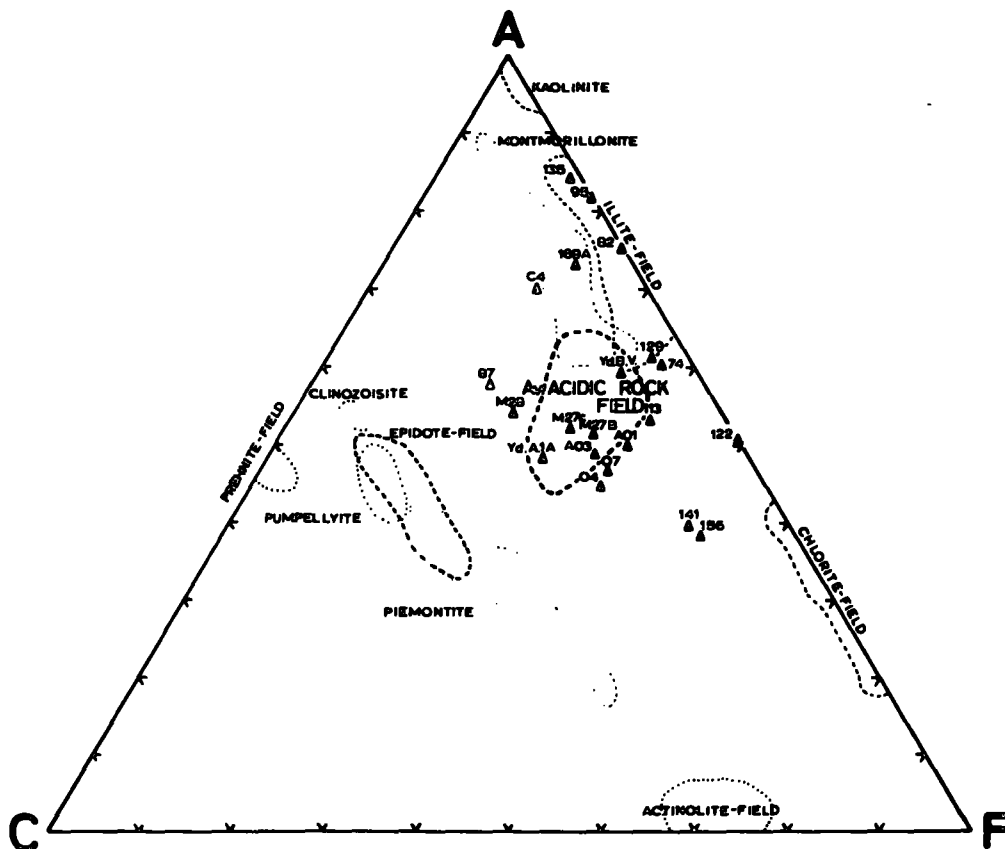


FIG.8E...ACF diagram showing the relationship of dacites from the Lahanos area to the compositional fields of average acidic rock and common alteration products

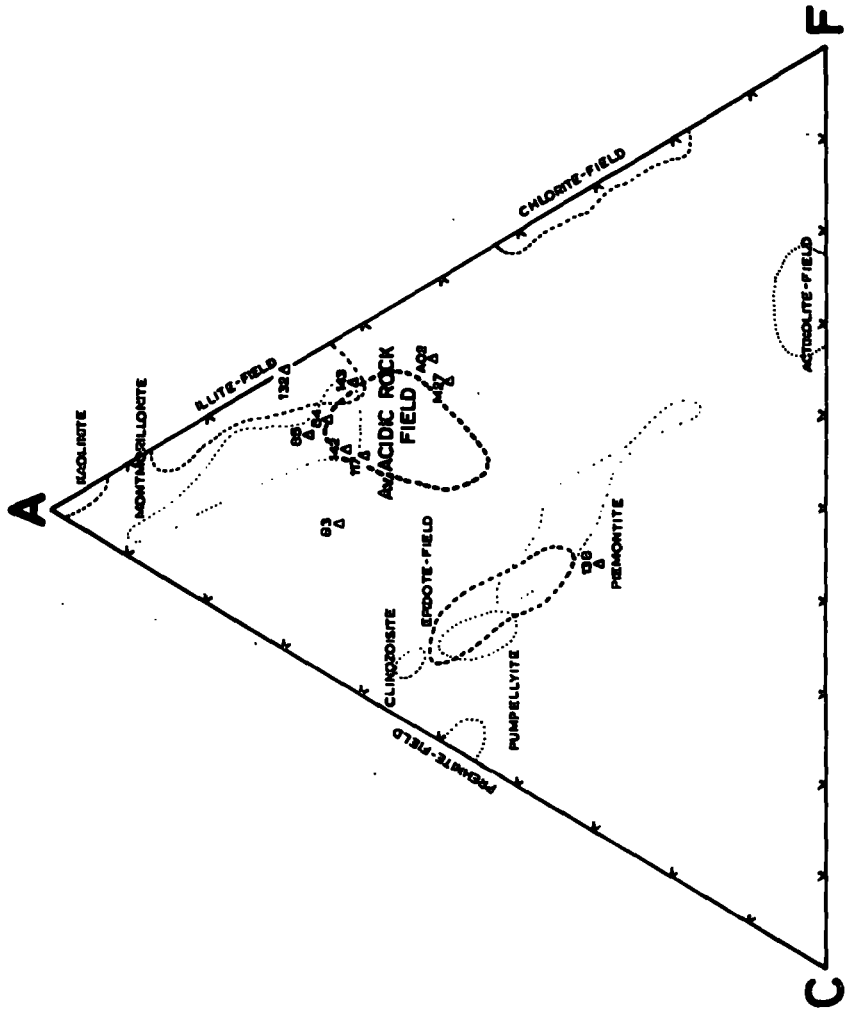


FIG. 8F. - ACF diagram showing the relationship of rhyodacites from the Lahanos area to the compositional fields of average acidic rock and common alteration products

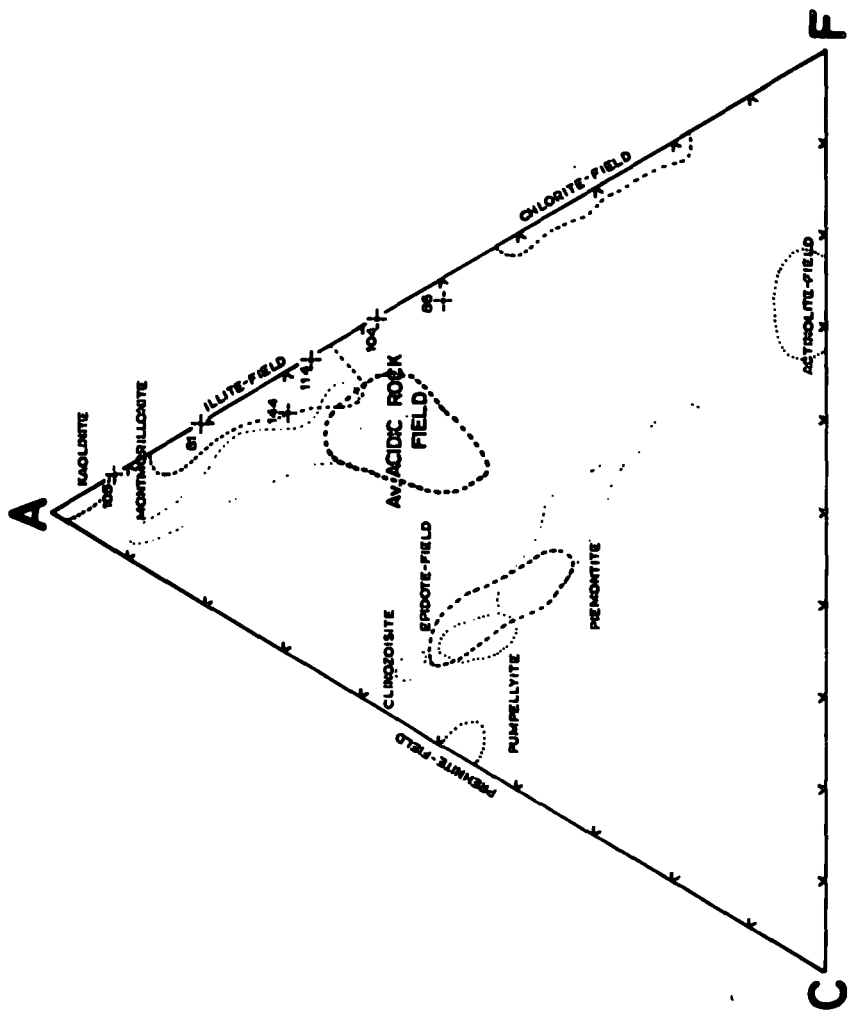


FIG. 86.--ACF diagram showing the relationship of rhyolites from the Lahanos area to the compositional fields of average acidic rock and common alteration products

D.IIb2 - Effects Of Alteration On The Variation of Major Oxides

In this subheading the chemistry of the volcanic rocks of the Lahanos area will be discussed in detail. To some extent comparisons are made with other volcanic areas of the world. The chemical analyses of major and minor elements and their C.I.P.W. norms in the Lahanos volcanic rocks have been given in Tabs. 4 and 5.

Variation of Oxides with SiO_2

Variation of oxides with SiO_2 provides a simple method for illustrating graphically the proportions of the major elements in a group of igneous rocks but its use has been criticised by Chayes (1962 and 1964) who has emphasised that the silica variation diagram is "of little use in discriminating between the effects of nearly all the processes thought to be of major importance in the differentiation of volcanic rocks". Despite this, such diagrams are still in common use. The variations of oxides with $\text{SiO}_2\%$ in the rocks of the Lahanos area have been plotted in Figs. 9 and 10 in which the amount (atomic weight per cent) of the given element is plotted against the $\text{SiO}_2\%$ (Fig. 9) and the Larsen function i.e. $1/3 \text{SiO}_2 + \text{K}_2\text{O} - (\text{FeO} + \text{MgO} + \text{CaO})\%$ where FeO represents the total iron as oxide (Larsen, 1936). (Fig. 10 and Tab. 3). The variation trends of K_2O , Na_2O , CaO , Fe_2O_3 and MgO against the Larsen function have a more linear relationship in spite of various alterations, when compared with variation against $\text{SiO}_2\%$. This is due to the inclusion of values for Fe_2O_3 , CaO , MgO , Na_2O , K_2O in the key variable.

TABLE 5

Trace element analysis in rocks from the Lahanos area

	Latite-basalt			Latite	Alkali basalt						Andesite-Tholeiite basalt						Yd.1B
	161	169C	169D	110	112	162	164	169E	H3	108	111	136	137	146	160	166	
Ba (ppm)	57	176	406	158	125	305	92	677	151	320	228	69	150	409	151	99	308
Sr "	94	77	196	66	124	122	158	573	153	85	183	274	67	296	101	360	189
Rb "	22	46	38	70	14	1	5	16	2	29	13	2	2	25	19	5	23
Zr "	31	319	334	77	79	62	126	133	321	112	142	48	79	115	75	97	126
Ni "	14	64	70	35	17	19	36	29	21	1	4	nil	nil	nil	18	52	nil
Cu "	93	15	31	59	113	111	373	240	22	61	79	46	22	22	22	152	25
Zn "	90	111	107	127	88	94	94	85	136	97	nil	91	141	114	94	75	85
S %	0.29	0.07	0.10	2.37	0.50	0.29	0.15	0.18	0.15	0.60	0.84	0.15	0.65	0.45	0.17	0.13	0.77

	Quartz-andesite										
	64	65	66	67	106	130	153	159	Yd.1A	P4	P3B
Ba (ppm)	89	87	123	128	48	29	60	96	48	87	114
Sr "	231	164	231	224	126	61	96	255	108	227	63
Rb "	4	6	5	5	8	8	2	13	7	nil	1
Zr "	95	79	107	89	146	75	89	217	159	347	53
Ni "	nil	2	2	nil	nil	nil	nil	4	4	3	12
Cu "	51	32	46	65	16	17	20	12	28	43	63
Zn "	128	130	179	103	96	153	247	57	486	55	286
S %	4.56	3.63	0.87	6.49	0.77	0.45	0.23	0.07	0.39	0.22	0.56

TABLE 5 (Contd.)

Trace element analysis in rocks from the Lahanos area

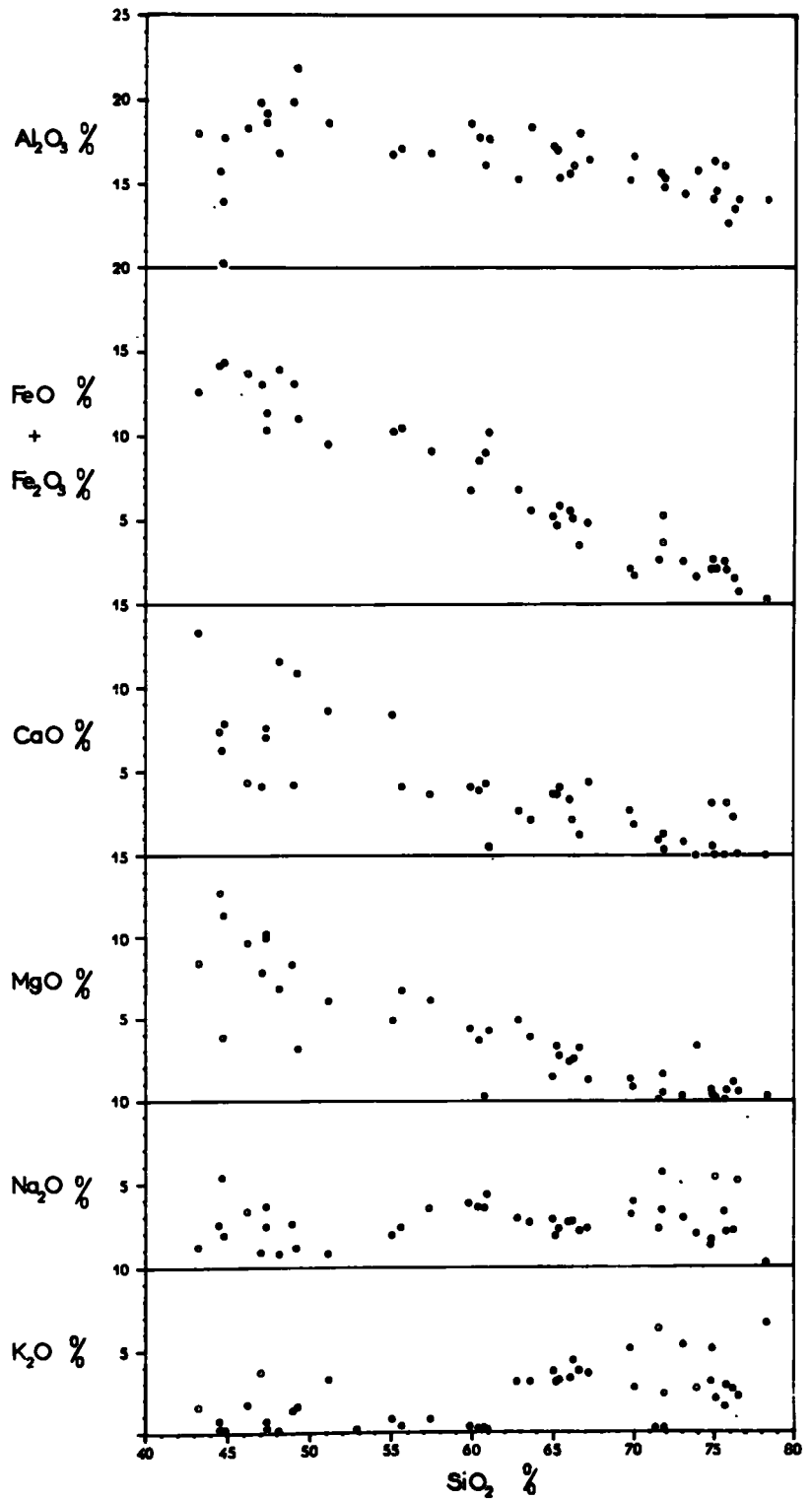
	D A C I T E																				
	74	82	87	95	113	122	129	135	141	156	169A	Yd. Ag. 1A	Yd. Bed vd.	G4	04	07	A01	A03	m27B	M27C	M28
Ba (ppm)	126	157	646	160	675	160	68	276	1033	253	870	516	249	183	720	718	128	98	133	130	29
Sr "	130	79	310	24	227	39	52	98	188	367	148	6	92	200	210	241	174	92	123	238	184
Rb "	18	26	47	22	113	18	17	21	95	35	41	89	50	n.d.	n.d.	n.d.	28	26	74	66	20
Zr "	182	277	274	200	265	206	163	260	211	272	156	170	235	189	173	188	119	90	176	177	221
Ni "	8	6	3	6	52	23	nil	6	37	7	7	12	6	1	2	2	0.2	0.3	5	2	4
Cu "	17	10	8	9	36	39	17	21	36	12	18	59	13	66	85	120	94	572	212	22	193
Zn "	170	67	55	108	97	152	86	35	128	62	42	65	80	87	71	69	191	120	266	49	96
S %	0.22	0.05	0.34	0.08	0.17	0.24	0.14	0.16	0.39	0.03	0.04	0.19	0.10	1.406	0.06	0.11	0.24	0.45	0.18	0.06	0.53

	R h y o d a c i t e										R h y o l i t e s					
	83	84	85	117	132	138	142	143	A02	M27	81	86	104	105	114	144
Ba (ppm)	101	177	379	1105	146	137	367	452	131	225	374	97	1213	804	688	373
Sr "	957	91	100	360	54	347	113	58	179	182	23	39	36	34	293	82
Rb "	42	43	70	21	50	30	39	33	44	82	56	65	29	73	105	67
Zr "	392	226	189	109	247	118	206	156	131	180	277	66	176	138	254	190
Ni "	4	9	5	1	4	31	4	5	nil	11	4	15	6	8	41	7
Cu "	6	14	10	110	15	38	16	34	42	25	11	36	15	19	14	19
Zn "	54	69	50	52	58	73	97	121	340	85	27	53	89	42	97	51
S %	0.24	0.05	0.09	0.31	0.17	1.95	1.11	0.68	0.16	0.06	0.03	0.17	1.40	0.06	0.54	0.09

FIG. 9

VARIATION DIAGRAM FOR BASALT-ANDESITE-DACITE-RHYOLITE

AROUND ESPIYE IN THE BLACK SEA REGION, NE TURKEY



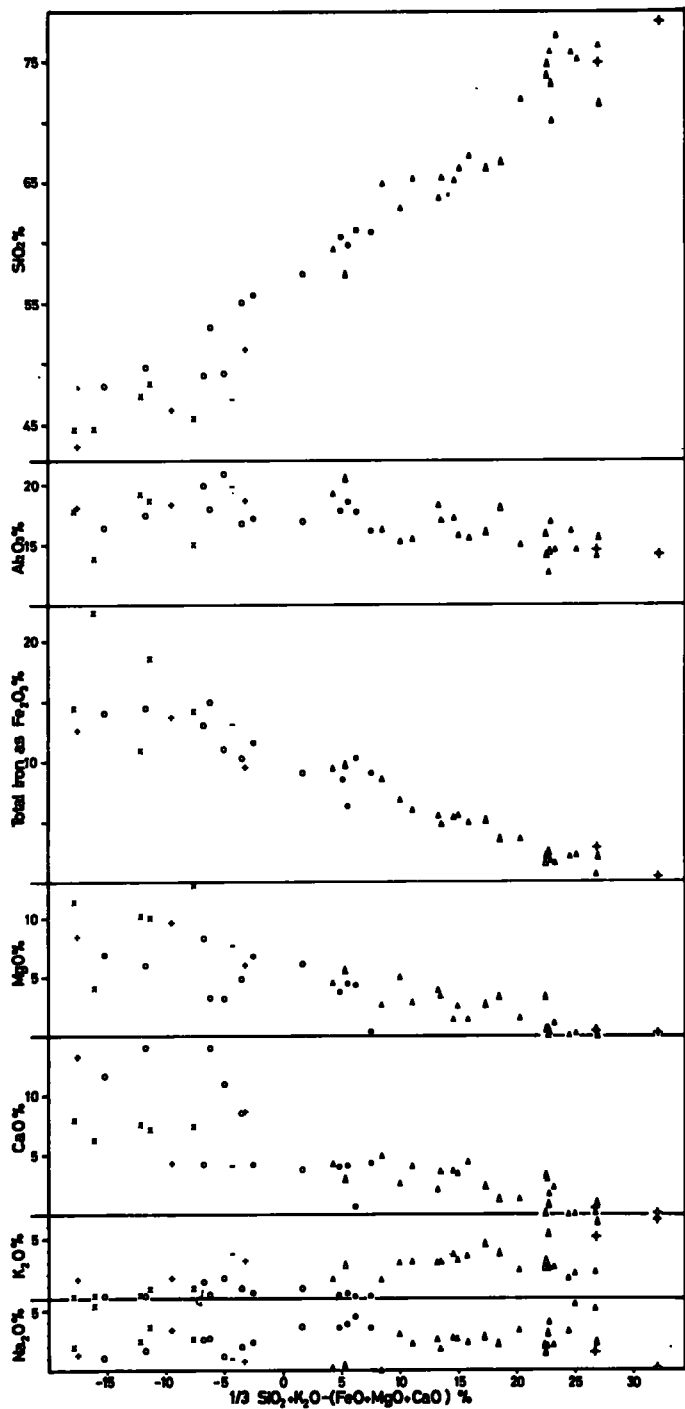
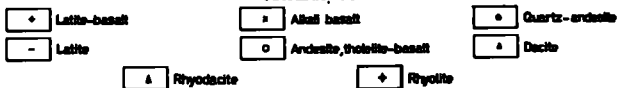


FIG.10... Variation in oxides with the Larsen's function in the Lahavos volcanic rocks.



The following principal features can be deduced from the variation diagrams of the Lahanos area volcanic rocks.

(i) Examination of both variation diagrams showed that there is hardly any gap in SiO_2 range except for a small gap between 51-55% SiO_2 which might be due to insufficient sample collection rather than due to the natural phenomena. However, Taneda (1962) points out a very few Japanese volcanic rocks show similar gap of silicon range about 54 to 55%.

(ii) There are pronounced concentrations of points in the range 43 to 47, 59.50 to 61.00 and 70 to 77% SiO_2 for the Lahanos area volcanic rocks. Again Taneda suggested that there is concentration of Japanese volcanic rocks having silica contents between 58 and 61%. These figures reflect the predominance of basalt, andesite, dacite, rhyodacite and rhyolite among the rock types found in the Lahanos area.

(iii) A certain amount of scattering is possibly due to various alterations, - hardly any oxide shows a linear trend; but some of them approximate to fairly regular trends.

In spite of scattering, an attempt has been made to compare Fig. 10 to the variation diagrams for volcanic rocks of the Yellowstone Volcanic province and plutonic rocks of the Lower Californian batholith Turner and Verhoogen (1960, pp. 349, Fig. 52). The variation of the different oxides against the Larsen's function shows a somewhat similar general trend to those found in the Lahanos volcanic rocks.

Variation in Al_2O_3

The alumina contents in the Lahanos area reach a maximum of 20.90% at about -6 and +5 (Fig.10) or 49% SiO_2 (Fig. 9) in the basalts which are very similar to the high-alumina basalts described by Kuno (1960) from Japan (Fig. 5 and Tab. 6). The general variation trend of Al_2O_3 shows some resemblance to the Lassen Peak (Bowen, 1956, Fig. 25, pp.95 and Williams, 1932) and Yellowstone Volcanic provinces (Turner and Verhoogen, 1960).

Variation in Iron Oxides

In Fig. 9 the total iron is plotted as $Fe_2O_3 + FeO$ and expressed as Fe_2O_3 . The overall picture of the total iron variation decreases as SiO_2 (acidity) increases which is similar in general behaviour to the iron variation trends of Yellowstone Park and Lassen Peak. Scattering in total iron is due mainly to pyritisation.

Variation in CaO

The general outline of the lime variation in both Fig. 9 and 10 suggests a gradual fall from the basic end to the acidic end. Scattering of lime is due to secondary carbonatisation and in other cases due to infilling of the vesicles by calcite and aragonite. One might suggest a broad resemblance to the Yellowstone province but it is somewhat different from the Lassen Peak volcano trend. The lime content shows more erratic scattering in the tholeiitic alkaline and latite- basalts compared to more acidic members of the Lahanos volcanic rocks.

TABLE 6

	Tholeiite			High Alumina Basalt						Alkali Basalt			
	108	136	166	137	160	161	162	164	169C	112	169D	169E	H3
SiO ₂	49.24	48.17	49.75	53.00	49.02	43.24	44.71	47.41	51.20	44.55	46.24	47.34	44.68
Al ₂ O ₃	20.98	16.87	17.45	18.00	19.97	18.09	17.78	19.24	18.65	15.88	18.19	18.67	13.91
Fe ₂ O ₃	8.27	10.29	5.93	3.30	8.97	4.20	8.11	9.20	6.67	10.24	11.05	6.80	6.66
FeO	1.73	3.71	3.32	3.95	4.07	8.40	6.30	2.27	2.83	3.93	2.61	4.68	15.77
MgO	3.15	6.91	5.84	3.15	8.28	8.49	11.35	10.13	6.05	12.73	9.70	10.00	4.00
CaO	10.91	11.59	14.02	13.95	4.16	13.25	7.93	7.58	8.66	7.44	4.39	7.07	6.34
Na ₂ O	1.17	0.93	1.57	2.63	2.53	1.27	1.94	2.45	0.80	2.52	3.27	3.56	5.42
K ₂ O	1.60	0.09	0.11	0.31	1.38	1.58	0.11	0.24	3.21	0.75	1.71	0.73	0.12
TiO ₂	1.19	1.09	0.87	1.41	1.09	0.71	0.94	1.11	1.55	1.14	2.13	0.66	2.79
MnO	0.12	0.13	0.12	0.38	0.17	0.29	0.29	0.15	0.06	0.29	0.10	0.18	0.15
S	0.60	0.15	0.13	0.65	0.32	0.47	0.49	0.18	0.27	0.50	0.35	0.27	0.13
Ba	0.0320	0.0069	0.0099	0.0150	0.0150	0.0057	0.0305	0.0092	0.0176	0.0125	0.0406	0.0677	0.0151
Sr	0.0085	0.0274	0.0360	0.0067	0.0101	0.0094	0.0123	0.0158	0.0077	0.0124	0.0196	0.0573	0.0153
Rb	0.0029	0.0002	0.0005	0.0002	0.0019	0.0022	0.0001	0.0006	0.0046	0.0013	0.0038	0.0016	0.0002
Zr	0.0112	0.0048	0.0097	0.0079	0.0075	0.0031	0.0062	0.0126	0.0319	0.0049	0.0334	0.0133	0.0321
Cu	0.0061	0.0046	0.0152	0.0022	0.0022	0.0093	0.0111	0.0373	0.0015	0.0113	0.0031	0.0239	0.0022
Ni	0.0001	nil	0.0052	nil	0.0018	0.0014	0.0019	0.0036	0.0064	0.0017	0.0070	0.0029	0.0021
Zn	0.0097	0.0091	0.0075	0.0141	0.0094	0.0090	0.0093	0.0096	0.0111	0.0088	0.0107	0.0085	0.0136
Norm. Quartz	9.62	10.68	7.86	8.58	7.74	nil	nil	0.88	7.76	nil	nil	nil	nil
Norm. Olivine	nil	nil	nil	nil	nil	8.09	6.15	nil	nil	15.10	7.58	15.26	2.40

Variation in MgO

Although the MgO- variation trend descends in somewhat linear fashion with increasing silica, some scattering occurs at the basic end of the Lahanos volcanic rocks. Values for a given silica percentage are comparable to those of many volcanic suites of the Island arc and orogenic belts; though the rocks of the Lahanos area have slightly higher MgO% owing to the hydrothermal mineralisation and alteration, i.e. formation of dolomite or dolomitic gangues and veinlets.

Variation in Na₂O

The soda variation trends are somewhat similar in both Fig. 9 and 10, but in the latter figure, the soda variation gave a better and smoother trend compared to Fig. 9. The soda content of the Lahanos volcanic rocks ranges from 0 to 5.50% Na₂O. In spite of over 5% range the soda variation trend showed little systematic variation throughout from the basalts to the rhyodacites, though it tends to be higher in the dacite and rhyodacite range. However, the soda trend towards the +30 Larsen's function gave distinct descendant pattern which suggest some similarity to the Yellowstone volcanic province trend in spite of albitisation and soda metasomatism of the Lahanos area volcanic rocks due to later hydrothermal activities.

Variation in K₂O

The variation trend for potash rises steadily from the basic end to the acidic end which is completely different in character from the soda trend. Plotting of oxides against the Larsen's function gave

better and smoother trend compared to the $\text{SiO}_2\%$ parameter. The accumulation of scattered potash values can be seen particularly in the tholeiitic basalts and andesite at basic end, and dacite to rhyodacite at the less acidic end (Fig. 10). Towards the acidic end the potash values move up which is somewhat comparable to the potash trend of the Yellowstone volcanic province and the Larsen Peak potash trends.

Both potash and soda (particularly) give slightly higher values comparing them to the other similar volcanic provinces especially at both the basic and acidic ends, which might be due to soda and potash metasomatism owing to the later hydrothermal activities in the Lahanos area.

Fe : Mg : (Na + K) Ratios

The relative proportions of iron magnesium and alkalis as atomic percentages in volcanic rocks from the Lahanos area are plotted on a triangular diagram in Fig. 11, shown alongside variation trends from the Hakone Volcano (data from Nockolds and Allen, 1958, pp. 48-50) lavas from the Crater Lake (Nockolds and Allen, 1953, pp. 111), Lassen Peak (Nockolds and Allen, 1953, pp. 114) and the Skaergaard intrusion (Wager and Deer, 1939).

Owing to intense alteration in the Lahanos volcanic rocks, scattering of results might be due to either enrichment in alkalis or consequently impoverishment in iron and magnesium or vice versa. The acidic series is relatively poor in iron, falling almost between the Crater Lake and the Hakone Hypersthenic Trends, and some of these

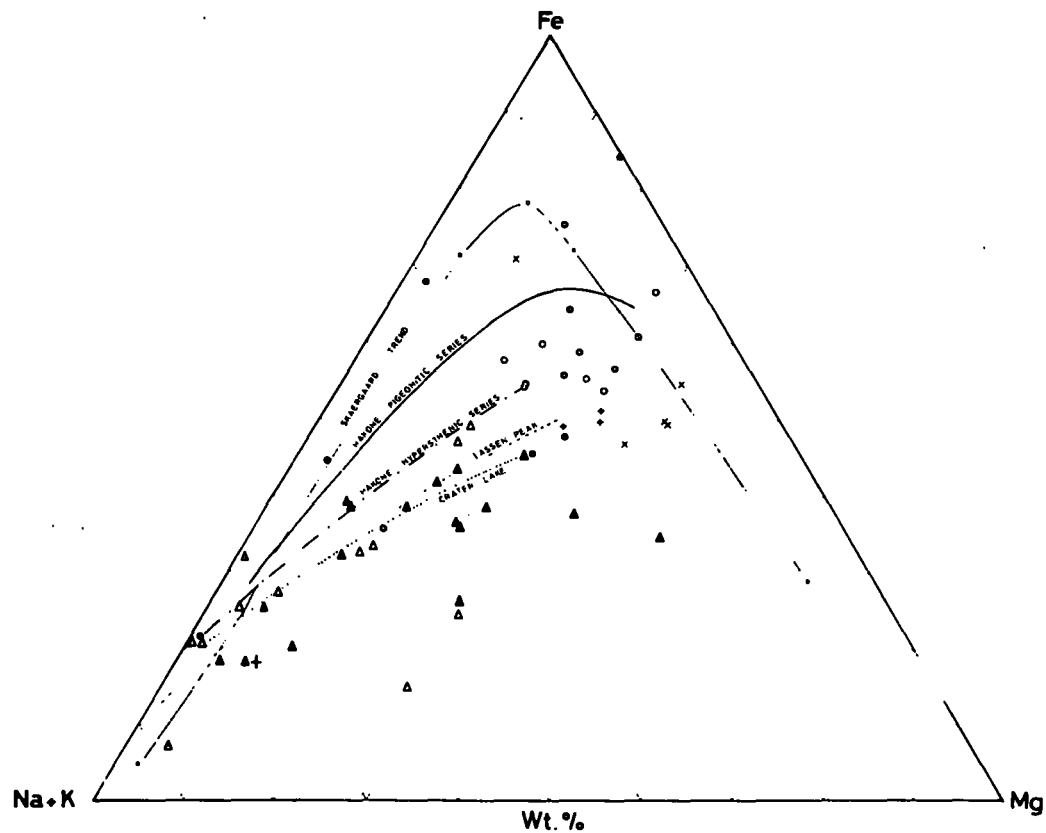


FIG. 11.—Variation of Fe:Mg (Na+K) in rocks of the Lahanos area Espiye, Eastern Black Sea, Turkey. Skaergaard Trend, Crater Lake, Lassen Peak, Hakone Hypersthene & Pigeonitic Series for comparison.

- | | |
|-----------------------------|--------------|
| • Latite-basalt | ▲ Dacite |
| × Alkali basalt | △ Rhyodacite |
| ○ Andesite tholeiite basalt | + Rhyolite |
| ● Quartz andesite | |

acidic rocks are enriched in alkalis and magnesia, so that some acidic volcanic rocks fall further down from the Crater Lake Trend. Iron enrichment in quartz andesite and some basalts is due to mineralisation i.e. pyritisation in general. The basic members of the Lahanos area often lie in between the Hakone Pigeonitic Trend and the Lassen Peak. Despite the considerable scattering of the Lahanos volcanic rocks, their general distribution pattern approximates to the Calc-alkaline Trend.

K : Na : Ca Ratios

The relative proportions of potassium, sodium and calcium as atomic percentages in the rocks of the Lahanos area are plotted in Fig. 12. The same plots are shown alongside trends from St. Kitts (Tomblin, 1964, Fig.29), the Hakone Hypertheneic Series, Crater Lake and Lassen Peak. The Lahanos volcanic rocks show considerable scatter over the whole area and it is therefore very difficult to suggest any kind of trend. Due to alteration (i) enrichment in Ca is more pronounced in quartz-andesite and to a less extent in basalt, andesite and rhyodacite; (ii) an enrichment in Na is very common in quartz-andesite and to a less extent in dacite; and finally (iii) an enrichment in K is more distinct in rhyolite, rhyodacite and to a less extent in the latite-basalt and tholeiite basalt and andesite.

Al : Ca : Na Ratios

Matsumoto (1963, pp.52-54) has plotted the Pigeonitic, Hypersthenic and alkali rock series of Japan on a diagram showing

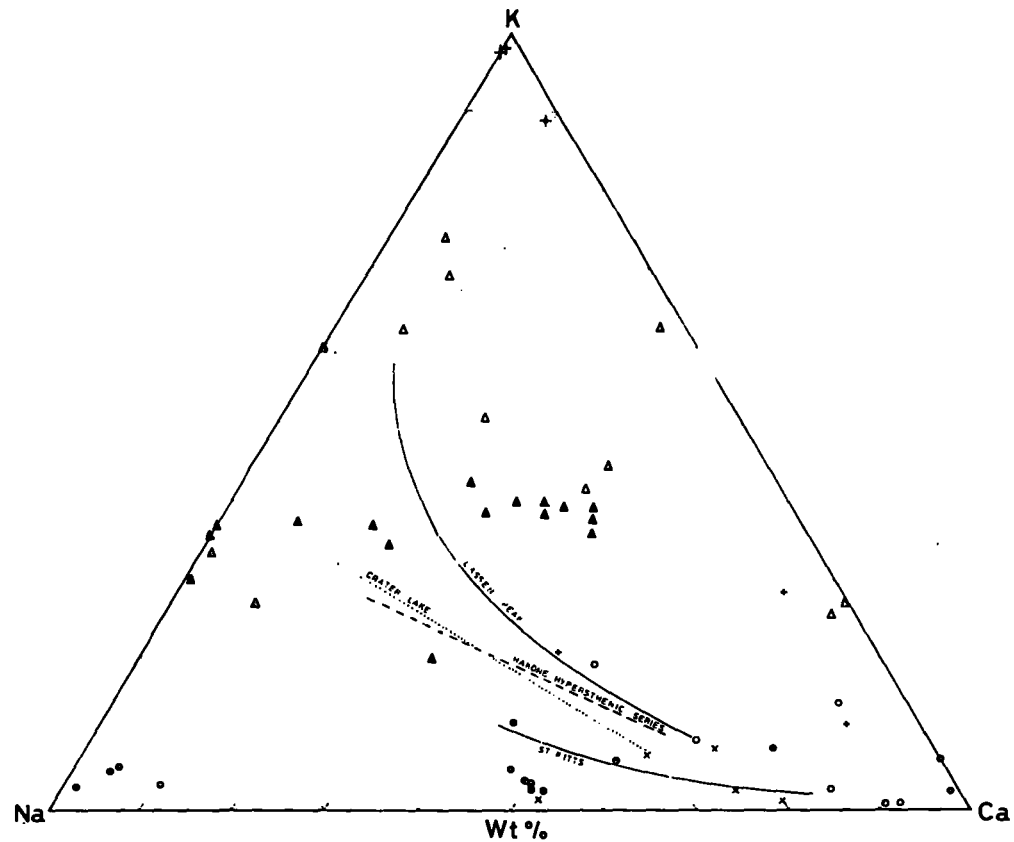


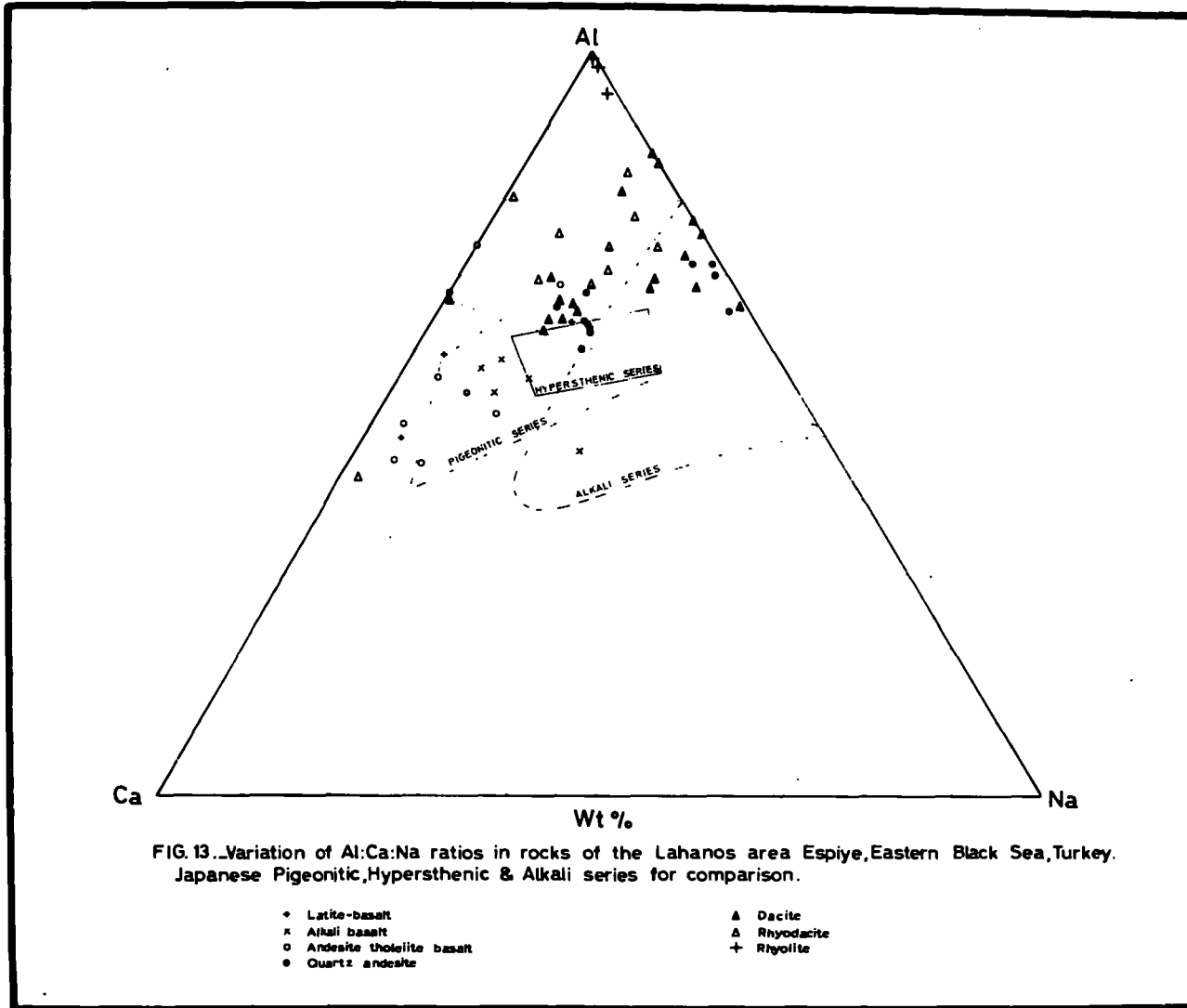
FIG. 12.—Variation of K:Na:Ca ratios in rocks of the Lahanos area Espiye, Eastern Black Sea, Turkey. Lassen Peak, Crater Lake, Hakone Hypersthene Series & St Kitts for comparison.

- | | |
|-----------------------------|--------------|
| ◆ Latite-basalt | ▲ Dacite |
| × Alkali basalt | △ Rhyodacite |
| ○ Andesite tholeiite basalt | + Rhyolite |
| ● Quartz andesite | |

the ratios of aluminum, calcium and sodium. In Fig. 13 the Lahanos rocks are plotted on a similar diagram which also shows the approximate fields occupied by the three series of Matsumoto. The study of Fig. 13 shows the close correspondence of the basic rocks of the Lahanos area with the Japanese Pigeonitic Series, whereas the more acidic members of the Lahanos area stay partly in the Alkali Series or in the Hypersthene Series and outside of these three Japanese series. As pointed out earlier in the chemical and mineralogical alteration sections, the predominant and common alteration product of the Lahanos acidic rocks, i.e. kaolinite, has also once more reflected in this triangular plotting (Fig. 13).

Total Iron Oxide - Magnesia Ratio and Iron Enrichment - Total Mafic Ratios

When total iron oxides are plotted against magnesia and when iron enrichment (expressed as $\frac{\text{FeO} + \text{Fe}_2\text{O}_3}{\text{MgO} + \text{FeO} + \text{Fe}_2\text{O}_3}$) is plotted against total mafic ($\text{FeO} + \text{Fe}_2\text{O}_3 + \text{MgO}$), Yoder, et al., (1964) have shown that the Hawaiian Tholeiite and Alkali Series show concentration trends. Figs. 14 & 15 show the variation of MgO with $(\text{FeO} + \text{Fe}_2\text{O}_3)$ and iron enrichment with total mafics for the rocks of the Hawaiian Alkali & Tholeiite Series, the Skaergaard intrusion and the Japanese Pigeonitic Series. The Skaergaard trend represents strong iron enrichment at slightly increasing total mafics until the final stages of fractionation where total mafics fall with no iron enrichment. The Hawaiian Tholeiitic Trend also shows strong iron enrichment at constant mafic but the trend is limited



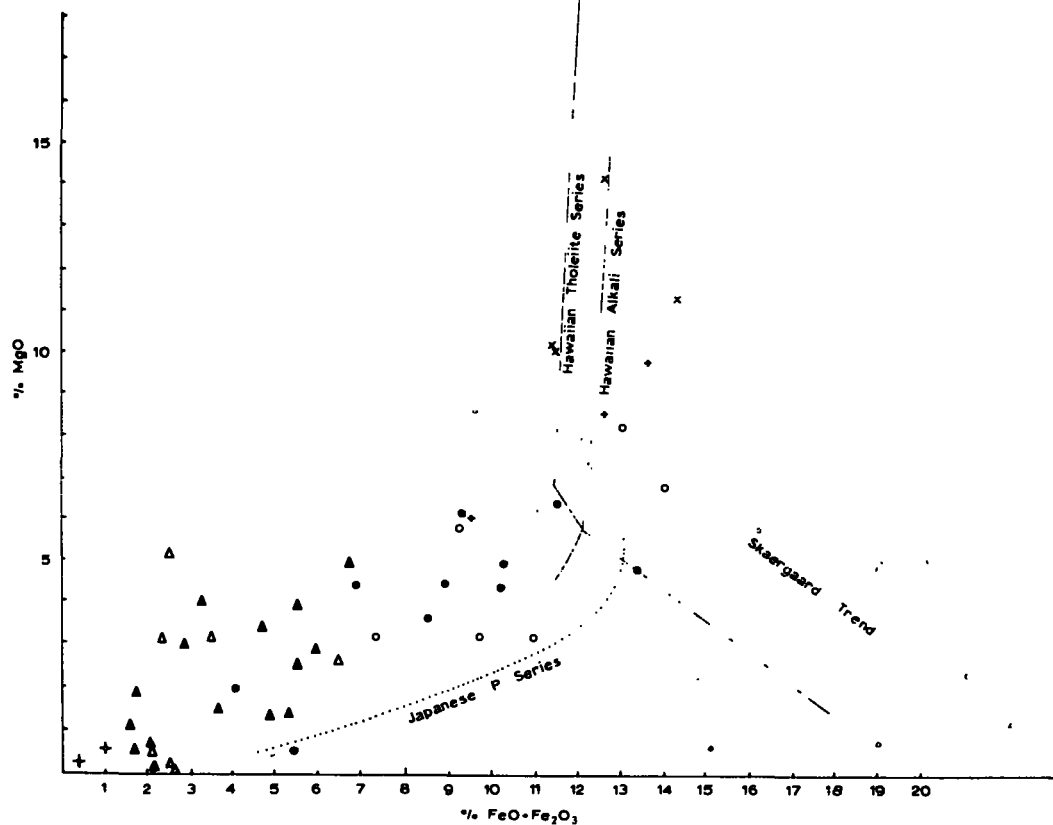


FIG. 14. Variation in MgO-(FeO+Fe₂O₃) ratios for volcanic rocks of the Lahanos area and their comparison to other volcanic areas. (After Wager & Deer 1939, Kuno 1959, Yoder & others 1965).

- | | |
|-----------------------------|--------------|
| ◊ Latite-basalt | ▲ Dacite |
| × Alkali basalt | △ Rhyodacite |
| ○ Andesite tholeiite basalt | + Rhyolite |
| ● Quartz andesite | |

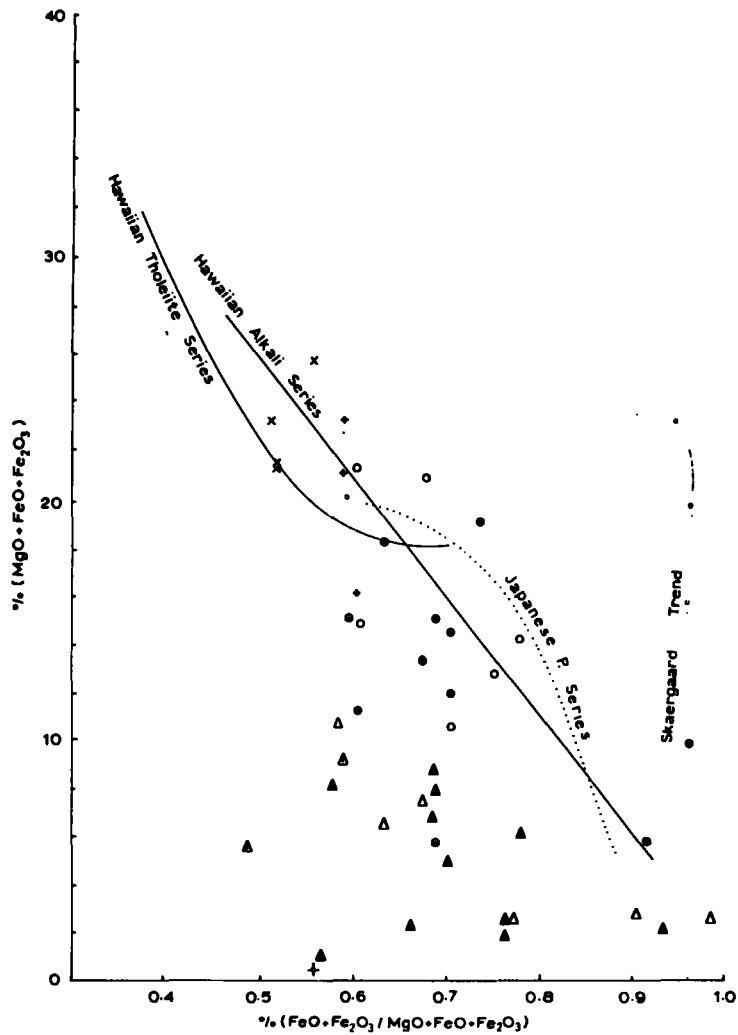


FIG. 15...Plot of iron enrichment ($\text{FeO} \cdot \text{Fe}_2\text{O}_3 / \text{MgO} \cdot \text{FeO} \cdot \text{Fe}_2\text{O}_3$) against total mafics ($\text{MgO} \cdot \text{FeO} \cdot \text{Fe}_2\text{O}_3$) for the rocks of the Lahanos area. Japanese Pigeonitic Series, Skaergaard Trend, Hawaiian Tholeiite & Alkali Series for comparison.

(After Wager 1960, Wager & Deer 1939, Kuno 1959, Yoder & others 1965).

- | | |
|-----------------------------|--------------|
| ◆ Latite-basalt | ▲ Dacite |
| × Alkali basalt | △ Rhyodacite |
| ○ Andesite tholeiite basalt | + Rhyolite |
| ● Quartz andesite | |

compared to the Skaergaard Trend. Kuno et al., (1951) showed an iron enrichment trend closer to that of the Japanese Pigeonitic Series, of which enrichment is in the intermediate stages only. The Hawaiian Alkali Series and the Calc-alkali Series of Japan show continuous iron enrichment with continuously falling total mafics.

The trend of the Lahanos, despite alterations, is roughly parallel to that of the Hawaiian Alkali Series and the Japanese Pigeonitic Series without any gap from the basalt to the rhyolites. Alkali- and latite-basalts of the Lahanos area show enrichment in iron in comparison with the Hawaiian Alkali and the Japanese Pigeonitic Series.

Yoder et al., (1965) have attributed differences in the iron enrichment trends of the Hawaiian Alkali and Tholeiitic Series to differences in the crystallisation and movement of olivine, plagioclase and pyroxene. Another possible cause of the variation trend of iron enrichment might be due to crystallisation and accumulation of magnetite. As it can be seen from Figs. 14 and 15 the Upper parts of both the Hawaiian Alkali and Tholeiite Series have probably been controlled by the separation of olivine. As Osborn (1959 and 1962) pointed out, the separation of magnetite would only be expected under conditions of high oxygen pressure which would result in the liquid being depleted in iron and enriched in SiO_2 , and the Calc-alkali Trend will occur.

D.III VARIATION IN MINOR ELEMENTS

Analyses of eight minor elements from Sixty two volcanic rocks of the Lahanos area are shown in Tab. 5. The volcanic rocks include basalts, andesites, dacites, rhyodacites and rhyolites. In spite of different alteration processes and products in the Lahanos volcanic rocks it is possible to make comparisons with other somewhat similar volcanic provinces particularly the Lassen Peak, the Crater Lake (Nockolds and Allen, 1953), the Polynesian Island and the Scottish Tertiary province (Turner and Verhoogen, 1960). T test analysis of minor elements in the Lahanos volcanic rocks did not show any particular significance, i.e. linear relationship except for zirconium and zinc, owing to addition of some minor elements by mineralisation.

Minor element analyses were made by an X-ray Fluorescence technique (See appendix). In order to compare the results from the Lahanos area with other volcanic provinces, the atomic concentrations in ppm are plotted against the modified Larsen's function (Fig.16).

Variation in Barium

The general distribution of barium in the rocks of the Lahanos area shows a very erratic distribution pattern from basic to acidic end because of addition of barium during the mineralisation. Barite forms one of the main gangue minerals associated with mainly sphalerite-galena rich ore. Therefore closer to the sulphide mineralisation one gets higher barium concentration. Barium varies from 57 to 677 ppm

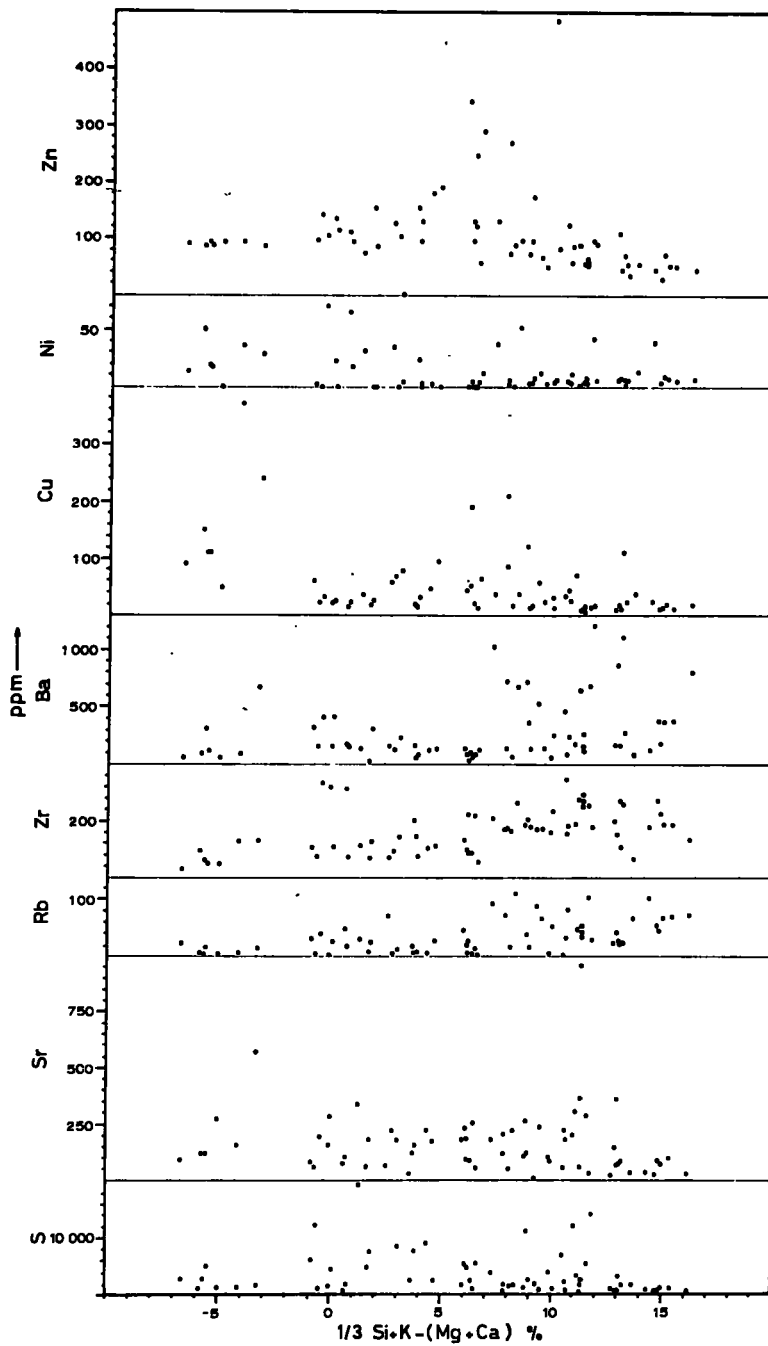


FIG. 16. Variation in S, Sr, Rb, Zr, Ba, Cu, Ni & Zn contents of the Lahanos volcanic area Espiye, Eastern Black Sea, Turkey.

in the various basalts, 29 to 128 ppm in the quartz-andesite, 29 to 1033 ppm in the dacite, 101 to 1105 ppm in the rhyodacite and 97 to 1213 ppm in the rhyolite of the Lahanos area (Tab 5 and Fig. 16). However, these figures suggested that at the basic end barium values are higher than the intermediate rock field, but after the +5 of $\frac{1}{3} \text{Si} + \text{K} - (\text{Mg} + \text{Ca}) \%$, barium values again increase with increasing acidity, and between + 7 and + 11 show very erratic concentration changes in particular for the enclosing silicate rocks of the sulphide deposit. The overall trend of the barium variation might suggest that towards the most acidic end there is an increase in the barium content, though it is not very clear, i.e. in the rhyolite. The barium content gives a generally rising trend which approximates to the general trend of volcanic rocks of the orogenic belt i.e. the calc-alkaline trend, rather than others.

Variation in Strontium

Distribution of strontium contents of the Lahanos area shows a more scattered pattern. Carbonate gangue minerals associated with sulphide mineralisation can possibly be responsible for this. A variation of 67 to 573 ppm in basalts, 61 to 255 ppm in quartz-andesites, 6 to 367 ppm in dacites, 54 to 957 ppm in rhyodacites and finally 23 to 293 ppm in rhyolites (Tab. 5 and Fig. 16). However, strontium contents, similarly to the barium contents, show somewhat higher values in the basic end, but as the acidity increases the strontium content slightly decreases at about + 11 to + 13 of the index of evolution; then a sudden and more distinct fall down towards the rhyolites. Because

of the very scattered concentration of strontium it is very difficult to suggest any kind of trend except for a broad sense of similarity to the general calc-alkaline trend.

Although Turekian and Kulp (1956, pp.294) state that strontium is independent of calcium in basaltic rocks whereas in granitic rocks there is a definite relation between strontium and calcium content; Nockolds and Allen (1953) commented on the variable behaviour of the strontium variation curve for different provinces and attribute the differences to the amount of plagioclase remaining from the magma. If much plagioclase is removed then the strontium content will decrease in the residual liquid, whereas if relatively little is removed, strontium will tend to increase. The presence of high strontium values in the less altered basalts of the Lahanos area can only be explained by Nockolds' and Allen's theory rather than by Turekian's and Kulp's suggestion.

Variation in Rubidium

In the Lahanos volcanic rocks rubidium contents show somewhat less scatter in comparison to the barium and strontium variation diagrams. Rubidium contents vary from 1 to 46 ppm in the basaltic rocks, 2 to 13 ppm in the quartz-andesitic rocks, 17 to 113 ppm in the dacitic rocks, 21 to 82 ppm in the rhyodacitic rocks and finally 29 to 105 ppm in the rhyolitic rocks. The general tendency of the rubidium is to increase with increasing acidity, with a very low gradient (Tab. 5 and Fig. 16). The potassium: rubidium ratios of the volcanic rocks of the Lahanos area are shown on Fig. 17.

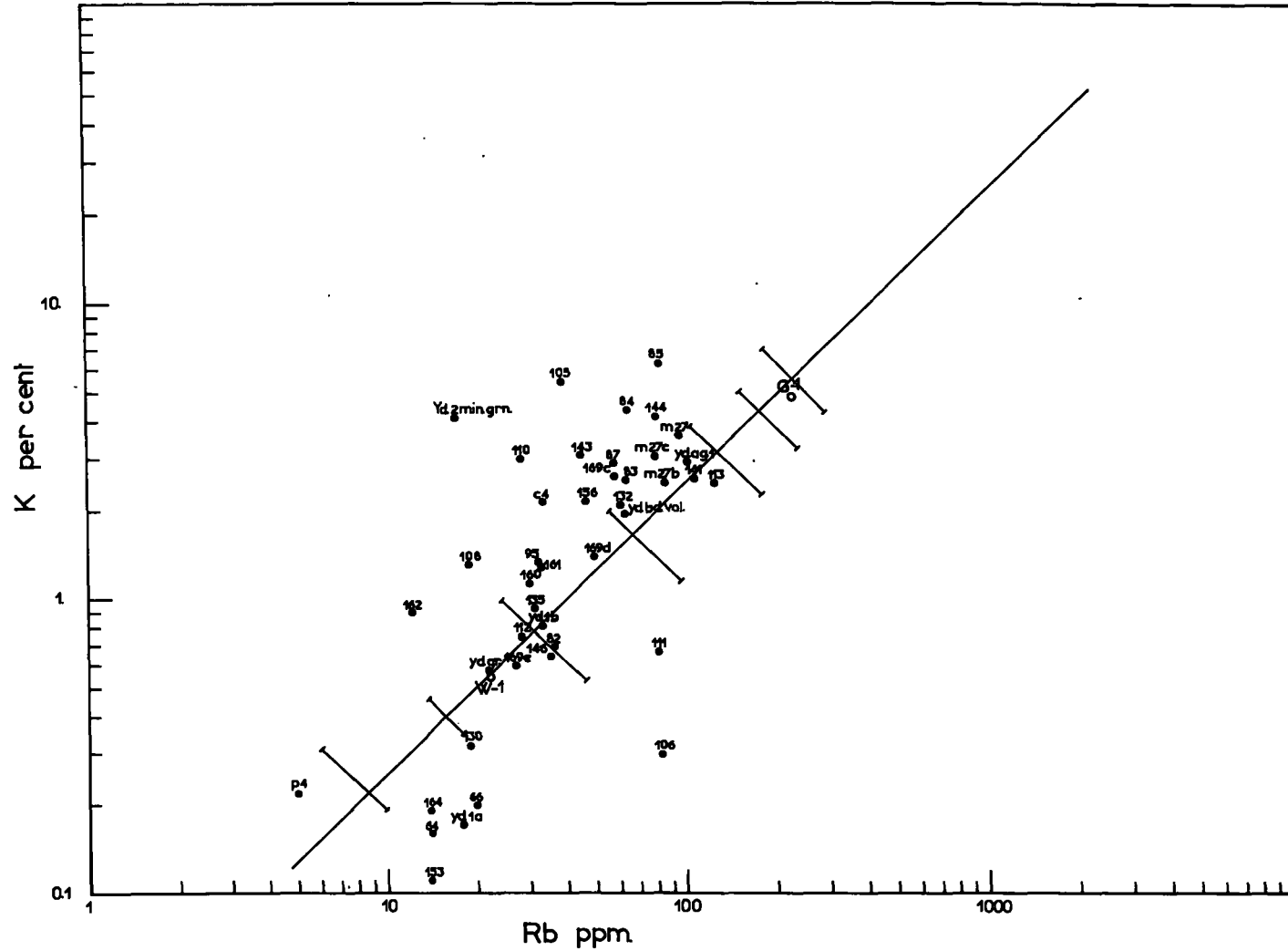


FIG.17.-K/Rb ratio in volcanic rocks around Espiye, NE Turkey

The igneous rocks from the Lahanos area cover the entire range of potassium:rubidium ratios of normal fractionation of the parental magma, i.e. there is no gap between the basic and acidic rocks, suggesting continuous differentiation products of the initial magma. The international standards of W-1 and G-1 were also shown for comparison.

In spite of the effect of potash metasomatism on the rubidium content, the general trend of the Lahanos area suggests some similarity to the trend of the Crater Lake and the Lassen Peak volcanoes and to a lesser extent to the Scottish Tertiary volcanic province, i.e. variation in the rubidium trend is quite similar to that of the calc-alkaline suite trend.

Variation in Zirconium

Zirconium is one of the elements less affected in comparison to other lithophile elements by the hydrothermal alteration and mineralisation, and its distribution therefore, gave a less scattered trend in spite of heavy rock alteration. Zirconium varies from 19 to 334 ppm in the basaltic rocks, 53 to 347 ppm in the quartz-andesitic rocks, 90 to 277 ppm in the dacitic rocks, 109 to 392 ppm in the rhyodacitic rocks and finally 66 to 277 ppm in the rhyolitic rocks (Tab. 5 and Fig. 16). The general trend of the zirconium shows a slight increase from the basic end to the intermediate rocks but it tends to increase with increasing acidity up to the rhyodacite where it reaches its maximum, and further increasing acidity yielded a slight decrease in the zirconium contents.

Variation in Nickel

The distribution pattern of nickel in the volcanics of the Lahanos area tends to give relatively higher contents in the basic rocks, particularly in the alkali- and latite-basalts, and intermediate or acidic intermediate rocks such as quartz-andesite and dacite (tab. 5 and Fig. 16). The nickel contents vary 13 to 70 ppm in the latite basalts, 17 to 36 ppm in the alkali basalt, 0 to 52 ppm in the tholeiitic basalt and andesite, 0 to 12 ppm in both quartz-andesite and dacite, 0 to 31 ppm in the rhyodacite and finally 4 to 15 ppm in the rhyolites of the Lahanos area. Concentrations are generally low with a few Ni-rich samples especially at the more basic end.

Variation in Copper

Distribution of copper shows somewhat similar to the nickel pattern and generally is more abundant in the basic rocks than in the acidic rocks. It occurs in close association with pyrite which is often visible. The range of values for basaltic rocks varies 15 to 373 ppm, for quartz-andesite 16 to 65 ppm, for dacitic rocks 8 to 572 ppm which is entirely due to late copper mineralisation, for rhyodacitic rocks 6 to 110 ppm and finally for rhyolitic rocks 11 to 36 ppm (Tab 5 and Fig 16). Except for those of high and erratic results, the general trend of the Lahanos area decreases with increasing acidity.

Variation in Zinc

The distribution pattern of zinc compared with copper and nickel

is less scattered. Zinc content increases with increasing acidity from the basic end up to the intermediate rocks (e.g. quartz-andesite and dacite), but further increases in the acidity corresponds with a decrease in zinc content of the Lahanos area, giving a peak at about + 6.5 of the evolution index (Fig. 16). Zinc contents range between 90 to 111 ppm in the Latite-basalt rocks, 85 to 136 ppm in the alkali basaltic rocks, 75 to 141 ppm in the tholeiitic andesite and basalts, 55 to 486 ppm in the quartz-andesitic rocks, 35 to 266 ppm in the dacitic rocks, 51 to 340 ppm in the rhyodacitic rocks and finally 27 to 97 ppm in the rhyolitic rocks (Tab. 5 and Fig. 16). The distribution of zinc, as with Ba, Sr, Cu, Ni, K has been affected by hydrothermal mineralisation in the Lahanos area. Some of the very high results are possibly due to proximity to the pyritic sulphide mineralisation.

Variation in Sulphur

Sulphur contents of most of the Lahanos area volcanic rocks are again very closely controlled by the pyritic sulphide mineralisation either with visible pyrite grains or tiny pyritic veinlets. However, the sulphur contents of various volcanic rocks of the Lahanos area vary as follows: 0.07 to 0.29% in the latite-basalt rocks, 0.15 to 0.50% in the alkali basaltic rocks, 0.13 to 1.23% in the tholeiitic andesite and basalts, 0.07 to 6.49% in the quartz-andesitic rocks, 0.03 to 1.40% in the dacitic rocks, 0.05 to 1.95% in the rhyodacitic rocks and finally 0.03 to 1.40% in the rhyolitic rocks (Tab. 5 and Fig. 16). The variation of sulphur content is vaguely followed by

zinc, copper, barium, nickel and strontium i.e. all followed the pyritic sulphide mineralisation. In other words correlation with the Crater Lake, the Lassen Peak etc. has little of relevance, because of the mineralisation overprinting at Lahanos.

D.IIIa Summary Of The Petrochemistry of
The Volcanic Rocks of the Lahanos area

The most dominant petrochemical features of the volcanic rocks of the Lahanos area are outlined as follows:

1. Chemically, there is a broad similarity with the rocks of the Calc-alkaline Series and volcanic associations of orogenic regions (Figs. 6, 7, 11, 12, 13, 14, 15 and 16).

2. The analysed rocks of the Lahanos area are basalts with 43.27 to 51.21% SiO_2 , andesites with 55.11 to 61.00% SiO_2 , dacites with 57.49 to 76.51% SiO_2 , rhyodacite with 66.26% to 73.91% SiO_2 and rhyolites with 64.72 to 78.29% SiO_2 (Some of the high and low silica contents of Tab.4 are due to included pyroclastic and altered rocks. Figures mentioned above represent the average rock types). Basic and acidic members are almost equally distributed in the field around the Lahanos area. However quartz-andesites and dacites predominate over basalts and tholeiite basalt-andesites in the mineralised area.

3. Comparison with other well-known volcanic provinces showed that the rocks of the Lahanos area are slightly rich in Al_2O_3 and MgO , while potash, soda, lime and iron contents show no difference relative to the world-wide calc-alkaline suites.

4. In comparison with the rocks of other Calc-alkaline and orogenic belt volcanic associations the rocks of the Lahanos area (particularly samples away from the hydrothermal mineralisation) are comparable in barium, strontium, rubidium, Copper, nickel, zirconium and zinc content. However, there is often some enrichment in the content of chalcophile and siderophile elements and some impoverishment in lithophile elements due to the effect of hydrothermal mineralisation.

5. Basalts of the Lahanos area are chemically similar to the High-alumina basalts of Kuno (1960) (Fig. 5 and Tab. 6). The basic volcanic rocks of the Lahanos area i.e. latite-basalts, alkali-basalts, tholeiite basalt-andesites and some of the quartz-andesites, are comparable to the Japanese alkaline and calc-alkaline and tholeiite rocks (Figs. 7 and 6) Fig 6 also includes the acidic members of the Lahanos area.

D.IIIb The Possible Origin of Basalts of the Lahanos Area

It would appear from the work carried out on the rocks of the Lahanos area that the principal types of basalt are porphyritic basalt chemically close to the average high-alumina basalts of Japan (Tab 6 and Fig 5). Some of the basalt-andesites contain a high percentage of normative quartz and pyroxene, and their features correspond closely to tholeiite (Fig. 3). Occurrence of calc-alkaline together with alkaline and tholeiitic basalts in the Lahanos area is very similar to the Japanese field occurrences of the alkali, calc-alkali

and tholeiite basalts which were described by Kuno (1959).

According to Kuno (1960, pp.141-142) high-alumina basalt is a primary magma, generated at depths in the mantle intermediate between those of tholeiite and alkali basalt formation. However Yoøer and Tilley (1962, pp. 419) regard the high-alumina basalts as important members of both tholeiite and alkali olivine basalt groups. They concluded that forthemost part a concentration of the plagioclase phenocrysts to give a porphyric rocks rich in alumina, followed by resorbtion of the phenocrysts to produce an aphyric high-alumina basalt.

It might be possible that the high-alumina basalts have been yielded by the accumulation of plagioclase phenocrysts in a tholeiitic magma. Only chemical classification rather than descriptive petrography has been used for the classification of basalts from the Lahanos area. However the occurrence of porphyritic basaltic rocks containing large phenocrysts of plagioclase up to several ten millimeters in size might support the possible explanation given just above.

D.IIIc The Possible Origin Of The Andesite-Dacite - Rhyodacite of the Lahanos Area.

Even today there is still no straight answer to the origin of intermediate volcanic rocks. There are many opinions on the origin of the intermediate volcanic rocks of the orogens which has often been ascribed to a process of fractional crystallisation of basaltic

magma, combined with the assimilation of granitic or sialic material. Wager and Deer (1939, pp. 323) said that they are "not usually produced by fractional crystallisation of basalt, acting alone." Tilley (1950, pp. 59) suggests that the intermediate rocks developed from "basaltic magma modified by sialic contamination to set it on its course of variation which fractional crystallisation appears most competent to yield". Kuno (1959, pp 70-71) concluded that the calc-alkaline series of Japan has been developed by fractional crystallisation of a tholeiitic or alkali basalt magma contaminated by granitic material. On the other hand, Osborn (1959 and 1962) and Roeder and Osborn (1966) suggested that the calc-alkaline series may result from fractional crystallisation of basaltic magma, in which a high oxygen pressure caused the early separation of magnetite and hence the liquid becomes enriched in silica and relatively depleted in iron. O'Hara (1965) pointed out that contamination of basaltic magma with granitic magma, or perhaps partial melting of sedimentary material, is important in the evolution of calc-alkaline rocks, and he also gives emphasis on partial fusion of peridotite at depth, under saturated conditions in a low pressure regime to give an andesitic liquid. The presence of hypabyssal dacite and extruded andesitic lavas would suggest that there was a time available for fractional crystallisation during the ascent of calc-alkaline suites in the Lahanos area.

Some large, rounded quartz crystals (xenocrysts) which occur in some of the Lahanos quartz-andesite and dacites may perhaps be

regarded as an indication of contamination. Kuno (1954) described similar quartz crystals from the Omuru-Yama volcanic zone, North Izu as xenocrysts.

Minute crystalline, dusty and glassy inclusions, similar to those common in plagioclase of the quartz-andesitic rocks of the Lahanos area can be attributed from the explanations of the other authors as (e.g. Kuno, 1950) ⁿ due to incipient remelting of feldspar suspended in a magma with which they were not in equilibrium. The oscillatory zoning shown by plagioclases in calc-alkaline rocks can be taken as further evidence of non-equilibrium.

Holmes (1932) describes the mixing of a granitic magma, which formed by partial fusion of the crust to account for the formation of andesites and this mechanism would explain the shortage of xenoliths in calc-alkaline rocks and would also clarify the need for assimilation during the rise of the magma through the crust, rather than whether a basaltic magma could assimilate on the way up towards the surface of the Earth, a sufficiently large amount of granitic material in order to produce high proportions of acidic rocks often seen orogenic belts.

Study of trace elements show that due to the mixing of average basaltic magma and granitic material in any reasonable proportions would give material much richer in certain elements particularly potash, rubidium, barium, uranium and thorium, than the average andesite (Taylor and White, 1965). Comparison of average minor elements of the Lahanos area showed that they lie within the normal

concentration of an average andesite and dacite. The further study of strontium isotopic ratios might explain or will throw a light on whether andesite and dacite were formed from mixing of two magmas, or not.

D.IIIId Stratigraphy-Modification of Field Observation

Following Laboratory Work

Petrographic and petrological studies of the Lahanos area volcanic rocks showed that the volcanic activity started with alkali olivine and latite-basalts passing upwards into the high-alumina basalt → tholeiite basalt-andesite (in places) → quartz-andesite → dacite → rhyodacite → rhyolite. Similar sequences have been described from Japan in the Honsyū and Izu Islands by Kuno (1960). This association formed probably through the fractional crystallisation of the high-alumina basalt magma contaminated by available acidic rocks possibly the Palaeozoic granitic and granodioritic rocks.

The only lithological modifications arises after petrographic and particularly petrochemical studies of dark green agglomerate, that overlies the Upper Dacitic, Rhyodacitic Series at the Lahanos copper mine. These dark green agglomerates have been described as basic in composition but their chemistry and C.I.P.W. norms showed that they are more acidic in composition and their plotting in Figs. 3 and 4 gave us dacitic and rhyodacitic composition rather than basic.

The presence of high-alumina basalt at Lahanos is now recog-

nised for the first time after detailed laboratory work, and detailed petrographical and petrological study of the volcanic rocks has shown their broad similarity to the Calc-alkaline suites of other orogenic belts.

CHAPTER E ~ MINERALISATION OF THE LAHANOS AREA

E. MINERALISATION OF THE LAHANOS AREAE.I LAHANOS

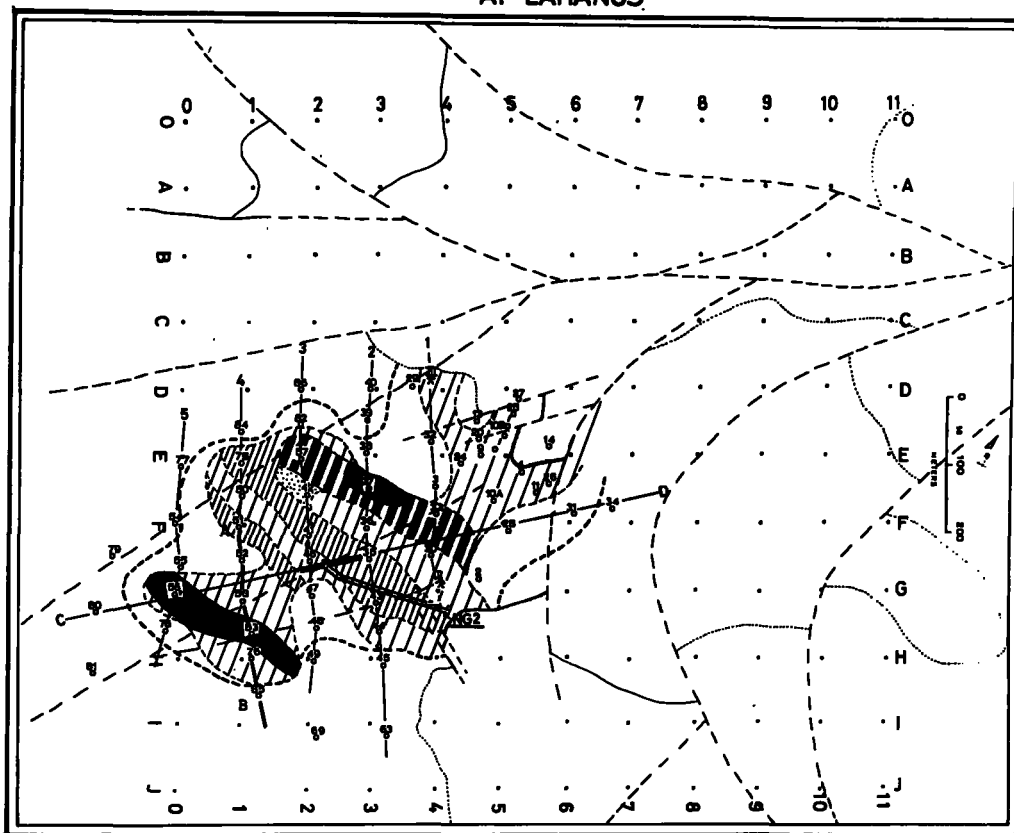
The first exploration of the Lahanos pyritic sulphide deposit started twenty five years ago and was mainly based on the self potential method of geophysical survey. The results were not very useful owing to the lack of any detailed geological map or geological knowledge of the deposit. The extensive alteration of the country rocks associated with the mineralisation was a further complication. Later, during the period 1957 - 1962, about seventy boreholes were put down on a grid pattern above the mineralisation during exploration work described by Pollak (1961) (See Map 8). These early boreholes proved 8.6 million metric tons of pyritic sulphide ore, containing 2.3 million metric tons assaying 3% copper and 2.3% zinc, and 0.3 million metric tons assaying 0.5% copper and 0.3% zinc. Sulphur assays showed 2.6 million metric tons assaying 44% sulphur and 6 million metric tons assaying 30% Sulphur. The average copper assays vary from 0.5% up to 13% Cu and similarly the average zinc assays vary from 0.1% up to 9.31% Zn (Pollak, 1961).

In 1966, Etibank, the state owned mining company, began operations to bring the deposit into production.

A 1:500 scale underground map of the workings prepared by the present author is shown on Map 7. The position of geological features is plotted at waist height. Because of the poor standing qualities of the altered rocks, the workings are timbered through

MAP_8

KEY MAP FOR OLD BOREHOLES & GEOCHEMICAL STUDY LOCATIONS AT LAHANOS



- | | | | |
|--|---------------------------------------|--|---|
| | Old borehole locations & section line | | Grid sampling points & their coordinates |
| | Main sulphide mineralisation | | Inferred limit of the Cu-Zn sulphide mineralisation |
| | 100-500 Kg/m ² Cu | | 500-1000 Kg/m ² Cu |
| | 1000-2000 Kg/m ² Cu | | >2000 Kg/m ² Cu |
| | 50-100 Kg/m ² Cu | | |

From A. Potlak, 1961

-out, which renders mapping difficult.

Although over 6000 meters of drilling was carried out under Pöllak's supervision, the cores have not been preserved and so no information could be obtained, nor any check of Pöllak's conclusions. In recent work by Etibank, boreholes A and B have been drilled and the writer was able to log and sample the cores. No information on the exact location and altitude of the holes was obtainable from Etibank, but their position was surveyed as accurately as possible by tape and compass during the field work.

The mineralisation in the Lahanos area is always located near to what has been mapped as the junction between the Lower and Upper Volcanic series. To assess the significance of this observation it is necessary to reconsider briefly the basis of the mapping. In general, the junction coincides with the strongest topographic feature in the area. Beds below are porphyritic dacites, beds above non-porphyritic in general. Beds above are reddened and commonly show columnar jointing (See Plate 6), beds below are brecciated, silicified and sericitised, but not reddened and do not show columnar jointing. At any given point, however, there may be some difficulty in deciding the exact position in the vertical sequence, due to alteration or slightly atypical features of the rocks. The amount of alteration increases considerably towards the mineralisation and it is therefore increasingly difficult to map the position of the junction with certainty. There is therefore a tendency at such places to take the junction as the horizon of

the mineralisation, so that the above general statements could seem to be merely the result of a circular argument. However, it is believed that the dangers of this approach have largely been avoided during the field mapping, and by abandoning Pollak's concept of a single "Ore dacite" in which mineralisation occurs. In cores from the Lahanos 'A' and 'B' boreholes, the main horizon of mineralisation is entirely within rocks of the Upper Volcanic Series. The cores from these boreholes provide the only specimens obtained during the present investigation in which the relationship of mineralisation to the host rocks is clearly seen, unaffected by surface weathering processes. They will be described in detail after the nature of the economic mineralisation itself has been described. It is necessary however, to point out that this observation is at variance with the relationships shown in Pollak's sections, where the ore bodies are all shown as lying at or below the junction of the Upper and Lower Series (Section C). (Geo. Sec. 3)

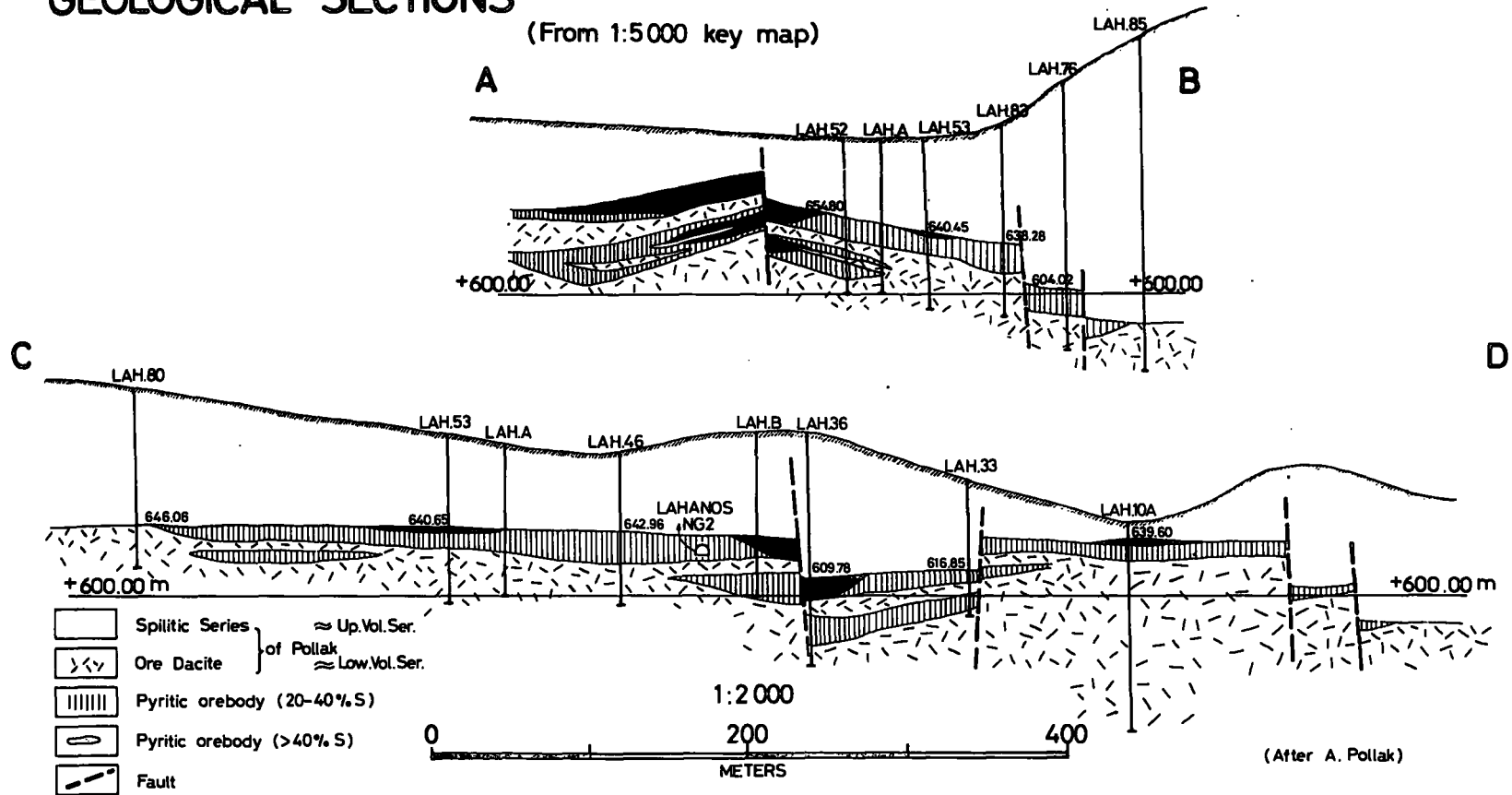
E.1a MODE OF OCCURRENCE OF THE ORE

The pyritic sulphide deposit, though fairly large in size, shows very little outcrop in the field. Outcrops can be seen only at the mouth of New Gallery two (See Plate 12) and a better and larger one in the northern outcrop of the Lahanos mine where the pyritic ore body gives an almost massive pyrite outcrop about 50 meters thick (See Map 6, 43.000 - 30.200). Where the Lahanos ore body is seen at surface, the only visible sulphide is pyrite.

Geo.Sec...3

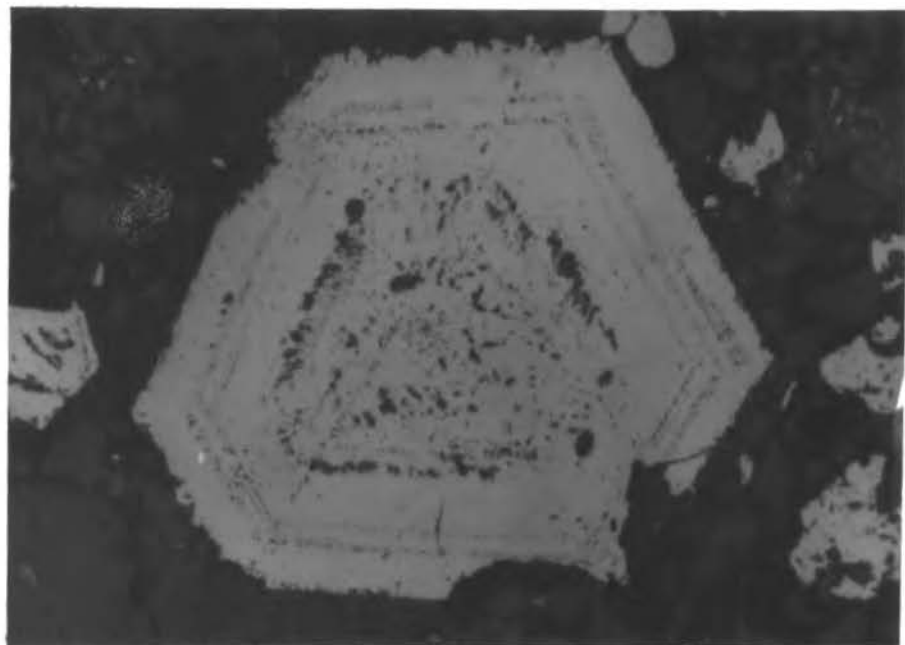
GEOLOGICAL SECTIONS

(From 1:5000 key map)





Pl. 13. General view, looking from NE of the Lahanos copper mine, Hydrothermally altered Lower Volcanic Series in the stream valley.



Pl. 14. Zoning in ore Zone IV pyrite. 350 x

A strong sulphurous smell is always noticeable near the outcrop. As one follows the main pyritic body downwards in the field i.e. towards the River Kizil in the footwall series, the main massive ore passes into a sulphide stock-work and further down into disseminated pyrite (See Plate 13). In the foot-wall series these are always associated with dense silicification, sericitisation and brecciation of the host-rock. The greyish white leached rock adjacent to the stock-work and disseminated mineralisation is often stained yellow by films of jarosite (confirmed by X-ray powder film).

The general shape of the ore body as established by Pollak's boreholes is shown on Map 8. From observations on the cores of boreholes A and B and of relationships underground in New Gallery 2, it seems that there is a downward zoning in the ore as follows:-

Ore Zone (i) Bornite, chalcopyrite, galena, pyrite with minor tennantite, marcasite and gold.

Ore Zone (ii) Sphalerite, galena-chalcopyrite, tetrahedrite-tennantite, enargite, pyrite.

Ore Zone (iii) Massive pyrite subordinate chalcopyrite and traces of bornite and tellurium minerals.

(i) and (ii) are dark coloured ores, (iii) is yellow.

Underground, a thin green clay layer is seen at the top of the ore body, but evidence is insufficient to show whether this is a general or only local feature.

The "nested saucer" relationship between the ore zones can be appreciated from Figs. 19 and 18.

FIG 18.-DISTRIBUTION OF S,Zn,Cu IN THE LAHANOS PYRITIC SULPHIDE DEPOSIT
(After A. Pollak)

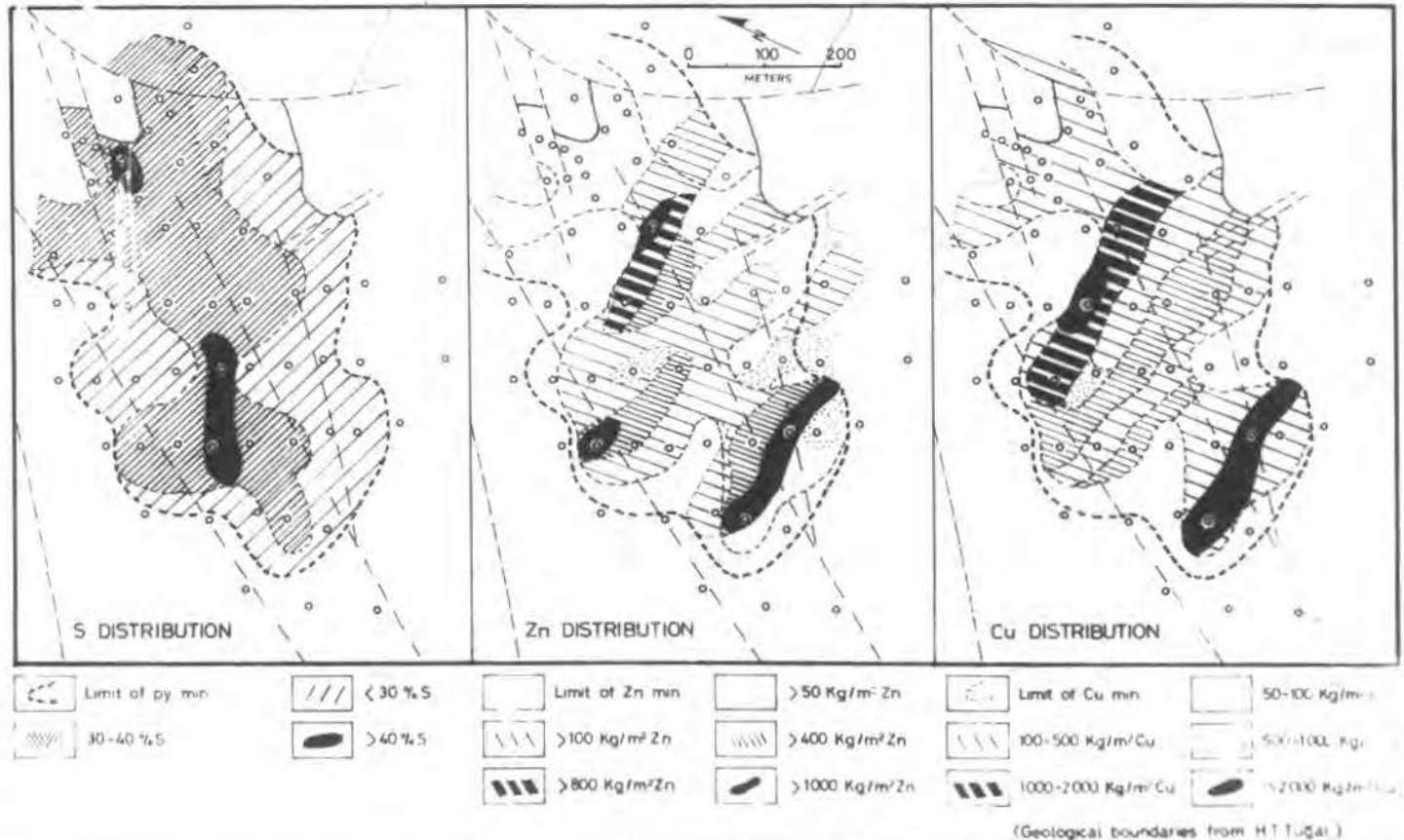
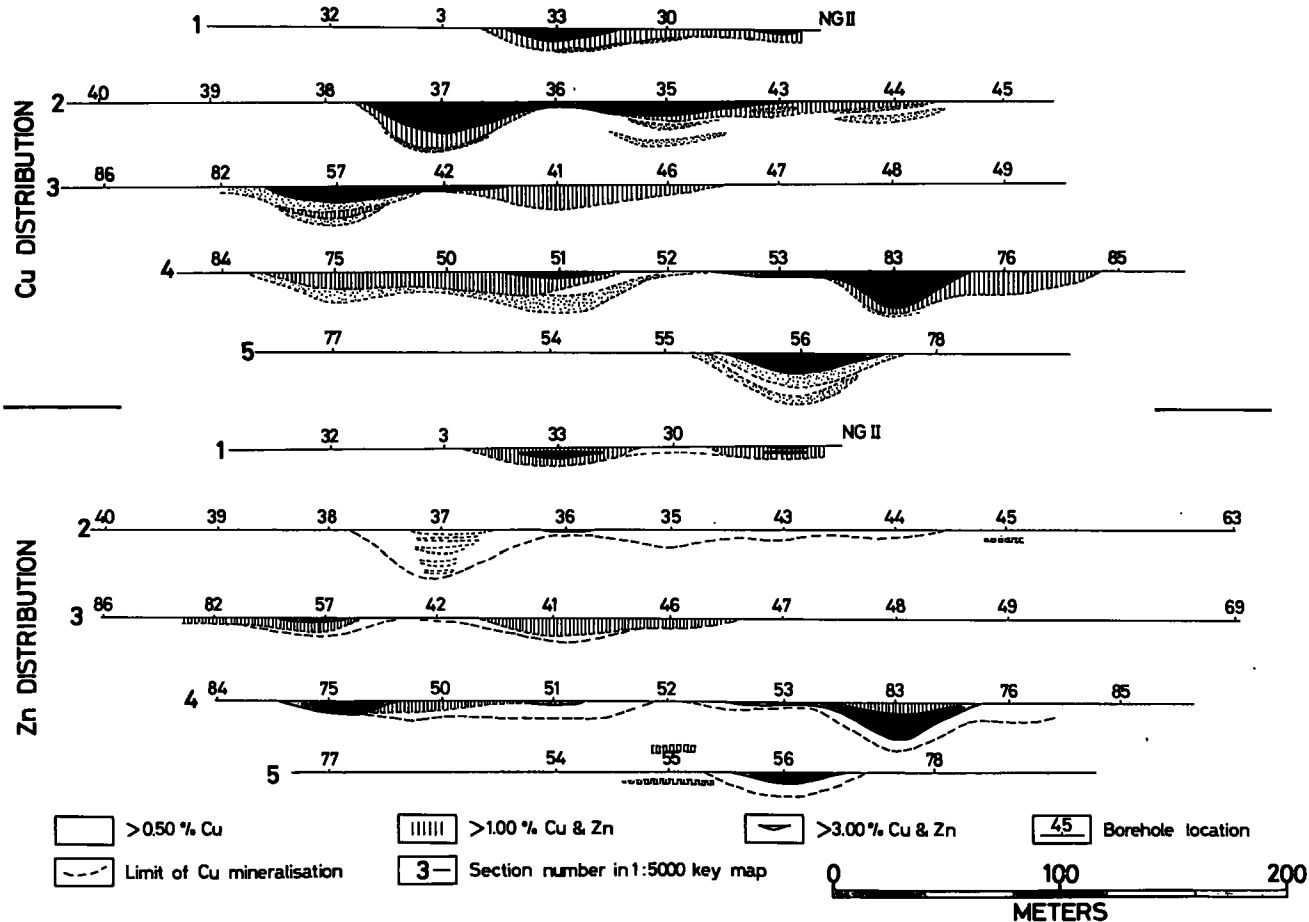


FIG 19.-DISTRIBUTION OF Cu & Zn % IN THE LAHANOS OREBODY
(After A. Pollak)



E.Ib METHODS OF STUDY

Polished specimens were prepared for initial examination of the ore, but because of the limited amount available in 'A' and 'B' borehole cores, these were prepared as polished thin sections, so as to be suitable both for reflected and transmitted light examination and for use with the microprobe. See appendix - for notes on the preparation technique.

From the more abundant underground ore samples, concentrates for X-ray and chemical analysis were prepared by a flotation technique, described in Appendix. Small amounts of material for X-ray examination were removed from the polished specimens using a hand held mounted needle, or a dental drill. The powder is collected on a glass hair dipped in collodion. With care, grains as small as 100 microns diameter can be sampled in this way.

E.Ic OREMICROSCOPY

117 polished specimens and 34 polished thin sections of selected ore samples from different parts of the Lahanos pyritic sulphide deposit have been examined to determine the mineral content and study textural and structural relations. Throughout both ore microscopy studies, and microphotography Leitz Panphot and Carl Zeiss Ultraphot II microscopes and their accessories have been used.

The following descriptions are mainly qualitative-quantitative

results on particular minerals are given in later sections.

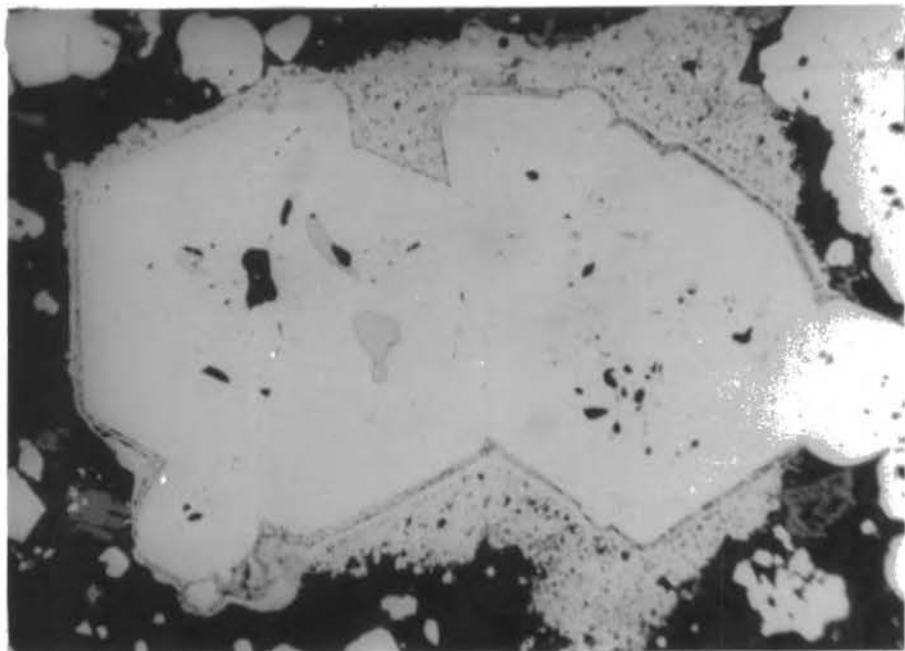
Where the identification of a mineral was uncertain from optical properties alone, X-ray powder patterns or study with the electron microprobe have been used for confirmation.

E.Ic1 Marginal Stockwork and Disseminated Mineralisation: This is the outermost zone of the mineralisation, within which pyrite is the only abundant sulphide mineral, associated with a gangue of quartz and minor amounts of sericite, clay minerals and carbonate.

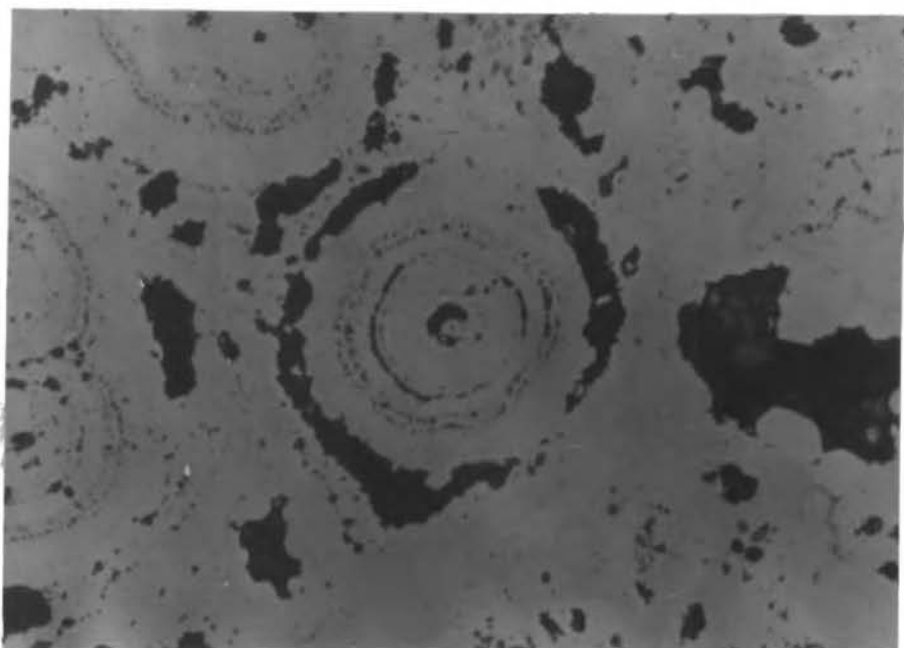
The pyrite shows hypautomorphic granular and aggregate textures and its grain size averages about 100 microns, with a range from less than one micron to over 125 microns. Zoning of the euhedral pyrite is quite common (See Plate 14) and it is usually brought out by inclusions of gangue minerals. Pyrite preferentially replaces feldspars of the host rock in the disseminated mineralisation and is often associated with quartz, sericite and rarely chlorite. Replacement of rutile and possibly hematite in the host rock by pyrite is also occasionally common. Cataclastic texture in the pyrite is sometimes seen. In the marginal stock-work and disseminated mineralisation there is a gradual change in the dominant gangue mineral towards Zone III, the quartz gradually giving place to dolomite, which may locally replace pyrite.

Small traces of other sulphides occur as inclusions in pyrite. Chalcopyrite, sphalerite, covellite, galena and possibly pyrrhotite occur in this way. Chalcopyrite and sphalerite also occur alone in small patches. Quartz often replaces phenocrysts and the ground-mass of the host rock and forms cross cutting veinlets.

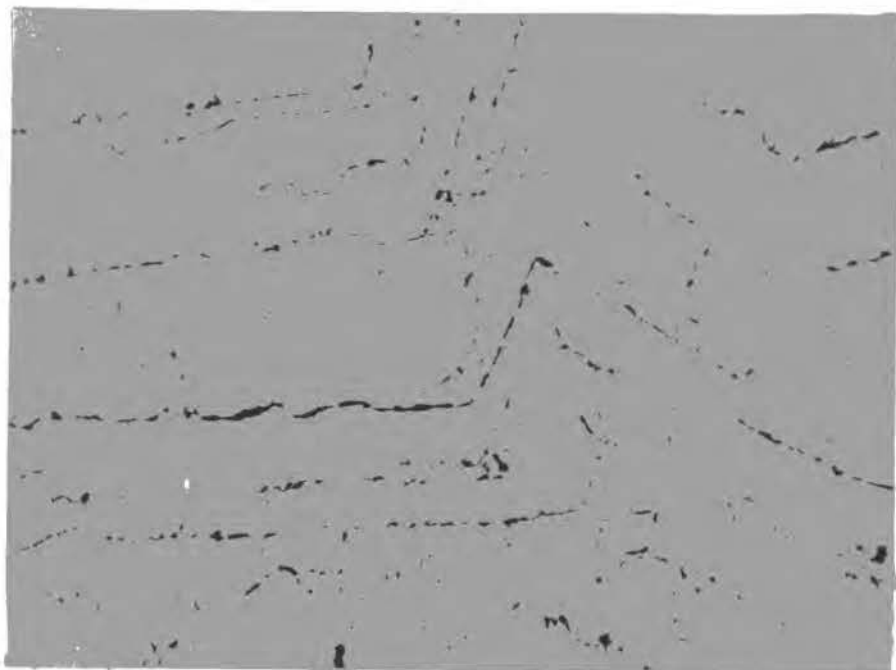
E.Ic2 Ore Zone III: This is the outer casing of the massive pyritic ore body of the Lahanos mine and it is mainly composed of massive



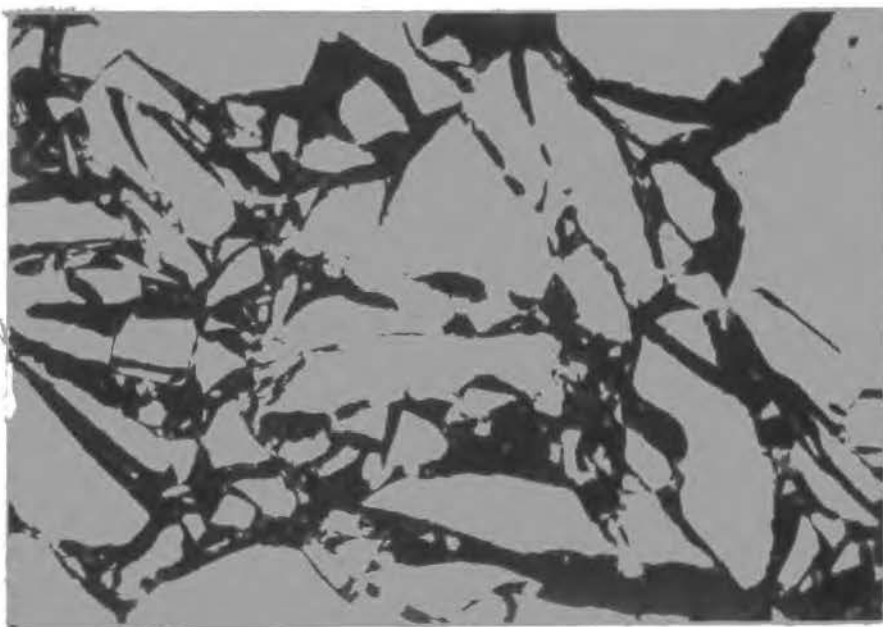
Pl. 15. Colloidal and granular pyrite relationships, ore Zone III
160 x.



Pl. 16A. Botryoidal texture in colloidal pyrite, ore Zone III
875 x.



Pl. 16B. Colloform banding in colloidal pyrite, ore Zone III. 73 x



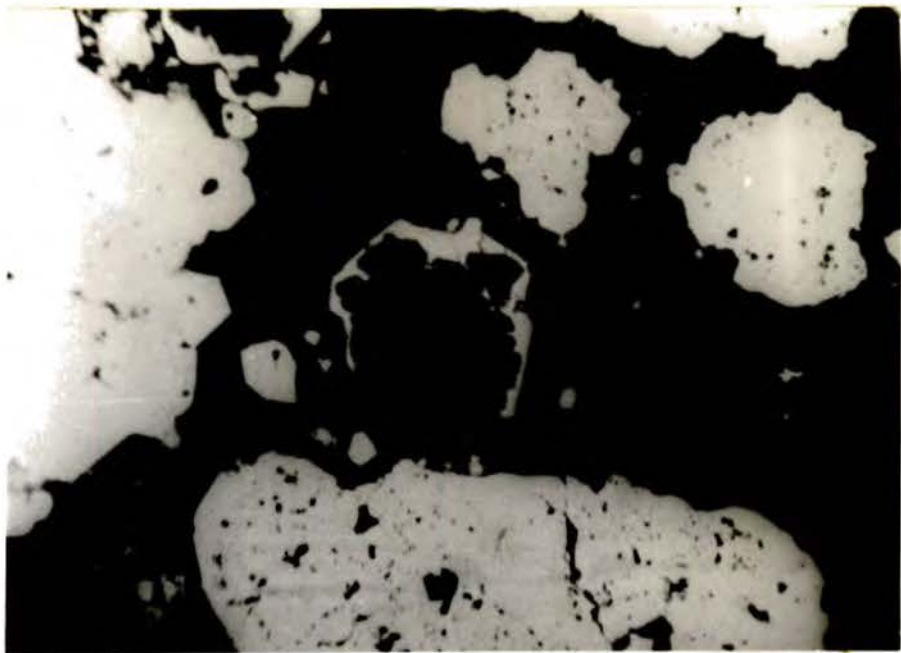
Pl. 17. Shattered pyrite replaced by gangue and chalcopyrite
(Cataclastic or mottled texture in pyrite, ore Zone III)
350 x.

pyrite and locally abundant chalcopyrite, tennantite and bornite. Closer to ore zone II sphalerite and traces of galena are abundant.

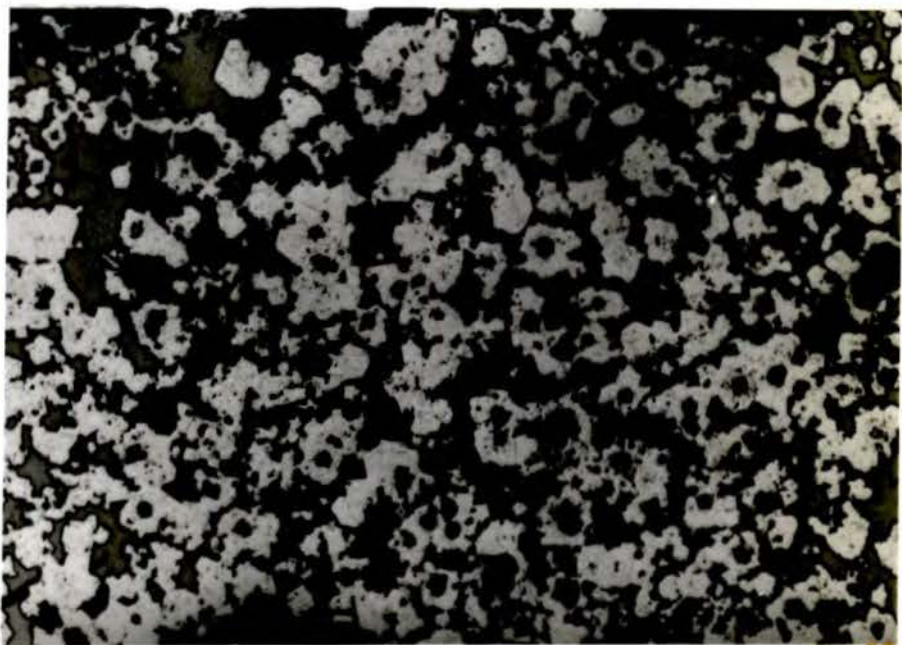
Pyrite in ore zone III forms massive pyritic bodies showing hypautomorphic granular texture or in many cases aggregates, and in addition colloform texture is commonly present. Weak to moderate anisotropism with brick red to dark navy blue colours can be seen with the highest light intensity. A general discussion of this phenomenon is given later (p 108).

Plate 15 shows both forms of pyrite. Colloidal pyrite forms botryoidal (See Plate 16A) and colloform banding (See Plate 16B) texture. In parts of ore zone III pyrite is shattered and recemented by gangue and partly by chalcopyrite (See Plate 17) so giving cataclastic texture. Zonal texture in pyrite is often brought out by many tiny bleb-like inclusions of bornite with neodigenite and covellite, chalcopyrite, sphalerite and gangue. The edges of the granular pyrite are occasionally rimmed by a second generation pyrite which then was followed by later sulphides and gangue minerals. Advanced stage replacement of pyrite yielded often an atoll texture (See Plate 18).

Marcasite occurs in trace amounts in Ore zone III and is usually associated with later mineralisation. Marcasite-quartz veins with a little chalcopyrite cut across the early pyrite and are often associated with carbonate gangue (dolomite). Marcasite is sometimes converted into pyrite along its edges, except where it has been embedded in chalcopyrite. Because of its distinct



Pl. 18. Atoll texture in pyrite due to replacing gangue mineral, ore Zone III. 160 x



Pl. 19. Tennantite replaces and infills the interstices of granular pyrite, ore Zone III. 350 x

pleochroism, sometimes slightly higher reflectivity than pyrite and strong anisotropism, marcasite is easily distinguished from the pyrite. Marcasite often forms the core of colloidal pyrite.

Chalcopyrite in places forms the major constituent after pyrite and usually infills the interstices of pyrite aggregates. Occasionally, closer to ore zone II, chalcopyrite together with tennantite (Plate 19) cements the intergranular spaces of pyrite, but where pyrite is the more abundant sulphide then chalcopyrite and bornite form inclusions in the pyrite. Tennantite inclusions in pyrite are not seen. Although sphalerite is not a common sulphide in ore zone III, it is occasionally present and often replaced by chalcopyrite. Bornite and chalcopyrite may show a mutual boundary relationship in inclusions in pyrite and less commonly in sphalerite. Bornite also commonly shows very fine grained ex-solution lamellae of chalcopyrite.

Often anhedral tennantite grains contain tiny patches of pink enargite ($\text{Cu}_3 \text{AsS}_4$) and rims of a bluish pink mineral which may be seligmannite (Pb Cu As S_3). Rarely patches of grayish blue anisotropic bournonite (Pb Cu Sb S_3) are also seen. These identifications have not been checked by microprobe.

Sphalerite and galena normally occur as tiny replacement patches in pyrite or along the individual pyrite boundaries. However, some large patches of sphalerite occur independent from the pyrite of ore zone III. Closer to ore zone II the frequency of irregular sphalerite patches gets higher and sometimes sphalerite is associated with chalcopyrite. Occasionally shattered sphalerite



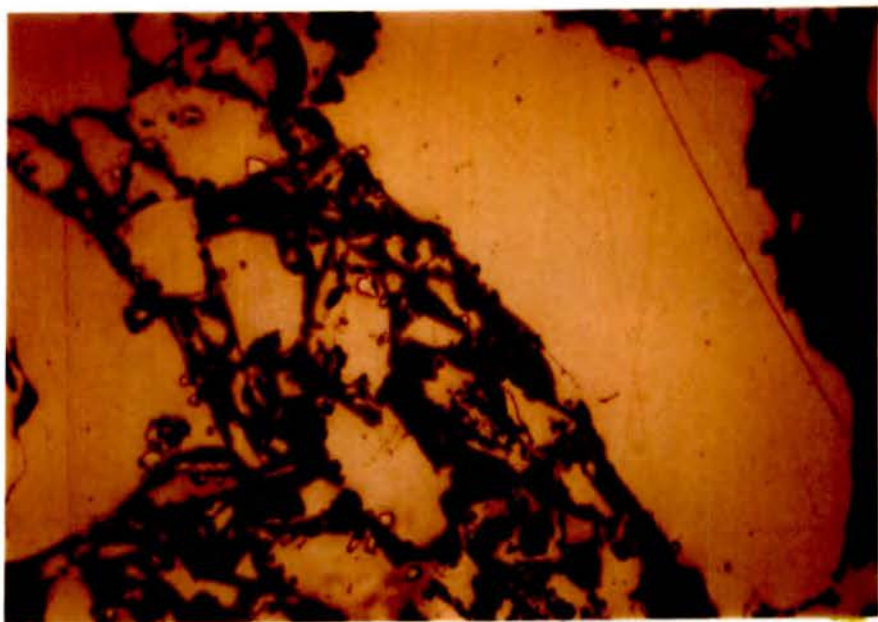
Pl. 20A. Sphalerite, gangue, barite relationships, ore Zone II. 160 x



Pl. 20B. Sphalerite, gangue, barite relationships, ore Zone II. 160 x



Pl. 20C. Sphalerite, gangue, barite relationships, ore Zone II. 160 x



Pl. 21A. Sphalerite chalcopyrite relationship, ore Zone II. 160 x

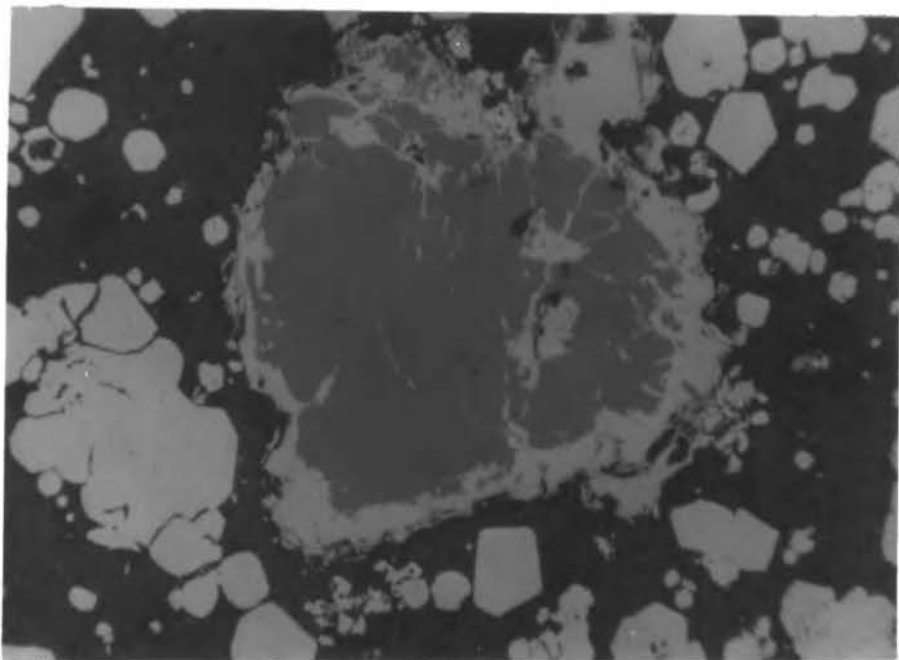
was infilled by gangue.

The main gangue mineral of this zone is dolomite and quartz is less abundant. Dolomite (which is confirmed by XRD) is usually later than the sulphides and often shattered pyrite and less often chalcopyrite were cemented by it.

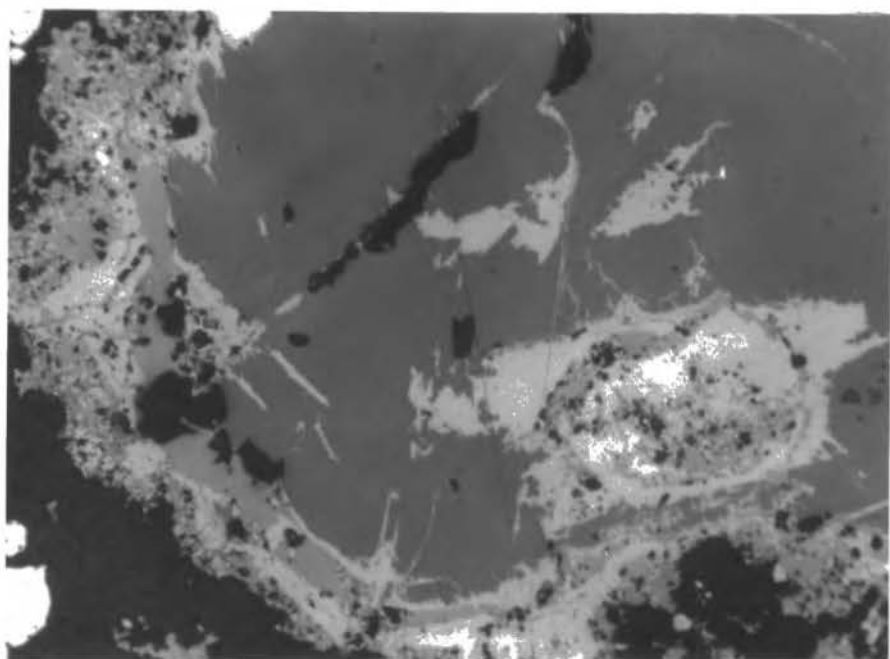
E.Ic3 Ore Zone II: The yellow ore of zone III passes fairly sharply into the speckled dark grey ore of ore zone II, within a distance usually less than a meter.

Sphalerite and pyrite are the major constituents of this zone but important amounts of galena, and chalcopyrite occur together with minor amounts of tennantite, enargite and seligmannite. Bornite, marcasite and colloform pyrite appear and become more abundant towards the junction with ore zone I.

Sphalerite, which is later than granular pyrite shows anhedral to subhedral granular texture, and has quite distinct internal reflection colours of red to yellow depending on its iron content. Various textural relationships with the barytes gangue are seen - Plates 20A, 20B, 20C. Sphalerite is usually older than and replaced by galena, but occasionally sphalerite replaces galena, indicating some overlap of deposition. The relationship between sphalerite and chalcopyrite is less well defined. Each mineral can be seen replacing the other, although usually chalcopyrite replaces sphalerite. This may indicate more than one period of deposition of either or both these minerals. (Plate 21A, 21B, 21C). What seems to be a guided replacement of sphalerite by chalcopyrite and tennantite is



Pl. 21B. Sphalerite chalcopyrite relationship, ore Zone II. 160 x



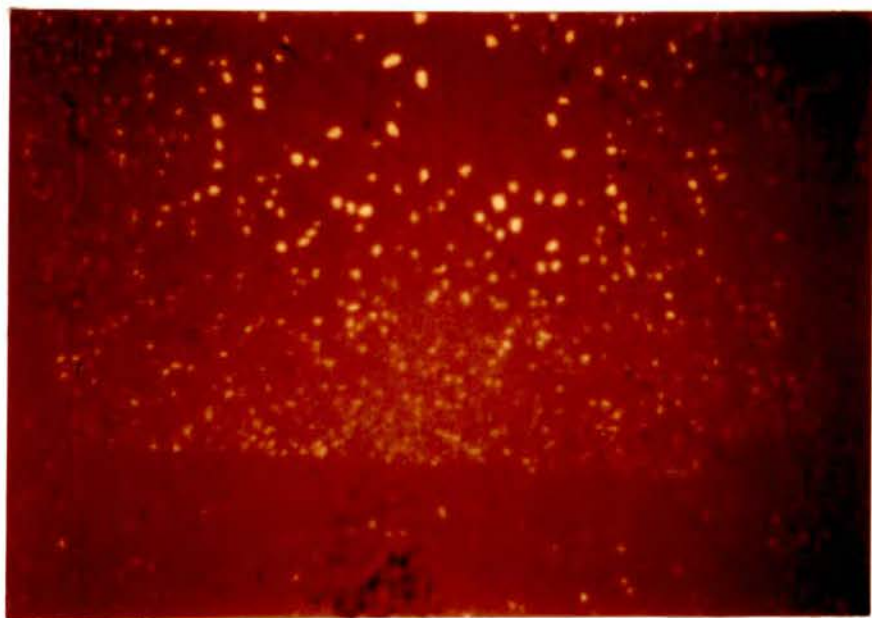
Pl. 21C. Sphalerite chalcopyrite relationship, ore Zone II. 160 x

also seen (Plate 22). Sphalerite older than chalcopyrite often shows emulsion type ex-solution blebs of chalcopyrite. Plate 23A from the Kepçelik deposit (See Map 2) which is about 2.5 kilometers SE of the Lahanos mine, shows this texture. Plate 23B from another part of the same section shows lamellar chalcopyrite ex-solution bodies - a form which does not seem to have been described by other authors. The emulsion type of ex-solution texture is also observed between sphalerite (host) and tennantite. Colloform pyrite of later origin than the granular pyrite (plate 24) is a striking feature of the Zone II ore (Plate 25, 26). Its relationship to other minerals varies, as can be seen in Plates 27A, 27B. In addition to colloform banded pyrite, a striking framboidal pyrite, probably also of colloidal origin (Rust, 1935 and Bastin, 1950) occurs in Zone II (Plate 28). In addition to separate framboidal spheres, this plate also shows framboidal nuclei within an area of coarser pyrite with shrinkage cracks. Relationships similar to the "radial bomb type" texture of Rust, 1935 are locally seen. Plate 29 shows a unique grain of pyrite with a contorted banded texture, reminiscent of graining in wood, found in sample 40A from the Lahanos Old Gallery. In the absence of further evidence, the significance of this grain is uncertain.

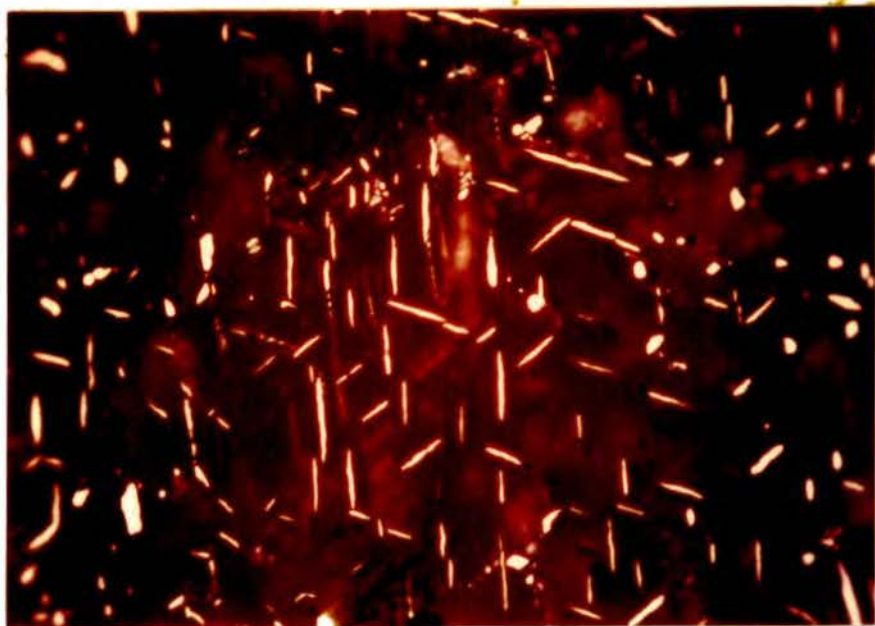
Galena frequently includes small patches of greenish grey tennantite and occasionally small areas of seligmannite. These have not been checked by microprobe because of their small grain size (about 3 microns) but the galena has been checked by microprobe for the presence of silver. None was detected.



Pl.22. Guided replacement of sphalerite by chalcopyrite (whitish gray) and tennantite (gray), ore Zone II. 160 x



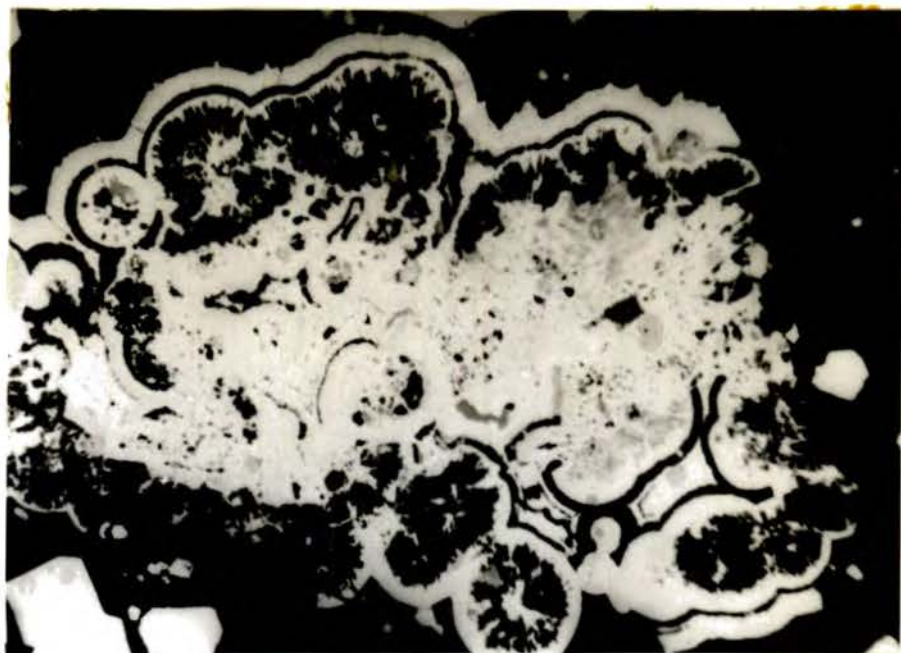
Pl. 23A. Emulsion type ex-solution blebs of chalcopyrite in sphalerite from the Keppelik mine, Lahanos area. 875 x



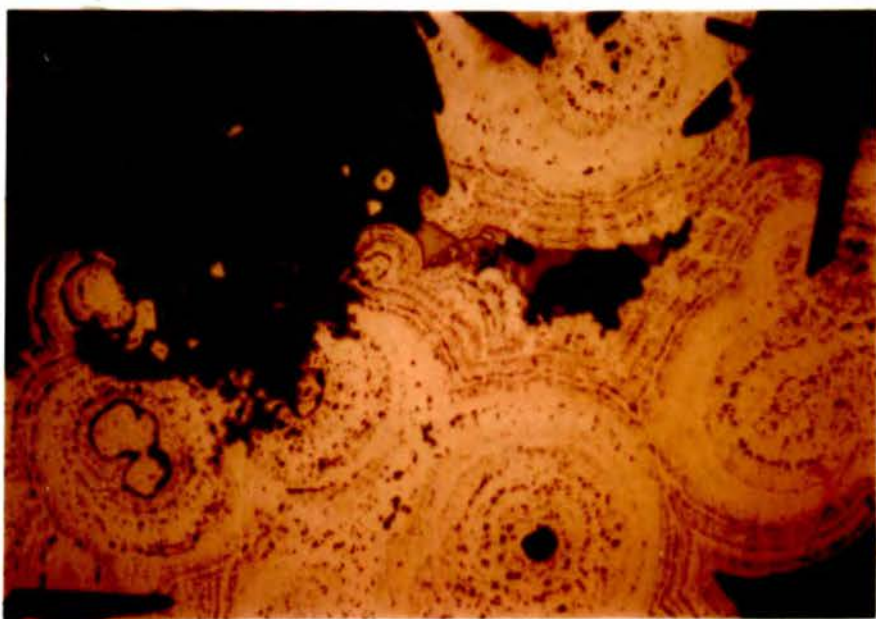
Pl. 23B. Ex-solution lamellae of chalcopyrite in sphalerite from the Kepeçelik mine, Lahanos area. 2200 x



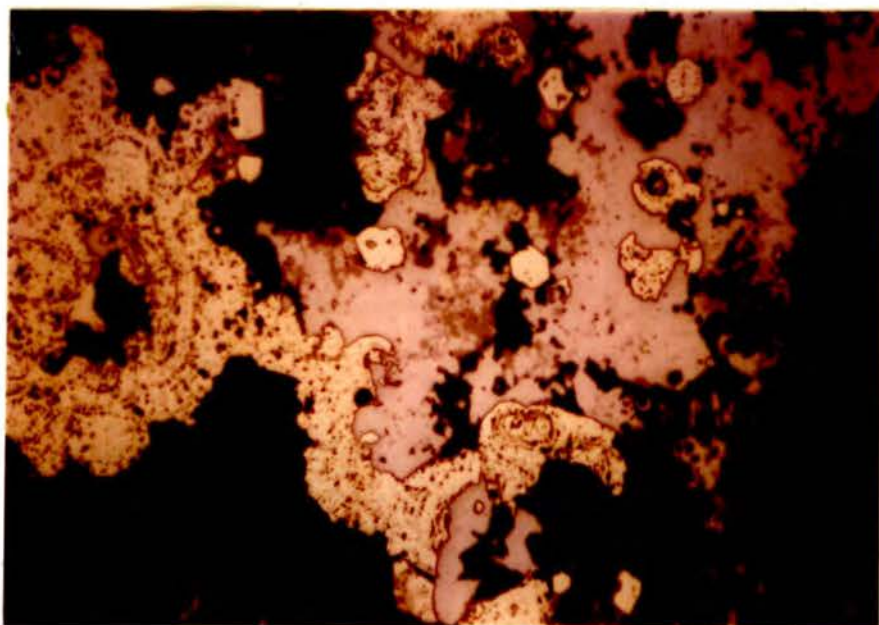
Pl.24. Colloidal pyrite-pyrite and sphalerite relationships, ore Zone II. 73 x



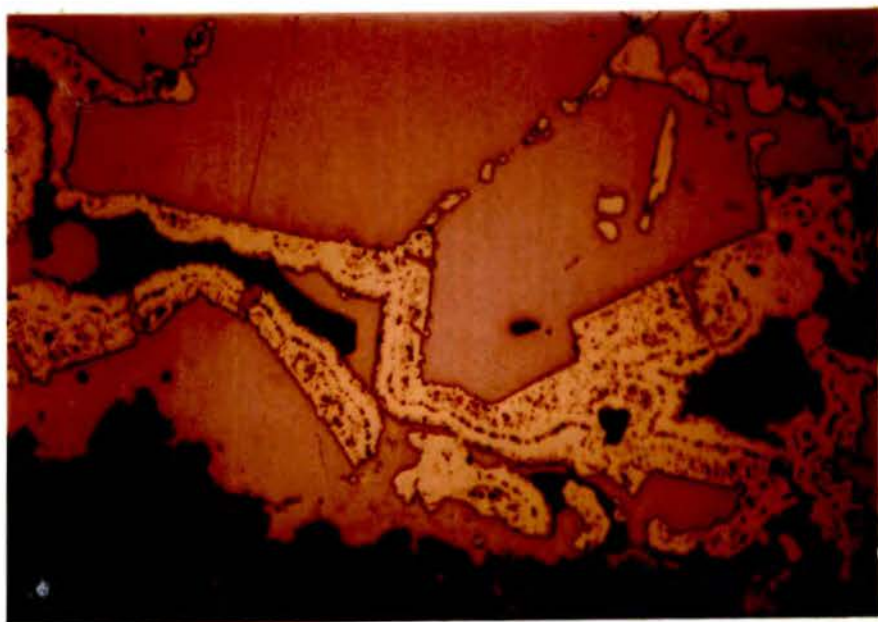
Pl. 25. Shelly colloform texture in pyrite, ore Zone II. 160 x



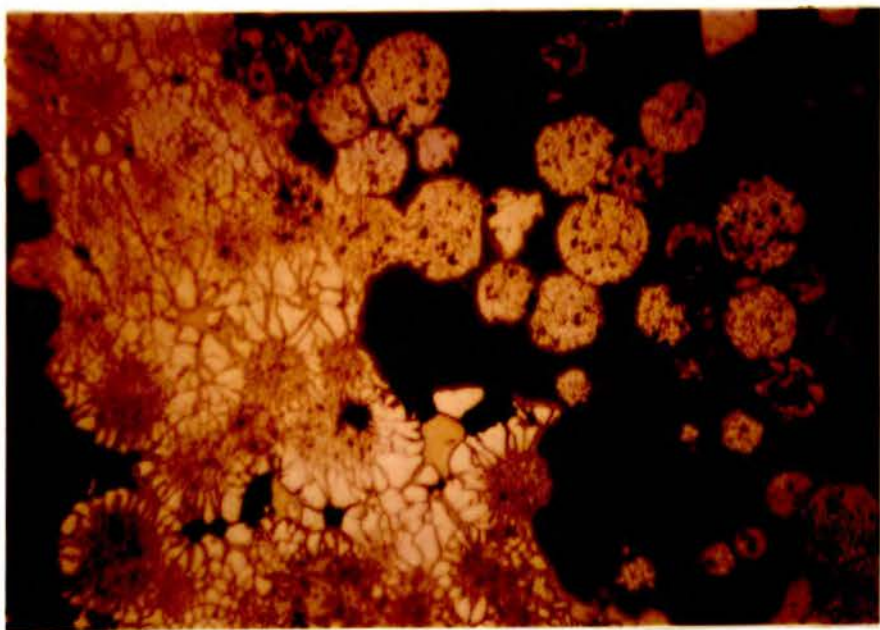
Pl. 26. Colloidal pyrite-sphalerite-galena-tennantite-barite relationships, Ore Zone II. 350 x



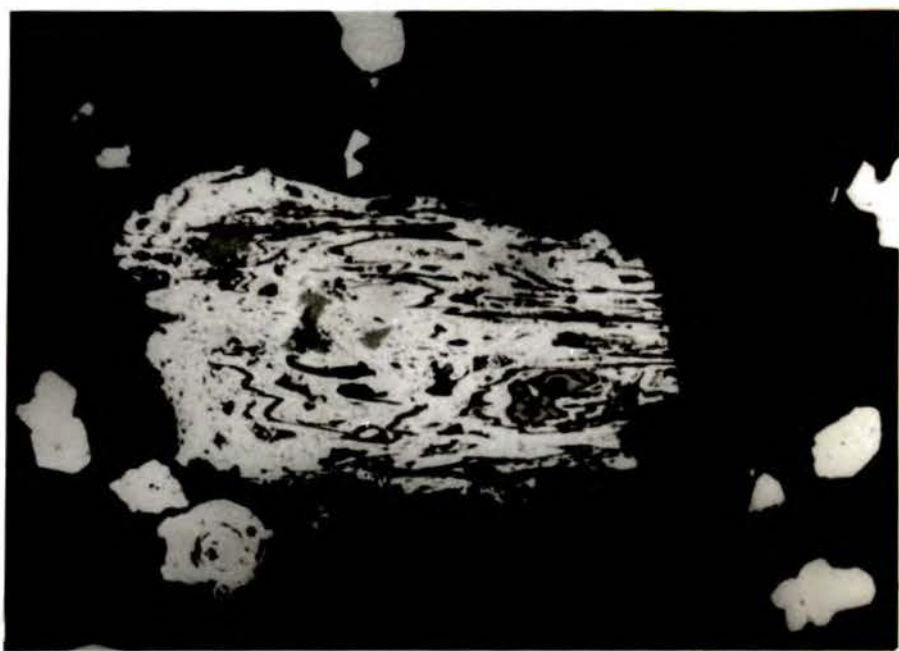
Pl. 27A. Age relationships between colloidal pyrite and galena, gangue and tennantite, ore Zone II. 350 x



Pl. 27B. Age relationships between colloidal pyrite and galena, gangue, ore Zone II. 350 x



Pl. 28. Framboidal pyrite-sphalerite relationships, ore Zone II.
875 x



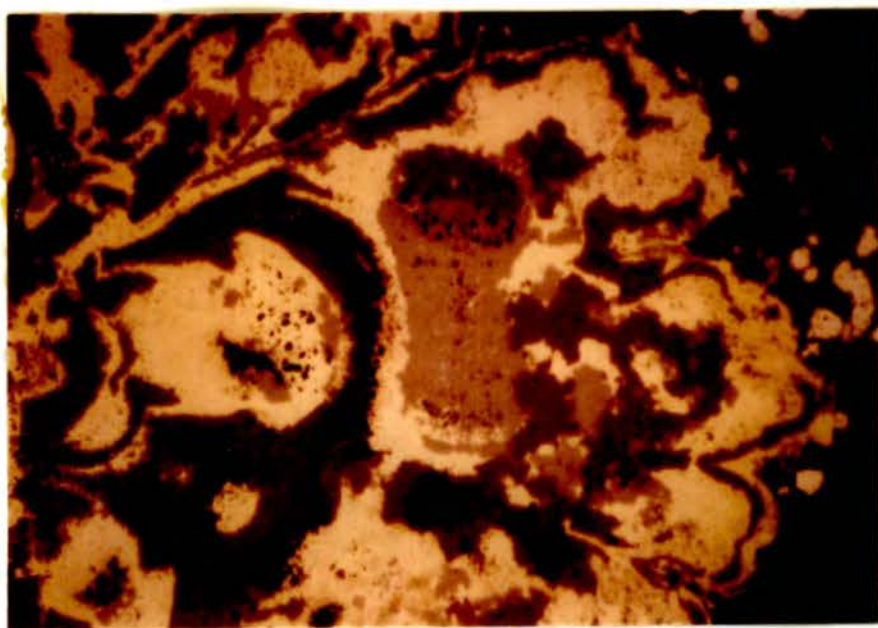
Pl. 29. Contorted banded texture in colloidal pyrite, ore Zone II.
160 x

In addition to its normal anhedral occurrence, infilling spaces and replacing various minerals, chalcopyrite also occasionally occurs in colloform banding with sphalerite (Plate 30).

Tennantite: According to certain authors, there is a variation of colour from greenish grey to bluish green grey with composition in the tetrahedrite-tennantite series. However, in the writers' experience, the apparent colour of these minerals can vary considerably depending on the colour of adjacent minerals. The colour relative to galena and sphalerite is distinctly different from the colour relative to pyrite and chalcopyrite. The X-ray powder pattern and quantitative electron microprobe analysis have confirmed that the mineral is usually tennantite, with only a very small amount of antimony in solid solution. Tennantite is more abundant towards ore zone III. (Plates 19, 31, A and B). However a grain of slightly more bluish gray colour associated with sphalerite was also analysed quantitatively by microprobe and found to be tetrahedrite (See Section E.Ie2).

Enargite-"Famatinite" ($\text{Cu}_3\text{As S}_4 - \text{Cu}_3\text{Sb S}_4$). Material having optical properties indicative of members of this series occurs in grains up to a maximum size of 100 microns and in irregular patches. The nomenclature of these minerals has been discussed recently by C. Lévy (1966), who adopts the nomenclature of H. Strunz (1957) given below:

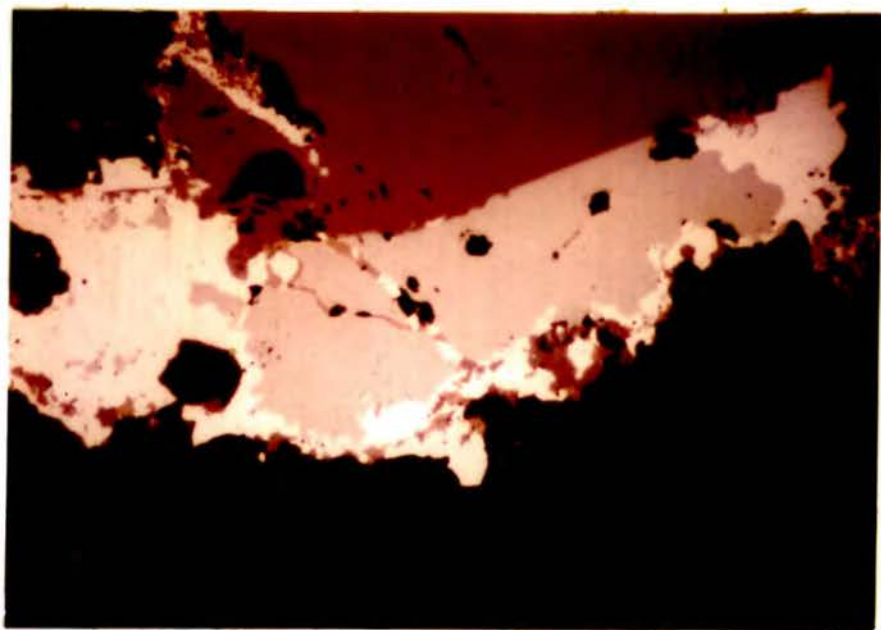
Orthorombic isotypes	}	Enargite $\text{Cu}_3\text{As S}_4$
	}	Stibioenargite $\text{Cu}_3\text{Sb S}_4$



Pl. 30. Colloform banding of chalcopyrite, sphalerite, associated tennantite and gangue, ore Zone II. 350 x



Pl. 31A. Shattered pyrite replaced by tennantite, ore Zone II closer to the ore Zone III. 600 x



Pl. 31B. Tennantite-galena-bornite-gangue age relationship, ore Zone II closer to the ore Zone I. 875 x



Pl. 32. Enargite phenocryst, ore Zone II. 875 x

Tetragonal isotypes } Luzonite Cu_3AsS_4
 } Stibioluzonite Cu_3SbS_4

in which the name famatinite is abandoned.

Partial phase relationships in this system are given by Barton and Skinner in "Geochemistry Of Hydrothermal Ore Deposits" (Ed. H.L. Barnes, 1967, p.306). The inversion of low temperature luzonite to high temperature enargite is given as 320°C . It is interesting to note that whilst higher temperature polymorphs usually have higher symmetry than low temperature forms, the reverse seems to be the case in this system.

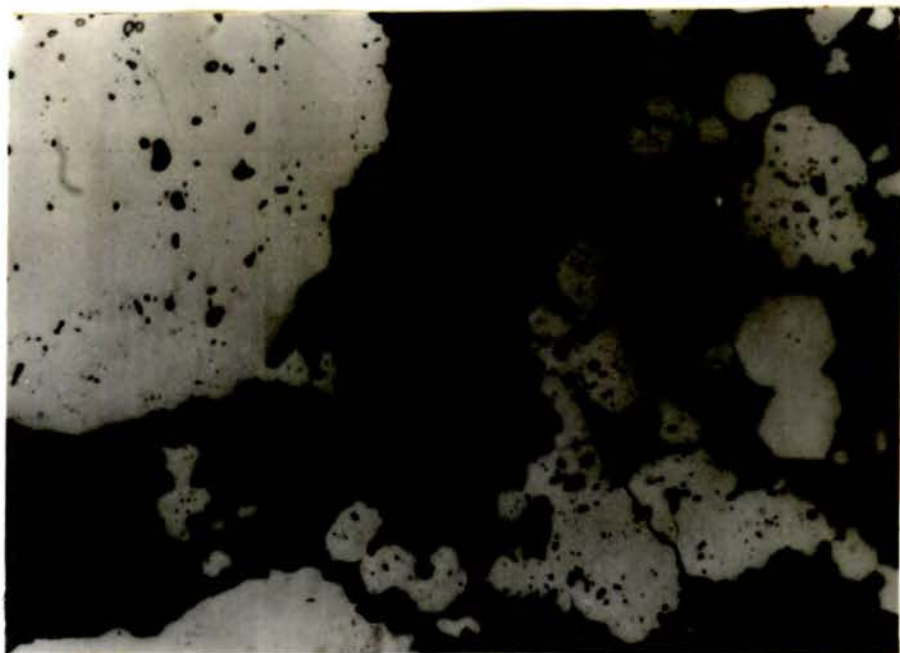
Lévy states that the existence in nature of stibioenargite is not established, and that the optical properties of the remaining three members are sufficiently distinctive to allow easy identification from qualitative observations. His microprobe analysis of material from Famatina shows compositions that would now be described both as luzonite and as stibioluzonite. It seems therefore, that the name "famatinite" may have been used in the past with an unduly wide meaning and should be avoided until its status is more thoroughly examined.

Reflectivity measurements (F104) and microprobe analysis (p97) show that the material in the Lahanos Zone II ore is enargite, the high temperature polymorph, with a negligible amount of antimony in solid solution (Plate 32 and 49 A - D). Some of the grains, because of orientation effects, show slightly different colours and anisotropy and were thought at first possibly to be of different

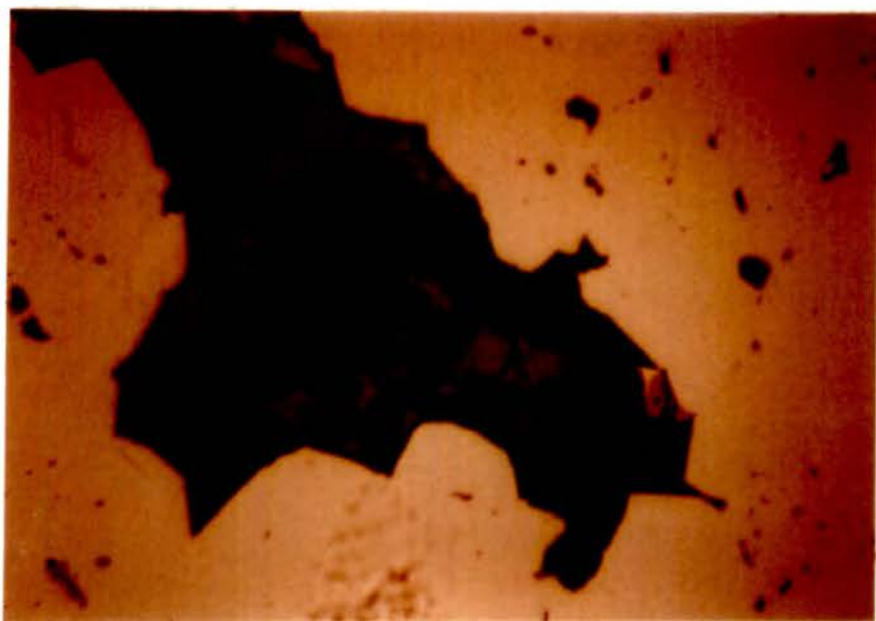
composition. However, when checked by microprobe and reflectivity measurement they proved to be enargite.

Enargite is usually associated with sphalerite, bornite, galena and to a less extent with pyrite. It definitely replaces pyrite (Plate 33) and sphalerite. However it is possible to see in the latter inclusions or blebs of enargite. The age relation of enargite with bornite is somewhat controversial i.e. in some cases enargite is definitely replaced by bornite, but also in a few cases the relationship is reversed. Occasionally bornite and neodigenite form segmented vein replacement texture in enargite.

Bornite in ore Zone II is present in minor quantity and usually occurs as tiny inclusions particularly in pyrite with an average grain size of about 20 microns. Similar inclusions and replacement patches are also common in sphalerite. Some of the larger replacement patches of bornite show tiny ex-solution lamellae of chalcopyrite developed in three directions i.e. along (111) planes. Often chalcopyrite and bornite show mutual boundary relationship in these inclusions. Sometimes when bornite replaces galena, it shows a reticulated replacement texture, which can often also be seen when bornite is being replaced by neodigenite and covellite. Bornite replaced by covellite often infills the interstices of pyrite (See Plate 34A and 34B). As seen in Plate 35A bornite forms bleb like inclusions in galena, and in Plate 35B an irregular intergrowth of bornite replacing galena is illustrated.



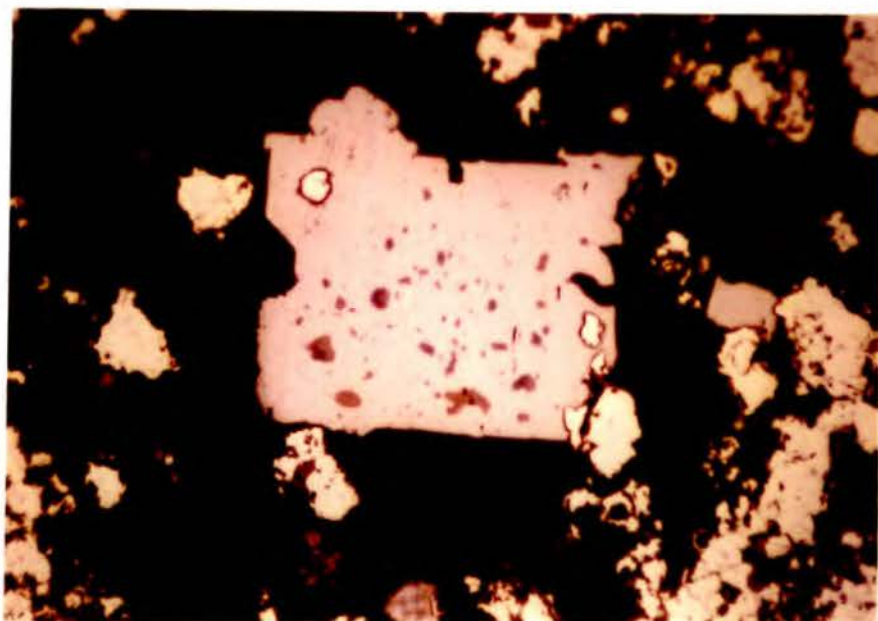
Pl. 33. Enargite replaces interstices of pyrite, ore Zone II. 350 x



Pl. 34A. Covellite-bornite-pyrite relation, ore Zone II, closer to the ore Zone I. 875 x



Pl. 34B. Covellite-bornite-pyrite relation, under cross nicols, ore Zone II, closer to the ore Zone I. 875 x



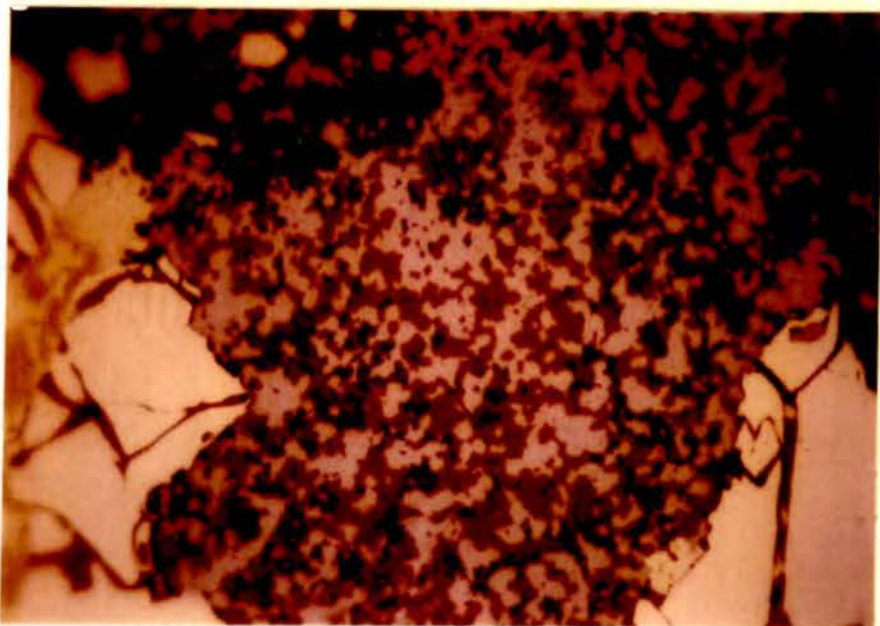
Pl. 35A. Galena-bornite relation, ore Zone II closer to the ore Zone I. 875 x

Covellite is an accessory copper sulphide mineral and tends to replace pyrite, galena, sphalerite and bornite rather than chalcopyrite, in fact no example of covellite replacing chalcopyrite has been seen anywhere in the Lahanos ore. In Plate 34A and 34B covellite replaces bornite and both infill the interstices of pyrite. Under crossed nichols, covellite is one of the easiest minerals to recognise owing to its vivid orange red polarisation colours. In Plate 36 covellite with colloidal pyrite shows beautiful colloform banding. Sometimes covellite occurs as tiny inclusions in banded colloform pyrite (Plate 16B).

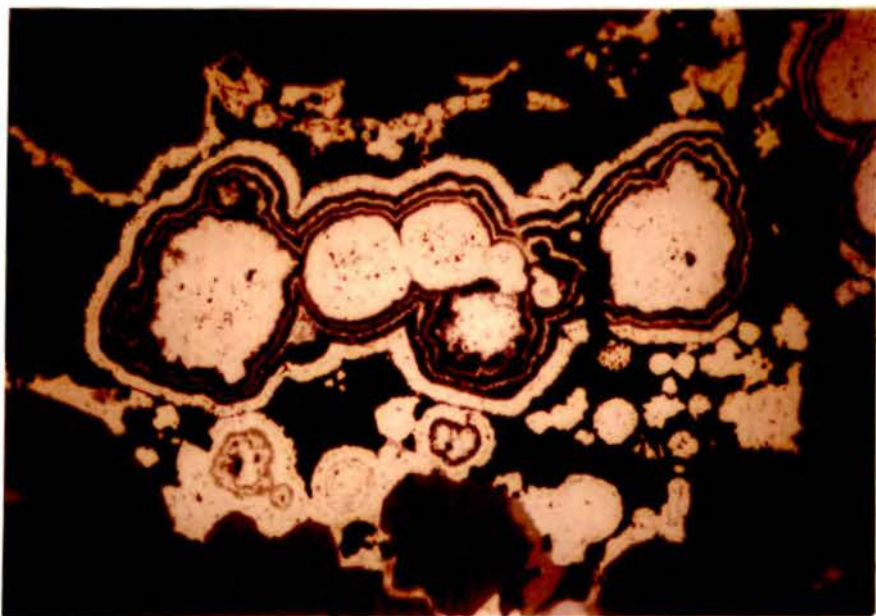
Neodigenite shows similar occurrences to covellite, Although it is usually an obvious secondary mineral, it is sometimes seen without any other associated copper mineral, and may therefore also be partly of primary formation.

Marcasite is usually associated with colloidal pyrite Plate 37A and 37B. Marcasite becomes more abundant closer to ore zone I, and is also seen in small quartz veinlets cutting across ore zone II.

Gangue minerals The commonest and characteristic gangue of ore zone II is barytes, forming blade like euhedral crystals or aggregates, and spherulitic arrangements of barytes blades (Plate 36). It is quite often possible to see that barytes replaces pyrite, colloidal pyrite, sphalerite, galena, chalcopyrite, but in some cases the reverse relationship occurs e.g. in Plate 23, 20 barytes blades were replaced by sphalerite. Other gangue minerals are quartz and dolomite in minor quantity. Both dolomite and barytes



Pl. 35B. Galena-bornite relation, ore Zone II closer to the ore Zone I.
2200 x



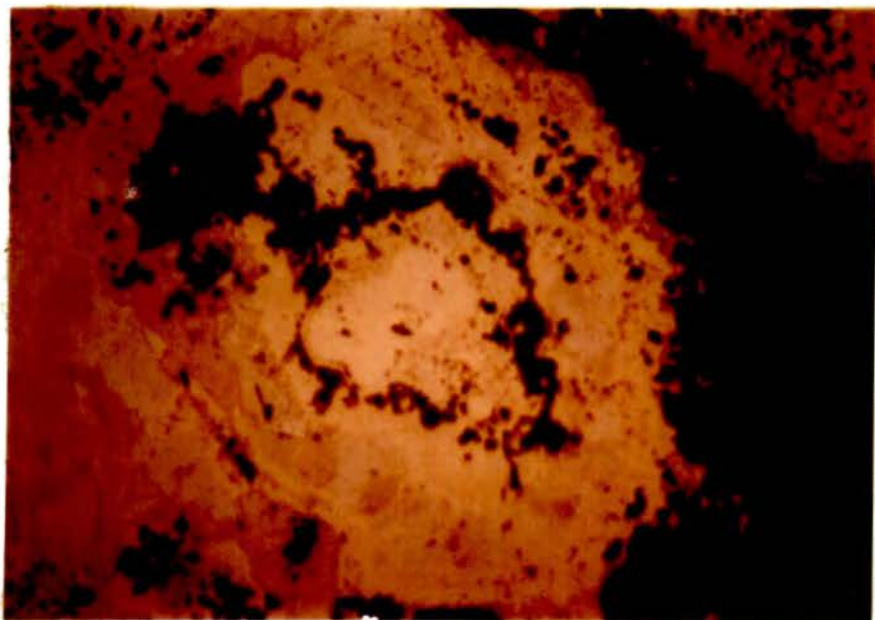
Pl. 36. Colloform banding of covellite and pyrite, ore Zone II. 875 x

clearly replace quartz. In some occasions dolomite seems to be replacing barytes i.e. optically continuous barytes blades were cut across by dolomite and in addition relicts of barytes occur in dolomite. However in sample NG 38 barytes is also replaced by deuteric quartz and possibly jasper.

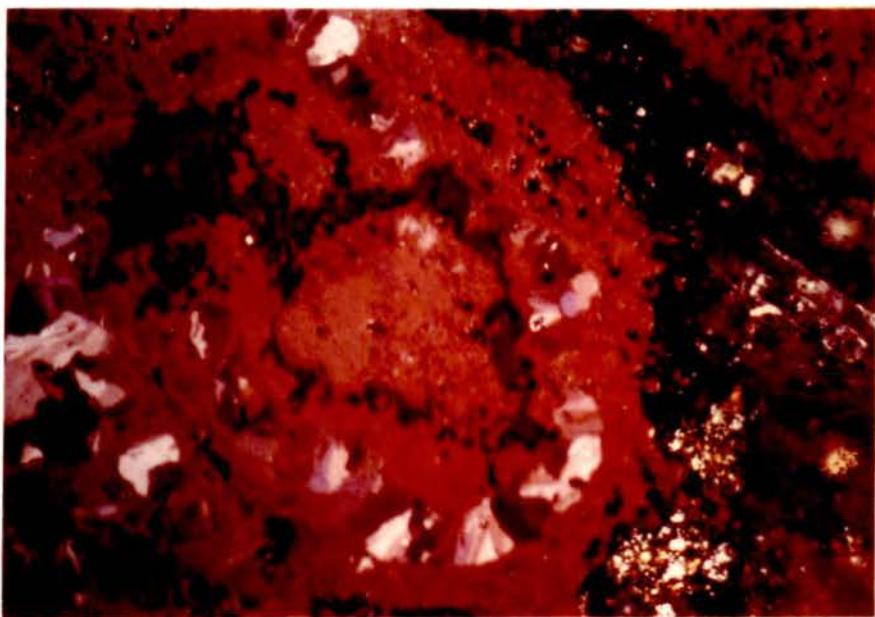
E.Ic4 Ore Zone I: This uppermost zone, not everywhere present, shows the highest copper values. Bornite, chalcopyrite, pyrite and colloidal pyrite are the most abundant sulphide minerals, whilst galena and marcasite are minor constituents.

Bornite is the second most important copper mineral in the Lahanos deposit as a whole, but is more abundant than chalcopyrite in Zone I, particularly towards the Upper contact of the pyritic ore body, just below the hanging-wall. The bornite of ore zone I shows weak to distinct reflection pleochroism and weak anisotropism with tan to reddish purplish brown polarisation colours under strong illumination. Its ordinary light colour is also noticeably slightly different, from the bornite of the other zones. X-ray powder photography confirmed its identity as bornite - quantitative details are given later. Bornite replaces galena, pyrite, chalcopyrite and tennantite, Plates 38, 39, 40, 41, 42. It is locally replaced by small amounts of neodigenite. Native Gold has been found for the first time in small amounts in polished sections of the Zone I ore (Plate 43). In every case, it is included in bornite.

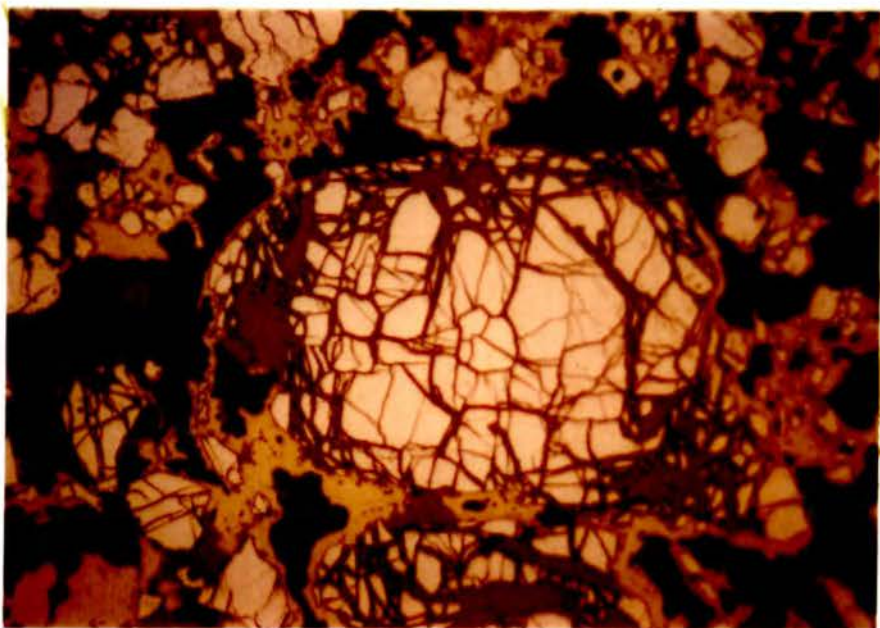
Chalcopyrite, the main copper mineral of the Lahanos deposit,



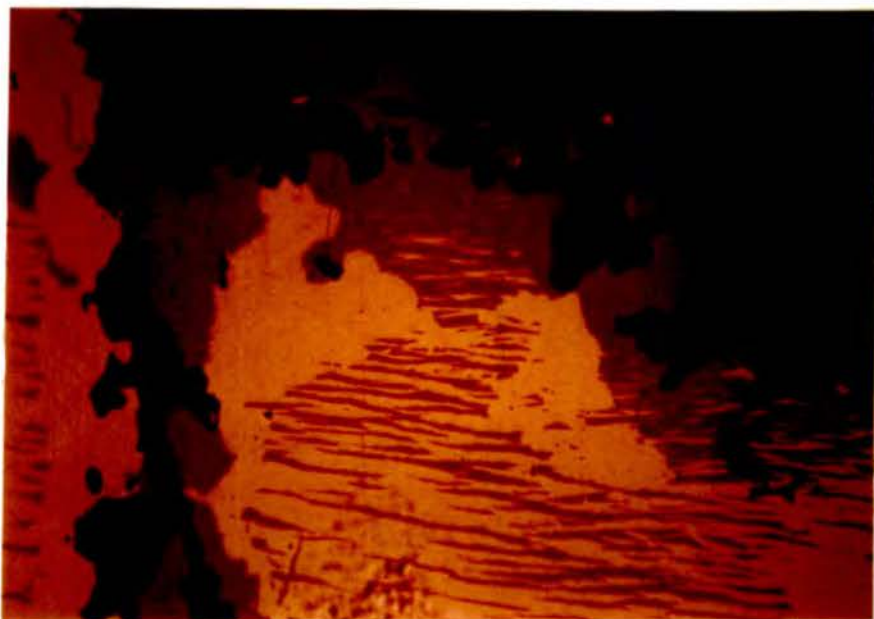
Pl. 37A. Colloidal pyrite-marcasite relationship. 375 x



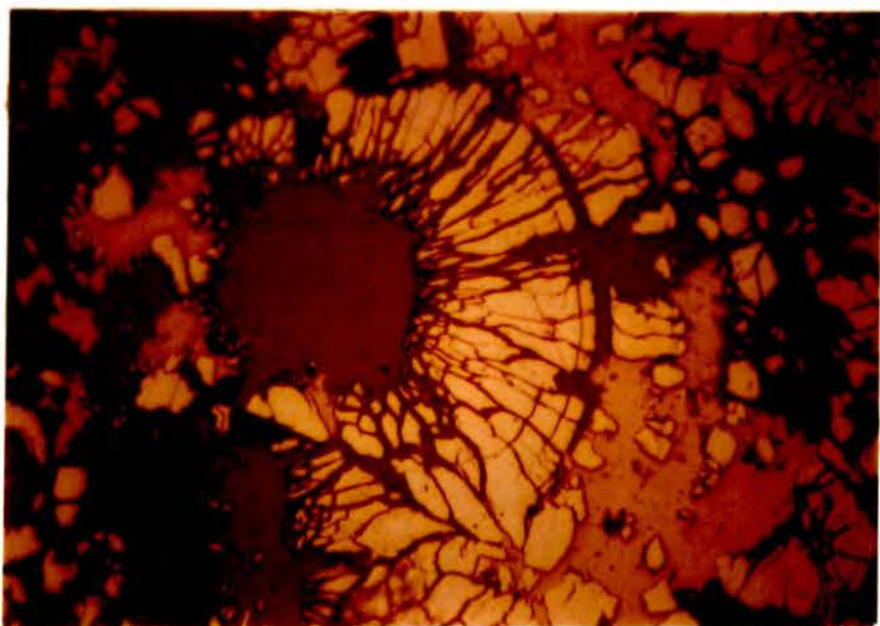
Pl. 37B. Colloidal pyrite-marcasite relationship, under cross nicols. 375 x



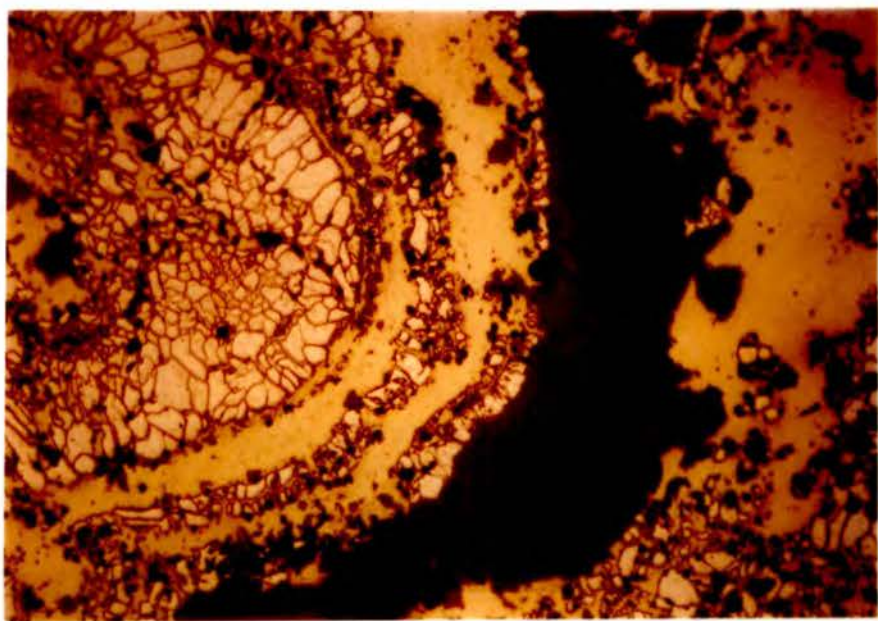
Pl. 38. Matching wall texture in between pyrite and bornite, ore Zone I. 375 x



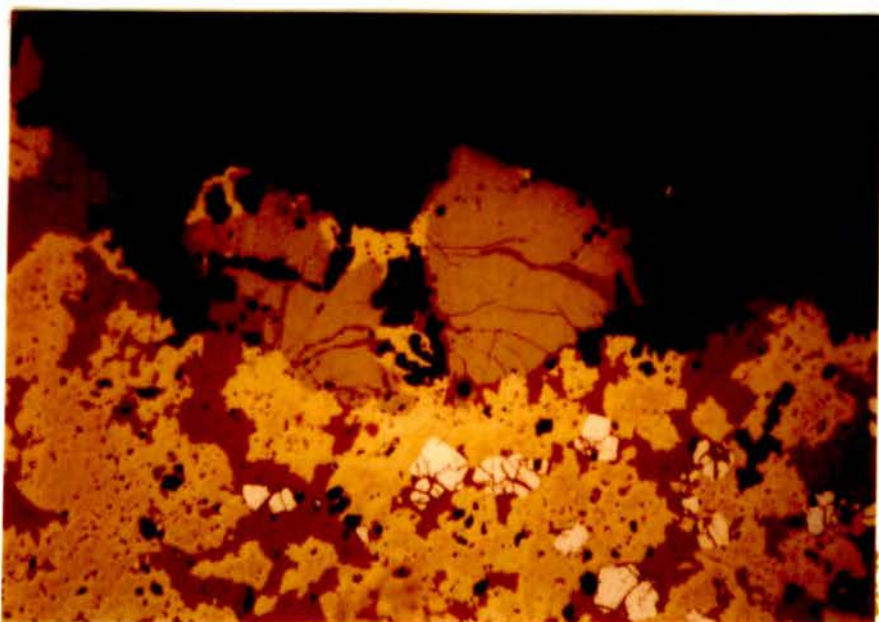
Pl. 39. Chalcopyrite-bornite relation, ore Zone I. 875 x



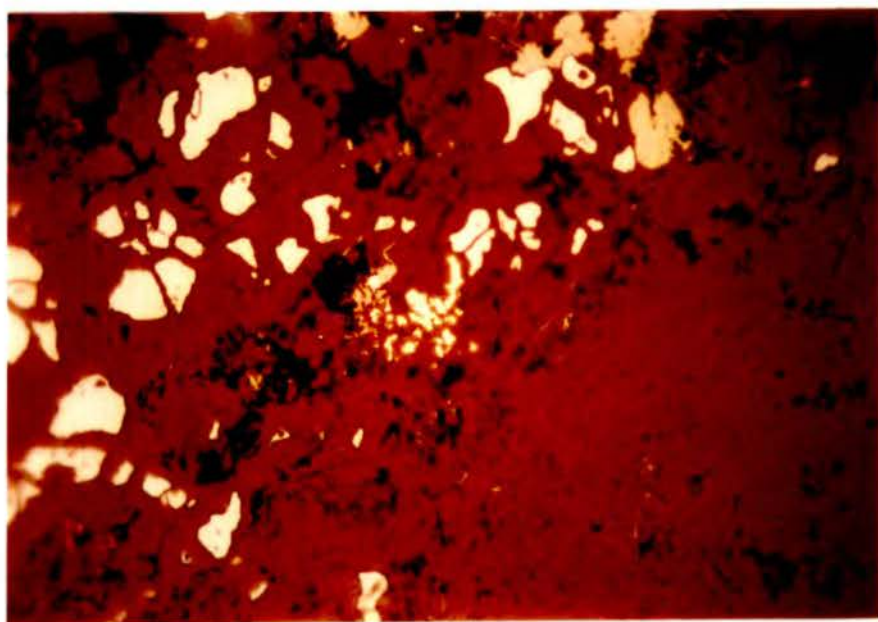
Pl. 40. Advance replacement of colloidal pyrite by bornite associated with chalcopyrite, ore Zone I. 875 x



Pl. 41. Bornite and colloidal pyrite relationship, ore Zone I. 375 x



Pl. 42. Tennantite-chalcopyrite-bornite relationship, ore Zone I. 375 x

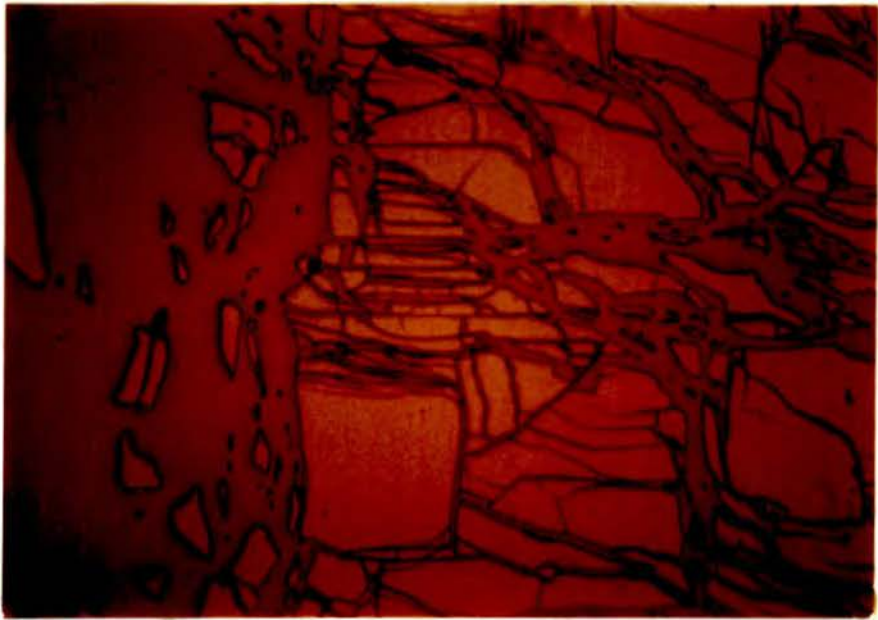


Pl. 43. Occurrence of native gold in bornite, ore Zone I. 2200 x

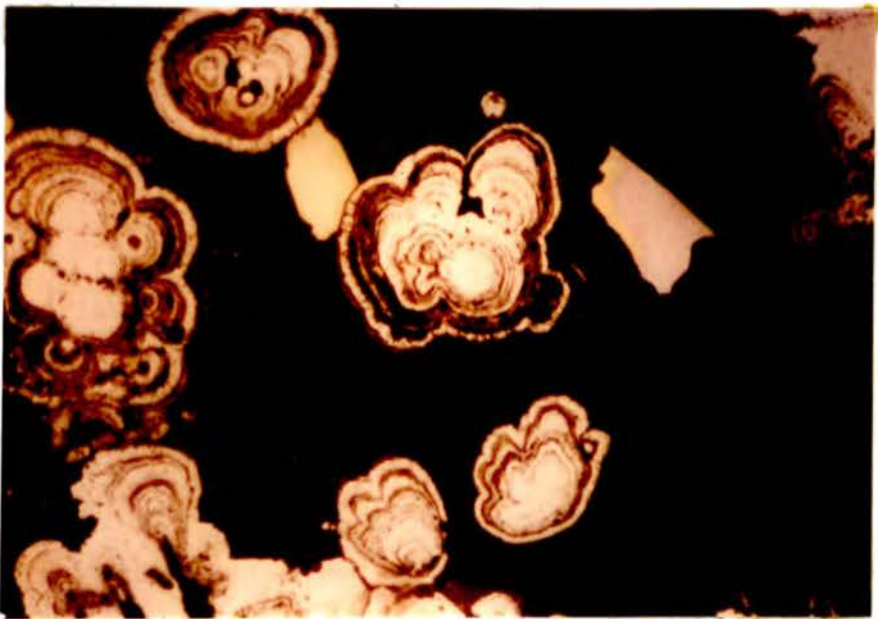
is somewhat less abundant than bornite in Zone I. Its relationships to bornite and pyrite have already been seen in previously mentioned plates. Plate 44 shows it replacing pyrite.

Colloform and massive pyrite are also abundant components of ore zone I. Colloform pyrite forms a second generation pyrite and usually surrounds the massive early pyrite. It often displays primary botryoidal, colloidal banding and spherulitic texture (Plate 45). Framboidal pyrite spheres, usually thought to be of colloidal origin, occur in isolation (Plate 46A, 46B) and various intermediate combinations of colloform textures are seen (Plate 47A, 47B), with a transition to textures that could be regarded as a zoned crystalline texture (Plate 48A, 48B).

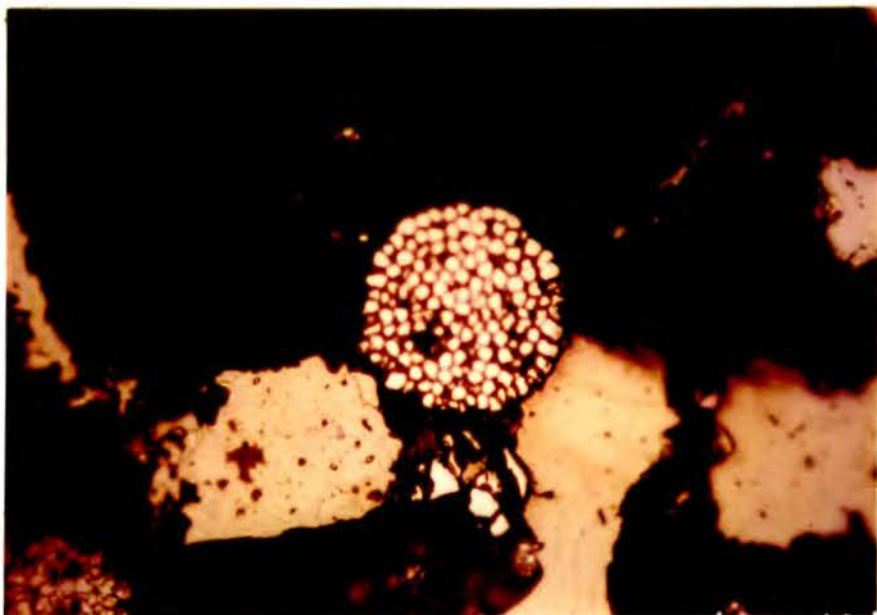
The main gangue mineral of ore zone I is lath shaped barytes, often associated with quartz and dolomite.



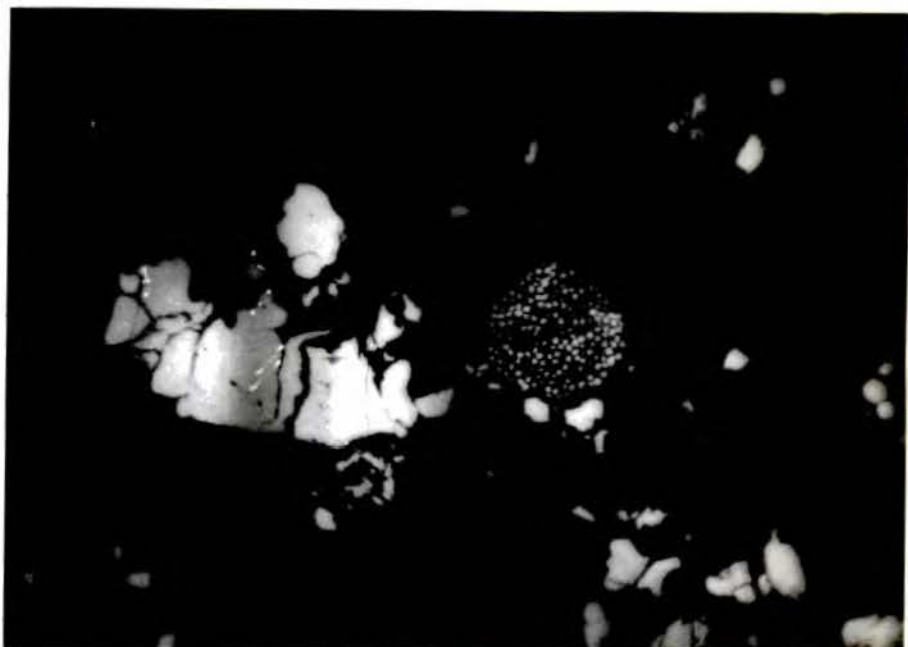
Pl. 44. Matching wall texture between pyrite and chalcopyrite, ore Zone I. 375 x



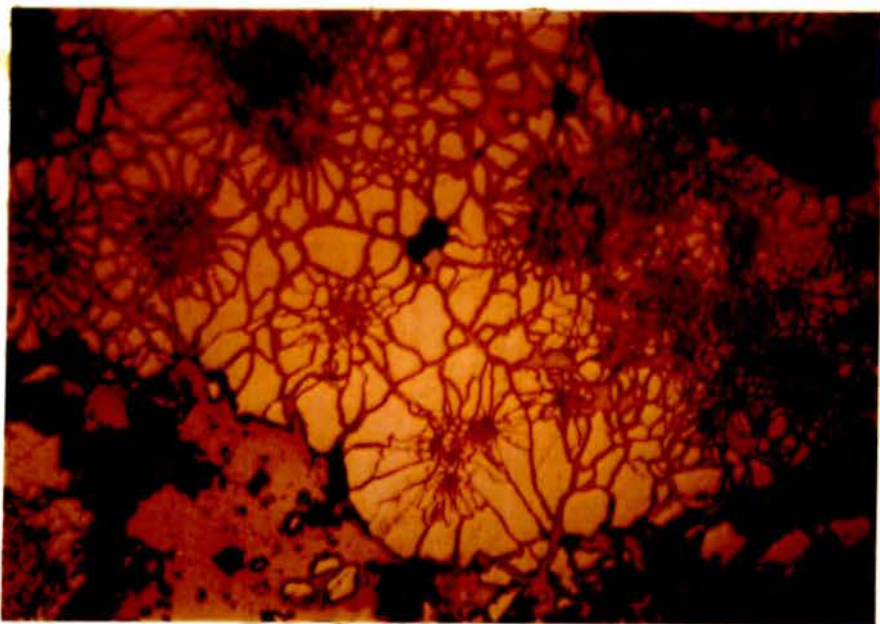
Pl. 45. Spherulitic texture of colloidal pyrite, ore Zone I. 375 x



Pl. 46A. Framboidal pyrite sphere, ore Zone I. 2200 x



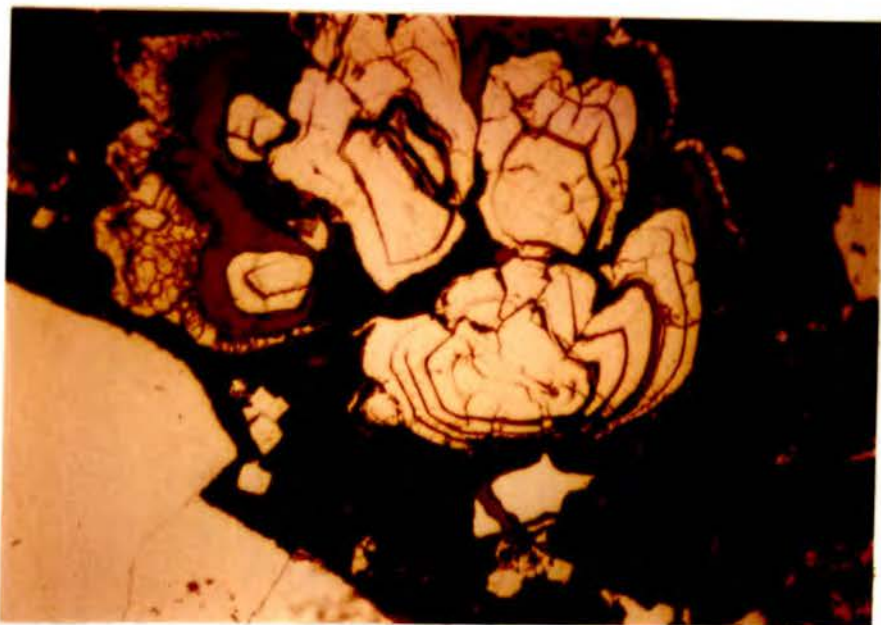
Pl. 46B. Framboidal pyrite sphere, ore Zone I. 600 x



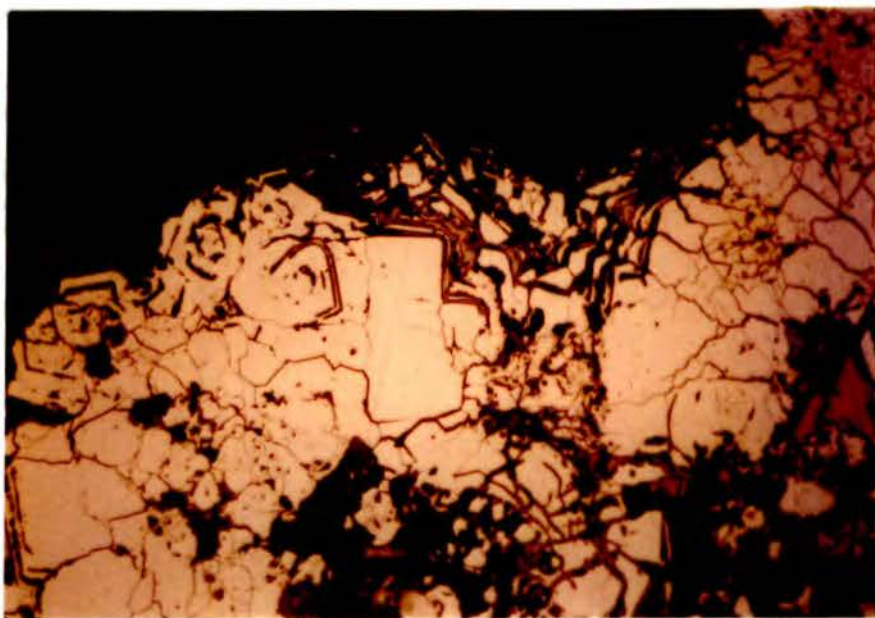
Pl. 47A. Colloidal pyrite-bornite-chalcopyrite relationship, ore Zone I. 875 x



Pl. 47B. Colloidal pyrite-bornite relationship, ore Zone I. 600 x



Pl. 48A. Zoned-crystalline texture in pyrite associated with bornite,
Ore Zone I. 875 x



Pl. 48B. Zoned-crystalline texture in pyrite associated with bornite,
Ore Zone I. 2200 x

E.I.d QUANTITATIVE PHYSICAL MEASUREMENTS ON LAHANOS ORESE.I.d1 X-ray Diffraction

X-ray studies of various sulphide minerals were undertaken on the Philips high angle XRD (P.W. 1051) or in some cases (particularly where only small amounts of material were available) with a 114.6 mm diameter powder camera. Calculations of accurate lattice parameters were made from film measurements, since the extrapolation procedures are better established than for diffraction chart measurements. Filtered copper or cobalt radiation were used as appropriate in each case. A standard Hilger and Watts film measuring scale with vernier capable of reading to 0.05 mm was used for film measurement and the results corrected for film shrinkage. Cell sizes of the cubic minerals were determined using a computer programme (M. George, 1968) based on the Cohen least squares extrapolation method. Results of this programme agreed with a check calculation carried out with a hand calculator. Details of the various diffraction patterns are given in Table 7.1-24 and a comparative table of cell sizes is given in Table 8.

E.I.d2 Electron Microprobe Analysis

The optical properties of opaque minerals are usually insufficiently well known to establish with any certainty the composition within a solid solution series. In such cases, following identification of the mineral group by optics, qualitative or semiquantitative

TABLE 7.1

X-ray diffraction data for various sulphide minerals

Sphalerite - NG39 light coloured sphalerite, Lahanos mine,
Ore Zone II, New Gallery.

$$a_0 = 5.4125 \pm 0.0005 \text{ \AA}$$

2θ (Co)	d	I/Ia. (Visual Est.)	hkl
33.271	3.126	10 ^I	111
38.588	2.709	5	002
55.735	1.915	9 ^{II}	022
66.468	1.633	8 ^{III}	113
69.873	1.563	3	222
82.767	1.353	4	004
92.241	1.241	5	133
95.386	1.2094	3	024
108.116	1.1048	7	224
118.449	1.0410	4	(115)
138.442	0.9567	4	(333)
155.764	0.91484	6	044
165.074	0.9021	2	135
			(006)
			(244)

(I, II, III indicate the three strongest lines
in order)

TABLE 7.2

X-ray diffraction for various sulphide minerals

Sphalerite - NG39 dark coloured sphalerite, Lahanos Mine,
Ore Zone II, New Gallery

$$a_{A0} = 5.4118 \pm 0.0005 \text{ \AA}$$

$2\theta(\text{Co})$	d	I/I ₀ (Visual est.)	hkl
33.288	3.125	10 ^I	111
38.619	2.707	5	002
55.755	1.913	9 ^{II}	022
66.421	1.633	8 ^{III}	113
82.483	1.3568	3	004
92.161	1.2418	5	133
95.443	1.2088	3	024
108.258	1.1038	6	224
118.350	1.04165	4	(115) (333)
138.434	0.9565	4	044
155.795	0.91478	6	135
165.366	0.90180	1	(006) (244)

(I, II, III indicate the three strongest lines in order)

TABLE 7.3

X-ray diffraction for various sulphide mineralsGalena - NGD16 associated with sphalerite, Lahanos mine,
Ore Zone II, New Gallery

$$a_0 = 5.9367 \pm 0.0005 \text{ \AA}$$

$2\theta(C^\circ)$	d	I/I ₀	hkl
30.302	3.424	9 ^{II}	111
35.160	2.963	10 ^I	002
50.554	2.1956	8 ^{III}	022
60.065	1.7882	7	113
63.074	1.7113	5	222
74.245	1.4832	5	004
82.192	1.3756	3	133
84.866	1.3266	6	024
95.359	1.2106	4	224
103.106	1.1420	3	(115) (333)
117.176	1.0481	2	044
126.122	1.0033	3	135
129.371	0.99949	4	(006) (244)
144.715	0.93859	4	026
162.258	0.90529	1	335

(I, II, III indicate the three strongest lines in order)

TABLE 7.4

X-ray diffraction for various sulphide minerals

Galena - NGD17 associated with sphalerite and chalcopyrite, Lahanos mine,

Ore Zone II, New Gallery

$$a_0 = 5.9359 \pm 0.0005 \text{ \AA}^0$$

2 θ (Co)	d	I/I ₀ (Visual est.)	hkl
30.275	3.428	9 ^{II}	(111)
33.373	3.118	2	Sph (111)
35.171	2.962	10 ^I	(002)
50.559	2.19505	8 ^{III}	(022)
55.830	1.9115	3	Sph (022)
60.051	1.7886	7	(113)
63.049	1.7118	6	(222)
66.561	1.630	2	Sph (113)
74.165	1.4835	4	(004)
82.199	1.3606	5	(133)
84.782	1.3267	6	(024)
92.131	1.2421	1	Sph (133)
95.293	1.2103	6	(224)
103.087	1.1422	5	(115)
			(333)
108.158	1.1045	1	Sph (224)
116.996	1.0491	4	(044)
			(115)
118.400	1.04135	1	Sph (333)
			(135)
126.144	1.0032	5	(006)
129.460	0.9891	5	(244)
			(026)
144.754	0.9385	5	Sph (135)
155.820	0.91307	1	(335)
162.265	0.90528	2	

The impurity is sphalerite

(I; II, III indicate the three strongest lines in order)

TABLE 7.5

X-ray diffraction data for various sulphide minerals

Chalcopyrite - NGD8 associated with bornite, Lahanos mine, Ore
Zone 1, New Gallery

$$a_0 = 5.2895 \pm 0.0006, c = 10.423 \pm 0.003 \text{ \AA}^0$$

2θ (Co)	d	I/I ₀ (Visual est.)	hkl
34.286	3.037	10 ^I	(112)
39.584	2.644	3	(004) (020)
56.777	1.882	7	(220)
57.726	1.8538	9 ^{II}	(024)
68.447	1.5914	8 ^{III}	(132)
69.297	1.5742	5	(116) (033)
72.246	1.5184	1	(224)
85.215	1.322	4	(040)
86.740	1.3035	2	(008)
95.134	1.2119	2	(332)
95.959	1.2039	5	(136) (143)
112.303	1.0899	6	(244)
114.152	1.0656	4	(228)
123.123	1.01725	3	(152)
124.073	1.01275	3	(336)
126.072	1.00355	2	(1.1.10)

(I, II, III indicate the three strongest lines in order)

TABLE 7.6

X-ray diffraction data for various sulphide
minerals

Chalcopyrite - NG 36 associated with bornite, Lahanos mine, Ore

Zone I, New Gallery

$$a_0 = 5.288 \bar{\pm} 0.001, c = 10.428 \bar{\pm} 0.003 \text{ \AA}^{\circ}$$

2 θ (Co)	d	I/I ₀ (Visual est.)	hkl
34.260	3.0395	10 ^I	(112)
39.575	2.644	2	(004) (020)
57.165	1.871	6	(220)
57.675	1.85505	9 ^{II}	(024)
68.310	1.5942	7 ^{III}	(132)
69.150	1.5773	3	(116) (033)
72.925	1.5062	3	(224)
86.625	1.3039	2	(008)
95.165	1.2124	3	(332)
95.925	1.2051	3	(136) (143)
112.275	1.0772	5	(244)
113.575	1.0691	2	(228)
123.125	1.0172	2	(152)

(I, II, III indicate the three strongest lines in order)

TABLE 7.7

X-ray diffraction data for various sulphide minerals

Chalcopyrite - NG39 associated with sphalerite and pyrite, Lahanos mine, Ore Zone II, New Gallery

$$a_0 = 5.2901 \bar{\pm} 0.0007, c = 10.421 \bar{\pm} 0.002 \text{ \AA}^{\circ}$$

$2\theta(\text{Co})$	d	I/I ₀ (visual est.)	hkl
34.300	3.036	10 ^I	(112)
39.600	2.6425	3	(004) (020)
57.225	1.868	8 ^{III}	(220)
57.800	1.852	9 ^{II}	(024)
68.450	1.5914	7	(132)
69.300	1.573	6	(116) (033)
72.300	1.4996	1	(224)
85.200	1.3223	5	(040)
86.825	1.3015	2	(008)
95.125	1.2118	5	(332)
95.925	1.2042	6	(136) (143)
112.350	1.0777	6	(244)
113.625	1.0688	5	(228)
123.125	1.0172	4	(152)
124.075	1.0127	4	(336)
125.975	1.00395	3	(1.1.10)

(I, II, III indicate the three strongest lines in order)

TABLE 7.8

X-ray diffraction data for various sulphide minerals

Bornite - NGD8 associated with chalcopyrite, Lahanos mine, Ore Zone
I, New Gallery.

$$a_0 = 10.948 \bar{\pm} 0.004, c = 21.912 \bar{\pm} 0.006 \text{ \AA}^0$$

2 θ (Co.)	d	I/I ₀ (Visual est.)	hkl
25.424	4.068	3	(105) (213)
31.018	3.348	9 ^{II}	(026)
31.453	3.303	5	(116) (312)
32.892	3.162	8 ^{III}	(224)
34.930	2.983	1	(107) (321)
37.212	2.805	3	(305) (323)
38.136	2.740	7	(008) (400)
39.685	2.637	1	(217) (411)
42.057	2.494	4	(413) (325)
49.775	2.127	1	(425) (511)
50.274	2.1075	2	(336) (1.1.10)
55.094	1.9350	10 ^I	(440) (408)
57.692	1.855	1	(2.1.11)
65.609	1.6520	3	(624) (2.2.12)
69.005	1.5802	1	(448)
71.403	1.5339	1	(712) (1.1.14)
76.248	1.4497	3	(3.1.14) (5.3.10)
81.493	1.3713	2	(800) (0.016)
90.890	1.2553	1	(6.2.12)
96.309	1.2006	1	(844)
98.282	1.1826	1	(6.4.12)
106.374	1.1172	3	(4.4.16) (848)

(I, II, III, indicate the three strongest lines in order)

TABLE 7.9

X-ray diffraction data for various sulphide minerals

Bornite - NG36 associated with chalcopyrite, Lahanos Mine, Ore
Zone I, New Gallery

$$a_0 = 10.938 \pm 0.003, c = 21.887 \pm 0.005$$

2θ (Co)	d	I/I ₀ (visual est)	hkl
25.414	4.069	4	(105) (213)
31.487	3.2985	6	(116) (312)
32.896	3.161	9 ^{II}	(224)
34.511	3.018	1	(107) (321)
37.210	2.805	4	(305) (323)
38.184	2.737	7 ^{III}	(008) (400)
39.734	2.634	3	(217) (411)
41.383	2.534	6	(413) (325)
50.354	2.1045	4	(336) (1.1.10)
55.127	1.933	10 ^I	(440) (408)
57.876	1.850	3	(2.1.11)
65.698	1.650	5	(624) (2.2.12)
69.022	1.5798	2	(448)
71.496	1.532	3	(712) (1.1.14)
74.845	1.4731	2	(705) (723)
77.868	1.4242	4	(3.1.14) (5.3.10)
81.742	1.3679	4	(800) (0.0.16)
90.941	1.2547	2	(6.2.12)
93.740	1.2257	1	(4.0.16) (840)
96.309	1.2007	2	(844)
99.558	1.1714	1	(6.4.12)
116.166	1.0538	3	(2.2.20) (6.6.12)

(I, II, III indicate the three strongest lines in order)

TABLE 7.10

X-ray diffraction data for various sulphide minerals

Pyrite - NGD17 associated with sphalerite, chalcopyrite and galena,
Lahanos mine, ore zone II, New Gallery

$$a_0 = 5.4172 \pm 0.0005 \text{ \AA}$$

2 θ (Co)	d	I/I ₀ (visual est)	hkl
30.243	3.431	2	gl
33.293	3.125	5	(111)
34.218	3.043	1	Cpy
35.122	2.966	2	gl
38.627	2.7065	10 ^I	(200)
43.876	2.396	9 ^{II}	(210)
47.790	2.210	8 ^{III}	(211)
50.514	2.098	1	gl
55.773	1.913	7	(220)
59.513	1.8035	1	(300) (221)
66.486	1.6326	10 ^I	(311)
69.861	1.5632	4	(222)
73.160	1.50205	5	(320)
76.484	1.446	6	(321)
82.783	1.3538	1	(400)
85.857	1.3141	1	(410) (322)
89.052	1.2766	1	(411) (330)
91.626	1.2474	3	(331)
95.232	1.2109	4	(420)
98.402	1.1816	4	(421)
101.516	1.1548	3	(332)
107.985	1.1057	4	(422)
111.289	1.0835	1	(500) (430)
114.664	1.0626	1	(510) (431)
118.113	1.0429	7	(511) (333)
125.536	1.0060	6	(520) (432)
129.461	0.98902	6	(521)
138.114	0.9577	7	(440)
143.083	0.94295	1	(522) (441)
148.657	0.9290	1	(530) (433)
155.30	0.91563	2	(531)
164.354	0.90287	6	(600) (442)

Impurities are galena and chalcopyrite

(I, II, III indicate the three strongest lines in order)

TABLE 7.11

X-ray diffraction data for various sulphide minerals

Pyrite - NG18 anisotropic pyrite, Lahanos Mine, Ore Zone III,
New Gallery.

$$a_0 = 5.4183 \pm 0.0005 \text{ \AA}^0$$

2 θ (Co)	d	I/I ₀ (visual est.)	hkl
14.300	7.182	1	Kaolinite
23.100	4.47	1	Kaolinite
33.250	3.1285	5	(111)
38.700	2.702	7	(200)
40.900	2.562	7	Kaolinite?
43.150	2.434	8 ^{III}	(210)
47.775	2.2105	9 ^{II}	(211)
55.710	1.9157	5	(220)
59.520	1.8035	1	(300) (221)
66.459	1.6333	10 ^I	(311)
69.800	1.5644	2	(222)
73.225	1.50095	1	(320)
76.350	1.4481	5	(321)
82.700	1.3548	1	(400)
85.925	1.3133	1	(410) (322)
88.800	1.2794	1	(411) (330)
92.210	1.2422	2	(331)
95.326	1.2108	2	(420)
98.426	1.1822	2	(421)
101.626	1.1548	2	(332)
108.300	1.1035	2	(422)
111.310	1.08335	1	(500) (430)
118.066	1.04315	6	(511) (333)
125.576	1.0057	4	(520) (432)
129.466	0.98905	2	(521)
138.126	0.9577	3	(440)
148.650	0.9290	1	(530) (433)
155.126	0.91594	1	(531)
164.206	0.90302	3	(600) (442)

(I, II, III indicate the three strongest lines)

TABLE 7.12

X-ray diffraction data for various sulphide minerals

Pyrite - 94 massive pyrite, Lahanos mine, Ore Zone III, surface sample

$$a_0 = 5.4166 \pm 0.0005 \text{ \AA}$$

2 θ (Co)	d	I/I ₀ (visual est).	hkl
33.478	3.108	5	(111)
38.928	2.686	9 ^{II}	(200)
43.628	2.409	8 ^{III}	(210)
47.978	2.2015	8 ^{III}	(211)
55.930	1.908	7	(220)
59.654	1.7997	1	(300) (221)
66.780	1.6263	10 ^I	(311)
70.030	1.560	5	(222)
73.280	1.4998	6	(320)
76.532	1.4452	6	(321)
82.932	1.3518	1	(400)
86.032	1.312	1	(410) (322)
89.182	1.2751	1	(411) (330)
92.232	1.2411	4	(331)
95.342	1.2099	5	(420)
98.494	1.1808	5	(421)
101.644	1.1538	4	(332)
108.094	1.1050	5	(422)
111.420	1.08265	2	(500) (430)
114.870	1.0614	1	(510) (431)
118.246	1.0422	7	(511) (333)
125.546	1.0059	6	(520) (432)
129.546	0.98875	6	(521)
138.196	0.9575	7	(440)
143.098	0.9428	1	(522) (441)
148.622	0.92905	1	(530) (433)
155.374	0.91552	1	(531)
164.374	0.90285	6	(600) (442)

(I, II, III indicate the three strongest lines in order)

TABLE 7.13

X-ray diffraction data for various sulphide minerals

Sphalerite - M2 honey coloured sphalerite, Murgul mine.

$$a_0 = 5.4109 \pm 0.0005 \text{ \AA}$$

2 θ (Co)	d	I/I ₀ (visual est.)	hkl
33.323	3.1215	10 ^I	(111)
38.619	2.707	3	(200)
55.756	1.913	8 ^{III}	(220)
66.472	1.6319	9 ^{II}	(311)
69.819	1.5624	2	(222)
82.809	1.3524	3	(400)
92.301	1.2428	5	(331)
95.318	1.2101	1	(420)
173.129	1.0718	7	(422)
118.374	1.0415	4	(511) (333)
138.458	0.95656	3	(440)
155.919	0.91456	5	(531)
165.442	0.90172	1	(600) (244)

(I, II, III indicate the three strongest lines in order)

TABLE 7.14

X-ray diffraction data for various sulphide minerals

Sphalerite - M2 dark coloured sphalerite, Murgul mine.

$$a_0 = 5.4101 \pm 0.0005 \text{ \AA}$$

2 θ (Co)	d	I/I ₀ (visual est)	hkl
30.256	3.429	2	gl
33.280	3.125	10 ^I	(111)
34.229	3.042	1	Cpy
35.103	2.9675	2	gl
38.651	2.705	4	(200)
50.494	2.098	2	gl
55.791	1.9132	9 ^{II}	(220)
60.063	1.7884	1	gl
62.987	1.7132	1	gl
66.585	1.6306	8 ^{III}	(311)
69.933	1.5619	2	(222)
82.825	1.3532	4	(400)
84.749	1.3280	1	gl
92.233	1.24195	6	(331)
95.351	1.2098	2	(420)
108.044	1.10535	7	(422)
118.412	1.0413	5	(511) (333)
138.500	0.9565	5	(440)
156.040	0.91437	7	(531)
165.409	0.90175	1	(600) (244)

Impurities are gl and cpy

(I, II, III indicate the three strongest lines in order)

TABLE 7.15

X-ray Diffraction data for various sulphide minerals

Galena - M2 associated sphalerite and little chalcopyrite, Murgul mine.

$$a_0 = 5.9353 \pm 0.0005 \text{ \AA}$$

$2\theta(\text{Co.})$	d	I/I_0 (visual est)	hkl
30.325	3.421	9 ^{II}	(111)
35.161	2.9625	10 ^I	(200)
50.549	2.0965	8 ^{III}	(220)
60.061	1.7884	7	(311)
62.999	1.713	5	(222)
74.235	1.4832	5	(400)
82.184	1.3619	4	(331)
84.842	1.3269	6	(420)
95.139	1.2118	5	(422)
103.062	1.14245	4	(511) (333)
117.046	1.0488	3	(440)
126.094	1.0034	6	(531)
129.441	0.9892	6	(600) (442)
144.729	0.93855	6	(620)
162.415	0.9051	1	(533)

(I, II, III indicate the three strongest lines in order)

TABLE 7.16

X-ray Diffraction Data for various sulphide minerals

Chalcopyrite - M12 associated with sphalerite, Murgul Mine.

$$a_0 = 5.2888 \pm 0.0022, c = 10.4252 \pm 0.005 \text{ \AA}$$

2θ (Co.)	d	I/I ₀ (visual est.)	hkl
29.413	3.523	10 ^I	(112)
33.086	3.144	3	Sph
33.861	3.074	3	(004) (020)
34.436	3.024	2	(112)
43.182	2.433	2	py
47.505	2.222	2	py
48.705	2.1705	9 ^{II}	(220)
49.130	2.153	1	(024)
56.352	1.8957	3	
57.876	1.850	8 ^{III}	(132)
58.576	1.8297	7	(116) (033)
71.246	1.5367	4	(040)
72.421	1.5153	2	(008)
78.893	1.4087	6	(332)
79.568	1.3987	6	(136) (143)
91.401	1.2498	5	(244)
92.201	1.2414	2	(228)

Impurities are pyrite and sphalerite

(I, II, III indicate the three strongest lines in order)

TABLE 7.17.

X-ray diffraction data for various sulphide minerals

Chalcopyrite - M15 associated with sphalerite and pyrite, Murgul mine

$$a_0 = 5.2888 \pm 0.0017, c = 10.4171 \pm 0.005 \text{ \AA}$$

2θ (Co)	d	I/I ₀ (visual est.)	hkl
34.315	2.034	10 ^I	(112)
39.635	2.640	3	(004) (020)
57.192	1.8702	7	(220)
57.767	1.853	9 ^{II}	(024)
66.558	1.6532	1	sph
68.481	1.5907	8 ^{III}	(132)
69.330	1.5737	5	(116) (033)
72.327	1.5169	2	(224)
85.214	1.3222	4	(040)
86.813	1.3026	2	(008)
95.185	1.2113	3	(332)
95.960	1.20395	5	(136) (143)
112.358	1.0767	6	244
113.677	1.0685	5	228
118.212	1.0424	1	Sph
123.157	1.01705	3	(152)
124.081	1.01270	3	(336)
126.054	1.00362	2	(1.1.10)

Impurity is sphalerite

(I, II, III indicate the three strongest lines in order)

TABLE 7.18

X-ray diffraction data for various sulphide minerals

Sphalerite - Kd. brownish sphalerite, Karadere mine, Ünye

$$a_0 = 5.4124 \pm 0.0005 \text{ \AA}$$

2 θ (Cu)	d	I/I ₀ (visual est.)	hkl
28.569	3.1242	10 ^I	(111)
33.068	2.7087	4	(200)
47.540	1.9126	9 ^{II}	(220)
56.228	1.6359	8 ^{III}	(311)
59.033	1.5635	1	(222)
69.386	1.3532	4	(400)
76.734	1.2410	7	(331)
79.109	1.2095	1	(420)
88.377	1.1050	7	(422)
95.417	1.0412	4	(511) (333)
107.740	0.95366	5	(440)
114.689	0.91486	6	(531)
128.366	0.85564	6	(620)
137.904	0.82533	3	(533)
160.914	0.78107	2	(444)

(I, II, III indicate the three strongest lines in order)

TABLE 7.19

X-ray diffraction data for various sulphide minerals

Sphalerite - Kd. honey coloured sphalerite, Karaders mine, Unye "

$$a_0 = 5.4119 \pm 0.0005 \text{ \AA}^0$$

2θ (Co)	d	I/I ₀ (Visual est.)	hkl
30.043	3.454	1	g1
33.318	3.122	10 ^I	(111)
36.152	2.8845	1	g1
38.642	2.7055	3	(200)
55.788	1.913	9 ^{II}	(220)
59.613	1.801	1	py
60.847	1.7675	1	g1
66.561	1.6312	8 ^{III}	(311)
69.926	1.5618	2	(222)
82.783	1.3528	4	(400)
92.113	1.2432	6	(331)
95.342	1.20985	3	(420)
108.075	1.10505	7	(422)
118.293	1.04196	6	(511) (333)
138.409	0.9568	5	(440)
155.780	0.91481	7	(531)
165.153	0.902015	2	(600) (244)

Impurities are galena and pyrite

(I, II, III indicate the three strongest lines in order)

TABLE 7.20

X-ray diffraction data for various sulphide minerals

Sphalerite - Kd. Greenish translucent sphalerite, Karadere mine, Unye

$$a_0 = 5.4119 \pm 0.0005 \text{ \AA}$$

2θ (Co)	d	I/I ₀ (visual est.)	hkl
30.050	3.4525	1	g1
33.248	3.1285	10 ^I	(111)
38.644	2.706	4	(200)
55.780	1.91035	9 ^{II}	(220)
57.279	1.8675	1	Cpy
60.326	1.7812	1	g1
66.496	1.6324	8 ^{III}	(311)
69.894	1.5626	2	(222)
82.858	1.3517	3	(400)
92.251	1.2409	6	(331)
95.293	1.21035	2	(420)
108.158	1.10465	7	(422)
118.355	1.0416	5	(511) (333)
138.459	0.95664	5	(440)
155.785	0.91480	6	(531)
165.187	0.901975	2	(600) (244)

Impurities are galena and Cpy

(I, II, III indicate the three strongest lines in order)

TABLE 7.21

X-ray diffraction data for various sulphide mineralsSphalerite - Kd. dark coloured sphalerite, Karadere mine,
Unye

$$a_0 = 5.4142 \pm 0.0005 \text{ \AA}$$

2θ (Cu)	d	I/I ₀ (visual est.)	hkl
28.563	3.125	10 ^I	(111)
33.061	2.7094	4	(200)
47.505	1.9122	9 ^{II}	(220)
56.402	1.6313	8 ^{III}	(311)
59.126	1.561	1	(222)
69.547	1.3505	4	(400)
76.644	1.2425	6	(331)
79.043	1.2104	1	(420)
88.339	1.10545	7	(422)
95.359	1.03175	4	(511) (333)
107.180	0.95718	4	(440)
114.652	0.91505	5	(531)
117.226	0.90225	1	(600)
128.246	0.85607	5	(620)
137.777	0.82567	4	(533)
141.391	0.81867	3	
160.608	0.78142	2	(444)

(I, II, III indicate the three strongest lines in order)

TABLE 7.22

X-ray diffraction data for various sulphide minerals

Galena - Kd. galena from mixed ore, Karadere Mine, Ünye

$$a_0 = 5.9355 \pm 0.0005 \text{ \AA}$$

2θ (Co)	d	I/I ₀ (visual est.)	hkl
30.337	3.420	9 ^{II}	(111)
35.210	2.9604	10 ^I	(200)
50.579	2.097	8 ^{III}	(220)
60.140	1.7862	7	(311)
63.099	1.7106	4	(222)
74.295	1.4827	4	(400)
82.342	1.3597	3	(331)
84.941	1.3256	6	(420)
95.359	1.21055	5	(422)
103.231	1.14195	4	(511) (333)
117.201	1.04795	2	(440)
126.172	1.0031	5	(531)
129.471	0.98905	5	(600) (244)
144.790	0.93840	5	(620)
162.383	0.90773	1	(533)

(I, II, III indicate the three strongest lines in order)

TABLE 7.23

X-ray diffraction data for various sulphide minerals

Galena - Kd. galena rich ore, Karadere mine, Unye "

$$a_0 = 5.9352 \pm 0.0005 \text{ \AA}$$

2θ (Co)	d	I/I ₀ (visual est.)	hkl
30.350	3.4196	9 ^{II}	(111)
35.225	2.9575	10 ^I	(200)
50.625	2.0932	8 ^{III}	(220)
60.175	1.7852	7	(311)
63.085	1.7109	2	(222)
74.325	1.4818	1	(400)
82.300	1.3602	2	(331)
84.850	1.3268	7	(420)
95.400	1.2102	4	(422)
103.275	1.14155	3	(511) (333)
117.225	1.0479	2	(440)
126.175	1.00305	6	(531)
129.500	0.98895	6	(600) (244)
144.775	0.93842	5	(620)
162.475	0.90502	1	533

(I, II, III indicate the three strongest lines in order)

TABLE 7.24

X-ray diffraction data for various sulphide minerals

Chalcopyrite - Kd. in mixed ore, Karadere mine, Ünye

$$a_0 = 5.2909 \bar{\pm} 0.0011, c = 10.423 \bar{\pm} 0.003 \text{ \AA}^{\circ}$$

2θ (Co)	d	I/I ₀ (visual est.)	hkl
30.200	3.4355	1	g1
34.247	3.0405	10 ^I	(112)
35.921	2.902	1	g1
37.170	2.8085	1	
39.518	2.648	3	(004) (020)
55.905	2.0825	2	Sph
57.129	1.872	7	(220)
57.703	1.855	9 ^{II}	(024)
68.356	1.5932	8 ^{III}	(132)
69.269	1.5749	7	(116) (033)
72.207	1.5192	1	(224)
85.231	1.3219	4	(040)
86.855	1.3021	2	(008)
95.143	1.21265	4	(332)
95.993	1.20365	5	(136) (143)
112.280	1.07718	6	(244)
113.529	1.0694	3	(228)
123.121	1.01705	3	(152)
124.020	1.0130	3	(336)
125.869	1.00445	1	(1.1.10)

(I, II, III indicate the three strongest lines in order)

TABLE 8

Comparative cell-size determination of various sulphide minerals
from Eastern Pontus Ore Province

<u>SPHALERITE</u> (Sph), ZnS, Z = 4, F $\bar{4}$ 3m pure ZnS. Ivanov, 1964 <u>LAHANOS</u> light coloured sphalerite NG39 Associated with cpy. NGD8 Associated with cpy. NG36	a_0 5.3985 \pm 0.0001 5.4125 \pm 0.0005 { $a_0 = 10.948 \pm 0.004$ $c = 21.912 \pm 0.006$ $a_0 = 10.938 \pm 0.003$ $c = 21.887 \pm 0.005$
<u>PYRITE</u> (py), FeS ₂ , Z = 4, P3a pure FeS ₂ . Berry and Mason, 1959 <u>LAHANOS</u> Associated with Sph, cpy. and gl. NGD17 Anisotropic pyrite NG18 Massive pyrite ore 94	5.417 5.4172 \pm 0.0005 5.4183 \pm 0.0005 5.4166 \pm 0.0005
<u>TETRAHEDRITE</u> , Cu ₁₂ Sb ₄ S ₁₃ , Z = 2, I $\bar{4}$ 3m pure Cu ₁₂ Sb ₄ S ₁₃ . Berry and Mason, 1959 <u>INKÖY</u> associated gl. and sph. H.A.I.A.	10.37 - 10.48 10.317 \pm 0.0005

microprobe work can be used to fix the composition more accurately. In some cases, the optical properties of a very small grain are insufficiently measurable for exact diagnosis and here again the probe can be used for identification, without the need for a full quantitative study. Finally, the optical properties of a mineral may differ sufficiently from those of known and expected minerals that a quantitative analysis is required for identification. A Cambridge Instrument Company 'Geoscan' electron microprobe analyser was therefore used for qualitative and quantitative study of certain minerals in the Lahanos ore. Examples of its use to obtain qualitative or semiquantitative results are now fairly common in the literature, so although such techniques were used, they will not be described here. The methods used for quantitative analysis will be described by Greenwood (1969) and details of the operating conditions used in the present work are given in Table 9. Correction of the raw counter data for background, drift and dead time was carried out using the Olivetti "Programma 101" desk computer. A computer programme for atomic number, fluorescence and mass absorption corrections in silicates based on Long's method and written in KDF9 Algol by Padfield and Aucott was modified by inserting the appropriate values for elements in sulphide minerals. These were obtained from Philibert, (1963); Reed, (1965); Duncomb and Shields, (1966), and Duncomb and Reed, (1967).

Quantitative results obtained are as follows -

TABLE 9

Operating conditions for electron microprobe analyser

<u>Element</u>	<u>kv</u>	<u>Crystal</u>	<u>2θ</u>	<u>Back-ground</u>	<u>E</u>	<u>ΔE</u>	<u>Lines</u>	<u>Slit</u>	<u>Counter</u>	<u>Time sec.</u>
Pb	15	Quartz	104.29	$\bar{+}$ 1.00	1.90	2.40	M	Out	FC	20
Bi	20	LiF	32.45	$\bar{+}$ 1.30	7.80	2.10	L	Out	SC	20
Au	15	LiF	36.49	$\bar{+}$ 1.30	5.47	1.80	L	Out	SC	20
Te	15	Quartz	58.52	$\bar{+}$ 1.30	1.75	0.95	L	Out	SC	20
Sb	15	Quartz	61.53	$\bar{+}$ 1.20	0.93	1.00	L	Out	SC	20
Ag	15	Quartz	76.49	$\bar{+}$ 1.30	0.85	2.00	L	Out	SC	20
As	15	LiF	33.57	$\bar{+}$ 1.30	7.10	2.30	K	Out	SC	20
Zn	15	LiF	41.37	$\bar{+}$ 1.30	4.71	2.10	K	Out	SC	20
Cu	15	LiF	44.59	$\bar{+}$ 1.30	3.75	2.50	K	Out	SC	20
Ni	15	LiF	48.37	$\bar{+}$ 1.30	3.20	2.50	K	Out	SC	20
Co	15	Quartz	31.20	$\bar{+}$ 1.30	2.60	1.20	K	Out	SC	20
Fe	15	Quartz	33.40	$\bar{+}$ 2.0	2.73	2.50	K	In	SC	20
Cr	15	Quartz	40.30	$\bar{+}$ 1.30	2.70	0.70	K	Out	SC	20
S	15	Quartz	106.44	$\bar{+}$ 1.30	2.00	2.60	K	Out	FC	20

Enargite

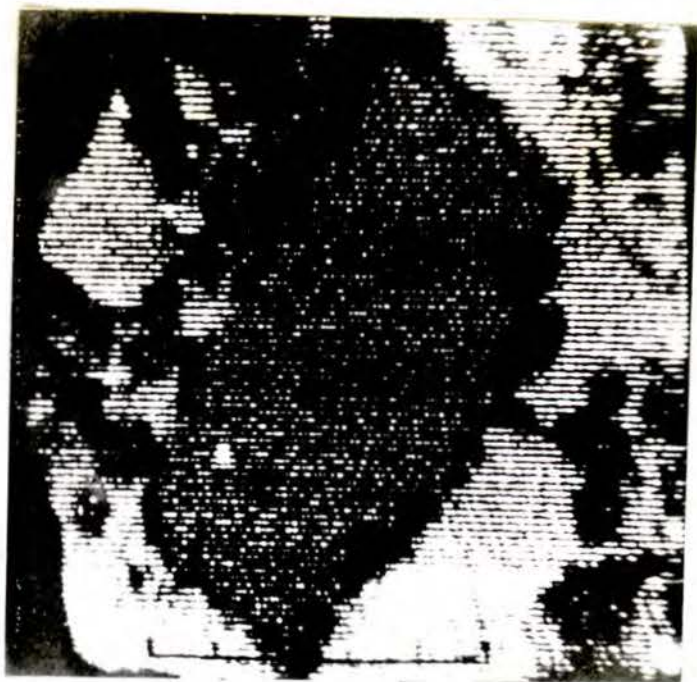
Tables 10. 1-6 give the corrected analysis for six enargite specimens from Zone II together with recalculations of the corresponding atomic formulae for comparison with the theoretical formula $\text{Cu}_3 \text{As S}_4$. In each case the result is regarded as in satisfactory agreement with this formula, since the numbers of atoms are mainly within 10% of the theoretical value. Qualitative X-ray images for an enargite are shown in Plate 32, 49 A-C.

Tetrahedrite - Tennantite

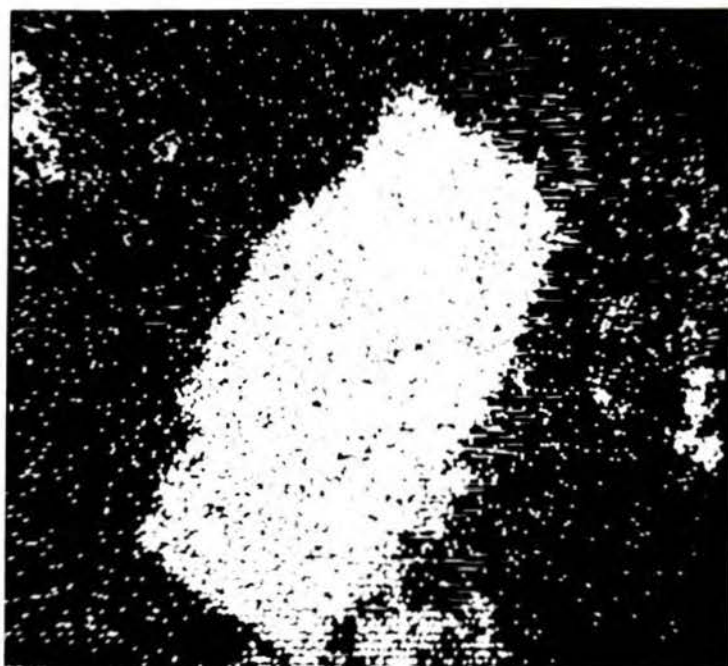
The mineralogy of the sulphosalt minerals has not in the past been well known because of the difficulty of obtaining sufficiently pure material for chemical analysis. As a result, many of the formulae given for particular species can be regarded only as approximations to the true formula. Thus, for tetrahedrite the formulae $\text{Cu}_3 \text{Sb S}_3$ and $\text{Cu}_{12} \text{Sb}_4 \text{S}_{13}$ are both quoted.

As written, the second of these formulae suggests a slight excess of sulphur over 4 ($\text{Cu}_3 \text{Sb S}_3$), but in fact it is more than likely that this might result from cation deficiencies. This can be suggested by writing the formula as $\text{Cu}_{2.77} \text{Sb}_{0.92} \text{S}_3$.

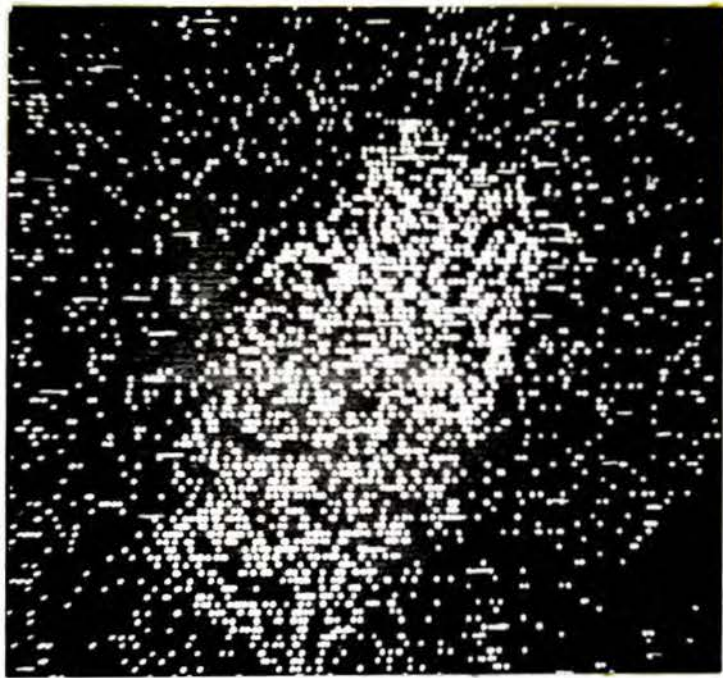
The structure of tetrahedrite and principles governing substitution of one element for another in the structure are insufficiently well known for firm conclusions to be made on the extent to which a given analysis represents a possible tetrahedrite composition. In the case of analysis by microprobe the results are calculated to a total of 100% , and this would be so even if



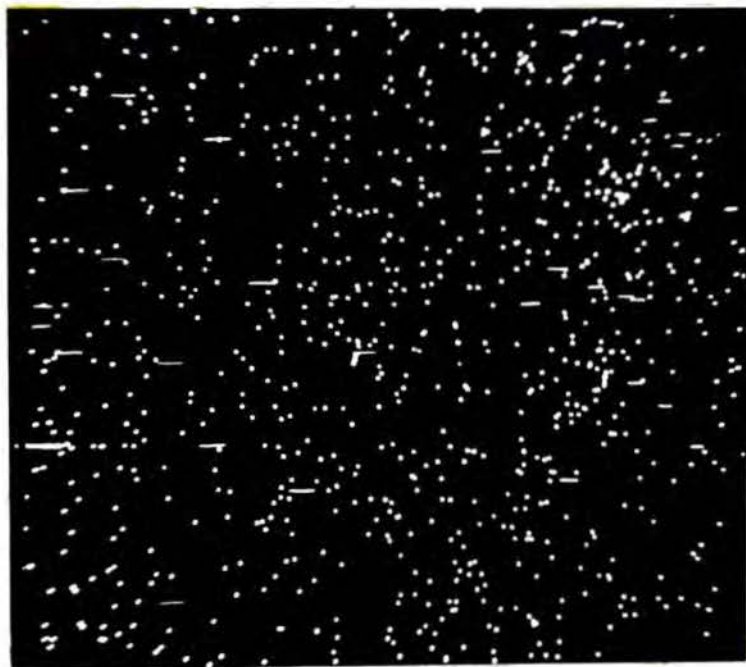
Pl. 49. The electron image of Plate 32, ore Zone II. 225 x



Pl. 49A. The X-ray image of Cu in Plate 32, ore Zone II. 225 x



Pl. 49B. The X-ray image of As in Plate 32, ore Zone II. 225 x



Pl. 49C. The X-ray image of Sb in Plate 32, ore Zone II. 225 x

TABLE 10.1

Enargite No. 49 II, Lahanos, Ore Zone II

<u>Element</u>	<u>Wt.%</u>	<u>Atomic Wt.</u>	<u>Atomic Proportions</u>	<u>Atoms to One Sulphur</u>	<u>Atoms to 4 Sulphur</u>
S	32.65	32.064	1.0180	1	4
Se	n.d.				
Te	nil	127.60			
As	19.07	74.94	0.2545	0.2500	1.000
Sb	0.15	121.75	0.0012	0.0012	0.0048
Bi	nil	208.98			
Cu	47.90	63.54	0.7538	0.7405	2.9624
Ag	nil	107.87			
Au	0.11	196.96	0.0006	0.0006	0.0024
Fe	0.12	55.84	0.0021	0.0021	0.0084
Co	nil	58.94			
Ni	nil	58.71			
Mn	n.d.				
Zn	nil	65.37			
Pb	nil	207.19			

Atomic formula = $\text{Cu}_{2.96} \text{As S}_4$

TABLE 10.2

Enargite No.48 I, Lahanos, Ore Zone II

<u>Element</u>	<u>Wt. %</u>	<u>Atomic Wt.</u>	<u>Atomic Proportions</u>	<u>Atoms to One sulphur</u>	<u>Atoms to 4 Sulphur</u>
S	34.8	32.064	1.0629	1	4
Se	n.d.				
Te	nil	127.60			
As	18.82	74.94	0.2512	0.2363	0.9456
Sb	0.14	121.75	0.0011	0.0010	0.0040
Bi	0.21	208.98	0.0010	0.0009	0.0036
Cu	46.74	63.54	0.7356	0.6921	2.7684
Ag	nil	107.87			
Au	nil	196.96			
Fe	nil	55.84			
Co	nil	58.94			
Ni	nil	58.71			
Mn	n.d.				
Zn	nil	65.37			
Pb	nil	207.19			

Atomic formula = $\text{Cu}_{2.77} \text{As}_{0.95} \text{S}_4$

TABLE 10.3

Enargite, No. 48 II, Lahanos, Ore Zone II

<u>Element</u>	<u>Wt.%</u>	<u>Atomic Wt.</u>	<u>Atomic Proportions</u>	<u>Atoms to One Sulphur</u>	<u>Atoms to 4 Sulphur</u>
S	34.86	32.064	1.0872	1	4
Se	n.d.				
Te	nil	127.60			
As	18.61	74.94	0.2484	0.2285	0.9140
Sb	nil	121.75			
Bi	0.36	208.98	0.0016	0.0001	0.0004
Cu	45.55	63.54	0.7169	0.6594	2.6376
Ag	nil	107.87			
Au	0.62	196.96	0.0031	0.0003	0.0012
Fe	nil	55.84			
Co	nil	58.94			
Ni	nil	58.71			
Mn	n.d.				
Zn	nil	65.37			
Pb	nil	207.19			

Atomic formula = $\text{Cu}_{2.64} \text{As}_{0.91} \text{S}_4$

TABLE 10.4

Enargite No.48.IIIA, Lahanos Ore Zone II

<u>Element</u>	<u>Wt.%</u>	<u>Atomic wt.</u>	<u>Atomic proportions</u>	<u>Atoms to one sulphur</u>	<u>Atoms to four sulphur</u>
S	34.79	32.064	1.0850	1	4
Se	n.d.				
Te	nil	127.60			
As	17.90	74.94	0.2389	0.2202	0.8808
Sb	nil	121.75			
Bi	nil	208.98			
Cu	47.02	63.54	0.7400	0.6820	2.7280
Ag	nil	107.87			
Au	0.29	196.96	0.0015	0.0001	0.0004
Fe	nil	55.84			
Co	nil	58.94			
Ni	nil	58.71			
Mn	n.d.				
Zn	nil	65.37			
Pb	nil	207.19			

Atomic formula = $\text{Cu}_{2.72} \text{As}_{0.88} \text{S}_4$.

TABLE 10.5

Enargite No. 48IIIB, Lahanos, Ore Zone II

<u>Element</u>	<u>Wt.%</u>	<u>Atomic Wt.</u>	<u>Atomic Proportions</u>	<u>Atoms to one sulphur</u>	<u>Atoms to 4 sulphur</u>
S	33.99	32.064	1.0601	1	4
Se	n.d.				
Te	nil	127.60			
As	18.43	74.94	0.2460	0.2321	0.9284
Sb	0.06	121.75	0.0005	0.0005	0.0020
Bi	nil	208.98			
Cu	47.09	63.54	0.7411	0.6991	2.7964
Ag	nil	107.87			
Au	0.42	196.96	0.00213	0.0020	0.0080
Fe	nil	55.84			
Co	nil	58.94			
Ni	nil	58.71			
Mn	n.d.				
Zn	nil	65.37			
Pb	nil	207.19			

Atomic formula = $\text{Cu}_{2.80} \text{As}_{0.92} \text{S}_4$

TABLE 10.6

Enargite No. 43 I, Lahanos, Ore Zone II

<u>Element</u>	<u>Wt. %</u>	<u>Atomic wt.</u>	<u>Atomic Proportions</u>	<u>Atoms to one sulphur</u>	<u>Atoms to 4 sulphur</u>
S	33.07	32.064	1.0314	1	4
Se	n.d.				
Te	nil	127.60			
As	17.43	74.94	0.2326	0.2255	0.9024
Sb	1.67	121.75	0.0137	0.0133	0.0532
Bi	nil	208.98			
Cu	47.83	63.54	0.7528	0.7299	2.9196
Ag	nil	107.87			
Au	nil	196.96			
Fe	nil	55.84			
Co	nil	58.94			
Ni	nil	58.71			
Mn	n.d.				
Zn	nil	65.37			
Pb	nil	207.19			

Atomic formula = $\text{Cu}_{2.92} \text{As}_{0.95} \text{S}_4$

some one or more elements present had not been determined, so that the microprobe analyses do not fix the composition with certainty. Because of these problems it is not at present possible to compare a sulphosalt formula as carefully with the theoretical formula as is possible, for example, in the case of various silicate minerals.

The analyses given in Tables 11.1 - 11.5 are therefore recalculated to a basis of three sulphur atoms and quoted without attempting to explain in each case the departure from theoretical $\text{Cu}_3 \text{Sb S}_3$. The case of the mineral named "ferroan tennantite" (Table 11.3) is, however worth further discussion. Its ordinary light colour is a bluish gray, suggestive of a member of the tetrahedrite-tennantite series. However, it is slightly pleochroic and shows strong anisotropism with pinkish red brown to yellow polarisation colours. This would then suggest a member of the bournonite-seligmannite group, but the probe shows that lead is not present. The formula recalculated to three sulphur atoms is $\text{Cu}_{2.79} \text{As}_{0.65} \text{S}_3$. For comparison theoretical tennantite is $\text{Cu}_{2.77} \text{As}_{0.92} \text{S}_3$ (assuming $\text{Cu}_{12} \text{As}_4 \text{S}_{13}$) and theoretical enargite $\text{Cu}_{2.25} \text{As}_{0.75} \text{S}_3$ (assuming $\text{Cu}_3 \text{As S}_4$). Thus, this mineral has anisotropy similar to enargite and less As than enargite, but the colour of tennantite and almost exactly the copper content of tennantite. If one could regard iron as a possible substitution for arsenic as well as copper, the formula could be written to correspond with a solid solution of composition intermediate between

TABLE II.1.

Zincian tetrahedrite No.49 III, Lahanos,
Ore Zone II

<u>Element</u>	<u>Wt.%</u>	<u>Atomic Wt.</u>	<u>Atomic Proportions</u>	<u>Atoms to 3 sulphur</u>
S	23.23	32.064	0.7244	3
Se	n.d.			
Te	nil	127.60		
As	4.21	74.94	0.0562	0.0221
Sb	21.86	121.75	0.1795	0.7437
Bi	nil	208.98		
Cu	46.91	63.54	0.7383	3.0576
Ag	nil	107.87		
Au	0.02	196.96	0.0001	0.0003
Fe	0.06	55.84	0.0011	0.0045
Co	nil	58.94		
Ni	0.02	58.71	0.0003	0.0012
Mn	n.d.			
Zn	3.69	65.37	0.0564	0.2337
Pb	nil	207.19		

Atomic formula = $\text{Cu}_{3.30} \text{Sb}_{0.77} \text{S}_3$

Table 11.2

Zincian tennantite-tetrahedrite ('Zanbergerite') No. 48 IV,
Lahanos, Ore Zone II

<u>Element</u>	<u>Wt.%</u>	<u>Atomic Wt.</u>	<u>Atomic Proportion</u>	<u>Atoms to 3 sulphur</u>
S	27.61	32.064	0.8611	3
Se	n.d.			
Te	nil	127.60		
As	9.53	74.94	0.1272	0.4434
Sb	15.30	121.75	0.1257	0.4380
Bi	0.84	208.98	0.0040	0.0138
Cu	39.95	63.54	0.6287	2.1903
Ag	nil	107.87		
Au	nil	196.96		
Fe	0.20	55.84	0.0036	0.0126
Co	nil	58.94		
Ni	nil	58.71		
Mn	n.d.			
Zn	6.58	65.37	0.1007	0.3507
Pb	nil	207.19		

Atomic formula = $\text{Cu}_{2.55} (\text{As Sb})_{0.90} \text{S}_3$

TABLE 11.3

Ferroan tennantite No. 43 III, Lahanos, Ore Zone II

<u>Elements</u>	<u>Wt.%</u>	<u>Atomic Wt.</u>	<u>Atomic proportions</u>	<u>Atoms to 3 sulphur</u>
S	30.02	32.064	0.9363	3
Se	n.d.			
Te	nil	127.60		
As	15.30	74.94	0.2042	0.6546
Sb	0.14	121.75	0.0011	0.0036
Bi	nil	208.98		
Cu	45.24	63.54	0.7120	2.2812
Ag	0.14	107.87	0.0013	0.0042
Au	0.40	196.96	0.0020	0.0063
Fe	8.55	55.84	0.1531	0.4905
Co	nil	58.94		
Ni	0.20	58.71	0.0034	0.0108
Mn	n.d.			
Zn	nil	65.37		
Pb	nil	207.19		

Atomic formula = $\text{Cu}_{2.79} \text{As}_{0.65} \text{S}_3$

TABLE 11.4

Zincian Tetrahedrite H.A.1A, Ink8y

<u>Elements</u>	<u>Wt.%</u>	<u>Atomic Wt.</u>	<u>Atomic Proportions</u>	<u>Atoms to 3 sulphur</u>
S	28.11	32.064	0.8767	3
Se	n.d.			
Te	nil	127.60		
As	3.87	74.94	0.0516	0.1766
Sb	26.98	121.75	0.2216	0.7584
Bi	nil	208.98		
Cu	36.24	63.54	0.5703	1.9517
Ag	0.03	107.87	0.0003	0.0010
Au	nil	196.96		
Fe	0.84	55.84	0.0150	0.0513
Co	nil	58.94		
Ni	0.05	58.71	0.0008	0.0027
Zn	3.89	65.37	0.0595	0.2036
Mn	n.d.			
Pb	nil	207.19		

Atomic formula = $\text{Cu}_{2.21} \text{Sb}_{0.94} \text{S}_3$

TABLE 11.5

Zincian Tetrahedrite H.A.1B, Inköy

<u>Elements</u>	<u>Wt.%</u>	<u>Atomic wt.</u>	<u>Atomic Proportions</u>	<u>Atoms to 3 sulphur</u>
S	26.7	32.064	0.8162	3
Se	n.d.			
Te	nil	127.60		
As	6.10	74.94	0.0814	0.2992
Sb	21.16	121.75	0.1738	0.6387
Bi	nil	208.98		
Cu	38.04	63.54	0.5987	2.2003
Ag	0.13	107.87	0.0012	0.0044
Au	nil	196.96		
Fe	1.09	55.84	0.0195	0.0717
Co	nil	58.94		
Ni	nil	58.71		
Mn	n.d.			
Zn	7.30	65.37	0.1117	0.4105
Pb	nil	207.19		

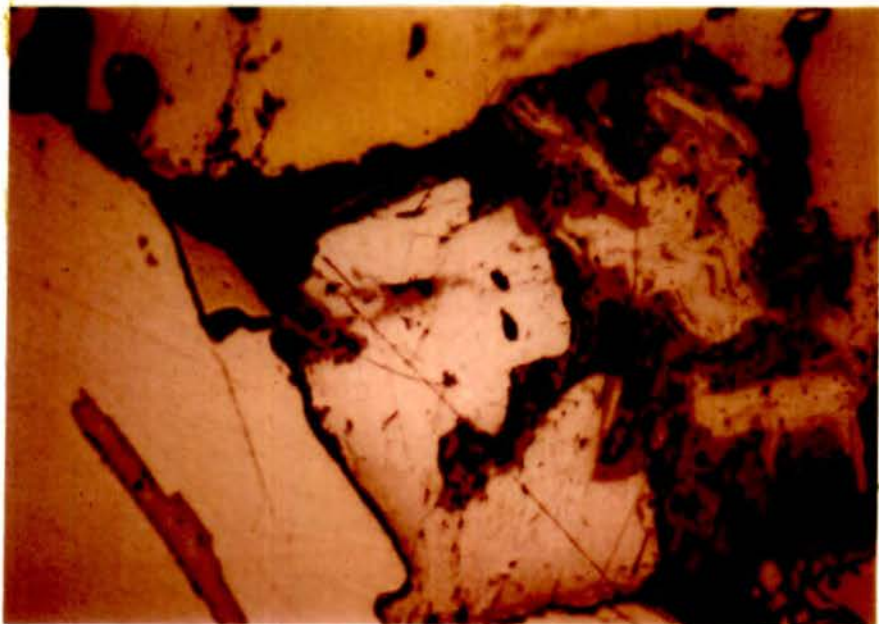
Atomic formula = $\text{Cu}_{2.68} \text{Sb}_{0.94} \text{S}_3$

enargite and tennantite. Obviously, more work on these minerals is required, preferably in cases where more material is available than in the present ore.

The "Zincian tetrahedrite-tennantite" shows essentially equal amounts of As and Sb. According to Batley and Tomkeieff (1957) a similar mineral has been called Zandbergerite by Kostov (1957).

Bismuth-Tellurium-Sulphur minerals

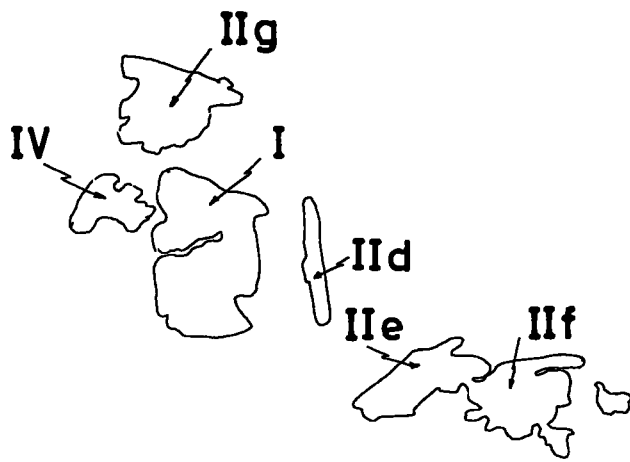
Within and marginal to the pyrite of ore zones II and III, whitish coloured grains up to $\frac{1}{2}$ mm in size and of similar reflectivity to pyrite may occasionally be seen (Plates 50A, 50B and 50C). The grains are strongly anisotropic, with grey white polarisation colours at both 45 degree positions and straight extinction. Their optical properties suggest tetradymite, $\text{Bi}_2\text{Te}_2\text{S}$. Plate 51 shows grains of this type, several of which have been analysed quantitatively with the microprobe. The results are given in Tables 12.1 - 12.9 and recalculated in various ways. Plates 51 A-E are qualitative pictures of one of the grains. Calculated on the basis of one sulphur atom in the formula the amounts of bismuth and tellurium approximate to the expected values for tetradymite, but nevertheless show differences that are thought to be significant. Recalculation to $(\text{S} + \text{Te}) = 3$ and $(\text{S} + \text{Te}) = 4$ gives no closer approach to any recognised Bi - Te - S mineral. The variation between analyses is such that taking an average composition seems to be justified. The result of this calculation is shown in Table 12.6 and can be regarded as indicating tetradymite with 8% solid

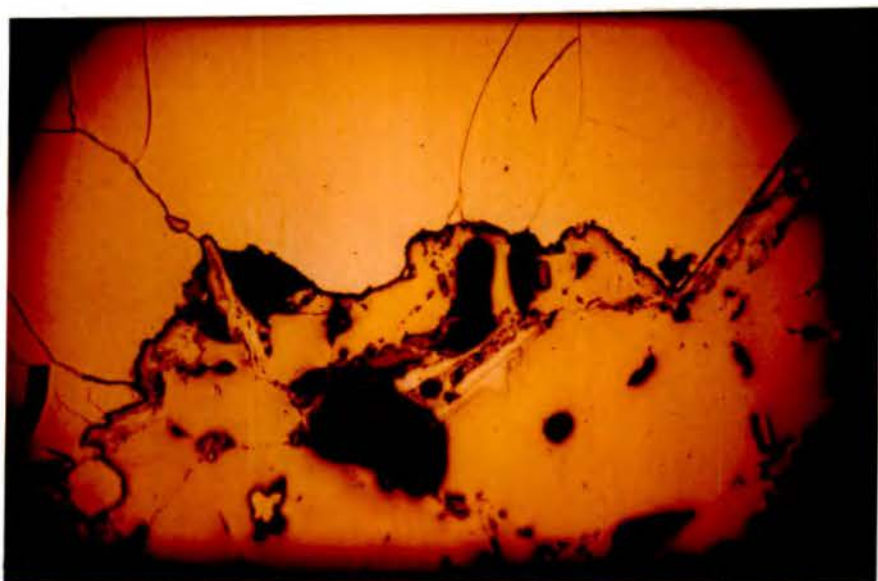


Pl. 50A. General view of tetradymite (Bi-Te-S) mineral in association with pyrite, chalcopyrite and tennantite. 375 x

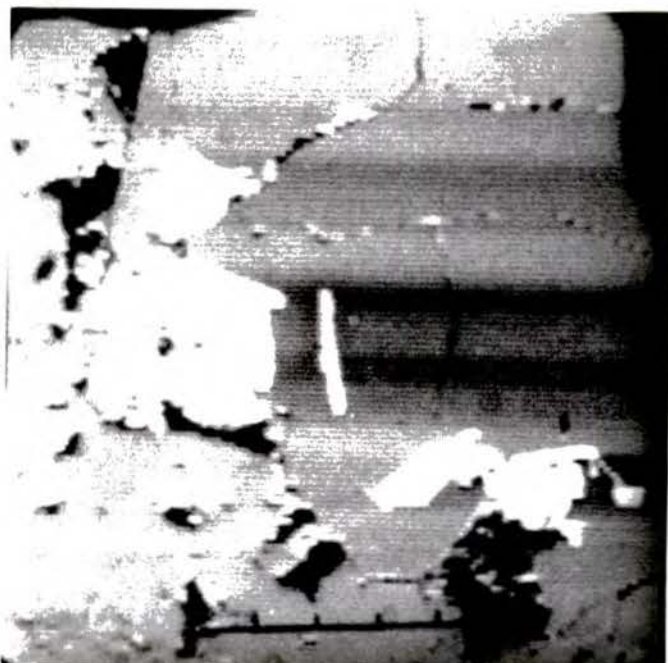


Pl. 50B. Right hand corner of Plate 50 at higher magnification. 875 x





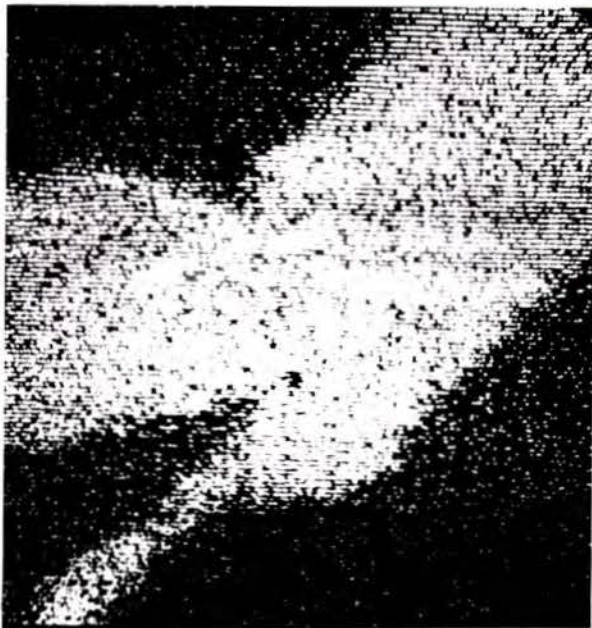
Pl. 50C. The second group of (Bi-Te-S) mineral association with pyrite and chalcopyrite. 70 x



Pl. 51. The backscattered electron image of Plate 50A, Lahanos mine. 125 x



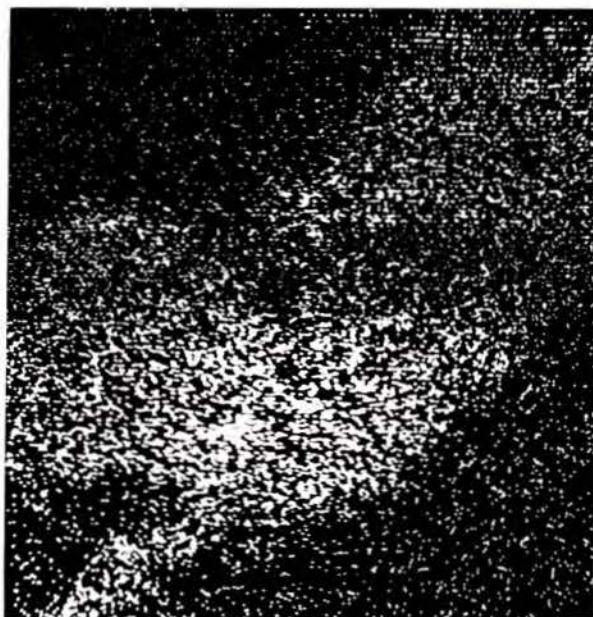
Pl. 51A. The backscattered electron image of the grain IIe. 1000 x



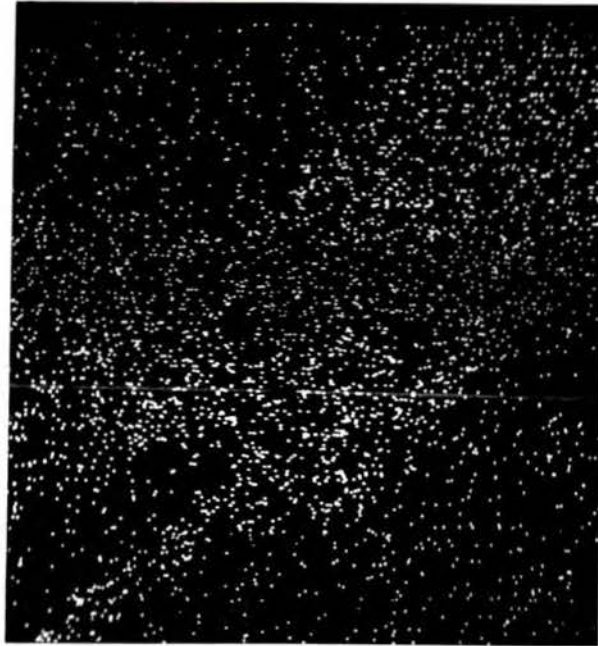
Pl. 51B. The X-ray image of Bi in the sample IIe. 1000 x



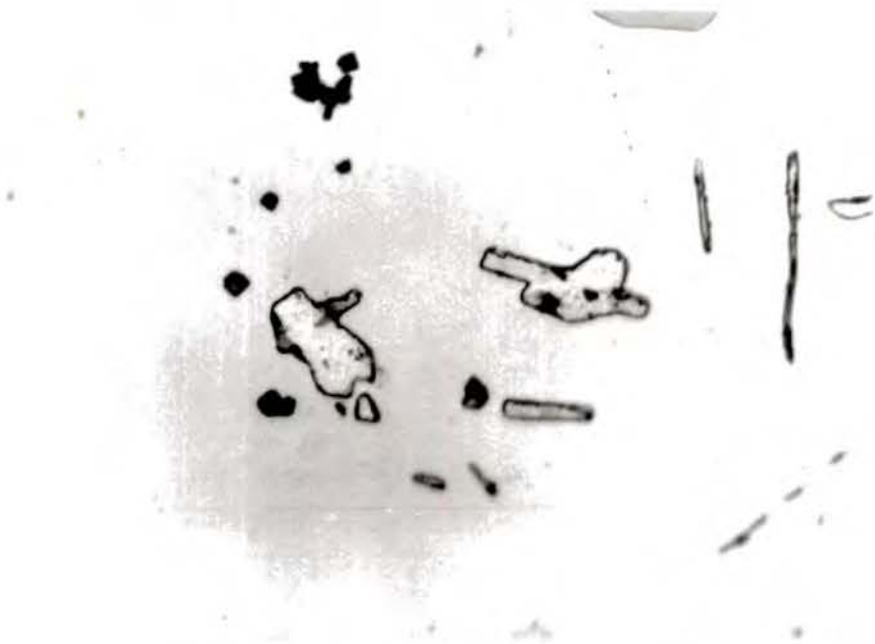
Pl. 51C. The X-ray image of Te in the sample IIe. 1000 x



Pl. 51D. The X-ray image of As in the sample IIe. 1000 x



Pl. 51E. The X-ray image of Au in the sample IIe. 1000 x



Pl. 52. Occurrences of Te-S-(Bi) mineral in ore Zone III pyrite, Lahanos. 875 x



solution of hedleyite $\text{Bi}_2 \text{Te}_3 \text{Bi}_5$. However, the status of these bismuth-tellurium minerals is in some doubt because of limited information. The average gold content of this mineral (0.04%) is of some interest. It should be noted that whilst native gold has been found in Zone I, the gold content of the Zones II and III ores must come partly from the tetradymite.

The analyses of two further grains, of similar appearance to the above and occurring in the same polished section are given in Tables 12.7 and 12.8. Compared with the average analysis of Table 12.6 and with each other these show slight but probably significant differences in the ratio of sulphur to tellurium.

Finally, a grain again optically similar to the remaining grains gave the analysis shown in Table 12.9. In this case, the amount of sulphur relative to tellurium is again increased, and there is a notable decrease in the amount of bismuth. The formula can be represented as 18% $\text{Bi}_2 \text{S}_3$, 82% $\text{Bi}_2 \text{Te}_2 \text{S}$ again a variation not covered by the existing nomenclature.

Within the pyrite of ore zone III, and also to a less extent in pyrite of zones II and IV, occasional small grains (5 to 40 microns) are seen of a white mineral similar colour to tetradymite but having a reflectivity noticeable higher than that of pyrite. (Plate 52). The grains are too small for reflectivity measurement with the apparatus at present available, but the reflectivity is estimated to be about 60%. The mineral is pleochroic and strongly anisotropic, showing blue or bluish yellow polarisation colours

TABLE 12.1

Tetradymite No. Ed, Lahanos

<u>Element</u>	<u>Wt.%</u>	<u>Atomic Wt.</u>	<u>Atomic Proportions</u>	<u>Atoms to one sulphur</u>	<u>Atoms to 3 (S + Te)</u>
S	3.80	32.064	0.1185	1	0.922
Se	n.d.				
Te	34.10	127.60	0.2672	2.255	2.078
As	0.73	74.94	0.0097	0.0818	0.076
Sb	0.16	121.75	0.0013	0.011	0.010
Bi	60.14	208.98	0.2877	2.427	2.237
Cu	0.08	63.54	0.0012	0.010	0.009
Ag	nil	107.87			
Au	0.99	196.96	0.0050	0.042	0.039
Fe	nil	55.84			
Co	nil	58.94			
Ni	nil	58.71			
Mn	n.d.				
Zn	nil	65.37			
Pb	nil	207.19			

TABLE 12.2

Tetradymite No. Ee, Lahanos

<u>Element</u>	<u>Wt.%</u>	<u>Atomic Wt.</u>	<u>Atomic Proportions</u>	<u>Atoms to one sulphur</u>	<u>Atoms to 3(S+Te)</u>
S	3.60	32.064	0.1122	1	0.898
Se	n.d.				
Te	33.50	127.60	0.2625	2.339	2.102
As	0.88	74.94	0.0117	0.1043	0.094
Sb	0.13	121.75	0.0010	0.009	0.008
Bi	60.46	208.98	0.2893	2.578	2.316
Cu	0.08	63.54	0.0012	0.011	0.010
Ag	0.03	107.87	0.0003	0.002	0.002
Au	1.32	196.96	0.0067	0.597	0.054
Fe	nil	55.84			
Co	nil	58.94			
Ni	nil	58.71			
Mn	n.d.				
Zn	nil	65.37			
Pb	nil	207.19			

TABLE 12.3

Tetradymite No. Ef, Lahanos

<u>Element</u>	<u>Wt.%</u>	<u>Atomic Wt.</u>	<u>Atomic Proportions</u>	<u>Atoms to one sulphur</u>	<u>Atoms to 3 (S + Te)</u>
S	3.88	32.064	0.1210	1	0.951
Se	n.d.				
Te	33.27	127.60	0.2607	2.154	2.049
As	0.09	74.94	0.0012	0.0099	0.094
Sb	0.24	121.75	0.0019	0.016	0.016
Bi	61.49	208.98	0.2942	2.431	2.312
Cu	0.24	63.54	0.0038	0.031	0.029
Ag	nil	107.87			
Au	0.82	196.96	0.0041	0.034	0.032
Fe	nil	55.84			
Co	nil	58.94			
Ni	nil	58.71			
Mn	n.d.				
Zn	nil	65.37			
Pb	nil	207.19			

TABLE 12.4

Tetradymite No. Eg, Lahanos

<u>Element</u>	<u>Wt.%</u>	<u>Atomic Wt.</u>	<u>Atomic Proportions</u>	<u>Atoms to one sulphur</u>	<u>Atoms to 3 (S + Te)</u>
S	3.49	32.064	0.1088	1	0.872
Se	n.d.				
Te	33.87	127.60	0.2654	2.439	2.128
As	0.19	74.94	0.0025	0.023	0.020
Sb	0.60	121.75	0.0049	0.045	0.039
Bi	61.15	208.98	0.2926	2.689	2.346
Cu	0.15	63.54	0.0023	0.021	0.018
Ag	0.09	107.87	0.0008	0.007	0.006
Au	0.46	196.96	0.0023	0.021	0.018
Fe	nil	55.84			
Co	nil	58.94			
Ni	nil	58.71			
Mn	n.d.				
Zn	nil	65.37			
Pb	nil	207.19			

TABLE 12.5

Tetradymite No. Ei, Lahanos

<u>Element</u>	<u>Wt.%</u>	<u>Atomic Wt.</u>	<u>Atomic Proportions</u>	<u>Atoms to one sulphur</u>	<u>Atoms to 3 (S+Te)</u>
S	4.00	32.064	0.1247	1	0.981
Se	n.d.				
Te	32.74	127.60	0.2566	2.058	2.019
As	0.48	74.94	0.0064	0.051	0.050
Sb	0.19	121.75	0.0016	0.013	0.013
Bi	61.42	208.98	0.2939	2.357	2.312
Cu	0.71	63.54	0.0112	0.090	0.088
Ag	0.09	107.87	0.0008	0.006	0.006
Au	0.36	196.96	0.0018	0.014	0.010
Fe		55.84			
Co		58.94			
Ni		58.71			
Mn					
Zn		65.37			
Pb		207.19			

TABLE 12.6

Average of Ed, Ee, Ef, Eg and Ei

<u>Elements</u>	<u>Wt.%</u>	<u>Atomic Wt.</u>	<u>Atomic Proportions</u>	<u>Atoms to one sulphur</u>	<u>Atoms to 3 (S+Te)</u>
S	3.75	32.064	0.1170	1	0.925
Se	n.d.				
Te	33.50	127.60	0.2625	2.2436	2.075
As	0.47	74.94	0.0063	0.0538	0.050
Sb	0.26	121.75	0.0021	0.0179	0.016
Bi	60.93	208.98	0.2916	2.4923	2.305
Cu	0.25	63.54	0.0039	0.0333	0.031
Ag	0.04	107.27	0.0004	0.0034	0.003
Au	0.79	196.96	0.0040	0.0361	0.033
Fe	nil	55.84			
Co	nil	58.94			
Ni	nil	58.71			
Mn	n.d.				
Zn	nil	65.37			
Pb	nil	207.19			

TABLE 12.7Tetradymite, No. Ej, Lahanos

<u>Element</u>	<u>Wt.%</u>	<u>Atomic Wt.</u>	<u>Atomic Proportions</u>	<u>Atoms to one sulphur</u>	<u>Atoms to 3 (S+Te)</u>
S	4.38	32.064	0.1366	1	1.0299
Se	n.d.				
Te	33.34	127.60	0.2613	1.913	1.9701
As	0.40	74.94	0.0053	0.039	0.040
Sb	0.08	121.75	0.0006	0.004	0.005
Bi	61.33	208.98	0.2935	2.148	2.212
Cu	0.44	63.54	0.0069	0.050	0.051
Ag	0.04	107.87	0.0004	0.003	0.003
Au	nil	196.96			
Fe	nil	55.84			
Co	nil	58.94			
Ni	nil	58.71			
Mn	n.d.				
Zn	nil	65.37			
Pb	nil	207.19			

TABLE 12.8

Tetradymite No. Eh, Lahanos

<u>Element</u>	<u>Wt. %</u>	<u>Atomic Wt.</u>	<u>Atomic Proportions</u>	<u>Atoms to one sulphur</u>	<u>Atoms to 3(S + Te)</u>
S	5.50	32.064	0.1715	1	1.232
Se	n.d.				
Te	31.43	127.60	0.2463	1.436	1.768
As	0.46	74.94	0.0061	0.036	0.044
Sb	0.18	121.75	0.0015	0.009	0.011
Bi	60.53	208.98	0.2896	1.689	2.080
Cu	1.54	63.54	0.0242	0.141	0.174
Ag	0.04	107.87	0.0004	0.002	0.002
Au	nil	196.96			
Fe	0.32	55.84	0.0057	0.033	0.041
Co	nil	58.94			
Ni	nil	58.71			
Mn	n.d.				
Zn	nil	65.37			
Pb	nil	207.19			

TABLE. 12.9

Tetradymite No. Ek, Lahanos

<u>Element</u>	<u>Wt.%</u>	<u>Atomic Wt.</u>	<u>Atomic Proportions</u>	<u>Atoms to one sulphur</u>	<u>Atoms to 3 (S+Te)</u>
S	6.71	32.064	0.2092	1	1.351
Se	n.d.				
Te	32.14	127.60	0.2552	1.2198	1.649
As	0.30	74.94	0.0040	0.019	0.026
Sb	0.20	121.75	0.0016	0.008	0.011
Bi	59.75	208.98	0.2859	1.3666	1.847
Cu	0.90	63.54	0.0142	0.0678	0.092
Ag	nil	107.87			
Au	nil	196.96			
Fe	nil	55.84			
Co	nil	58.94			
Ni	nil	58.74			
Mn	n.d.				
Zn	nil	65.37			
Pb	nil	207.19			

TABLE 12.10

Tellurium - Sulphur mineral OG 37, Lahanos

<u>Element</u>	<u>Wt.%</u>	<u>Atomic Wt.</u>	<u>Atomic Proportions</u>	<u>Atoms to one Sulphur</u>
S	14.58	32.064	0.4547	1
Se	n.d.			
Te	67.06	127.60	0.5255	1.1557
As	0.40	74.94	0.0053	0.0116
Sb	0.49	121.75	0.0040	0.0088
Bi	16.47	208.98	0.0788	0.1733
Cu	0.77	63.54	0.0121	0.0266
Ag	nil	107.87		
Au	0.23	196.96	0.0011	0.0024
Fe	nil	55.84		
Co	nil	58.94		
Ni	nil	58.74		
Mn	n.d.			
Zn	nil	65.37		
Pb	nil	207.19		

and complete extinction. These properties suggest tellurobismuth but the microprobe analysis shown in Table 12.10 does not confirm this. The composition is unlike that of any established mineral and the microprobe results are believed to be reliable. The re-calculated analysis suggests slightly impure TeS. However, in the absence of more abundant material or the opportunity for additional work, it is not possible to consider this further.

E.Id3 Reflectivity:

The reflectivity apparatus described by Phillips and Nichol (1965), Nichol (1962) and Phillips and Bradshaw (1966), with later modification of the photomultiplier tube attachment and circuit constants by Burton (1967) to improve linearity and stability, was used to measure the spectral reflectivity of various minerals. The continuous interference filter monochromator (Veril B-200, Jena Glassworks, Mainz No B-34716) has the following characteristics -

Wave length	450	550	650
Transmission%	37	36	30
Half height width (nm)	26	26	34

Linearity of response of the photomultiplier was checked by the method described by Phillips & Bradshaw (1966) and results are given in Tab. 13. No significant departure from linearity was detected. The apparatus was left switched on continuously over a period of several days whilst the measurements were being made to ensure greater stability. Measurements were made at intervals of 20 nm from 440 nm up to 660 nm.

When the optical system and the photomultiplier are ready, a black box reading is taken - this is the correction (C) for primary glare due to reflection from the back of the objective. Readings were first taken for the standard then for the specimen (G'_{sp}) and again for the standard. The arithmetic mean of the readings for the standard is expressed as (G'_{st}). Then the desired

TABLE 13

Linearity of response of the photomultiplier

<u>Stage Readings</u> <u>θ (in degrees)</u>	<u>Galvo Readings</u> <u>v (in millivolts)</u>
90	141.0
85	119.0
80	100.0
75	80.0
70	59.8
65	42.4
60	27.3
55	15.0
50	6.32
45	1.32
44	0.81
43	0.43
42	0.24
41	0.20
40	0.31
39	0.605
38	1.10
37	1.66
35	3.35
30	10.50
25	21.20
20	35.10
15	52.50
10	71.10
5	92.00
0	111.20
355	113.20

value (R_{sp}) for the reflectivity of the specimen is obtained from the following equation:

$$\frac{R_{sp}}{R_{st}} = \frac{(G'_{sp} - C)}{(G'_{st} - C)} \quad \text{or}$$

$$\frac{R_{sp}}{R_{st}} = \frac{G_{sp}}{G_{st}}$$

Standards calibrated by N.P.L. were used, namely Black glass No. 2538.4, Carborundum No. 2538.27, Silicon No. 2538.37 and their reflectivity values are given in Tab. 14.

Results obtained for chalcopyrite from the Lahanos mine are shown in Table 15 and Figs. 20 and 20A. None of the measured Lahanos specimens showed any detectable anisotropy, so that it was not possible to relate the measurements to a specific optical or crystallographic direction. The spread of results seen in Fig. 20A may be due to differences in the quality of polish and other errors of measurement, since no significant difference in cell size was found in the cases where this data was available. However, there are slight differences in colour visible under the microscope between some of these specimens and it is believed that the differences in measured reflectivity, particularly between 600 and 660 nm, are significant. It may be that small amounts of certain trace elements can appreciably affect the reflectivity, without any corresponding detectable difference in the cell parameters. There is insufficient information to check this thoroughly, but the results given for NG31, NGD43-46, and K in Table 23 suggest that arsenic and silver might act in this way. Chalcopyrite

TABLE 14

N.P.L. Reflectivity values for Standards

<u>Wave-length</u> <u>n.m.</u>	<u>Black glass</u> <u>No. 2538.4</u>	<u>Carborundum</u> <u>No. 2538.27</u>	<u>Silicon</u> <u>No. 2538.37</u>
440	4.52	21.0	43.1
460	4.50	20.8	41.3
480	4.49	20.6	39.9
500	4.47	20.5	38.9
520	4.46	20.4	38.0
540	4.44	20.3	37.2
560	4.43	20.2	36.6
580	4.42	20.1	36.0
600	4.41	20.0	35.5
620	4.40	20.0	35.1
640	4.39	19.9	34.8
660	4.38	19.9	34.4

TABLE 15

Reflectivity measurements of
Chalcopyrite

Sample No.	<u>440 nm</u>	<u>460 nm</u>	<u>480 nm</u>	<u>500 nm</u>	<u>520 nm</u>	<u>540 nm</u>	<u>560 nm</u>	<u>580 nm</u>	<u>600 nm</u>	<u>620 nm</u>	<u>640 nm</u>	<u>660 nm</u>
OG39(1) NGD4 (light)	26.680	32.033	37.256	40.888	43.588	45.709	47.717	49.045	49.187	48.884	48.599	49.910
NGD4 (dark)	27.634	32.665	37.751	41.618	44.213	46.505	48.109	49.226	49.746	49.535	49.805	50.166
NG31(1)	27.634	33.261	38.468	42.047	44.177	46.552	48.109	49.138	49.082	49.839	49.166	48.733
NG31(2)	24.925	30.508	35.695	39.881	42.614	44.980	46.943	47.860	48.571	48.046	48.842	49.536
NG32	24.776	29.940	35.644	39.881	42.732	45.025	47.511	48.027	48.571	48.334	48.842	49.536
NG35	18.309	23.896	29.417	34.341	37.792	40.500	42.709	44.622	45.196	45.172	45.755	45.866
NG39	25.035	30.687	35.792	39.894	42.700	44.859	46.744	48.085	48.746	49.169	49.092	48.160
NGD	26.534	32.332	37.466	41.468	44.054	46.176	47.954	49.195	49.351	49.465	49.092	48.160
43-46m	19.973	25.472	31.161	35.984	39.239	41.810	43.769	45.536	46.165	46.043	46.607	46.784
E	26.221	31.801	37.004	41.232	44.052	46.385	48.412	49.294	49.517	49.675	49.092	48.160
K	26.673	32.048	37.215	40.982	43.531	45.742	47.481	48.517	48.602	48.485	48.471	48.160
M1	25.262	30.608	36.234	40.417	43.063	45.502	47.330	48.319	48.870	48.808	48.720	48.160
M2	26.390	31.742	37.063	41.062	44.097	46.135	47.767	48.910	49.046	49.140	49.622	48.168
M3	25.766	31.316	36.466	40.719	43.440	45.900	47.767	48.734	49.201	49.140	49.622	48.168
M12	25.922	31.572	36.739	40.762	43.399	45.900	47.588	48.822	49.201	49.140	49.622	48.168
M24(max)	25.922	31.316	36.577	40.891	43.645	46.323	47.886	48.910	49.513	49.140	49.622	48.168
M24(min)	26.078	31.486	36.685	40.805	43.358	45.712	47.648	48.734	49.201	48.834	48.977	46.784
Kd 2c	26.078	31.486	36.631	40.426	43.029	45.288	47.171	47.764	48.267	48.834	48.977	46.784

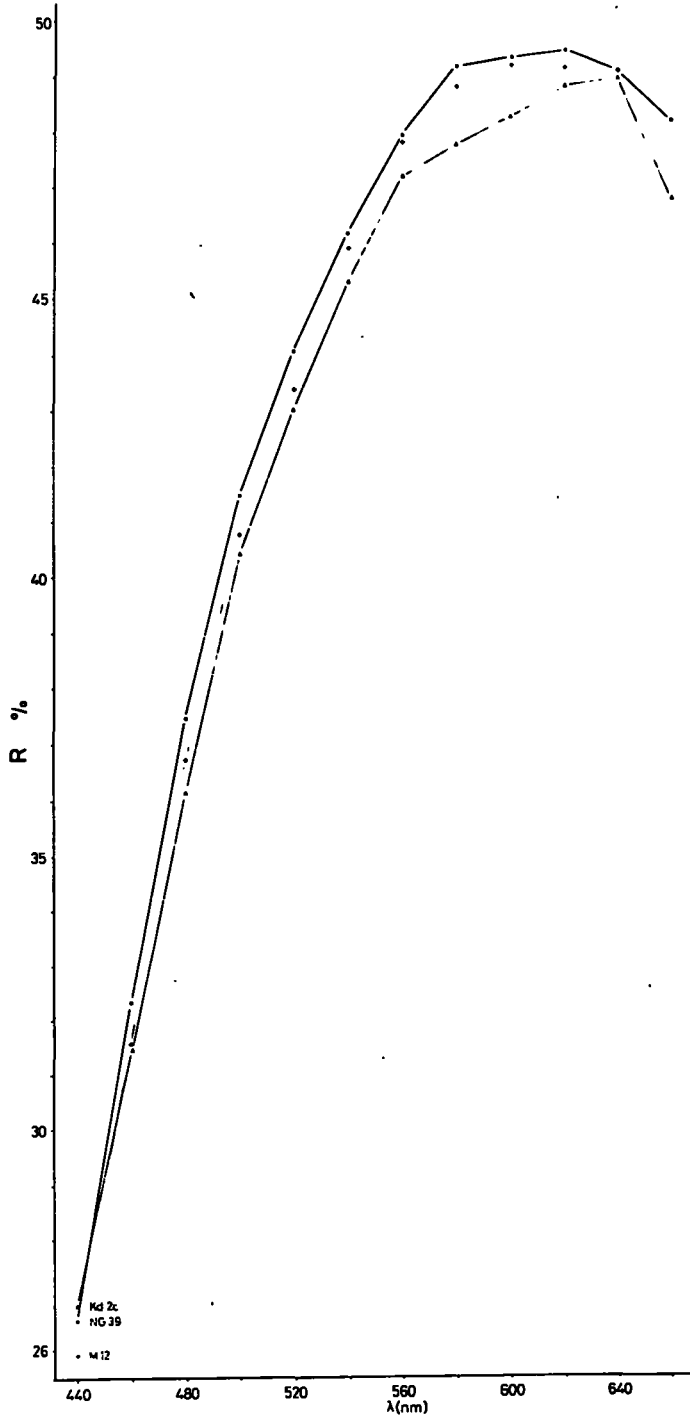


FIG 20 - Dispersion curves of chalcopyrite from the Karadere, Lahanos and Murgul mines.

• Karadere chalcopyrite $a=522 \text{ \AA}$, $c=104230 \text{ \AA}$ • Lahanos chalcopyrite $a=52901$, $c=104215 \text{ \AA}$ • Murgul chalcopyrite $a=52887$, $c=104252 \text{ \AA}$

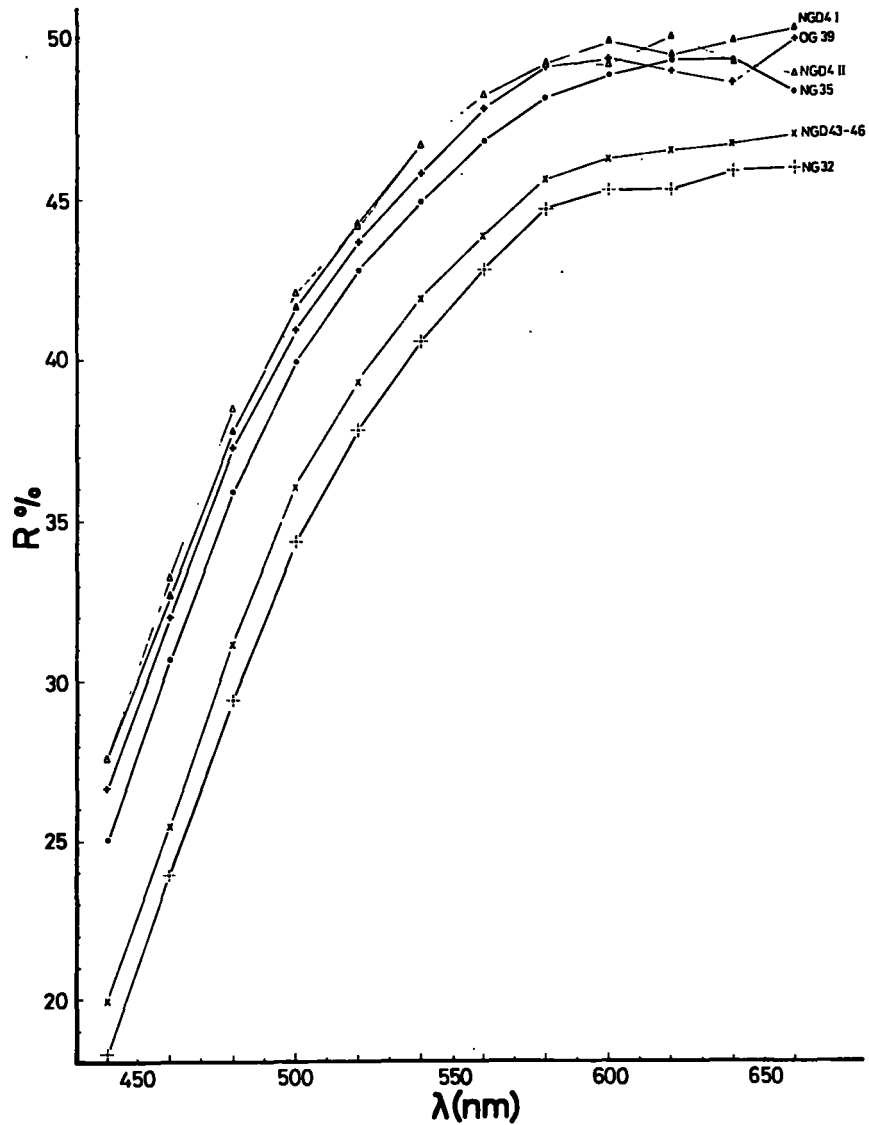


FIG. 20A...The spectral reflectivity of chalcopyrites from the Lahanos mine

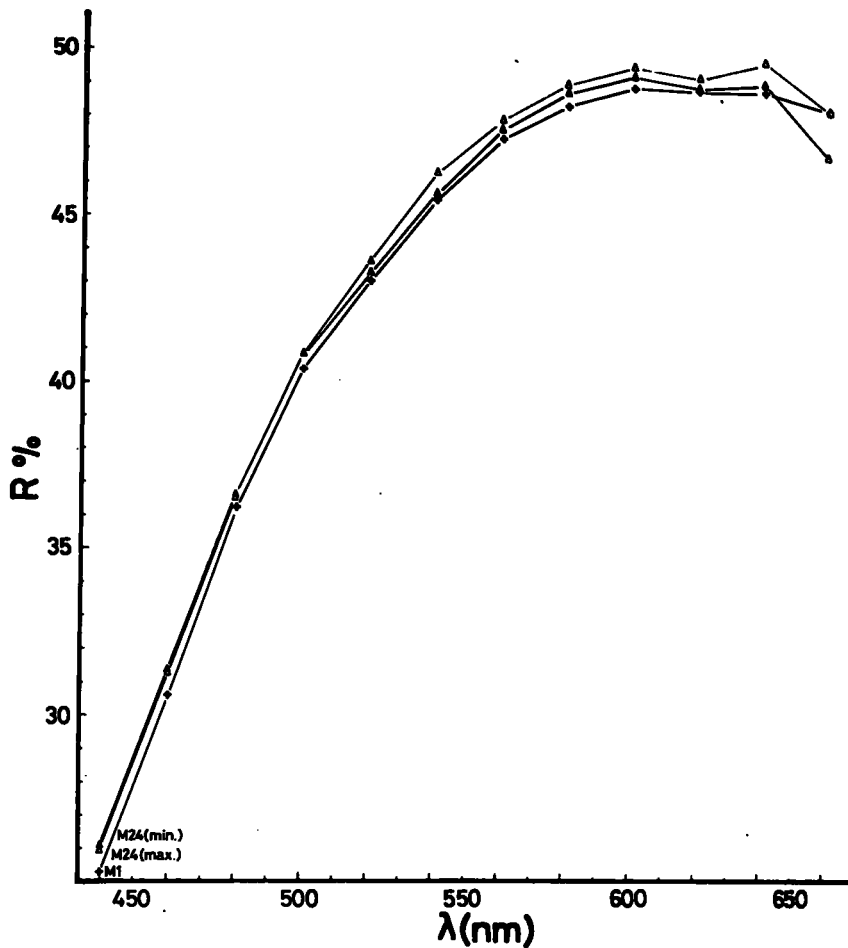


FIG. 20B...The spectral reflectivity of chalcopyrites from the Murgul mine

associated with pyrite from Zone III seems to have a significantly lower reflectivity than chalcopyrite from Zones I and II.

Enargite ($\text{Cu}_3 \text{AsS}_4$) - Reflectivity measurements on two grains from ore Zone II are shown in Tab. 16 and Fig. 21A. The values are lower than those given by Ramdohr (1950, pp. 398 and 402) and OrceI (1935), but compare closely with those given by Lévy (1966, pp. 109-110) and shown in Fig. 21B for comparison. The orientation of the grains is not known and Lévy's values are also for randomly oriented grains. The observed bireflection is therefore likely to be less than the true maximum for enargite. There was an insufficient number of measurable grains to use the method of Phillips and Ware (1967). Lévy's curves for luzonite and stiboluzonite are very different in form from those for enargite. Thus, the Lahanos material is identified as the higher temperature form, enargite, and not low temperature luzonite, and must have been formed at a temperature above 320°C (Barton and Skinner, 1967).

Bornite ($\text{Cu}_5 \text{FeS}_4$) - Tab. 17. According to Morimoto and Kullerud (1961), the form of bornite stable at room temperature is a tetragonal polymorph, but owing to twinning, the apparent symmetry may also be cubic or orthorhombic. In the present study, bornite examined by X-ray powder diffraction was insufficiently pure to allow these detailed aspects of the structure to be examined. In polished section the bornite at Lahanos normally appears isotropic, but using very strong illumination, a weak anisotropy can sometimes be seen, as described for example, in the account of ore Zone I.

TABLE 16

Spectral reflectivity measurements
of enargite

<u>Sample No.</u>	<u>440 nm</u>	<u>460 nm</u>	<u>480 nm</u>	<u>500 nm</u>	<u>520 nm</u>	<u>540 nm</u>	<u>560 nm</u>	<u>580 nm</u>	<u>600 nm</u>	<u>620 nm</u>	<u>640 nm</u>	<u>660 nm</u>
OG48 (max)	29.236	28.735	28.369	28.425	28.331	28.295	27.945	28.124	28.110	28.034	28.111	28.743
OG48 (min)	26.652	26.694	26.423	26.010	25.449	24.907	24.507	24.182	24.160	24.482	24.761	25.715
OG49 (max)	26.011	26.093	26.069	26.118	25.979	25.773	25.635	25.491	25.781	26.159	26.700	27.107
OG49 (min)	25.681	25.730	25.724	25.550	25.124	25.054	24.173	23.962	24.641	24.289	24.741	24.256

TABLE 17

Reflectivity measurements of bornite

<u>Sample No.</u>	<u>440 nm</u>	<u>460 nm</u>	<u>480 nm</u>	<u>500 nm</u>	<u>520 nm</u>	<u>540 nm</u>	<u>560 nm</u>	<u>580 nm</u>	<u>600 nm</u>	<u>620 nm</u>	<u>640 nm</u>	<u>660 nm</u>
NG-D3	17.448	17.086	17.675	18.647	19.808	20.756	22.085	23.160	24.746	25.893	27.473	27.784
NG-D6	16.703	16.600	17.262	18.482	19.414	20.655	21.402	22.489	23.421	24.167	25.031	26.461
NG-36	18.213	18.714	19.828	21.336	22.516	23.534	24.498	25.401	26.182	27.046	27.450	28.666
OG-48	17.368	17.160	17.423	18.185	18.917	19.889	20.839	21.836	22.853	24.164	24.761	25.715
A55m(1)	18.023	16.536	15.670	15.653	15.942	16.507	17.476	18.608	20.175	21.692	23.199	23.869
A55m(2)	17.553	16.367	15.723	15.993	16.675	17.478	18.506	19.834	21.407	22.897	24.454	25.273

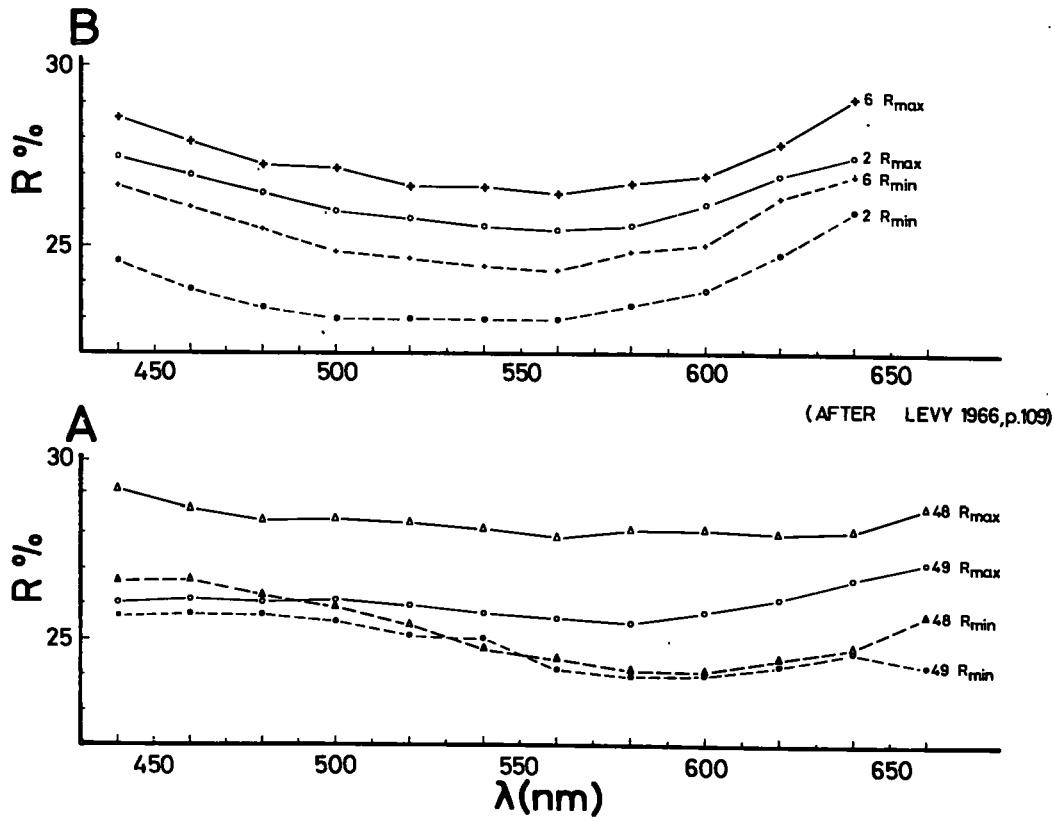


FIG. 21.—The spectral reflectivity of enargite from the Lahanos mine(A)

In measuring the reflectivity, it was not possible to use a sufficiently high light intensity to detect this anisotropy and consequently the grain were measured as if isotopic. Although the observed reflectivity varies in different grains, as shown in Fig. 22, the form of the curves is similar for most grains with the exception of NGD3. It should of course, be remembered that experimental work at the Geophysical Laboratory has shown that various bornite solid solutions can exist. However, it has not been possible in the time available to check the composition of the measured grains by microprobe.

Tetrahedrite-Tennantite - Table 18, Fig. 23A. The values given by Lévy (1966) and shown in Fig. 23B indicate a general increase in reflectivity with increasing antimony content in this series (the cell parameters increase similarly). Results for the Lahanos specimens cover a similar range.

Pyrite (FeS₂) - Table 19. Values for different specimens from the Lahanos mine are shown in Tab. 19 and Fig. 24A. They tend to give somewhat higher values than Ramdohr's and Orcel's measurements (Ramdohr 1950, pp. 572) and also higher than pyrite and anisotropic pyrite described from the Basal Reef of the Witwatersrand System by Saager and Mihálik (1967). They are lower than the results of Demirsoy (1968) and Nichol and Phillips (1965), but similar to those of Santok Singh (1965). Two of Santok Singh's specimens were polished together in the same mount and yet showed a marked difference in reflectivity. Thus it seems that there are

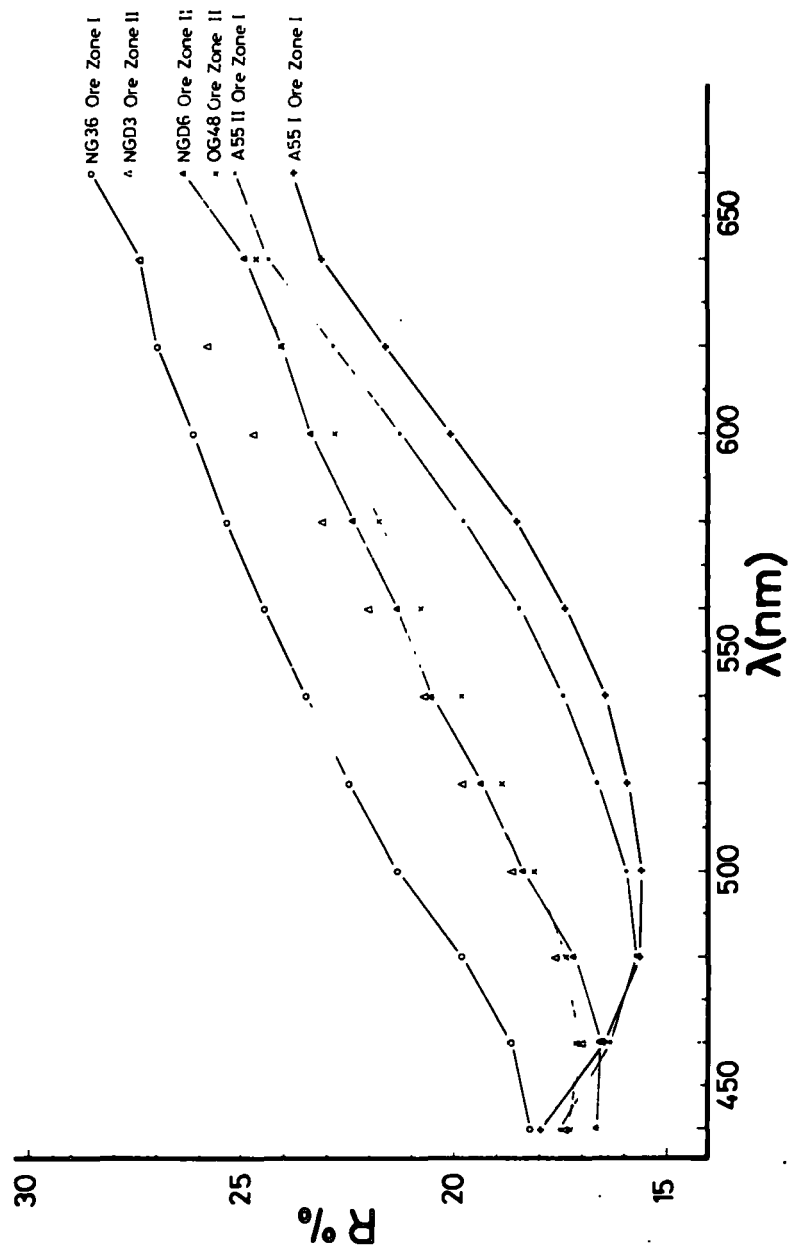


FIG. 22..The spectral reflectivity of bornite from the Lahanos mine

TABLE 18

Reflectivity measurements of tennantite-tetrahedrite

Sample No.	<u>440nm</u>	<u>460 nm</u>	<u>480 nm</u>	<u>500 nm</u>	<u>520 nm</u>	<u>540 nm</u>	<u>560 nm</u>	<u>580 nm</u>	<u>600 nm</u>	<u>620 nm</u>	<u>640 nm</u>	<u>660 nm</u>
OG40	28.526	28.453	28.953	29.254	29.716	29.778	29.610	29.043	28.157	27.718	27.066	26.144
OG47(1)	29.255	28.818	29.049	29.464	29.818	29.695	28.910	28.360	27.362	27.025	25.845	24.962
OG47(2)	29.085	28.725	28.654	29.284	29.621	29.656	29.092	28.635	27.842	27.025	26.504	26.421
OG49(1)	30.299	30.231	30.252	30.360	30.284	30.033	30.070	29.881	29.870	30.173	29.547	28.666
OG49(2)	29.584	29.440	29.593	29.781	30.071	30.131	30.011	29.451	28.782	28.337	27.360	27.107
OG51	28.853	28.786	28.733	29.014	29.165	29.079	28.771	28.002	27.659	26.968	26.228	25.715
E	30.193	29.927	30.088	30.467	30.801	31.007	31.124	30.945	30.361	29.911	29.271	28.081
H.Ag1A	29.725	29.564	29.615	29.752	30.189	30.380	30.625	30.548	29.983	29.885	28.021	28.743

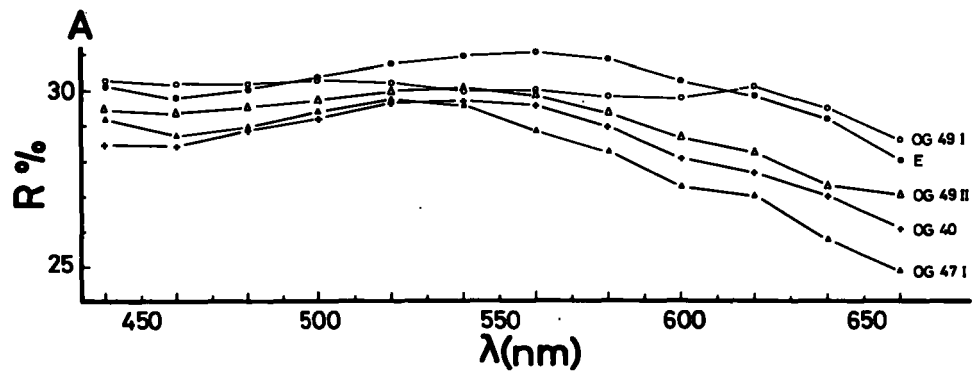
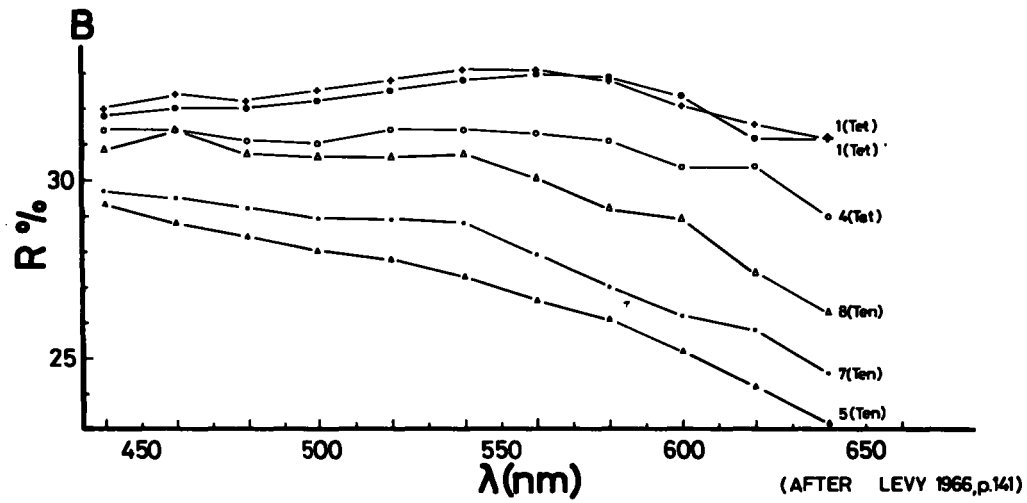


FIG. 23...The spectral reflectivity of tetrahedrites-tennantites from the Lahanos mine(A)

TABLE 19

Reflectivity measurements of pyrite

<u>Sample No.</u>	<u>440 nm</u>	<u>460 nm</u>	<u>480 nm</u>	<u>500 nm</u>	<u>520 nm</u>	<u>540 nm</u>	<u>560 nm</u>	<u>580 nm</u>	<u>600 nm</u>	<u>620 nm</u>	<u>640 nm</u>	<u>660 nm</u>
NGD10(1)	42.635	45.336	47.678	48.941	50.423	52.035	53.328	54.318	53.474	54.890	53.474	54.133
NGD10(2)	41.369	44.082	46.330	47.284	48.790	51.511	52.448	53.350	52.796	53.536	52.778	54.133
NG18 (min)	41.246	44.025	46.443	48.158	49.476	50.964	52.374	53.208	53.498	53.527	53.905	53.836
NG18 (max)	41.246	44.108	46.683	48.391	49.742	51.224	52.630	53.496	53.498	53.527	53.905	53.836
OG94	40.465	43.589	45.793	47.095	48.495	50.181	51.600	52.458	52.288	53.536	52.778	54.133

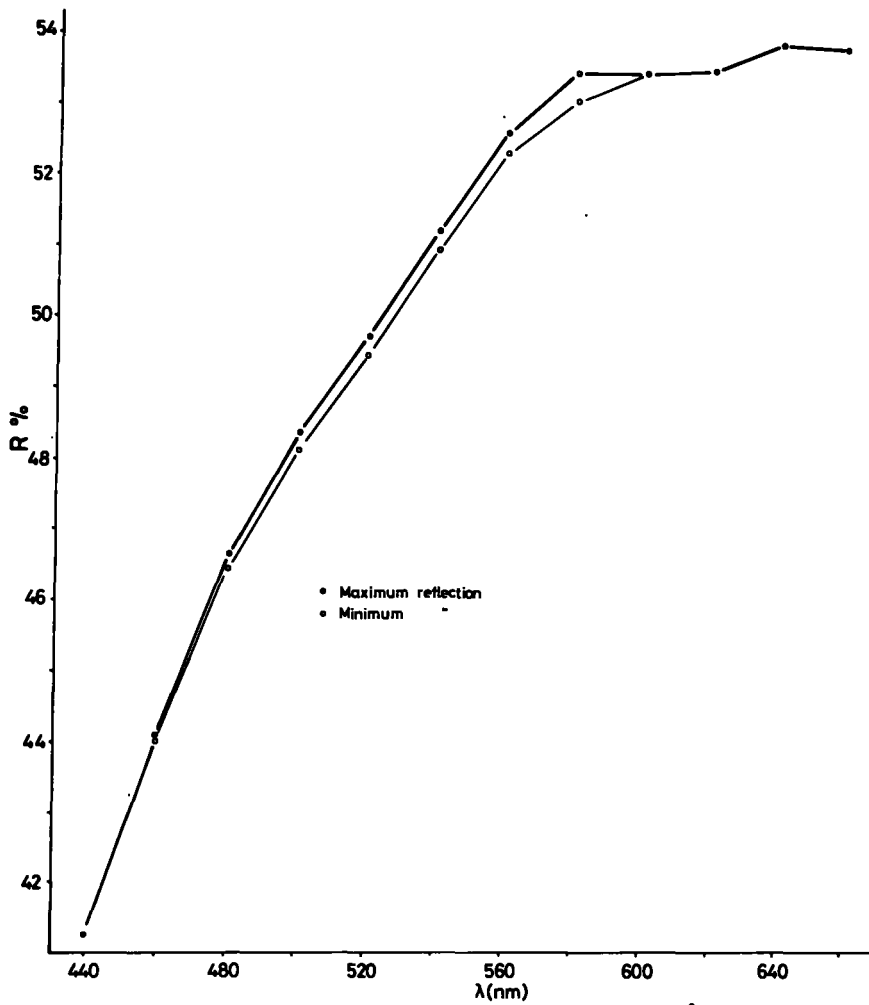


FIG. 24.—Dispersion curves of anisotropic pyrite with a cell size of $a=5.4174 \text{ \AA}$ from Lahanos mine.

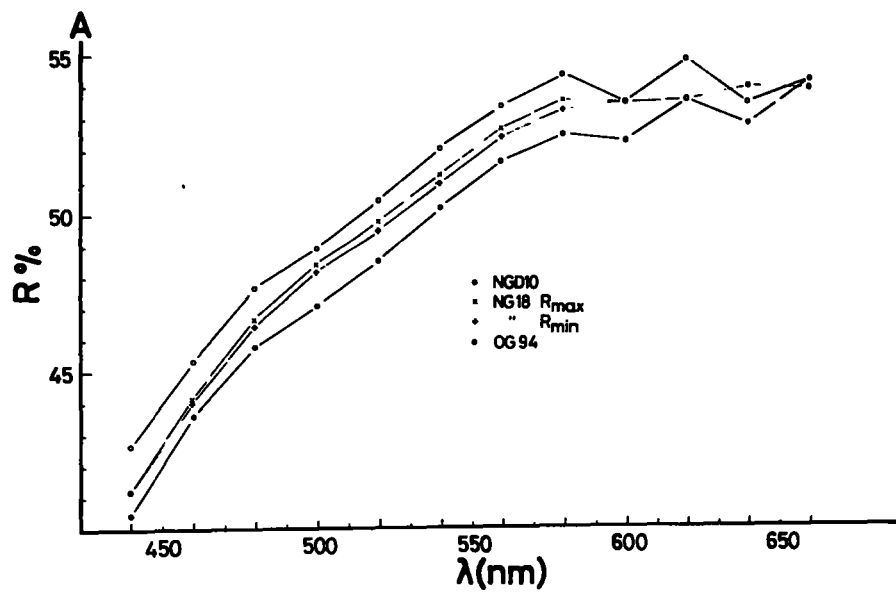
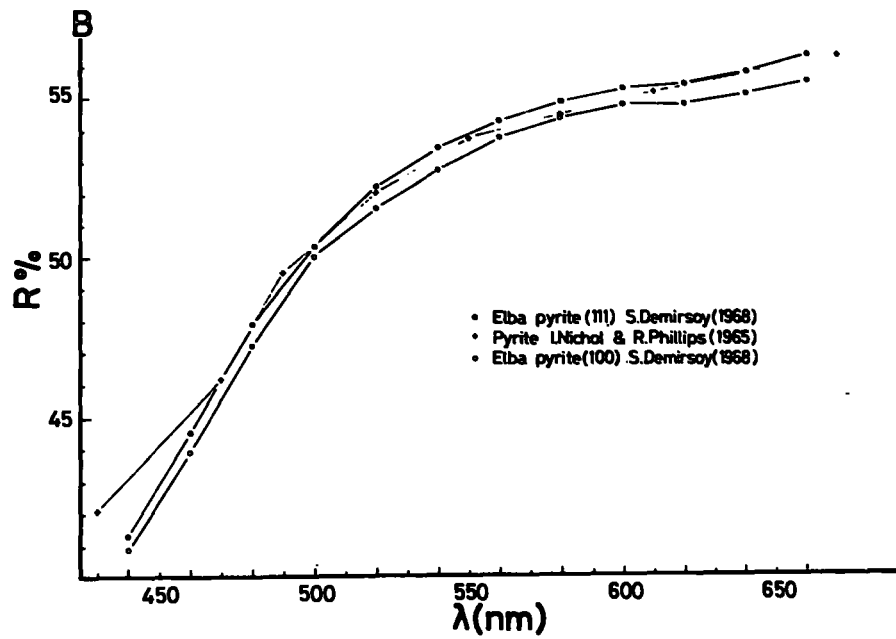


FIG. 24(A&B)...The spectral reflectivity of pyrites from the Lahanos mine(A)

real differences in reflectivity between different specimens of pyrite that cannot be ascribed to differences in the quality of the polish, although a reliable explanation for the differences has not yet been found. Anisotropic pyrite has been reported by various authors - Stanton (1955 and 1959), Uytendogaardt (1951), Santok Singh (1965), Saager and Mihalik (1967) and Gibbons (1967) and was also found in polished specimens from the various ore zones at Lahanos. Measurements of the maximum and minimum reflectivity were made on NG18, as shown in Tab. 19, and the maximum bireflection was found to be 0.3%. This is similar to the values found by Gray (1961) and Hallimond and Bowie (1964). However when the same sample (NG18) was sent a second time for repolishing, there was no sign of anisotropism in the pyrite. This supports the view that the observed anisotropism may be a polishing artefact, although Stanton's (1959) conclusion is the reverse of this. The cell size of NG18 (Tab. 7.11) is slightly larger than those of two other pyrite specimens from Lahanos, but it is doubtful whether the difference is significant. Similarly there is no obvious anomaly in the trace element content of the specimen (Tab 24). Reflectivity measurements on the anisotropic pyrite show minimum bireflection at the red and blue ends of the spectrum, yet these are the observed polarisation colours. From theory, the polarisation colours observed should be those for which the bireflection is a maximum. Further investigation is required before this puzzling phenomenon can be explained.

Marcasite (Fe S₂) The reflectivity values for R max and R min on the two grains in specimen NGD9 are given in Tab. 20 and Fig. 25. No other grains large enough to measure with the available apparatus were found. No published figures for the spectral reflectivity of marcasite have been found for comparison and it must be emphasised that the present figures give only partial information, since the optical properties of marcasite vary appreciably with orientation.

Sphalerite (ZnS) Table 21, Fig. 26. As would be expected, the values obtained for the low iron content Lahanos specimens are somewhat smaller than those found by Nichol and Phillips (1965) for Trepča, which are shown on Fig. 26 for comparison. Values given by Demirsoy (1968) for a polished cleavage surface of zincblende are given for comparison in Tab. 21. As they lie in the middle of the Lahanos range of values, they are not shown on Fig. 26 in the interests of clarity.

Galena (Pbs) Table 22, Fig. 27, gives values for various galena specimens from the ore Zone II. For comparison, the values given by Demirsoy (1968) for a fresh (100) cleavage face are given. Demirsoy's Fig. 40 shows that after polishing, the observed reflectivity drops by about 2% which gives values comparable with those of the Lahanos specimens.

TABLE 20

Reflectivity measurements of marcasite

Sample No.	<u>440 nm</u>	<u>460 nm</u>	<u>480 nm</u>	<u>500 nm</u>	<u>520 nm</u>	<u>540 nm</u>	<u>560 nm</u>	<u>580 nm</u>	<u>600 nm</u>	<u>620 nm</u>	<u>640 nm</u>	<u>660 nm</u>
NGD9 (1)(min)	44.980	45.983	47.717	48.528	49.543	50.556	51.478	51.629	51.397	50.971	40.911	50.166
NGD9(1) (max)	45.921	48.112	49.997	51.150	51.885	52.860	53.560	54.878	53.250	53.413	52.844	51.600
NGD(2) (min)	45.764	46.409	47.825	48.614	49.297	49.897	50.525	50.224	48.156	49.445	49.622	48.733
NGD9(2) (max)	45.450	47.090	48.802	49.642	50.324	51.167	51.716	51.629	51.243	50.971	50.266	50.166
Kd 1b (min)	42.014	42.564	43.595	44.378	45.234	46.291	47.485	47.710	45.915	47.699	47.688	45.408
Kd 1b (max)	46.200	48.127	50.611	51.640	52.346	53.156	53.781	53.783	51.489	53.099	53.488	50.912

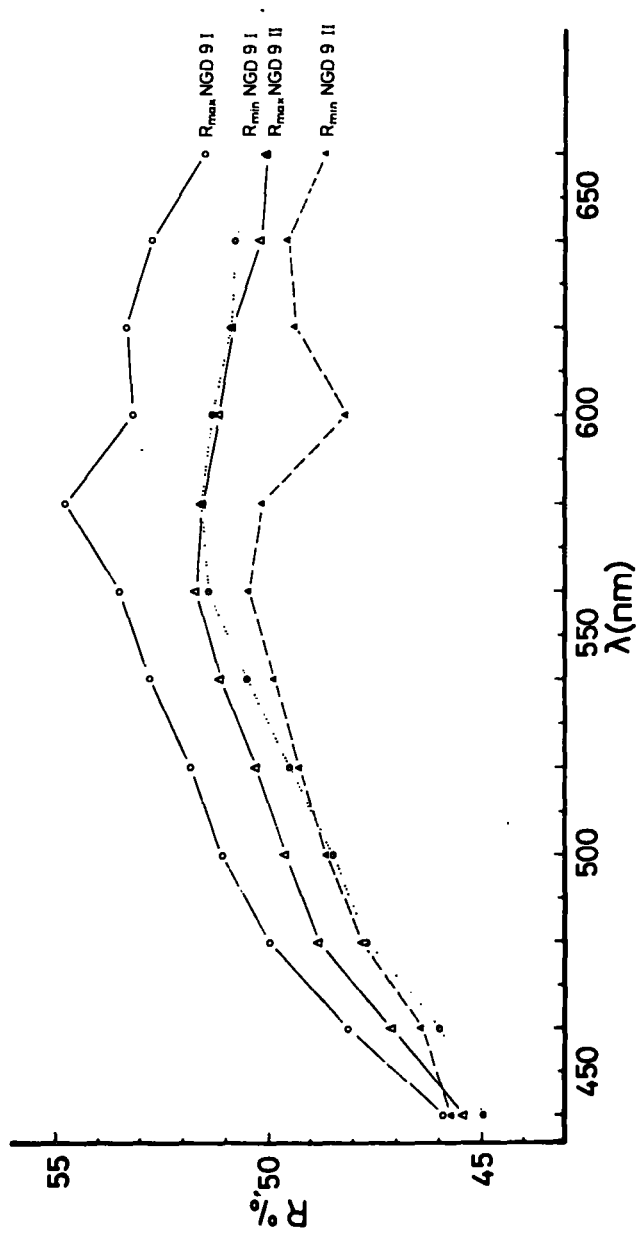


FIG. 25.—The spectral reflectivity of marcasites from the Lahanos mine

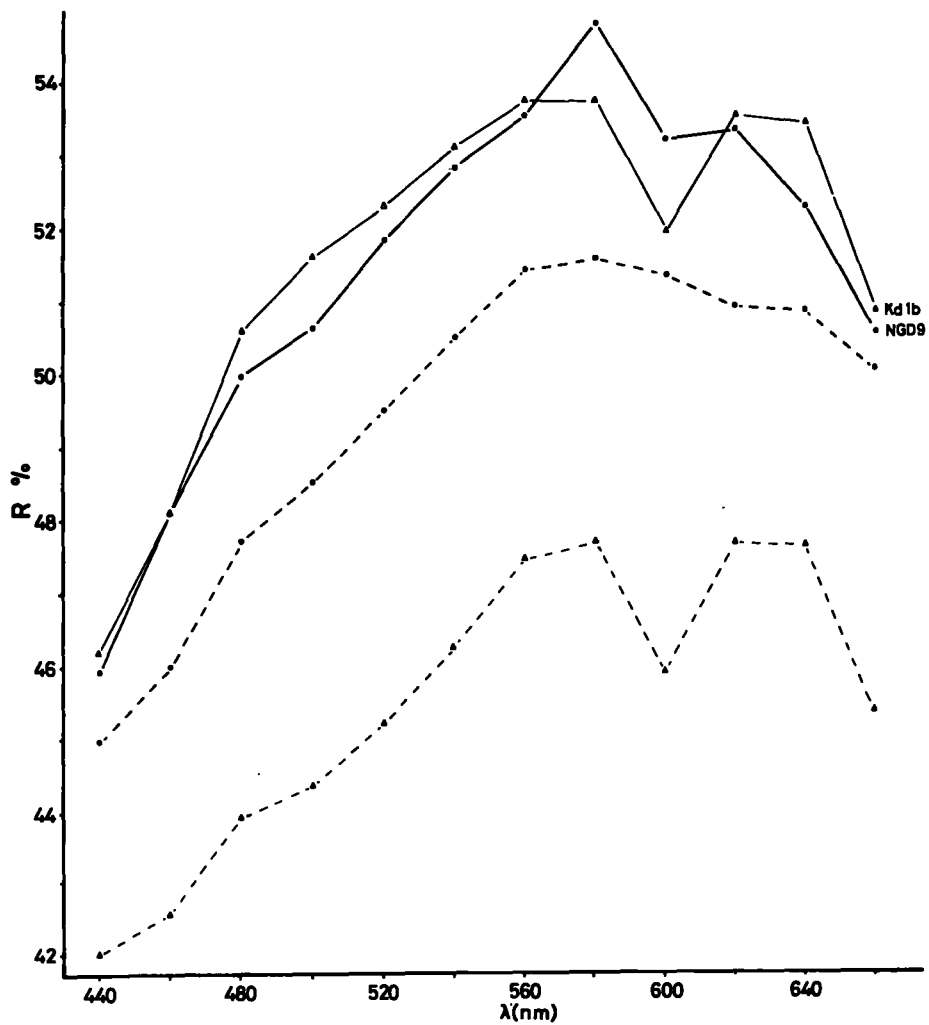


FIG. 25A... Dispersion curves of marcasite from Karadere(•) and Lahanos(•) mine. Solid lines for maximum reflection & dashed lines for minimum reflection.

TABLE 21

Reflectivity measurements of
Sphalerite.

Sample No.	<u>440 nm</u>	<u>460 nm</u>	<u>480 nm</u>	<u>500 nm</u>	<u>520 nm</u>	<u>540 nm</u>	<u>560 nm</u>	<u>580 nm</u>	<u>600 nm</u>	<u>620 nm</u>	<u>640 nm</u>	<u>660 nm</u>
OG39(1)	17.161	17.061	16.868	16.451	16.186	16.114	16.102	15.983	15.880	15.963	15.466	15.847
OG39(2)	17.740	17.391	17.349	17.236	17.204	17.058	17.094	17.471	16.770	16.949	16.180	16.541
OG40(1)	17.622	17.498	17.310	17.129	16.897	16.665	16.479	16.377	16.325	16.239	15.944	15.670
OG40(2)	17.388	17.413	17.225	17.111	16.902	16.725	16.627	16.435	16.260	16.318	16.103	15.670
OG41	18.185	18.061	17.759	17.496	17.250	17.076	16.928	16.931	16.662	16.798	16.574	16.541
NGD16(1)	18.198	17.732	17.454	17.262	17.030	16.885	16.815	16.641	16.334	16.667	15.866	16.024
NGD16(2)	18.340	18.040	17.740	17.451	17.293	17.068	16.823	16.675	16.498	16.502	15.952	15.134
NG34(1)	17.894	17.724	17.446	17.278	17.104	16.885	16.575	16.567	16.426	16.529	16.574	16.541
NG34(2)	17.489	17.260	17.134	16.937	16.826	16.573	16.565	16.339	16.231	16.389	16.375	16.541
NG39(1)	17.978	17.612	17.471	17.201	17.077	16.858	16.641	16.577	16.367	16.319	16.022	16.024
NG39(2)	17.967	17.676	17.611	17.255	17.157	16.940	16.784	16.693	16.424	16.536	16.188	16.024
M1	17.979	17.866	17.630	17.354	17.212	17.060	16.846	16.697	16.728	16.631	15.952	16.024
M2	18.394	18.181	17.887	17.653	17.704	17.591	17.386	17.366	17.238	17.297	16.449	16.024
M3	18.951	18.505	18.374	18.241	18.400	18.024	17.828	17.670	17.474	17.327	17.179	17.119
Kd 2a	18.323	18.044	17.947	17.779	17.705	17.541	17.381	17.348	17.115	17.448	17.248	16.412
Kd 2c	18.220	17.861	17.731	17.534	17.363	17.089	16.949	16.832	16.556	16.585	16.816	16.412

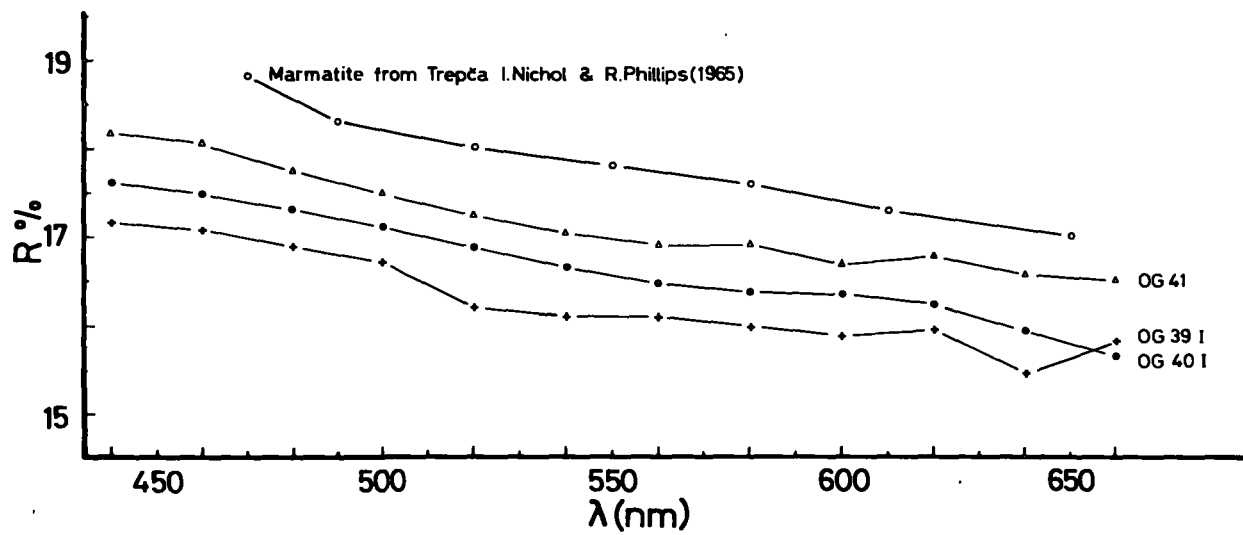


FIG. 26...The spectral reflectivity of sphalerites from the Lahanos mine

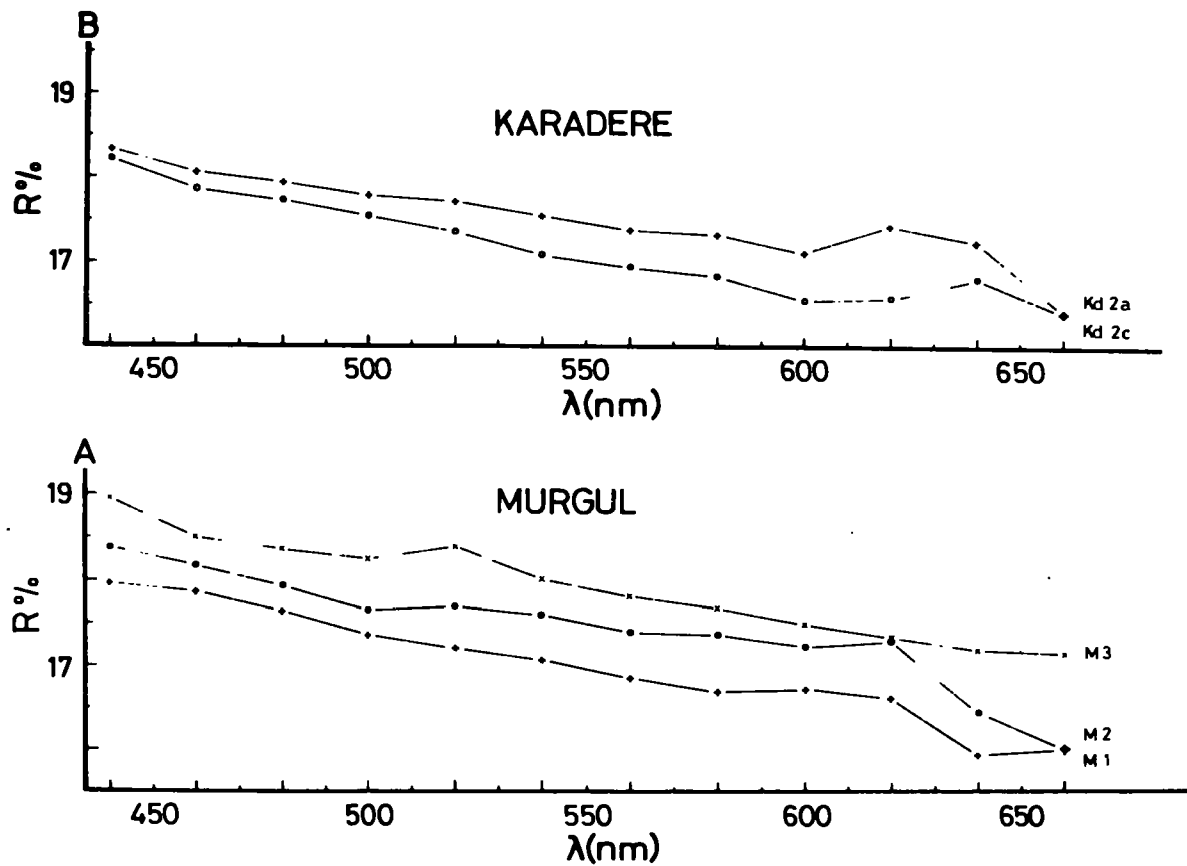


FIG. 26...The spectral reflectivity of sphalerites from the Murgul(A)& Karadere(B) mines (A&B)

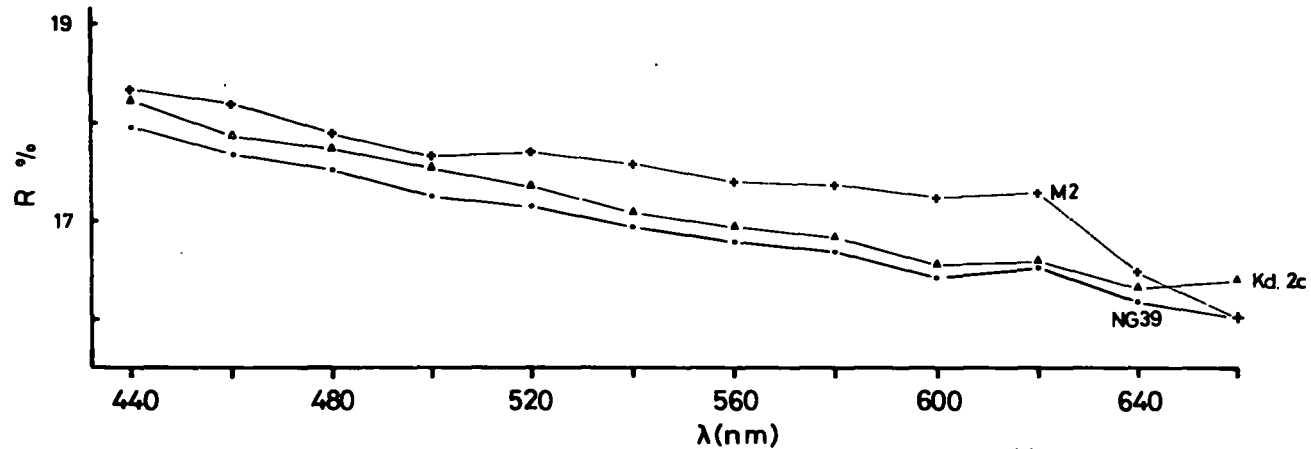


FIG. 26C...Dispersion curves of sphaerite from the Karadere, Lahanos and Murgul mines.

▲ Karadere sphaerite. $a = 5.4119 - 5.4141 \text{ \AA}$

● Lahanos sphaerite. $a = 5.4118 - 5.4123 \text{ \AA}$

◆ Murgul sphaerite. $a = 5.4101 - 5.4112 \text{ \AA}$

TABLE 22

Reflectivity measurements of galena

<u>SAMPLE NO.</u>	<u>440 nm</u>	<u>460 nm</u>	<u>480 nm</u>	<u>500 nm</u>	<u>520 nm</u>	<u>540 nm</u>	<u>560 nm</u>	<u>580 nm</u>	<u>600 nm</u>	<u>620 nm</u>	<u>640 nm</u>	<u>660 nm</u>
OG39	46.809	45.888	44.271	43.252	42.205	41.823	41.705	41.735	41.163	41.299	41.419	40.908
OG40(1)	46.935	45.636	44.427	43.396	42.363	41.794	41.533	41.647	41.598	41.406	41.502	40.908
OG40(2)	46.463	45.318	44.122	43.126	42.409	42.031	41.777	41.494	41.260	41.204	41.629	41.566
OG41	46.894	44.866	43.716	42.921	42.287	41.253	41.059	40.863	40.852	40.597	40.890	39.978
NGD16	46.821	45.845	44.384	43.244	42.408	42.024	41.975	41.797	41.406	41.575	41.069	40.770
NGD17	47.366	45.625	44.326	43.114	41.861	41.725	41.551	41.312	41.149	41.458	41.075	40.770
NG34	47.328	45.888	44.428	43.298	42.548	41.978	41.783	41.578	41.258	41.312	40.974	40.770
M1	46.927	45.613	44.262	43.165	42.297	41.748	41.758	41.222	41.015	41.343	41.414	40.770
M3	47.495	46.457	47.705	43.676	42.713	42.220	42.084	41.621	41.334	41.620	41.414	40.770
Kd2a	46.927	45.449	44.360	43.222	42.486	41.913	41.813	41.382	41.475	41.620	41.414	40.770
Kd2c	46.502	45.216	44.064	43.008	42.146	41.662	41.541	41.382	41.053	41.343	40.389	40.770

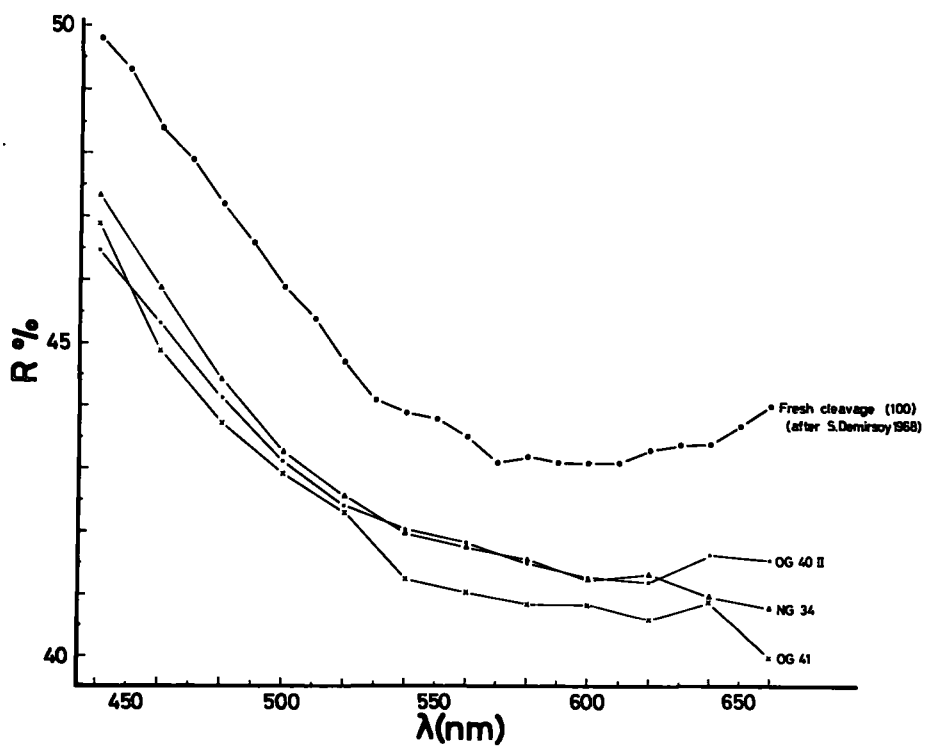


FIG. 27...The spectral reflectivity of galenas from the Lahanos mine

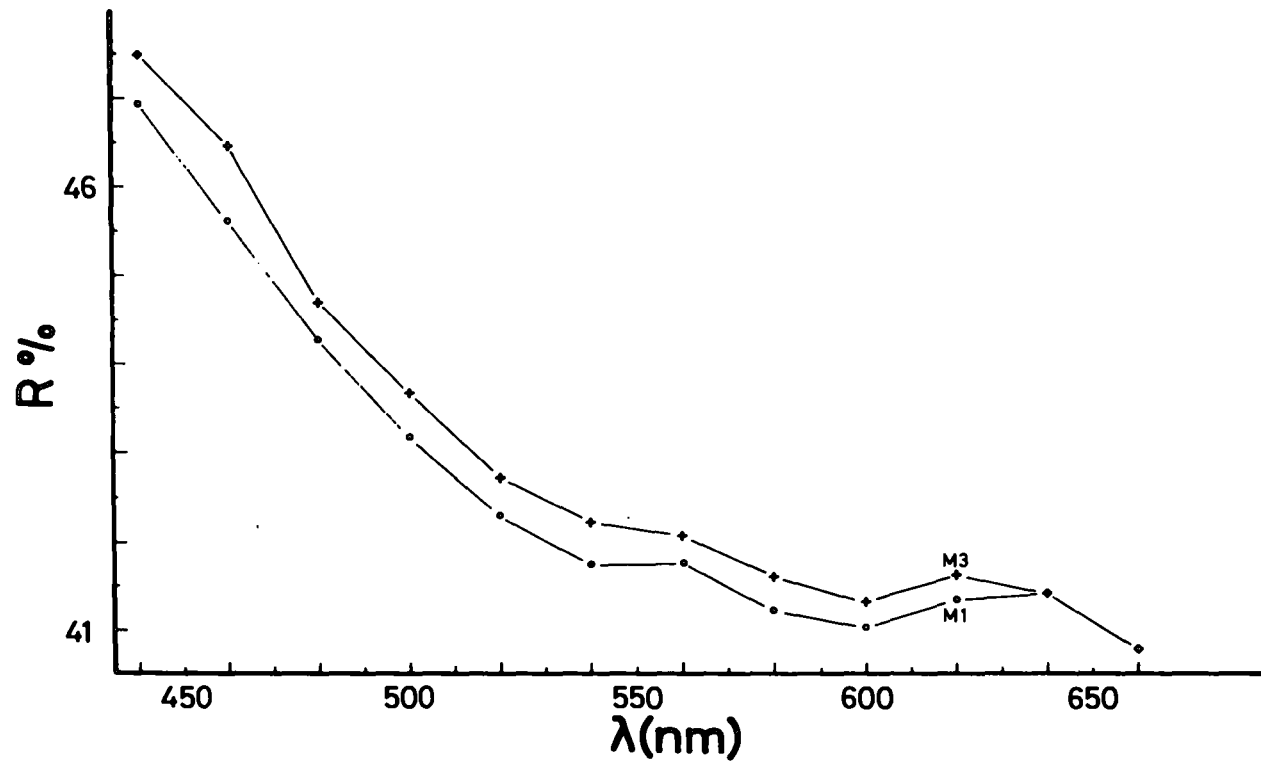


FIG. 27A._The spectral reflectivity of galenas from the Murgul mine

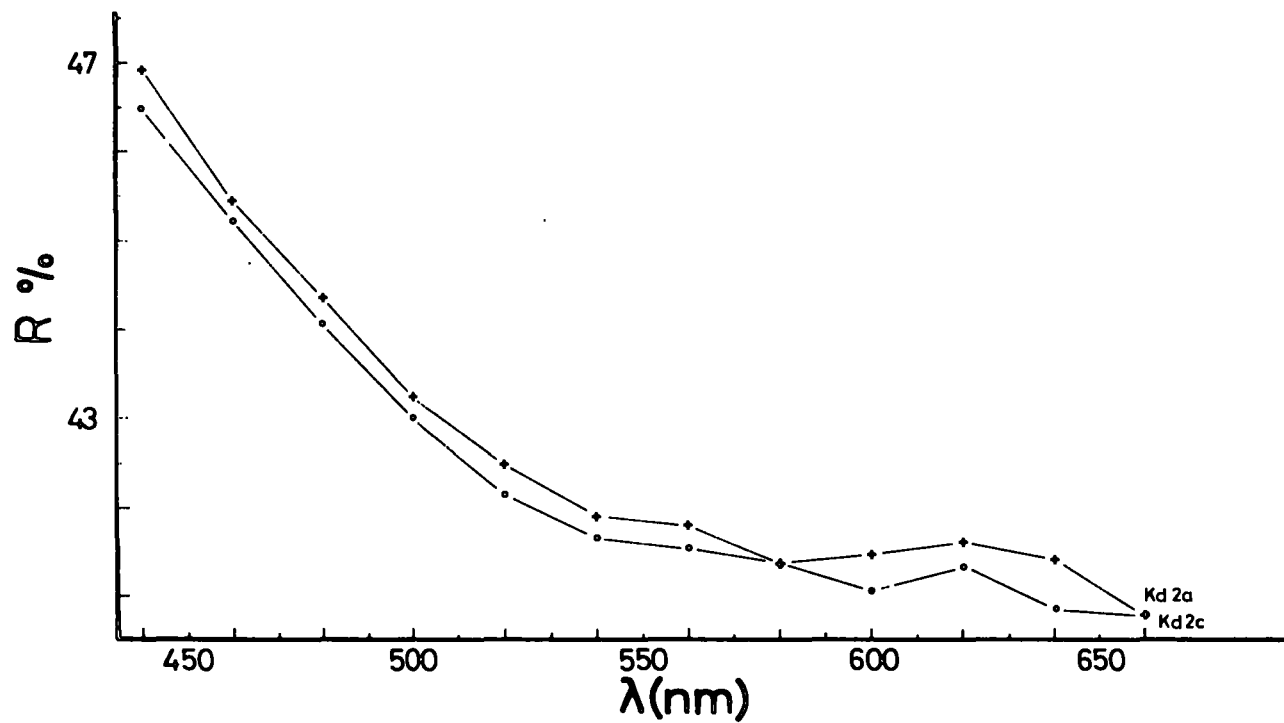


FIG. 27B._The spectral reflectivity of galenas from the Karadere mine

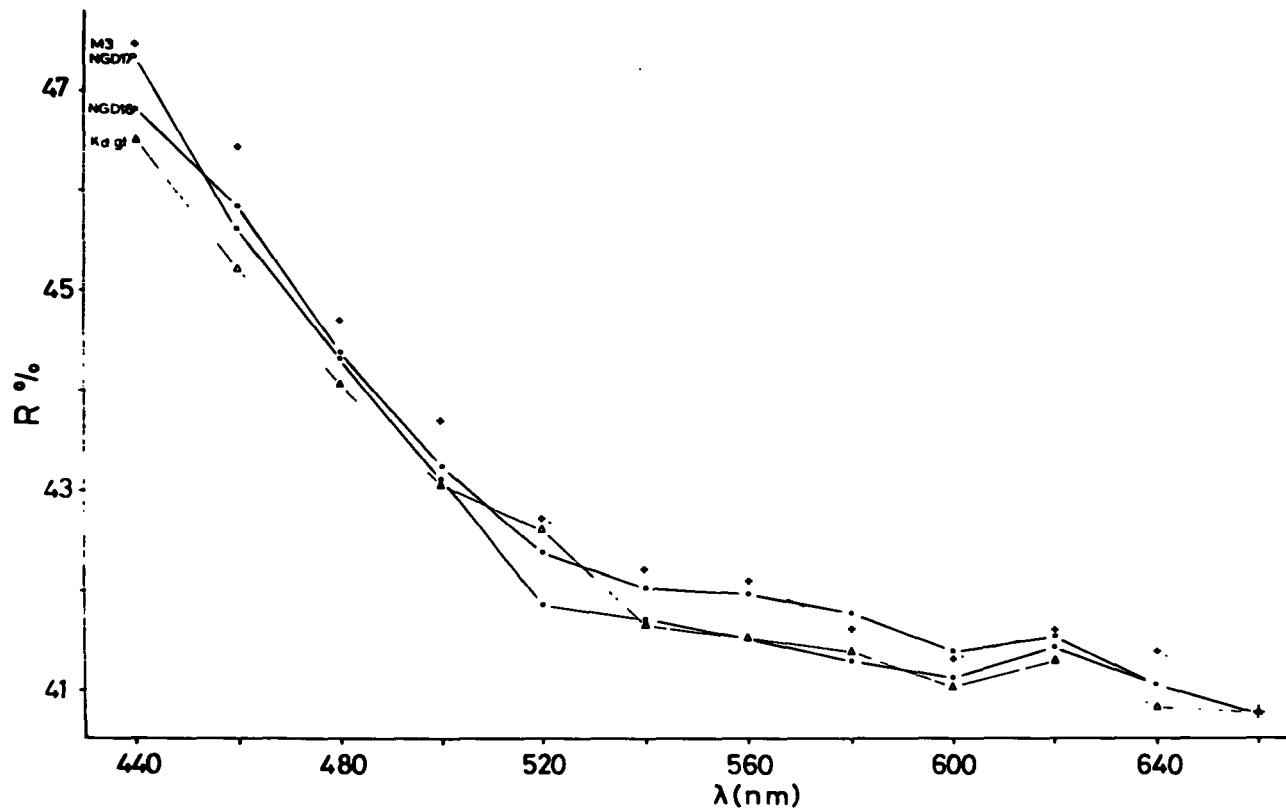


FIG. 27C...Dispersion curves of galena from the Karadere, Lahanos and Murgul mines.

▲ Karadere galena. $a=5.9351-5.9354 \text{ \AA}$

○ Lahanos galena. $a=5.9359-5.9367 \text{ \AA}$

◆ Murgul galena. $a=5.9353 \text{ \AA}$

E.Ie Wall-rock Petrography

Petrographical study of cores from boreholes A and B gave the opportunity of examining the wall-rocks of the Lahanos mineralisation relatively free from normal surface weathering effects. The two boreholes showed different lithological units above the mineralisation, except for just above the main mineralisation; below the mineralisation both boreholes showed similar rock units (See Section 4 and Map 6). Hence these two boreholes will be described separately.

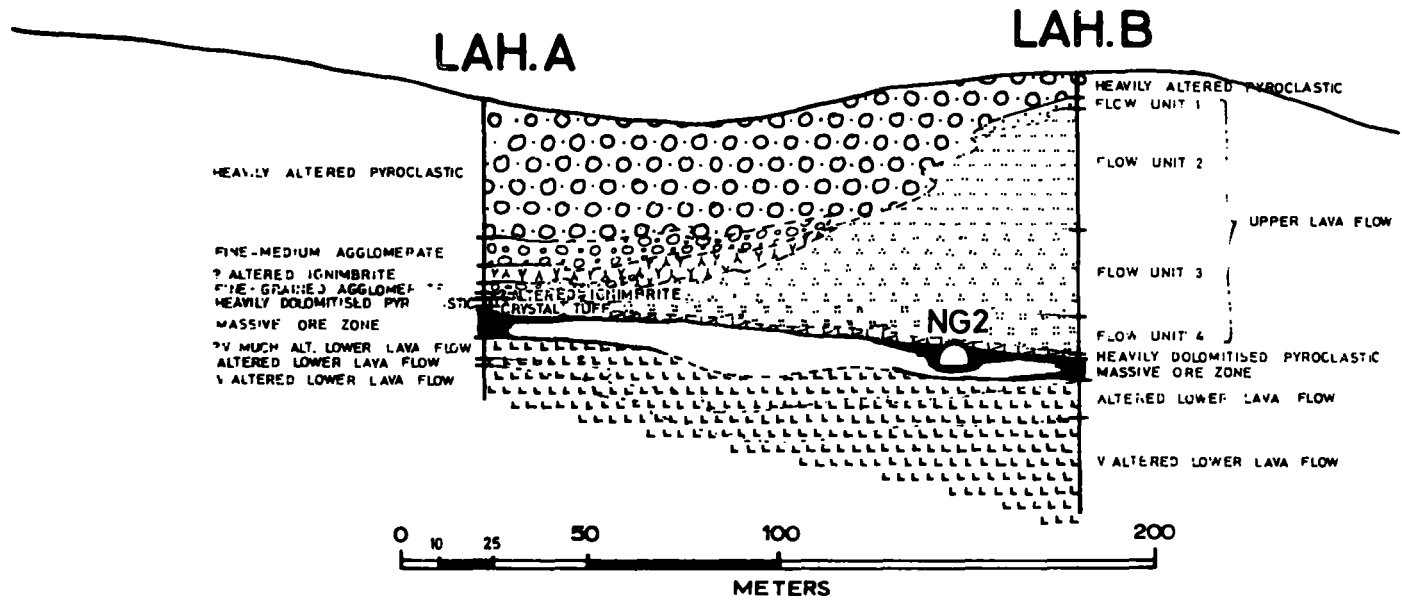
E.Ie1 Borehole A: Nine samples, representing 18 meters of core, were collected and 24 thin sections were examined. The first 38 m could not be sampled because of no core recovery. The first 5 samples represent the roof rocks while the rest represent less mineralised host-rock within the mineralised horizon.

0.00 - 38.00m: From surface observations and comparison with the fragments of core recovered, this consists of heavily altered coarse green-gray sometimes bluish dark gray agglomerate and other fine grained pyroclastic rocks.

38.00 - 45.00m: Fine to medium grained agglomerate containing different fragments of lava flows and some altered crystals with small amounts of altered volcanic glass. Some of the plagioclase, in spite of alteration, shows zoning. Kaolinisation, chloritisation and carbonatisation are common alteration processes. Vesicles of different flow fragments were mainly infilled by chloritic material. Very much altered dark coloured fragments were thought to be altered glass.

Geo.Sec.4

GEOLOGICAL SECTION (THROUGH THE LAHANOS BOREHOLES A&B)



45.00 - 50.00m: Heavily altered fine grained agglomerate or medium to coarse grained tuff. Plenty of deuteric quartz and dolomite veinlets cutting across the rock. Relicts of altered glass and quartz can be seen in spite of heavy dolomitisation, as seen in Sample A03 (2). Sample A03 (3) represents a fine grained vitric pyroclastic rock, and the presence of angular glass shards would suggest an ignimbritic pyroclastic. The entire groundmass is completely made of very fine grained dark opaque material. All angular glass fragments are devitrified and sometimes altered to chlorite. The common alteration is dolomitisation.

50.00 - 53.00m: Fine grained agglomerate containing lava and volcanic glass fragments with an extensive dolomitisation.

53.00 - 54.00m: Another horizon of angular fragments containing pyroclastic rocks (? ignimbrite), which are very similar in appearance and characters to those offound at 45 - 48 meters.

54.00 - 55.35m: Very distinct in hand specimen, with a violet reddish brown colour and looks like a limestone. X-ray diffractometer and optical studies suggested that it is a fine grained dolomitic rock containing very small amounts of volcanic glass and other volcanic material. Dark brown coloured amorphous cement surrounds the individual small grains averaging about 60 by 80 microns in size. Volcanic devitrified glasses reach about 0.5 mm grain size. Sample A05 (54 - 55) represents the average chemical analysis of this rock (Table 27A).

55.35 - 55.50m: This is the rock unit which overlies the

Lahanos pyritic sulphide deposit. In hand specimen it is quite compact and also quite distinct from the dolomitic horizon and appears to be well bedded crystal tuff. It is entirely made of angular quartz averaging 200 by 100 microns in size and devitrified glass averaging 200 by 250 microns in size. The cementing material appears to be the same as in the dolomitic horizon. Dolomitisation along the bedding plane is quite well developed. Closer to the main ore zone contact intensive dolomitisation of the crystalline tuff is seen, in which only relicts of altered glass are present. Dolomitisation is also associated with some ore and gangue minerals (e.g. chalcopyrite, bornite, pyrite and barytes). These epigenetic minerals are much more abundant closer to the ore contact. In spite of well developed bedding of the crystal tuff, the Lahanos ore body does not show a flat upper contact (see Plate 53), on the contrary it shows, as seen in Plate 53, a quite irregular contact.

55.50 - 64.00m: The Lahanos massive pyritic sulphide horizon.

64.00 - 70.00m: Very much altered host-rock containing dolomite, deuteric quartz, sericite and pyrite as alteration products.

70.00 - 72.00m: A fine grained lava flow, which is quite similar to those found in borehole B, with an interlocking groundmass mainly consisting of quartz, altered feldspar and some patches of altered volcanic glass. Due to mineralisation there are a large number of dolomitic veinlets cutting through the fine grained lava flow in addition to patches of dolomite in the groundmass.

72.00 - 78.00m: Very much silicified and sericitised wall-rock.



Pl. 53. Ore-Hanging-wall relationship in borehole A.

There are also small quantities of dolomite present as an alteration product. It appears that the entire primary texture and structure of the host rock is completely destroyed, but in hand specimen some porphyritic texture relicts can be seen. This altered porphyritic lava is very similar to those found below the ore horizon in borehole B between 94 and 118 meters.

E.1e2 Borehole B: During the study of borehole B about 34 thin sections were examined. The first 26 of them were collected above the mineralisation and the rest were collected below the ore horizon. Because of no core recovery from the first 7m no sample was collected.

0.00 - 7.00m: No core recovery owing to the presence of altered pyroclastic rocks somewhat similar to those found in borehole A 0 to 38 meters.

7.00 - 77.00m: The study of thin sections, taken with the chemical analyses, suggest that this is a thick composite lava flow including four different lava flow units. Changes in the chemical analysis could however be just a reflection of different alteration products.

Flow unit 1. (7.00 to 10.00m) This is a fine grained porphyritic lava flow. Complete alteration of phenocrysts to mainly dolomite and to a less extent sericite, kaolinite, chlorite and xenomorphic quartz. The groundmass is composed of well rounded felsitic grains of mainly quartz with a little sericite and feldspars and with an average grain size of about 35 by 35 microns.

Flow Unit 2 (10.00 to 43.00m) This second flow unit is somewhat similar to the first flow unit in hand specimen and even in thin sections, but it has a more angular felsitic groundmass than the first flow unit. Samples of this flow unit were also affected by dense alteration of dolomitisation, sericitisation, silicification etc.

Flow unit 3 (43.00 to 67.00m) The microscopic characters are quite similar to the first flow unit i.e. its groundmass shows well rounded felsitic texture as described from the first flow unit. All phenocrysts and volcanic glasses were altered to mainly dolomite and to a less extent to kaolinite and sericite. However, as an accessory mineral there are some unaltered long prismatic apatite grains occurring in the groundmass or in some opaque grains. Closer to the ore body the number of dolomitic veinlets and intensity of dolomitisation increases and devitrified glass becomes more abundant.

Flow unit 4 (67.00 - 77.00) This is the bottom flow unit of the thick porphyritic composite lava flow, with microscopic characters very similar to the second flow unit, but the presence of coarser interlocking felsitic groundmass and a small number of altered phenocrysts makes it quite clearly distinct from the flow units 2 and 3. The main alteration products are dolomite and, closer to the ore, xenomorphic quartz. However, there is also some altered glass and a few accessory apatite grains.

77.00 - 78.00m: This is another pyroclastic rock which occurs just above the Lahanos ore body and its general appearance is quite

similar to that described from borehole A at 54 to 55.35 meters. From the relict texture, it seems to be a vitric tuff containing mainly volcanic glass and a very small amount of quartz fragments. At present, it is a pyroclastic rock heavily altered owing to mineralisation. The principal alteration mineral is dolomite associated with some kaolinisation, sericitisation and a very small amount of chloritisation.

78.00 - 84.00m: The Lahanos massive pyritic sulphide horizon.

84.00 - 94.00m: Another fine grained porphyritic lava flow horizon. The felsitic groundmass shows interlocking texture rather than rounded. The presence of a little more abundant altered phenocryst relicts makes it quite easily distinct from the flow unit 4 (i.e. 67 to 77 meters). But this lava flow is very similar to those already described in borehole A at 70 to 72 meters. The main alteration product is dolomite with a little sericitisation. It is possible to see a few larger patches and veinlets of dolomite.

94.00 - 118.00m: Severely sericitised, silicified and pyritised, possibly a lava flow. Microscopic studies of these rocks revealed some similarity to those previously described from borehole A (between 72 to 78m). Strained xenomorphic deuteric quartz patches are quite common. Due to heavy alteration and alteration products, closer to the ore body, there are no relicts of the original texture. Therefore in such cases, it is very difficult to say whether they were lava or pyroclastic; however the presence of relict porphyritic texture, particularly in sample B33 110, very much

favours the possibility that it is a lava and less altered interlocking felsitic groundmass may suggest that these are very much altered members of the lava flow described between 84 to 94 meters in borehole B i.e. a porphyritic lava horizon with interlocking felsitic groundmass occurs just below the Lahanos massive pyritic deposit.

The petrographic studies of both Lahanos boreholes showed that the Lahanos pyritic massive sulphide deposit occurs in between pyroclastic rocks on top and an altered porphyritic lava flow below. Examination of the upper contact of the ore body showed an irregular boundary against the pyroclastic rocks (Plate 53), indicating that advancing ore solutions penetrated for some distance into the pyroclastic rocks.

E.Ie["] Mineralogy of Alteration Halo

It is evident that variations in host-rock composition, both mineralogical and chemical, are important factors controlling the nature of hydrothermal alterations. The acidity of hydrothermal fluids or of ore-forming solutions causing reaction with unstable wall-rocks will induce physical and chemical changes tending towards the establishment of equilibrium under the prevailing conditions. The alteration products may range from simple recrystallisation to the addition, removal or rearrangement of chemical components. Conspicuous and widespread alterations of the hanging-wall and foot-wall series in close association with the pyritic sulphide

deposit at Lahanos and particularly at the Karaerik and Karilar mines, old mines which are 8km N of the Lahanos mine, (Map 2), can very often be seen from some distance away from the deposit. A general feature of the alteration is an area of bleaching above the main ore, in the hanging-wall (Plates 12, 13, 54).

The outer and most widespread alteration is propylitisation of the Upper Volcanic Series. Because it is found over large areas, it can not be used as a precise indicator of the location of sulphide mineralisation. The second alteration halo of kaolinisation and sericitisation often associated with tiny euhedral pyrite crystals is closer to the ore body and it is this halo that can be seen at a distance. The innermost halo or the outer casing of the ore body, particularly in the foot-wall series, is dense silicification often with sericitisation and pyritisation. Its appearance and mineral assemblage is very similar to those described for "Keiko" or siliceous ore from Japan (Kato, 1928; Geological survey of Japan, 1960). However, in the hanging-wall series alteration products are somewhat different from the foot-wall series. It is possible to see locally a well developed thin green kaolinite-dickite layer associated with pyrite, just above the massive sulphide body. A good deal of dolomitisation, associated with fluorapatite, of the Upper Volcanic Series closer to the main sulphide body has been observed from the borehole cores and their presence was confirmed by both XRD and thin section studies.

Wall-rock alteration and zoning in the alteration products

are well established at Butte, Montana by Sales (1950) and Sales and Mayer (1948). Their experimental studies on wall-rock alteration products indicated that the critical temperature for the development of sericitisation lies between 340°C and 360°C and the acidity is near 0.1N HCl.



Pl. 54 The general
view of
the
alteration
above the
Lahanos
Mine.

E.II CHEMISTRY

The chemistry of the Lahanos ore and adjacent rocks has been thoroughly investigated and will now be described in the following order -

- A. (i) Trace elements in purified individual sulphide minerals.
- (ii) Major and trace element distribution in Lahanos New Gallery 2.
- B. Major and trace elements in wall-rocks
 - (i) Borehole geochemistry
 - (ii) Surface geochemistry

E.II A Trace Elements in Sulphides

Trace element studies of the Lahanos pyritic sulphide deposit have been carried out both on purified individual sulphide minerals and on unseparated whole ore samples, using the Philips 1212 Automatic XRF spectrograph and a Hilger large quartz emission optical spectrograph. Following a qualitative XRF examination to see which elements were detectable, standards were prepared according to methods described by Ahrens and Taylor (1961) (See Appendix for operating conditions of both XRF and emission optical spectrograph and Fig. 28 A-D). The optical spectrograph was used only to determine Co:Ni ratios on purified minerals. Although native gold and gold bearing minerals have been found in the ore, gold was not determined because of the low sensitivity of the XRF method.

FIG. 28A...CALIBRATION GRAPHS FOR XRF SPECTROGRAPHY
(MAJOR ELEMENTS IN SILICATES)

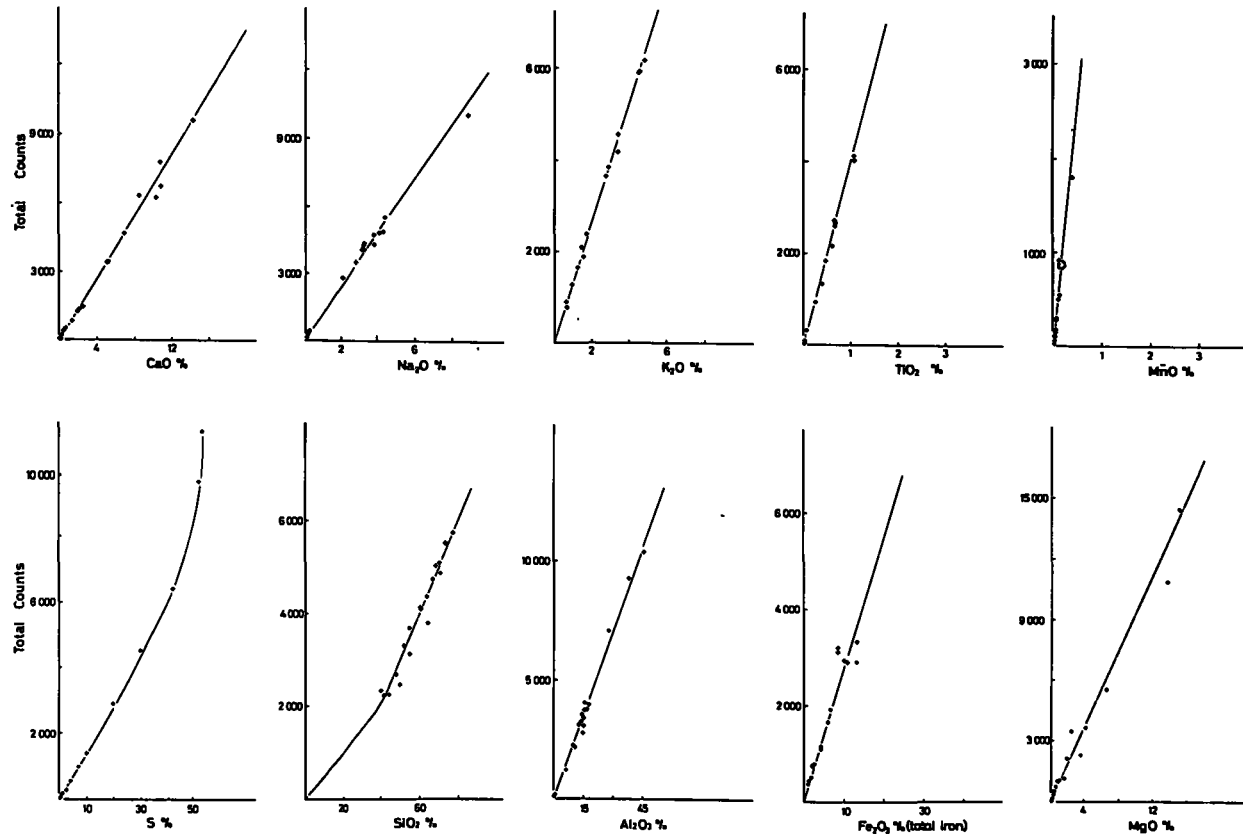


FIG. 28B...CALIBRATION GRAPHS FOR XRF SPECTROGRAPHY
(TRACE ELEMENTS IN SILICATES)

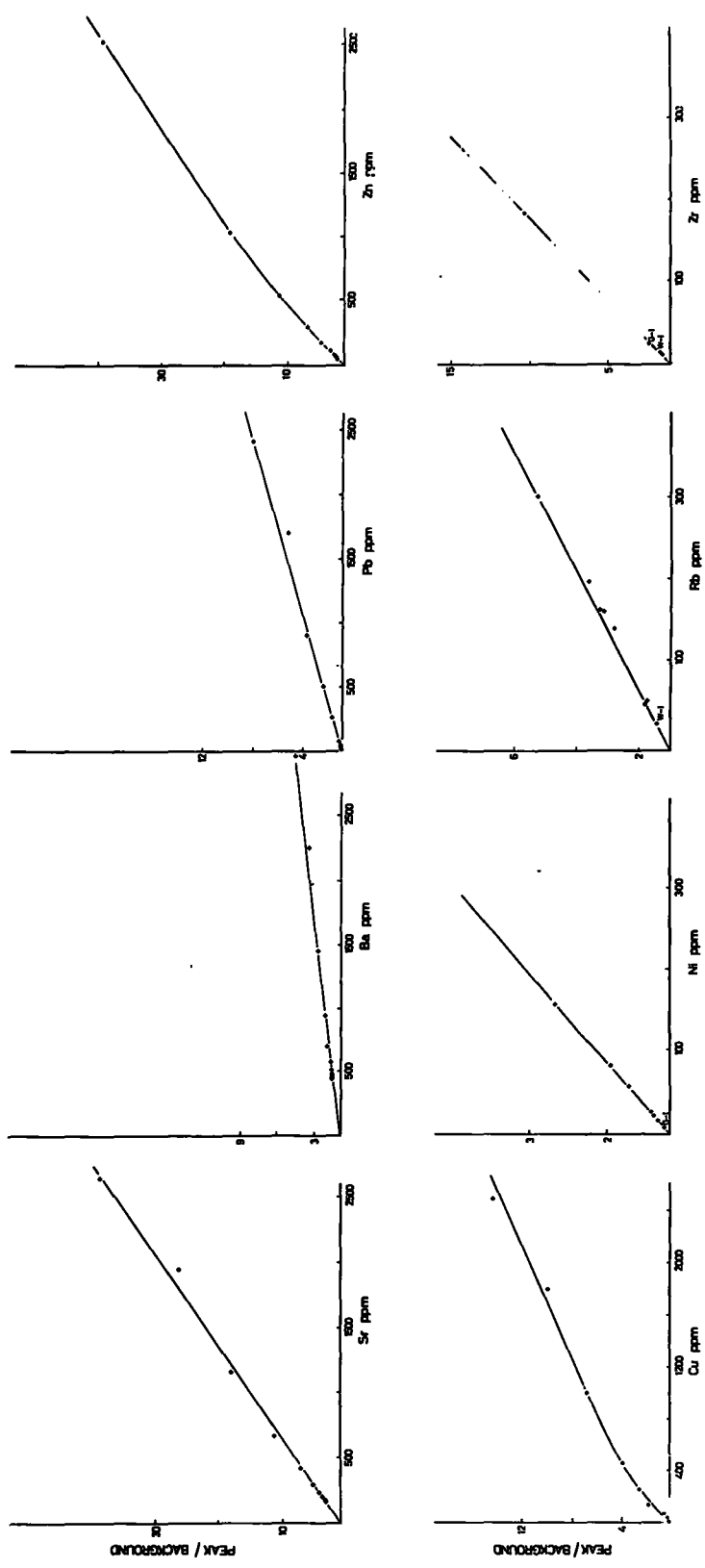
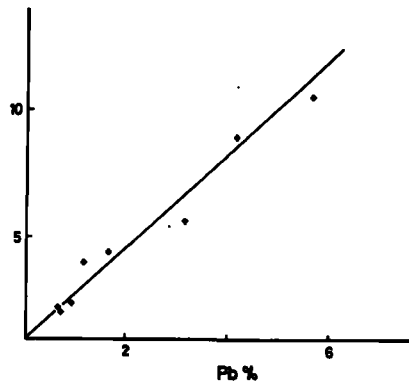
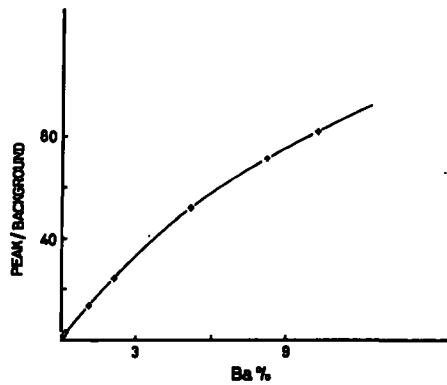
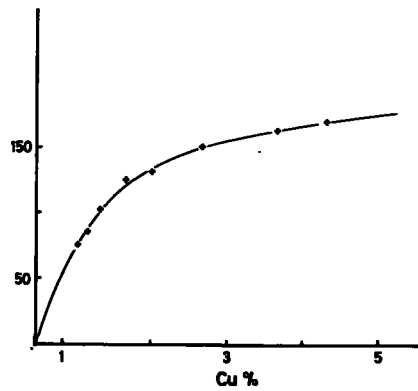
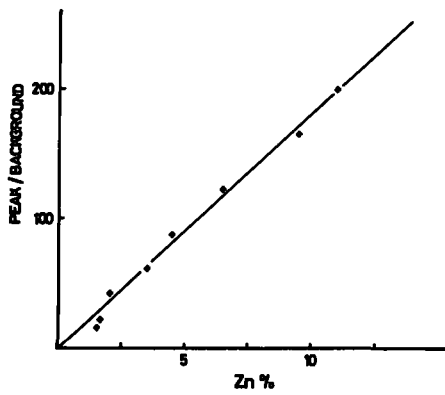


FIG. 28C...CALIBRATION GRAPHS FOR XRF SPECTROGRAPHY
(MAJOR ELEMENTS IN SULPHIDES)



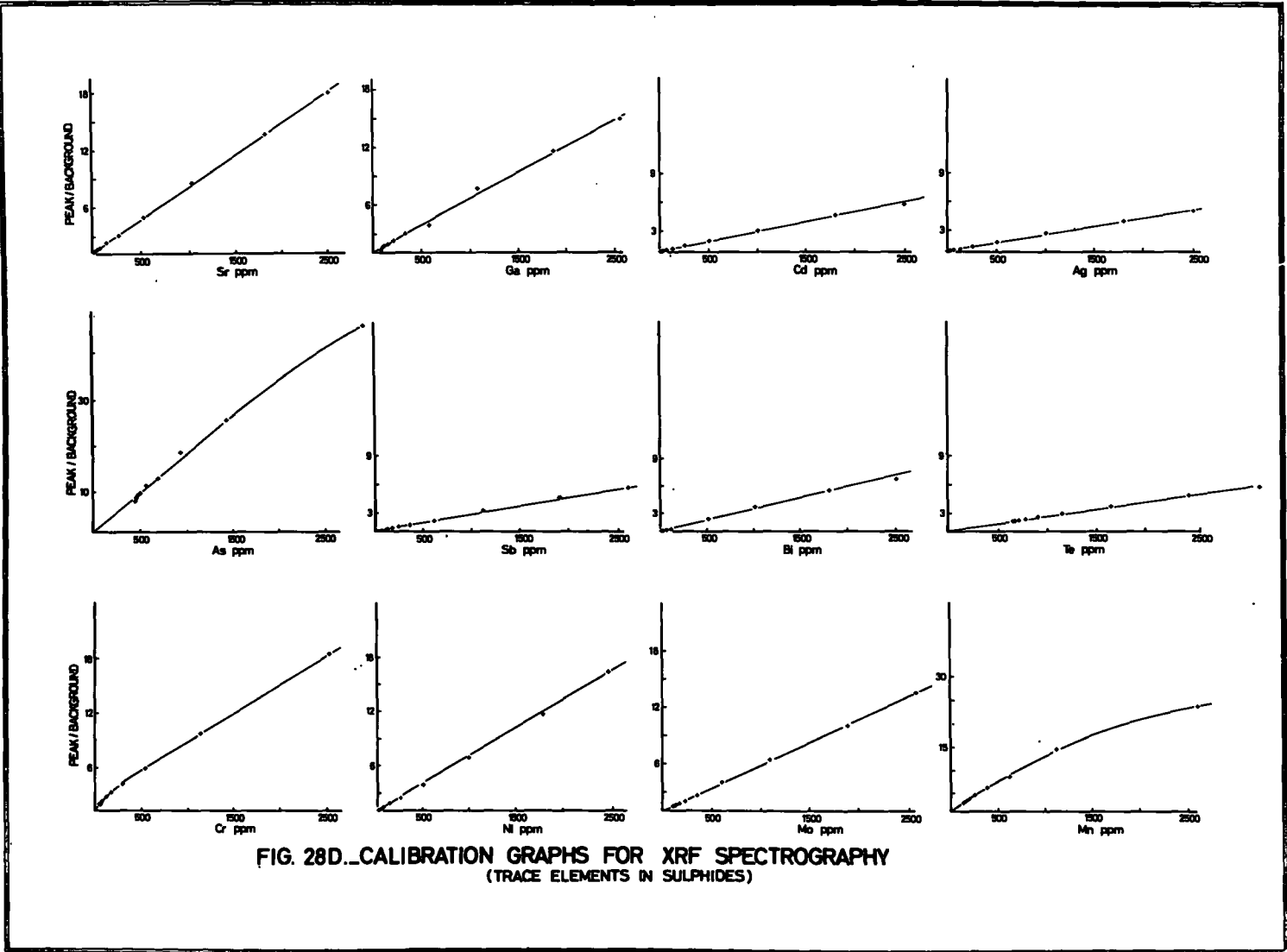


FIG. 28D...CALIBRATION GRAPHS FOR XRF SPECTROGRAPHY
(TRACE ELEMENTS IN SULPHIDES)

E.II Ai TRACE ELEMENT DISTRIBUTION IN PURIFIED INDIVIDUALSULPHIDE MINERALS

Results are set out in Tables 23 and 24.

It must be pointed out that although efforts were made to secure purified specimens of the various minerals discussed below, the nature of the ores is such that a strictly monomineralic concentrate would be almost impossible to achieve. As discussed and illustrated previously, most of the minerals contain small inclusions of other minerals that may profoundly affect the apparent trace element content. The results are nevertheless thought to be of interest in particular cases - as for example the results for chromium.

Pyrite:

Arsenic - The presence of arsenic in pyrite has been reported by many workers e.g. Fleischer (1955) gave summary tables for trace element content in pyrite and other sulphide minerals. Although in some cases this may be due to the presence of arsenopyrite or other arsenic bearing minerals, Neuhaus (1942) and Hoehne (1952) have shown that arsenic is present in "pure" pyrite. The first author found that optically homogenous pyrite containing about 5% and 2.70%. As had a larger unit cell ($a_0 = 5.442 \text{ \AA}$) than that of pure pyrite ($a_0 = 5.411 \text{ \AA}$) and he concluded that arsenic was present in True solid solution. In the case of the Lahanos pyrite, unit cell sizes vary from $a_0 = 5.416$ to $a_0 ; 5.418 \text{ \AA}$, which is also slightly larger than the value given for pure pyrite by Neuhaus. Pyrite from the Lahanos mine gave 487 ppm of As; which falls into the hydrothermally formed pyrite group described by Carstens (1941 a, b and c). According to Hawley (1952), the arsenic content

TABLE 23

Trace element distribution of pyrite, chalcopyrite, sphalerite and galena in the Lahanos, Murgul & Karadere mines

	<u>Sample No.</u>	<u>As</u>	<u>Sb</u>	<u>Bi</u>	<u>Cd</u>	<u>Cr</u>	<u>Co</u>	<u>Ga</u>	<u>Mn</u>	<u>Mo</u>	<u>Ni</u>	<u>Ag</u>	<u>Te</u>
PYRITE	NG 32	n.d.	140	n.d.	32	n.d.	n.d.	53	n.d.	71	21	19	360
	NG 33A	n.d.	133	n.d.	32	n.d.	n.d.	56	n.d.	102	22	13	450
	NG 37	n.d.	112	n.d.	42	n.d.	n.d.	56	n.d.	80	75	13	155
	NG(43-46)m	487	133	96	27	52	n.d.	44	329	125	37	32	348
CHALCOPYRITE	K	47	107	60	37	64	12	15	114	43	8	1	257
	NG(43-46)m	nil	122	nil	27	nil	58	29	n.d.	92	21	26	298
	NG 31	59	254	nil	17	35	257	11	647	61	9	1	225
	M12	33	68	nil	57	64	nil	nil	3	28	nil	19	132
	M15	nil	117	nil	90	nil	nil	5	nil	254	28	32	193
	M15	309	145	12	157	36	34	40	15	450	24	44	183
SPHALERITE	NG 39	2388	510	558	2537	42	nil	208	26	773	19	39	175
	NGD16	4920	640	1864	2270	31	44	270	18	281	11	146	247
	M12	893	608	160	2350	26	n.d.	131	11	265	n.d.	89	182
	Kd.P	1180	616	260	3730	nil	95	117	180	37	22	39	175
	Kd.Mix	n.d.	640	n.d.	3070	n.d.	n.d.	128	n.d.	47	n.d.	44	175
BORNITE	NGD8	5022	833	1080	42	38	25	35	nil	141	9	438	385
GALENA	Kd	12990	117	3870	104	nil	12	128	nil	47	nil	180	175

TABLE 24.

Co and Ni analysis of concentrated sulphides from the Lahanos,
Murgul and Karadere mines

<u>Sulphide Min.</u>	<u>Min. Deposit</u>	<u>Sample No.</u>	<u>Co</u>	<u>Ni</u>	<u>Co/Ni</u>	<u>Av.Co/Ni for each mine</u>
<u>PYRITE</u>	Lahanos	NGD4	20	19	1.05	
		NG10	12	23	0.52	
		NG18	66	8	8.25	
		NG20	46	9	5.11	
		NG32	nil	3	nil	
		NG34	254	83	3.06	
		93	94	9	10.44	
		94	111	12	9.25	
		102	143	5	28.60	8.29
		Kizilkaya	134	34	14	2.43
	Boztepe	150/3	873	43	20.30	20.30
	Karilar & Karaerik	KR2	157	10	15.70	
		KR3	34	5	6.80	11.25
	Çatak	Ct	84	4	21.00	21.00
	Murgul	M(210)py	27	3	9.00	
		M(111)py	99	1	99.00	
		X M 23A	71	9	7.89	38.63
Pillarcivat	P	512	5	102.10	102.40	
<u>CHALCO- PYRITE</u>	Lahanos	K	12	8	1.50	
		NG31	257	9	28.56	
		NG(43-46)m	59	21	2.81	10.96
	Murgul	M15	34	24	1.42	1.42
<u>BORNITE</u>	Lahanos	NGD8	25	9	2.78	2.78
<u>SPHALER- ITE</u>	Lahanos	NGD16	44	11	4.00	
		NG34	nil	20	nil	
		NG39	nil	19	nil	1.33
	Murgul	M2	nil	nil	nil	
	Karadere	Kd	95	22	4.32	4.32
<u>GALENA</u>	Karadere	Kd	12	nil	-	-

of pyrite decreases with increasing temperature of formation.

Antimony and Bismuth - The antimony values of 112 to 140 ppm and bismuth 96 ppm are probably due to sulphosalt impurities.

Cadmium - The cadmium content of pyrite from the Lahanos mine showed a variation of 27 to 42 ppm of Cd. Noddack and Noddack (1931) reported only one pyrite with about 10 ppm of Cd. The presence of cadmium in all pyrite samples of the Lahanos mine could well be due to tiny inclusions of sphalerite.

Chromium - The chromium concentration was determined in only one sample which gave 52 ppm of Cr. Hawley and Nichol (1961) mentioned the presence of chromium in all samples from Sudbury with a steady range between 10 to 20 ppm. This result from Lahanos is therefore rather anomalous, but as will be seen, it is repeated in other ores of this study.

Cobalt and Nickel - The cobalt and nickel contents of pyrite and other sulphides have been determined by the emission optical spectrograph because of iron $K\beta$ and Co $K\alpha$ interference in the XRF technique (conditions for Co and Ni in optical spectrograph - see appendix). Results are tabulated with Co:Ni ratios in Tab. 24. The significance of Cobalt content and Co:Ni ratios have been discussed by Hawley (1952) and Gavelin and Gabrielson (1947) who suggested that a Co:Ni ratio greater than one indicates a hydrothermal origin for pyrite. The results in Tab. 24 with one exception all suggest on this basis that the Lahanos pyrite is of hydrothermal origin. It should be noted that Fleischer (1955) has shown that exceptions

to this rule can occur.

Gallium - Although the geochemistry of gallium is mainly related to that of aluminium, it is partly chalcophile and occurs in sulphides of tetrahedral structure (Goldschmidt, 1954, pp.329). Thus the 44 to 56 ppm found in the Lahanos pyrite is probably from small inclusions of sphalerite.

Manganese - The presence of manganese in pyrite is to be expected since Hauerite MnS_2 is isostructural with pyrite. The only result available for the Lahanos-pyrite gave 329 ppm Mn. Gavelin and Gabrielson (1947) found no appreciable differences in the manganese content of pyrite from higher or lower temperature deposits, but they indicated a slight tendency of doubtful significance for pyrite associated with sphalerite rich ore to contain more manganese than pyrite associated with copper ores.

Molybdenum - Analysis of Mo in the Lahanos pyrite showed a variation from 71 to 125 ppm, compared to six pyrites from North America with a range 20 to 42 ppm of Mo (Stanton, 1967).

Silver - Tab. 23. Pyrite associated with chalcopyrite shows higher silver values than the massive pyrite. This may well be explained by the presence of tetrahedrite - tennantite and other sulphosalt minerals in close association with pyrite and chalcopyrite and their inclusion in pyrite.

Tellurium - Tellurium contents of the Lahanos-pyrite are given in Tab. 23 with a variation from 155 to 450 ppm of Te. As shown previously however, small inclusions of various tellurium containing minerals do occur.

Chalcopyrite:

Three separated Lahanos chalcopyrites have been analysed for As, Sb, Bi, Cd, Cr, Co, Ga, Mn, Mo, Ni, Ag and Te and their quantitative values are given in Tables 23 and 24.

Arsenic - Arsenic contents of 0, 47 and 59 ppm were found. These are probably due to the small inclusions of enargite and tennantite detected in the study of polished sections.

Antimony - Although the principal sulphosalt minerals present at Lahanos are arsenic rich, it is interesting to find that the trace antimony content of chalcopyrite is in each case higher than the amount of arsenic, suggesting that the chalcopyrite itself may carry a relative concentration of antimony. The amounts are much greater than the 20 ppm Sb quoted for a chalcopyrite by Noddack and Noddack (1931).

Bismuth - Bismuth has been found in one sample, which is known from polished section studies to contain tetradyomite. Noddack and Noddack (1931) found 5 ppm in chalcopyrite.

Cadmium - The cadmium content of chalcopyrite from the Lahanos mine varies from 17 to 37 ppm. Noddack and Noddack (1931) gave 180 ppm Cd from an analysed single chalcopyrite. The presence of sphalerite inclusions probably accounts for the observed values.

Chromium - As mentioned by Hawley and Nichol (1961) the chromium content of chalcopyrite is erratic, but where it is present or detectable it is almost constant, and they found a relatively high chromium content in Sudbury-chalcopyrite with a value of 79 ppm.

The Lahanos-chalcopyrite showed a similar chromium concentration.

Cobalt and Nickel - Hawley and Nichol (1961) suggested a range of 55 to 490 ppm Co for hydrothermally deposited chalcopyrite, therefore the cobalt content of the Lahanos mine falls into the hydrothermal range with a variation of 12 to 257 ppm Co. The Co:Ni ratio is higher than one.

Gallium - The gallium content of the Lahanos - chalcopyrite is apparently slightly less than chalcopyrite from the Soviet Union, for which Borovik et al. (1941) found 0 to 100 ppm.

Molybdenum - Noddack and Noddack (1931) and Yanishevsky (1934) found 70 - 70 - 900 ppm of Mo in three chalcopyrites compared with 43, 61, 92 in the present study.

Sphalerite:

There is general agreement that in addition to Fe, Mn and Cd, the elements Ga, Co and some others all occur in sphalerite substituting for zinc. Evrard (1945) stated, "the governing factor as to the presence of rare elements in sphalerite is the original composition of the parent magma. The variations resulting from modifications of temperature and pressure are then superimposed".

Antimony and Arsenic - The observed values are almost certainly due to inclusions of tennantite, enargite and tetrahedrite, all of which have been identified as inclusions in sphalerite during the examination of polished specimens.

Bismuth - Although bismuth minerals have been found in the Lahanos ore, they are not normally associated with sphalerite or

galena, yet specimen NGD16 contains almost 0.2% of bismuth. This could be produced by only 0.3% of tetradymite and such an amount cannot be excluded as a possible contaminant.

Cadmium - As mentioned by many other previous investigators cadmium is one of the most common trace elements that occur in sphalerite. The observed content of around 2000 ppm is therefore not particularly unusual.

Chromium - In common with other Lahanos minerals, sphalerite shows an unexpectedly high concentration of chromium. Its significance will be discussed later.

Cobalt and Nickel - To explain the observed Cobalt and nickel content of the sphalerite as resulting from inclusions of pyrite would require a much greater contamination by pyrite than is thought to be likely. It therefore seems probable that these elements may resemble iron in entering the sphalerite structure. O^ftedahl (1940) found no correlation between the cobalt and iron contents in sphalerite and Kullerud (1953) found no correlation between cobalt content and temperature of formation.

Gallium - As mentioned previously, gallium tends to enter sulphide minerals of tetrahedral structure and this is supported by the high gallium content of the sphalerite as compared with the other sulphides.

Manganese - Kullerud (1953), Gabrielson (1945), Launay and Urbain (1910) and many other previous investigators agree that the manganese content of sphalerite varies with the iron content and is highest in samples from high temperature deposits. The iron

content of the Lahanos sphalerite deduced from cell size measurements is relatively low (See Page.97) but even so the manganese contents found seem to be surprisingly low.

Molybdenum - Semi-quantitative analyses of molybdenum in sphalerite given by Fleischer (1955) showed a variation from 10 to 100 ppm. The value of 773 ppm Mo found for specimen NG39 is therefore rather high, and especially higher than for the other sulphide minerals. No molybdenite has been found in these ores and it therefore seems that Mo may preferentially enter the sphalerite structure.

Silver - Oftedahl (1940) suggested that all sphalerite samples, containing more than 50 ppm silver, must contain impurities such as galena or silver bearing sulphosalts. Because of the presence of these minerals at Lahanos, a similar explanation is probable.

Bornite:

It was not found possible to develop an effective flotation method for the separation of bornite. The sample for which results are given in Tables 18 and 19 was obtained by hand picking of the -48 + 60 mesh crushed ore. The observed trace element content has no outstanding feature that demands comment additional to those already made for other minerals.

E.II Aii MAJOR AND TRACE ELEMENT DISTRIBUTION IN LAHANOS

NEW GALLERY 2

Map 7 shows the location of specimens collected from New Gallery 2. It was not possible with the resources and time available to

collect truly representative samples of the type used to assess the grade of an ore body. However, each of the specimens collected was selected as being, as far as possible, representative of the ore body at that point.

To establish whether the ore zones tentatively recognised in the field represent real differences in the composition of the ore, the above specimens were analysed by XRF to establish their major and trace element contents. Because the computer correction programme of Holland and Brindle (1966) had not been used for sulphide rich materials and no analysed sulphide rich standards were available, the following methods were used.

For the nine major silicate rock elements Si, Al, Mg, Fe (total) Ca, Na, K, Ti and Mn count rates were compared with a series of 19 standards (including W1, G1 etc.) normally used in the department for silicate rock analysis. In the case of count rates less than the range covered by these standards, a linear variation passing through zero on both count rate and concentration axes was assumed, as shown in the working curves, Figs. 28 A-D.

For the remaining major elements S, Pb, Zn, Cu, Ba the addition method of Ahrens and Taylor, (1961, pp. 158) was used taking as base material NG11 from zone III, selected as satisfying the requirements for a base material as detailed by Ahrens and Taylor.

The results obtained (Table 25) are regarded as semi quantitative only, for the major elements, but the totals obtained suggest that the relative amounts are certainly significant.

TABLE 25

Major and trace element analyses of the NG-2 & OG-2 ore samples including other deposits

		NG1	NG2	NG3	NG4	NG5	NG6	NG7	NG8	NG9	NG10	NG11	NG12	NG14	NG15	NG16
SiO ₂	(%)	45.269	54.400	52.142	32.194	61.076	5.253	8.665	9.778	7.675	0	0	0.086	0.028	5.182	4.250
Al ₂ O ₃	"	23.079	12.693	11.185	30.520	7.806	3.399	4.678	9.810	5.347	0.145	0.266	1.050	0.633	2.822	23.906
Fe ₂ O ₃ (total)	"	12.542	12.499	13.865	16.011	11.351	35.946	29.450	19.870	27.332	33.238	36.574	34.032	41.972	35.276	29.641
MgO	"	0.009	0.018	0.629	0.129	0.370	0.878	2.126	1.665	0.079	4.645	3.072	1.136	0.371	0.876	0.652
CaO	"	0	0.027	0.527	0.060	0.699	0.791	2.020	2.388	0	4.778	3.059	1.346	0.275	0.730	0.060
Na ₂ O	"	0	0.097	0	0	0.329	0	0.978	0.157	0	0.567	0	0	0	0.730	1.654
K ₂ O	"	0	0	0.153	0.017	1.209	0.396	0.638	0.181	0	0	0	0	0	0.365	2.656
TiO ₂	"	0.373	0.451	0.179	0.661	0.107	0.037	0.128	0.188	0.208	0.072	0.027	0.074	0.151	0.255	0.338
MnO	"	0	0	0.002	0	0	0	0.002	0.008	0.001	0.049	0.016	0.015	0.004	0.010	0
Ba	"	0.150	0.115	0.095	0.094	0.128	0.095	0.193	0.930	0.930	0.104	0.092	0.100	0.093	0.095	0.104
Sr	(ppm)	790	11312	55	298	55	276	10	33	15	13	7	67	0	22	7
Mn	"	155	0	68	82	22	25	27	108	28	466	120	125	30	88	23
Ga	"	144	123	5	127	108	114	76	85	71	71	76	37	42	79	99
Cr	"	38	75	46	108	44	20	40	61	50	78	55	51	n.d.	41	27
Co	"															
Mo	"	37	40	45	40	45	48	80	131	96	115	98	98	57	88	67
Ni	"	46	40	22	22	26	0	7	31	31	35	17	24	6	0	6
S	(%)	17.62	17.10	20.59	19.25	15.79	52.10	50.38	42.45	48.12	51.25	51.37	47.70	52.725	52.12	34.85
Pb	"	0.525	0.950	0.400	0.475	0.775	0.529	0.512	0.725	0.825	0.988	1.400	0.850	1.150	0.875	0.888
Zn	"	0.073	0.145	0.095	0.075	0.200	0.302	0.082	0.145	0.150	0.875	0.868	0.405	0.587	0.125	0.673
Cu	"	0.200	0.275	0.132	0.350	0.087	0.194	0.082	11.575	9.150	3.025	3.087	13.125	1.925	0.413	0.251
Te	(ppm)	252	262	262	270	247	240	274	430	1075	590	732	410	415	422	262
As	"	0	253	1	5	51	0	8	183	208	445	422	393	166	328	140
Sb	"	112	173	108	100	100	95	117	100	122	133	128	128	133	122	95
Bi	"	0	0	0	0	0	0	0	128	108	240	48	56	n.d.	44	0
Cd	"	22	17	17	17	22	22	17	13	22	37	37	22	27	27	22
Ag	"	0	1	0	0	0	1	1	1	8	32	13	13	19	1	8

TABLE 25 (Contd.)

Major and trace element analyses of the NG2 & OG2 ore samples including other deposits

		<u>NG35</u>	<u>NG36</u>	<u>NG39</u>	<u>OG32</u>	<u>OG33</u>	<u>OG34</u>	<u>OG35</u>	<u>OG36</u>	<u>OG37</u>	<u>OG38</u>	<u>OG39</u>	<u>OG40</u>	<u>OG41</u>	<u>OG42</u>	<u>OG43</u>
SiO ₂	(%)	10.109	7.370	9.390	48.851	58.912	80.212	26.135	57.797	0	25.631	1.465	0.002	0	0	4.124
Al ₂ O ₃	"	45.691	22.363	2.309	19.585	11.241	14.155	18.208	12.122	22.890	19.480	15.958	5.397	4.877	0.749	20.106
Fe ₂ O ₃ (total)	"	4.569	12.114	12.130	12.678	11.300	1.437	21.062	5.387	16.792	18.700	9.347	0.258	0.001	43.222	13.610
MgO	"	0.096	0.090	0.043	0.009	0.008	0.116	0.009	4.836	0.018	0.024	0.005	0.002	0.001	0.561	0.028
CaO	"	0	0	0	0	0	0.017	0	8.914	0.018	0	0	0	0	0.893	0
Na ₂ O	"	0.442	0	0	0.162	0.152	0	0.606	1.689	0	0	0	0	0	0.273	0
K ₂ O	"	0.038	0.110	0.030	0	0	1.204	0.108	1.383	0	0.0006	0.071	0	0	0	0.097
TiO ₂	"	0.442	0.220	0.012	0.495	0.252	0.233	0.670	0.428	0.282	0.631	0.201	0.052	0.049	0.014	0.269
MnO	"	0	0.004	0.004	0	0	0	0.001	0.391	0	0	0	0	0	0.008	0.0006
Ba	"	16.950	13.550	1.520	0.110	0.198	0.095	0.128	0.095	12.075	0.201	12.400	23.150	24.325	0.098	13.900
Sr	(ppm)	3005	1913	183	805	5290	863	1048	1646	1679	144	2433	2850	1528	20	2760
Mn	"	0	0	0	17	10	8	25	5280	35	10	43	0	7	59	37
Ga	"	13	0	112	137	129	73	141	215	1434	1501	1	127	151	83	218
Cr	"	26	35	47	15	105	35	71	67	0	42	33	21	54	35	23
Co	"															
Mo	"	59	54	184	57	40	39	147	34	57	90	67	37	40	135	71
Ni	P	52	48	49	65	37	193	108	74	22	24	0	55	61	17	48
S	(%)	17.52	25.75	41.05	17.08	15.05	1.67	31.06	4.75	42.92	29.13	35.40	19.12	10.87	52.75	28.37
Pb	"	2.463	2.450	13.300	0.625	1.262	0.525	1.012	1.050	0.900	0.785	5.037	29.095	35.095	0.688	6.550
Zn	"	0.561	0.101	14.650	0.087	0.570	0.092	0.120	0.285	3.400	1.900	17.750	21.400	23.375	0.373	9.550
Cu	"	5.438	15.550	5.383	0.162	0.437	0.087	0.663	0.098	0.350	3.062	1.862	0.562	0.362	0.238	3.150
Te	(ppm)	193	132	410	262	262	207	270	220	167	332	232	45	37	360	247
As	"	312	684	2990	24	117	0	184	41	111	1501	1631	5241	6707	347	1556
Sb	"	95	163	425	122	133	91	117	91	38	825	216	340	287	107	262
Bi	"	96	164	532	0	0	0	0	0	0	20	176	1055	1392	64	16
Cd	"	0	0	438	27	22	22	17	22	0	32	172	269	162	22	52
Ag	"	0	55	95	0	0	0	0	0	0	0	0	0	8	39	0

TABLE 25 (Contd.)

Major and trace element analyses of the NG2 & OG2 ore samples including other deposits

		OG44	OG45	OG 46	OG47	OG48	OG49	OG50	OG51	OG52	OG53	OG54	OG55	OG56	92
SiO ₂	(%)	0.135	4.494	2.134	0.875	2.226	8.839	16.450	22.865	41.680	13.249	9.464	1.183	6.197	1.121
Al ₂ O ₃	"	9.406	22.470	5.427	30.678	22.562	39.400	32.450	18.723	38.952	32.401	6.448	9.071	5.994	0.374
Fe ₂ O ₃ (total)	"	24.219	7.862	34.883	3.771	4.392	19.914	18.812	16.278	8.957	14.131	29.485	31.192	27.176	44.56
MgO	"	0.448	0.029	0.036	0.020	0	0.046	0.045	0.024	0.019	0.035	0.031	0.048	0.051	0.015
CaO	"	3.773	0	0.024	0	0	0	0	0	0	0	0	0	0.132	0
Na ₂ O	"	0	0	0.561	0	0	0	0.198	0	0.828	0	0	0.418	0	0
K ₂ O	"	0	0.029	0.170	0	0	0.002	0	0	0	0	0	0.155	0.325	0
TiO ₂	"	0.118	0.314	0.073	0.350	0.276	1.379	1.595	0.325	1.157	0.821	0.364	0.466	0.173	0.120
MnO	"	0.016	0	0.001	0	0	0.004	0.003	0	0.001	0.0005	0.001	0.002	0.0004	0.001
Ba	"	3.700	13.900	1.875	18.400	16.500	0.117	0.101	1.305	0.093	6.550	0.092	4.325	1.825	0.095
Sr	(ppm)	579	2186	490	3275	3175	1228	192	695	199	1657	152	547	228	0
Mn	"	745	74	0	0	15	65	50	0	30	118	25	0	0	8
Ga	"	56	90	83	69	90	350	253	107	227	116	110	69	94	77
Cr	"	39	43	34	21	26	194	45	60	51	41	62	61	194	39
Co	"														
Mo	"	75	67	43	61	258	129	178	102	59	80	40	65	39	53
Ni	"	30	59	7	51	54	51	51	28	48	40	0	12	0	0
S	(%)	45.30	27.60	52.05	21.90	23.70	29.30	28.85	30.60	6.95	26.32	51.35	51.45	50.90	52.75
Pb	"	1.087	3.287	1.312	6.512	10.087	0.450	0.875	0.850	1.113	1.175	1.625	1.150	0.837	0.750
Zn	"	4.000	15.250	1.000	14.000	16.000	0.195	0.382	1.483	0.075	3.350	0.505	0.174	5.975	0.070
Cu	"	7.275	4.237	0.300	2.913	3.537	0.087	0.100	6.375	0.074	1.550	0.488	0.238	0.262	0.087
Te	(ppm)	397	189	274	140	215	291	286	1105	232	415	257	207	247	232
As	"	2750	1545	402	1651	2365	199	188	5220	21	1315	402	171	83	38
Sb	"	417	780	112	308	603	112	122	4290	112	370	168	88	95	95
Bi	"	28	44	20	128	220	28	4	52	0	16	200	44	0	0
Cd	"	42	184	13	90	162	17	17	32	27	8	32	8	31	22
Ag	"	32	0	19	0	0	0	0	26	0	0	26	0	1	7

TABLE 25 (Contd.)

Major and trace element analyses of the NG2 & OG2 ore samples including other deposits

		<u>93</u>	<u>94</u>	<u>102</u>	<u>134</u>	<u>150/3</u>	<u>151</u>	<u>KR2</u>	<u>KR3</u>	<u>PL1</u>	<u>PM2</u>	<u>PU3</u>	<u>Pl</u>	<u>Qt 1</u>	<u>Qt 3</u>
SiO ₂	(%)	0	0	0.370	30.744	0	18.508	0	3.177	n.d.	70.109	0	n.d.	52.966	61.684
Al ₂ O ₃	"	0.295	2.513	0.602	8.252	0.029	12.754	2.538	1.689	n.d.	4.069	0.755	n.d.	1.859	6.612
Fe ₂ O ₃ (total)	"	45.388	41.953	44.888	15.046	42.575	11.565	43.870	42.237	n.d.	18.241	3.151	n.d.	7.130	11.549
MgO	"	0.016	0.072	0.015	0.037	0.044	0.364	0.013	0.072	n.d.	0.959	0	n.d.	1.974	0.027
CaO	"	0	0	0.009	0	0	0.058	0.044	0	n.d.	0	0	n.d.	3.463	7.554
Na ₂ O	"	0	1.508	0.540	0.769	1.721	0	0.058	0	n.d.	0	0	n.d.	3.832	0
K ₂ O	"	0	0.004	0.031	0.087	0	2.445	0.015	0.202	n.d.	0	0	n.d.	0	0
TiO ₂	"	0.404	0.029	0.003	0.025	0	0.211	0.073	0.101	n.d.	0.023	0.003	n.d.	0.255	0.299
MnO	"	0.002	0.001	0	0	0.0006	0.006	0	0.012	n.d.	0.117	0.040	n.d.	0.166	0.036
Ba	"	0.125	0.120	0.099	0.095	0.092	0.750	0.100	0.107	0.095	0.095	0.093	0.093	0.092	0.093
Sr	(ppm)	76	0	0	0	0	5	0	0	0	0	0	39	38	565
Mn	"	19	0	15	1	26	0	21	5	250	228	245	2210	1148	618
Ga	"	74	89	90	106	71	125	87	89	127	107	130	46	96	130
Cr	"	35	68	41	38	410	39	26	57	33	35	40	47	59	113
Co	"				34	873									
Mo	"	75	34	43	61	43	69	39	71	48	86	39	33	53	57
Ni	"	10	2	0	12	35	40	1	1	49	0	54	18	0	42
S	(%)	52.85	52.84	52.60	42.95	53.00	24.50	52.55	51.70	29.75	0.52	27.99	42.60	12.15	11.30
Pb	"	0.672	0.525	0.688	1.675	0.812	0.600	0.500	0.537	3.375	0.580	26.450	0.512	0.525	0.473
Zn	"	0.102	0.077	0.055	0.120	0.015	24.975	0.073	0.040	24.350	0.615	23.150	0.185	0.160	0.127
Cu	"	0.163	0.260	0.053	0.136	1.075	3.037	0.106	0.066	0.625	5.375	2.363	4.600	0.544	0.050
Te	(ppm)	270	257	215	240	281	167	270	240	45	220	215	220	207	262
As	"	495	15	0	94	55	37	50	0	438	0	4755	1	0	0
Sb	"	140	95	80	127	95	321	91	100	160	188	302	91	87	100
Bi	"	16	8	0	0	12	0	0	0	240	0	1339	0	0	54
Cd	"	32	22	17	22	27	1450	22	32	1665	27	1294	22	22	17
Ag	"	13	13	0	0	7	8	13	1	0	39	204	1	0	0

Fig. 29 shows graphically the results for the major ore elements related to the position of each specimen in the New Gallery and the ore zone boundaries estimated during the field work.

There is a general agreement between the results and what would be expected from the descriptions of the mineralogy of the various ore zones as previously given.

E.II Bi VERTICAL DISTRIBUTION OF MAJOR AND TRACE ELEMENTS

As previously mentioned, cores from the large number of boreholes at Lahanos have not been preserved, but it was possible to obtain partial core samples from the two recent Lahanos boreholes A and B. The samples obtained from the ore horizons in the core were necessarily limited because of the amount needed for assay purposes, but more complete sampling was possible from the unmineralised country rock.

Analysis was carried out as described in E.II Aii for major and trace element contents of the ore horizon, whilst the country rock results were corrected by the Holland and Brindle (1966) procedure. The results are given in Tables 26 and 27 A and B, and Figs. 30-36 show the results graphically. Petrographic descriptions of the rocks have been given previously. The principal features of interest are as follows -

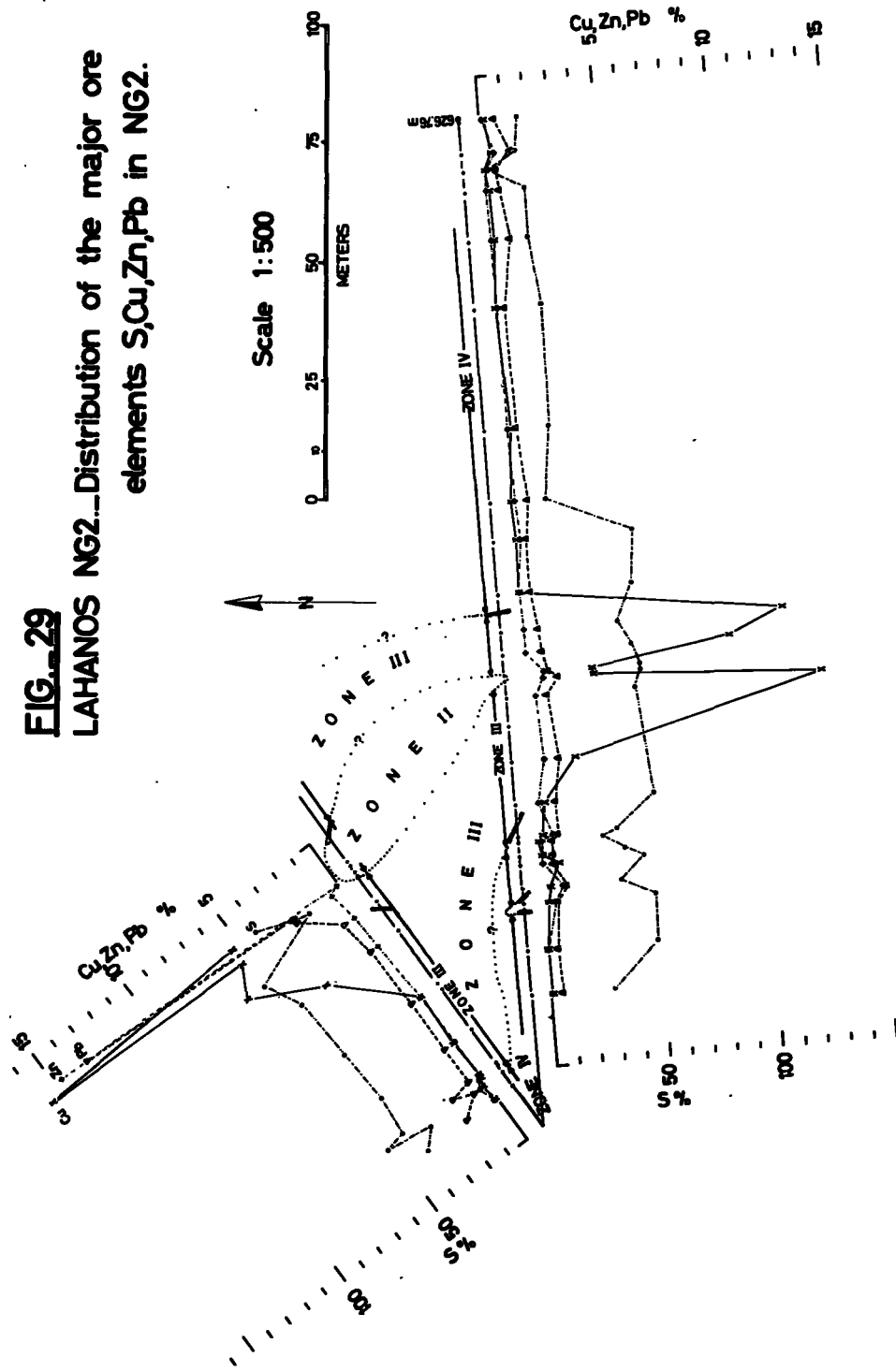
1. Lithophile major elements (Fig. 30 A and B). Aluminium increases appreciably in amount near the upper margin of the ore horizon, particularly in borehole B. This corresponds with the

TABLE 26

Major and trace element analyses of the boreholes A & B ore samples

		A5500	A5550	A5555	A5660	A6050	A6400	A6500	B7800	B7900	B8000	B8100	B8200	B8300	B8350	B8900	B9500	B11800
SiO ₂	(%)	2.006	0	0	1.770	20.282	22.057	33.796	17.142	0.213	6.131	4.172	7.400	4.998	23.356	18.270	8.718	45.168
Al ₂ O ₃	"	27.566	2.614	1.847	13.238	15.084	16.451	21.676	2.316	0.695	0.229	0.368	0.156	1.527	2.910	0.559	3.464	2.702
Fe ₂ O ₃	"																	
(total)	"	12.867	7.760	6.590	13.068	21.901	19.944	15.535	20.397	33.065	28.709	31.099	30.536	30.261	18.405	25.634	28.363	11.462
MgO	"	0.619	0.925	1.205	0.041	1.534	4.513	1.708	0.148	0.056	0.020	0.022	0.063	4.998	3.084	2.125	6.789	0.100
CaO	"	0.759	0.689	1.586	0	1.756	6.286	1.895	0	0.003	0	0	0	6.206	4.126	2.750	13.159	0
Na ₂ O	"	1.849	0	0	0	0.588	1.700	2.310	0	0	0	0	0	0.337	0	0	0	0.100
K ₂ O	"	0	0	0	0.010	0.003	0.124	2.643	0.218	0.020	0	0.001	0	0.232	0.402	0.718	0.513	0.469
TiO ₂	"	0.305	0.035	0.023	0.170	0.315	0.256	0.438	0.016	0.017	0.004	0.008	0.009	0.013	0.027	0.022	0.045	0.066
MnO	"	0.006	0.019	0.029	0.001	0.03	0.006	0	0.007	0.012	0.009	0.009	0.005	0.233	0.142	0.652	0.453	0
Ba	"	13.450	3.925	2.700	10.025	0.095	0.099	0.145	0.543	0.210	0.095	0.092	0.070	0.090	0.093	0.095	0.099	0.104
Sr	(ppm)	2746	688	556	1255	97	61	37	44	0	0	0	0	7	0	1	10	0
Mn	"	97	88	208	104	53	85	35	n.d.	103	95	97	41	2870	1630	821	4878	8
Ga	"	46	117	3	77	3	129	117	63	0	58	58	0	87	107	89	0	63
Cr	"	259	73	19	84	0	163	0	199	43	54	53	59	213	249	691	1215	42
Co	"																	
Mo	"	50	48	61	75	111	84	141	258	302	173	244	76	215	160	206	86	57
Ni	"	63	49	52	55	7	3	8	39	55	28	26	16	9	7	4	9	13
S	(%)	32.60	42.75	36.70	41.62	36.37	27.90	18.95	45.40	51.58	50.55	50.45	50.87	48.55	45.20	48.75	37.12	39.12
Pb	"	5.088	18.876	24.587	5.825	0.525	0.375	0.563	2.787	3.325	4.037	2.637	1.262	0.650	0.575	0.550	0.425	0.525
Zn	"	0.423	19.225	20.050	10.775	0.337	0.100	0.232	0.250	2.600	1.575	3.602	0.735	0.952	0.337	0.132	0.140	0.073
Cu	"	2.012	2.587	3.788	2.988	1.138	0.079	0.138	10.562	8.162	8.400	7.313	8.750	0.837	0.725	0.094	0.056	0.055
Te	(ppm)	305	450	760	558	274	305	283	240	352	305	298	347	340	317	274	233	252
As	"	793	2970	4268	1598	36	7	23	806	1371	1283	1085	508	545	197	144	20	5
Sb	"	0	308	440	630	91	108	100	298	233	198	163	128	140	122	95	91	91
Bi	"	124	467	796	164	0	52	0	92	164	124	140	212	68	0	16	0	0
Cd	"	0	681	490	103	22	27	17	22	90	66	90	37	27	17	22	22	32
Ag	"	0	13	60	0	0	1	0	60	83	26	26	19	19	0	1	0	0

FIG. 29
LAHANOS NG2...Distribution of the major ore
elements S, Cu, Zn, Pb in NG2.



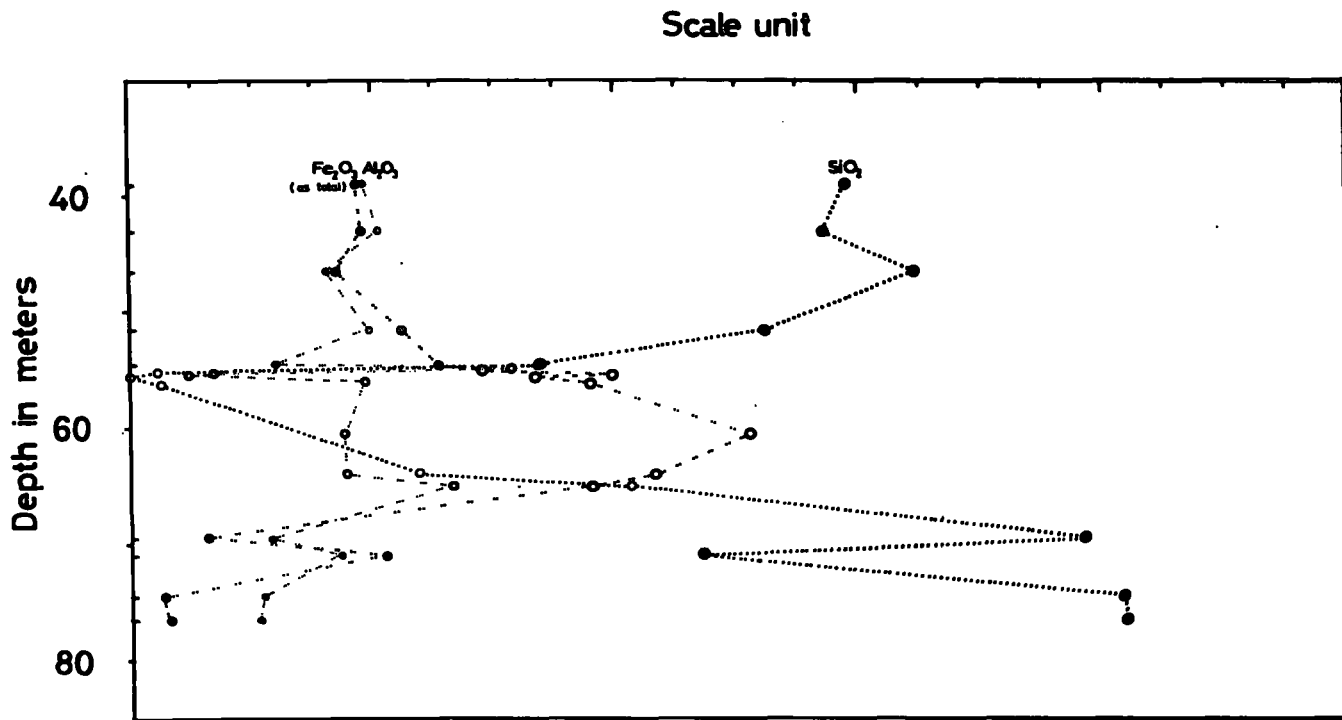
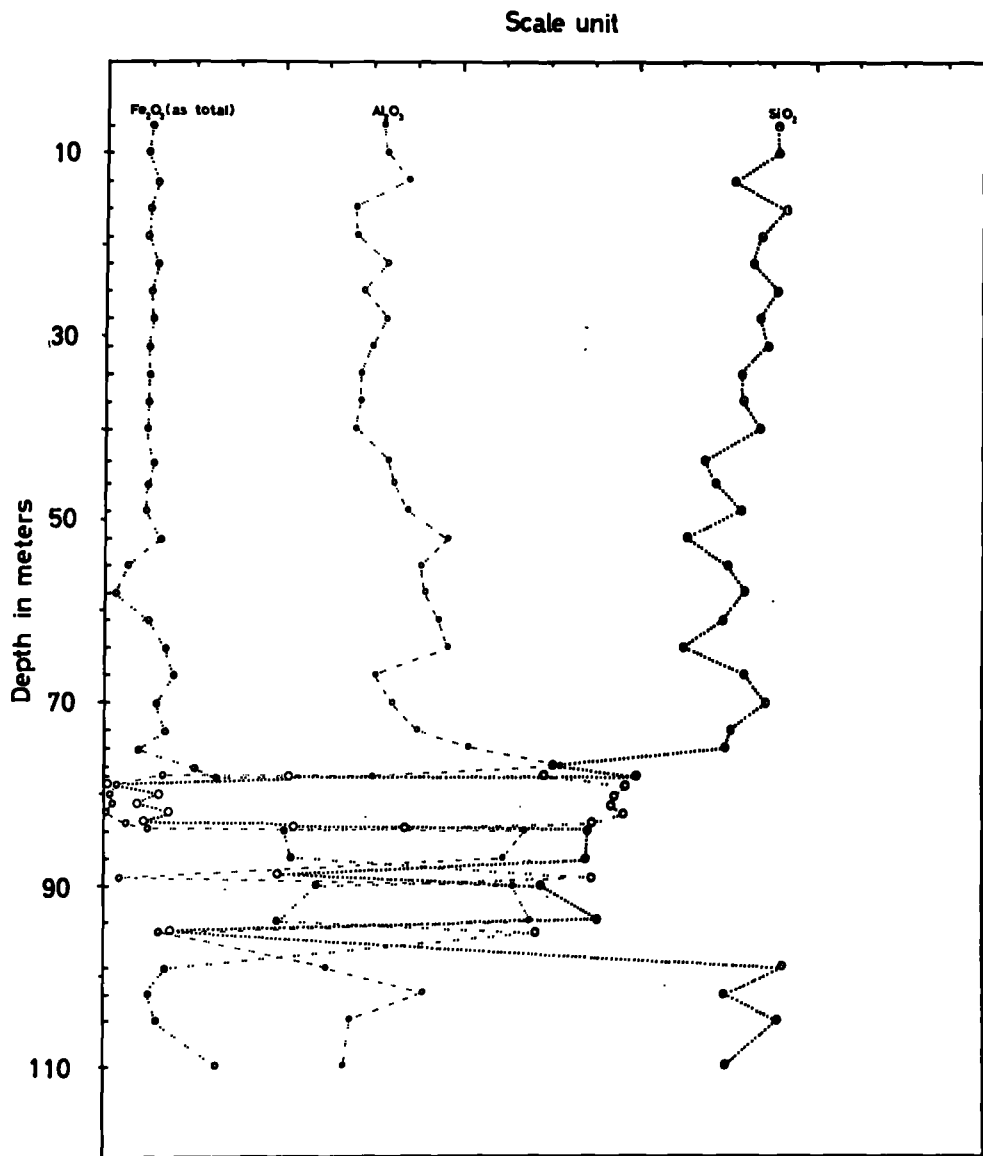


FIG. 30A
 LAHANOS BOREHOLE A. Distribution of the lithophile elements SiO₂, Al₂O₃, total iron as Fe₂O₃ with depth. Solid symbols=rock, open symbols=ore.
 One scale unit for SiO₂ & Al₂O₃ = 5.00%
 " " " " Fe₂O₃ = 2.50%



FIG_30B

LAHANOS BOREHOLE B.-Distribution of the lithophile elements SiO₂, Al₂O₃, total iron as Fe₂O₃ with depth. Solid symbols=rock, open symbols=ore.

One scale unit for SiO₂ = 5.00%

" " " " Al₂O₃ & Fe₂O₃ = 2.50%.

presence of kaolinite-dickite as alteration products, referred to elsewhere.

2. Lithophile minor and trace elements (Figs. 31 A,B; 32 A,B). Mg, Ca, Ti, Mn, Ga, Ba, and Sr also show a marked increase corresponding with the increase in Al referred to above. Potassium shows a maximum value in borehole B, some 30 meters above the ore horizon. It is not possible to determine with certainty whether this is due to a difference in the original rock chemistry or to an upward migration of K following hydrothermal mineralisation. It is interesting to note that in borehole A, Ba occurs as a major element accompanying the sulphide mineralisation, whilst remaining a minor element in B (Fig. 33 A, B).

3. Chalcophile major and trace elements (Figs. 33 A,B; 35, A,B; 36 A,B). The principal feature of interest is the distinct increase in trace zinc some 10 meters above the top of the ore horizon.

4. Siderophile major and trace elements (Fig. 34 A,B) Molybdenum is regarded by Goldschmidt (1954) as a siderophile element and it is convenient to show its distribution on this figure. Its maximum in the ore horizon^{is} of interest and also the fact that the position of the maximum within the ore horizon is different in the two boreholes.

E.II Bii SURFACE GEOCHEMISTRY

During the last three decades, applied geochemical studies have mainly been concerned with secondary dispersion patterns and primary geochemical dispersion patterns have received less attention (Ginzberg,

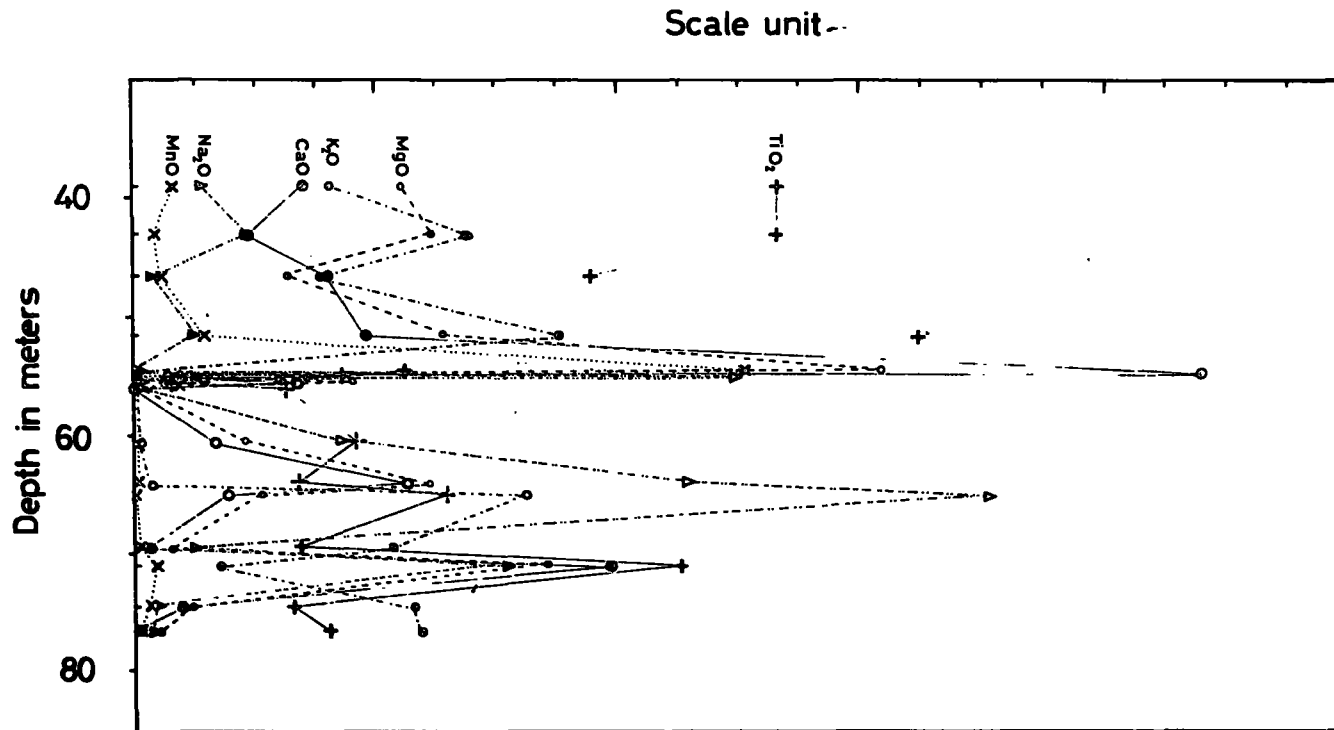


FIG._31A

LAHANOS BOREHOLE A.-Distribution of the lithophile elements MgO,CaO,K₂O,Na₂O,MnO,TiO₂ with depth. Solid symbols=rock, open symbols=ore.

One scale unit for CaO & K₂O = 1.50 %

" " " " MgO= 1.00 %

" " " " Na₂O= 0.20 %

" " " " MnO & TiO₂%.

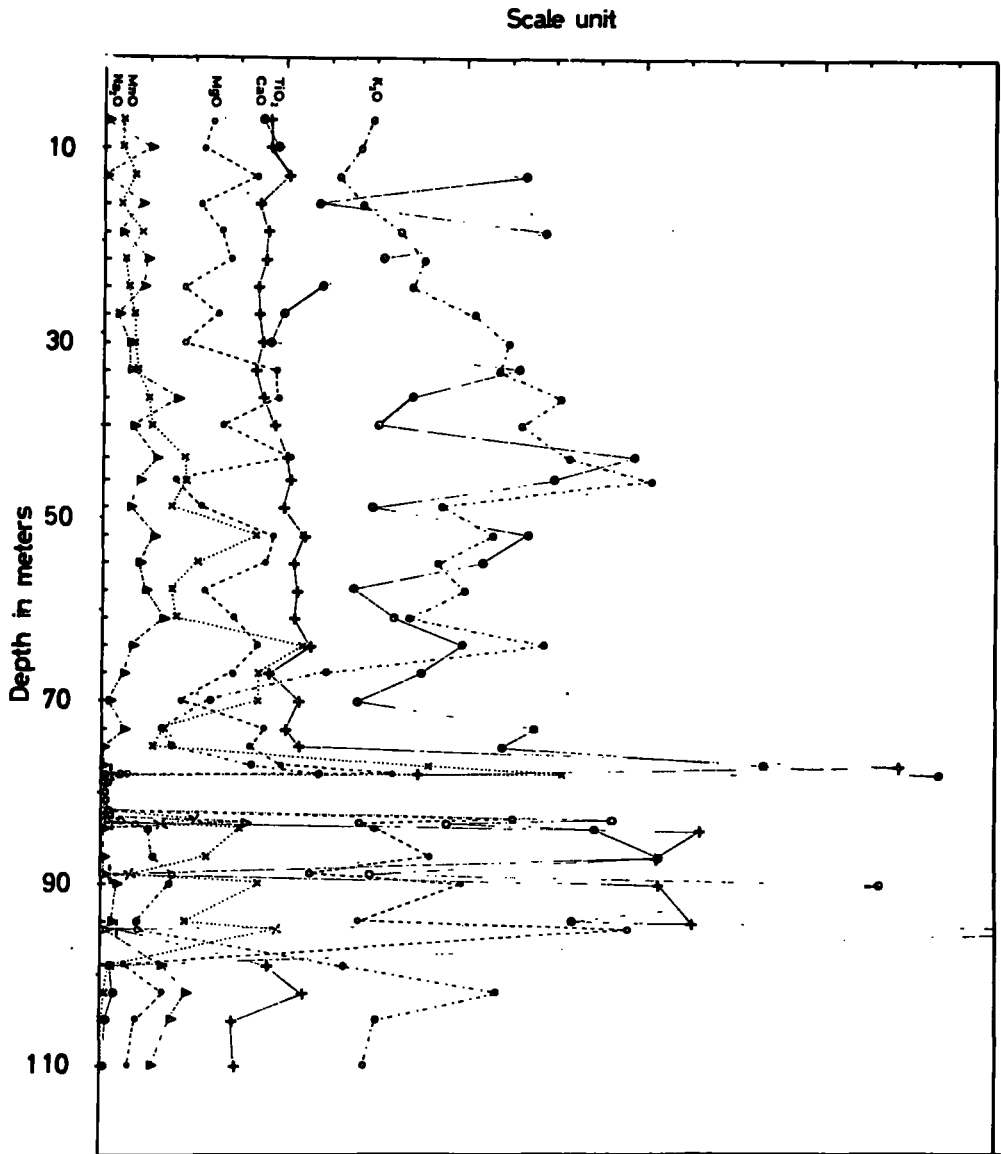


FIG. 31B
 LAHANOS BOREHOLE B. - Distribution of the lithophile elements MgO, CaO, K₂O, Na₂O, MnO, TiO₂
 with depth. Solid symbols=rock, open symbols=ore.
 One scale unit for MgO, CaO & K₂O=0.50%
 " " " " Na₂O, MnO & TiO₂=0.10%.

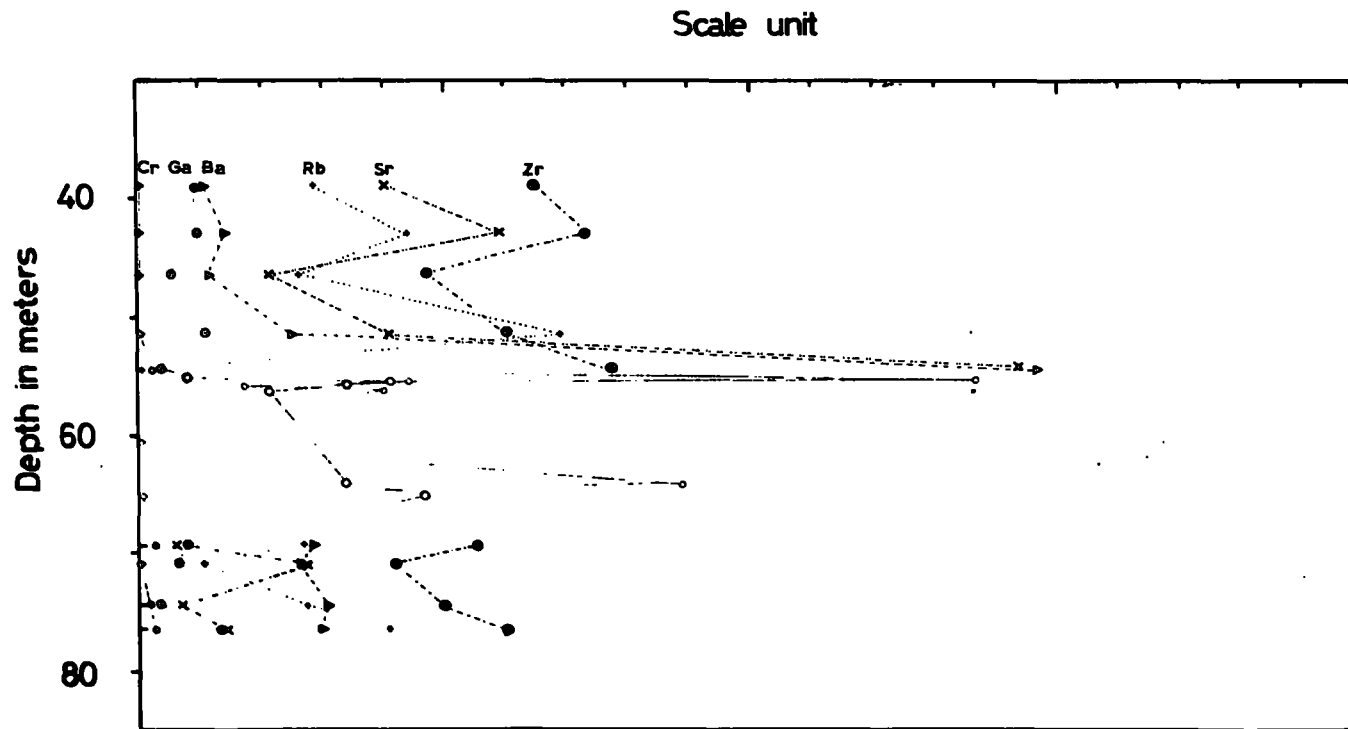


FIG._32A

LAHANOS BOREHOLE A. Distribution of the trace lithophile elements Ba,Sr,Cr,Zr,Ga,Rb with depth.

One scale unit for Ba=100 ppm.(Solid symbols=rock, open symbols=ore)

" " " " Sr= 40 ppm

" " " " Cr,Zr & Ga= 20 ppm

" " " " Rb= 10 ppm

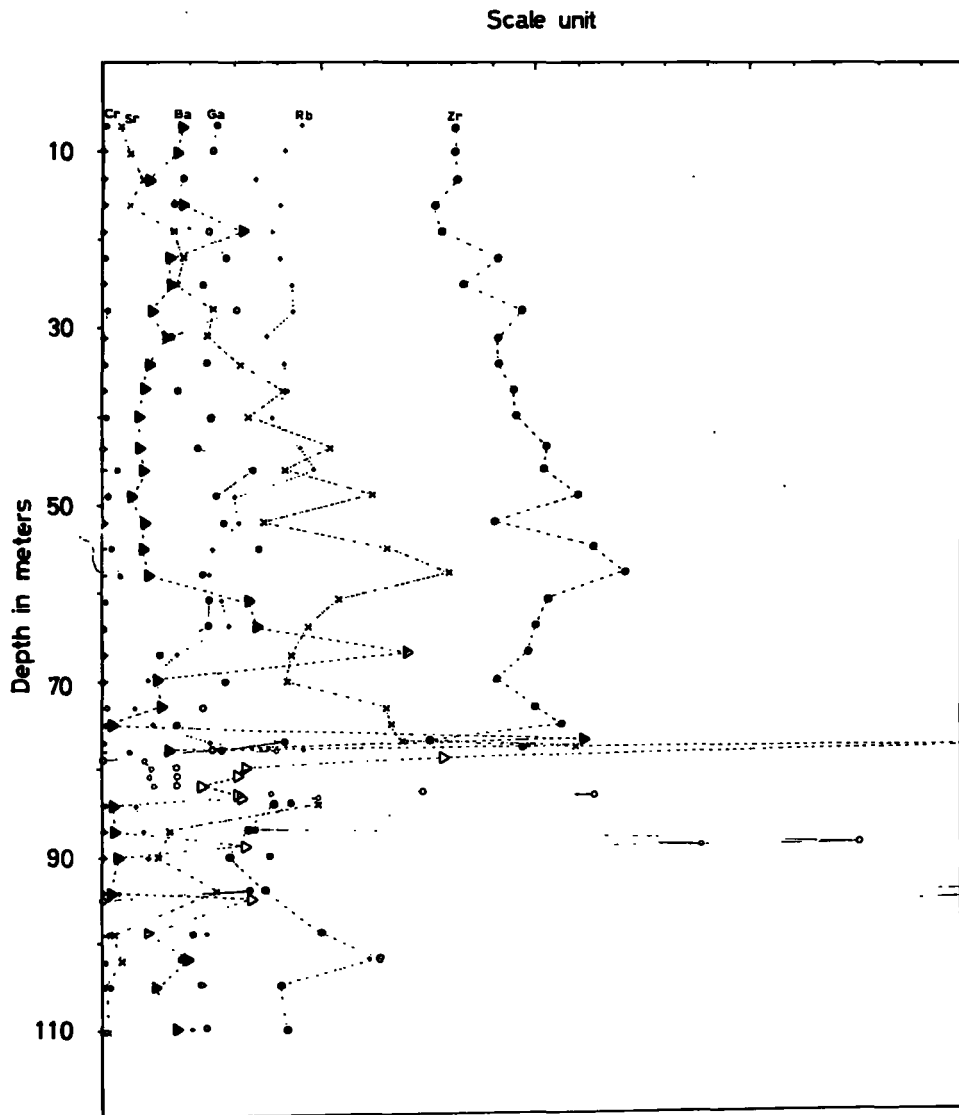


FIG. 32B
LAHANOS BOREHOLE B.—Distribution of the trace lithophile elements Ba, Sr, Cr, Zr, Rb, Ga with depth.

One scale unit for Ba=250 ppm.(Solid symbols=rock, open symbols=ore)
 " " " " Sr & Cr = 50 ppm
 " " " " Zr = 20 ppm
 " " " " Rb = 10 ppm
 " " " " Ga = 5 ppm.

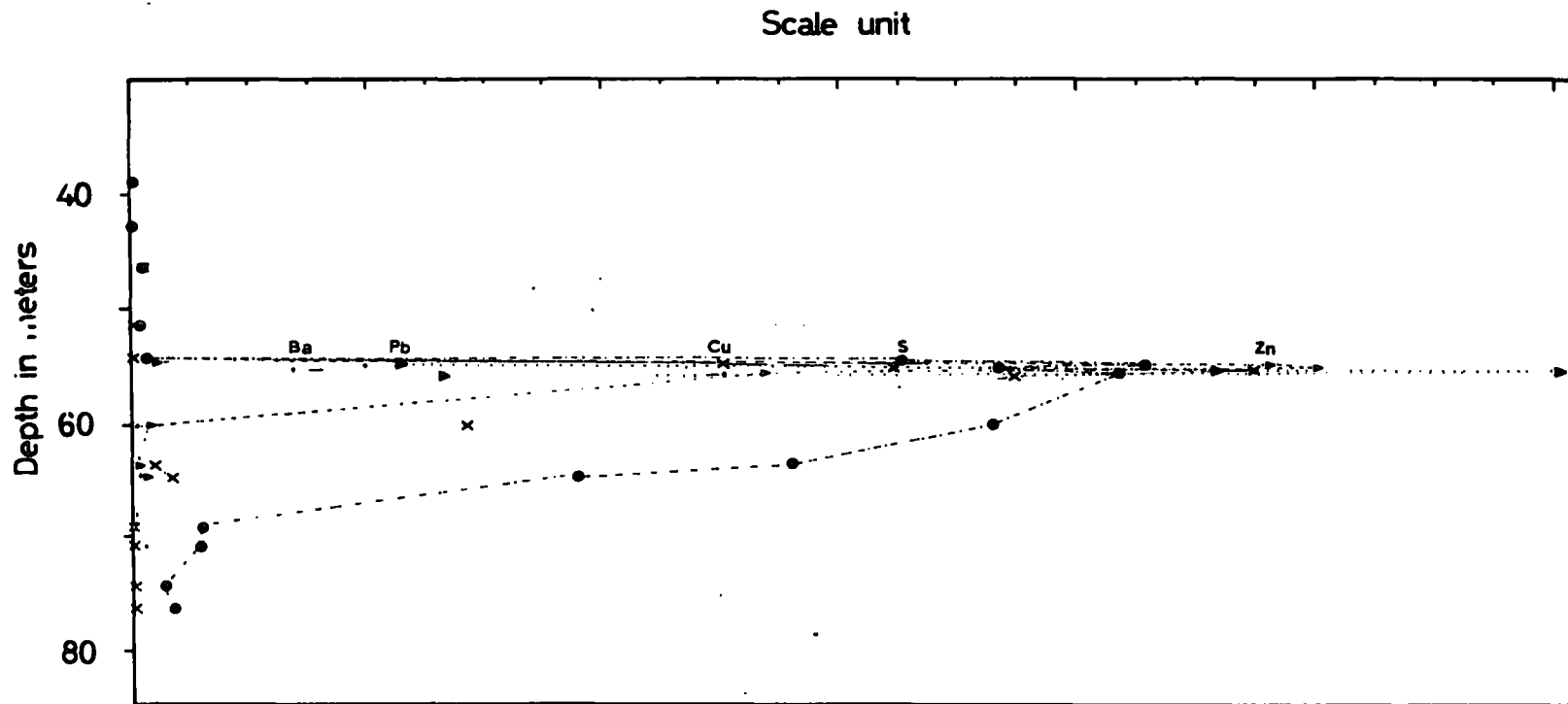


FIG. 33A

LAHANOS BOREHOLE A.—Distribution of the major elements S,Pb,Zn,Ba,Cu with depth in the ore horizon.

One scale unit for S=2.50%

" " " " Pb,Zn,Ba=1.00%

" " " " Cu=0.20%

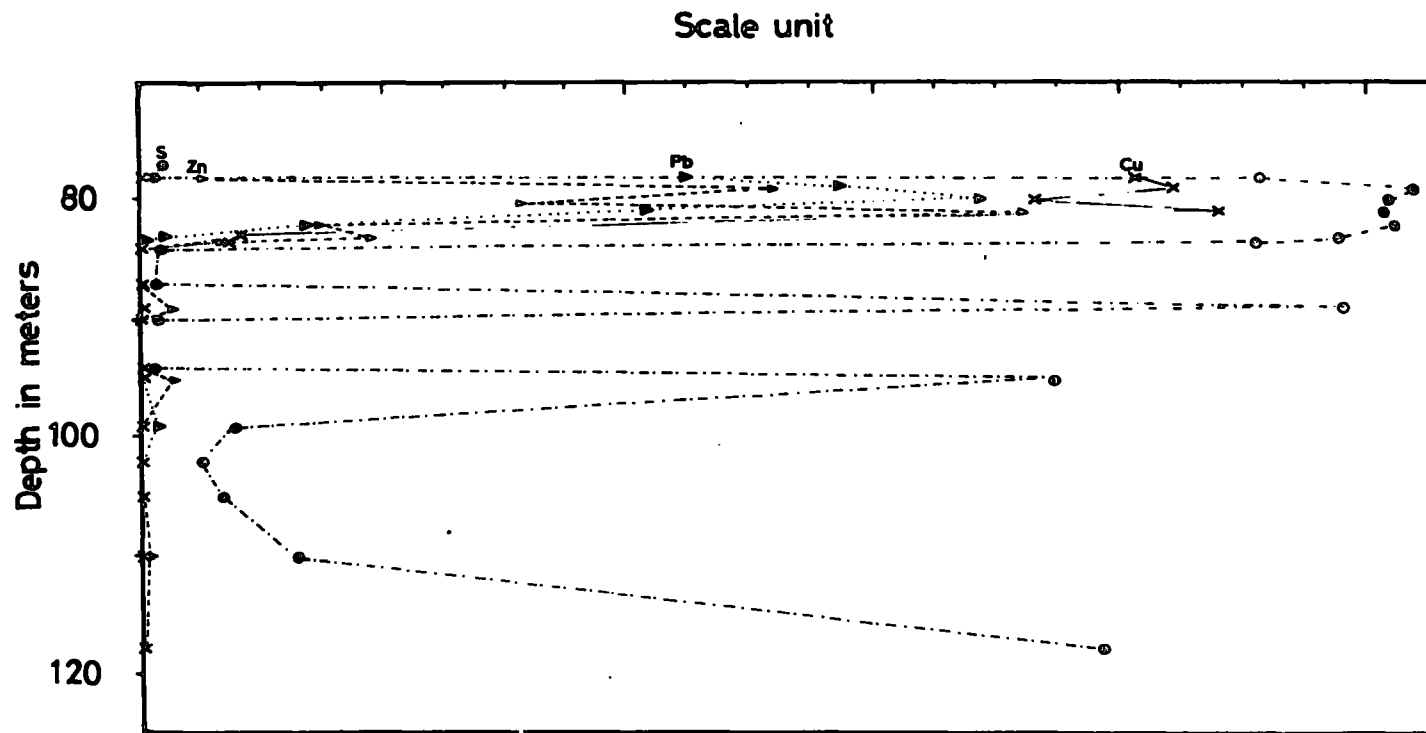


FIG. _33B

LAHANOS BOREHOLE B.-Distribution of the major elements S,Cu,Pb,Zn with depth in ore horizon.

One scale unit for S=2.50%

" " " " Cu=0.50%

" " " " Pb & Zn=0.25%

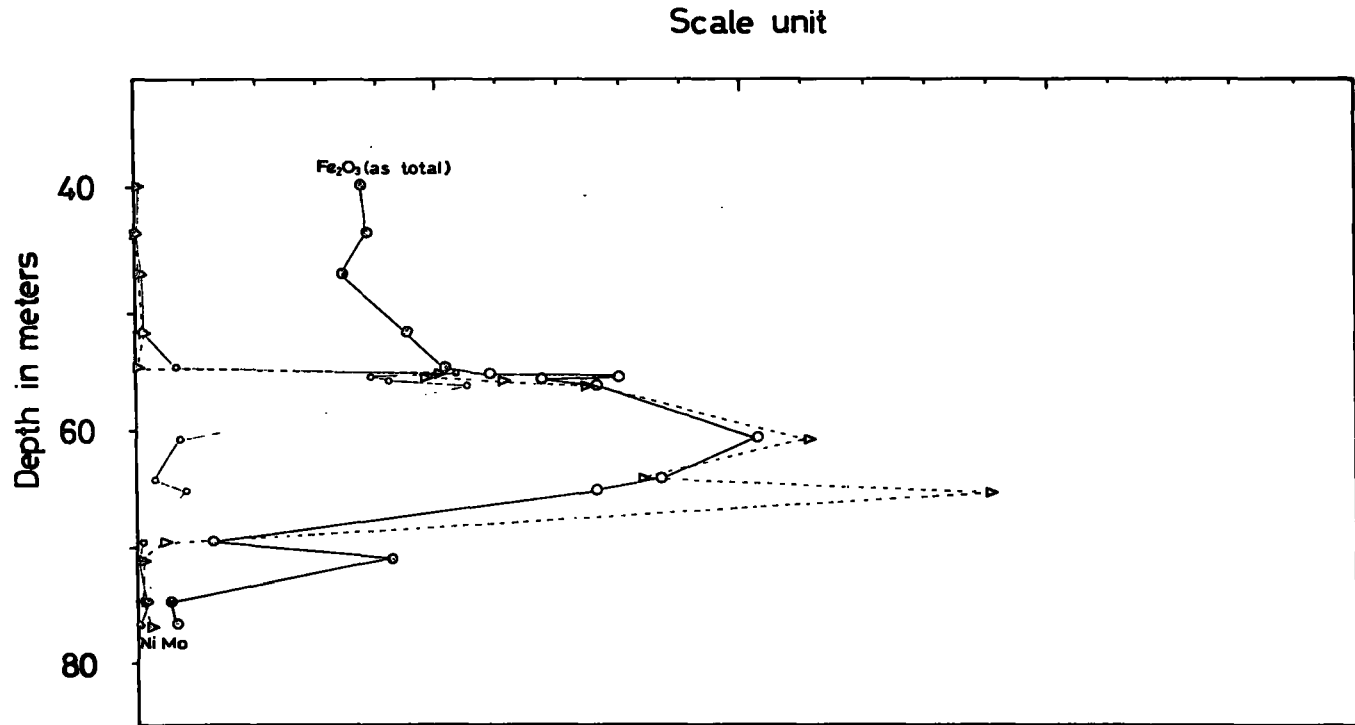


FIG. 34A

LAHAHANOS BOREHOLE A.—Distribution of the siderophile elements total iron as Fe₂O₃, Mo, Ni with depth. Solid symbols=rock, open symbols=ore.

One scale unit for Fe₂O₃ = 2.50%
 " " " " Mo & Ni = 10 ppm.

Scale unit

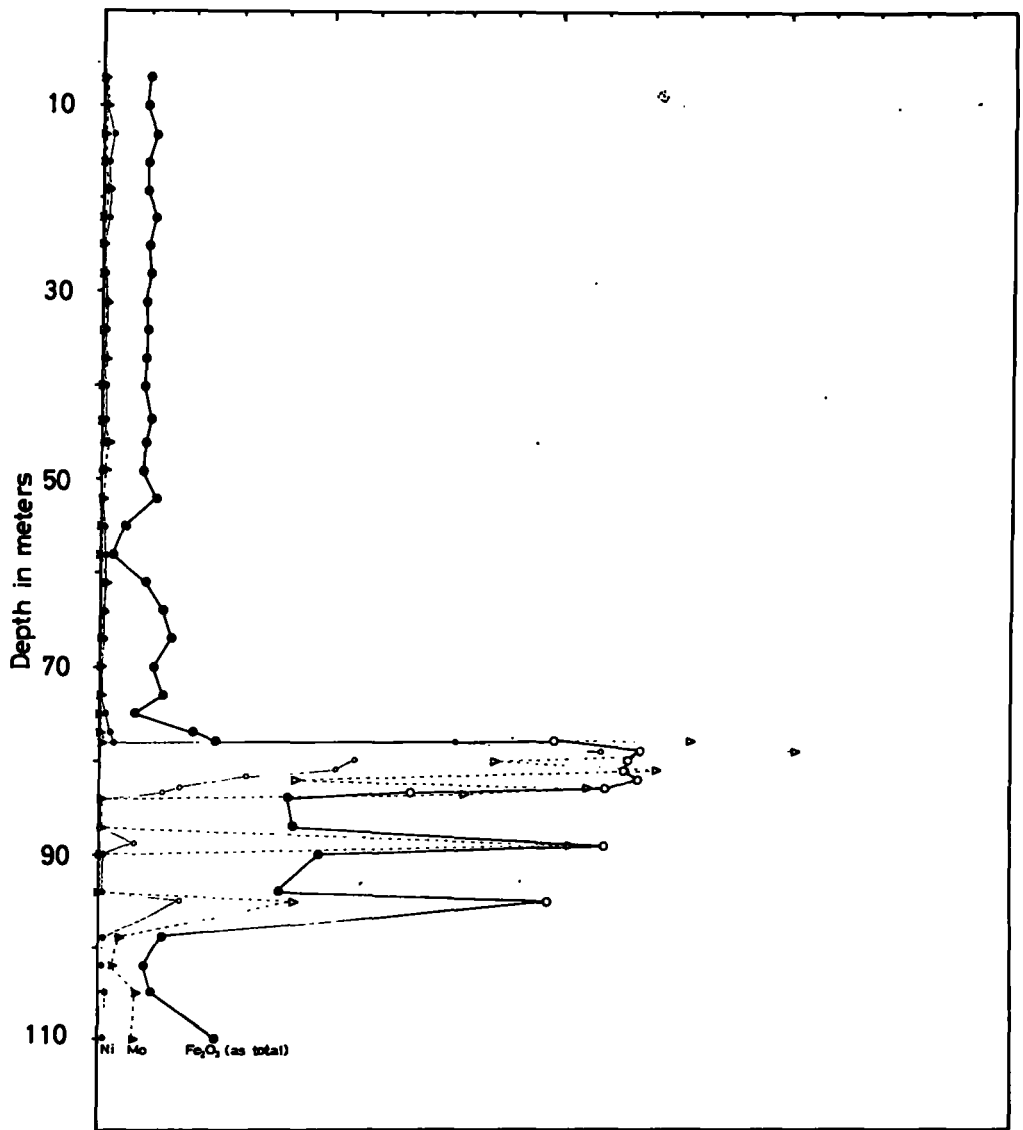


FIG. 34B

LAHANOS BOREHOLE B.-Distribution of the siderophile elements total iron as Fe_2O_3 , Mo, Ni with depth. Solid symbols=rock, open symbols=ore.

One scale unit for Fe_2O_3 = 2.50 %

" " " " Mo = 20 ppm

" " " " Ni = 5 ppm.

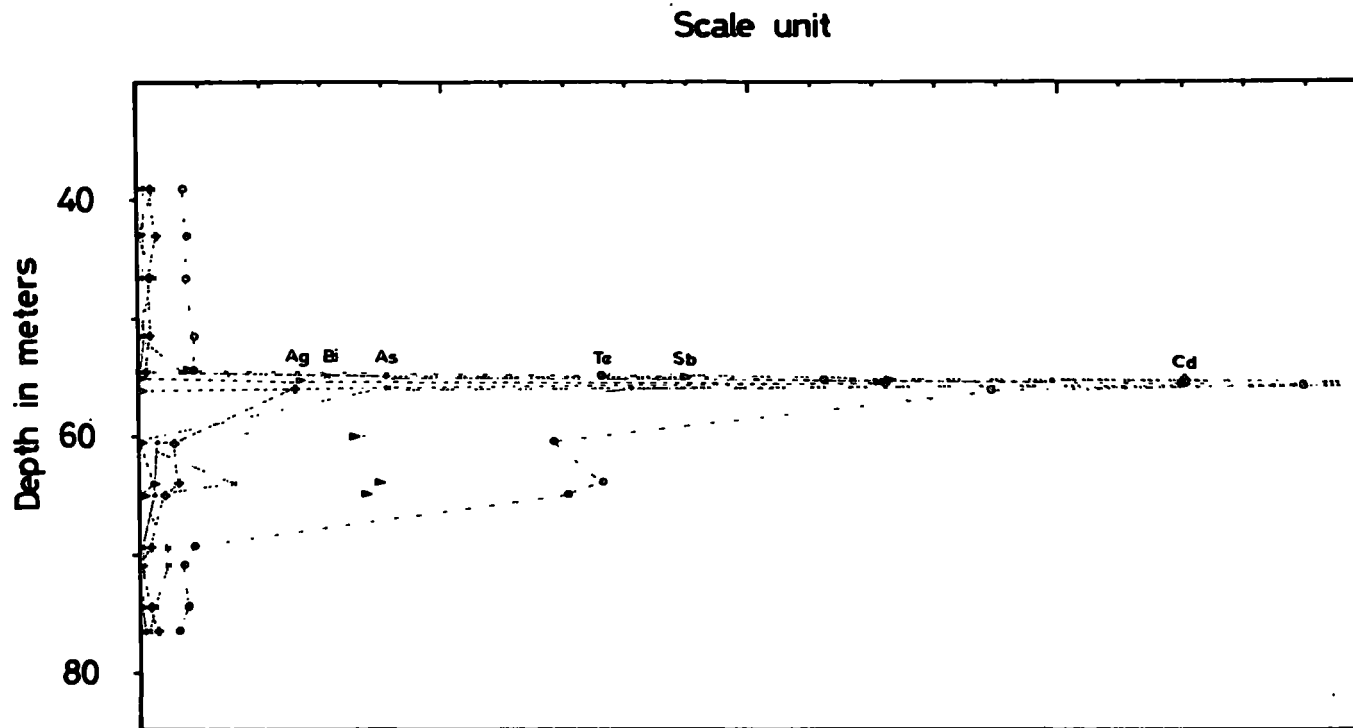


FIG. _35A

LAHANOS BOREHOLE A.—Distribution of the trace chalcophile elements As,Sb,Bi,Cd,Te,Ag with depth in the ore horizon.

One scale unit for As=200 ppm

" " " " Sb,Bi,Cd & Te=40 ppm

" " " " Ag= 5 ppm.

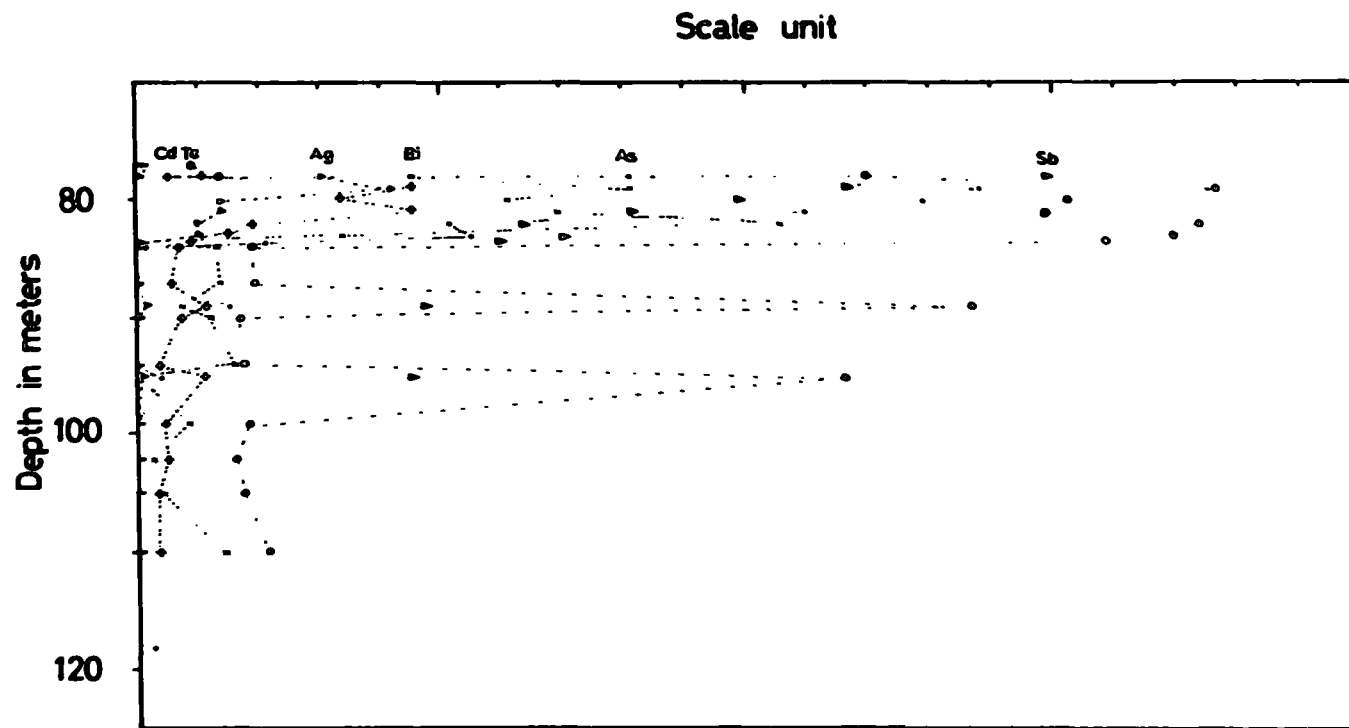


FIG._35B

LAHANOS BOREHOLE B.-Distribution of the trace chalcophile elements As,Sb,Bi,Ag,Cd,Te with depth in the ore horizon.

One scale unit for As= 100 ppm

" " " " Sb,Bi,Ag,Cd & Te=20 ppm.

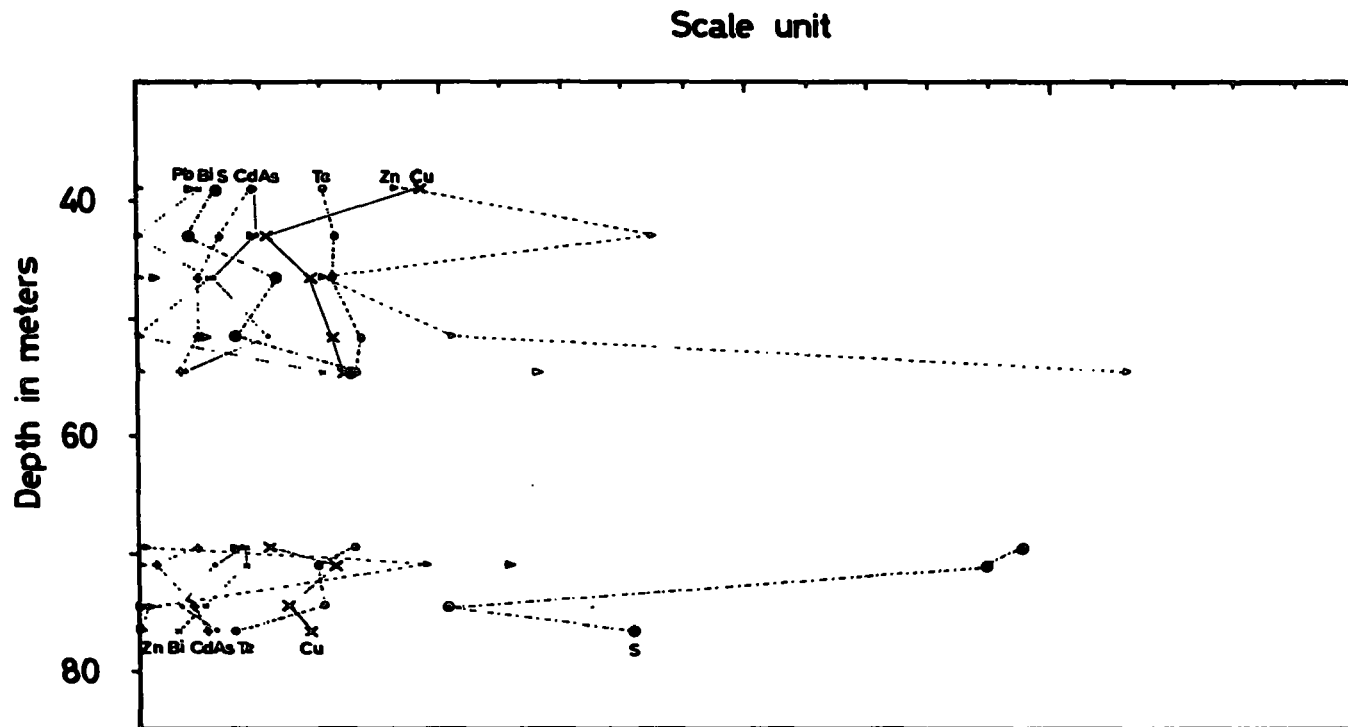


FIG._36A

LAHANOS BOREHOLE A..Distribution of the trace chalcophile elements S,Zn,Cu,Pb,Bi,As,Cd,Te with depth.

One scale unit for S=0.20%

" " " " Zn=40 ppm

" " " " Cu=20 ppm

" " " " Pb,Bi,As,Cd & Te=10 ppm.

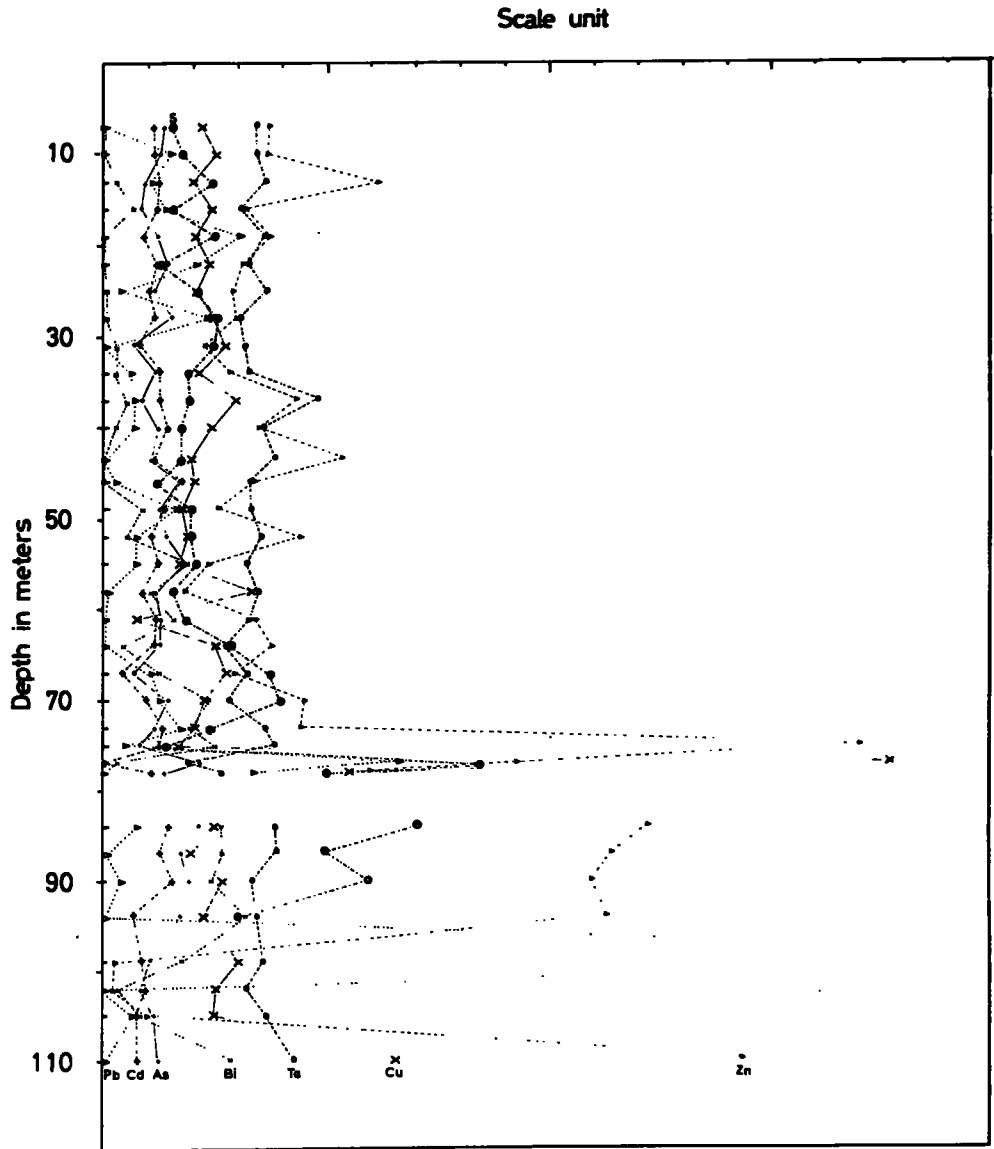


FIG. -36B

LAHANOS BOREHOLE B.-Distribution of the trace chalcophile elements S,Cu,Zn,Pb,Bi,As,Cd,Te with depth.

One scale unit for S=0.10 %

" " " " Cu & Zn=20 ppm

" " " " Pb,Bi,As,Cd & Te=10 ppm.

1960; Hawkes and Webb, 1962). In an attempt to discover whether any detectable geochemical dispersion anomaly exists in association with the Lhanos mineralisation that might prove to be useful in prospecting, samples were collected on a grid pattern as shown on Map 7. Since the object was to look for a primary dispersion pattern, the samples collected were all of solid rock. Geobotanical work (Pollak, 1962) has already shown that a secondary copper anomaly can be detected.

The results are shown and contoured on Figs. 37, 38 and 39. Although anomalous values appear at certain points for particular elements, the general conclusion to be drawn from this work seems to be that in this area primary geochemical anomalies are of doubtful value as indicators of the exact location of economic mineralisation.

In seeking to understand the genesis of the Lahanos mineralisation, it was thought to be important to make comparisons with other mineralised areas in the Eastern Pontic ore province. The nature of the mineralisation in the more important of these areas is described in the following sections before considering the conclusions to be drawn from the preceding details of the Lahanos ores.

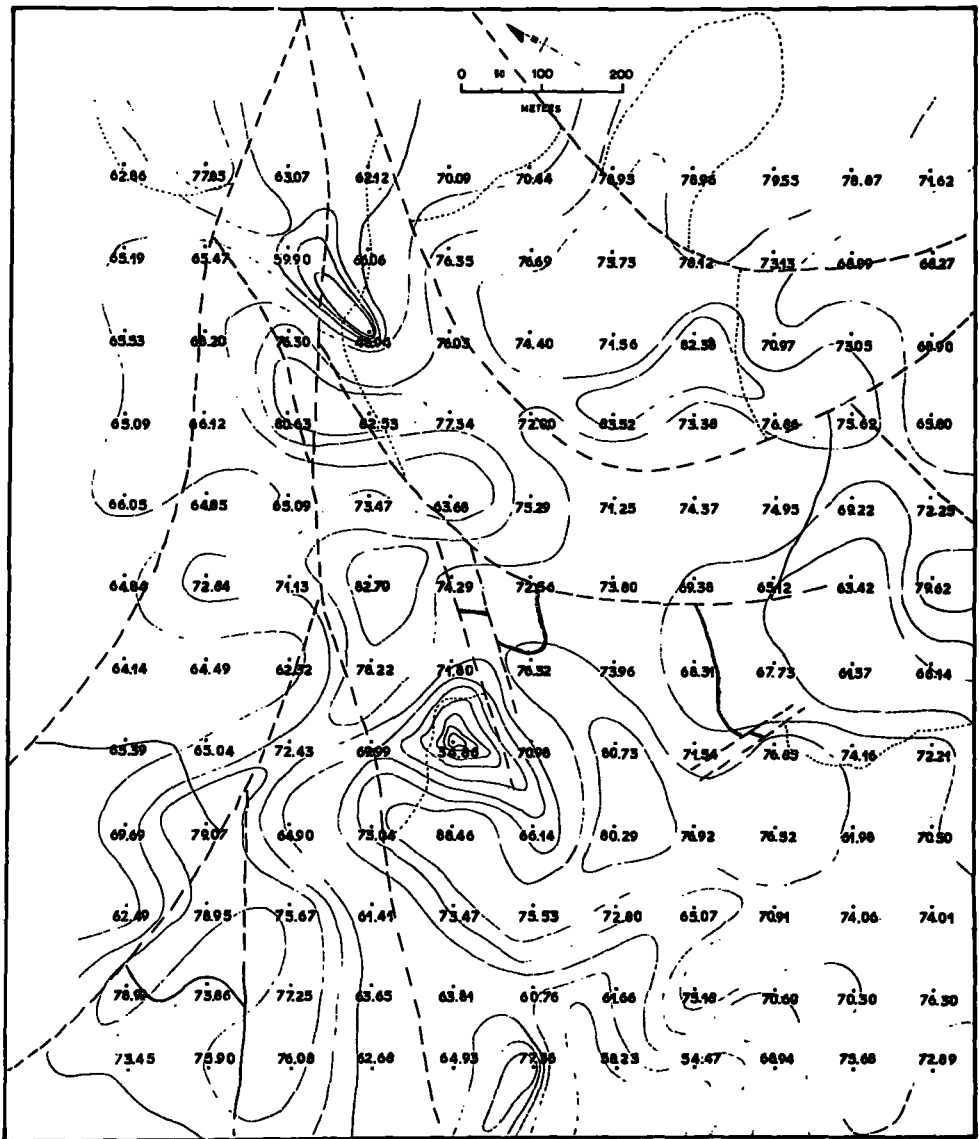


FIG.37A...Distribution of SiO_2 in surface values above the mineralization at Lahanos, Espiye. Values in per cent. Contour interval 5.00%. Scale is 1:5000.

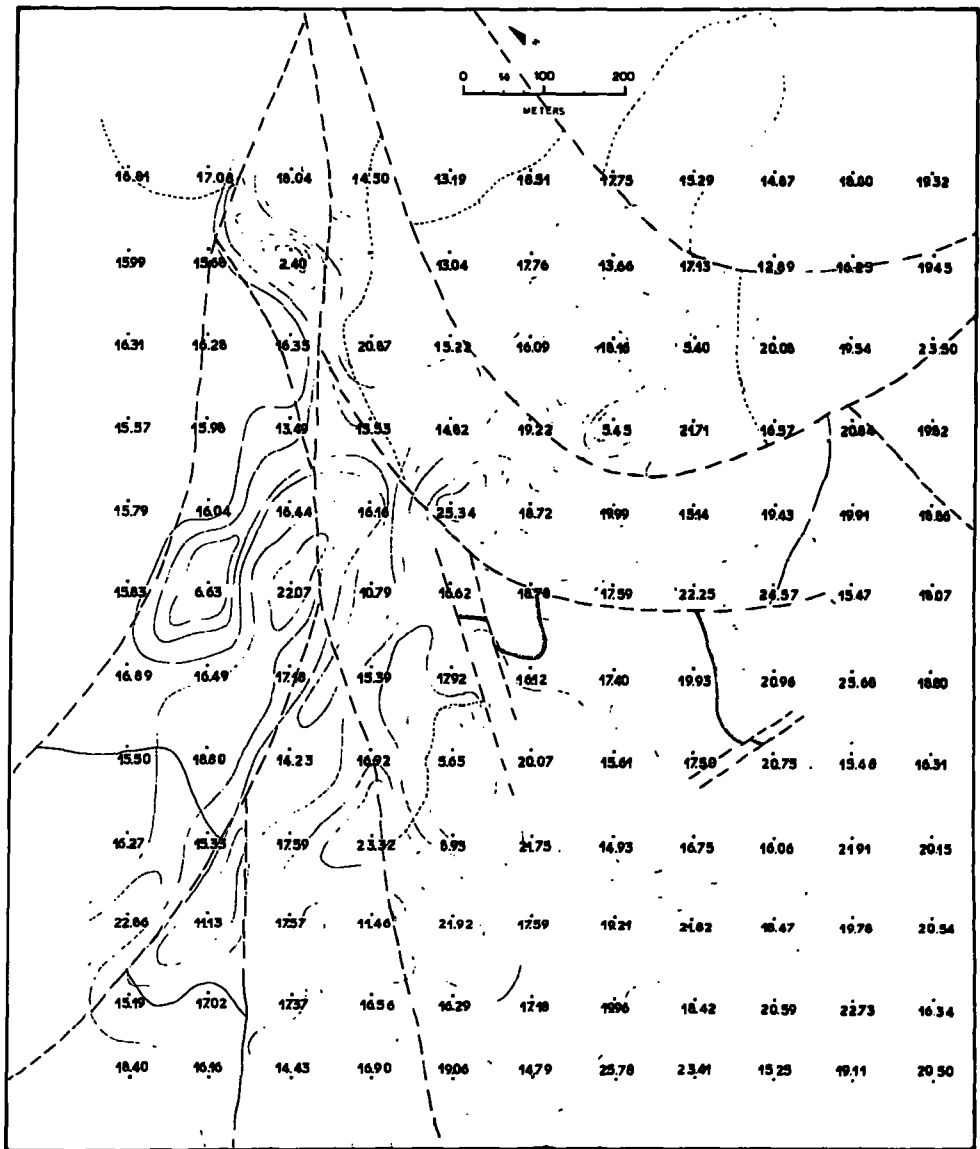


FIG. 37B._Distribution of Al_2O_3 in surface values above the mineralization at Lahanos, Espiye. Values in per cent. Contour interval 3.00%. Scale is 1:5000.

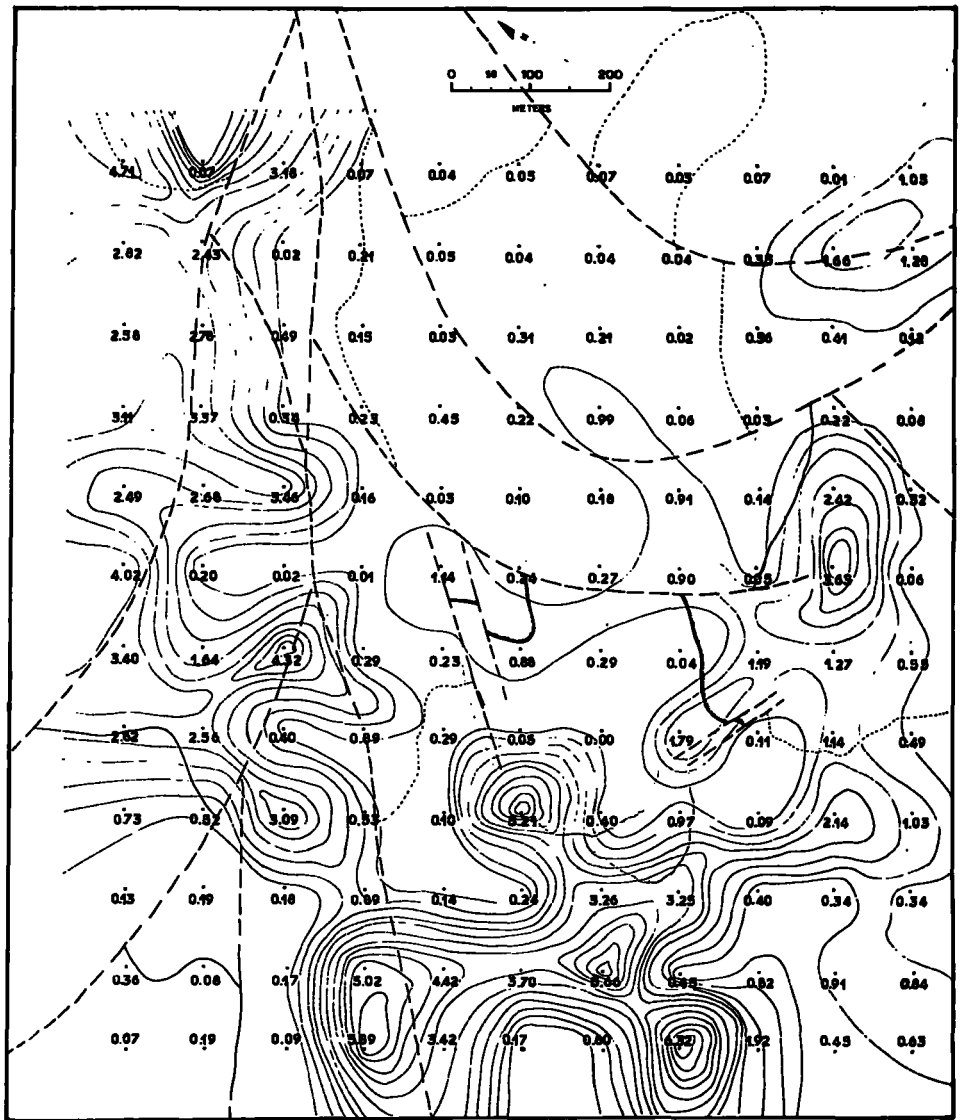


FIG.37C...Distribution of MgO in surface values above the mineralization at Lahanos, Espiye. Values in per cent. Contour interval 0.50%. Scale is 1:5000.

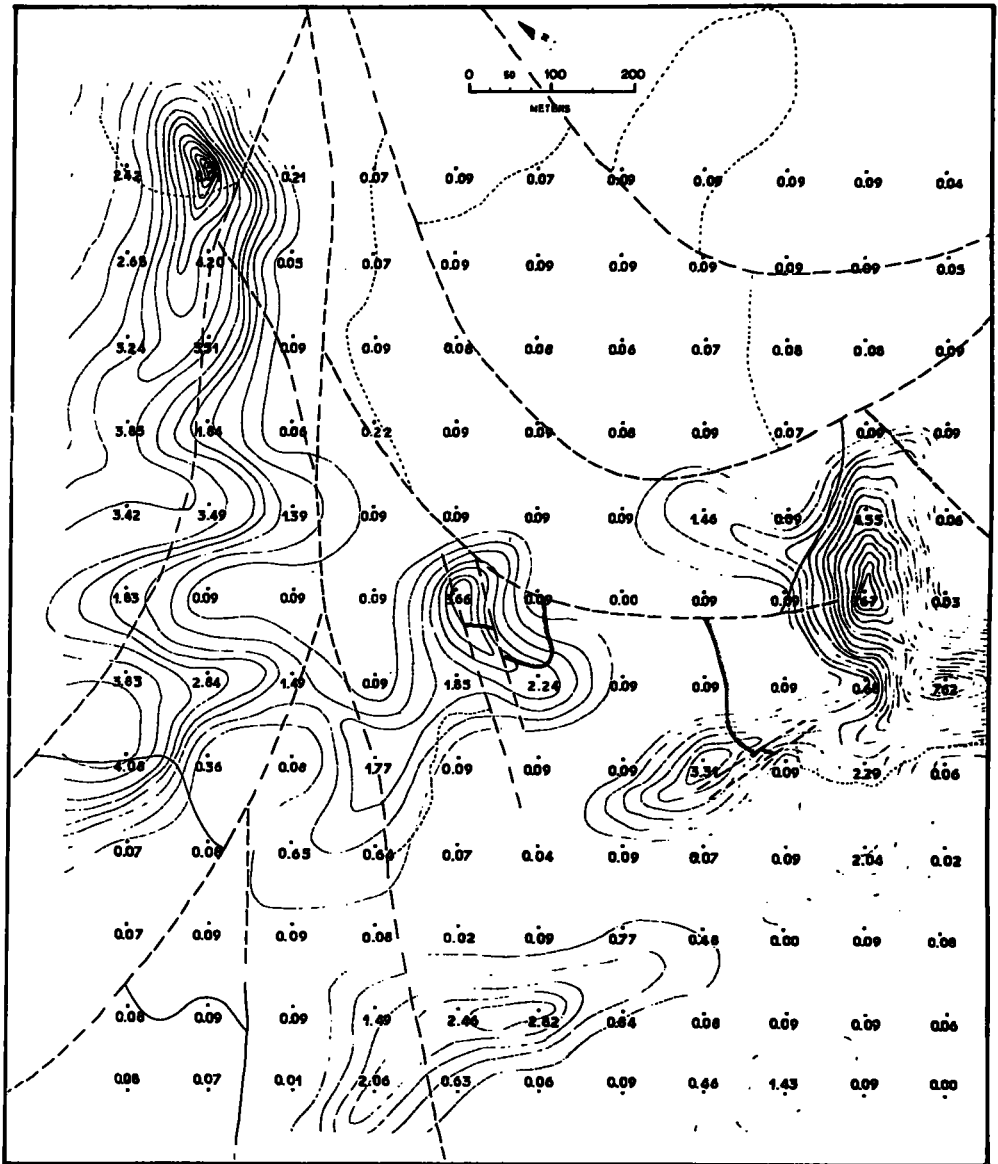


FIG.37D._Distribution of CaO in surface values above the mineralization at Lahanos, Espiye. Values in per cent. Contour interval 0.50%. Scale is 1:5000.

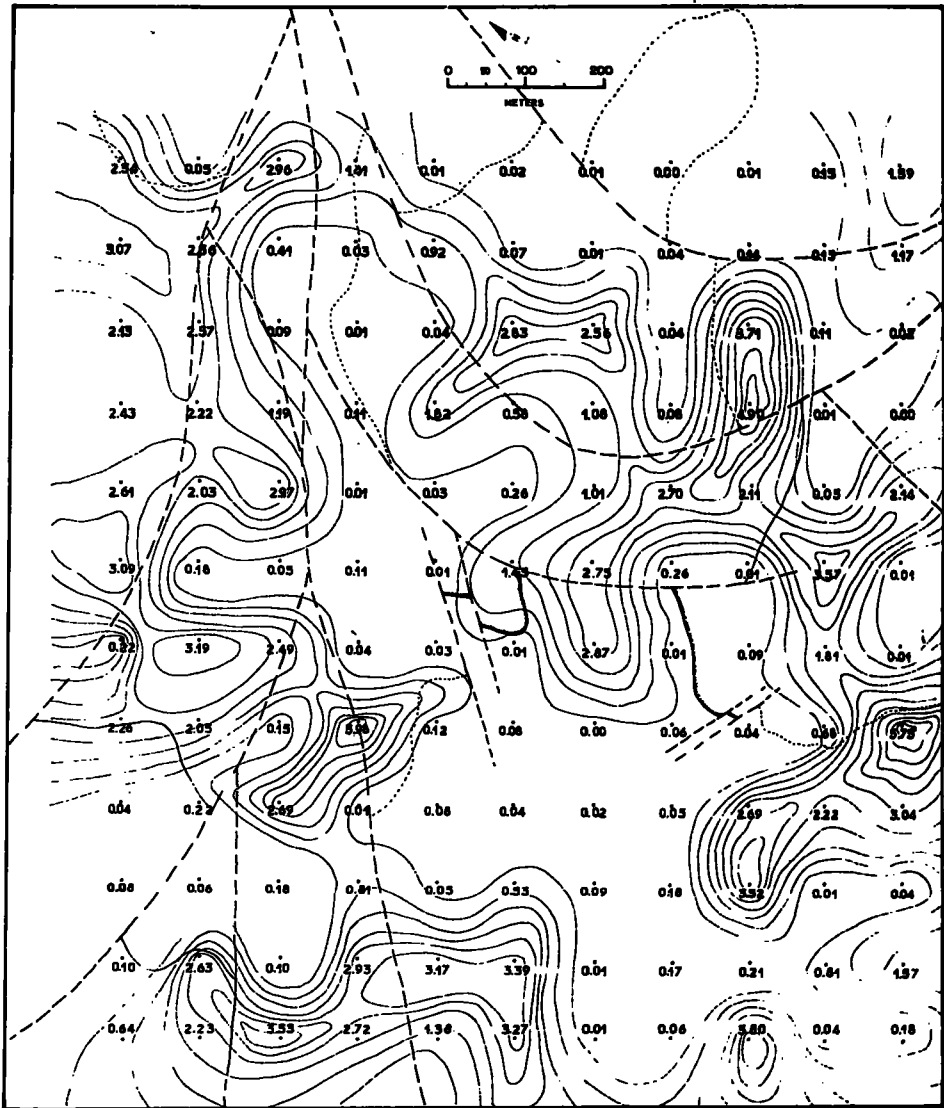


FIG. 37E.—Distribution of Na₂O in surface values above the mineralization at Lahanos, Espiye. Values in per cent. Contour interval 0.50%. Scale is 1:5000.

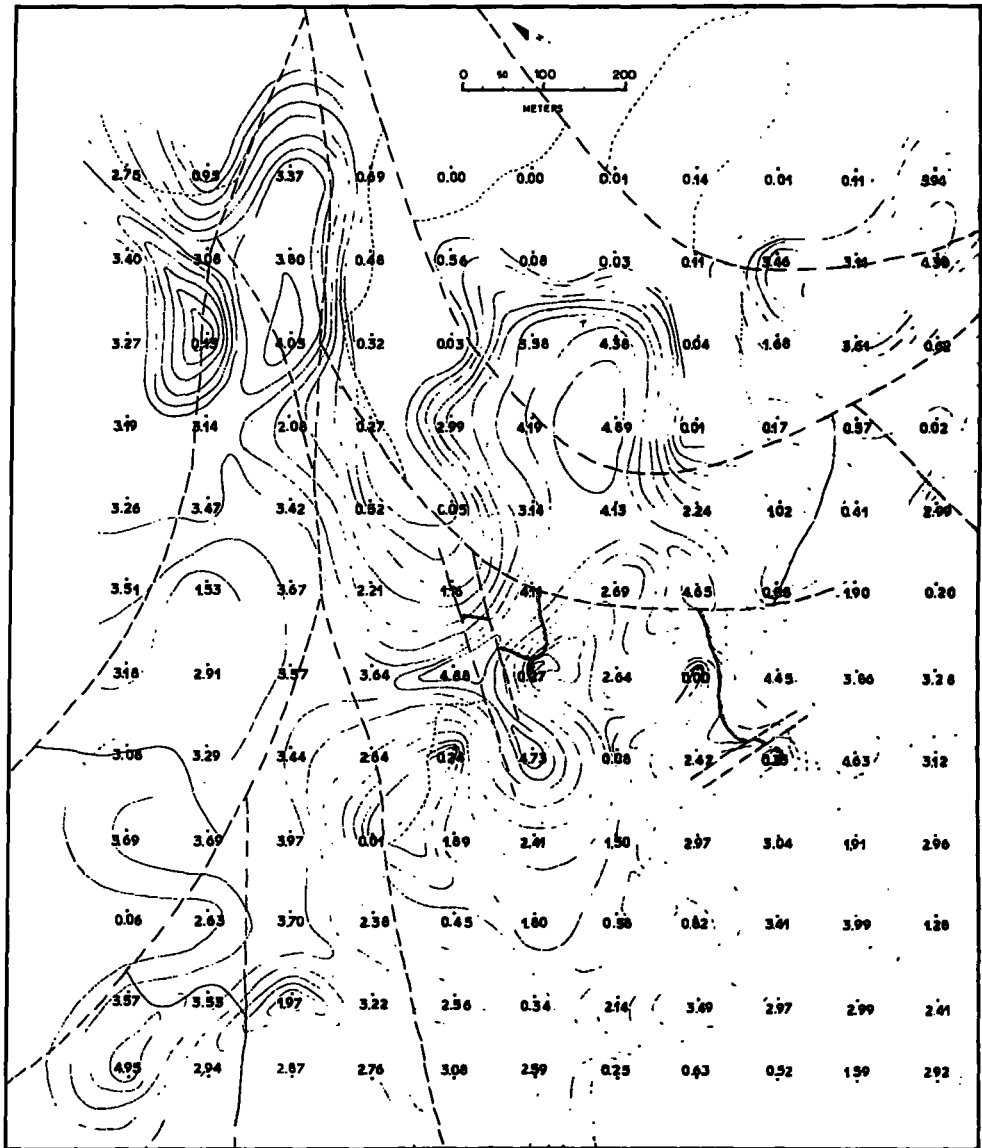


FIG.37F...Distribution of K₂O in surface values above the mineralization at Lahanos, Espiye. Values in per cent. Contour interval 0.50%. Scale is 1:5000.

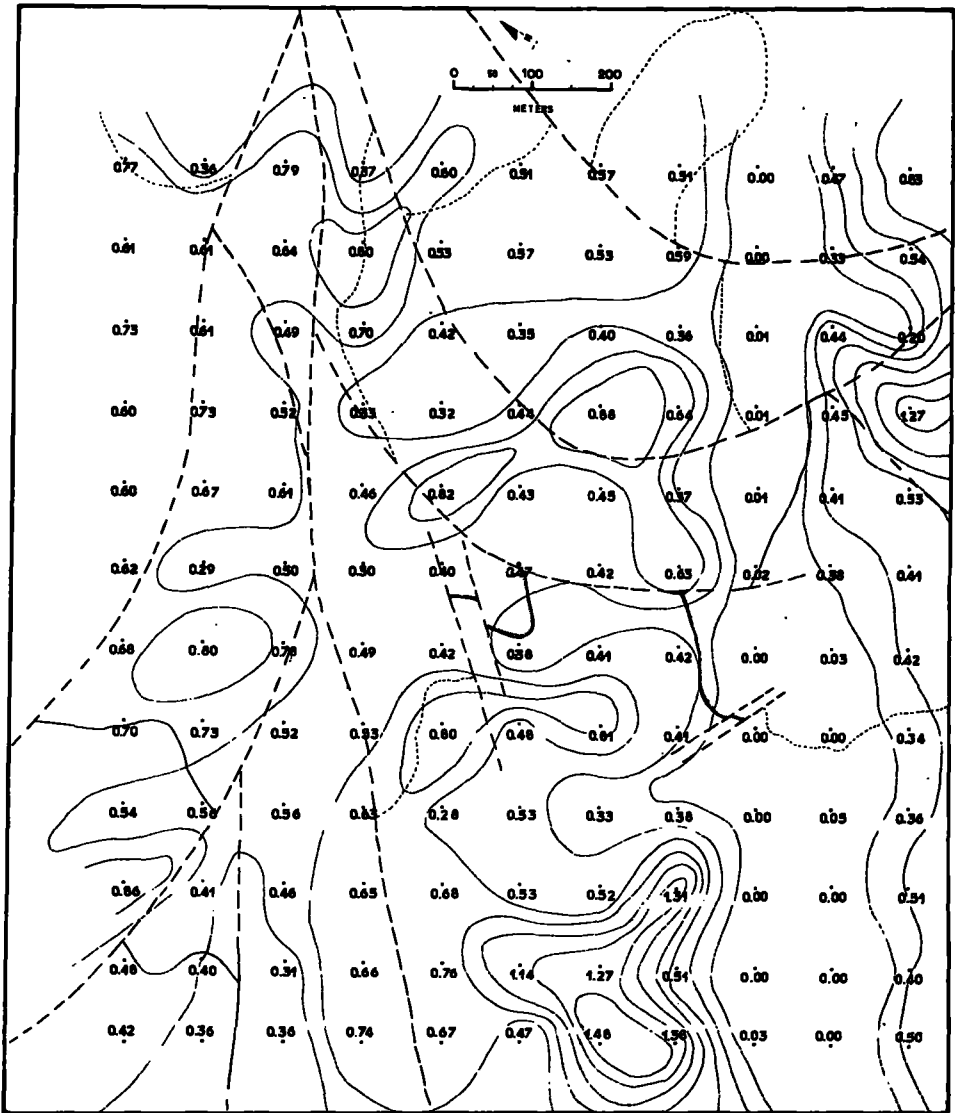


FIG.37G...Distribution of TiO₂ in surface values above the mineralization at Lahanos, Espiye. Values in per cent. Contour interval 0.20%. Scale is 1:5000.

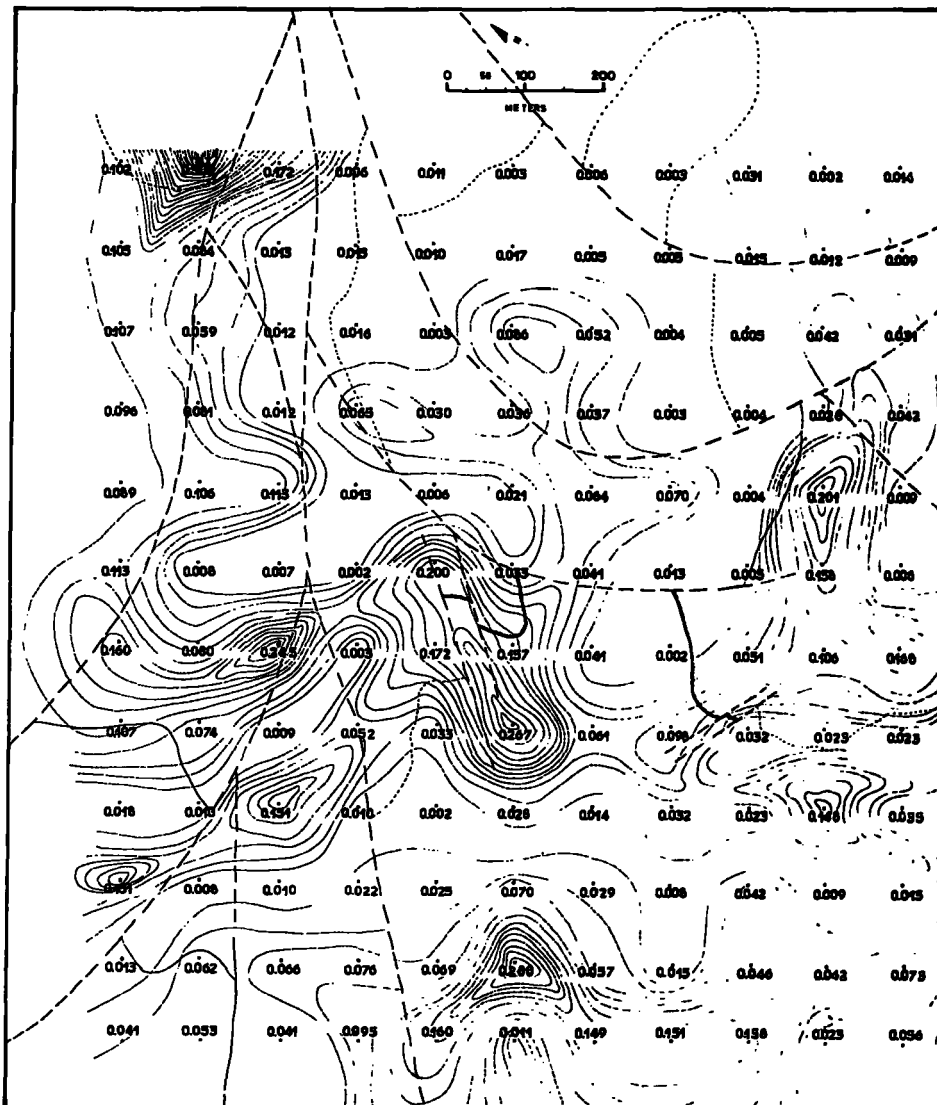


FIG.37H...Distribution of MnO in surface values above the mineralization at Lahanos, Espiye. Values in per cent. Contour interval 0.02%. Scale is 1:5000.

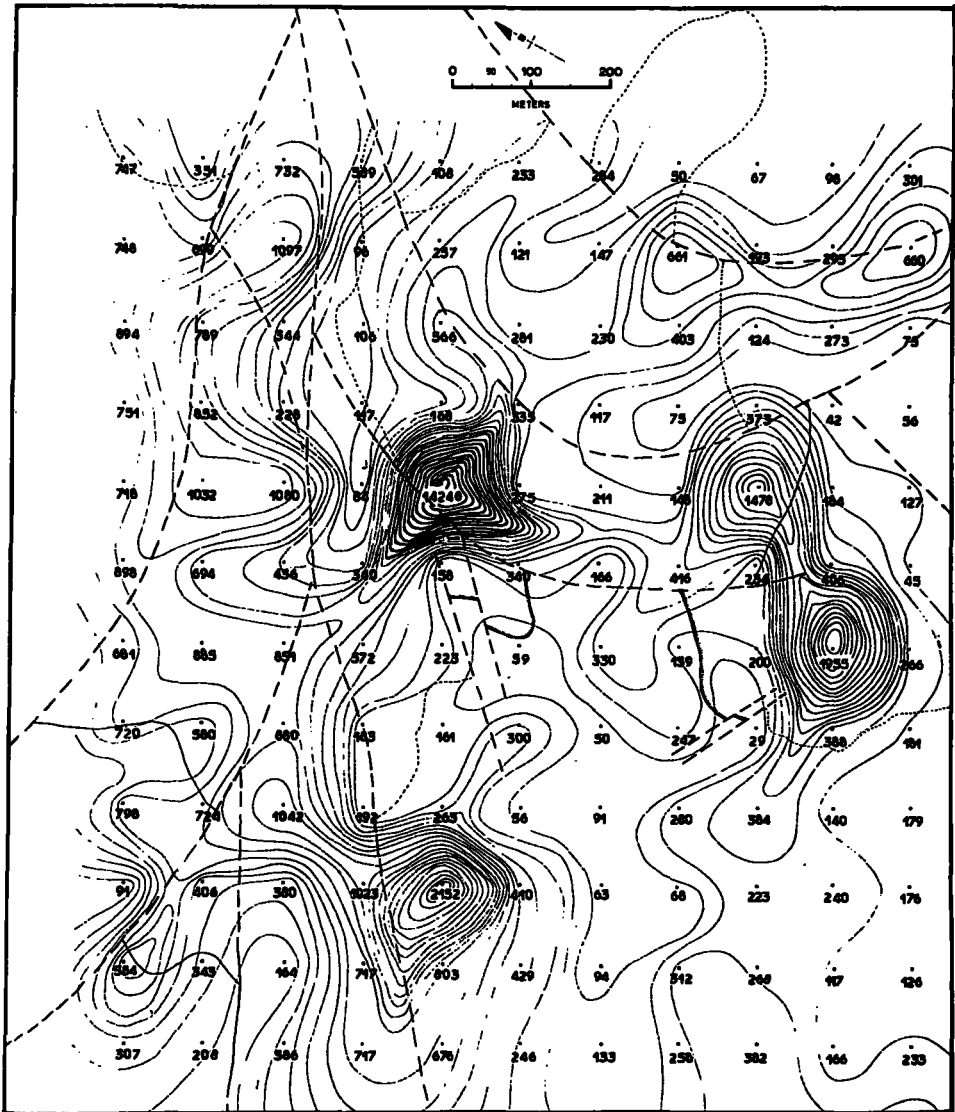


FIG.371._Distribution of Ba in surface values above the mineralization at Lahanos,Espiye. Values in ppm. Contour interval 1000 ppm for thick lines,100 ppm for thin lines.

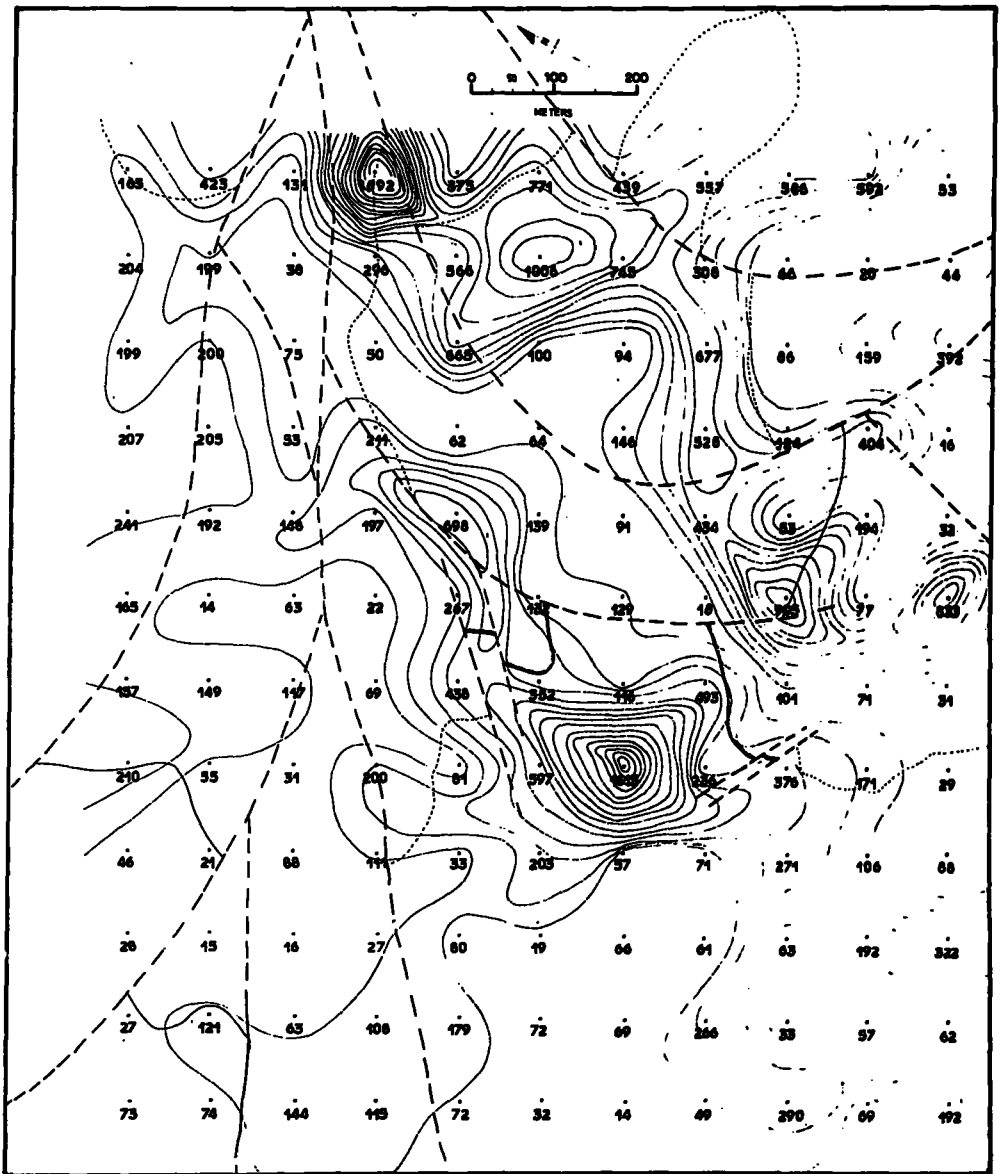


FIG.37J._Distribution of Sr in surface values above the mineralization at Lahanos, Espiye. Values in ppm. Contour interval 100 ppm.

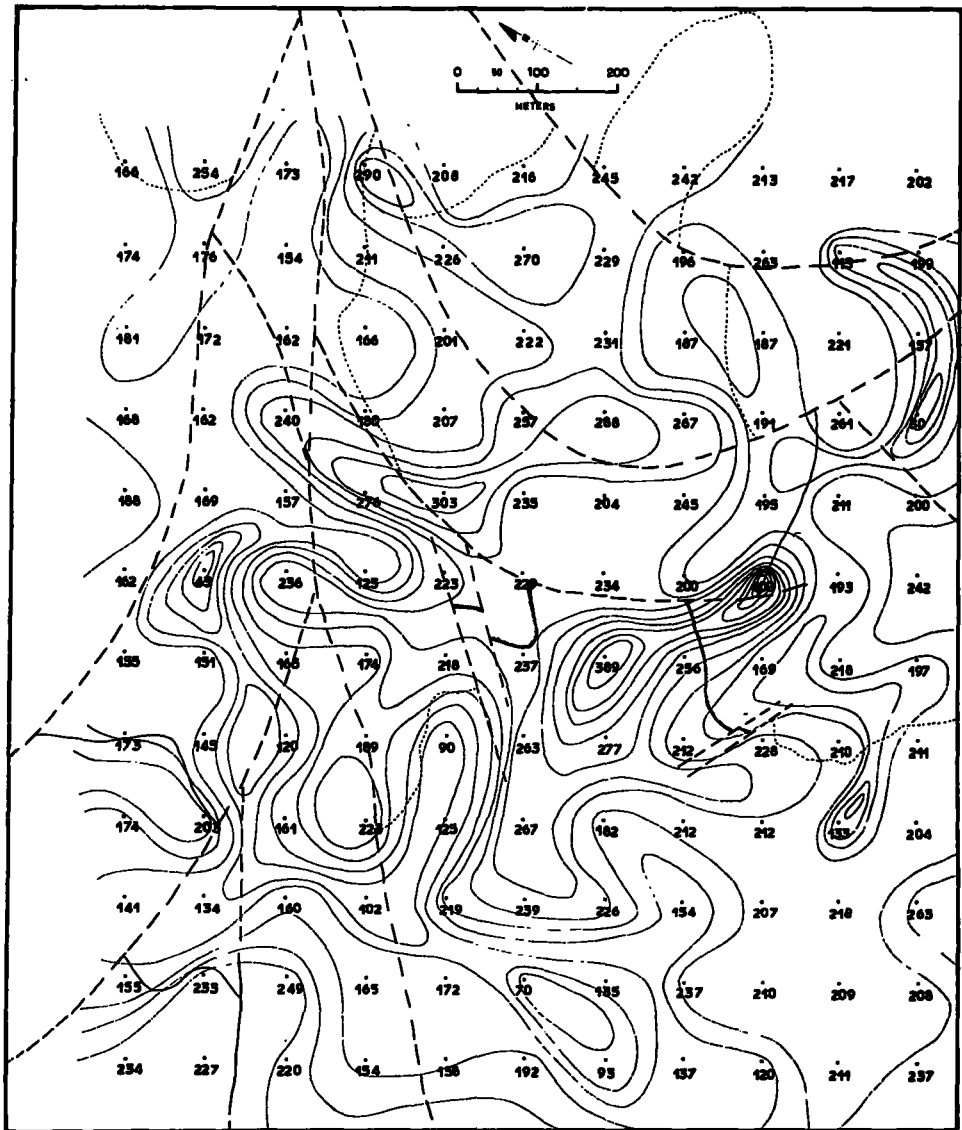


FIG 37K..Distribution of Zr in surface values above the mineralization at Lahanos, Espiye. Values in ppm. Contour interval 25 ppm.

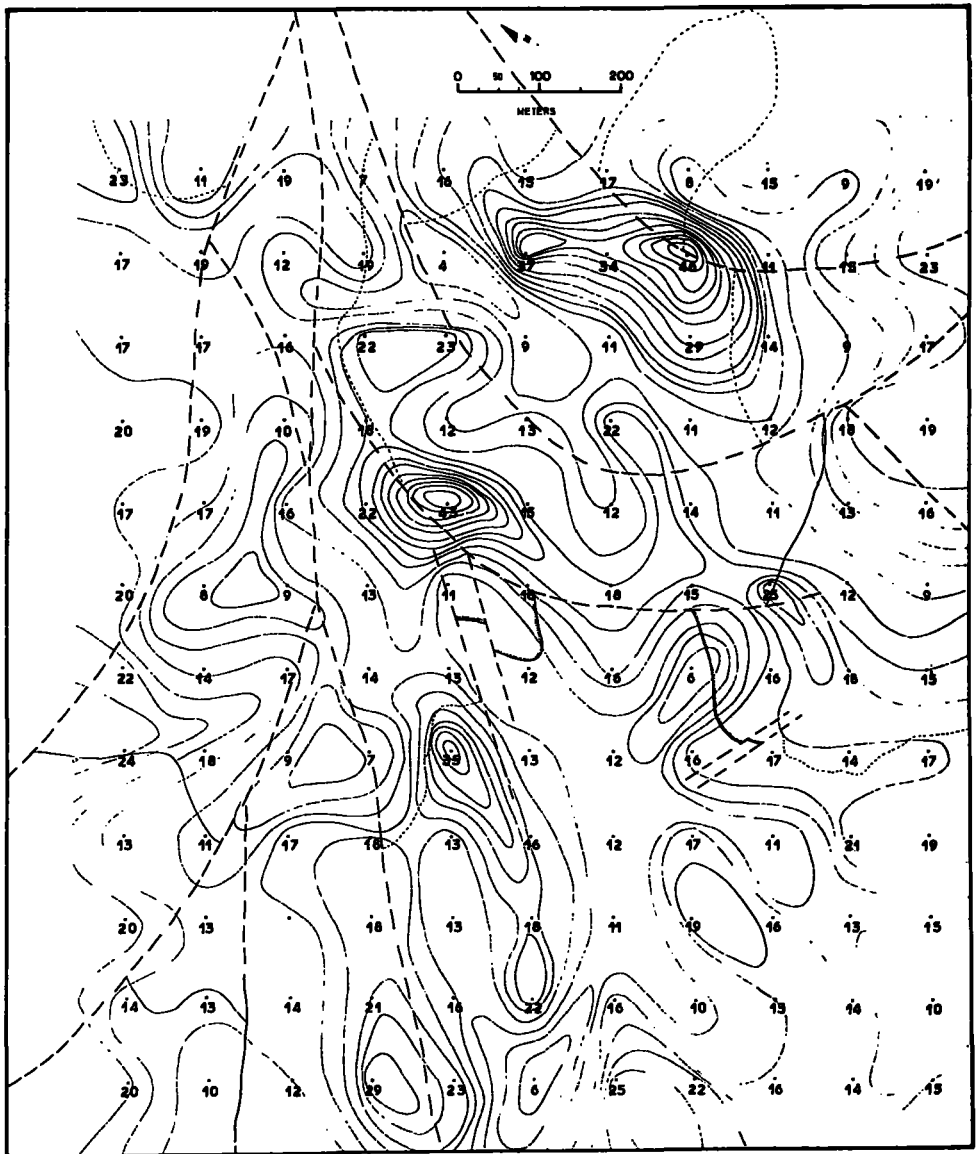


FIG.37L..Distribution of Ga in surface values above mineralization at Lahanos, Espiye. Values in ppm. Contour interval 3 ppm.

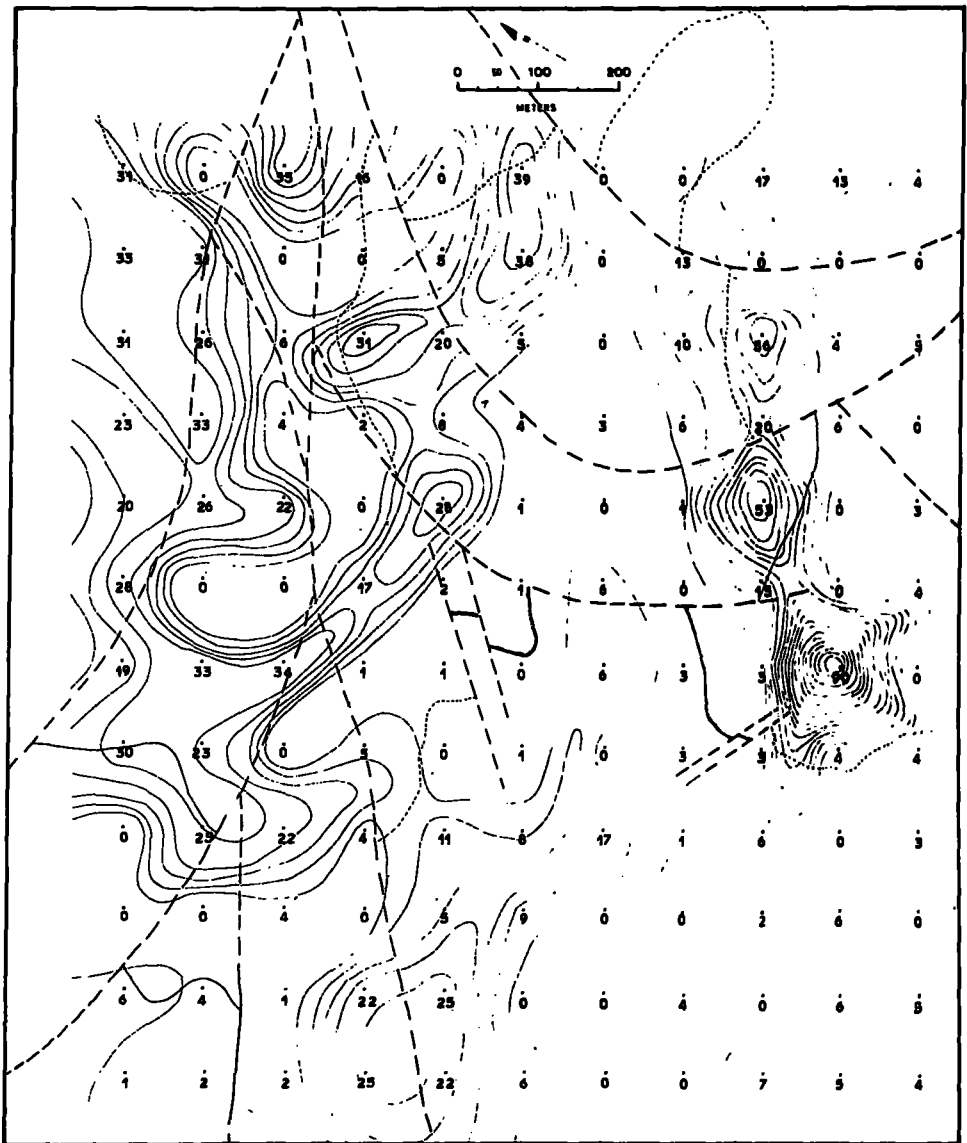


FIG 37M..Distribution of Cr in surface values above mineralization at Lahanos,Espiye. Values in ppm. Contour interval 5 ppm.

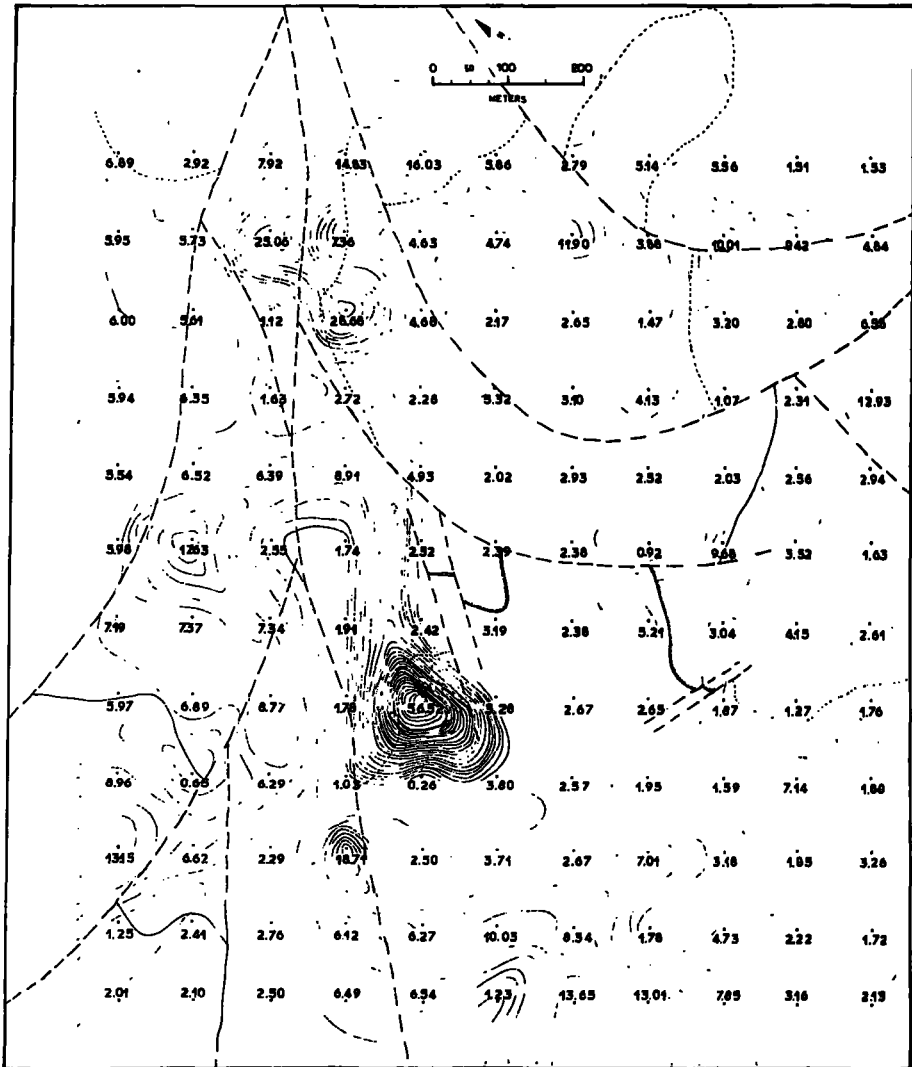


FIG.38A...Distribution of FeO+Fe₂O₃ in surface values above the mineralization at Lahanos, Espiye. Values in per cent. Contour interval 2.00%. Scale is 1:5000.

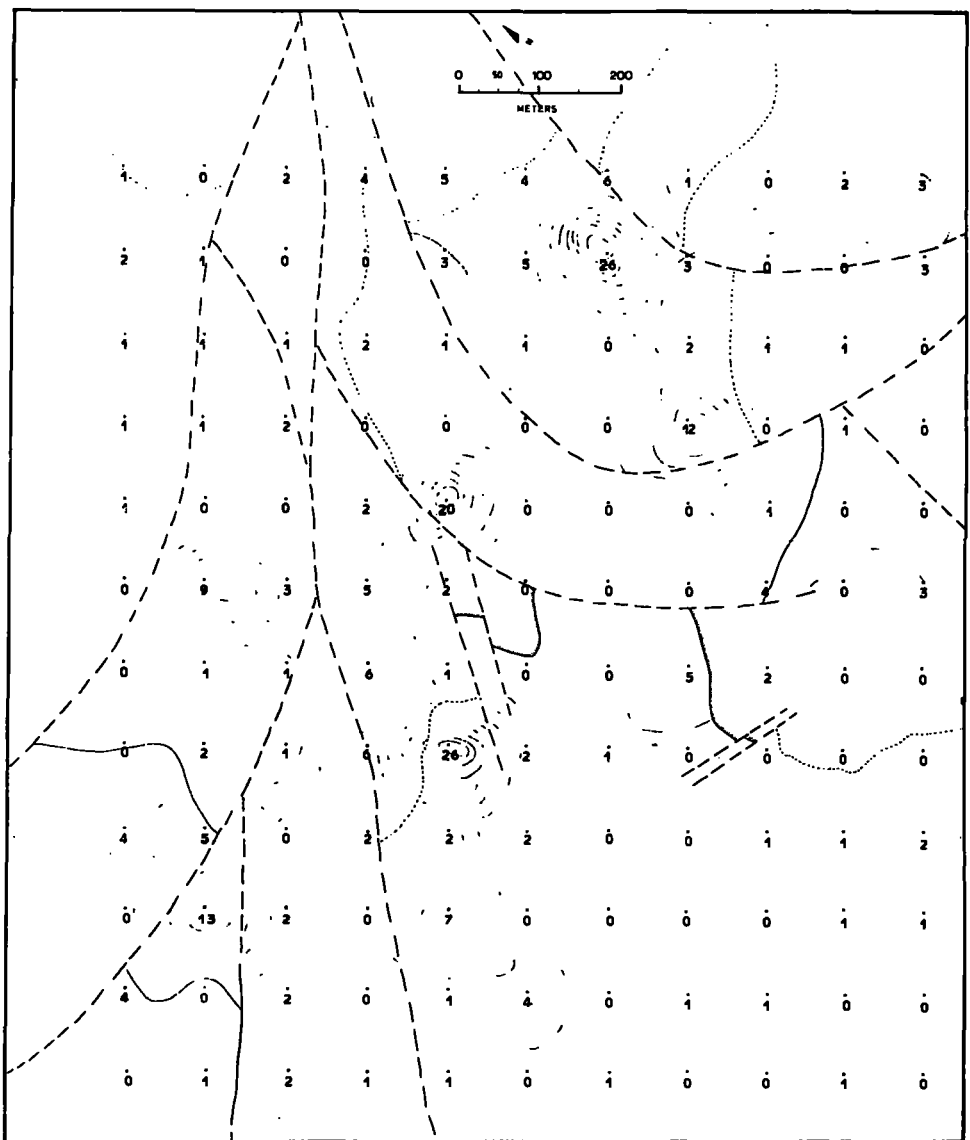


FIG.38B._Distribution of Mo in surface values above the mineralization at Lahanos, Espiye. Values in ppm. Contour interval 3 ppm.

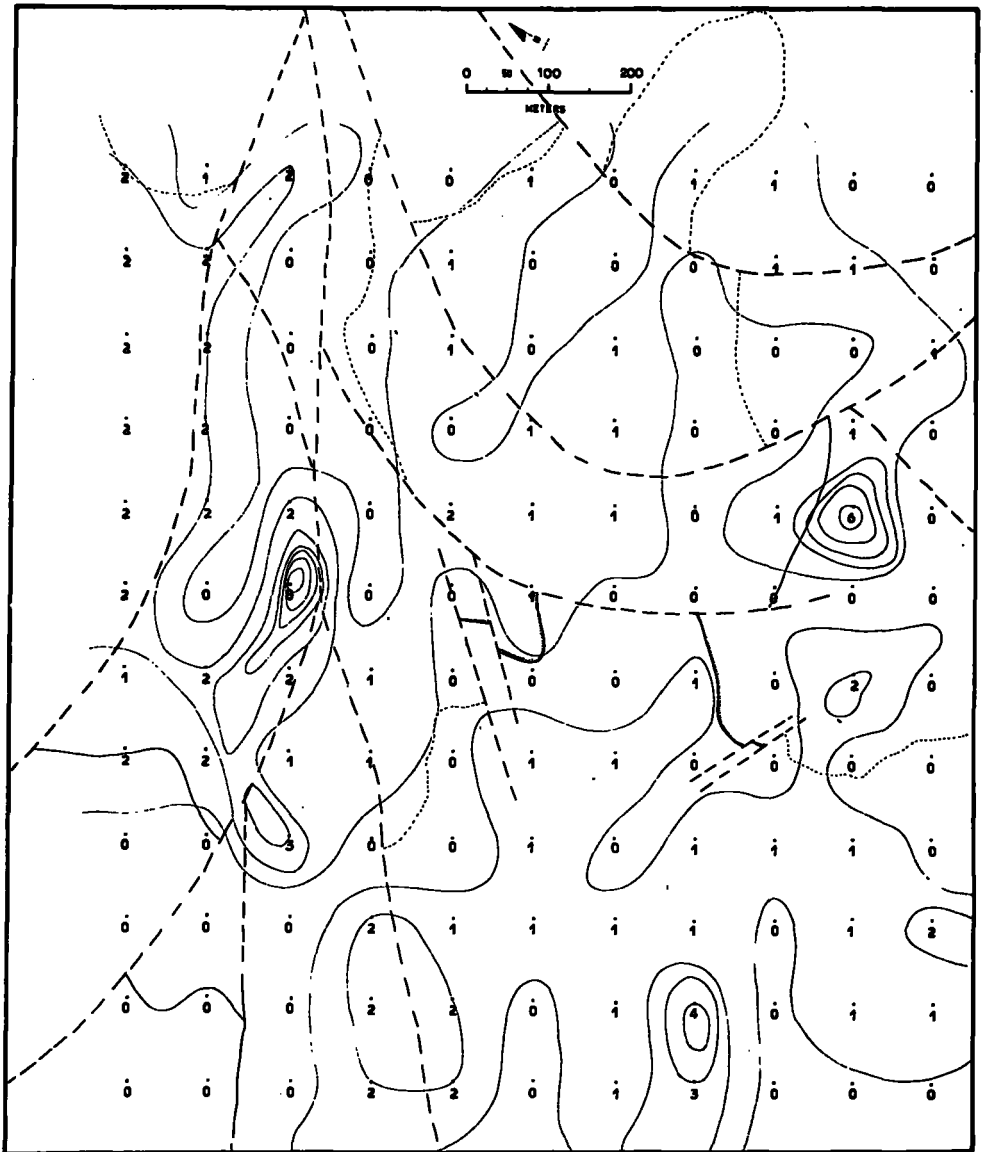


FIG.38C._Distribution of Ni in surface values above mineralization at Lahanos, Espiye. Values in ppm. Contour interval 1 ppm.

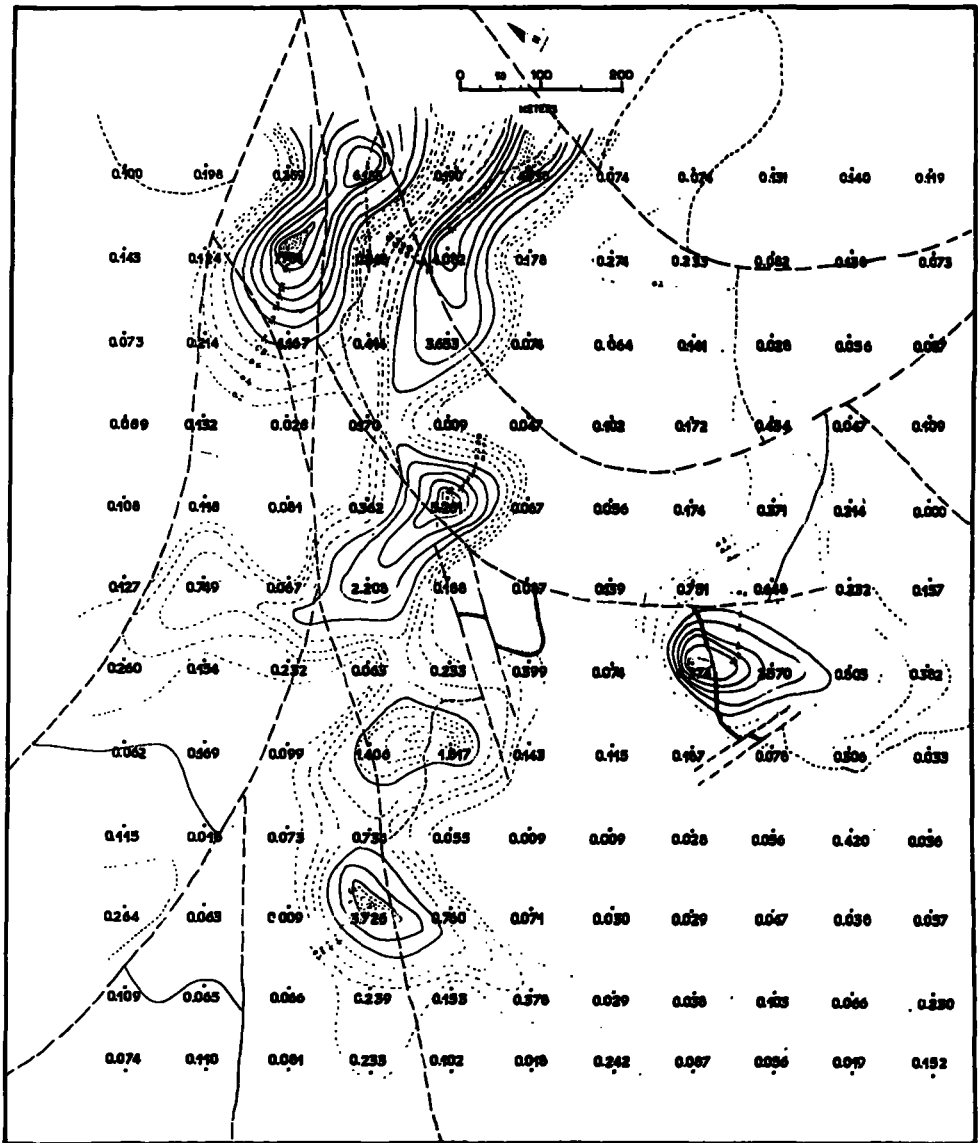


FIG.39A..Distribution of S in surface values above the mineralization at Lahanos, Espiye. Values in per cent. Contour interval 1% for solid lines,0.2% for dashed lines. Scale is 1:5000.

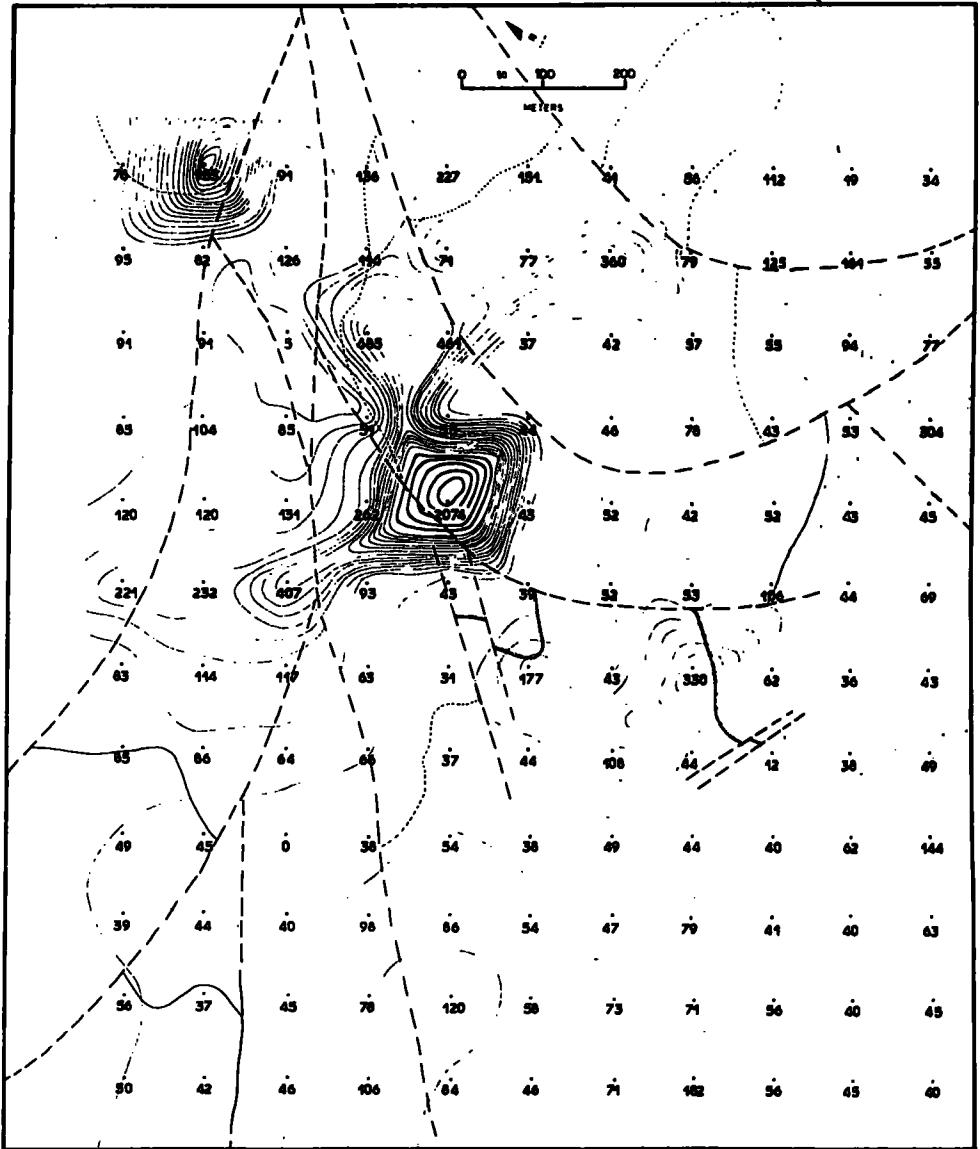


FIG.39B._Distribution of Cu in surface values above the mineralization at Lahanos,Espiye. Values in ppm. Contour interval 250 ppm for thick lines,50 ppm for thin lines.

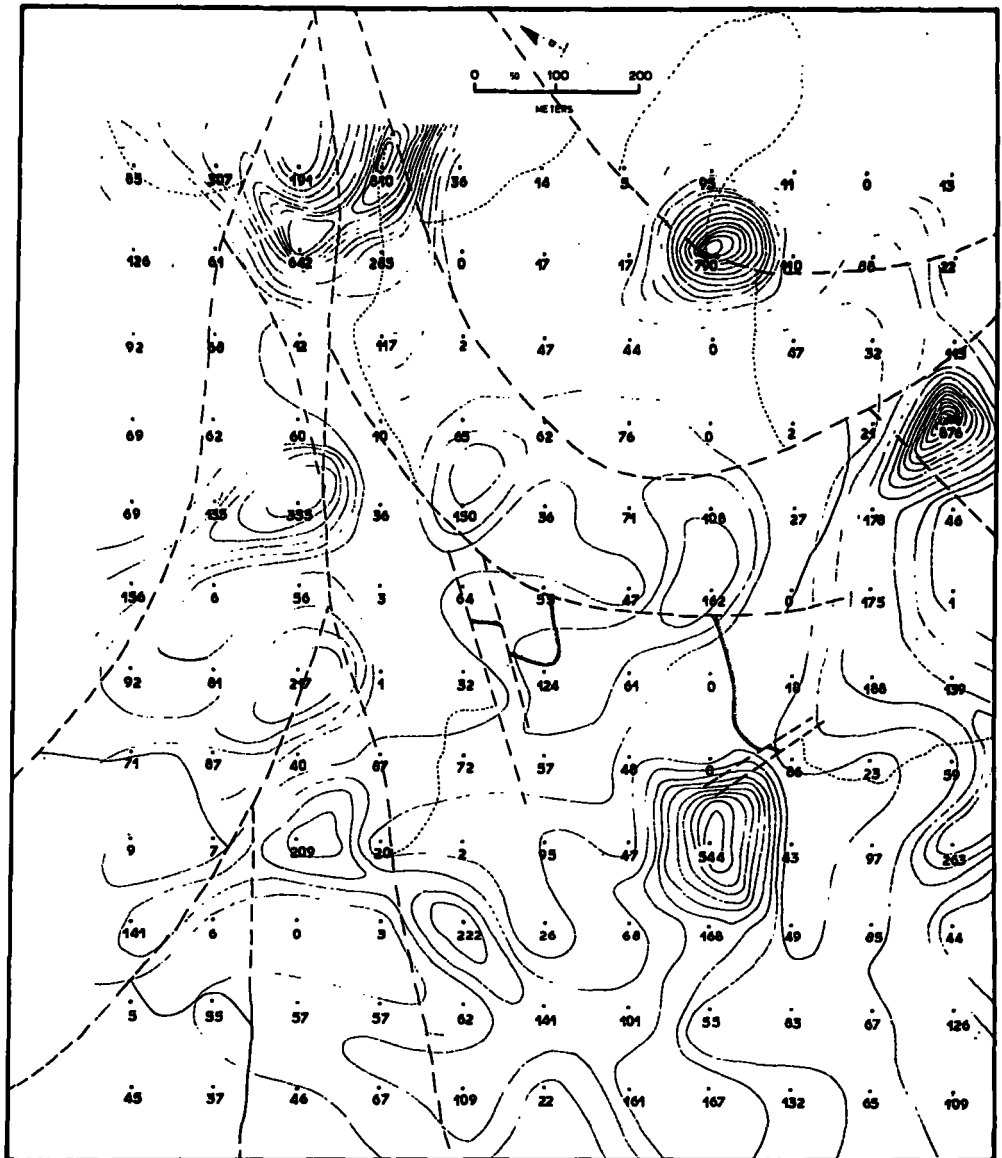


FIG.39C...Distribution of Zn in surface values above the mineralization at Lahanos,Espiye. Values in ppm. Contour interval 50 ppm.

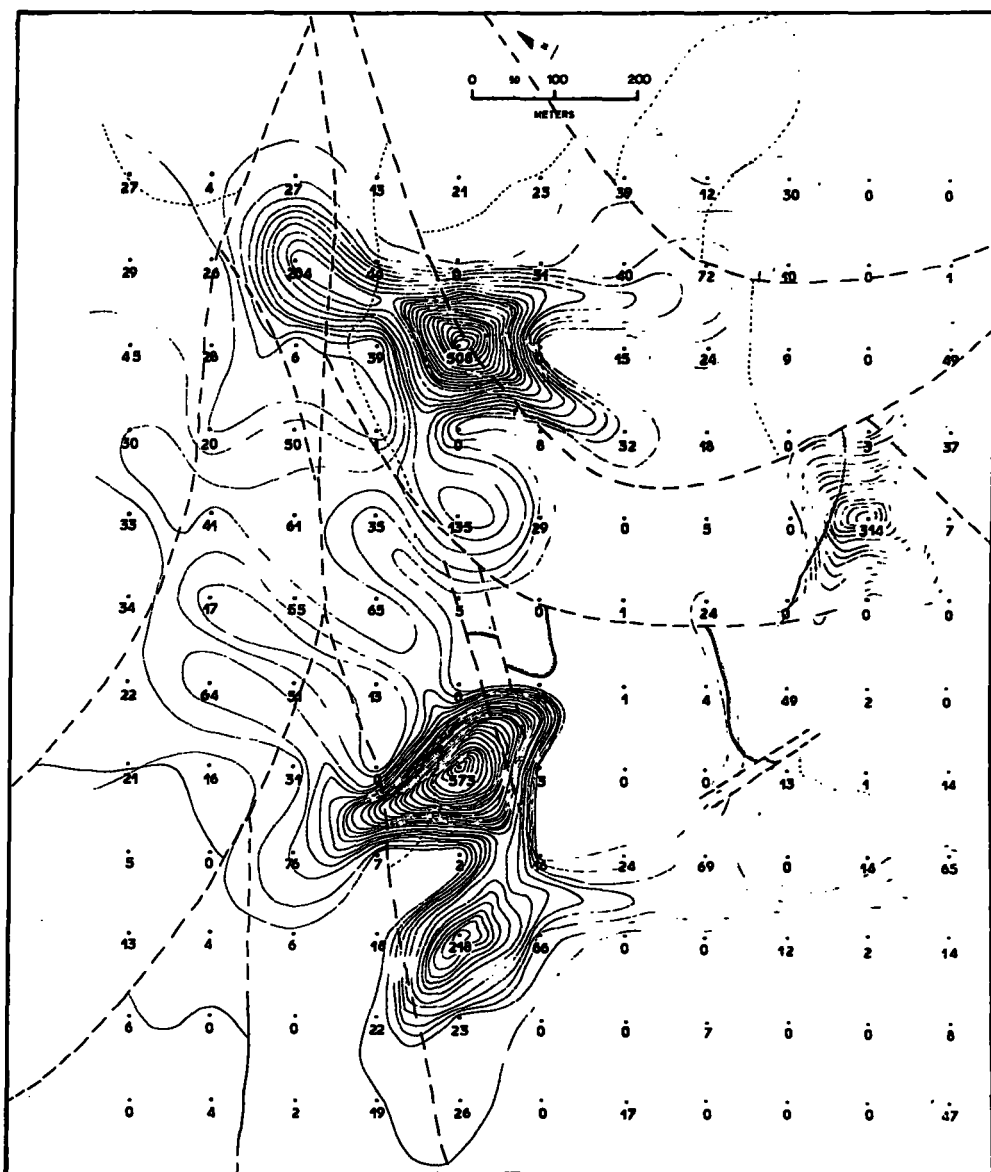


FIG. 39D._Distribution of Pb in surface values above the mineralization at Lahanos, Espiye. Values in ppm. Contour interval 20 ppm.

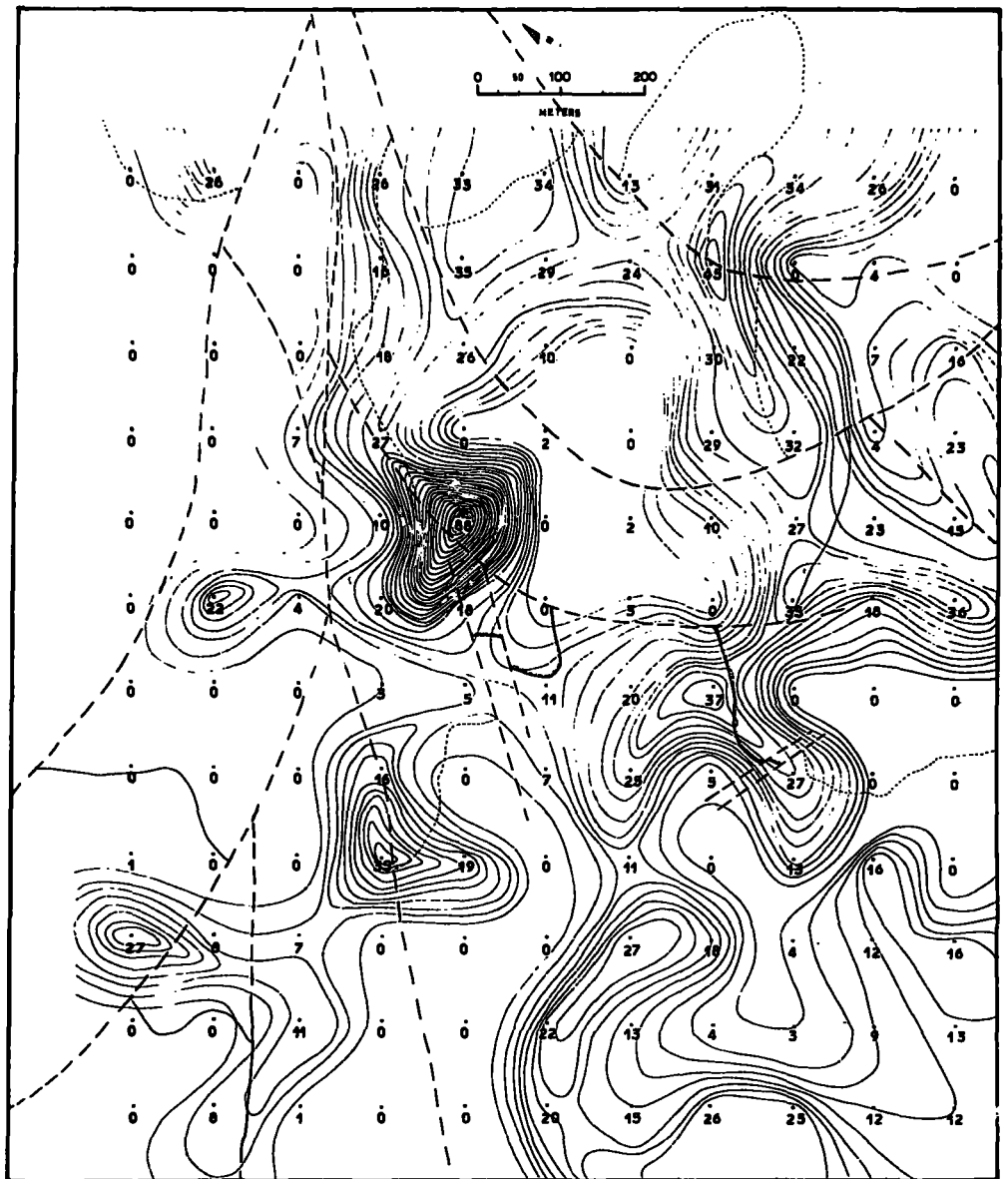


FIG. 39E.—Distribution of Bi in surface values above mineralization at Lahanos, Espiye. Values in ppm. Contour interval 3 ppm.

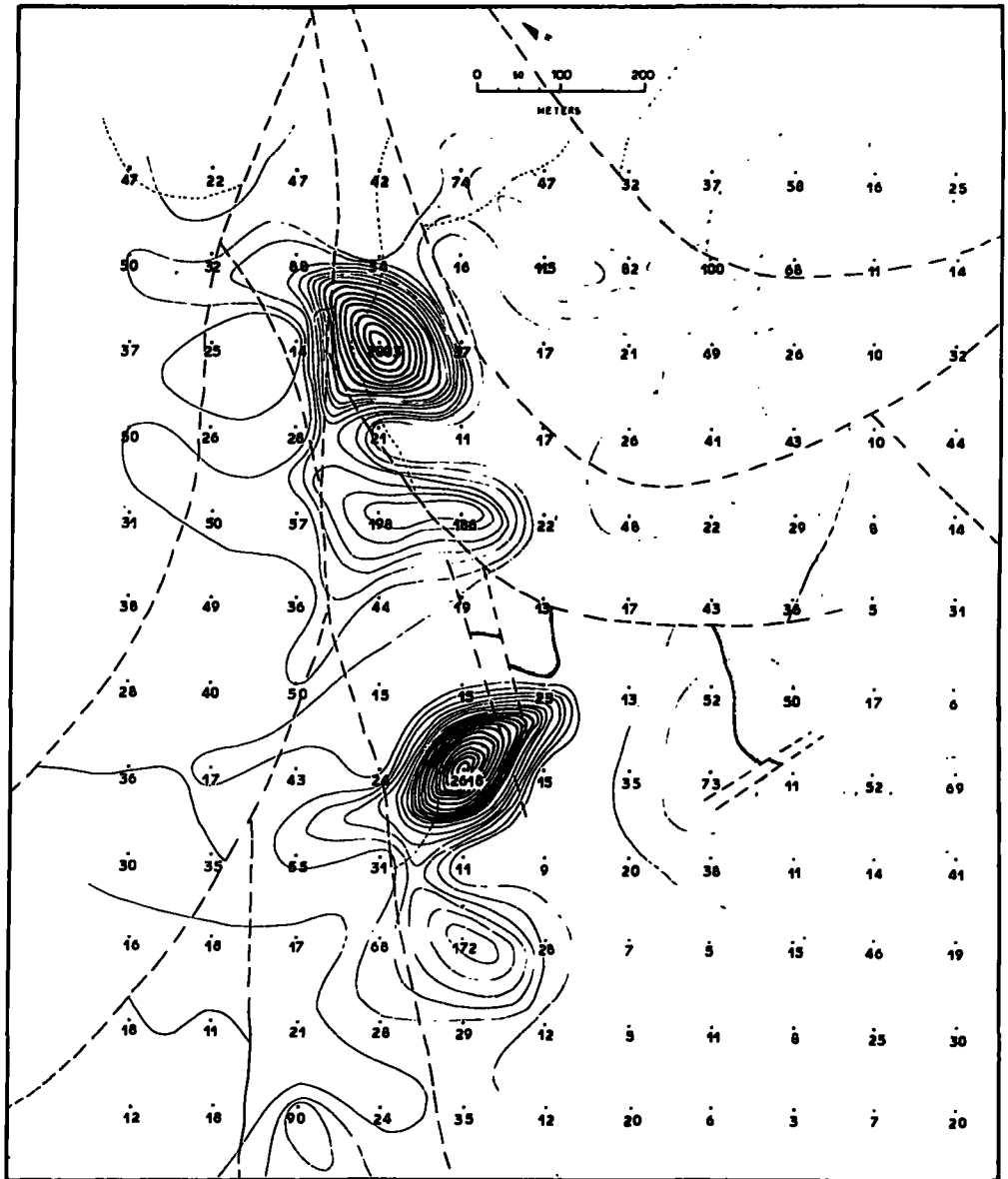


FIG.39F._Distribution of As in surface values above mineralization at Lahanos, Espiye. Values in ppm. Contour interval 25 ppm for thin and 200 ppm for thick lines.

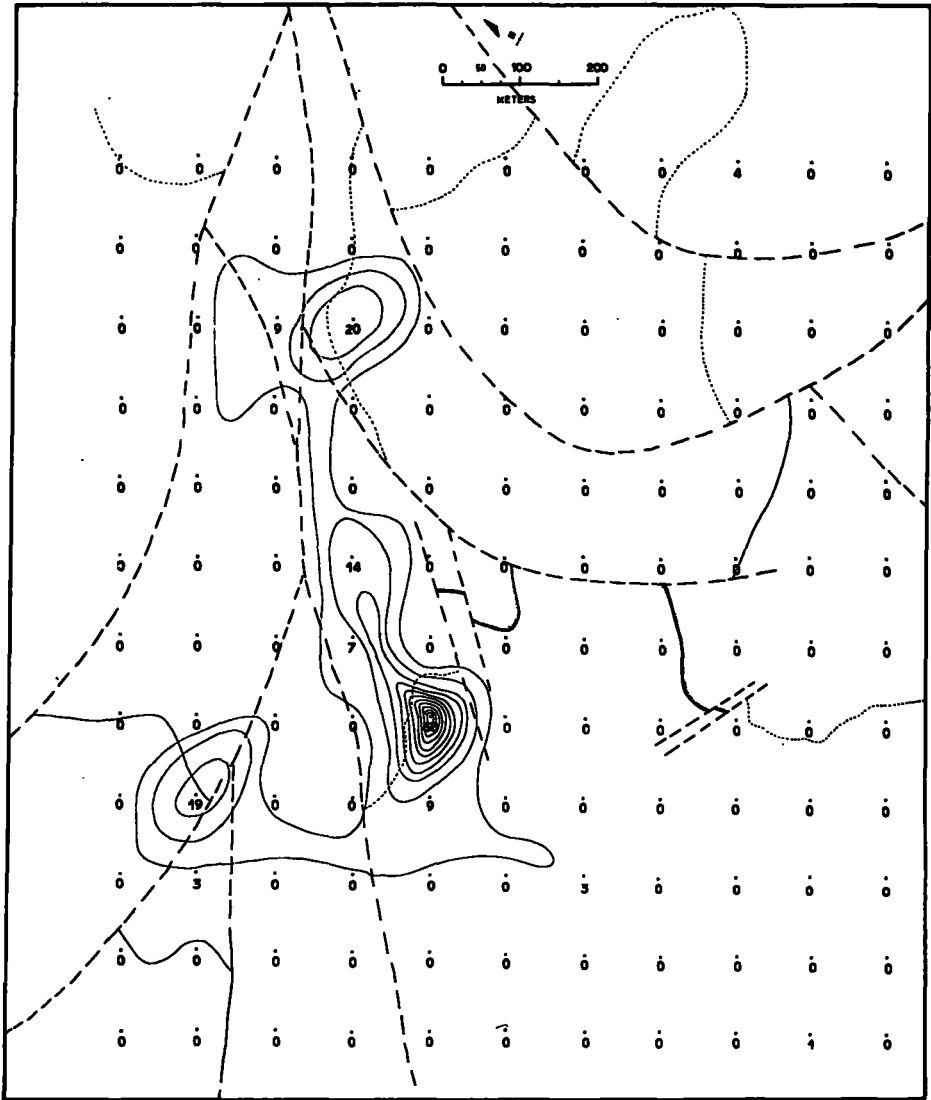


FIG.39G._Distribution of Sb in surface values above the mineralization at Lahanos, Espiye. Values in ppm. Contour interval 5 ppm.

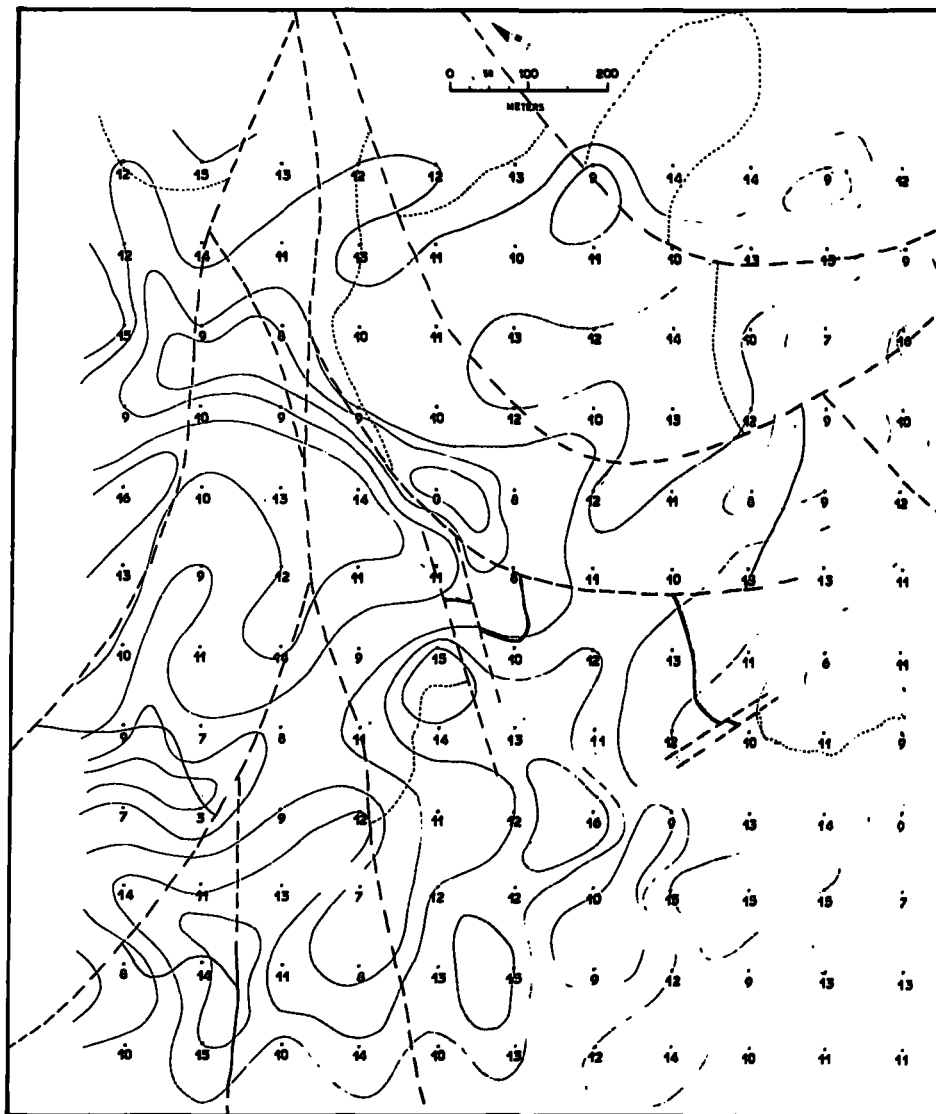


FIG.39H._Distribution of Cd in surface values above the mineralization at Lahanos, Espiye. Values in ppm. Contour interval 3 ppm.

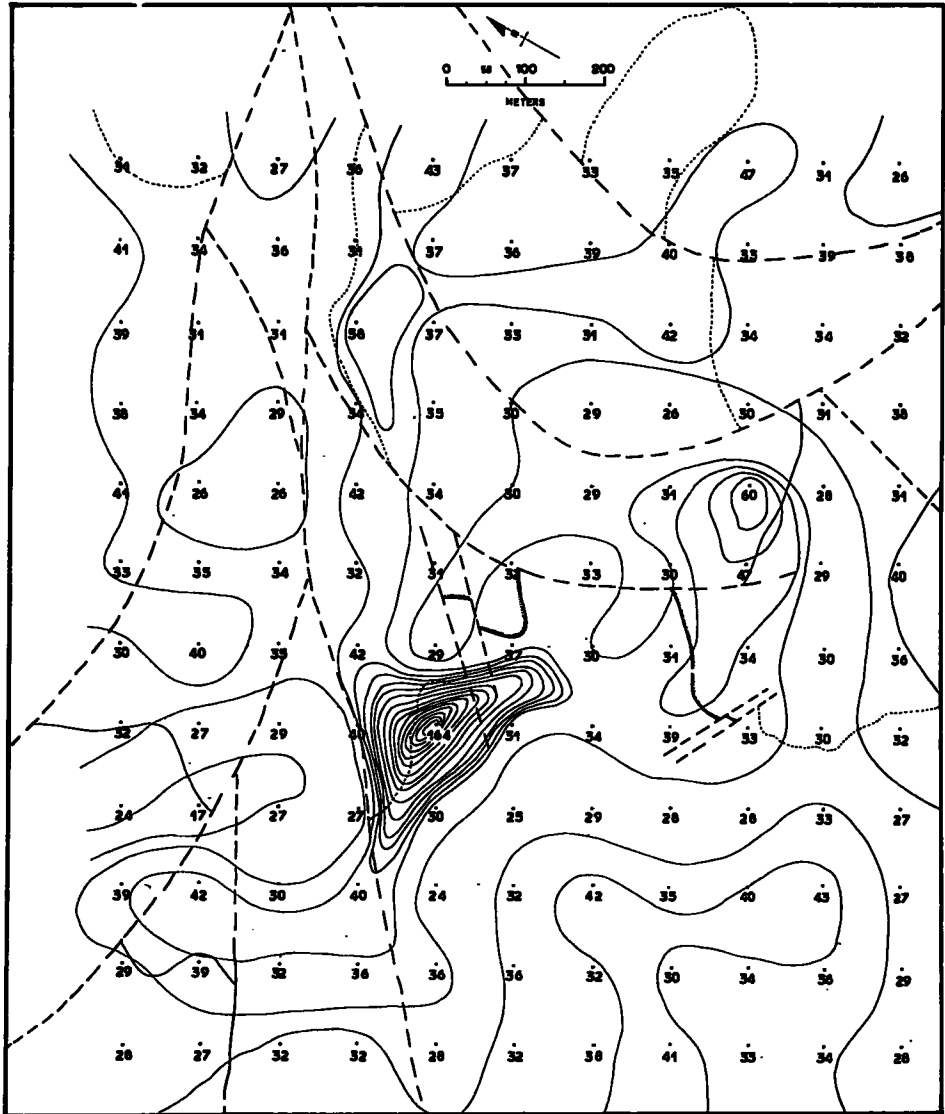


FIG.39I._Distribution of Te in surface values above the mineralization at Laňanos, Espiye. Values in ppm. Contour interval 10 ppm.

CHAPTER F - MINERALISATION OF MURGUL MINE

F. Murgul

Murgul copper mine, Borçka, Artvin Vilayeti, NE Turkey (See Maps 1, 3) is the second biggest working copper mine in Turkey, located at a distance of about three kilometers SE of Murgul town. During the field study, Murgul mine was twice visited for a short period of time to collect ore and host rock samples and to see the mode of occurrence of the copper mineralisation, since its general setting is similar to that of the Lahanos occurrence.

Mining activity has gone on here since medieval times (possibly Genoese). The first systematic exploration of the area was carried out in 1898 and eventually in 1900 the "Caucasus Copper Company" (A British company) was founded, and produced during the period between 1907 and 1914 with an output of 16,000 metric tons of blister copper. The first Turkish interest was started by Etibank (the state owned mining company) in 1938 after a break of 24 years. Murgul copper mine started regular production in 1951 after the establishment of a concentration plant and copper smelter. An underground mining system was first employed, but later this method was abandoned. Today an open-cast mining method is being employed, and therefore the production of blister copper has been increased. At present 1034 labourers are employed by Etibank, of whom 560 work on the mine site, 60 on the aerial ropeway and 160 on plant and administration. The concentration plant and smelter employ 254 workers. Daily ore output is 2000 metric tons and yearly about

600,000 metric tons. Daily output of the smelter is 39 metric tons of blister copper. The overall grade of ore is 2.08% Cu, with a reserve of 16 million metric tons. Recent exploration activities of Etibank has discovered an ore body at Çakmak Kaya location in the vicinity of Murgul mine with an ore reserve of 20.8 million metric tons assaying 1.08% Cu.

Sulphide mineralisation is located in between totally silicified Lower Dacitic Series (i.e. porphyritic dacite) and the Upper Dacitic pyroclastics, but the ore body is mainly in the Lower Dacitic Series (Pollak, 1962; Kraeff, 1963b) and consists of hydrothermally brecciated quartz masses containing numerous veins and veinlets with an averaging thickness of a few millimeters up to a few tens of centimeters i.e. a stock-work of pyrite and chalcopyrite. Beside pyrite and chalcopyrite it is also possible to see some accessory sphalerite, galena and sulphosalts mainly of the tetrahedrite-tennantite group. This recognition of the present ore body as a stock-work results from the present author's examination of the deposit and has not previously been mentioned by other workers in the area. It is probable that more massive ore existed in the previously worked parts of the deposit, and that this also showed a zone of secondary copper enrichment, since these features are referred to by previous authors. However, no sign of these features is now to be found. The existence of abundant gypsum with disseminated (?) pyrite and pyrite veinlets, above the ore body has also not been recorded by previous workers.

The geology and general setting of the area is not very complicated and the following stratigraphic column can be deduced by compiling the results of previous workers (e.g. Pollak, Kahrer, Kraeff, Klay, etc.)

8. Alluvial - Pleistocene deposits and debris,
7. The Young Basic Series (same as the Lahanos area),
6. The Tertiary Granitic Intrusions (All belong to the Tatos Batholith),
5. Post-Cretaceous dacite III (= Hypabyssal dacite of the Lahanos area),
4. The Upper Basic Series
 - (d) Tuff Series
 - (c) Limestone-marl Series
 - (b) Hippuritic limestones
 - (a) Spilite II
3. The Upper Dacitic Series (= Upper Volcanic Series of Lahanos),
 - (b) Albite dacite II
 - (a) Dacitic tuffs
2. The Lower Dacitic Series (= Lower Volcanic Series of Lahanos),
1. The Lower Basic Series (= same as Lahanos).
 1. The Lower Basic Series which is called 'Spilitic Series I' by Kraeff (1963b) consists of a series of spilites and soda keratophyre

spilites, with tuffs and agglomerates, in the river Murganihevi and Scutari (Maps 3 and Section 5). Some pyritic impregnations have been pointed out by Kahrer (1958) within this series.

2. The Lower Dacitic Series is similar to that at Lahanos, represented by porphyritic dacite (lavas mainly), characterised by quartz and albite phenocrysts lying in a quartz-bearing ground-mass which may contain laths of albite. Due to mineralisation this series is very much altered, the main alteration processes being secondary silicification, sericitisation, a little kaolinisation and pyritisation. The Murgul ore body mainly occurs within this porphyritic dacite as a replacement body dipping into the side of the mountain Karataş (Section 5).

3. The Upper Dacitic Series consists of two different units i.e. dacitic tuff and porphyritic dacite II. The dacitic tuffs are very similar to the Lahanos dacitic pyroclastics. They have also red as the dominant colour and are fairly thin, overlying the Lower Dacitic Series and showing secondary silicification and local calcification. Porphyritic dacite II (Albite dacite II) directly overlies the dacitic tuffs and the Lower Dacitic Series and sulphide body with unconformity. The albite dacite II is characterised by coarse grained texture and greenish colour, but sometimes near the sulphide mineralisation they do show red violet colours which might be due to disseminated ore minerals. It is also possible to see xenoliths of the Lower Basic Series. Chemical analysis of these rocks suggested a Rhyodacitic composition rather

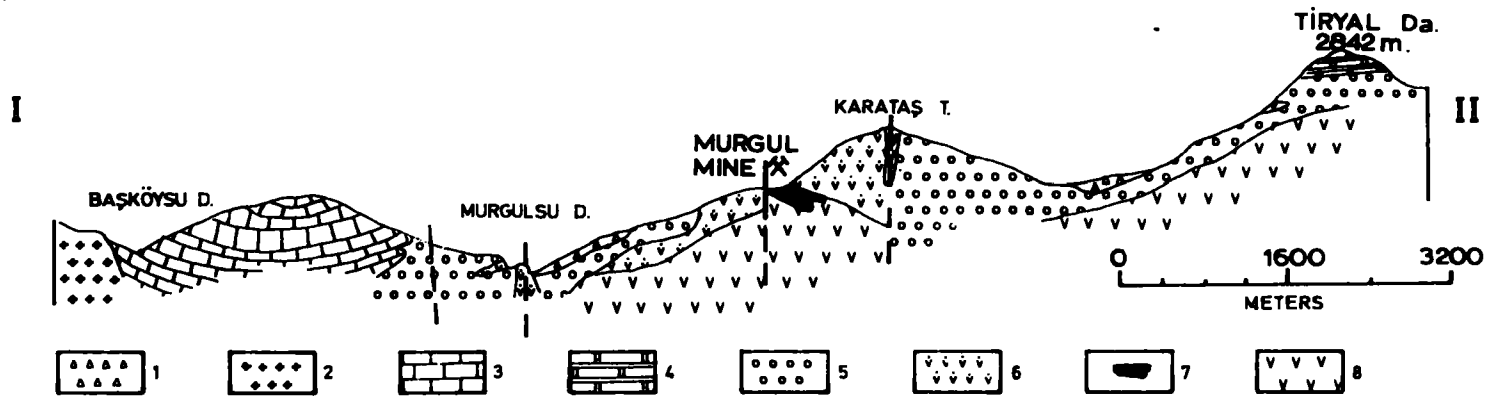
Geo.Sec._5

GEOLOGICAL SECTION OF THE MURGUL AREA

(AFTER L. KLÄY)

NW

SE



1. Debris & landslide masses, 2. Albite tonalite, 3. Limestone-marl series, 4. Hippuritic limestone series, 5. Spilitic series II, 6. Albite dacite II, 7. Orebody, 8. Albite dacite I.

than dacitic, similar to those of the Lahanos area. This fact is also supported by the microscopic evidences i.e. abundance of rounded and corroded phenocrysts of quartz (Samples M27, M27B and C, M28 in Tab. 4).

4. The Upper Basic Series is mainly composed of a series of sub-marine volcanics and sediments. At the bottom it mainly consists of Spilite II containing soda keratophyre spilites, agglomerates, tuffs, and sometimes inclusions of the Upper Dacitic Series. A good outcrop of this series can be seen NE of Murgul town (Map 3). The Hippuritic limestone series (Turonian - Lower Campanian) consists of reddish layered limestone with beds of massive white limestones. These beds are fossiliferous and contain a micro fauna e.g. *Globotruncana laperenti laperenti* and *Globotruncana laperenti tricarinata* etc. (Kraeff, 1963b). There is an unconformity present between the Hippuritic limestone and its overlying limestone marl series. A good outcrop of the Hippuritic limestones can be seen SE of Murgul town (Map 3 and Section 5). The limestone-marl series of Upper Campanian-Maestrichtian-? Eocene age consists of limestone, marly limestone, marl, sandstone and tuff containing *Globotruncana c.f. Stuarti*, *Globotruncana c.f. Conica*, *Globotruncana c.f. rosetta* etc. and its passage upwards into the Nummulitic Eocene is seen at the Kuvarshan copper mine (Kovenko, 1942). The limestone-marl series is overlain by pyroclastics.

5. The post-Cretaceous dacite III, which is the equivalent of the Hypabyssal dacite at Lahanos, contains some important pyrite and

other sulphide mineralisation in the Gölbaşı and Operkment areas near Murgul.

6. Tertiary granitic intrusions are mainly made of albite tonolite, granodiorite, granite and characterised by euhedral phenocrysts of albite with a little quartz intergrown with albite v^emicular forms. At Başköy, NE of Murgul (Map 3) one of these bodies is intruded into the limestone-marl series.

7. The Young Basic Series mainly consists of various andesitic and basaltic dykes.

8. Alluvial-Pleistocene deposits and debris are exposed SE of Murgul town, on the flank of the Murgul Suyu Stream (Klay, 1962).

F.Ia MINERALISATION

F.Ial Mode of Occurrences of Ore

The Murgul ore body is said to be composed of three different ore shoots known as (i) Çangara, (ii) Sosveni and (iii) Satep. At the +1150m level the size of Çangara and Sosveni ore shoots together is 450m by 300m with an average thickness of 100m. Below this level, the copper content of the ore body is lower than 0.8% which is at present an unworkable grade. The general appearance and mode of occurrence of the Murgul sulphide mineralisation shows broad similarity to those of Japanese "OkO" (=Yellow Ore) (Japan, 1960) with main mineral assemblages of pyrite and chalcopyrite associated with subordinate amounts of tetrahedrite-tennantite, sphalerite and little galena. There seems to be no development of zoning within the ore body.

F.Ia2 Methods of Study

Sulphide samples from the Murgul mine have been treated in the same way as previously described for the Lahanos samples.

F.Ia3 Ore Microscopy

Ten polished specimens were prepared from the 26 ore samples selected as being representative of the Murgul mineralisation.

Pyrite is the earliest and most abundant sulphide mineral. It shows little or no corrosion, occasional zonal replacement, and forms hypidiomorphic crystals which may be replaced by sphalerite, chalcopyrite, galena and gangue minerals, generally along the grain boundaries between different pyrite grains. Within the copper rich parts of the ore body individual rounded and idiomorphic crystals of pyrite show a grain-size variation between 80 by 60 microns to 500 by 500 microns. The size of pyrite aggregates also changes in size from 300 by 250 microns up to 800 by 1300 microns. There is also colloidal pyrite which is later than granular pyrite but it too is replaced by sphalerite, chalcopyrite and galena.

Sphalerite occurs in two generations in the Murgul ore. The early sphalerite is the second oldest sulphide mineral after pyrite and forms local concentrations within the ore body. The second generation sphalerite very clearly replaces chalcopyrite (Plate 55). The early sphalerite often forms xenomorphic (or allotriomorphic) granular texture and its intersertal spaces are often replaced by interstitial galena, chalcopyrite and gangue. Chalcopyrite in early



55. The second generation sphalerite (dark gray) and chalcopyrite relationship, Murgul mine. 160 x



56. Chalcopyrite lamellae in sphalerite, Murgul mine. 2700 x

sphalerite exhibits a very nice emulsion type of ex-solution texture which would indicate a temperature range of formation from 350° to 650°C (Buerger, 1934; Borchert, 1934 and Schwartz, 1931) and chalcopyrite often forms blebs and also blades (lamellae on the (111) planes of sphalerite (Plate 56). There is a tendency for these blebs and lamellae to accumulate near the grain margins of the sphalerite.

Chalcopyrite occurs as the main copper sulphide and forms xenomorphic (or allotriomorphic) rounded granular texture. Occasionally in small cavities in the host rock alone or with other sulphide and gangue minerals, it forms euhedral crystals. Chalcopyrite replaces early sphalerite, pyrite and tennantite, but is mainly replaced by galena, late sphalerite (Plate 55) covellite and gangue. Tennantite-tetrahedrite and chalcopyrite often show a mutual boundary relationship, but sometimes it is possible to see tiny veinlets of chalcopyrite replacing tennantite-tetrahedrite, particularly in sphalerite, i.e. tennantite-tetrahedrite is a little earlier than chalcopyrite and both showed overlapping growth. Chalcopyrite and galena are often associated, isolated patches of chalcopyrite commonly occurring in galena, but sometimes the reverse is seen. In general, galena replaces chalcopyrite, showing the same kind of age relationship as the chalcopyrite tennantite-tetrahedrite association i.e. another overlapping intergrowth texture. Chalcopyrite sometimes contains tiny specks of native gold.

Galena is the only lead sulphide mineral and forms xenomorphic interstitial texture with sphalerite. It often replaces pyrite, sphalerite and partly chalcopyrite and tennantite-tetrahedrite but is sometimes replaced by chalcopyrite and selectively by neodigenite and covellite, forming a ramifying replacement texture. Zonal replacement of pyrite by galena is also present.

The tennantite - tetrahedrite $(\text{Cu}_{10} (\text{Cu, Fe})_2 \text{As}_4 \text{S}_{13} - \text{Cu}_{10} (\text{Cu, Fe})_2 \text{Sb}_4 \text{S}_{13})$ group of copper arsenic and copper antimony sulphosalts are common minor minerals in Murgul mine, where tennantite often predominates over tetrahedrite and both show rounded patches and mutual boundary relationships against chalcopyrite, but there are some areas where chalcopyrite veinlets cut across tennantite-tetrahedrite. A significant texture of tennantite or tetrahedrite is that blebs of tennantite in sphalerite display a similar texture to the emulsion ex-solution texture of chalcopyrite in sphalerite.

Neodigenite $(4 \text{Cu}_2\text{S Cu S})$ selectively replaces galena forming a ramifying replacement texture, and occasionally replaces tennantite, chalcopyrite, sphalerite and pyrite. Small veinlets of neodigenite cut across tennantite and chalcopyrite and sometimes surround chalcopyrite where neodigenite may well be a pseudomorph after galena. Tiny fractures in sphalerite are sometimes infilled with neodigenite. Finally small rounded inclusions of neodigenite occur in pyrite.

Covellite (CuS) is present in small quantity and is often seen as replacing veinlets in chalcopyrite. An association of covellite with neodigenite in chalcopyrite is also observed.

Due to extensive opencast mining it is not now possible to see the secondary enrichment zone which is already worked out. However, there is some recent formation of malachite, azurite and chalcantite^h. Kahrer (1961) describes the following minerals from the secondary enrichment zone: bornite, rhombic chalcocite, covellite and lamellar chalcopyrite.

From ore microscopy studies in Murgul mine the following paragenetic table can be suggested for sulphide mineralisation: As primary ore mineralisation pyrite - sphalerite - tennantite (-tetrahedrite) - chalcopyrite - galena - sphalerite - ?gold - neodigenite - covellite - and followed by various gangue minerals i.e. barytes - ankerite - dolomite. In the secondary enrichment zone, according to Kahrer's (1961) paragenetic table the sequence bornite - rhombic chalcocite - neodigenite - covellite - lamellar chalcopyrite - azurite - malachite was found.

F.1a4 X-ray Diffraction

X-ray studies of sulphides from Murgul mine were carried out by methods already described for the Lahanos sulphides (See E.1el).

Sphalerite (ZnS , $F\bar{4} 3m$, $a_0 = 5.3985 \text{ \AA}$ according to Kudenko and Stetsenko, 1964): On examination with a binocular microscope of a sphalerite concentrate prepared by flotation, two distinct varieties were seen, respectively lighter and darker in colour.

Small samples of each were hand picked for powder photography.

For the lighter coloured sphalerite a cell size of $5.4109 \bar{\pm} 0.0005$ A° was found, and for the darker one $5.4101 \bar{\pm} 0.0005$ A° (Table 7). There is thus no significant difference in cell size between the two. According to Kullerud (1953) and Skinner et al. (1959) a solid solution of 11 mole per cent FeS is indicated which corresponds with a minimum formation temperature of about $200 - 360^\circ\text{C}$, which is lower than that found for the Lahanos-sphalerite.

Galena (PbS , $\text{Fm}3\text{m}$, $a_0 = 5.94$ A° given by Wasserstein, 1951; Swanson and Fuyat, 1953): Cell-size determination of galena in Murgul mine gave a value of $a_0 = 5.9353$ A° which is slightly different from Karadere-galena, but noticeably smaller than Lahanos-galena (Table 7).

Chalcopyrite (Cu Fe S_2 , $\text{I } \bar{4} 2\text{d}$): In the literature, various values are given for the cell size. According to Deer et al. (1962) $a_0 = 5.25$ and $C = 10.32$ A° for pure chalcopyrite. Cell-size determination of Murgul-chalcopyrite associated with sphalerite gave a cell-size of $a_0 = 5.2887$ and $C = 10.425$ A° , and a second one from chalcopyrite rich ore without sphalerite gave a cell size of $a_0 = 5.2888$ and $C = 10.4171$ A° . Both cell-sizes are distinctly higher than the values quoted by Deer et al. The difference may be due to the trace element content of the Murgul specimens, which is given in Tables 23 and 24.

F.Ia5 Reflectivity

Measurements on samples from the Murgul deposit were made

using methods and standards as previously described for the Lahanos deposit. Results given in Tables 15, 21, 22 and Figs. 20, 20B, 27A, 27C, 26 A and B, 26 C are distinguished by the prefix M. The reflectivity values for chalcopyrite, sphalerite and galena in yellow ore (i.e. Murgul type) seem to be slightly higher than for the same minerals occurring in Black ore (i.e. Lahanos type) and black vein type ore (i.e. Karadere type).

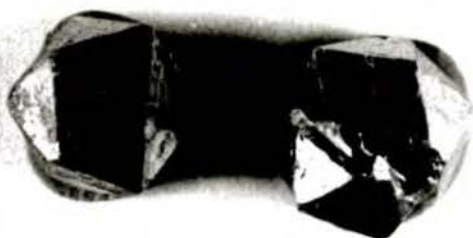
F.Ia6 Wall-Rock Alteration

Beneath the Murgul ore body, the wall-rocks are extensively silicified, with the development of jasper, and sericitised. Above the ore body about one meter of propylitised volcanic wall-rock passes upwards into a massive and banded gypsum horizon from 2 to 10 meters in thickness containing veinlets and scattered crystals of pyrite, and this in turn grades into altered country rock with clay minerals, then unaltered country rock. The association is similar to that described at the Wanibuchi mine, Japan by Iwao (1956).

F.Ia7 CHEMISTRY

Trace element contents of separated Murgul sulphide minerals and Co:Ni ratios in the pyrite have been determined by methods previously described for Lahanos and are shown in Tables 23 and 24. Bornite, enargite, marcasite and bismuth/tellurium minerals have not been detected in any of the Murgul ores studied, but with these exceptions, Murgul mineralogy is similar to that at Lahanos, so that comments on the trace element distribution at Lahanos apply equally, to the Murgul ore and are therefore not separately discussed here.

It is however, interesting to note that the Mo content of the Murgul chalcopyrite is much higher than found in this mineral elsewhere. The Co:Ni ratios of Murgul pyrite are much greater than unity and therefore indicate a hydrothermal origin. Large euhedral pyrite crystals are abundant within the silicified foot-wall parts of the ore body. Two distinct morphologies occur—the pyritohedron (210) and octahedron (111). Co/Ni ratios were determined for each type and as shown in Table 24, the ratio in crystals of octahedral habit is an order of magnitude greater than in pyritohedral crystals. The reasons for this difference are not understood at the time of collecting the samples, no attention was paid to the distribution of morphology, and in many crystals combinations of the two forms occur. In some cases, relative development of the two forms is such as to produce a crystal which resembles a regular icosahedron, with an apparent five fold symmetry (Plate 57).



57. Icosahedron pyrite crystal from Murgul mine.



58. The general field occurrence of the Black vein type mineralisation at Inkoy, Tirebolu.

F.II KARADERE AND INKÖY (BLACK VEIN TYPE DEPOSITS)

Karadere (Pb-Zn-Cu) mine, Kumarli, Ünye, Ordu Vilayeti and Inköy (Pb-Zn-Cu) mine, Tirebolu, Giresun Vilayeti (See Map 1) both represent a third type of base metal sulphide deposition within the same volcanic environment in the Eastern Pontus Ore Province. The general characteristics of these deposits are that they occurred in shear and fault zones forming veins of base metal sulphide, and are of smaller size than the Lahanos and Murgul mines. The main sulphide minerals are galena, sphalerite and a little chalcopyrite, pyrite and lead-copper sulphosalts.

F.IIa KARADERE (Pb-Zn-Cu) MINE Kumarli, Ünye, Ordu Vilayeti which is situated about 1.5 km W of Kumarli village in the river Kara. The lead-zinc-copper deposit is composed of three parallel E-W veins some 100m apart, cutting through silicified dacitic tuff, passing up into a dark green agglomerate (believed to be equivalent to the Upper Basic Series at Lahanos) which is overlain in turn by a sedimentary limestone. In addition to the main E-W fracture system, dipping 50° to the N, a subsidiary N-S fracture zone dipping W is also developed and contains a weaker mineralisation than the main veins. The deposit was first worked by an English Company about ninety years ago and recently worked by the "Dedehan" private company. Now Etibank has been exploring this Pb-Zn-Cu sulphide deposit for its copper content. However, copper is a subsidiary sulphide mineral, though in this type of mineral deposit, one does get locally enriched chalcopyrite with pyrite and marcasite. Unless the lead-zinc rich

upper part passes downwards into a copper rich zone, the main potential of the veins seems to be for lead and zinc. Geophysical work has recently been carried out by Etibank to endeavour to discover more about the extent of the mineralisation.

F.IIa1 MINERALOGY OF THE ORE

The general appearance of the Karadere mixed sulphide ore is in between the two leading types i.e. Lahanos Black Ore and Murgul Yellow Ore. It is not as dark as Lahanos ore nor as light as Murgul ore; but the presence of galena and sphalerite makes the Karadere deposit closer in appearance to the Lahanos Black Ore.

The Karadere mixed sulphides were treated in the same way as the Lahanos and Murgul Sulphides for further chemical and X-ray studies.

F.IIa2 Ore Microscopy

Selected ore samples from the galena rich and galena poor parts of the main vein have been studied in polished section and show quite different mineral assemblages from the Murgul Yellow Ore, but are closely comparable with the Lahanos Black Ore.

Pyrrhotite (Fe S_{1+x}) appears to be the earliest sulphide and is mainly replaced by marcasite, pyrite, sphalerite and galena. Occasionally pyrrhotite and marcasite show clean cut boundary relationships, but marcasite often replaces pyrite. It is possible to see relicts of pyrrhotite in pyrite and sphalerite. Although the amount of pyrrhotite is very small ($\ll 1\%$), it is nevertheless more abundant than at Lahanos.

Marcasite (FeS_2): Marcasite-pyrrhotite and pyrite associations are quite common in the galena poor ore. Marcasite replaces pyrrhotite of which relicts are often seen in Marcasite, but marcasite is replaced by colloidal pyrite, in association with sphalerite and chalcopyrite, in a segmented vein replacement.

Pyrite (FeS_2) is the commonest iron sulphide present in the galena rich ore. Two distinct varieties of pyrite occur in the Karadere ore which are quite similar to those of Lahanos - and Murgul pyrite i.e. massive or granular pyrite and colloidal pyrite. The latter is later than granular pyrite and occasionally rims around the marcasite. Granular early pyrite is replaced by sphalerite, tennantite and other sulphides.

Sphalerite (ZnS) is less abundant than galena. It is earlier than galena and other copper sulphides, including sulphosalts, but it replaces iron sulphides. Chalcopyrite and sphalerite sometimes show a mutual boundary relationship, but often emulsion type exsolution blebs of chalcopyrite occur in sphalerite as well. Mutual boundary texture is also found between sphalerite and tennantite.

Enargite ($\text{Cu}_3 \text{As}_4 \text{S}_{13}$) is present in subordinate amounts in the Karadere ore. It clearly replaces sphalerite and marcasite but is replaced by tennantite.

Tennantite ($\text{Cu}_{10} (\text{Cu}, \text{Fe}) \text{As}_4 \text{S}_{13}$) is present in amounts greater than enargite, but still $< 1\%$ in the Karadere deposit. It replaces all iron sulphides including the colloidal pyrite in which tiny veins of tennantite cut across the banding. It is also possible to

see colloidal pyrite relicts in tennantite. Galena and tennantite often show replacement texture in which tennantite is often replaced by galena, but it is possible to see replacement of galena by tennantite in the galena rich ore. These two minerals also exhibit a myrmekitic texture. All these observations would suggest a successive mineralisation in which tennantite is a little earlier than galena. Tennantite and chalcopyrite relationships are somewhat similar to those of galena and tennantite i.e. tennantite a little earlier than chalcopyrite or both contemporaneous. Tennantite clearly replaces sphalerite and enargite.

Chalcopyrite (Cu Fe S_2) is the common copper iron sulphide in the Karadere deposit and locally shows enrichment, but in the lead-zinc ore body it is often present in only subordinate amounts. Sphalerite and chalcopyrite often show emulsion ex-solution texture, which indicates a temperature range about $650^\circ - 350^\circ\text{C}$ according to Schwartz (1931), Buerger (1934) and Borchert (1934). The presence of mutual boundary texture between chalcopyrite and sphalerite may indicate that after chalcopyrite had completely ex-solved, it migrated towards the outside of the sphalerite grains. The second and main generation of chalcopyrite is earlier than galena, gangue, covellite and neodigenite. Both galena and associated chalcopyrite often replace sphalerite.

Galena (PbS) and sphalerite are the main sulphide minerals of the Karadere ore deposit, galena being more abundant than sphalerite and other sulphides, and it replaces all iron sulphides and sphalerite.

It is possible to see relicts of pyrite in galena. Both chalcopyrite and galena display relicts or patches of one in the other, though chalcopyrite is more usually being replaced by galena.

Covellite (CuS) and Neodigenite (Cu₉ S₅) These copper sulphide minerals are the latest sulphides. They replace other early sulphide minerals and are often associated together.

From the study of polished sections, the following order of formation is suggested for the Karadere minerals - Quartz - pyrrhotite - marcasite-pyrite - ? Colloidal pyrite - Sphalerite (chalcopyrite) - enargite - tennantite - chalcopyrite - galena-gangue - neodigenite and covellite.

F.IIa3 X-ray Diffraction

X-ray studies of different sulphides have been undertaken under similar conditions to those of Lahanos - and Murgul-sulphides.

Sphalerite: Cell size determinations of sphalerite from the Karadere deposit have been carried out on the basis of differences in colour. Selected different coloured grains (i.e. brown (opaque), brownish yellow, honey coloured and green translucent) were examined by powder photography and cell sizes calculated. The results from these different sphalerites are given in Tab. 7. The smallest cell size was obtained from honey coloured semi-translucent sphalerite with $a_0 = 5.4118 \pm 0.0005 \text{ \AA}$, followed by translucent green sphalerite with $a_0 = 5.4119 \pm 0.0005 \text{ \AA}$, and brownish yellow almost opaque

sphalerite with $a_0 = 5.4123 \pm 0.0005 \text{ \AA}^\circ$, whilst the largest cell size was obtained from opaque dark brown sphalerite with $a_0 = 5.4141 \pm 0.0005 \text{ \AA}^\circ$. The transparency of sphalerite closely follows the cell size variation which is a function of substitution by Fe^{++} , Cd and Mn (Kudenko and Stetsenko, 1964; Kullerud, 1953; Skinner et al., 1959 etc.). Using Kullerud's method for sphalerite as a geothermometer, for Karadere-sphalerite 7 to 12 mol per cent FeS is obtained from Henrique's chart, which corresponds to a temperature range of c. 240° to 400°C . With this range of temperature, the Karadere-sphalerite appears to be formed at a higher temperature than the Murgul type yellow ore and Lahanos type black ore. The presence of pyrrhotite in association with sphalerite in the Karadere deposit would indicate that in the system Zn-Fe-S there was no iron deficiency so that the temperature obtained is more reliable than in the case of Lahanos- and particularly Murgul-sphalerite, where the non-existence of pyrrhotite in association with sphalerite may indicate an iron deficiency, so that only a minimum temperature of formation is indicated. Even after corrections were made, particularly for the Cd and Mn content of the sphalerite, according to Kudenko and Stetsenko (1964), this did not alter the relative sequences of temperature range found by Kullerud's method.

Galena: Cell-size determination of two galenas associated with galena rich ore and galena poor ore from the Karadere deposit gave a slightly smaller cell-size in the galena rich ore i.e. $a_0 = 5.9352 \pm 0.0005 \text{ \AA}^\circ$ compared to galena poor mixed ore i.e. $a_0 = 5.9355 \pm$

0.0005 A° (see Tab. 7). Higher cell-sizes were obtained for the Lahanos-galena which is often associated with sphalerite and chalcopyrite.

Chalcopyrite: The Karadere chalcopyrite cell size is slightly larger than that from the other deposits.

F.IIa4 Reflectivity Measurements On Karadere Sulphides

Reflectivity measurements of different sulphide ores from the Karadere deposit have been carried out by using the technique which has already been described in (E.1e3). Results are given in Tables 15, 20, 21, 22. In comparison with the Lahanos-type (i.e. Black ore) and Murgul-type (i.e. Yellow ore), the Karadere ore (i.e. Black vein type ore) gave higher reflectivity values for marcasite, intermediate values for sphalerite and lower reflectivity values for chalcopyrite and galena.

F.IIa5 Chemistry

Trace element contents of separated Karadere sulphide minerals and Co:Ni ratios in the pyrite were determined by methods previously described for Lahanos ores and are shown in Tables 23 and 24.

The cadmium and cobalt contents of the Karadere sphalerite are distinctly higher than found at Lahanos and Murgul. The Karadere galena is the only one for which trace element contents have been determined, because of the difficulty of separating a sufficient quantity of galena from the other ores.

F.IIb INKOY (Pb-Zn-Cu) MINE: This is another vein type deposit which is situated 4 km E of Tirebolu at the junction of the Tirebolu-Trabzone and Tirebolu-Harşit roads, on the west bank of the river Harşit estuary, where mineralisation occurs in a fault zone in the Upper Volcanic Series (See Map 1 and 2 and Plate 58). The deposit is being worked at present by a private Company - no information is available about the mining method, and it is worked for lead and zinc content rather than copper. The main ore minerals are galena, sphalerite, chalcopyrite, pyrite and sulphosalts. Ore microscopy studies of the Inkoy deposit suggested the following paragenetic sequence: pyrite-sphalerite-galena-tetrahedrite-tennantite group (i.e. tetrahedrite-tennantite-seligmanite $2\text{PbS Cu}_2\text{S As}_2\text{S}_3$, occurring near the boundaries of tennantite and galena) - chalcopyrite-gangue as primary sulphide mineralisation. Covellite occurs as a secondary mineral.

Electron probe analysis showed that although both tetrahedrite and tennantite are present, tetrahedrite is the more abundant. Quantitative probe results for tetrahedrite are shown in table 11.6-7 and its cell-size in Table 8; the identity of the seligmannite was checked by X-ray diffraction.

F.III OTHER DEPOSITS OF THE EASTERN PONTUS ORE PROVINCE

Within the Eastern Pontus Ore Province there are mineral deposits other than those already described, but they usually have no economic value, except for certain manganese deposits. They can be grouped into:

1. Syngenetic or syn-sedimentary submarine exhalative ore deposits including pyrite and manganese.

2. Contact metasomatic deposits, mainly iron oxides.

1. Syngenetic or Syn-Sedimentary Submarine Exhalative Ore Deposits

This group of mineral deposits can be divided into 1a - Pyrite and 1b - Manganese deposits. Both are supposed to have a close genetic relation to the submarine volcanic activity that took place during the development of the Eastern Pontids.

1a - The pyrite deposits of this group have no economic value, but they occur throughout the Eastern Pontids, locally developed and often associated with the common autoalteration products of silicification, propylitisation and kaolinisation of the volcanic series. They are usually lenticular in shape with a thickness from a few centimeters up to several meters, according to Geoffroy (1960), who has described good examples of this sub group from the Rize and Çayeli districts.

1b - The manganese ore deposits are of syn-sedimentary volcanic exhalative type according to Borchert (1958), and they are found principally in the area between Rize and Murgul. According to Kraeff (1963b) they are formed at the end of the second of the four magmatic cycle he recognises. The best examples of this type of manganese ore deposit has been described by Kraeff (1963b) from Peronit, Hopa, Rize (Map 8), where manganese nodules occur in violet coloured silicified dacitic tuffs, dipping NW at 30°. Small manganese nodules of pyrolusite and polianite with accessory opal-chalcedony (1 - 2 cm in diameter) are located at the upper part of the tuff. This Peronit manganese deposit has similar features to those of the manganeseiferous sedimentary formations of the porphyry

series associated with volcanism of trachyte-Liparite type (including dacite) described by Verentsov (1964) from Russia. There are other manganese occurrences associated with spilites of the Lower Basic and Upper Basic series in the Hopa-Murgul region and this second group will also fall into Varentsov's second group of manganeseiferous sedimentary-volcanic formations i.e. manganese deposits associated with a greenstone series of spilite-keratophyres.

According to the present author's observations during the brief visits to Pilarcivat, Ardeşen area and Latum, Çayeli area, the sphalerite, galena, chalcopyrite mineralisation found together with the manganese ores may well have a separate later origin.

2. Contact Metasomatic Or Contact Pneumatolitic Deposits:

The occurrence of this group of deposits has apparently a genetic relation to the emplacement of the Pontid Batholith (Tatos Batholith). They contain mainly specularite, (hematite), magnetite and pyrite with very small specks of chalcopyrite and they are characterised by

(i) Association of skarn minerals and the presence of garnet, epidote and actinolite,

(ii) chloritisation and calcification of the host rock.

Representatives of this group of mineral deposits are well developed at the contacts of the intrusive bodies and limestones. However a similar kind of deposit occurs in volcanic rocks as well e.g. at Çatak, Yağlıdere, Camiyani, Giresun (See Map 2 and 4 (Grid

ref I5)) within the Lower Basic Series. Small lenses of specularite, magnetite and epidote occur, which are cut by late pyrite and quartz veins. These contact metamorphosed and mineralised volcanics were possibly lime and marl enriched parts of volcanic pyroclastics, or they were limestone and marl lenses.

Ore microscopy studies of the Çatak mineralisation showed that lamellae of earlier specularite are replaced by magnetite. Magnetite replaces along the edges of the specularite lamellae and advanced replacement produces pseudomorph lamellae of magnetite after specularite. Replacement of iron oxide by later sulphide and quartz is also common. Pyrite shows hypidiomorphic granular aggregates and contains embedded hematite grains and also sometimes infills intersertal spaces of specularite. The Co:Ni ratio of pyrite from the Çatak deposit given in Table 24 indicates a high temperature origin.

CHAPTER G - CONCLUSION AND DISCUSSION ON
ORIGIN OF THE LAHANOS PYRITIC
SULPHIDE DEPOSIT

G. CONCLUSIONS AND DISCUSSION ON ORIGIN
OF THE LAHANOS PYRITIC SULPHIDE DEPOSIT

As previously mentioned (Section BIV), two principal theories have been suggested to explain the origin of deposits of the Lahanos type in the Eastern Pontus ore province - the syngenetic submarine exhalative and epigenetic hydrothermal theories. The outstanding feature of these deposits is that they belong to the class of so-called "strata bound" sulphide deposits. The attraction of the syngenetic theories is that they provide a ready explanation for the "strata bound" feature, whilst epigenetic theories so far apparently do not. Nevertheless, the results of the present study as given in preceeding pages seem to provide strong support for an epigenetic hydrothermal origin. The main lines of evidence can be divided as follows -

- (a) Field observation
- (b) Microscopic study of the ores
- (c) Chemistry of the ore

(a) Field Observations

In addition to the foot-wall stockwork, veinlets of mineralisation can be seen underground penetrating into the hanging-wall. This feature, which was also noticed by Pollak (1961), is unlikely to appear in syngedimentary ores, but would be expected in epigenetic ore formation.

In a broad sense, the ore body zoning at Lahanos is somewhat similar to a well described and known zoning due to hydrothermal

mineralisation and alteration at Butte, Montana by Sales and Mayer (1948 and 1949). The distribution of the zones is the reverse of what Garlick has described as to be expected in syn-genetic deposits, using the Zambian copperbelt as his example (in Mendelsohn, 1961). Finally, the alteration halo seen so clearly in the field at Lahanos can only be of epigenetic origin. From the work of Sales and Mayer (1950), the sericitisation in these rocks has probably taken place at temperatures above 340°C .

(b) Oremicroscopy

The occurrence of undoubted ex-solution textures in various minerals at Lahanos, Murgul and Karadere is indicative of a relatively high temperature of formation for the ores. The pairs (host mineral named first) sphalerite-chalcopyrite, and bornite-chalcopyrite in particular suggest temperatures between 300 and 650°C , according to Schwartz (1931), Beurger (1934), Borchert (1934), Sugaki and Yamae (1950) and Brett (1964).

According to Skinner (1960), the presence of enargite rather than luzonite indicates a formation temperature above 320°C .

Such temperatures are only likely to have occurred in epigenetic mineralisation. Furthermore, the evidence of replacement of one mineral by another, seen in polished specimen, points to an extended period of mineralisation and high temperatures, unlikely to occur in syn-sedimentary mineralisation.

(c) Chemistry of the Ore

Co:Ni ratios determined for pyrite and chalcopyrite at Lahanos, Murgul, Karadere etc. all indicate a high temperature of formation (See Fleischer (1955), Hawley and Nichol (1961)).

Using sphalerite as a geothermometer, vide Kullerud (1953), Henrique (1957), Skinner (1959), Kudenko and Stetsenko (1964), a range of minimum temperatures from 200° - 470°C is indicated for these deposits.

On the basis of the foregoing summarised lines of evidence, it is possible to conclude that the Lahanos mineralisation is epigenetic, that it was deposited from solutions of high initial temperature entering a pre-existing rock sequence. The constituents of the various minerals were present in the solution and deposited successively, although not regularly, with falling temperature. Evidence for the age of the mineralisation is less distinct - it can only be said that with the possible exception of some dykes, the mineralisation is apparently later than all of the rocks in the Lahanos mine area.

Control of the location of the mineralisation seems to have been by the presence of a fine grained pyroclastic horizon of restricted permeability, below which the ore solutions were at least partially ponded back. As a consequence, no primary heavy metal geochemical anomaly occurs over the Lahanos ore body. The highest copper anomaly in the area (500 ppm) was found on Killik Tepe (See section 2) but boreholes there found no economic

mineralisation. The rocks are lavas with no appreciable interbedded pyroclastics. Thus, at Killik Tepe the hydrothermal solutions were able to pass on upwards without obstruction through the well jointed lavas, giving a geochemical anomaly but no ore deposition.

Two major aspects of the above comments require further discussion - the exact nature of the hydrothermal solutions and the mechanism causing precipitation when the travel of such solutions is impeded.

Although the principal ore minerals in these deposits are sulphides, it is most unlikely that they were transported in solution as simple sulphides, because of the very limited solubilities of the sulphides and because the order of solubilities provides no explanation for the observed order of deposition in many sulphide deposits. The arguments relative to the problem are summarised by Krauskopf (1967, p.499 et seq.).

Various authors (Kinkel, 1966; White, 1968; Anderson, 1969) in considering the origin of similar deposits have recently suggested alternative explanations to overcome this difficulty, whilst objections to some of their theories can be summarised by the following quotation from Barnes (1967, p.339) -

"The well-known low solubilities of sulphides in many aqueous solutions has led to the suggestion that transport occurs in a sulphur-deficient chloride solution in which the metals are soluble, followed by deposition caused by either mixing with a separate sulphide rich

solution or exposure to a host rock containing abundant iron sulphides (Lowering, 1961). Such a thesis is untenable for textural reasons because the depositional process would be rapid, tending to dump all sulphides together at the interface of the two environments. In addition, the sequence of precipitation in such circumstances would be controlled primarily by the solubility products and cannot match that commonly observed. For these and other reasons, this mechanism of ore transport and deposition is inadequate for nearly all hydrothermal deposits."

Recent experimental work on the nature of hydrosulphide complexes of heavy metal ions has, however, shown that several metals can be kept in solution at concentrations well above those allowed by the solubility product if the solution is near neutral and contain abundant H_2S (Krauskopf, 1967, p.502). Under these conditions the principal sulphur ion is HS^- and Barnes (1960) has shown that the enhanced solubility of zinc in H_2S solutions between 25 and 195° can be accounted for by formation of the ion $ZnS(HS)^-$. Even in chloride solutions, if the solution is saturated with H_2S and the pH is in the neutral region, Hinnert and Holland (1963) have shown that complexes of the above type are formed in preference to chloride complexes of the metal. However, the necessary experimental results that would allow a detailed thermodynamic consideration of the problem, such as that of Helgeson (1964) for lead chloride complexes, are not yet available, particularly for temperatures above $250^\circ C$. Thus Krauskopf (1967) states "This long discussion

of magmatic fluids, which has occupied the better part of three chapters, has left us without a satisfactory explanation for the origin of ore deposits" and Barnes (1967) "Many more experimental data are needed to begin to understand sphalerite transport at 400°C and above".

There is nevertheless a sufficient background of experimental detail to allow a reasonable quantitative explanation to be attempted.

First of all, information on the composition of gases from volcanic fumaroles and hot springs in volcanic areas shows according to Krauskopf (1967) "a remarkable similarity in the kinds of substances present and a still more remarkable variation in the proportions of these substances". Tables 28 and 29 give the compositions of gases collected from the basalt volcano Kilauea, Hawaii and Showa-Shinzan, a dacite dome in northern Japan. Next to water vapour, carbon dioxide is usually the most abundant gas. Various sulphur gases and HCl are present and their relative amounts vary widely. Thus, the hydrothermal waters associated with volcanic activity contain both chloride and hydrosulphide ions, the two principal complexing agents suggested as capable of transporting heavy metals in solution.

Despite this fact, there is characteristically no mention of heavy metal sulphides being deposited from the evaporating hydrothermal fluids in most recent volcanoes. Sulphur may be so abundant that for example the Siretoko - Iosan volcano in Hokkaido, Japan produced a

TABLE 28

Analysis of gases from Kilavea. Analyses are given in volume percent. All chlorine calculated as Cl₂

<u>Sample</u>	<u>J8</u>	<u>J11</u>	<u>J13</u>	<u>J16</u>	<u>S3</u>	<u>S9</u>
CO ₂	47.68	20.93	16.96	18.03	33.48	8.32
CO	1.46	0.59	0.58	0.56	1.42	0.82
H ₂	0.48	0.32	0.96	0.67	1.56	1.82
N ₂	2.41	4.13	3.35	3.11	12.88	8.92
Ar	0.14	0.31	0.66	0.08	0.45	0.29
SO ₂	11.15	11.42	7.91	8.53	29.83	16.80
S ₂	0.04	0.25	0.09	0.15	1.79	2.48
SO ₃	0.42	0.55	2.46	2.53		
Cl ₂	0.04	0.00	0.10	0.08	0.17	1.01
H ₂ O	36.18	61.56	67.52	66.25	17.97	59.97

(Source : Krauskopf, 1967, Tab. 16-1)

TABLE 29

Analyses of gases from Showa-Shinzon

The "active" gases include all gases other than H₂O, air, excess N₂ and the inert gases. The figures for the active gases are in volume percent, recomputed to total 100%. The last three lines of the table give the total of the active gases, excess N₂, and H₂O also in volume percent and totalled to 100%

<u>Temperature, °C</u>	<u>750</u>	<u>700</u>	<u>645</u>	<u>464</u>	<u>328</u>	<u>194</u>
* CO ₂	65.0	61.1	64.3	91.1	89.5	76.4
* CH ₄	0.08	0.14	0.14	0.14	0.15	0.16
* NH ₃	0.06	0.007	0.01	0.10	0.007	0.01
* H ₂	25.0	24.5	21.3	5.12	6.96	13.6
* HCl	5.39	8.61	8.61	1.51	1.48	4.66
* HF	2.76	3.54	3.51	0.88	0.65	0.43
* H ₂ S	0.10	0.62	0.53	1.07	1.05	4.27
* SO ₂	1.66	1.52	1.60	0.12	0.14	0.50
Total active gases	0.723	0.592	0.569	0.859	0.948	0.258
N ₂	0.026	0.019	0.021	0.042	0.052	0.026
H ₂ O	99.25	99.39	99.41	99.10	99.00	99.72

*"Active Gases"

(Source : Krauskopf, 1967, Tab. 16-2)

sulphur flow nearly a mile in length with thicknesses of more than 16 feet and widths up to 85 feet. (Watanabe, 1940). Other volcanoes in Hokkaido have formed sulphur ore bodies as sublimation deposits at active solfataras, and in addition replacement bodies of sulphur and iron sulphide are found (Jenks, 1966). They are related to Cenozoic calderas of Krakatao type with andesitic and dacitic flows and pyroclastics. The only other mineral of importance is opaline silica and there is some kaolinisation of the host-rocks. Therefore whilst volcanic fluids contain complexing agents capable of transporting heavy metals, and may form sulphur and iron sulphide ore bodies, either at surface (sulphur only) or as subsurface, essentially concordant replacements in dacitic tuff, the volcanic environment does not provide the heavy metals, other than iron. Suggestions that the source of heavy metals may be by leaching from the volcanic rock pile are not supported by these observations.

It might be argued that the Japanese volcanic area is in some way different from the Lahanos volcanic area, so that the above observations are not relevant to Lahanos. However, in northern Honshu, mineral deposits closely similar to Lahanos are found in the "Kuroko" ores of the green tuff region (Fig. 40). Details of the kuroko ores are given by Kato, 1928 and 1934; Japanese Geol. Surv., 1960; Jenks, 1966; Maruyama, 1967, but the principal features of interest are well summarised by Jenks (loc.cif.). In vertical sequence kuroko or black ore (with mainly sphalerite, galena and barite, and smaller amounts of pyrite, chalcopyrite, tetrahedrite

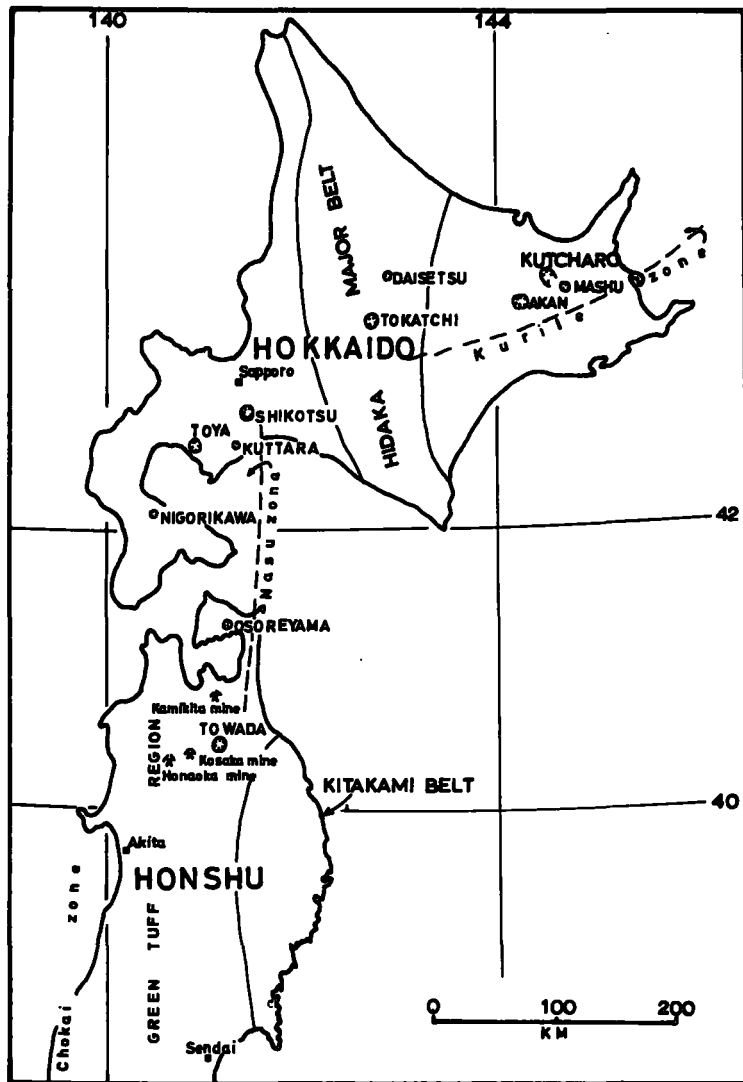


FIG.40. Map of Hokkaido and northern Honshu, showing location of old massifs (shaded), volcanic zones, principal calderas, and selected black ore mines.

(AFTER JENKS, 1956)

etc.) is underlain by Oko or Yellow ore (pyrite and chalcopyrite) then Keiko or siliceous ore (quartz, pyrite, chalcopyrite - sometimes in stockwork form). Large masses of anhydrite and gypsum are found in some of the ore bodies. The ore bodies are semi concordant deposits in dacitic to rhyolitic tuffs of middle Miocene age. The sequence is believed to have been largely deposited under marine conditions and Late Miocene clastic sediments overlies the volcanic sequence.

A very close similarity with the Lahanos deposit and other deposits of the Eastern Pontus ore province exists, even to the general tectonic setting and relationship to the Alpine orogenic belt, and the common occurrence of greenish propylitic alteration in the stratified volcanic rocks. There seems to be no significant difference in rock types between the Cenozoic volcanics of Hokkaido, which do not have kuroko ores, and the Kuroko bearing Miocene volcanics of Honshu. Thus, again, it seems unlikely that the volcanicity or the volcanic rocks are the source of the mineralisation. One difference that may be significant is that the Miocene rocks formed below the sea "in irregular marine depressions somewhat sheltered among islands and peninsulas chiefly of volcanic origin" (Jenks, 1966, p.464) whilst the recent volcanoes discussed above formed on land.

It is therefore necessary to find some source for the copper, lead, and zinc other than the volcanic activity. In Anätolia, and particularly to the south of the mapped area at Lahanos, bodies of granite are found intruded into the base of the volcanic rocks

(See Map 2). It is a common observation that such granitic bodies may produce hydrothermal solutions carrying copper, lead, zinc, gold, bismuth, arsenic and other elements such as are found in the Lahanos deposit. Occasional veinlets of sulphide mineralisation are found in the Lower Basic Series in the Lahanos area, far below the level of the main ore bodies, and in the granite itself. The occurrence in the area of economic vein deposits has been described, of a type commonly associated with granitic intrusions.

As these hydrothermal solutions moved up into the volcanic rocks, they presumably encountered warm volcanic waters carrying CO_2 , HCl , and H_2S - complexing ions that would increase the solubility of the dissolved metal ions and at the same time prevent their precipitation by a simple cooling process (Barnes, 1967, p.376). In the case of pyrite, experimental work (Barnes, 1967, p.365) shows that hydrosulphide or chloride complexes do not greatly increase the solubility, but when ammonium is present with H_2S , solubility is increased and this increases enormously at temperatures above 250°C . Ammonium is present in volcanic waters (see Table 29), and this probably explains the abundance of pyrite in the kuroko ores and the pyrite deposits of Cenozoic age in Hokkaido. This is the one case where the metal is probably derived by leaching of the volcanic rocks.

Because of the submarine formation of the Lhanos volcanics (the occurrence of pillow lavas, absence of signs of subaerial weathered surfaces on the lava flows, presence of interbedded limestones), sea water trapped in the rocks will be a further source

of chloride complexing agents. With upward movement, the solutions will cool and this is normally taken as a sufficient condition to produce precipitation from hydrothermal solutions. Experimental work shows that in fact this is not so - the solubility of the zinc hydrosulphide complex is nearly independent of temperature up to 200°C (Barnes, 1967, p.354) and the solubility of various compounds can increase with falling temperature (Helgeson, 1964, p. 96; Barnes, 1967, p. 405). Thus, where the solutions were able to move upwards with relative ease through cooling cracks and joints in the lavas, no deposition took place. It was only when the free upward travel was impeded by fine grained pyroclastic beds of restricted permeability that a precipitation mechanism could operate. This mechanism has been described in detail by Helgeson (1964) for the case of lead chloride complexes and involves hydrothermal alteration of the wall-rock, a consequent change in composition of the solution and this in turn leads to precipitation of sulphides. Fig. 41 is Helgeson's diagram showing that the solubility of galena is sensitive to the Na/H ratios in solution at a given temperature, from his calculations of equilibria in the system $PbS - NaCl - HCl - H_2O$. Superimposed stability fields for K-feldspar, K-mica and kaolinite are shown, relative to the K/H abscissa, which is positioned relative to the Na/H abscissa so as to give Na/K ratios consistent with those common in fluid inclusions.

Consider a solution represented by A on the diagram travelling freely along a vertical fissure. On cooling to C, it alters feldspar

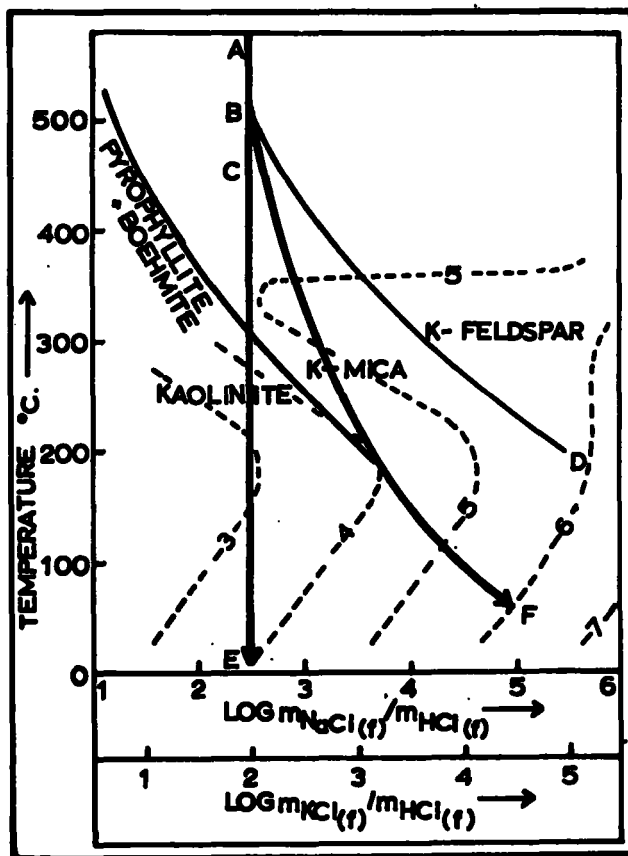


FIG.41. Calculated "A" isosolubility curves for galena in NaCl-HCl-H₂O solutions at fixed $m_{\text{NaCl}(f)} = 3.0$ with superimposed phase relations in the system K₂O-Al₂O₃-SiO₂-H₂O at 15,000 psi after Hemley.⁽⁷⁾ Light solid lines are phase boundaries, dashed lines isosolubility curves, and heavy solid lines represent various compositional trends of solutions moving along a given geothermal gradient. The numbers indicate log $m_{\text{Na}(f)}$.

(AFTER HELGESON, 1964)

in the fissure walls to sericite, loses H in the process and so its Na/H ratio moves slightly to the right along curve BD. Further solution passing this point is in equilibrium with the sericite and so passes up the fissure, eventually finding unaltered wall to react with at a lower temperature. Thus, apart from a thin alteration skin, most of the solution passes up without any appreciable reaction with the wall rock.

The solution encountering a horizontal layer of pyroclastic rock has much more opportunity for reaction - the larger surface area of the fine grained pyroclastic and the increased time for reaction caused by the restricted permeability - and must pass through the rock rather than along open channels. As a consequence of the reaction its composition will change along a curve such as BF, towards a region of low solubility for the sulphide, which will therefore be precipitated. It is interesting to note that because of the form of the solubility curves for the sulphide, after precipitating sulphide with falling temperature, the curve BF may enter a zone where the solubility increases with decreasing temperature. Thus, sulphide already precipitated may be re-dissolved, which gives a reason for the replacement phenomena so commonly seen in these ores, and for the successive formation of the same mineral at different times. Helgeson (1964, p.105) shows that the total H^+ added to a wall-rock during hydrothermal alteration is commensurable with the amount of lead in the vein and that alteration of wall-rock to a depth of one meter can account for a vein of galena more than 12 cm wide. The

process described therefore seems to give a satisfactory quantitative as well as qualitative explanation of observations.

Calcite and dolomite also have increasing solubility with decreasing temperature so that simple cooling is again inadequate to explain their formation. Boiling of the solution with loss of CO_2 can cause their precipitation, but if the pressure were low enough to allow this, deposition of these minerals in all rocks at the same level would occur, and this is not found. Loss of H from the solution and its exchange for K, Na, Ca and Mg in the country rock, does also however cause precipitation of these carbonates, so the same mechanism is operative as with the sulphides. Barnes (1967, p.413) gives reasons why highly magnesium rich solutions are not necessary to form dolomite at temperatures above 250°C and why it may be formed in preference to calcite in alteration zones caused by hydrothermal fluids in silicate rocks.

Barite requires no detailed consideration, since its solubility decreases with decreasing temperature, but the presence of gypsum is less easily explained. As Barnes (1967, p. 419) points out, gypsum should only occur in hydrothermal deposits formed below 57°C or in the zone of secondary alteration. Anhydrite can however be formed at temperatures above 400°C due to the reaction $4\text{SO}_2 + 4\text{H}_2\text{O} \rightleftharpoons \text{H}_2\text{S} + 3\text{H}_2\text{SO}_4$ which takes place in hydrothermal fluids during cooling from 600°C to 400°C . The formation of gypsum would then occur from the anhydrite at temperatures below 57° . This explanation for the gypsum at Lahanos and Murgul is supported by the observed occurrence

of anhydrite and gypsum in some of the Japanese Kuroko ores.

Thus a mechanism has been described to account for the observed mineralogy and location of the Lahanos deposit and other deposits of similar type including the Japanese kuroko ores. Whilst submarine pyroclastics are important in providing complexing ions and a precipitation mechanism, the ultimate origin of the economic metals is mainly in hydrothermal solutions arising from subjacent granitic bodies.

REFERENCES

- ADAMIAN, A.A. (1966). The problem of the genesis of tuff-tufflava formations in Armenia. Tufflavas and ignimbrites, p.41-45. American Elsevier Publishing Company, Inc, New York.
- AHRENS, L.H. and TAYLOR, S.R. (1961). Spectrochemical Analysis: Addison-Wesley Series in the Earth Sciences. p.454.
- ANDERSON, C.A. (1969). Massive sulphide deposits and volcanism: Econ. Geol. vol. 64, p.129-146.
- ARNI, P. (1939). Tektonische Grundzüge Ostanatoliens und benachbarter Gebiete: M.T.A. Publ., Serie B, No. 4, Ankara.
- BADGLEY, P.C. (1959). Structural methods for the exploration geologist and a series of problems for structural geology students: Harper and Brothers, publishers, New York.
- BANNISTER, F.A. (1940). Bravoite from Mill Close mine, Derbyshire: Min. Mag., vol. 57, p.227.
- BARNES, H.L. (1960). Ore solutions, Carnegie Institution of Washington, Geophysical Laboratory Yearbook 59, p.137-141. Experimental evidence for the solubility of sphalerite in hydrosulphide solutions.
- BARNES, H.L. (1967). Geochemistry of hydrothermal ore deposits, 670p: Holt, Rinehart and Winston, Inc.
- BARTON, P.B. and KULLERUD, G. (1958). The Fe-Zn-S System: Carnegie Inst., Washington, Ann. Rep. Dir. Geophys. Lab., 1957-1958, Vol. 57, p.227.
- BARTON, P.B., Jr. (1959). The chemical environment of ore deposition and the problem of low-temperature ore transport; in Researches in Geochemistry: P. Abelson, Ed., John Wiley and Sons, New York, p. 279-299.
- BARTON, P.B. Jr. and SKINNER, B.J. (1967). Sulphide mineral stabilities: Geochemistry of hydrothermal ore deposits, p. 236-333; Edited by Barnes, H.L. Holt, Rinehart and Winston, Inc.
- BASTIN, E.S. (1950). Interpretation of ore textures: Geo. Soc. Amer. Mem. 45.
- BASTIN, E.S. et al. (1931). Criteria of age relations of minerals: Econ. Geol. Vol. 26, p.561-610.
- BATEMAN, M.A. (1956). Economic mineral deposits: John Wiley and Sons Inc.

- BERRY, L.G. and MASON, B (1959). *Minerology, Concepts, descriptions, determinations*: W.H. Freeman and Company, San Francisco, California.
- BLUMENTHAL, M.M. (1946). Die neue geologische Karte der Türkei und einige ihrer Stratigraphisch-tettonischen Grundzüge: *Eclogae Geol. Helv.*, vol. 39, No. 2.
- BORCHERT, H. (1934). Über Entmischungen im system Cu-Fe-S und ihre Bedeutung als geologische Thermometer; *Chem. der Erde*, Vol. 9, p. 145-172.
- BORCHERT, H. (1951). Die Zonengliederung der Mineralparagenesen in der Erdkruste: *Geologische Rundschau*, Vol. 39, No. 1, p.81-94.
- BORCHERT, H. (1958). Türkiyede inisiyal ofiyolitic magmatizmaya ait krom ve bakir cevheri yataklari: *M.T.A. Ens. Yayinlari Ankara*.
- BOROVIK, S.A., LIZUNOV, N.V. and SHCHERBINA, V.V. (1941). Gallium in the minerals and ores of the Soviet Union: *Acad. Sci. U.R.S.S. Bull., Ser. Geol.*, No. 3, p.150-158.
- BOWEN, N.L. (1956). *The Evolution of the igneous Rocks*: Dover Publ. Inc., New York.
- BOWIE, S.H.U. and HENRY, N.F.M. (1964). Quantitative measurements with the reflecting polarizing microscope: *Trans. Inst. Min. Metall.*, Vol. 73, p. 467-478.
- BRETT, R. (1964). Experimental data from the system Cu-Fe-S and their bearing on exsolution textures in ores: *Econ. Geol.*, Vol. 59, No. 7, p.1241-1269.
- BROWN, J.S. (1948). *Ore Genesis*: The Hopewell Press, p. 27-31, 126-132.
- BRUNN, H. (1952). Les éruption ophiolitique dans le NW de la Grèce, leur relation avec l'oro genèse: *Internant. Geol. Congr. Alger Sect XV*, p. 19-27.
- ✓ BUERGER, N.W. (1934). The unmixing of chalcopyrite from sphalerite: *Amer. Mineral.*, Vol. 19, p. 525-530.
- BURTON, C. (1967). M.Sc. thesis, University of Durham. Unsubmitted.
- CANN, J.R. and VINE, F.J. (1966). An area on the crest of the Carlsberg Ridge: Petrology and magmatic survey. *The Philosophical Transactions of the Royal Society of London, A*, Vol. 259, p.199-217.
- CARSTENS, C.W. (1941a). Om geokjemiske underspkelser av malmer; *Norsk Geol Tids.*, Vol. 21, p.213-221.

- CARSTENS, C.W. (1941h). Zur Geochemie einiger norwegischen Kiesvorkommen: Kgl. Norsk Videnskabs. Selskabs, Forh., Vol. 14, p. 36-39.
- CARSTENS, C.W. (1941c). Über sedimentäre Schwefelkiesvorkommen: Kgl. Norsk Videnskabs. Selskabs, Forh., Vol. 14, p. 120-122.
- CARSTENS, C.W. (1942a). Ein neuer Beitrag zur geochemischen charakteristischen norwegischer Schwefelkieserze: Kgl. Norske Videnskabs. Selskabs, Forh., Vol. 15, p. 165-168.
- CARSTENS, C.W. (1942b). Über den Co-Ni-Gehalt norwegischer Schwefelkiesvorkommen: Kgl. Norske Videnskabs. Selskabs., Forh., Vol. 15, p. 165-168.
- CHAYES, F. (1962). Numerical correlation and petrographic variation: J. Geol., Vol. 70, p. 440-452.
- CHAYES, F. (1964). Variance - covariance relation in some published Harker diagram of volcanic suites: J. Petrol., Vol. 5, p. 219-237.
- COOK, E.F. (1966). Tufflavas and ignimbrites: American Elsevier Publishing Company, Inc., New York.
- DEER, W.A., HOWIE, R. and ZUSSMAN, J. (1962). Rock Forming Minerals, Vol. 1, 2, 3, 5: Longmans.
- DEMIRSOY, S. (1968). Untersuchungen über den einfluss der chemischen zusammensetzung auf die Spektralen Reflexions funktionen und Mikroeindruckhärten : Im Spinell - Dreistoffsystem unter besonderer Berücksichtigung der chromspinell. Im system $FeS_2-NiS_2-CoS_2$, an Zonen eines natürlichen Bravoit-Kristalls: Van der Fakultät für Bergbau und Huttenwesen der Rheinisch - Westfalischen Technischen Hochschule Aachen, West Germany.
- DUBERTRET, L. (1953). Geologie des roches vertes du Nord-Ouest de la Syrie et du Hatay (Turquie): Notes et Memoires sur le Moyen-Orient, Vol. VI. Paris.
- DUNCOMB, P. and SHIELDS, P.K. (1966). The effect of excitation potential on the absorption corrections: 'The Electron Microprobe', p. 284: John Wiley and Sons, New York.
- DUNCOMB, P. and REED, S.T.B., (1967). The calculation of sloping power and backscatter effects in electron probe microanalysis: Tube Investments Research Laboratories Technical Report No. 221.
- EDWARDS, A.B. (1947). Textures of the Ore Minerals and their Significance: Aust. Inst. Min. Met. (Inc.), Melbourne.
- EGERAN, E.N. (1947). Tectonique de la Turquie et relations etc. G. Thomas, Nancy.

- EGERAN, EBN. and LAHN, E. (1951). Kuzey ve Orta Anadolunun tektonik durumu hakkında not: M.T.A. Mecm. No. 41, Ankara.
- ERENTÖZ, C. (1966). Contribution à la stratigraphie de la Turquie: Bull. M.T.A., No. 66, Ankara.
- EVARD, P. (1945). Minor elements in sphalerite from Belgium: Econ. Geol., Vol. 40, p.568-574.
- FLEISCHER, M. (1955). Minor elements in some sulphide minerals: Econ. Geol., Fiftieth Ann. Vol., p. 970-1024.
- GABRIELSON, O. (1945). Studier över element fördelningen zinklanderna från Svenska fyndorter: Sver. Geol. Undersokn., Ser. C, No. 468, Arsbok 39, No. 1, p. 1-52 (English Summary).
- GATTINGER, T.E., ERENTÖZ, C. and KEVIN, I. (1961). Explanatory text of the Geological Map of Turkey, Sheets Trabzon, Samsun and Sinop (1:5000000): M.T.A. Publ. Ankara.
- GAVELIN, S., and GABRIELSON, O. (1947). Spectrochemical investigation of sulphide minerals from ores of the Skellefte district. The significance of minor constituents for certain practical and "theoretical problems of economic geology: Sver. Geol. Undersokn., Ser.C, No. 491, Arsbok 41, No. 10, p.1-45.
- GEOFFROY, J. de (1960). Çayeli, Pazar ve Ardeşen bölgelerinin jeolojisi ve Maden Yatakları: M.T.A. raporu, Ankara.
- GEORGE, M. (1969). M.Sc. Thesis, University of Durham.
- GIBBONS, G.S. (1967). Optical anisotropy in pyrite: Amer. Min., Vol. 52, p.359-370.
- GINZBERG, I.I. (1960). Principles of geochemical prospecting: Trans. from Russian by V.P. Sokoloff. New York and London Pergamon. 311p.
- GOLDSCHMIDT, V.M. (1954). Geochemistry; Edited by Alex Muir: Oxford Univ. Press, London.
- GORSHKOV, G.S. (1967). Volcanic phenomena and the upper Mantle: Chemistry of the earth's crust, Vol. II, p. 41-51; Printed by S. Manson, Jerusalem. Binding: Wiener Bindery Ltd.
- GRAY, I.M. (1961). Unpublished Ph.D. thesis, Univ. of London.
- GRAY, I.M. and MILLMAN, A.P. (1962). Reflection characteristics of ore minerals: Econ. Geol., Vol. 57, p. 325-349.
- GREENWOOD, P.B. (1969). In preparation Ph.D. thesis, Univ. of Durham.

- HOLLAND, J.G. and BRINDLE, D.H. (1966). A self consistent mass absorption correction for silicate analysis by X-ray fluorescence: *Spectrochimica Acta.*, Vol. 22, p. 2083-2093.
- HOLMES, A. (1932). The origin of igneous rocks: *Geol. Mag.*, Vol. 69, p.543-558
- INESON, P.R. (1967). Trace element geochemistry of wall-rock alteration in the Pennine orefield and Cumberland ironfield: Unpublished Ph.D thesis, Univ. of Durham.
- IVANOVE, V.V. (1964). Distribution of Cadmium in ore deposits: *Geochemistry international 1964 volume*, p. 757-768.
- IWAO, S. (1956). Hydrothermal Gypsum Deposits of the Wanibuchi mine, Japan, with special reference to alteration of Wall-Rocks: *Jap. Journ. Geol. Geogr.*, Vol. 27, p.105-131.
- JAPAN GEOLOGICAL SURVEY (1960). *Geology and Mineral Resources of Japan*, 2d ed., Dai-Nippon Printing Co., Ltd., 304p.
- JENKS, W.F. (1966). Some relations between Cenozoic volcanism and ore depositions in northern Japan: *New York Acad. Sci. Trans.*, Ser. 2, vol. 28, No. 4, p. 463-474.
- JOHANNSEN, A. (1937). A descriptive petrography of the igneous rocks, vols. I, II, III: The Univ. of Chicago press Chicago, Illinois.
- KAHRER, C. (1958). Die Kupferlagerstätte Murgul in der nordöstlichen Türkei: M.T.A. Publ., Ankara.
- KAHRER, C. (1960). M.T.A. Raporu, Ankara.
- KANEHIRA, K. and BACHINSKI, D. (1967). Framboidal pyrite and concentric textures in ores of the Tilt Cave mine, northeastern Newfoundland: *The Canadian min.*, vol. 9, part. 1, p.124-128.
- KANIA, T.E.A. (1936). Some notes on the origin of pyritic copper deposits of the mesothermal type: *Econ. Geol.*, Vol 31, p. 453-471.
- KATO, T. (1928). Some characteristic features of the ore deposits of Japan related genetically to the late Tertiary volcanic activity: *Japan Jour. Geol. and Geogr.*, Vol. 6, p. 41-43.
- KATO, T. (1934). The types of copper ore deposits of Japan: *Geol. Soc. Tokyo Jour.*, Vol. 41, No. 487, p. 155-160.
- KERR, P.F. (1959). *Optical Mineralogy*: Mc Graw Hill Book Company Inc., London.

- " "
- Gümüş A. (1964). Genesis of some Cupreous pyrite deposits of Turkey: Cento. Symposium on Mining Geol. the Base metals, Turkey. p.152-154.
- GUSTAFSON, L.B. (1963). Phase equilibria in the system Cu-Fe-As-S: Econ. Geol., Vol. 58. p. 667-701.
- HALLIMOND, A.F. (1957). Direct measurement of the standard reflectances with the microphotometer: Min. Mag., London, Vol. 31, p. 487-494.
- HALLIMOND A.F. and BOWIE, S.H.U. (1964). On the reflectivity of pyrite: Min. Mag. London, Vol. 111, p. 385-387.
- HARKER, A. (1964). Petrology for students, an introduction to the study of rocks under the microscope: Eighth edition, Cambridge Univ. Press.
- HAWKS, H.E. and WEBB, J.S. (1962). Geochemistry in Mineral Exploration: Harper's Geosc. Seris. New York. 415 p.
- HAWLEY, J.E. (1952). Spectrographic studies of pyrite in some Eastern Canadian gold mines: Econ. Geol., Vol. 47, p. 260-304.
- HAWLEY, J.E. and NICHOL, I. (1961). Trace elements in pyrite, pyrrhotite and chalcopyrite of different ores: Econ. Geol., Vol. 56, p.467-487.
- HAYCOCK, M. (1931). A method for sampling minerals in polished sections: Econ. Geol., Vol. 26, p. 414-420.
- HELGESON, H.C. (1964). Complexing and hydrothermal ore deposition: International Series of Monographs in the earth sciences, Vol. 17, p. 1-128. Macmillian Company, New York.
- HENRIQUES (1957). Arkiv for mineralogi och Geologi, vol. 2, p. 277.
- HINNERS, N.W. (1963). The solubility of sphalerite in aqueous solutions at 80°C: Unpublished Ph.D. dissertation, Dept. Geology, Princeton, Univ.
- HOEHNE, K. (1952). Die Verbreitung des Arsens auf den Erzlargerstätten des schlesischen geburges und sein Vorkommen in schlesischen Pyriten: Neus Jahrb. Mineral., Monatsh., p. 4-13.
- HOLLAND, H.D. (1956). The chemical composition of vein minerals and the nature of ore forming fluids: Econ. Geol., Vol. 51, p.781.
- HOLLAND, H.D. (1959). Some applications of thermochemical data to problems of ore deposits. I-stability relations among the oxides, sulphides, sulphates, carbonates of ore and gangue minerals: Econ. Geol., Vol. 54, p. 184-233.
- HOLLAND, H.D. (1965). Some applications of thermochemical data to problems of ore deposits. 2-Mineral assemblages and the composition of ore forming fluids. Econ. Geol., Vol. 60, p. 1101 - 1166

- KETIN, I. (1951). "Über die Geologie der Gegend von Bayburt in Nordost-Anatolien. Rev. Fac. Sci. Univ. Istanbul. Ser. B, Vol. XVI, Fasc 2, Ankara.
- KETIN, I. (1959). "Türkiyenin orojenik gelişmesi: M.T.A. mecm., No. 53, Ankara.
- KETIN, I. (1966). Tectonic units of Anatolia (Asia Minor): Bulletin of the Mineral Research and exploration Institute of Turkey, No. 66, Ankara.
- KIEFT, C. (1956). Harsit nehri vadisi havzasi metalik maden yataklari hakkında bazi mulahazalar: M.T.A. mecm. No. 48, Ankara.
- KINEŞ, M.T. (1969). The geology and the ore mineralisation in the Keban Area, East Turkey: unpublished Ph.D. thesis Univ. of Durham.
- KINKEL, A.R. (1966). Massive pyritic deposits related to vulcanism and possible methods of emplacement: Econ. Geol., Vol. 61, No. 4, p.673-694.
- KLAY, L. (1962). "Erenkoy-Başkoy-Yk. Potocur ve P 1711 (Murgul Suyu D.) arasindaki bolgeye ait jeolojik harita: M.T.A. raporu No. 3032, Ankara.
- KOSTOV, I. (1957). Trans. All. Union Min. Soc. No. 3, p. 336-342. Aspects of theoretical Mineralogy in the U.S.S.R. Battey and Tomkeieff 'International series of Monographs on edited Sciences, Vol. 18'.
- KOVENKO, V. (1942). Mines de Cuivere de Kuvarshan de la region d'Artvin. M.T.A. mecm. No. 2/27, Ankara.
- KOVENKO, V. (1943). "Giresun vilayetinde Espiye ve Gorele do llaylarindaki Karaerik, Agalik, Israil, Ilh.Madenleri: M.T.A. mecm. 1/29, Ankara
- KRAEFF, A. (1963a). A contribution to the geology of the region between Sirya and Ardanuç : Bulletin of the Mineral Research and Exploration Institute of Turkey, No. 60, Ankara.
- KRAEFF, A. (1963b). Geology and mineral deposits of the Hopa-Murgul region (western part of the province of Artvin), NE Turkey: Bulletin of the Mineral Research and Exploration Institute of Turkey, No. 60, Ankara.
- KRAUS, E.C. (1958). Dogu Anadolu orojenleri ve bunlarin şariyaj mesafeleri: M.T.A. mecm., No. 51, Ankara.
- KRAUSKOPF, K.B. (1967). Source rocks for metal-bearing fluids, p. 1-33, in Barnes, H.L., ed., Geochemistry of Hydrothermal Ore Deposits: Holt, Rinehart, and Winston, Inc., 670p. New York.

- KRAUSKOPF, K.B. (1967). Introduction to geochemistry, International series in the earth and planetary sciences: Mc Graw-Hill Book Company.
- KUDENKO, A.A. and STETSSENKO, V.P. (1964). The system ZnS + FeS as a geological thermometer: Geochemistry international 1964 volume, p. 1091 - 1095.
- KULLERUD, G. (1953). The FeS-ZnS system. A geological thermometer: Norsk Geol. Tids., vol. 32, p. 61-147.
- KULLERUD, G., VOKES, F.M. and BARNES, H.L. (1959). On exhalative-sedimentary ores: Geol. Foren. Stockholm Forh., vol. 81, no. 1, no. 496, p. 145-148.
- KULLERUD, G. (1967). Sulphide studies: Researches in geochemistry, vol. II, p 286-321; ed. by P.H. Abelson: John Wiley and Sons, Inc.
- KUNO, H. (1950). Petrology of Hakone Volcano and adjacent areas, Japan Bull. Geol. Soc. Amer., Vol. 61, p. 957-1020.
- KUNO, H. (1953). Plateau basalt lava of East Manchuria: Proc. 7th Pacific Sci. Cong. New Zealand, Vol. 2, P. 375-382.
- KUNO, H. (1954). Geology and petrology of Omuru-yama Volcanic group, North Izu: J. Fac. Sci. Univ. Tokyo 11, vol. 9, p. 241-266.
- KUNO, H. (1959). Origin of Cenozoic petrographic provinces of Japan and surrounding areas: Bull. Volcan. Ser II. 20, p. 37-76.
- KUNO, H. (1960). High-alumina basalt: J. Petrol., Vol. 1, P. 121-145.
- LARSEN, E.S. (1936). Petrologic results of a study of the minerals from the Tertiary volcanic rocks of the San Juan Region, Colorado: Amer. Min., Vol. 21, p.670-701.
- LAUNAY, L. de and URBAIN, G. (1910). Recherches sur la metallogenie des blendes et des minerais qui en derivent: Soc. Geol. France, Bull. Vol. 10, p. 787-795.
- LEPP, H. (1956). Precision measurements of the cell edge of synthetic pyrite: Amer. Min., Vol. 41, p. 347.
- LEVY, C. (1966). Contribution a la mineralogie des sulfures de cuivre du type $Cu_3 \times S_4$. Les Bioxydes de Manganese cristallographie et conditions de gisement: Publié dans le memoire du bureau de recherches geologiques et minières.
- LINDGREN, W. (1933). Mineral Deposits: Mc Graw-Hill Book Company, Inc., New York.

- LINDROTH, G.T. (1946). The crystal structure of pyrrhotite in iron sulphide ores of Sweden: Tek. Tid., Vol. 76, p. 383.
- LONG, J.V.P. (1966). Cambridge, Dept. Min. Pet., private publication.
- LOVE, L.G. (1957). Micro organism and the presence of syngenetic pyrite: Geol. Soc. London Quart. Jour., Vol. 113, p. 429-440.
- LOVE, L.G. (1962a). Biogenic primary sulphide of the Permian Kupferschiefer and Marlslate: Econ. Geol., Vol. 57, p. 350-366.
- LOVE, L.G. (1962b). Further studies on micro-organism and the presence of syngenetic pyrite: Paleontology. Vol. 5.
- LOVE, L.G. and AMSTUTZ, G.C. (1969). Framboidal pyrite in two andesites: N. Jb. Mineralogie. Monatshefte, Jg 1969, H.3, p. 97-108, Stuttgart.
- LOVERING, T.S. (1949). Rock alteration as a guide to ore, East Tintic district, Utah: Econ. Geol., Mono.
- LOVERING, T.S. (1961). Sulphide ores formed from sulphide-deficient solutions: Econ. Geol., Vol. 56, p. 68-99.
- MACKAY, R.A. (1946). The control of impounding structure on ore deposition: Econ. Geol. Vol. 41, p. 13-46.
- MALEYEV, E.F. (1966). Genetic types of clastolavas and their distinction from ignimbrites: Tufflavas and ignimbrites, p. 27-31. American Elsevier Publishing Company, Inc., New York.
- MANSON, V. and POLDERVART, A. (1964). Geochemistry of basalts and dolerites: (Abs). Spec. pap. Geol. Soc. Amer., Vol. 82, p. 127.
- MARPLES, J.A.C. and SHAW, J.L. (1966). Two crystallographic computer programmes for lattice parameter refinement and for calculating expected line position: United Kingdom Atomic Energy Authority Research Group Report AERE - R.5210.
- MARUYAMA, S. (1967). Kuroko Geology: World Mining, April, 1967, p.47-49.
- MATSUMOTO, I. (1963). On the origin of the Neogene Volcanic series in Southwest Japan: J. Geosci. Osaka City Univ., Vol. 7, p.49-79.
- MAUCHER, A. (1960a). Die Kieserze von Keltaş, ein Beispiel Submariner Gleitfalten in exhalative sedimentären Erzlagerstätten. Neues. Jahrb. f. Min. Abh. Bd. 94.
- MAUCHER, A. (1960b). 1960 senesinde Tirebolu ve Murgul'da yapılan tetkik gezileri hakkında seyyahat raporu (neşredilmemi), M.T.A., Ankara.

- MOORHOUSE, W.W. (1959). The study of rocks in thin sections: Harper International Student reprints.
- MORIMOTO, N. and KULLERUD, G. (1961). Polymorphism in bornite: Amer. Min., Vol. 46, p. 1270-1282.
- MORIMOTO, N. (1964). Structures of two polymorphic forms of Cu_5FeS_4 : Acta Cryst., Vol. 17, p. 351-360.
- MORONEY, M.J. (1967). Facts from Figures, p. 56-65: Penguin Books.
- McKINSTREY (1963). Mineral assemblages in sulphide ores: The system Cu-Fe-As-S: Econ. Geol., Vol. 58, p. 483-506.
- NESTEROVA, Y.S. (1958). The chemical composition of galena: Geochemistry (Geokhimiya) No. 7, p. 835. Geochem. Soc. Translation.
- NEUHAUS, A. (1942). Über die Arsenführung der dichten Schwefelkiese (Melnikowit-Pyrite) Gelpyrite von Wresloch, Baden, und Deutsch-Bleischarley, Oberschlesien: Metall. U. Erz, Vol. 39, p. 157-189.
- NICHOL, I. and PHILLIPS, R. (1965). Measurement of spectral reflectivity of manganese oxides: Mineralog. Mag., London Vol. 35, p.200-213.
- NOCKOLDS, S.R. and ALLEN, R. (1953). The geochemistry of some igneous rocks series: Geochim. Cosmochim. Acta, Vol. 4, p. 105-142.
- NOCKOLDS, S.R. (1954). Average chemical composition of some igneous rocks: Bull. Geol. Soc. Amer., vol 65, p. 1007-1032.
- NOCKOLDS, S.R. and ALLEN, R. (1955). The geochemistry of some igneous rock series: Geochim. Cosmochim. Acta, Vol. 4, p. 42-105.
- NOCKOLDS, S.R. and ALLEN, R. (1956). The geochemistry of some igneous rock series, part III: Geochim. Cosmochim. Acta, vol. 9, p.34-77.
- NODDACK, I. and NODDACK, W. (1931). Die Geochemie des Rheniums: Zeitschr. Phys. Chem., vol. 154A, p. 207-244.
- NOWACK, E. (1932). Kreide-Entwicklung und Grosstektonik in Nord. Anatoliens Zentralblatt f. Min. etc., B. Stuttgart.
- OFTEDAL, I. (1940). Untersuchungen über die Nebenbestandteile von Erzmineraleien norwegischer zinkblende-führender vorkommen: Norsk. Videnskap. Akad., Skrifter, Mat. - Naturwiss - Kl., No.8, p.103.
- OFTEDAHL, C. (1958). A theory of exhalative - sedimentary ores: Geologiska Föreningens I. Stockholm för handlingar. 492 Band 80, Hafte 1, p. 1 - 19.

- O'HARA, M.J. (1965). Primary magmas and the origin of basalts: Scot. Journ. Geol., part 1, Vol. 1, p. 19-40.
- ORCEL, J. (1935). L'éclat des minéraux et la mesure de leur pouvoir réflecteur au moyen du microscope photoélectrique: Arch. du Muséum (5^e), Vol. 12, p. 171 - 189.
- OSBORN, E.F. (1959). Role of oxygen pressure in the crystallisation and differentiation of basaltic magma: Amer. Jour. Sci., Vol. 257, p. 609-674.
- OSBORN, E.F. (1962). Reaction series for subalkaline igneous rocks based on different oxygen pressure conditions: Amer. Min., Vol. 47, p. 211 -226.
- OSWALD, F. (1912). Armenien Handbuch d. regional: Geologie, Bd. V/3, Heidelberg.
- OZEROVA, N.A. (1959). On the use of primary dispersion halos of quick-silver in search for lead-zinc deposits (in Russian): Geokhimiya, 1959, p. 638-645.
- PADFIELD, T. and AUCOTT, J.W. (1968). KDF9 correction procedure: Dept. Geol. Univ. Durham.
- POLACHE, C. BERMAN, H. and FRONDEL, C. (1944). The system of mineralogy of J.D. Dana and E.S. Dana: John Wiley and Sons, Inc., Vol. 1, (7th Ed.)
- PARK, C.F. Jr (1955). The zonal theory of ore deposits: Econ. Geol. 50th Ann. volume, p. 226-248.
- PARK, C.F. Jr (1957). The problem of vertical zoning: Econ. Geol., Vol. 52, p.477-481.
- PAULING, L. and BROCKWAY, L.O. (1932). The crystal structure of chalcopyrite $CuFeS_2$: Zeit. Krist., Vol. 82, p. 188.
- PEACOCK, M.A. and SMITH, F.G. (1941). Precise measurements of the cube edge of common pyrite and nickeliferous pyrite: Univ. Toronto Stud., Geol. Ser., Vol. 46, p. 107.
- PETROV, V.P. (1966). Petrologic properties of ignimbrites and tuffaceous lavas and their place among rocks intermediate between lavas and tuffs: Tufflavas and ignimbrites p. 16-26. Amer. Elsevier Publ. Company, Inc., New York.
- PHILIBERT, J. (1963). A method for calculating the absorption correction in electron-probe microanalysis. in 'X-ray optics and X-ray micro-analysis'. Ed. H.E. Pattee, V.E. Cosslett and A. Engström, Vol. 3, p. 379. Academic Press, New York.

- PHILLIPS, F.C. (1954). The use of stereographic projection in structural geology: Edward Arnold (Publishers) Ltd., London.
- PHILLIPS, R. and BRADSHOW, P.M.D. (1966). A test of the linearity of a photomultiplier used for reflectivity measurement: *Mineralogical Magazine*, London, Vol. 35, p. 756-758.
- PHILLIPS, R. and WARE, N.G. (1967). The spectral reflectivity of synthetic calcium monoferrite: *Mineralogical Magazine*, London, Vol. 36, p.422-424.
- POLLAK, A. (1961). Karadeniz sahilinde, Giresun vilayeti dahilinde Lahanos cevher yataklari: M.T.A. Mecm., No. 56, Ankara.
- POLLAK, A. (1961). M.T.A. raporu Ankara.
- POLLAK, A. (1962). M.T.A. raporu, No. 2908, Ankara.
- POLLAK, A. (1962). M.T.A. raporu, No. 14944, Ankara.
- PRYOR, E.J. (1965). *Mineral Processing*: Elsevier Publishing Co. Ltd., (3rd Ed.).
- RAMDOHR, P. (1950). *Die Erzminerale und ihre Verwachsungen*: Akademie-Verlag, Berlin.
- REED, S.J.B. (1965). Characteristic fluorescence corrections in electron-probe microanalysis: *Br. Journ. Appl. Physics*, Vol. 16, p. 913-926.
- REVIEWS (1969). *Econ. Geol.*, Vol. 64, p. 120: Geology of ore deposits (Academy of Sciences of U.S.S.R., Jan-Feb., 1966, Vol. 8, No. 1, in Russian).
- RILEY, L.B. (1936). Ore body zoning: *Econ. Geol.*, Vol. 31, p. 170-184.
- ROEDER, P.L. and OSBORN, E.F. (1966). Experimental data for the system $MgO-FeO-Fe_2O_3-Ca Al_2Si_2O_8 - SiO_2$ and their petrologic implications: *Amer. J. Sci.*, Vol. 264, p. 428-496.
- RUST, G.W. (1935). Colloidal primary copper ores at Cornwall mines, Southeastern Missouri: *Jour. Geol.*, Vol. 43, p. 398-426.
- SAAGER, R. and MIHALIK, P. (1967). Two varieties of pyrite from the Basal Reef of the Witwatersrand system: *Econ. Geol.*, Vol. 62, p. 719-731.
- SANTOKH SINGH, D. (1965). Measurement of Spectral Reflectivity with the Reichert Microphotometer: *Transactions of the Institutions of Mining and Metallurgy*, Vol. 74, part 14, p. 901-916.
- SALES, R.H. and MAYER, C. (1948). Wall-rock alteration at Butte, Montana: A.I.M.M.E. Technical Pub., No. 2400.

- SALES, R.H. and MAYER, C. (1949). Results from preliminary studies of vein formation at Butte, Montana: Econ. Geol., Vol. 44, p. 465-484.
- SALES, R.H. and MAYER, C. (1950). Interpretation of wall-rock alteration at Butte, Montana: Colorado School of Mines Quart., Vol. 45, No. 113, p. 261-273.
- SCHMINCKE, H.U. (1967). Fused tuff and peperites in South-Central Washington: Geol. Soc. Amer. Bull., Vol. 78, p. 319-330.
- SCHNEIDERHOHN, H. (1941). Lehrbuch der Erzlagerstättenkunde, Vol. 1, Jena, 858 p.
- SCHOUTEN, C. (1934). Structure and texture of synthetic replacements in ore spaces: Econ. Geol., Vol. 29, p. 611-658.
- SCHOUTEN, C. (1946). The role of S bacteria in the formation of the so-called sedimentary Cu-ores and pyritic ore bodies: Econ. Geol., Vol. 41, p. 517-538.
- SCHOUTEN, C. (1962). Determination Tables for Ore Microscopy: Elsevier Publishing Co.
- SCHROLL, E. (1951). Spurenelementparagenese (Mikroparagenese) Ostalpiner Bleiglanze; Oesterr Akad. Wiss. Anz. math. - naturw. K., p.6-12.
- SCHROLL, E. (1955). Über das Vorkommen einiger Spurenmetalle in Blei-Zink-Erzen der ostalpinen Metallprovinz: Min. Petr. Mitt. (Tschermak), Vol. 5, p. 183.
- SCHULTZE-WESTRUM, H.H. (1960). Giresun-Trabzon vilayetlerinde yapılan harita çalışmaları hakkında rapor (neşredilmemiş) M.T.A., Ankara.
- SCHULTZE-WESTRUM, H.H. (1961). Giresun civarındaki Aksu deresinin Jeolojik profili: M.T.A. Mecm., No. 57, Ankara.
- SCHWARTZ, G.M. (1931a). Intergrowths of bornite and chalcopyrite: Econ. Geol., Vol. 26, p. 186-201.
- SCHWARTZ, G.M. (1931b). Texture due to unmixing of solid solutions: Econ. Geol., Vol. 26, p. 739-763.
- ✓ SCHWARTZ, G.M. (1942). Progress in the study of ex-solution in ore mineral: Econ. Geol., Vol. 37, p. 345-364.
- ✓ SCHWARTZ, G.M. (1951). Classification and definition of texture and mineral structure in ores: Econ. Geol., Vol. 46, p. 578-591.
- SHAPIRO, L. and BRANNOCK, W.W. (1962). Rapid analysis of silicate, carbonate and phosphate rocks. U.S. Geol. Surv. Bull. No. 1144 - A.

- SHIRINIAN, K.G. (1966). Ignimbrites and tufflavas (principles of classification and conditions of formation particularly in Armenia): Tufflavas and ignimbrites, p. 32-40. Amer. Elsevier Publishing Company, Inc., New York.
- SKINNER, B.J. (1959). Effect of manganese on the sphalerite geothermometer (Abstr.): Geol. Soc. Amer. Bull. Vol. 70, p. 1676.
- SKINNER, B.J., BARTON, P.B. and KULLERUD, G. (1959). Effect of FeS on the unit cell edge of sphalerite, a revision: Econ. Geol., Vol. 54, p. 646.
54
- SKINNER, B.J. (1960). Assemblage enargite-famatinite, a possible geologic thermometer (Abs): Geol. Soc. Amer., Vol. 71, p. 1975.
- SLEMMONS, D.B. (1962). Determination of volcanic and plutonic plagioclases using a three - or four - axis universal stage. Revision of Turner method: Geol. Soc. Amer. Special paper, N.69.
- SMITH, R.E. (1967). Segregation vesicles in basaltic lava: Amer. Journ. Sci., vol. 265, p. 696-713.
- STANTON, R.L. (1955). The anisotropism of pyrite: Australian Journ. Sci., Vol. 18, p. 88-89.
- STANTON, R.L. (1957). Studies of polished surface of pyrite and some implications: Canadian Minerologist, vol. 6, part 1, p. 87-103.
- STOČES, B. (1934). How to determine probable changes in primary mineralisation with increasing depth: Econ. Geol., Vol. 29, p. 93-95.
- STRUNZ, H. (1957). Mineralogische Tabellen. Leipzig.
- STRECKEISEN, L.A. (1967). Classification and nomenclature of igneous rocks: N. Jb. Miner. Abh. 107, 2 und 3, S. 144-240, Stuttgart, Sept. und Okt.
- SUGAKI, A. and YAMEA, N. (1950). Thermal study of copper ores from the Akayama Mine, Japan: Jour. Japanese Assoc. Min. Pet. Econ. Geol. vol. 34, p. 173-178.
- SWANSON, H.E. and FUYAT, R.K. (1953). Standard X-ray diffraction powder pattern: U.S. Bur. Stds., circ. 539, Vol. 2, p. 16.
- SUTHERLAND, K.L. and WARK, I.W. (1955). Principles of Flotation: Austr. Inst. Min. Met., p. 118.
- TAGGART, A.F. (1951). Elements of Ore Dressing: John Wiley and Sons, Inc., New York.

- TANEDA, S. (1962). Frequency distribution and average chemical composition of the volcanic rocks in Japan. Mem. Fac. Sci. Kyushu Univ. Ser. D, Geol., Vol. XII, No. 3, p. 237-255.
- TAYLOR, S.R. EMELEUS, C.H. and EXLEY, C.S. (1956). Some anomalous K/Rb ratios in igneous rocks and their petrological significance: Geochim. et cosmechim. Acta, Vol. 10, p. 224-229.
- TAYLOR, S.R., and WHITE, A.J.R. (1965). Geochemistry of andesite and the growth of continents: Nature 208, p. 271-273.
- TILLEY, C.E. (1950). Some aspects of magmatic evolution: Quart. J. Geol. Soc. London, vol. 106, p. 37-62.
- TOMBLIN, J.F. (1964). The volcanic history and petrology of the Soufriere region, St. Lucia. D. Phil. Thesis Oxford (unpublished).
- TUREKIAN, K.K. and KULP, J.L. (1956). The geochemistry of Strontium? Geochim. et. Cosmochim. Acta, Vol. 10, p. 245-296.
- TURKIYE (1966). "Turkiye Bakir, kurşun ve Çinko Yataklari: M.T.A. yayinlari, No. 133, Ankara.
- TURNER, F.J. and VERHOEGEN, J. (1960). Igneous and metamorphic Petrology: McGraw-Hill Book Company, New York (2nd Ed.).
- UYTENBOGAARDT, W. (1951). Tables for microscopic identification of ore minerals: Princeton Univ. Press, Princeton, New Jersey.
- VARENTSOV, I.M. (1964). Sedimentary manganese ore: Elsevier Publishing Company, Amsterdam-London-New York.
- VLODAVETZ, V.I. (1966). The problem of Tufflavas and ignimbrites: Tufflavas and igimbrites, p. 1-15: Amer. Elsevier Publing Company, Inc., New York.
- WAGER, L.R. and DEER, W.A. (1939). Geological investigation in East Greenland. Part III. The petrology of the Skaergaard intrusion, Kangerd-Lugssuak: Medd. Om. Grønland. 105, no. 4, p. 1-352.
- WAGER, L.R. (1960). The major element variation of the layered series of the Skaergaard intrusion and a re-estimation of the average composition of the Hidden Layered Series and of the successive residual magmas: Journ. Petrol., Vol. 1, p. 364-398.
- WARK, I.W. (1938). Principles of Flotation: Australasian Inst. Min. and Met. (Inc.).
- WASSERSTEIN, B. (1951). Precision lattice measurements of galena: Amer. Min., Vol. 36, p. 102.
- WHITE, D.E. (1968). Environments of generation of some base-metal ore deposit: Econ. Geol., Vol. 63, p. 301-335.

- WIJERSLOOTH, P. de (1946). Karadeniz doğu sahilleri çevresinde "bilhassa kuvarshane bakir yataklari (vilayet Çoruh) hakkında bazı malumat: M.T.A. Mecm. No. 1/35, Ankara.
- WIJKERSLOOTH, P. De and MARKUS, R. (1959). M.T.A, raporu (neşredilmemiş), Ankara.
- WILLIAMS, H. (1932). Geology of the Lassen Volcanic National Park, California: Bull. Dep. Geo. Univ. California, vol. 21, p. 195-385.
- WILLIAMS, H. (1942). The geology of Crater Lake National Park, Oregon: Pub. Carneg. Inst., 540, p. 162.
- WILLIAMS, H., TURER, F.J., and GILBERT, G.M. (1954). Petrography, an introduction to the study of rocks in thin sections: W.H. Freeman and Company, San Francisco.
- WINCHELL, A.N. and WINCHELL, H. (1964). Elements of Optical Mineralogy, An introduction to microscopic petrography: John Wiley and Sons Inc. (4th Ed.).
- YANISHEVSKY, E.M. (1934). The question of the joint occurrences of molybdenum and vanadium in the oxidation zone of ore deposits: Problemy Soviet Geol., vol. 2, p. 135-141.
- YODER, H.S., and TILLEY, C.E. (1962). Origin of basalt magmas and experimental study of natural and synthetic rock systems: Journ. Petrol., vol. 3, p. 342-352.
- YODER, H.S., SHAIRER, J.F., and TILLEY, C.E. (1964). Melting relations of volcanic tholeiite and alkali rock series: Ann. report Geophys. Lab. 1964-1964, p. 69-82.
- ZANKLE, H. (1961). Magmatismus and Bauplan des ostpontischen Gebirges im Querprofil des Harşit Tales, NE Anotalien: Geol. Rundschau, Bd. 51.

APPENDIX

X-ray Fluorescence Technique

10 major elements analysis of the volcanic rocks have been run on the Philips P.W. 1051 semi-automatic and P.W. 1212 automatic spectrograph against the four international standards of G-1, W-1, S-1, T-1 and plus 28 secondary standards supplied by the Geology Department of Durham University. The operating conditions are tabulated in the following tables.

Operating Conditions for 1051 Semi-automatic XRF
- Major Element Analysis

<u>Element</u>	<u>Peak 2θ</u>	<u>Tube</u>	<u>Generator KV</u>	<u>m.A</u>	<u>Crystal</u>	<u>Path</u>	<u>Collimator</u>	<u>Counter</u>	<u>Counter Voltage</u>	<u>Time (Sec)</u>	<u>Discrim.</u>	<u>Attenuation</u>	<u>Amplifier</u>	<u>Ch. Width</u>
Si	78.01	Cr	40	20	E.D.D.T.	Vac	Coarse	flow	1625	50	no	-	-	-
Al	112.65	Cr	32	30	E.D.D.T.	Vac	Coarse	flow	1625	40	no	-	-	-
Fe	57.41	W	40	20	LiF	Air	Fine	flow	1625	20	no	-	-	-
Mg	106.49	Cr	32	30	A.D.P.	Vac	Coarse	flow	1650	80	yes	2	4.14	20 volt
Ca	44.84	Cr	30	20	E.D.D.T.	Vac	Coarse	flow	1625	30	no	-	-	-
Na	72.73	Cr	40	20	Gypsum	Vac	Coarse	flow	1660	100	yes	2	2.80	20 volt
K	106.60	Cr	34	20	LiF	Vac	Coarse	flow	1625	30	no	-	-	-
Ti	55.90	Cr	40	20	LiF	Vac	Coarse	flow	1625	40	no	-	-	-
Mn	62.89	W	40	20	LiF	Air	fine	flow	1575	30	no	-	-	-
S	44.83	Cr	36	20	E.D.D.T.	Vac	fine	flow	1625	40	no	-	-	-

Operating Conditions for 1212 automatic XRF - Major Element Analysis

<u>Element</u>	<u>Peak 2θ</u>	<u>Tube</u>	<u>Generator</u>	<u>Kv</u>	<u>mA</u>	<u>Crystal</u>	<u>Path</u>	<u>Collimator</u>	<u>Counter</u>	<u>Counts</u>	<u>Time (Sec.)</u>
Si	109.15	Cr.	1575	60	32	LiF 110	V+G	Coarse	flow	FC	40
Al	145.13	Cr.	1575	60	32	LiF 110	V+G	Coarse	flow	FC	40
Fe	85.72	Cr.	1575	60	8	LiF 110	air	Fine	flow	FT	20
Mg	79.05	Cr.	1575	50	40	LiF 110	V+G	Coarse	flow	FC	40
Ca	45.07	Cr.	1575	60	8	LiF 110	V+G	Coarse	flow	FC	40
Na	105.05	Cr.	1575	50	40	LiF 110	V+G	Coarse	flow	FC	40
K	50.58	Cr.	1575	60	8	LiF 110	V+G	Coarse	flow	FC	40
Ti	36.58	Cr.	1575	60	8	LiF 110	V+G	Coarse	flow	FC	40
Mn	62.89	W	1575	70	30	LiF 110	air	Fine	flow	FT	20
S	73.50	Cr.	1575	50	40	LiF 110	V+G	Coarse	flow	FC	40

Operating Conditions for Trace Element analysis in Silicates

<u>Element</u>	<u>Peak 2θ</u>	<u>Tube</u>	<u>Generator</u>	<u>Kv</u>	<u>mA</u>	<u>Crystal</u>	<u>Path</u>	<u>Collimator</u>	<u>Counter</u>	<u>Counts</u>	<u>Time</u>
Ba	15.60	W	1675	60	32	LiF 110	V+G	Coarse	S	FT	40
Te	18.26	W	1675	60	32	LiF 110	V+G	Coarse	S	FT	40
Sb	19.08	W	1675	60	32	LiF 110	V+G	Coarse	S	FT	40
Cd	20.95	W	1675	60	32	LiF 110	V+G	Coarse	S	FT	40
Ag	22.68	W	1675	60	32	LiF 110	V+G	Coarse	S	FT	100
Zr	28.31	W	1675	60	32	LiF 110	V+G	Coarse	S	FT	40
Mo	28.93	W	1675	60	32	LiF 110	V+G	Coarse	S	FT	100
Sr	35.85	W	1675	60	32	LiF 110	V+G	Coarse	S	FT	100
Rb	37.78	W	1675	60	32	LiF 110	V+G	Coarse	S	FT	100
Bi	39.11	W	1675	60	32	LiF 110	V+G	Coarse	S	FT	100
Pb	40.70	W	1675	60	32	LiF 110	V+G	Coarse	S	FT	40
As	48.78	W	1675	60	32	LiF 110	V+G	Coarse	S	FT	100
Ga	56.20	W	1675	60	32	LiF 110	V+G	Coarse	F+S	FT	100
Zn	60.63	W	1675	60	32	LiF 110	V+G	Coarse	S	FT	40
Cu	65.62	W	1675	60	32	LiF 110	V+G	Coarse	F+S	FT	40
Ni	71.24	W	1675	60	32	LiF 110	V+G	Coarse	F+S	FT	100
Mn	95.20	W	1670	60	32	LiF 110	V+G	Coarse	F+S	FT	40
Cr	107.12	W	1670	60	32	LiF 110	V+G	Coarse	F+S	FT	100

X-Ray Fluorescence Trace and Major Element Analysis in Sulphides

Operating Conditions for trace element analysis in sulphide

<u>Element</u>	<u>Peak 2θ</u>	<u>Tube</u>	<u>Generator</u>	<u>Kv</u>	<u>mA</u>	<u>Crystal</u>	<u>Path</u>	<u>Collimator</u>	<u>Counter</u>	<u>Counts</u>	<u>Time (Sec)</u>
Ba	15.60	W	1675	60	32	LiF 110	V+G	Fine	S	FT	40
Te	18.26	W	1675	60	32	LiF 110	V+G	Fine	S	FT	40
Sb	19.08	W	1675	60	32	LiF 110	V+G	Fine	S	FT	40
Cd	20.95	W	1670	60	32	LiF 110	V+G	Coarse	S	FT	40
Ag	22.68	W	1675	60	32	LiF 110	V+G	Fine	S	FT	40
Mo	28.93	W	1675	60	32	LiF 110	V+G	Fine	S	FT	100
Sr	35.85	W	1675	60	32	LiF 110	V+G	Fine	S	FT	100
Bi	39.11	W	1675	60	32	LiF 110	V+G	Fine	S	FT	100
As	48.78	W	1675	60	32	LiF 110	V+G	Fine	S	FT	100
Ga	56.20	W	1675	60	32	LiF 110	V+G	Fine	F+S	FT	100
Cu	65.62	W	1675	60	32	LiF 110	V+G	Coarse	F+S	FT	40
Ni	71.24	W	1675	60	32	LiF 110	V+G	Fine	F+S	FT	100
Mn	95.20	W	1670	60	32	LiF 110	V+G	Coarse	F+S	FT	40
Cr	107.12	W	1670	60	32	LiF 110	V+G	Coarse	F+S	FT	100

Operating Conditions for Major Element analysis in sulphide

<u>Element</u>	<u>Peak 2θ</u>	<u>Tube</u>	<u>Generator</u>	<u>Kv</u>	<u>mA</u>	<u>Crystal</u>	<u>Path</u>	<u>Collimator</u>	<u>Counter</u>	<u>Counts</u>	<u>Time (sec)</u>
Ba	15.60	W	1675	60	32	LiF 110	V+G	Fine	S	FT	20
Pb	40.70	W	1675	60	32	LiF 110	V+G	Fine	S	FT	20
Zn	60.63	W	1675	60	32	LiF 110	V+G	Fine	S	FT	20
Cu	65.62	W	1675	60	32	LiF 110	V+G	Fine	S	FT	20

Operating Conditions for X-ray Powder Camera (in copper radiation)

Instrument : Philips PW 1051 Generator unit
 KV & mA : 40 KV, 20 mA
 Radiation : Cu K α , 1.54051
 Filter : Ni
 Collimator : Fine
 Camera : Large camera 114.59 mm in diameter
 Exposure time : 20 hours
 Film : Ilford industrial G fast or Industrial B.

Operating Conditions for X-ray Powder Camera (in Cobalt radiation)

Instrument : Norelco generator unit and Philips PW 1051 generator
 KV & mA : 34 KV, 11 mA
 Radiation : CoK γ (1.78892)
 Filter : Fe γ _{ca}
 Collimator : Fine
 Camera : Large camera with 114.59 mm in diameter
 Exposure time : 24 hours using point source, 40-50 hours using line source
 Film : Ilford industrial G fast or Industrial B.

<u>Minerals</u>	<u>Genera- tor</u>	<u>KV</u>	<u>MA</u>	<u>Radia- tion</u>	<u>Source</u>	<u>Fil- ter</u>	<u>Colli- motor</u>	<u>Expo- sure</u>	<u>Film</u>
NG39 Sph1	PW1051	34	10	CoK α	Point	Fe	Fine	24	Industrial G
NG39 Sph2	PW1051	34	10	CoK α	Line	Fe	Fine	48	Industrial G
M2 Sph1	PW1051	34	10	CoK α	Line	Fe	Fine	48	Industrial G
M2 Sph2	PW1051	34	10	CoK α	Point	Fe	Fine	24	Industrial G
Kd Sph1	PW1051	34	10	CoK α	Line	Fe	Fine	48	Industrial G
Kd Sph2	PW1051	34	10	CoK α	Point	Fe	Fine	24	Industrial G
Kd Sph3	PW1051	40	16	CuK α	Point	Ni	Fine	22	Industrial G
Kd Sph4	PW1051	40	16	CuK α	Line	Ni	Fine	48	Industrial G
NG43-46Cpy	PW1051	40	16	CuK α	Point	Ni	Fine	23	Industrial G
NGD8 Cpy	PW1051	40	16	CuK α	Line	Ni	Fine	48	Industrial G
NGD17 Cpy	PW1051	40	16	CuK α	Point	Ni	Fine	22	Industrial G
M12 Cpy	PW1051	40	16	CuK α	Point	Ni	Fine	24	Industrial G
NGD8 Cpy	PW1051	34	10	CoK α	Line	Fe	Fine	48	Industrial G
NGD17 py	PW1051	34	10	CoK α	Point	Fe	Fine	24	Industrial G
NG39 Cpy	PW1051	34	10	CoK α	Point	Fe	Fine	24	Industrial G
M15 Cpy	PW1051	34	10	CoK α	Line	Fe	Fine	48	Industrial G
Kd Cpy	PW1051	34	10	CoK α	Point	Fe	Fine	24	Industrial G
Kd gl 1	PW1051	34	10	CoK α	Point	Fe	Fine	24	Industrial G
Kd gl 2	PW1051	34	10	CoK α	Point	Fe	Fine	24	Industrial G
NGD8 Brn	PW1051	34	10	CoK α	Point	Fe	Fine	24	Industrial G
NG36 Brn	PW1051	34	10	CoK α	Point	Fe	Fine	24	Industrial G
NGD16 gl	PW1051	34	10	CoK α	Point	Fe	Fine	24	Industrial G
NGD17 gl	PW1051	34	10	CoK α	Line	Fe	Fine	48	Industrial G
M2 gl	PW1051	34	10	CoK α	Point	Fe	Fine	24	Industrial G
NG36 Cpy	PW1051	34	10	CoK α	Line	Fe	Fine	48	Industrial G
NG36 brn	PW1051	34	10	CoK α	Point	Fe	Fine	30	Industrial B

OPERATING CONDITIONS FOR THE DETERMINATION OF CO AND NI
IN DIFFERENT SULPHIDES

Charge Preparation

Internal Standard : Johnson Matthey 'Specpure' Ammonium chloropalladinite
 Buffer : National Carbon Co. - Graphite (SP2)
 Ratio, sample to Internal Standard/Buffer : 3 part sample to 1 part Internal Standard/Buffer
 Standard/Buffer : mixed in a plastic vial using Spex Mixer Mill No. 8000.

Electrode type

Anode : National Special spectroscopic products: Graphite (L1138P 120 x 12, Lot No. 36E)
 Dimension of Crater : 1/8" x 2.5 mm.
 Cathode : Johnson Matthey Carbon sheets (Cat. No. L1205) diameter: 5 mm.

Optical System

Quartz prism Wave-length range : 2750 A° - 4650 A°
 Lens system : Hilger E 958 focussed on slit 7 step filter using 7 steps (Log 2 differences)
 Slit : Height: 9 mm. Width: 0.8 micron
 Camera diaphragm : 14 mm.
 Plate : Kodak B10
 Analytical Gap : 5 mm.

Exposure

Special Conditions : arc in an atmosphere of Argon: Oxygen (ratio 80:20) - at a flow rate of 4 litres/min - through a modified stallwood jet.
 Current : 6.8 A d.c. short circuit
 Burn : 8 A d.c.
 Timing : Preburn: 15 Sec. Exposure: 50 secs.

Photographic

Developer : Kodak DX-80
 Fixer : Kodak AM 33+H for 3 min
 Washing : 25 Minutes
 Finishing : Plates rinsed in distilled water containing Kodak photo-flo solution to ensure drying free from spots.

Lines

Analyses : Co: 3453.505. Ni: 3414.765
 Internal Standard : Pd: 3481.152

Instrument

: A Hilger and Watts Automatic Large Spectrograph E 742 with Quartz Optical System.

THE PREPARATION OF POLISHED SECTIONS

The specimen to be polished is placed in a 37 mm diameter brass cylinder 18 mm high, on a glass plate in a vacuum desiccator. After evacuation with a water pump, Geemar resin (No. ER264) is run into the mould and allowed to set overnight. After removal from the mould, the Geemar disc is ground down by hand on rotating metal laps using first a medium carborundum (Carb. Co. Ltd., grade 3F. RA grit) then fine carborundum (800 grit), washing well with water between stages. The rear face of the disc is then turned down on a lathe to parallelism with the ground specimen face.

Various lapping stages follow - first of all the specimen is lapped with fast cutting alumina grade No 5/20 for about a minute; then with diamond paste abrasive (Hyprez diamond compound 6-W-42 medium and Y4-W-475 fine), each for up to 24 hours, and finally for less than a minute with 'finish polishing' alumina. 6" diam. Pellon polishing discs are used on a metal base lap and oil or demineralised water as lubricant. Specimens from the last lap are cleaned in carbon tetrachloride in an ultrasonic cleaning bath. Finally for electron probe microanalyser study the resin block is turned down to 8 mm. in height in order to fit the microprobe specimen holder.

PREPARATION OF POLISHED THIN SECTIONS

Following preparation of a polished specimen, as described in the previous page, a thin slice is cut from the disc, excess resin is removed by a wet diamond grinding wheel and the slice stored in a numbered envelope to await further treatment. This consists of mounting the slice on a normal 76 mm. microscope slide with Lakeside 70 resin, as when preparing a normal rock thin section, and carrying out the normal grinding processes. When this thin sectioning is completed a 48 mm glass slide is fixed to the ground surface of the specimen with Araldite epoxy resin, then both slides are heated on a hotplate and the slide on the polished surface is removed. A 45 degree bevel is ground on the back of the slide at the end opposite the numbered end to facilitate mounting in the microprobe specimen holder. Remove the excess resin from the slide with a razor blade, wash the specimen in methylated spirit using light friction of the thumb to remove the heat sensitive resin from the specimen surface and then leave the section to dry or dry with an air jet.

Polished and polished thin sections for electron microprobe analyser study have to be carbon coated in the usual form of vacuum coating apparatus.

FLOTATION TECHNIQUE

A laboratory scale design which consists of a one litre buchner separation funnel with porosity 4 is the main cell-tank. The lip was extended to facilitate overflow of the flotation concentrate into a smaller buchner funnel connected with vacuum. Compressed air is introduced through the stem of the flotation funnel. A glass plate and glass rod were used for collecting and skimming the froth manually into the small buchner funnel, to dry the concentrate. Washing with acetone assisted final purification and quick drying. The apparatus is illustrated by Kineş (1969).

This method was used to separate and concentrate chalcopyrite, bornite, galena, sphalerite, pyrite and gangue minerals from the mixed Lahanos ore. The conditions were adjusted to ensure maximum purity of the concentrate of each mineral, rather than maximum recovery of the mineral from the ore. After preliminary breakage of the ore sample with a hydraulic jack, further reduction was carried out in a jaw crusher. Taggart (1951), Pryor (1965) and Wark (1938) suggest that a suitable size range for flotation on the laboratory scale is -48 +60 mesh. Material from the jaw crusher treated in various automatic mills crushed very quickly to a much smaller size than this because of the very friable nature of the ore. It was therefore, necessary to treat the jaw crusher product in a simple percussion mortar and sieve to achieve the desired size range. For each flotation 100 grams -48 mesh + 60 mesh ore was used with a pulp dilution of 20%. After every flotation separation the flotation cell and small buchner funnel were cleaned thoroughly with aqua-regia followed by washing with water in order to prevent any possibility of contamination

by either concentrate or tailing and middlings of the previous run. Every run of concentrate was recycled several times in order to get a sufficient amount of pure concentrate for further study of particular minerals.

The methods and flotation reagents used for separation of the different sulphides and gangue minerals were based on recommendations in the books by Pryor, Sutherland, Wark and Taggart with slight modifications where necessary.

Separation of gangue from sulphides: 0.8 lt water with p.H. 8.5 was used in the one litre buchner flotation funnel. After introducing air gently into the flotation cell, 4.5 mgrs of Potassium ethyl-xapthate per 100 grs -48 and +60 mesh ore is added as collector. A few medicine drops of Cresol, $\text{CH}_3 \text{C}_6 \text{H}_4 \text{OH}$, as a frothing agent were also added and after waiting for even mixing to occur, the dried sample was added. The bubble rate was then increased to achieve flotation. The critical points throughout the process are:

(1) The rate and density of air bubbles. Cresol alone gives fewer and larger bubbles than a mixture of cresol and creosote, but the latter frothing agent also caused flotations of gangue, so cresol alone was used.

(2) p.H. of the pulp. If it is less than 8.5, gangue also floats with sulphides. This was checked by a Pye p.H. meter, using dilute sodium hydroxide or sulphuric acid for adjustments.

Sutherland's & Wark's method combined with Dow's method (Pryor, 1965) is used for chalcopyrite separation from other sulphides and gangue. 25 mgrs of potassium ethyl-xanthate per litre of pulp as collector, 0.45 grs

of $ZnSO_4$ with 0.15 grs of $Na_2 SO_3$ for sphalerite and 0.30 grs of CaO for pyrite per 100grs. of ore were used as a depressant. 6 or 8 medicine drops of cresol and 2 or 3 medicine drops of creosote were used as frothing agent. The acidity of the pulp was maintained at 5.5 with addition of sufficient dilute $H_2 SO_4$.

For sphalerite, 26.7 mgrs of sodium di-ethyl dithiocarbamate per litre of pulp were used as collector, 150 mgrs of CaO depressant for pyrite but activator of silicate; similarly 150 mgrs of $Na_2 SO_3$ per 100 grs of ore as depressant for pyrite, but again activator for silicate; 450 mgrs of $Cu SO_4$ (or copper acetate) per 100 grs of ore as activator for zinc, iron, cobalt, nickel sulphides; 6.8 mgrs of cresol per 100 grs of ore and 2 medicine drops of creosote were used as frothing agent. During the flotation test the acidity of the pulp was kept at about p.H. 5 but not greater than p.H. 6.2.



Consultation of Durham University Theses

A. TO BE SIGNED BY A MEMBER OF STAFF OF THE BORROWING LIBRARY

In handling the undermentioned thesis

.....
TUGAL, T. pyritic sulphide deposits of
.....

..... the Baharos mine area, Eastern Black Sea Region
..... Turkey

Place of deposit of thesis Watts library, Geology Department

I undertake

- (1) not to issue it for consultation until Section B of this form has been completed by the reader.
- (2) to keep it in the library under lock and key when not in use.
- (3) to ensure that the person consulting the thesis knows that it must not be removed from the library.
- (4) to observe strictly any conditions for the method of transport indicated by Durham University, and to return the thesis by registered post.

Signature Laura Barker

B. TO BE COMPLETED BY THE PERSON CONSULTING THE THESIS

In using the above mentioned thesis, I undertake

- (1) to handle it with great care and not to add to, alter or diminish it in any way, or interfere with its structure and arrangement.
- (2) to acknowledge any use made of it, or any quotation from it, in any work of my own.
- (3) not to publish (or in the case of a Music thesis perform) any part of the work without obtaining the consent of the author (or his representatives after his death) during the period of copyright.

Signature C. B. Leitch

Address Imperial College, Dept. of Geology

Date 22/10/74

Geo. Sec.-1

GEOLOGICAL SECTIONS

(From 1:25 000 map)

